International Conference on

Applied Electromagnetic Technology

1st AEMT

Lombok 11 - 15 April 2014

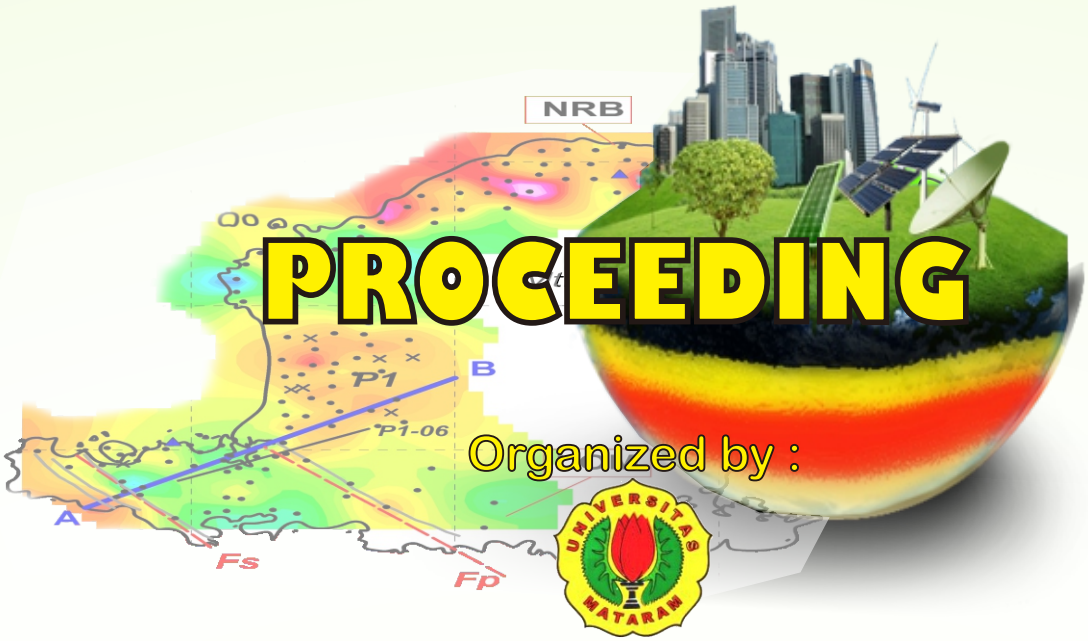

PROCEEDING

Organized by :

Faculty of Engineering
Mataram University

co. Organized by:

University of Indonesia & GFZ Postdam Germany

Universitas Indonesia

GFZ
Helmholtz Centre
POTSDAM

ISBN 978-602-70279-0-9

CONFERENCE ORGANIZER

Advisor

Dirjen Dikti Kemdikbud RI
Direktur Ditlitabmas Dirjen Dikti Kemdikbud RI
Deputy Jaringan & IPTEK Kemenristek RI
Gubernur Nusa Tenggara Barat
Bupati Lombok Tengah
Bupati Lombok Utara

Steering Committee

Prof. Ir. H. Sunarpi, Ph.D (Rector of Universitas of Mataram)
Prof. Ir. Suwardji, M.App.Sc., Ph.D (Vice Rector Universitas Mataram)
Yusron Saadi, ST., MSc., Ph.D (Dean of Faculty of Engineering, Unram)
Prof. Claudia Stolle (GFZ Potsdam Germany, Head of Geomagnetic Section)
Dr. Ir. Muhamad Asvial (Vice Dean I of Faculty of Engineering,UI)
Prof. Mioara Mandea (IAGA Secretary General)
Prof. Sri Widiyantoro (HAGI)
Prof. Hery Hardjono (LIPI)
Dr. Kyoko Nakano (JICA PREDICT)

Program Committee

Dr. Monika Korte (GFZ Potsdam, Germany)
Dr. Joachin Linthe (GFZ Potsdam, Germany)
Prof. Josaphat Tetuko Sri Sumantyo (Chiba University, Japan)
Prof. Katsumi Hattori (Chiba University, Japan)
Prof. Wolfgang Martin Boerner (University Illinois Chicago, USA)
Prof. Riri Fitri Sari (University of Indonesia)
Dr. Harry Arjadi (EMC Laboratory, SMTP-LIPI)
Dr. Fitri Yuli Zulkifli (University of Indonesia)
Ir. Gunawan Wibisono, Ph.D. (University of Indonesia)
Dr. Ir. Dodi Sudiana (University of Indonesia)
Dr. Teti Zubaidah (University of Mataram)
Cahyo Mustiko Octa Muvianto, ST., MSc., Ph.D (University of Mataram)

CONFERENCE ORGANIZER

Organizing Commettee

Chairman : Misbahuddin, ST., MT
Vice Chairman : Rosmaliati, ST., MT
Secretary : Ahmad Syamsul Irfan Akbar, ST., M.Eng
Treasurer : Bulkis Kanata, ST., MT

Secretariat :
Ahmad S. Irfan Akbar, ST., M.Eng
Abdullah Zainuddin, ST., Mt
Sultan, ST., MT
Supriyatna., ST., MT
Akhirudin, ST
Denek Bini Tindih Ring Ubaya
Pitaria Rahim Riani
Puji Hidayati Sari
Tirmizi Yassir Rozak
I Wayan Suwika
Sarah
Suliati Aini
Yuliana Fatmi

Ceremonial :
Abdul Natsir, ST., MT
Ni Made Seniari, ST., MT
Dian Wijaya Kurniawidi, S.Si., M.Si
M. Alfaris, SSi
Lily Maysari A. M.Si
Nurlaily Agustiarini
Tri Yulianti
Risca Arie Wahyuningsih
Aris Widyatmoko
Nurlaily Agustiarini
Rani Rahmawati Syafrin
Edwin Saleh
L. Wahyu Dedy Aprian
Restu Nopiandi Irawan
Dinar Yulyanti
Pahrurrozi
Rosmalita Arini

CONFERENCE ORGANIZER

Seminar	:	Atas Pracoyo, ST., MT., Ph.D Dr. Basari Dr. Arief Udhiarto Akmaludin, ST., MSc., Ph.D Ir. Didi Supriadi Agustawijaya, M.Eng., Ph.D Syahrul, ST., MA.Sc., Ph.D. Dr. Suhayat Minardi, M.Si. Dr. rer.nat Kosim Eko Prajoko, ST., M.Eng., Ph.D Dr. Oki Setyandito, ST., M.Eng. I Nyoman Wahyu Setiawan, ST., M.Eng., Ph.D. I Gede Pasek Suta Wijaya, ST., MT., D.Eng
Accomodation, Transportation, & Tour	:	I Made Ari Nrartha, ST., MT. I Made Budi Suksmadana, ST., MT. Ida Bagus Fery Citarsa, ST., MT. Heri Wijayanto, ST., MT. Cipta Ramadhani, ST., M.Eng. Zainul Ilham Andi Pramadana M. Junaedi
Venue and Facilities	:	Paniran, ST., MT. Dr. Ida Ayu Sri Adnyani, ST., MT. Syafaruddin Ch, ST., MT. Agung Budi Muljono, ST., MT. Sutami Aries Saputra, ST., M.Eng. Ahmad Yani Nawi Naufan Nada M. Sofian Azmi Yoga Samurdita Iqbal Chan Saputra Muliadi Fikri Jamal Heri Hidayat M. Majedi Adib Manggini Syahrullail I Wayan Putra

CONFERENCE ORGANIZER

Meal	:	Bulkis Kanata, ST., MT. Laili Mardiana, S.Si., M.Si Alfina Taurida Alaydrus, S.Si., Msi Aisyah Tatik Muliani Niswatun hasanah Yuli Hartini Yulia Pradewi
Publication and Documentation	:	Made Sutha Yadnya, ST., MT Dr. I Made Ginarsa Padlullah Izyad Fathin Ainul Hamdani Hendra Trisnayadi Susilawati riskia Agus Budi Hendra kurniawansyah p Dwi kurniawan
Sponsorship	:	Sudi Maryanto Al Sasongko, ST., MT. Giri Wahyu Wiriasto, ST., MT Lalu Wirahman Wiradarma, S.T., M.Sc. Agustono, S.T., M.Sc. Baiq Dewi Krisnayanti, M.P Ir. Didi S. Agustawijaya, M.Eng., Ph.D Ir. Miko Eniati, MT Rizal Bahteran Samsul Bahraen Arifatul Hidayati Yuda Pratama Putra Kesawa Edi Wiranata I Wayan Sujatmika Gessy Anggraeni M. Musfariawan At-Thoriq

CONFERENCE ORGANIZER

Security and Health	:	Giri Wahyu Wiriasto, ST., MT M. Bakti Adiguna Wahyu Surya permana Waesal Karni I Gusti Ayu Kusdiah Gameliarini Ari Rahmi Hermawati Handrayani Helni Septa Utani

Conference Organizer Committe:

Faculty of Engineering University of Mataram
Jalan Majapahit No.62 Mataram Kodepos 83115,
Phone : +62-370-636126
Fax : +62-370-636126
Email : aemt@emtech-geomagnetic.org
website : http://aemt2014.emtech-geomagnetic.org

PREFACE

WELCOME FROM THE DEAN OF FACULTY OF ENGINEERING

UNIVERSITY OF MATARAM

First of all, let us praise God Almighty who has bestowed upon us His blessing and thus allow us to participate in the very important event for academicians and scientists around the world. I am delighted that the EMTech Research Group of Faculty of Engineering University of Mataram in co-operation with University of Indonesia and GFZ Potsdam Germany are finally able to organize the strong academic tradition called the 1st International Conference on Applied.
Electromagnetic Technology. The 1st International Conference on AEMT is the culmination of more than one year hard works by the joint committee since the typical event needs a long and well preparation. As a very prestigious event involving many scientists and researchers from different continents, it is truly an honor to organize and to host this scientific event.

We have to admit that Indonesia only contributes a very small part in top-rated research. In our home countries, it can hardly go unnoticed that there is a serious lack of world-class scientific institutions, and yet disturbingly we also see that there is no lack of scientific talent. The existence of Lombok Geomagnetic Observatory can bridge this unusual and extraordinary imbalance. The observatory renders an important contribution for the scientific investigation of the Earth's interior and environment. In the future, the investigation from the observatory will benefit the global research community when the observatory joins the Intermagnet network.

The interest from researchers and scientist around the world is a clear signal that in the right term, global community and Indonesian government together with local authorities can expect to feel positive effect from this event. We are certainly looking forward to bringing this initial step of inauguration of the Lombok Geomagnetic Observatory to the world scientific community. This not beyond our reach if we can establish the links with other key players in the associated areas. The majority of participants who are representing higher institutions as well as research institutions show the importance of the role that the universities and research institutions have to play in bringing quality researches into global development.

Finally, I would like to express my sincere thanks and appreciation to all sponsors who contribute to this event. To all participants who have come from different continents, I would like to extend my very warm welcome to this conference. I wish you all to have a productive and fruitful discussion.

Yusron Saadi, ST., M.Sc., Ph.D
Dean
Faculty of Engineering, University of Mataram

PREFACE

WELCOME FROM THE 1st AEMT 2014 ORGANIZING COMMITTEE

Welcome to the 1st International Conference on AEMT (Applied Electromagentic Technology). It is a great pleasure for the Faculty of Engineering University of Mataram in collaboration with University of Indonesia to be able to hold this conference. This event is the first international conference held by Faculty of Engineering University of Mataram. it is a new spirit of strengthening to hold such a conference in the future, which would greatly support the success of the Faculty of Engineering University of Mataram towards "Go International" in 2025.

The theme of the 1st AEMT is" The Lombok Geomagnetic Observatory Inauguration": a support for environmental monitoring & discovery of new natural resources. Underlying this theme is the inauguration of the Lombok Geomagnetic Observatory that has launched on 11 April 2014 in Central Lombok District by Minister of Research and Technology.

The aim of this International Conference is to provide an international forum for exchanging knowledge and expertise as well as creating a prospective collaboration and networking on various fields of science, engineering, and especially, applied geomagnetic technology along with its supporting fields.

Although this first international conference is a specific themed conference, many of interested speakers participate to present and discuss their ideas related with geomagnetic and its various supporting fields such as New-Renewable Energy, Telecommunication, signal processing, Data Management & Information Systems, and Miscellaneous related aspect to Electromagnetic Technology.

This conference will have 3 keynote speakers, 4 invited spaekers, and has gathered 43 papers from various universities and intitutions from both domestic and overseas.

My deepest appreciation to our speakers, observers, sponsors, contributors, and supported parties who have given their generous supports. I would also like to thank all members of the Organizing Committee and our distinguished Reviewers for all of their supports and advices as well as the IJTech Journal of University of Indonesia that wiil publish some seleted papers.

Allow me to wish all of you a meaning and rewarding conference. We wish you a pleaseant and memorable stay in Lombok. Thanks you and we hope to meet you again at AEMT 2018.

Misbahuddin, ST., MT
Chairperson of 1st AEMT 2014 Organizing Committee

CONTENT

CONTENT

CONTENT

DATA MANAGEMENT & INFORMATION SYSTEMS

CONTENT

Telecommunication

CONTENT

ELECTROMAGNETIC TECHNOLOGY

INVITED SPEAKER

Prof. Dr. Claudia Stolle

Helmholtz Centre Potsdam
GFZ German Research Centre for Geosciences
claudia.stolle[at]gfz-potsdam.de

Since 1 July 2013, Prof. Claudia Stolle is the new head of section 2.3, Earth's Magnetic Field.

On 1st July 2013 Prof. Dr. Claudia Stolle was appointed head of Section 2.3, "Earth's Magnetic Field". As a joint appointment between GFZ and the University of Potsdam, Prof. Stolle commenced a position as professor of the "Earth's Magnetic Field" in the Faculty of Mathematics and Natural Sciences. Her research interests focus on the interaction of the Earth's magnetic field and phenomena and trends in the upper atmosphere, as well as the characterization of the sources of the geomagnetic field in the near-Earth space

Prof. Stolle has previously been 'Senior Scientist' a the Technical University of Denmark (DTU) in Copenhagen. During this time she was responsible for the scientific management of DTU's global network of ground magnetometers, and she worked on developing and defining scientific data products for the upcoming ESA satellite mission Swarm.

After obtaining a degree in meteorology at the Centre national de la recherche scientifique (CNRS) and the French weather service Météo France in Toulouse, Prof. Stolle completed her PhD at the University of Leipzig on the new possibility of imaging the ionosphere using GPS measurements.

Prof. Dr. Mioara Mandea

Mioara Mandea, Ph.D. is General Secretary of the European Geosciences Union and Programme Manager for the Solid Earth Observation / Directorate for Strategy and Programmes of Centre National d'Etudes Spatiales (French Space Agency), Paris.
Her research interests mainly concern measuring, mapping, and understanding the multitude of magnetic fields encountered in near Earth and near Earth-like planets. She has concentrated her work in important areas, participating in the general effort of measuring Earth's magnetic field from ground to space, developing new tools to model the geomagnetic field and its secular variations (with a special emphasis on geomagnetic jerks), and using the geomagnetic information to determine physical properties in the deep Earth's interior (with special studies on the lower mantle conductivity or motions at the core-mantle boundary). Her fields of research also include geopotential field mapping, on global or regional scales, with important implications for the understanding of rapid changes within the Earth's system.

INVITED SPEAKER

Prof. Wolfgang Martin Boerner

University of Illinois at Chicago

Wolfgang-Martin Boerner was born in Finschhafen, Papua New Guinea (formerly Deutsch-Ost Neu-Guinea) in 1937, spent his childhood in Oceania & Austral-Asia, received the B.S. (Abitur) degree from the August von Platen Gymnasium, Ansbach, Germany, the M.S. (Dipl.-Ing.) degree from the Technical University of Munich, Munich, Germany, and the Ph.D. degree from the Moore School of Electrical Engineering, University of Pennsylvania, Philadelphia, in 1958, 1963, and 1967, respectively.

From 1967 to 1968, he was a Research Assistant Engineer at the Department of Electrical and Computer Engineering, Radiation Laboratory, University of Michigan, Ann Arbor. From 1968 to 1978, he was with the Electrical Engineering Department, University of Manitoba in Winnipeg, MB, Canada. In 1978, he joined the Department of Electrical Engineering and Computer Science, University of Illinois at Chicago as Professor and Director of its Communications, Sensing & Imaging and Navigation Laboratory, where he serves now a Professor Emeritus and Distinguished Research Scientist.

Prof. KATSUMI HATTORI

Chiba University, JAPAN

hattori@earth.s.chiba-u.ac.jp

AREAS OF EXPERTISE: GPS Geosciences Applications, Signal Processing and Image Processing, Ground electromagnetic observation

PROFESSIONAL EXPERIENCE

Mar.1992 – Received Ph. D. in Electrical Engineering from Nagoya University
1992-1995 – Research Associate, Faculty of Engineering, Toyama Prefectural University
1995-1997 – Lecturer at Department, Gunma National College of Technology
1997-1998 - Researcher, International Frontier Research Program on Earthquakes
1998-2000 - Team Leader, International Frontier Research Program on
2001-2006 - Associate Professor of Marine Biosystems Research Center, Chiba University
2006-2007 - Associate Professor, Faculty of Science, Chiba University
July 2009-present – Professor of Earth Sciences, Graduate School of Science, Chiba University

INVITED SPEAKER

Dr. Monika Korte

Helmholtz Centre Potsdam
GFZ German Research Centre for Geosciences
monika.korte[at]gfz-potsdam.de

Research Interests:

- Geomagnetism and Paleomagnetism
- Recent and long term geomagnetic secular variation
- Global and regional geomagnetic field modeling
- Geomagnetic ground observations
- Separation of magnetic field sources

Career :

since 2009 Working Group Leader "Geomagnetic Observatories" within Section 2.3 of GFZ
since 2003 Scientific Director of Niemegk Geomagnetic Observatory at GFZ Potsdam

2002 – 2003	Postgraduate Researcher, GFZ Potsdam
2001 – 2002	Postgraduate Researcher, Scripps Institution of Oceanography, University of California, San Diego
1999 – 2001	Postgraduate Researcher, GFZ Potsdam
1997 – 1999	PhD student, GFZ Potsdam
1996 – 1997	Student research assistent, Geophysical Observatory Fürstenfeldbruck, LMU München.

Dr. Harry Arjadi

Pusat Penelitian Sistem Mutu dan Teknologi Pengujian

- Receive Ph.d from Salford University.
- Member of Barrier Removal to the cost-effective development and implementation of Energy efficiency Standards and Labelling

PRESENTATION GUIDELINES

ORAL PRESENTATION

Please note that the time allocated to each oral presentation is 15 minutes including questions and answers.

Powerpoint slides for presentation on a LCD video projector are recommended.

Oral presentation rooms will be equipped with the following items:

- Notebook computer running WINDOWS operating system, with MS Office 2007, Acrobat Reader 8.0
- An LCD vedio projector

We recommeded that presenters bring their presentation file in a format compatible with one of the above applications, and stored in a USB thumb drive (flash disk)

Due to limited time of presentation, presenters are not allowed to use their own notebook or laptop computers.

All presenters can upload their presentations files into the computer in their assigned presentation room during Registration on the morning of their presentation from 08.00 hrs onwards, or during the tea breaks. An assistant will be in the room to help you.

Note:

- AC Voltage is 220 V in Indonesia
- The connector from LCD projector to your computer is limited to a D-sub 15 pin male connection

JOURNAL PUBLICATION

Papers that are not presented at the AEMT Seminar on 14 April 2014 by one of the Authors will be deleted from the AEMT Proceeding, nor will be submitted to IJTech for publication.

PROGRAM OVERVIEW

Schedule of the 1st International Conference on Applied Electromagnetic Technology (AEMT). Grand Legy Hotel, Mataram, Indonesia, 11-15 April 2014

Date	Time	Programme	Venue
Monday, 14 April 2014	07.00 - 08.00	Registration	Pre-function Hall
	08.00 - 08.30	Opening Ceremony The Holly Qur'an Recitation	Kenanga Ballroom, Grand Legi Hotel-Mataram
	08.00 - 09.30	1. Welcome remarks by the Committee Chairperson (Mr. Misbahuddin, ST.MT.) 2. Speech of the Dean of Engineering Faculty of Mataram University (Yusron Saadi, ST., M.Sc., Ph.D.) 3. Opening Seminar by the Vice Rector of Mataram University: Prof. Ir. Suwardji	
	09.30 - 09.45	Photo Session	
	09.45 – 10.00	**Coffee break & Poster Session**	Pre-function Hall, Grand Legi Hotel Mataram
	10.00 - 11.30	Plenary Lecture 1 Moderator : I Gede Pasek Suta Wijaya, ST., MT., Ph.D. Speaker 1 : Dr. Monika Korte (The Helmholtz Centrum, GFZ Postdam, Germany) Speaker 2 : Prof. Wolfgang Martin Boerner (IEEE/University Illinois, Chicago-USA) Speaker 3 : Dr. Harry Arjadi (EMC Laboratory, SMTP-LIPI, Indonesia)	Kenanga Ballroom, Grand Legi Hotel-Mataram
	11 .30 - 11.45	Break – Traditional dance	
	11.45 - 1 3.00	Plenary Lecture 2 (by Skype) Moderator : Eko Pradjoko, ST., M.Eng., Ph.D. Speaker 1 : Prof. Katsumi Hattori (Chiba University, Japan) Speaker 2 : Prof. Mioara Mandea (CNES/ Université Paris Diderot, France)	
	1 3.00 - 1 4.00	Lunch, Pray	Restaurant, Grand Legi Hotel – Mataram
	14.00 - 17.30	Parallel Session (See the detailed schedule on the next pages)	Grand Legi Hotel Mataram

SCHEDULE OF PARALLEL SESSION

GROUP-1 : Geo- and Electromagnetism
Chair : Dr.rer.nat. Tety Zubaidah, ST., MT.
Moderator : Indira Puteri Kinasih, Wahyudi W Parnadi
Venue : Kenanga Room I

Time	ID	Authors	Affiliation	Title
01.30 - 01.45 pm	G101	L. M. Musafar K,Triyanta,W. Srigutomo,T. Jamaluddin,A. Yoshikawa, T. Uozumi	Dept. of Physics Bandung Institute of Technology, International Center for Space Kyushu University	Pc5 Magnetic Pulsations During Outer Electron Radiation Belt
01.45 - 02.00 pm	G102	Yosi Setiawan,Daryono	Meteorological and Geophysical Academy Meteorological, Climatological and Geophysics Agency Jakarta	AComparison Between Computer Derived (Adaptive Smoothing Method) and Hand Scaled K Indices at Tuntungan Geophysical Station
02.00 - 02.15 pm	G103	Angga Setiyo P, Boko Nurdiyanto, Suliyanti P, Hastuadi Harsa,Arafah,Katsumi Hattori	Research and Development Center, BMKG Pelabuhan Ratu Geophysics Observatory, BMKG Chiba University	Electromagnetic Anomaly As Earthquake Precursor In Pelabuhan Ratu, Sukabumi
02.15 - 02.30 pm	G104	Ayu Adi Justicea, Daryono	Academy of Meteorology and Geophysic AMG Jakarta	ULF Geomagnetic Pertubations Related With Earthquake Case Study: 9th January 2014
02.30 - 02.45 pm	G105	S.Ahadi, N.T Puspito, G.Ibrahim, S. Saroso	Institut Teknologi Bandung Meteorological Climatological and Geophysical Agency National Institute of Aeronautic and Space	Determinations Onset time of Earthquake Precursor by Analizing ULF-EM Emission Signal in Sumatra region, Case Studi Padang 2009 and Mentawai 2010
02.45 - 03.00 pm	G106	Relly Margiono, Mahmud Yusuf	Meteorology and Geophysical Academy Meteorology Climatology and Geophysical Agency Jakarta	On the Influence of DC Railway Noise on Variation Data from Tangerang Geomagnetic Observatories
03.30 - 03.45 pm	G107	Indira Puteri Kinasih, Giri Wahyu Wiriasto, Teti Zubaidah, Bulkis Kanata	Mathematics Computation Laboratory of IKIP Mataram Department of Electrical Engineering, Mataram University	Lesser Sunda Islands Earthquake Inter-Occurrence Times Distribution Modeling
03.45 - 04.00 pm	G108	I Putu Dedy Pratama, Yosi Setiawan, Daryono	Meteorological and Geophysical Academy Meteorological, Climatological and Geophysics	Horizontal Component Variation in Geomagnetic Stations During Annular Solar Eclipse on January 26th, 2009

SCHEDULE OF PARALLEL SESSION

Time	ID	Authors	Affiliation	Title
			Agency	
04.00 - 04.15 pm	G109	Bulkis Kanata, Teti Zubaidah, Cipta Ramadhani, Budi Irmawati	Department Of Electrical Engineering, Department Of Informatic University of Mataram	Changes of the Geomagnetic Signal linked to Tohoku Earthquake on March 11th 2011
04.15 - 04.30 pm	G501	Teti Zubaidah, Bulkis Kanata, Paniran	Electrical Engineering Dept. of Mataram University	Three Dim Mapping of Static Magnetic Fields over A Semi Anechoic Chamber
04.45 - 05.00 pm	G503	Warsa Warsa, Hendra Grandis, Wahyudi W Parnadi, Djoko Santoso	Applied Geophysics Research Group Faculty of Mining & Petroleum Engineering ITB	Three-dimensional Inversion of Magnetic Resonance Sounding (MRS) for Groundwater Detection

GROUP-2 : New-renewable Energy
Chair : Rosmaliati, ST., MT.
Moderator : I Nyoman Wahyu S, ST.,MT.,Ph.D; Niken Arumdati, ST.,M.Sc
Venue : Kenanga Room II

Time	ID	Authors	Affiliation	Title
01.30 - 01.45 pm	G201	Amien Rahardjo, Iwa Garniwa MK, Faiz Husnayain	Faculty of Engineering Universitas Indonesia	Analysis of Harmonic Distortion Effect on Deviation Measurement of Electrical Energy in kWh Meter
01.45 - 02.00 pm	G202	Niken Arumdati1 , J. F. G. Cobben	Energy and Mining Provincial Office of West Nusa Tenggara Electrical Engineering Dept, Technische Universiteit Eindhoven	Inrush Related Problems Caused by Lamps and Electric Vehicle
02.00 - 02.15 pm	G203	Faiz Husnayain, Putu Aditya, Kuo-Lung Lian	Faculty of Engineering Universitas Indonesia National Taiwan University of Science and Technology	Studies on Smart Charging Strategies for a Lead-Acid Battery
02.15 - 02.30 pm	G204	I Nyoman Wahyu Satiawan, Ida Bagus Fery Citarsa, I Ketut Wiryajati, Mohan V. Aware	Electrical Engineering, Mataram University	Performance comparison of PWM schemes of dual-inverter fed five-phase motor drives

SCHEDULE OF PARALLEL SESSION

Time	ID	Authors	Affiliation	Title
02.30 - 02.45 pm	G205	Ratna Ika Putri, Muhammad Rifa'i, Supriatna Adhisuwignjo	Electronic Department Malang State Polytechnic, Indonesia	Design of Buck Converter For Photovoltaic System Applications
02.45 - 03.00 pm	G206	N. Sulistiyanto , M. Rif´an, O. Setyawati	Electrical Engineering Brawijaya University	Development of a 20 V-LED driver based on the boost converter using a FPGA module
03.30 - 03.45 pm	G207	Teguh Utomo, Rini Nur Hasanah, Mohammad Bisri	Brawijaya University, Indonesia	Development of Microhydro Field Laboratory under the Program of Science and Technology on Campus Innovation and Creativity
03.45 - 04.00 pm	G208	Wahyudi W. Parnadi, Adhiarta P., Widodo, Toni Rahadinata	Geophysical Engineering Institut Teknologi Bandung Geological Resource Center (PSDG)	Resisistivity Structures in Mt. Batur Geothermal Prospect Area in Bali Province, Indonesia
04.00 - 04.15 pm	G209	Lie Jasa , IGA Raka Agung, I Putu Ardana, Ardyono ,Mauridhy Hery Purnomo	Electrical Engineering Udayana University Electrical Engineering ITS	Smart Grid Control with Fuzzy Integrator for Micro Hydro Connected to Low Voltage Distribution PT. PLN (Persero)
04.15 - 04.30 pm	G210	Rini Nur Hasanah, Hadi Suyono, Wijono, Moch Dhofir	Electrical Engineering Brawijaya University	A Building Audit Software to Support Energy Management and Conservation
04.30 - 04.45 pm	G502	Boko Nurdiyanto, Yunus Daud, Ahmad Zarkasyi	Post Graduate Program of Geophysics Reservoar FMIPA, UI Center for Geological Resources Geological Agency	Application Of Mt And Gravity Method To Potential Analysis Of Kepahiang Geothermal, Bengkulu
04.45 – 05.00 pm	G504	Wahyudi W. Parnadi, Widodo, Ryanti W. Savitri, Ahmad Zakarsyi	Geophysical Engineering Bandung Institute of Technology Subsurface Department Geological Resource Center	Magnetotelluric Investigations in Wai Umpu Geothermal Prospect Area Lampung Province, Indonesia
05.00 – 05.15 pm	G505	Syahrul Husain	Department Of EMechanical Engineering University of Mataram	Preliminary Study of Exergy Analysis of Magnetic Refrigeration

SCHEDULE OF PARALLEL SESSION

GROUP-3 : Data Management & Information Systems
Chair : Misbahuddin, ST.,MT
Moderator : I Gede Pasek Suta W, ST.,MT,.D.Eng, Cipta Ramadhani, ST.,M.Eng
Venue : Melati Room

Time	ID	Authors	Affiliation	Title
01.30 - 01.45 pm	G301	Cahyo Darujati, Syamsul Anam,, Hasan Dwi C, Agustinus Bimo G	Faculty of Computer Science Narotama University, Indonesia	Improvement Of Multi Resolution Digital Image Magnification Using Combined Low Pass Filter and Bilinear Interpolation
01.45 - 02.00 pm	G302	Dede Sutarya, Adhi Mahendra	Electrical Engineering Dept., Universitas Pancasila	Outlier Filtering For Hydrogen Temperature And Flow Rate Time Series Data In Sintering Process
02.00 - 02.15 pm	G303	Mokhammad Hendayun, Iwan Abadi, Marulan Heryanto Samosir	Departement of Informatics Engineering Langlangbuana University	The Implementation of the Advanced Encryption Standard (AES) Encryption Algorithm For Computer File Security
02.15 - 02.30 pm	G304	Dwijoko Purbohadi	Department of Information Technology, Universitas Muhammadiyah Yogyakarta	Intelligent Tutoring System for Mastery Learning:Development Method for Extensive Use
02.30 - 02.45 pm	G305	Emi Susilowati,Dwi Handoko	University of Muhammadiyah Jakarta Badan Pengkajian dan Penerapan Teknologi Balai IPTEKnet	Comparison of K-Means and Agglomerative Hierarchical Clustering Method with Principal Component Analysis in Research Document Analysis
02.45 - 03.00 pm	G306	Yusriel Ardian, Wiji Setiyaningsih	Faculty of Information Technology, University of Malang Kanjuruhan	Level Prediction Of Pneumonia In Children Time Range Based Breastfeeding, Immunization Status, Nutrition Using K-Means
03.30 - 03.45 pm	G307	Cipta Ramadhani, Wahyu Ramadhani	Jurusan Teknik Elektro Fakultas Teknik Universitas Mataram STMIK Syaikh Zainuddin NW Nadhatul Wathan Anjani NTB	Parallel Programming to Increase Performance of Binary Search Tree
03.45 - 04.00 pm	G308	Made Liandana, I Wayan Mustika, and Selo	Universitas Gadjah Mada	Fall Detection System for Elderly Based on Android Smartphone
04.00 - 04.15 pm	G309	Misbahuddin, Heri Wijayanto, Muhsyaf Saipul Arni	University of Mataram	Poverty Mapping in Mataram by Multi-Criteria Fuzzy Approach

SCHEDULE OF PARALLEL SESSION

Time	ID	Authors	Affiliation	Title
04.15 - 04.30 pm	G310	Falahah,Dewi Rosmala,Abraham Mikhael Dolok	Informatics Department Widyatama University Informatics Department Institut Teknologi Nasional	Socialization and Visualization of City Transport Using Google Maps API
04.30 - 04.45 pm	G311	Wina Witanti, Falahah,Yuliana	Basic Science Faculty Universitas Jenderal Achmad Yani Informatics Department, Universitas Widyatama	SIG-based Earthquake Information System
04.45 - 05.00 pm	G312	I Gede Pasek Suta Wijaya, Ni Nyoman Kencanawati	Engineering Faculty Mataram University	Denoising Acoustic Emission Signal Using Wavelet Transforsm for Determining the Source Location Micro Crack on Concrete

GROUP-4 : Telecommunication
Chair : Made Sutha Yadnya, ST., MT
Moderator : Dr. Yuli Fitri, Dr.. Asvial
Venue : Teratai Room

Time	ID	Authors	Affiliation	Title
01.30 - 01.45 pm	G401	Masjudin, I Wayan Mustika, Widyawan	Department of Electrical Engineering and Information Technology Universitas Gadjah Mada	Particle Swarm Optimization for Wireless Sensor Network Deployment Design by Taking Account of Barrier Position and Attenuation
01.45 - 02.00 pm	G402	Muhammad Fauzan Edy Purnomo	Faculty of Engineering University of Brawijaya	Circularly Polarized Stack-Patch Microstrip Array Antenna for Mobile Satellite Communications
02.00 - 02.15 pm	G403	SatriaGunawanZain,Adhi Susanto,Thomas Sriwidodo,Wahyu Widada	Electrical Engineering, GadjahMada University Electrical Engineering, Makassar State University National Institute of Aeronotics and Space	Angle of Arrival Using Cross Yagi-Uda Antennas
02.15 - 02.30 pm	G404	Made Sutha Yadnya, Haniah Mahmudah, Ari Wijayanti, I Wayan Sudiarta, Achmad Mauludianto	Universitas Mataram Politeknik Elektronika Negeri Surabaya Institut Teknologi Sepuluh November	Simulation Attenuation From Rain Cell Movement For Wimax Channel Transmission In Lombok

SCHEDULE OF PARALLEL SESSION

Time	ID	Authors	Affiliation	Title
02.30 - 02.45 pm	G405	Rijal Widhi Permadi, Maria Irmina P., Kanisius Karyono	Universitas Multimedia Nusantara, Tangerang, Indonesia	Android Based Indoor Navigation Application Using Earth's Magnetic Field Pattern Case Study: Universitas Multimedia Nusantara
02.45 - 03.00 pm	G406	Risanuri Hidayat, Sasmito Aji, Litasari	Department Electrical Engineering, Engineering Faculty University of Gadjah Mada	Implementation of Haar Wavelet Transform on Xilinx Spartan-3E FPGA
03.30 - 03.45 pm	G407	Priadhana Edi Kresnha,Aini Mukaromah	University of Muhammadiyah Jakarta Faculty of Computer Science University of Mercu Buana	A Robust Method of Encryption and Steganography Using ElGamal and Spread Spectrum Technique Based on MP3 Audio File
03.45 - 04.00 pm	G408	Gede Angga P, I Wayan Mustika, Selo	Universitas Gadjah Mada	Check Out System Using Passive RFID Technology in Wholesale Supermarket
04.00 - 04.15 pm	G409	Siti Sendari, Yuni Rahmawati	Engineering Faculty of Engineering State University of Malang	Instrumentation of Carbon Monoxide to Indentify Traffic Jams
04.15 - 04.30 pm	G410	Muhamad Asvial,Indra W Gumilang	Faculty of Engineering Universitas Indonesia	Channel Estimation using Least Square Estimation (LSE) Orthogonal Frequency Division Multiplexing (OFDM) System
04.30 - 04.45 pm	G411	Fitri Yuli Zulkifli, Eufrasia Inti Alphatia Putri, Basari,Eko Tjipto Rahardjo	Faculty of Engineering, Universitas Indonesia	Design of Low Noise Amplifier for 2.35 GHz Long Term Evolution (LTE) Application

We gratefully thank to our sponsors and contributors:

G101

Pc5 Magnetic Pulsations During Outer Electron Radiation Belt

L. Muhammad Musafar K., Triyanta, W. Srigutomo
Dept. of Physics, Graduate School of Science,
Bandung Institute of Technology
Jl. Ganesha 10, Bandung, Indonesia,
aurora@bdg.lapan.go.id

L. Muhammad Musafar K., T. Djamaluddin
Space Science Center, LAPAN
Jl. Dr. Djunjunan No, 133, Bandung, Indonesia, 40173

A. Yoshikawa, T. Uozumi, K. Yumoto
International Center for Space Weather Science and Education
Kyushu University 33
6-10-1 Hakozaki, Fukuoka, Japan, 812-8581

Abstract— **Since the discovery of radiation belt decades ago still remain some fundamental questions one of which is the mechanism responsible for the acceleration of electrons. Ground-based Pc5 magnetic pulsation during increasing of 2-MeV electron fluxes has been analyzed. A filter bandpass in the range period 150-600 seconds has been used to localize the Pc5 waves and then we applied wavelet transform where the Morlet function as a mother wavelet to analyze Pc5 wave packets. First, we show that dynamic pressure of solar wind controls power of Pc5 magnetic pulsations. Second, with performing cross-spectrum analysis of Pc5 wavelet during electron radiation belt we show wavelet power of Pc5 magnetic pulsations associated with maximum wavelet cross spectrum shows similar change of Pc5 pulsations during radiation belt events. Increasing of electron fluxes that initiated by presence of large power of Pc5 magnetic pulsations has been observed. This indicates that Pc5 magnetic pulsations play a role in acceleration and transport mechanism of electron radiation belt. Also, 4-5 days from the beginning of increasing of electron fluxes we observed globally depression the power of Pc5 magnetic pulsations as well as monotonically decreasing of solar wind dynamic pressure. In other side, in the end period of electron belt we also observed an increasing of Pc5 magnetic pulsations. We suggest that during expanding phase of outer electron radiation belt outward to interplanetary electron belt pressure reduce the solar wind dynamic pressure and consequently a decreasing in the power of Pc5 magnetic pulsation. And, in the end period of electron radiation belt the electron fluxes back to its normal level and consequently a sudden increasing of Pc5 solar wind dynamic pressure and that sudden increasing also drives sudden increasing power of Pc5 magnetic pulsations.**

Keywords—magnetic field; Pc5 magnetic pulsations; electron fluxes, radiation belt

G102

A Comparison Between Computer Derived (Adaptive Smoothing Method) and Hand Scaled K Indices at Tuntungan Geophysical Station

Yosi Setiawan, Daryono
Meteorology and Geophysical Academy
Meteorology, Climatology and Geophysical Agency
Jakarta
yosi.setiawan@yahoo.com

***Abstract*—Instrument transition at Tuntungan Geophysical Station from La Cour analog variograph to digital fluxgate magnetometer LEMI-018 change the way to derive K-indices value. This study is done to ensure that the K-indices value from manual hand scaled and the software derived with ASm (Adaptive Smoothing Method) is not differing enough. Using data from January until September 2010 minus July, confirm the results: about 17% of K-indices are in agreement and about 15% differ by more than one unit, the percentage of differences equal to 0 are varies for K=0-6 with 28%, 26%, 17%, 14%, 6%, 17%, and 100% for each K-value, the percentage of differences equal to 0 with the UT 3-hour interval have variation between 13% to 21%.**

Keywords—Geomagnetism, K-indices, ASm method

IV. INTRODUCTION

Tuntungan Geophysical Station (IAGA code: TUN),located at 3.517 N and 98.567 E with elevation 86 meters above sea level, is the Technical Implementation Unit of the Meteorology, Climatology and Geophysical Agency (BMKG) in North Sumatra (Fig. 1) that making observations in the field of geophysics, and one of them is geomagnetic observation.Data generated from the geomagnetic observations are including daily data of all components of the geomagnetic field, disturbed day data, and K-indices data.

Geomagnetic observations at Tuntungan began in 1982 with analog variograph La Cour. Then in 2003, it is received additional digital magnetometer DMI from BGS (British Geological Survey), but its condition is now broken. In 2008 Tuntungan received again an additional digital fluxgate magnetometer LEMI-018 that are still in service today, but it was only used as a backup of the analog variograph La Cour. This digital fluxgate magnetometer was stop working for several times because of sensor trouble.

Since September 2012 the analog variograph La Cour has discontinued for operations due to huge cost for treatment, so that the data of digital fluxgate magnetometer LEMI-018 are used as the main data. Consequently the calculation to obtain the variation values of each component, the disturbed days, and K-indices data has changed. It is not too difficult to get the variation values of each component and to determine the disturbed days. The problem is how to get the K-indices value.

As in [1], K-indices are an index designed to quantify the level of disturbances caused by the influence of the solar wind at a single location using magnetic observatory measurements and it is produced for eight three-hour segments in a UT day. K-indices measured in nT and denoted by a single digit code from 0 to 9 according to a quasi-logarithmic scale where K=0 indicates completely quiet conditions and K=9 indicates highly disturbed conditions. Reference [2] said that K=0–2 correspond toperiods of magnetic quietness; K=3–5 correspondto periods of moderate geomagnetic activity; and K=6–9 correspond to periods of intense to very intensegeomagnetic activity. Table 1 shows the K-indices scale at Tuntungan.

In Tuntungan previously, it was performed by manual measurement on the magnetogram (hand scaled), now it is used computer to get the K-indices from the digital data. The software used here is KAsm which uses Adaptive Smoothing Method.

The purposes of this study are to compare the K-indices data from manually measurement results (hand scaled) with the data from KAsm calculation and to determine the accuracy of the Adaptive Smoothing Method in K-indices calculation specially at Tuntungan Geophysical Station.

TABLE I. K-INDICES SCALE FOR TUNTUNGAN GEOPHYSICAL STATION. THE RANGE ARE EXPRESSED IN NT.

Range	0	4.5	9	18	36	63	108	180	297	450
K-value	0	1	2	3	4	5	6	7	8	9

V. DATA

To comparing the K-indices data, itneeds two data obtained from the same period. And to determine the quantitative estimation of an algorithm accuracy requires the K-indices data from manual measurements on the classical magnetogram by a well-trained observer. In the case of

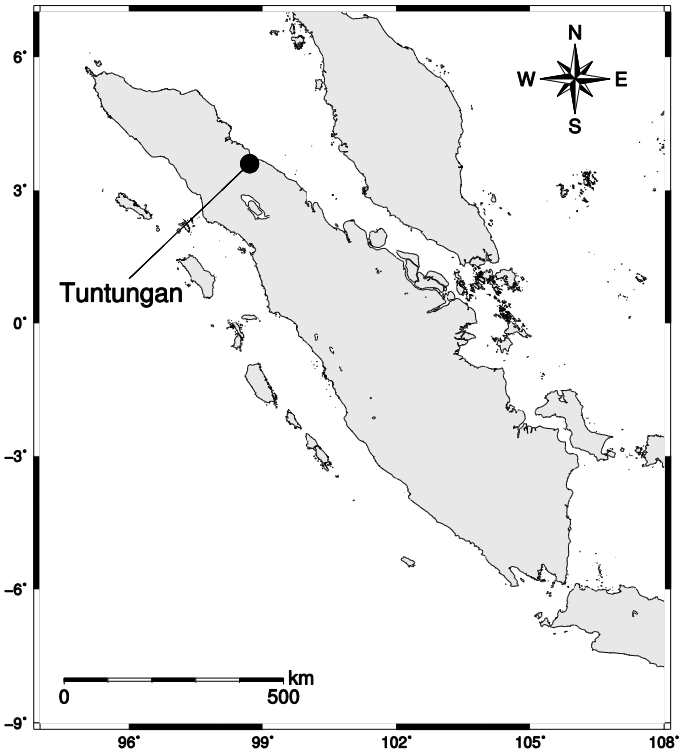

Fig. 1. Fig. 1. Location map of Tuntungan Geophysical Station

Tuntungan (TUN) observatories, the data from analog and digital magnetometer that operates at the same period is only at January until September 2010 minus July.

A. Hand Scaled K-indices

The analog variograph derived K-indices obtained from the variation amplitude of the horizontal component using a glass scale and the Solar Regular (S_R) variation must be eliminated. The analog variograph La Cour measures the HDZ component. These data are used as the reference data.

The lack of this data is there are alot of lost record data. These lost record are mostly caused by an error when washing the photographic paper in the dark room that made the paper to burn out. The other shortage is the K-indices was measured by different people that made the subjectivity level is relatively high.

B. Computer Derived K-indices

The digital fluxgate magnetometer LEMI-018 measures the XYZ component and has 1 second sampling rate and the resolution is 0.01 nT on each component. The measured range of total magnetic field at the display is ±65.000 nT and the temperature drift is less than0.2 nT/°C. To calculate the K-indices value using KAsm, the output text data from LEMI-018 must be converted into IMFV 1.22 format.

VI. METHOD

Reference [3] said that the problem in measuring the K-indices lies in how to identify the S_R variation ($S_R$for Solar Regular) in magnetogramwhich is the imagined curve for the day inquestion in quiet magnetic conditions. In the method called Adaptive Smoothing as in [4], the SR-curve is deduced from a least squares fit of one-minute values with an additional limitations on the second derivatives and with weight factors to make the influence of quiet periods greaterthan that of the disturbed ones. In the final algorithm, there are three free parameters to be adjusted (in reality, two of them are the same) for each observatory to achieve the best agreement with hand-scaled K-indices, two smoothing parameters and one involved in the definition of the weight factors.

The S_R is estimated through the minimization of the expression:

$$\min_{y_1,\ldots,y_n}\left\{\sum_{i=1}^{n} l_i^2\,(y_i-x_i)^2+\sum_{i=2}^{n-1}\lambda^2[(y_{i+1}-2y_i+y_{i-1})/h]^2\right\} \quad (1)$$

where λ is the smoothing coefficient, l=(l_i) (i=1,...n)are the weighting factors, x=(x_i) and y=(y_i) (i=1,...n) are the input (observed variations) and output (S_R);h=1, because the effect of h can be included inλ. The calculations are made with data series that represent 1 day with additional night weight (n=1440). The procedure has two steps. First, l_i=1 for i=1,...1440, and $\lambda=\lambda_1$. For every hour, differences between minimum and maximum values of (x-y) are calculated. Let V_j be these values (j=1,...24). In the second step, the procedure is used once more with the same smoothing factor λ_1, and the weights are defined as follows:

$$l_i = exp\left(1 - V_j/M\right) \quad (2)$$

where j=1,...24 and i=60(j-1)+1,...60j;λ_1 and M are the two parameters to be adjusted.

In this study, the K-indices data from the results of manually measurement abbreviated with K(HS) for hand scaled. While the K-indices data from the results of computer calculation abbreviated with K(ASM) for adaptive smoothing method. As in [5], in order to characterize the results obtained from the calculation method, we first compared the K(HS)and K(ASM) distributions for the whole data.We then studied the distribution of thedifferences using following formula:

$$DK = K(ASM) - K(HS) \quad (3)$$

where DK are the differences betweencomputer derived and hand-scaled K-indices. To illustrate the calculation results obtained from the ASm method, we make the plot of DK distribution. To determine the distribution pattern of DK toward the reference K-indices, DK is plotted against the K(HS) value. The last method is DK plotted against the time (in UT) with a 3-hour intervals to determine the pattern of the distribution.

VII. RESULTS AND DISCUSSIONS

All K-indices are showed at Fig. 2 and Fig. 3. K-indices from computer calculation results are plotted as blue bar, while manual measurement results are plotted as red bar. The values below zero line are the lost record data. It can concludes that there are alot of lost record data on both K-indices.

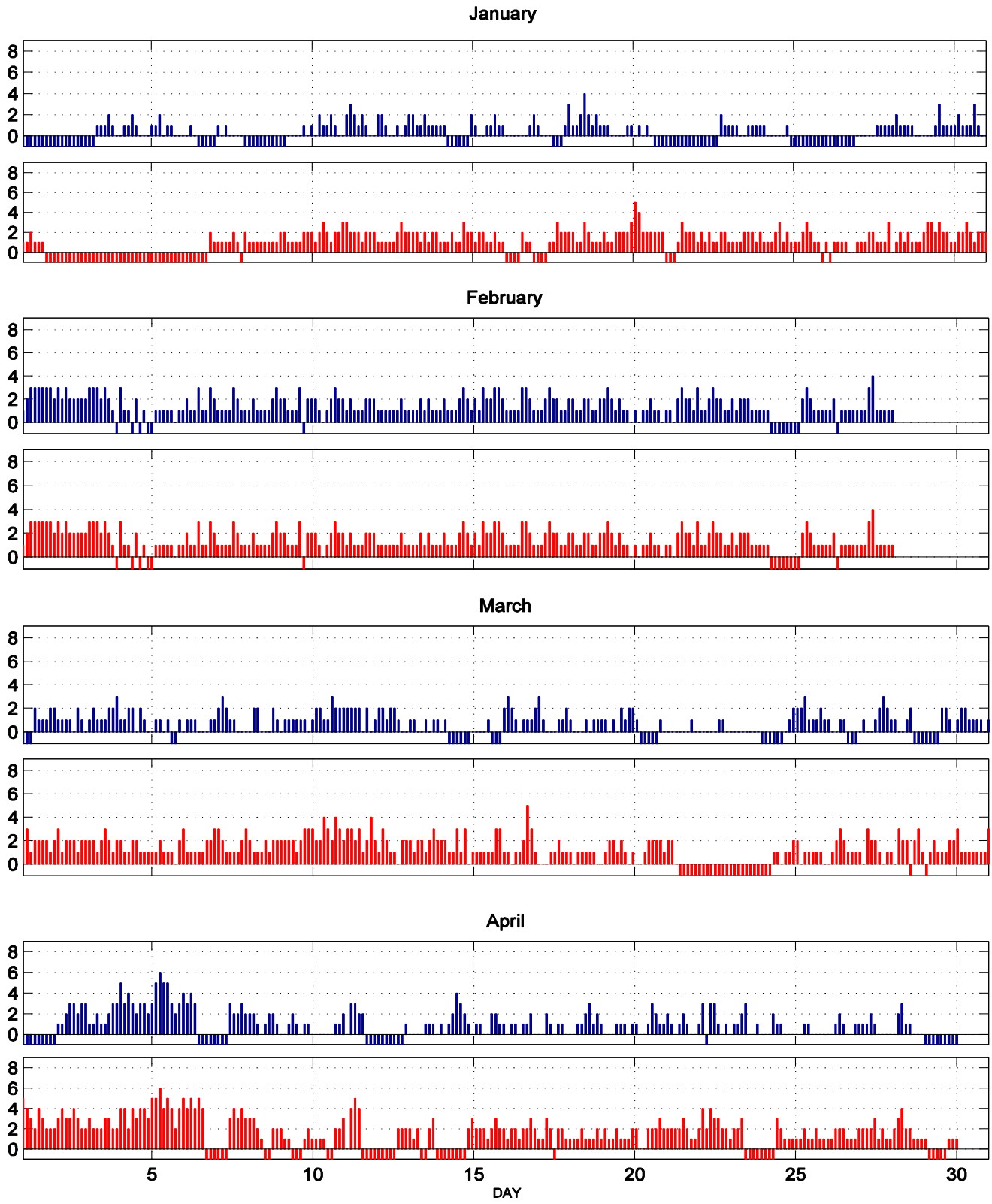

Fig. 2. K-indices in graphical form, January 2010 until April 2010. Blue bars are the computer calculation results while red bars are the manual measurement results. The values below zero line are the lost record data.

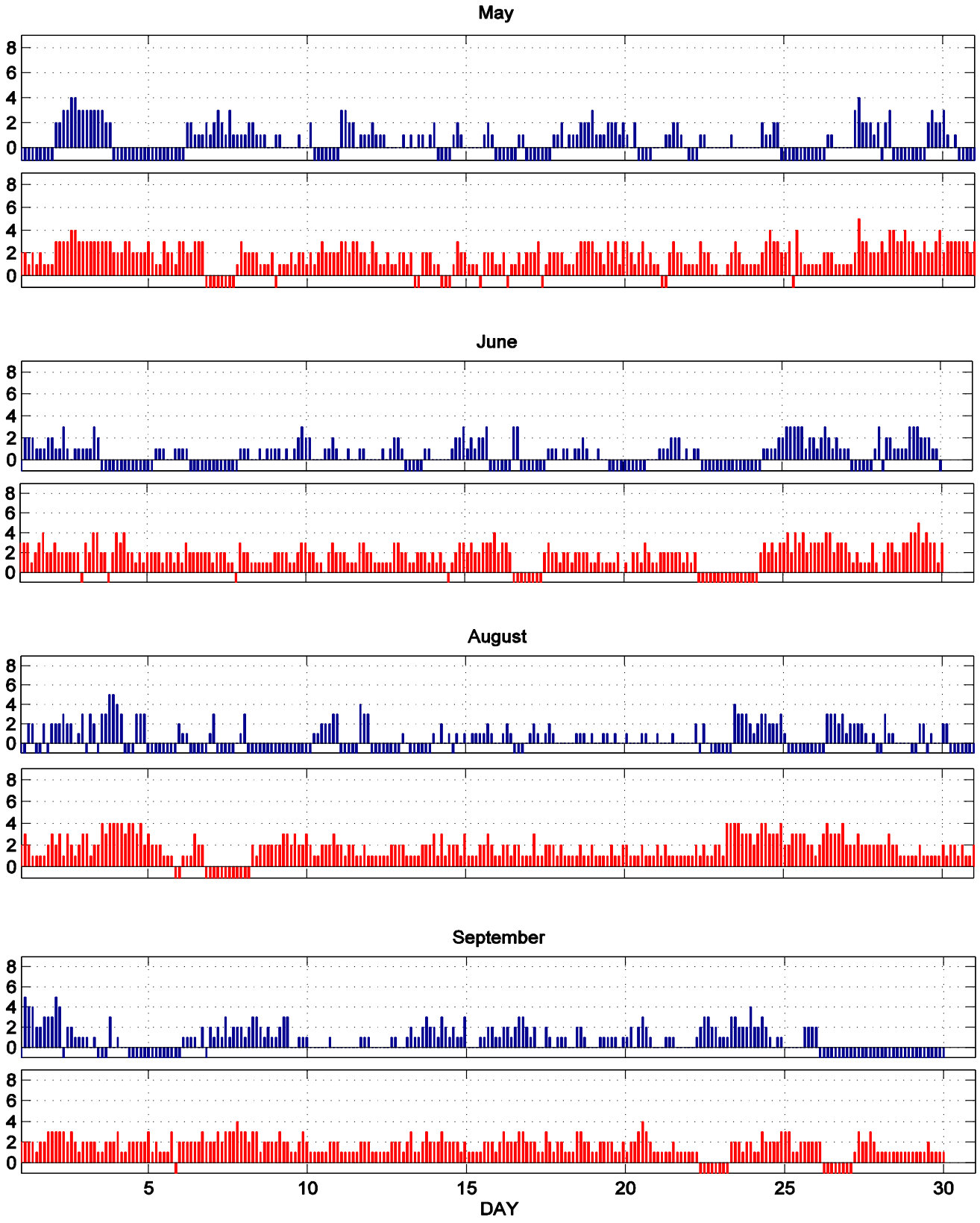

Fig. 3. K-indices in graphical form, May 2010 until September 2010 minus July 2010. Blue bars are the computer calculation results while red bars are the manual measurement results. The values below zero line are the lost record data.

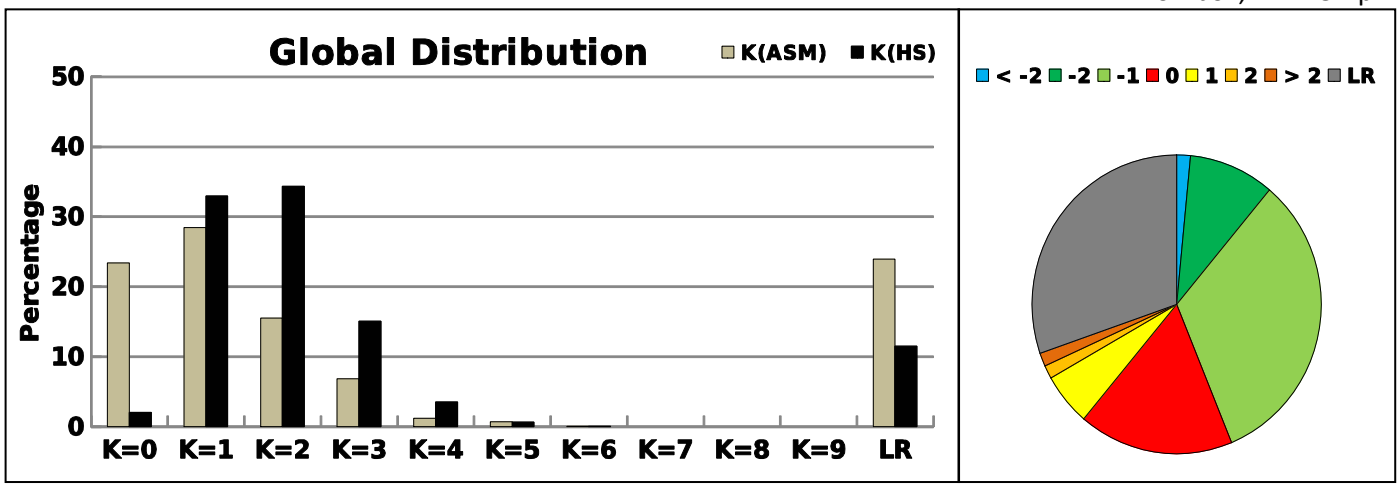

Fig. 4. Left: distribution of K-indices from manual measurement results and from computer calculation (LR is Lost Record data).Right: distribution of DK.

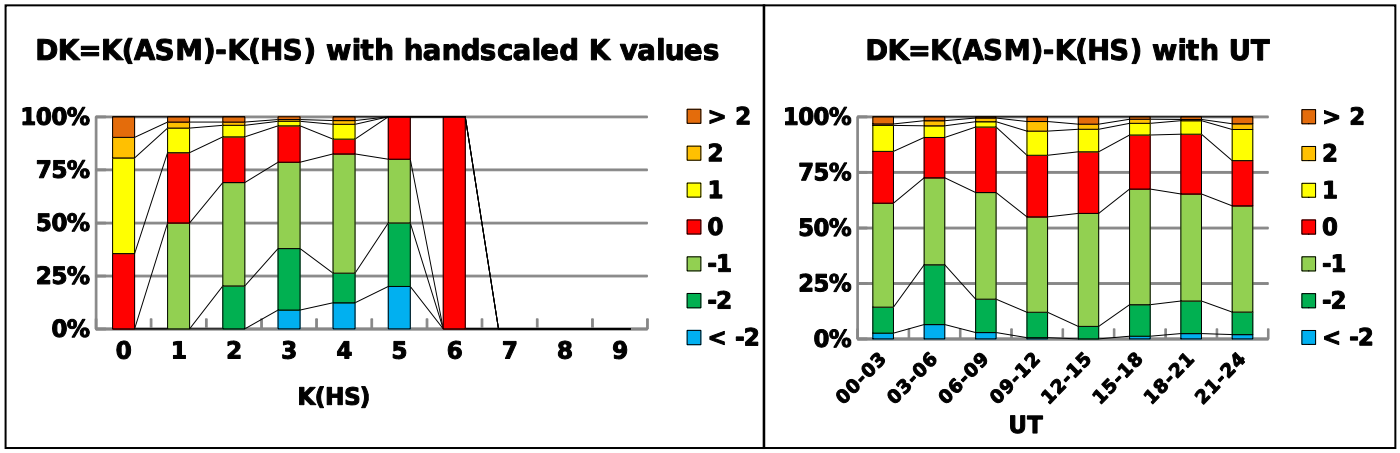

Fig. 5. Left: Distribution of DK with handscaled K values. Right: Distribution of DK with UT.

A. Global K-indices Distribution

Fig. 4 shows the distribution of K-indices from manual measurement results and from computer calculation.Overall, the maximum percentage of K(HS) is at K=2 and K(ASM) is at K=1. The difference of maximum percentage is probably caused by a false reading of the scale by observer. Also it mustbe considered that the percentage of the lost record data are relatively high and it will certainly affect the final result.

Fig. 4 also shows the distribution of difference value DK = K(ASM) – K(HS) or difference between K-indices from computer calculation results and manual measurement results. Overall, the percentage of K(ASM) and K(HS) which has equal value or DK=0 is 17%, while the DK is equal or greater than ±2 is 15% with 30% of missing data.

B. Hand-scaled KValue Dependance

Fig. 5 shows the distribution of DK value against the reference K-indices (K(HS)). The percentage of manual measurement K-indices which has the same value (DK=0) with the computer calculation K-indices varies on K=0-6 respectively 28%, 26%, 17%, 14%, 6%, 17%, and 100%. In this figure, the lost record data are not included in the graphic.

C. UT Dependance

Fig. 5 also illustrates the distribution pattern of DK value against time (in UT) in 3-hour intervals. The percentage of DK=0 against UT varies between 13% to 21%. K-indices varies from 00-24 UT with 3-hour interval respectively 15%, 13%, 21%, 21%, 20%, 17%, 18%, and 13%. In this figure, the lost record data also not included in the graphic.

VIII. CONCLUSION

The conclusions of this study can be summarized as follows: (1) there are some differences between K-indices from computer calculation results and the manual measurement results. This is likely due to error measurement by observer; (2) The accuracy of Adaptive Smoothing Method in K-indices calculation is not high enough in this study, but that must be considered is the high number of the loss record data.

REFERENCES

[1] S.J. Reay, E. Clarke, and B. Hamilton, " First steps towards K indices from South Atlantic Observatories: Port Stanley Observatory", Data Science Journal, Volume 30, 2011.

[2] M. Menvielle, T. Iyemori, A. Marchaudon, and M. Nosé,"Geomagnetic indices," inGeomagnetic Observations and Models, IAGA Special Sopron Book Series 5, M. Mandea and M. Korte, Eds. DOI 10.1007/978-90481-9858-_8,SpringerScience+BusinessMediaB.V.2011.

[3] J. Jankowski, and C. Sucksdorff, " Guide for magnetic measurements and observatory practice", IAGA, Warsaw, 1996.

[4] M. Menvielle, N. Papitashvili, L. Häkkinen,and C. Sucksdorff, "Computer production of K indices: review and comparison of methods", Geophys. J. Int. 123, 866-886, 1995.

[5] M. Bitterly, M. Menvielle, J. Bitterly, and A. Berthelier, "A comparison between computer derived (FMI method) and hand scaled K indices at Port Aux Francais and Port Alfred French Observatories", ISGI, 1997.

G103

Electromagnetic Anomaly As Earthquake Precursor In Pelabuhan Ratu, Sukabumi

Angga Setiyo Prayogo, Boko Nurdiyanto, Suliyanti Pakpahan, Hastuadi Harsa
Research and Development Centre
BMKG Jakarta, Indonesia
boko.nurdiyanto@gmail.com

Arafah
Pelabuhan Ratu Geophysics Observatory
BMKG
Sukabumi, Indonesia

Katsumi Hattori
Chiba University
Chiba, Japan

Abstract—**Research on electromagnetic anomalies related to earthquakes as early signs (precursors) of earthquake was performed in Pelabuhan Ratu Observatory. This research was part of BMKG's Integrated studies on earthquake precursors that carried out in stages and sustainable analysis of geophysical, geo-atmospheric and geochemical parameters. Research was focused on identifying physical parameters as an earthquake anomaly precursor in the Pelabuhan Ratu, West Java along 2013. Goals to be achieved in this research were improvement of the quality of BMKG information in the earthquake mitigation. Electromagnetic parameters used were magnetotelluric data observed at geophysical observatories of Pelabuhan Ratu in collaboration with Chiba University (Japan). The method of electromagnetic data processing was done by applying polarization ratio (ratio of spectral analysis) method and impedance of EM wave on the ULF (Ultra Low Frequency) spectrum. Results of magnetic polarization and impedance of EM wave were identification of 5-50 days anomaly before the main shock, these parameters included in short-term precursors were likely caused by electrokinetic and microcrack before the accumulation of energy released as earthquakes.**

Keywords: Pelabuhan Ratu, Electromagnetic, Earthquake Precursor)

IV. INTRODUCTION

Earthquake is a natural phenomenon that the occurrence of erratic and unpredictable consequences. Efforts to minimize the hazards of earthquakes needs to be done, one of which is to detect early signs (precursors) the occurrence of earthquakes. Earthquake precursor research requires a variety of observational data and methods, one of which is the data of the earth's magnetic.

If a material under tension / stress then some properties of these materials undergo changes that can be monitored, such as properties of magnetic, radioactive, electron content, temperature and so on. Relations regarding such phenomena in the ionosphere-atmosphere system and the lithosphere is described by reference [1] in which prior to the earthquake will be no accumulation of energy in lithosfir to micro-cracks occur (microfracturing) which resulted in the loss of ULF emissions, emissions of radon, as well as changes in conductivity [1].

Electromagnetic anomalies as earthquake precursors was one method that on progress to developed. Observation of electromagnetic waves (EM) in the earth's surface within the limits of ultra low frequncy (ULF) (f <10 Hz) is believed to be the most promising of the monitoring activity of the earth's crust due to penetrating power of electromagnetic can be compared with depth at which the activity takes place and fluctuations in the Earth's crust The electrical conductivity of the earth can be detected directly [2].

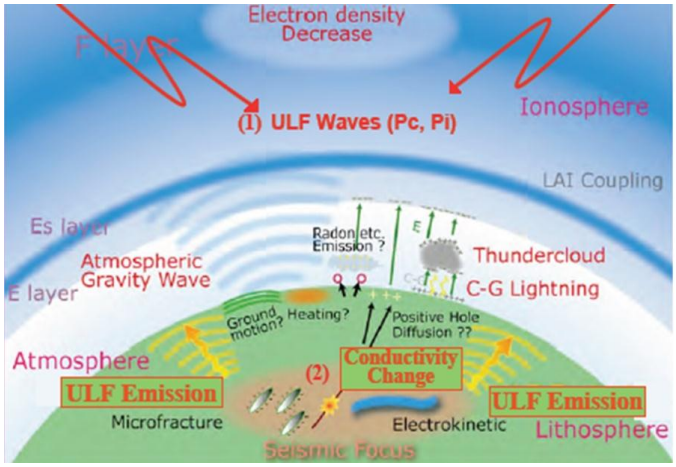

Fig. 1. **Relationship phenomena in the ionosphere-atmosphere system and the lithosphere [1]**

Yumoto et al. [3] introduced a new technique, namely the earthquake precursor studies and comparative polarization signal for the H and Z components of the technique makes it possible to separate the ULF emission of solar wind, magnetosphere, ionosphere or litosphere and derived from seismic origin (lithosphere) [3].

The purpose of this study was to analyze the characteristics of ULF electromagnetic signals in the spectrum and find anomalies that can be used to explain the phenomenon of earthquake precursors in the Pelabuhan Ratu.

V. RESEARCH METHOD

Data that used in this research was observational data magnetotelluric (MT) that consisting of electrical components Ex and Ey and also magnetic components X , Y , Z in January up to December 2013, that obtained from Geophysical Observatory, Pelabuhan Ratu . This station was formed from collaboration BMKG and Chiba University (Japan). Data obtained in the form of magnetic components H_X, H_Y, H_Z , and also electrical components E_X and E_Y. Ratio between electrical fields to magnetic fields (E/H) generating Electromagnetic Impedance that depend on the resistivity of medium or rock. Impedance as a function of the period provide information about the resistivity as function of depth.

Disturbance storm time (Dst) index during January up to December 2013 that obtained from WDC Geomagnetic models, Kyoto University was used as supporting data. This data is used to confirm the global external noise, which in case of magnetic storms, the magnetic anomalies encountered in the processing of data can be ignored.

Earthquake data that used as case study in earthquake precursors analysis was earthquake occurrence data from BMKG at Geophysical Observatory Pelabuhan Ratu area by calculating distance limitation based on Dobrovolsky research (1979), that the radius of the effective precursor manifestation zone depends on the earthquake magnitude and can be calculated using the empirical formula:

$$R_D = 10^{0.43 \times M_L} \quad (1)$$

With R_D is radius strain (Km) and M_L is earthquake local magnitude [4].

From January – November 2013, there were 9 event of earthquake with magnitude 3.7 until 5.5, that included in radius of precursor manifestation zone based on Dobrovolsky calculation. Earthquake data that used in this analysis was shown in Table 1 and Figure 2.

Table 1. Earthquake Data in 2013 (BMKG)

No	Date	Lat	Lon	Depth	Mag	Mag Type	Length	Radius
1	02/02/2013	-7.23	105.24	10	5.3	MLv	149	190
2	26/02/2013	-7.42	107.07	145	5.4	mb	73	210
3	06/03/2013	-6.59	106.24	132	4.6	M	58	95
4	08/04/2013	-7.29	105.95	48	5.2	Mw(mB)	75	172
5	16/04/2013	-6.25	104.72	48	5.5	MLv	221	232
6	14/05/2013	-6.8	106.62	10	3.7	MLv	24	39
7	21/07/2013	-7.43	106.15	26	4.4	M	66	78
8	24/10/2013	-7.25	106.38	108	4.7	MLv	34	105
9	13/11/2013	-6.59	106.37	139	4.9	Mw(mB)	51	128

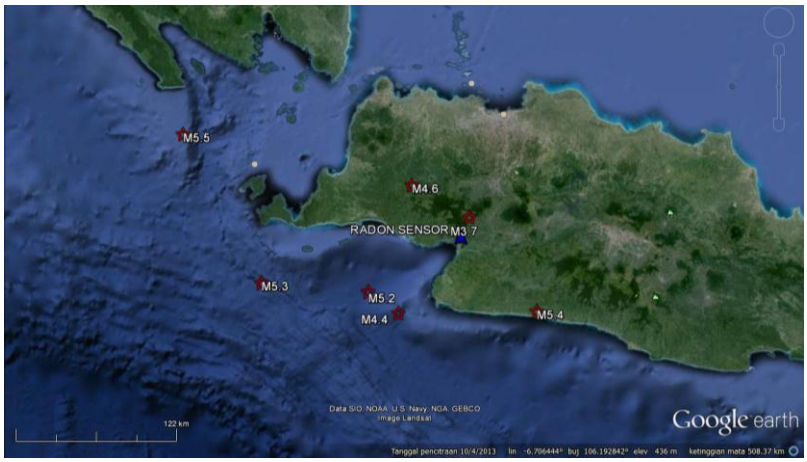

Fig. 2. **Plot distribution of Earthquake in January – November 2013**

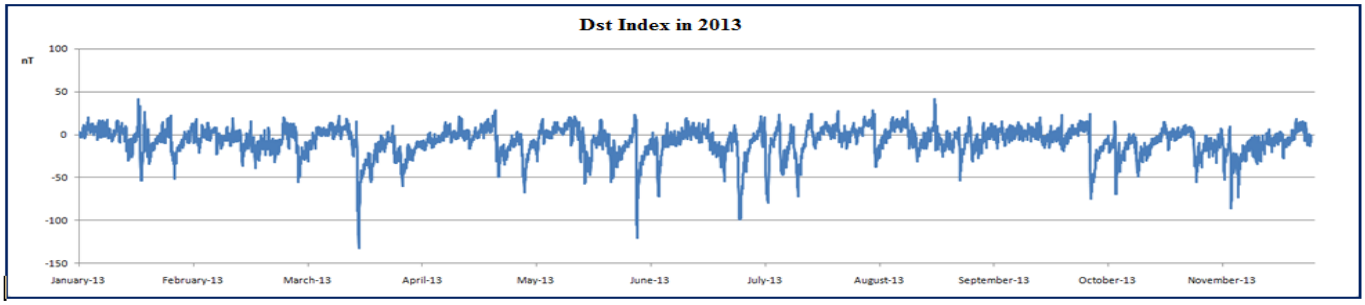

Fig. 3. **Dst Index plotting in January – November 2013 [5]**

Magnetic data processing performed using spectral polarization ratio (spectral density analysis) vertical and horizontal components (H_Z/H_H) in ULF spectrum (0.01 Hz) as introduced by Hayakawa, et. al. [6]. Analysis was performed in the evening hours 15:00 to 22:00 UTC (22:00 to 05:00 GMT) in order to avoid noise due to human activity. To convert signals from time domain to frequency domain using wavelet transform db5. In addition, the ratio of the horizontal component and annual mean (H_H/H_{HT}) and EM wave impedance changes (EX/HY) also analyzed [6].

VI. Result and Discussion

A. *Analyze of Magnetic Polarization Ratio*

Before analyze results of magnetic parameters, Dst index must be seen to determine the increase or decrease the intensity of the magnetic field variations caused by solar activity or other phenomena. Generally, negative magnetic field noise or magnetic storm indicates decrease of Earth's magnetic field [7].

In Dst index graphics (Figure 3), there are two times decrease in Dst index variations that relatively large and classified in powerful storm, on March 17th to 18th, 2013 and June 1st, 2013 so in this period should be careful to determine anomalies of magnetic data. If during a magnetic storm encountered significant anomalous magnetic data, the data can be ignored as precursors of earthquakes because the anomaly influenced by magnetic storms because most likely influenced by the anomalous magnetic storms.

Results of study show that anomaly of resistivity thought to be earthquakes precursors was impaired [8]. While polarization anomaly (Z/H) thought to be earthquake precursors according to research by Hayakawa [6], Hattori [9], and Yumoto [3] was value increase. In polarization ratio of horizontal component of magnetic variation of the annual mean (H/H_T), according to the Yumoto, et. al. [3] suspected anomalies as earthquakes precursors was value increase.

From graph in Figure 4 can be known some value increase of the magnetic polarization ratio H_Z/H_H. Then the earthquake occurrence data are also plotted as a case study at that time, so they can know the relationship between the occurrence of earthquake anomalies. ULF emissions anomaly with significant increase was found at February 9th until 19th or 7 days before earthquake event at February 26th (M 5.4) with distance 73 km and followed by earthquake at March 6th (M 4.6) with distance 58 km. On March 31th until April 2nd anomaly increase was found before earthquake at April 8th (M 5.2) with distance 75 km. Upon occurrence of this earthquake, the polarization values increased drastically which may be exacerbated due to the earthquake which happened to be near the station observations and shallow depth. This was anomaly for earthquake at April 16th (M 5.5) with distance 221 km. Then after significant increase anomaly at April 25th until 29th, earthquake was found at May 16th (M 3.7) with distance 24 km. Significant increase anomaly also found at May 30th until Juni 5th, but no earthquake after that. Then there was small ULF increase at Juni 21th until July 18th, after that earhquake was occured at July 21th (M 6.6) with distance 66 km. After this earthquake, ULF emissions tend to be stable. In August until October, there wasn't anomaly.

Figure 5 shows graph of magnetic variation ratio of horizontal component of the annual mean (H_H/H_{HT}) from January to November 2013. In the period from 7 to 16 March 2012 and the date of October 1 to 13 2012 looks absence of a significant increase in value (green) allegedly caused by solar activity as seen in the Dst index [9].

Study results of Yumoto, et. al. show that in this method the alleged polarization anomalies as earthquake precursors was value increase. From graph in Figure can be known some increase in magnetic polarization ratio H_H/H_{HT} value. Earthquake occurrence also plotted as case study at interval time, so known relationship between anomalies with earthquake event [3].

From graph in Figure can be known some increase of ratio H_H/H_{HT} value. Anomaly with significant increase was found at January 10th, January 29th, February 23th, March 14, April 7th, April 22th, August 8th, August 29th, Sept 24th and 26th, October 9th and 13th, Nopember 7th and 21th. Earthquake at February 2nd (M 5.3) with distance 190 km was occured after anomaly at January 29th or 5 days before event earthquake at February 26th (M 5.4) with distance 210 km occured after anomaly at February 23th or 3 days before events. Then earthquake at April 8th and 16th were occured after anomaly at March 14th, or 21 days before events. Earthquake at July 21th occured after anomaly at June. After that, also occured significant unstable anomaly at August until

early October, that was anomaly before earthquake at October 24th. Then the last anomaly was occured at Nopember 7th, 6 days before earthquake at November 13th.

Significant increase of polarization value that the probably caused by earthquake epicenter was shallow and near with observation station, so thus causing a very large effect. From plotting magnitud and ratio at graph, known that some distance occurs between anomaly on earthquake event were different. So, couldn't determine certainty long gains and interval time anomaly to earthquake event. The increase of polarization value to earthquake event occurred in ground, thus causing greater effect [10].

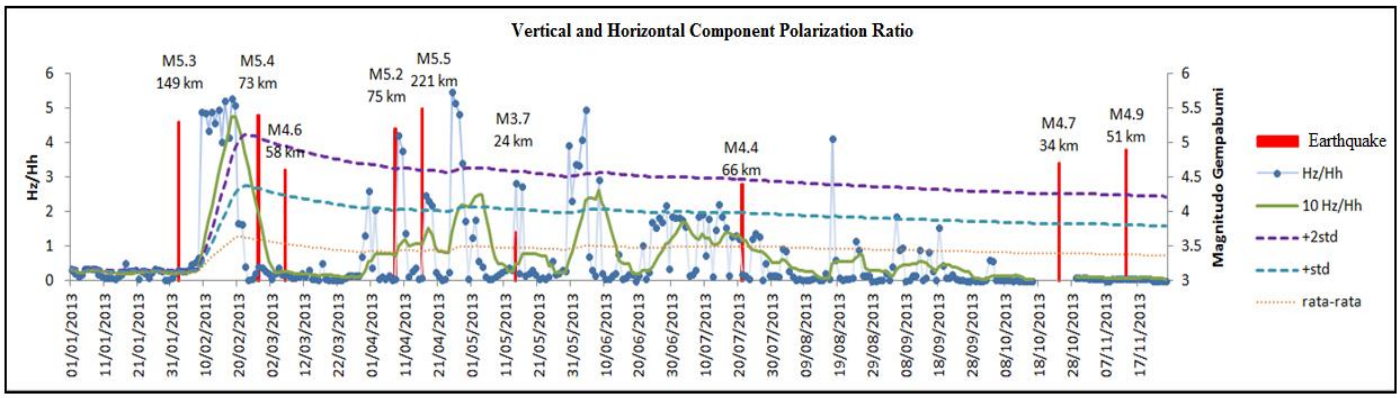

Fig. 4. **Results of electromagnetic data processing about ratio of vertical and horizontal polarization components**

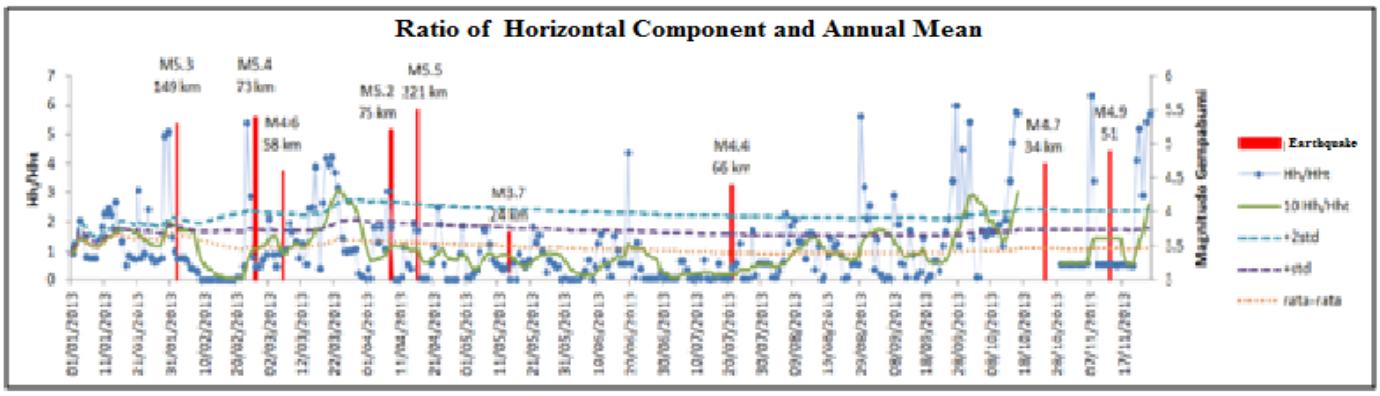

Fig. 5. **Results of electromagnetic data processing about ratio of horizontal component and annual mean**

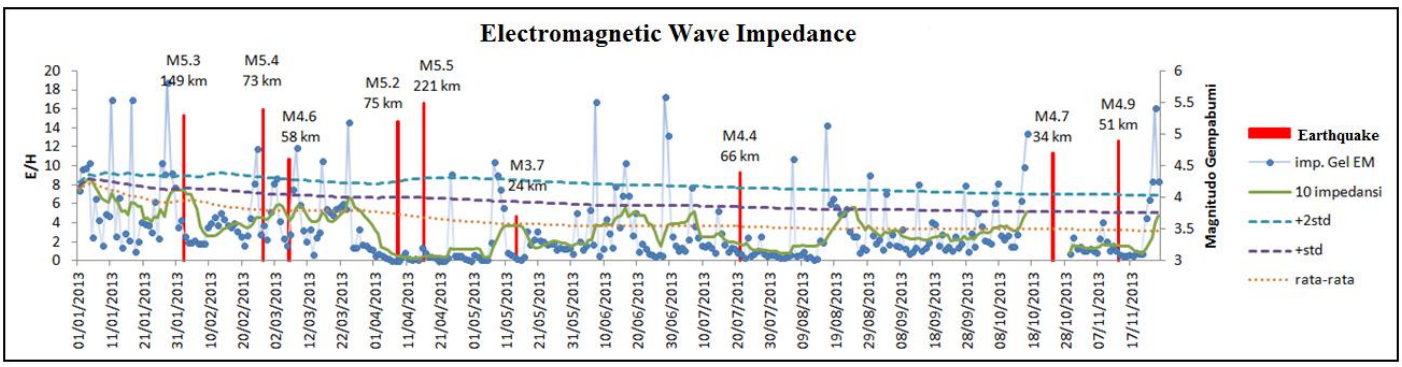

Fig. 6. **Results of electromagnetic data processing about electromagnetic wave impedance**

B. Analyze of Electromagnetic Wave Impedance

Figure 6 shows graph of electromagnetic waves impedance variation at January to November 2013. Impedance values obtained from comparative calculation of magnetic field divided magnetic field that perpendicular to the direction (E_X/H_Y). Has been discussed above that impedance or ratio between electric field (E) and magnetic (H) depend on resistivity of medium or rock. So, impedance as function of period provide information about resistivity of medium as depth function [9].

Previus results studies [8] show that anomaly of resistivity thought to be earthquake precursors was the value decrease. Existence of some decrease in impedance values was show in graph at Figure 6. Then the earthquake occurrence data also plotted at same graph as a case study at that time, so relationship between the impedance anomaly with earthquake events can be known directly. Some anomalies of impedance that occured at interval January – November was shown in figure 6. Anomaly of electromagnetic wave impedance parameters during January to November 2013 took place on February 2, February 23 - 24, March 1 - 2, May 7, June 13 and 28, August 17, October 14-15, and November 22-23. There are some events that happened after impedance anomaly, with different variational distance between anomaly to earthquake. But there are anomalies that occur without followed by earthquakes [8].

Earthquake at February 2 (M 5.3) with a distance of 149 km coincided with anomalies on February 2. Further anomalies at February 23 - 24 followed by earthquake at February 26, or 2 days later. Four days after anomaly on March 1 – 2, occured earthquake with magnitude 4.6 at 58 km length from magnetic station. Earthquake on April 8 and 16, there was no sign of electromagnetic impedance anomaly. Furthermore, earthquake at 14 May (M 3.7) with distance of 24 km occurred after the anomaly on the of May 7th. Anomaly on June 13 and 28 followed by earthquake on 21 July (M 4.4) at distance of 66 km. Anomaly on August 17 was not followed by earthquake events. But further anomalies on October 14 - 15 followed by earthquake on October 24 October (M 4.7) with distance of 34 km. There is an increase again on 22-23 november, but unfollowed by earthquakes, earthquake incident occurred prior to the anomaly, which is on the 13th november.

The results of the analysis of electromagnetic parameters using magnetic data (H_Z/D_D and D_D/H_{HT}) and impedance (E_X/H_Y) obtained precursor anomaly approximately 7-50 days before the earthquake occurred (Table 2), so that these parameters are included in short-term precursors that may be exacerbated elektrokinetis and microcrack process before the buildup of energy regardless as earthquakes. The closer the epicenter of the earthquake led to the emergence of a span of the longer detectable electromagnetic anomalies [9].

Table 2. Time interval about anomalies that as earthquake precursors

Parameters	Interval anomaly before earthquake (2013)						
	Febr 2nd	Febr 26th	March 6th	April 8th	April 16th	Oct 24th	Nov 13th
Magnetic							
H_Z/H_H	-	7 days	8 days	7 days	6 days	54 days	-
H_H/H_{HT}	5 days	3 days	-	3 days	20 days	11 days	6 days
Electromagnetic Impedance							
Ex/Hy	1 days	2 days	4 days	-	-	10 days	-

VII. CONCLUSION

Magnetic anomalies were detected 7 - 54 days before earthquake events. Electromagnetic wave impedance anomalies appear 1 - 10 days before earthquake events. Electromagnetic anomalies as earthquake precursors are classified as short-term precursors.

ACKNOWLEDGMENT

Conveyed gratitude to Mr. Noor Efendi for providing magnetic data for this study. And thanks to head of research and development for the guidance.

REFERENCES

[1] Yumoto, K. and The MAGDAS Group. (2006), *MAGDAS Project and Its Application For Earthquake Prediction*, Proceedings of the International Workshop on Integration of Geophysical Parameter as a Set of Large Earthquake Precursors, Research and Development Center BMG, Jakarta.

[2] Nurdiyanto, B., et al. (2011), *Integration of Geophysical Parameter Observation in the Earthquake Predictability*, JCM2011-031, Proceedings of the 36th HAGI and 40th IAGI Anual Convention and Exhibition, Makasar.

[3] Yumoto, K., Ikemoto S., Cardinal, M.G, Hayakawa, H., Hattori, K., Liu J.Y., Saroso, S., Ruhimat, M., Husni, M., Widarto, D.S., Ramos E., McNamara, D, Otadoy R.E, Yumul G., Ebora R., dan Servdano N. (2009), *A new ULF wave analysis for Seismo-Electromagnetics using CPMN/MAGDAS data Physics dan Chemistry of the Earth, Parts A/B/C* Volume 34, Issues 6-7, 2009, Hal. 360-366 Electromagnetic Phenomena Associated with Earthquakes dan Volcanoes.

[4] Dobrovolsky, I.P., Zubkov, S.I., & Miachkin, V.I. (1979), Estimation of the size of earthquake preparation zones. *Pure and Applied Geophysics*, Vol. 117, No. 5, pp. 1025–1044.

[5] WDC. World Data Center For Geomagnetic (2012), http://wdc.kugi.kyoto-u.ac.jp/aeasy/index.html

[6] Hayakawa, M., Kawate R., Molchanov O.A., dan Yumoto K. (1996), Result of Ultra-Low Frequency Magnetic Field Measurements during the Guam Earthquake of 8 augustus 1993, *Geophysical Research Lett.*, Vol 23, No.3, Hal.241-244.

[7] Gonzales, W.D., Joselyn, J.A., Kamide, Y., Kroehl, H.W., Rostoker, G., Tsurutani, B.T., Vasyliunas, V.M. (1994). What is a Geomagnetic Storm?, J. Geophys, Res 99, 5571.

[8] Xuemin, Z. and Xuhui, S. (2011), Electromagnetic Anomalies around TheWenchuan Earthquake and Their Relationship with Earthquake Preparation. *International Journal of Geophysics*, Volume 2011, Article ID 904132, 8 pages. Hindawi Publishing CorporationHattori, K. (2007), *ULF Electromagnetic Changes Possibly Associated with Crustal Activity*. Proceding Electromagnetics in Seismic and Volcanic Areas. Bilateral Seminar Italy-Japan July 25-27, 2007 Chiba Japan. Edited by Katsumi Hattori and Luciano Telesca. Hal. 41 – 56.

[9] Hattori, K. (2007), *ULF Electromagnetic Changes Possibly Associated with Crustal Activity*. Proceding Electromagnetics in Seismic and Volcanic Areas. Bilateral Seminar Italy-Japan July 25-27, 2007 Chiba Japan. Edited by Katsumi Hattori and Luciano Telesca. Hal. 41 – 56.

[10] Nurdiyanto, B., dkk. (2013), Studi Prekursor Gempabumi secara Terpadu Tahun 2012, *Laporan Tahunan Hasil-hasil Kegiatan Puslitbang BMKG*, 104-115.

G104

ULF Geomagnetic Pertubations Related With Earthquake

Case Study: 9th January 2014

Ayu Adi Justicea, S.T (*Author*)
Academy of Meteorology and Geophysic
AMG
Jakarta, Indonesia
ayujusticea2014@gmail.com

DR. Daryono
Academy of Meteorology and Geophysic
AMG
Jakarta, Indonesia
line 4-e-mail address if desired

***Abstract*— On midnight, 9th January 2014, 72 km from Southwest Pandeglang, Banten, Indonesia, an earthquake happen at 23:16:43 WIB, with Magnitude 5.2 Richter Scale, depth 10 km, and felt in Binuangeun (II-III MMI). West Java is a prone location for earthquake, it means that for research of short-term earthquake prediction.**

According to with many previous research on earthquake prediction, the extreme and full of research for many years, practical short-term for earthquake prediction still have conducted sustainable research. Research on earthquake-related electromagnetic phenomena in the earth have long conducted some research has shown that many such phenomena can answer one of the methods for earthquake prediction.

The ULF geomagnetic phenomena change is the one of the many phenomena that occur and can be proven in previous studies. To that end, this report first reviews previous observational facts and present the latest results in the detection of ULF geomagnetic change by signal analyzing by NOAA data. Finally, we will further study and determine the mechanism of propagation of ULF signals associated with an earthquakes.

Key words: Short-term earthquake prediction, Earthquake-related electromagnetic phenomena, ULF geomagnetic change, ULF emissions

I. INTRODUCTION

According to Daryono (2010) [18], West-Java region is part of Indonesia tectonic framework of the system. These areas include the Mediterranean and mountain paths are in the main zone of tectonic plate collision. Meeting these two plates are converging, where both collide and one of them, namely the Indo-Australian plate, slipped under the Eurasian plate. At the meeting of plate boundary is marked by oceanic trenches, as evidenced by the discovery of a trough in the southern West Java known as Java Trench.

Indo-Australian plate movement against the Eurasian plate resulted in West Java as one of the areas that have a high enough level of seismicity in Indonesia with regard to the activity of the collision plate (plate collision). This raises the plate movement of tectonic structures that are characteristic of subduction systems, namely Benioff Zone , ocean trenches , back beyond the arc (outer arc ridge) , outer arc basin (outer arc basin) , and the arc mountains (volcanic arc). In addition to the seismic vulnerability due to plate collision activity, this region is also highly vulnerable due to a local fault geological structure in the mainland. This structure is formed by the pressure of the ocean boundary Indo-Australian plate with the Eurasian continental shelf. Based on the tectonic conditions, then in almost all parts of the southern region of West Java, the earthquake disaster events can occur at any time but occur is hard to predict exactly when and where earthquakes will occur.

West Java is also a region with a typical island trough structure, with unique physiography characteristic, because it is on a mountain that lies on the Mediterranean island of Sumatra, Java, Bali and Nusa Tenggara. The interaction between the two plates and volcanic activity of the two systems mountain make this area as one of the country prone to earthquakes with a high level of seismicity.

From History record, since 1833 to 2008 have occurred at least 28 times the incidence of strong earthquakes in West Java and cause tsunamis. West Java has a long history of destructive earthquakes, including the 1875 earthquake Brass (7 people were killed, 628 houses collapsed), Tasikmalaya Earthquake 1979 (10 people killed, 1,430 houses collapsed), Earthquake Majalengka 1990 (8,000 homes collapsed), Earthquake Sukabumi, 2000 (35 people seriously injured, 633 houses were severely damaged), Earthquake Mount Halu 2005 (139 homes damaged), Earthquake and Tsunami Pangandaran 2006 (550 deaths).

The high frequency of the seismic activity, which needs serious attention given to each occurrence of natural disasters almost always arise casualties and material losses are not small. The catastrophic events can't be avoided, but we can do is minimize the loss of life, property and the environment. The

loss of life and property in the event of disasters that have been happening, more often due to lack of awareness and understanding of the government and the public against potential vulnerabilities and disaster mitigation efforts.

To reveal the high level of insecurity in the West Java earthquake disaster earth, necessary to study aspects of seismicity and tectonics local area as a whole. Because,in general, seismic activity can be viewed from the level of seismicity and regional tectonic conditions. If we observe the seismicity map of West Java, it was apparent the level of seismic activity in the area is very high . The earthquake that happens quite a lot in different variations of the magnitude and depth. Epicenter distribution in the western part of Java Island arc depth is generally dominated by variations in the depth of shallow earthquakes is less than 60 kilometers although not all shallow earthquakes that occurred vibration can be felt due to the relatively small magnitude . The distribution of earthquakes deeper appear more concentrated in the northern archipelago .

Distribution moderate earthquake had a depth of 60-300 kilometers is considered less dangerous . That is because hiposenternya quite deep and its influence on the surface is not very significant , except for the earthquake which happened to have a very large magnitude that its influence can be felt on the surface in a broad spectrum . Meanwhile , the earthquake had a depth of over 300 kilometers no harm given activity are very deep in the earth . Earthquakes of this type generally occur in the ocean plate subduction system . Earthquake in northern Java looks very tight distribution reflecting a seismic earthquake activity in high enough so that it can be explained that the earthquake hypocenter northward deeper patterns .
Based on a review of the aspects of seismicity and tectonics , it can be concluded that the high seismic activity of the region of West Java caused this archipelago has two generators of earthquake sources , ie from the south island arc in the form of plates subduction activity , and the presence of several active faults in mainland . Shallow earthquake is one of the main characteristics of earthquake activity due to the active faults . Seismicity and tectonics picture frame above would be enough to give a thorough overview that West Java is very vulnerable to terrestrial disasters , such as earthquakes and tsunamis .

Some research for possible correlations between the earthquakes, have many hypotesis, there are the variations of magnetic fields, Earth's horizontal and vertical currents in the atmosphere, was born when in early 1988, the historical data on the Black Sea was systemized [Mavrodiev, 1996].

The achievement in the Earth surface tidal potential modeling, with the ocean and atmosphere tidal influences being included, makes an essential part of the research. In this sense, the comparison of the Earth tides analysis codes (Venedikov et al., 2003; Milbert, 2011) is very useful. The possible tidal triggering of earthquakes has been investigated for a long period of time (Knopoff, 1964; Tamrazyan, 1967, 1968; Ryabl at al., 1968; Shlien, 1972; Molher, 1980; Sounau et al., 1982; Burton, 1986; Shirley, 1988; Bragin, 1999).

The last-years laboratory results in modeling the earthquake processes in increasing stress conditions support, at least qualitatively, the quantum mechanic phase shift explanation of the mechanism of generation of electromagnetic effects before and during earthquakes (Freund et al., 2002; St-Laurent et al., 2006; Vallianatos et al., 2003).
Some progress in establishing the geomagnetic filed and Eart tides variations as imminent precursors for increasing regional seismicity was presented in several papers (Mavrodiev, Thanassoulas, 2001; Mavrodiev, 2002a, b; 2003a, b, c; Mavrodiev, 2004; Mavrodiev, Pekevski, 2008; Mavrodiev, Pekevski, Jimseladze, 2008).

The model of earthquake-related part has to be infinitely repeated in the "theory–experiment–theory" process, using nonlinear inverse problem methods in looking for correlations between the different fields in dynamically changing space and time scales. Each approximate model supported by some experimental evidence should be included in the analysis (Varotsos et al., 2006; Thanassoulas et al., 2001a, b; Eftaxias at al., 2001, 2002; Duma, 2006). The adequate physical understanding of the correlations among electromagnetic precursors, tidal extremes and a impendant earthquake is related to the progress of an adequate Earth magnetism theory and electrical currenets distribution, as well as to the quantum mechanical understanding of the processes in the earthquake source volume before and during the earthquake. According to Strachimir,2008, geomagnetic earthquake precursor improvement formulation on the earthquake minimum ±1 day and maximum ±2 days before an earthquake occur.

The analysis of more accurate at space and time measuring sets for the Earth crust condition parameters, including the monitoring data of the electromagnetic field under and ver the Earth surface, from the temperature distribution and other possible precursors, would be the basis of nonlinear inverse problem methods. It could be promising for studying and solving the "when, where and how" earthquake prediction problem and in this paper we discuss some results reflect on ULF emissions observed few days prior to some of the recent seismic activities in Indonesia, especially West-Java. These Emissions are fund to occur as pertubations in the ionospheric and have been detected by Satellite (NOAA).

According to above, the research of seismo-electromagnetic effect refer to the magnetic and electric field disturbances that are observed during the earthquake. According that statement, there are many methods of studying and innovations such anomalies involve the application of space based technology by satellites data and using the ground based sensors to recording the continuous data to analyzing the results. In this paper, we present and analyze about the electromagnetic field disturbances in ULF range detected by satellite for some earthquakes that have occurred especially in West Java, Indonesia. The earthquake happen in the Indonesia region and the measured considerably strong magnitude on Richter Scale. The data we got from NOAA, and

implemented to form of magnetic and electric sensors that keep in line variations constantly.

II. OBSERVATIONAL METHOD

In this paper, observational method thats we used there is some encourage studis related with earthquake and and some phenomenon simultaneously by satellite (NOAA), this part for studies and investigation of the ionospheric pertubations related with major geophysical hazard. This paper explain about disturbations related to Satellite Environment, Solar Cycle Sunspot, Solar Cycle Radio Flux Progression, Solar Cycle Ap Progression, the results of Magnetometer, X-Ray Fluxs and Kp Indext.

The study case of this paper is an earthquake 9th January 2014, 72 km from Southwest Pandeglang, Banten, Indonesia, an earthquake happen at 23:16:43 WIB, with Magnitude 5.2 Richter Scale, depth 10 km, and felt in Binuangeun (II-III MMI).

Picture 1. The Earthquake event at 9th January 2014 (Source BMKG from Antara News.com)

III. RESULTS AND DISSCUSSION

The solar cycle (or solar magnetic activity cycle) is the periodic change in the sun's activity (including changes in the levels of solar radiation and ejection of solar material) and appearance (visible in changes in the number of sunspots, flares, and other visible manifestations). Solar cycles have an average duration of about 11 years. They have been observed (by changes in the sun's appearance and by changes seen on Earth, such as auroras) for hundreds of years. (Wikipedia)

Solar variation causes changes in space weather, weather, and climate on Earth. It causes a periodic change in the amount of irradiation from the Sun that is experienced on Earth. It is one component of solar variation, the other being aperiodic fluctuations. Evolution of magnetism on the Sun. Powered by a hydromagnetic dynamo process, driven by the inductive action of internal solar flows, the solar cycle:

- Structures the Sun's atmosphere, its corona and the wind;
- Modulates the solar irradiance;
- Modulates the flux of short-wavelength solar radiation, from ultraviolet to X-ray;
- Modulates the occurrence frequency of solar flares, coronal mass ejections, and other geoeffective solar eruptive phenomena;
- Indirectly modulates the flux of high-energy galactic cosmic rays entering the solar system. (Wikipedia)

We show that The Solar cycle resluts every day before and after the earthquake:

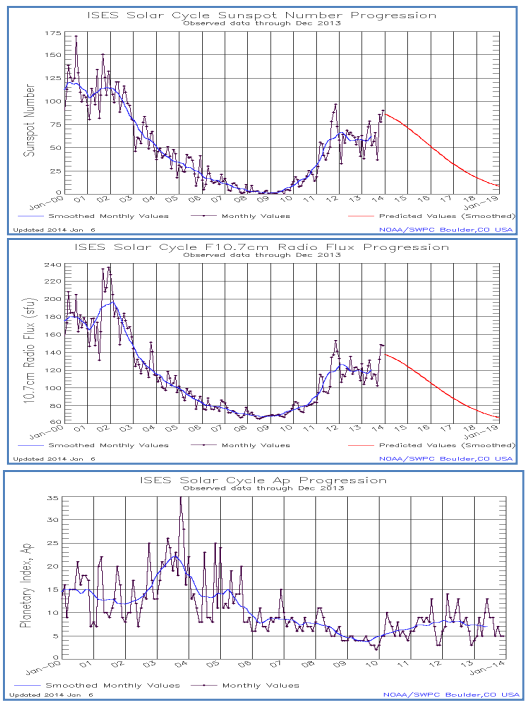

Picture 2. Diagram show the Solar Cycle from Satellite data of NOAA (a) Solar Cycle Sunspot Progression, (b) Solar Cycle Radio Flux Progession, (c) Solar cycle Ap Indext Progression

Picture 1 explain about Sunspots may exist anywhere from a few days to a few months, but they eventually decay, and this releases magnetic flux in the solar photosphere. This magnetic field is dispersed and churned by turbulent convection, and solar large-scale flows. These transport mechanisms lead to the accumulation of the magnetized decay products at high solar latitudes, eventually reversing the polarity of the polar fields. (Wikipedia).

The dipolar component of the solar magnetic field is observed to reverse polarity around the time of solar maximum, and reaches peak strength at the solar minimum. Sunspots, on the other hand, are produced from a strong toroidal (longitudinally directed) magnetic field within the solar interior. Physically, the solar cycle can be thought of as a regenerative loop where the toroidal component produces a poloidal field, which later produces a new toroidal component of sign such as to reverse the polarity of the original toroidal field, which then produces a new poloidal component of

reversed polarity, and so on. (Wikipedia). The results show that the Solar variations is decrease ± 1 day before an earthquake at 9th January 2014, it seems that this solar cycle can explain about precursor before an earthquake happen in Indonesia Region, especially West-Java Region.

The Geostationary Operational Environmental Satellite - R Series (GOES-R) is the next generation of geosynchronous environmental satellites which will provide atmospheric and surface measurements of the Earth's Western Hemisphere for weather forecasting, severe storm tracking, space weather monitoring, and meteorological research. GOES-R is a follow-on to the current GOES system which is utilized by NOAA's National Weather Service for weather monitoring and forecasting operations as well as by researchers for understanding interactions between land, ocean, atmosphere, and climate. The GOES-R series program is a collaborative development and acquisition effort between NOAA and NASA to develop, deploy, and operate the satellites. The overall program is managed by NOAA with an integrated NOAA-NASA program office organization co-located at NASA's Goddard Space Flight Center in Greenbelt, Maryland. GOES-R is scheduled for launch in early 2016. The GOES-R series of satellites (GOES-R, S, T, & U) will extend the availability of the operational GOES satellite system through 2036. (NOAA)

The GOES-R Magnetometer will provide measurements of the space environment magnetic field that controls charged particle dynamics in the outer region of the magnetosphere. These particles can be dangerous to spacecraft and human spaceflight. The geomagnetic field measurements will provide alerts and warnings to satellite operators and power utilities. GOES-R Magnetometer data will also be used in research. The GOES-R Magnetometer products will be part of NOAA space weather operations, providing information on the general level of geomagnetic activity and permitting detection of sudden magnetic storms. In addition, measurements will be used to validate large-scale space environment models that are used in operations.

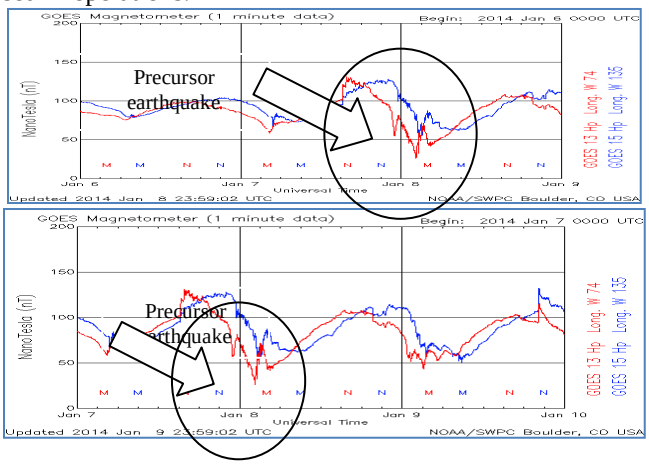

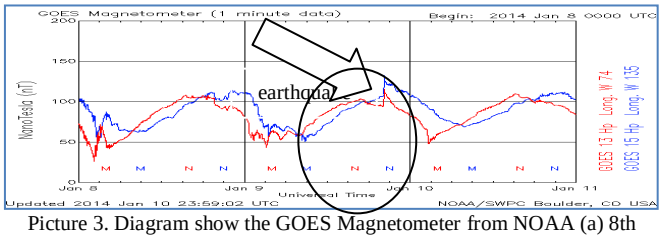

Picture 3. Diagram show the GOES Magnetometer from NOAA (a) 8th January 2014, (b) 9th January 2014, (c) 10 January 2014

Picture 2 explain about decrease of space magnetic field that controls charged particle dynamics in the outer region of magnetosfer before the earthquake at 9th January 2014. The general level of geomagnetic activity and permitting detection of sudden magnetic storms. In addition, measurements will be used to validate large-scale space environment used in operations by ULF/ELF studies. At 8th January 2014 models that are , it seems that the GOES Magnetometer recorded the space magnetic space with disturbance signal before the earthquake happen.

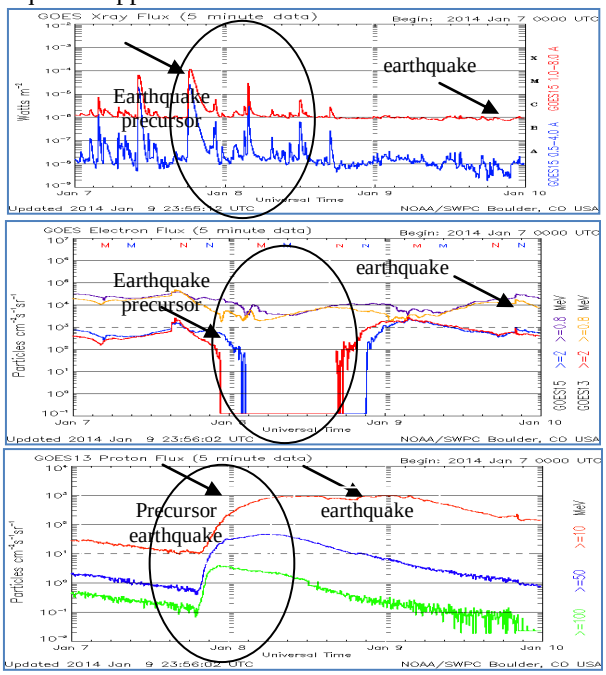

Picture 4. Diagram show the GOES from NOAA (a) Xray Flux 9th January 2014, (b) Electron Flux 9th January 2014, (c) Proton Flux 9th January 2014

Picture 3 explain about decrease of space magnetic field that controls charged particle dynamics in the outer region of magnetosfer before the earthquake at 9th January 2014. The general level of geomagnetic activity and permitting detection of sudden magnetic storms. In addition, measurements will be used to validate large-scale space environment models that are used in operations by ULF/ELF studies. It explain about increase of Xray Flux, Electron flux distubation and decrease of proton flux at 8th January 2014. It seems that this methods of ULF/ELF studies can improvement the earthquake precursor 1 day before an earthquake happens.

The K-index quantifies disturbances in the horizontal component of earth's magnetic field with an integer in the range 0-9 with 1 being calm and 5 or more indicating a geomagnetic storm. It is derived from the maximum fluctuations of horizontal components observed on a magnetometer during a three-hour interval. The official planetary **Kp index** is derived by calculating a weighted average of K-indices from a network of geomagnetic observatories. Since these observatories do not report their data in real-time, various operations centers around the globe estimate the index based on data available from their local network of observatories.

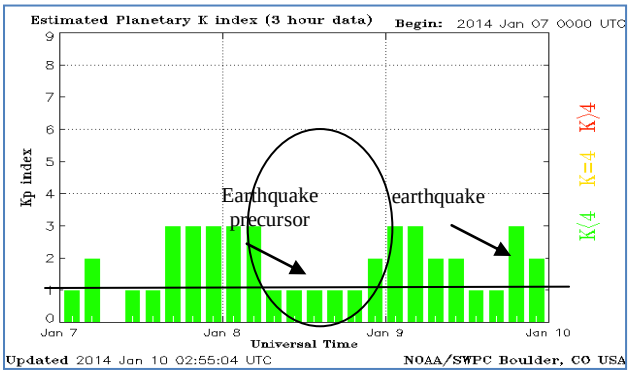

Picture 5. Diagram show the Estimated K indeks from NOAA, at 10th January 2014

Picture 4. Explain about The K_p index is used for the study and prediction of ionospheric propagation of high frequency radio signals. Geomagnetic storms, indicated by a K_p of 5 or higher, have no direct effect on propagation. However they disturb the F-layer of the ionosphere, especially at middle and high geographical latitudes, causing a so-called *ionospheric storm* which degrades radio propagation. The degradation mainly consists of a reduction of the maximum usable frequency (MUF) by as much as 50%.[6] Sometimes the E-layer may be affected as well. In contrast with sudden ionospheric disturbances (SID), which affect high frequency radio paths near the Equator, the effects of ionospheric storms are more intense in the polar regions. From the result, we can see that the increase of K index estimated ±1day before the earthquake occur.

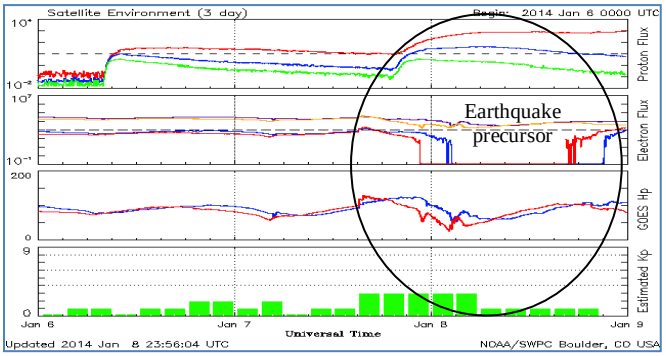

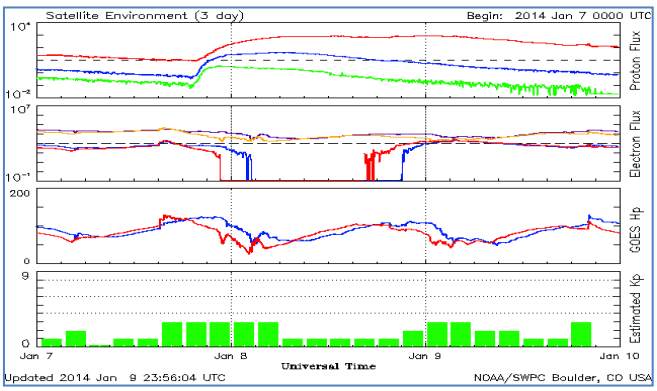

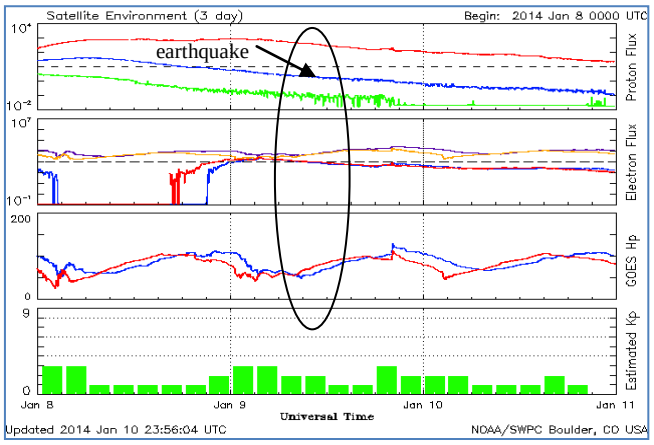

Picture 6. Diagram show the Satellite Environment from NOAA; (a) 8th January 2014, (b) 9th January 2014, (c) 10 January 2014

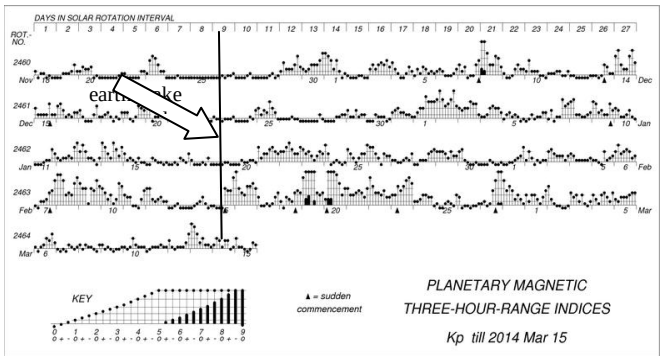

Picture 7. Plenetary Magnetic Three Hour Range Indices

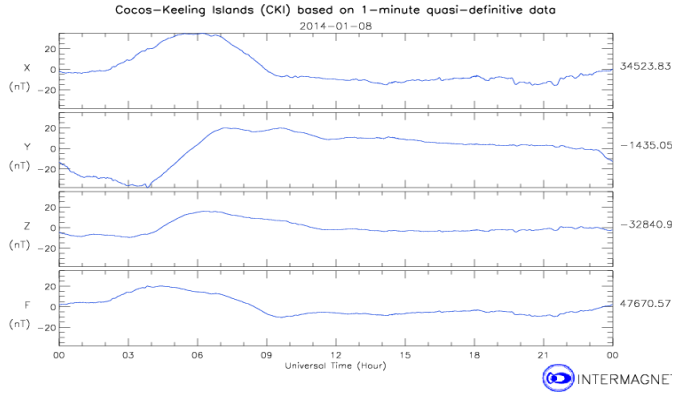

(a)

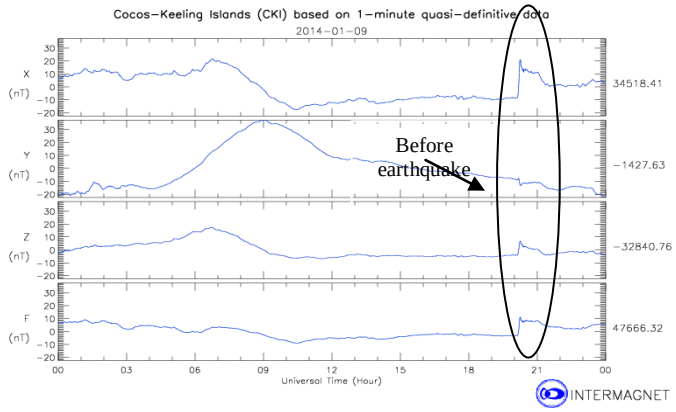

(b)

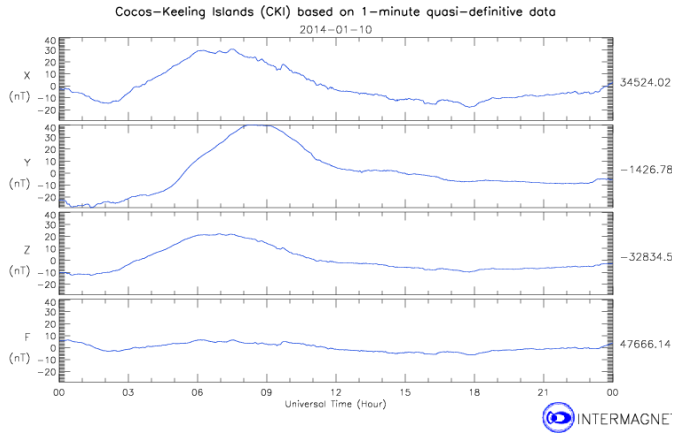

(c)

Picture 8. Diagram shows that COCOS (X, Y, Z, F magnetic component) (a) date 08th January 2014, (b) date 09th January 2014, and (c) date 10th January 2014 (Intermagnet)

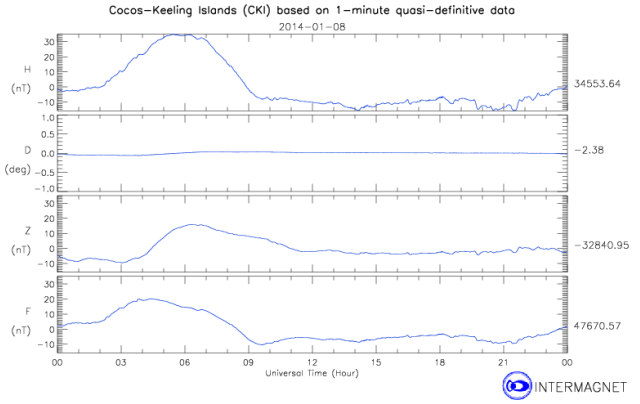

(a)

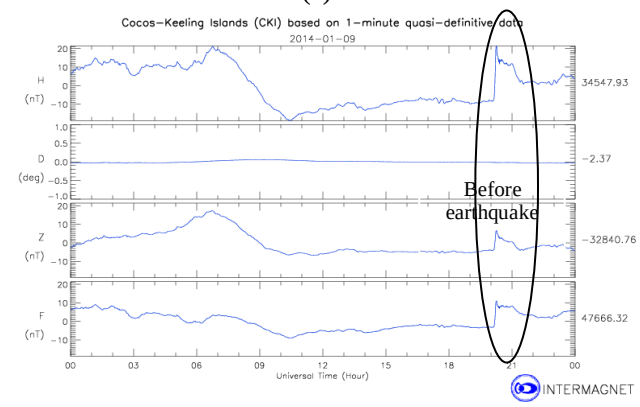

(b)

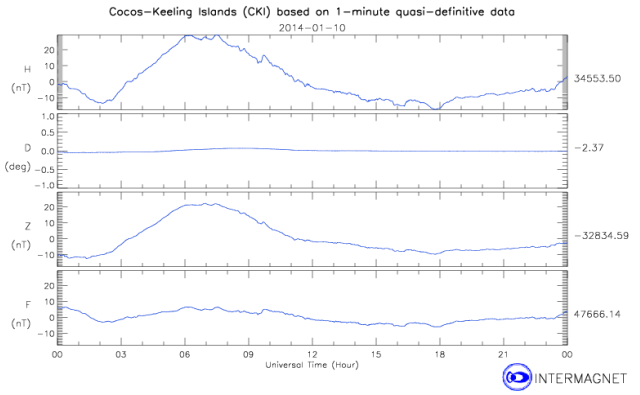

(c)

Picture 9. Diagram shows that COCOS (H, D, Z, F magnetic component) (a) date 08th January 2014, (b) date 09th January 2014, and (c) date 10th January 2014(Intermagnet)

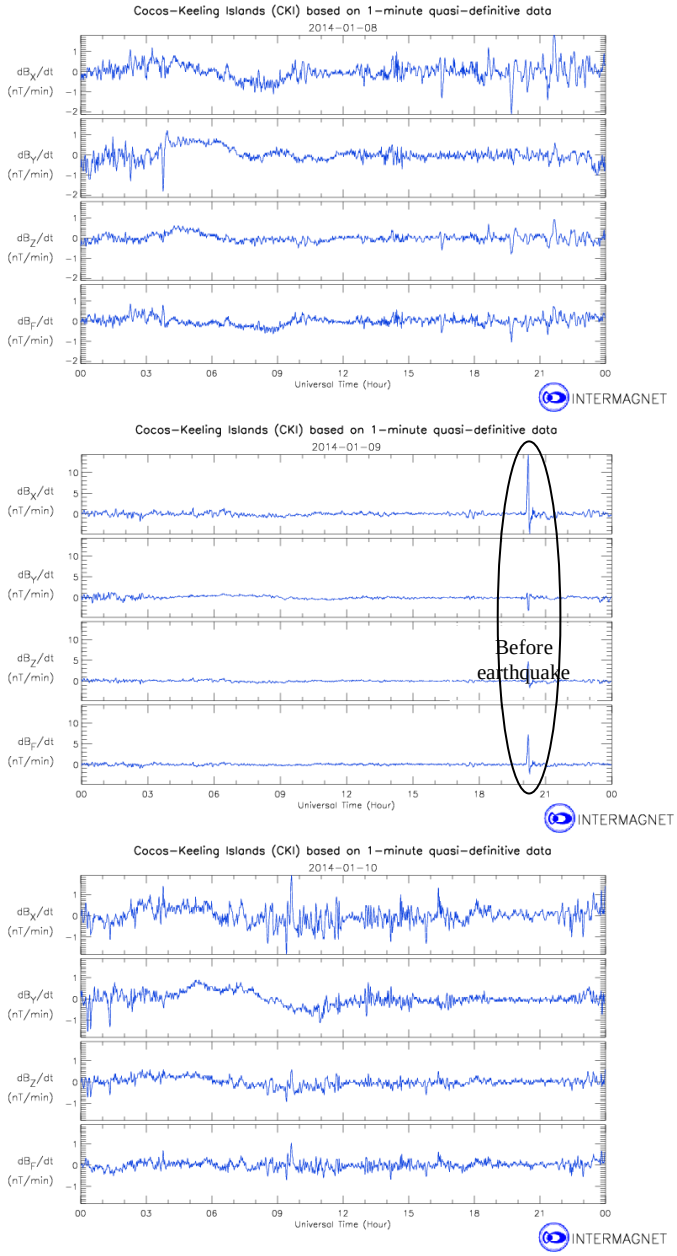

Picture 10. Diagram shows that COCOS (dBx/dt, dBy/dt, dBz/dt and dBf/dt magnetic component) (a) date 08th January 2014, (b) date 09th January 2014, and (c) date 10th January 2014(Intermagnet)

IV. CONCLUSION

The correlations between magnetism and electric field activities and incoming earthquakes, which occur in the time defined from the next minimum (±1 day) or maximum (±3days) of the Earth Satellite data observations is tested statistically. The distribution of the time difference between predicted and occurred events decrease in the time. This result can be interpreted like a possible first reliable approach for solving the "when" earthquakes prediction problem. On the basis of electromagnetic monitoring under, on and over Earth surface is proposed research for solution of "when, where" earthquake prediction probably by ULF/ELF results . Under the hypothesis the current has a big vertical component the data of two geomagnetic vector devices are enough for determination of the future epicenter. The three devices will permit to research the correlation between Earth surface distribution of precursor function Sig and the Magnitude of the incoming earthquake. The complex questions for solving the "when, where and how" earthquake prediction problem is very shortly presented.

ACKNOWLEDGMENT

Thanks to NOAA, INTERMAGNET

REFERENCES

[1] Mavrodiev S.Cht., Thanassoulas C., "Possible correlation between electromagnetic earth fields and future earthquakes", ISBN 954-9820-05-X, Seminar proceedings, 23-27 July, 2001, INRNE-BAS, Sofia, Bulgaria, 2001

[2] Knopoff, L, Earth tides as a triggering mechanism for earthquakes, Bull. Seism. Soc.Am. 54:1865–1870, 1964

[3] Tamrazyan G.P., Tide-forming forces and earthquakes, ICARUS, Vol.7, pp.59-65, 1967

[4] Tamrazyan G.P., Principal ragularities in the distribution of major earthquakes relative to Solar and Lubar tades and other Cosmic forces, ICARUS, Vol.9, pp.574-592, 1968

[5] Venedikov, A. and Arnoso, R.: Program VAV/2000 for Tidal Analysis of Unevenly Spaced Data with Irregular Drift and Colored Noise, J. Geodetic Society of Japan, 47,1, 281–286, 2001

[6] Venedikov, A. P., Arnoso, R., and Vieira, R.: A program for tidal data processing, Computer & Geosciences, 29, 4, 487–502, 2003

[7] Alexandrov L., Autoregularized Gauss-New-ton-Kantorovich iteration Process, Comm. JINR, P5-5515, Dubna, 1970

[8] Alexandrov L., Regularized computational process of Newton-Kantorovich type, J. Comp. Math. And Math. Phys., 11, Vol. 1, 36-43, 1971

[9] Alexandrov L., The program REGN (Regularized Gauss-Newton iteration method) for solving nonlinear systems of equations, Comm. JINR P5-7259, Dubna, 1973

[10] Alexandrov L., Program code REGN, PSR 165 RSIK ORNL, Oak Ridge, Tennessee, USA,1983

[11] Mavrodiev S. Cht., On the reliability of the geomagnetic quake as a short time earthquake's precursor for the Sofia region, Natural Hazards and Earth System Sciences (2004) 4: 433–447, SRef-ID: 1684-9981/nhess/2004-4-433

[12] Mavrodiev, S. Cht., and Pekevski, L., Complex Regional Network for Earthquake Researching and Imminent Prediction, Electromagnetic phenomena related to earthquakes and volcanoes, Editor: Birbal Singh, Publ., Narosa Pub. House, New Delhi, pp. 135-146, 2008

[13] Mavrodiev, S. Cht., Pekevski, L., and Jimseladze, T. Geomagnetic-Quake as Imminent Reliable Earthquake's Precursor: Starring Point for Future Complex Regional Network, Electromagnetic phenomena related to earthquakes and volcanoes, Editor: Birbal Singh, Publ., Narosa Pub. House, New Delhi, pp. 116-134, 2008,

[14] Mavrodiev S. Cht., Pekevski L., On the Balkan- Black Sea- Caspian Complex NETWORK for earthquake's Researching and Prediction, NATO Advanced research workshop management of urban earthquake risk in Central Asian ans Caucasus countries, Istanbul, 14-16 May, 2006

[15] Rusov, V. D.; Vaschenko, V. N.; Linnik, E. P.; Cht. Mavrodiev, S.; Zelentsova, T. N.;Pintelina, L.; Smolyar, V. P.; Pekevski, L., Mechanism of deep-focus earthquakes anomalous statistics,EPL (Europhysics Letters), Volume 91, Issue 2, pp. 29001 (2010)

[16] Rusov, V.D. et all, Solar Dynamo as host power pacemaker of Earth global climate, EU FP7 IRSES 2011 Project, "Complex research of Earthquake's Forecasting Possibilities, Seismicity and Climate Change Correlations", ISBN978-9989-631-04-7, Ohrid, Macedonia, BlackSeaHazNet Series, Volume 1, 2-5 May, 2011

[17] Daryono, Kerangka Tektonik dan Sejarah Panjang Gempabumi Jawa Barat, BMKG, 19 May, 2010

[18] Bhattacharya, et all. Study of ULF/ELF Pertubation Associated With Earthquake, Electromagnetic phenomenon related to earthquake an Volcanoes, 41-47, 2008.

[19] wikipedia.org

[20] noaa.usgs.gov

[21] R. Nicole, "Title of paper with only first word capitalized," J. Name Stand. Abbrev., in press.

[22] Y. Yorozu, M. Hirano, K. Oka, and Y. Tagawa, "Electron spectroscopy studies on magneto-optical media and plastic substrate interface," IEEE Transl. J. Magn. Japan, vol. 2, pp. 740-741, August 1987 [Digests 9th Annual Conf. Magnetics Japan, p. 301, 1982].

[23] M. Young, The Technical Writer's Handbook. Mill Valley, CA: University Science, 1989.

[24] www.intermagnet.org

[25]Hayakawa, Mashashi et.all. Monitoring ULF Geomagnetic Variation Associated With Earthquakes, Sensors, 2007

[26] Hatori, Katsumi. ULF Geomagnetic Changes Associated with The Large Earthquakes. TAO. Vol.15, No.3, 329-360, September, 2004

[27] www.bmkg.go.id

[28]www.antaranews.com(http://www.antaranews.com/berita/413377/gempa-52-sr-guncang-pandeglang-banten)

G105

Determinations Onset time of Earthquake Precursor by Analizing ULF-EM Emission Signal in Sumatra region,

Case Studi Padang 2009 and Mentawai 2010.

S.Ahadi
Faculty of Earth Sciences and Technology
Bandung Institute of Technology
Bandung, Indonesia
su4idi@yahoo.com

S. Saroso
National Institute of Aeronautic and Space
Bandung, Indonesia

N.T. Puspito and G. Ibrahim
Faculty of Mining and Petroleum Engineering
Bandung Institute of Technology
Bandung, Indonesia

S. Ahadi
Meteorological Climatological and Geophysical Agency
Jakarta, Indonesia

Absract-**Determination of onset time precursors of strong earthquakes for Padang 2009 and Mentawai 2010. We are using geomagnetic data from Geomagnetic station KTB, Sumatra and two station references DAV, Philippine and DAW, Australia. Separate techniques are required in its determination. Not the same as that recorded in the kinetic wave seismograms can be determined by direct time domain. Difficulties associated with electromagnetic waves seismogenic activities require analysis of the transformed signal in the frequency domain. Determination of the frequency spectrum will determine the frequency of emissions emitted from the earthquake source. We analize signal ULF emission with associated strong earthquake in sumatera period 2009 – 2010 for Padang earthquake 2009 and Mentawai earthquake 2010. The aim is to analyze the power amplitude of the ULF emissions in the horizontal component (H) and vertical component (Z). Polarization power ratio S_Z/S_H is used for determining the sign of earthquake precursors controlled by the standard deviation. The pattern recognition polarization ratio should be obtained which can differentiate emissions from seismogenic effects and geomagnetic activity. ULF emission patterns generated that seismogenic effect has duration > 1 days before event. The dominance of emission intensity recorded at the Z component and for the dominance of the emission intensity of geomagnetic activity recorded in the component H. The result shows that the onset time is determined when the polarization power ratio S_Z / S_H standard deviation over the limit ($p \pm 2 \sigma$) which has a duration of > 1 days .**

Keywords—component; *Earthquake precursor, polarization ratio, Onset time, ULF emission and Sumatra Earthquake,*

I. INTRODUCTION

Earthquake precursor studies using data geomagnetic has been widely reported by several researchers Hattori et al [1-4].The result is still the problem of how to determine the signature and how the onset time precursor as anomaly earthquake associated with ULF emissions determined?. This study tried to answer the earlier problems by analyzing the pattern of earthquake precursor emissions associated with ULF f = 0.023 Hz, it is based on reports from Ismaguilov et al. [5 and 6] report is the seismogenic frequency spectrum f = 0.02 - 0.05 Hz. it has also been strengthened by Hattori et al. [2] using frequencies in the range f = 0.01 Hz. Yumoto et al. [7] also uses frequencies in the range f = 0.01 - 0.022 Hz . This spectrum used to investigate a strong earthquake Padang 2009 and Mentawai 2010. Result of the earthquake investigation eventually led to a question of how relations earthquake magnitude and distance to the length of ULF emissions recorded in the magnetogram.

II. DATA AND METHOD

These research is to analyze the data geomagnetic with associated strong earthquake Padang 2009 and Mentawai 2010 using BMKG catalog previously been conducted by Ibrahim et al. [8]. This research uses data during nigthtime (23.00 – 04.00 local time) and an increase in the signal processing analysis. Data selection when a quiet day that the monitoring by geomagnetic index Dst (Distrubence Storm time). We are using geomagnetic reference station DAV (Davao in

Philippines) at the North and DAW (Darwin in Australia) at the south.

Our goal to observe the earthquake did not occur when storm or sub storm. in the same way we determine the precursor to a strong earthquake in Sumatra within ≤ 500 km from KTB. We also choose a quiet day at the station and for comparison the DAV (Davao, Philippines) in the north and DAW (Darwin, Australia) in our South also collected data on strong earthquake within ≤ 500 km from the station. And we selected earthquakes recorded at stations DAV does not occur simultaneously or ± 10 days when the earthquake occurred in Sumatra. From here we get an earthquake in Sumatra will be chosen completely clean of another earthquake disturbances in comparison with reference station.

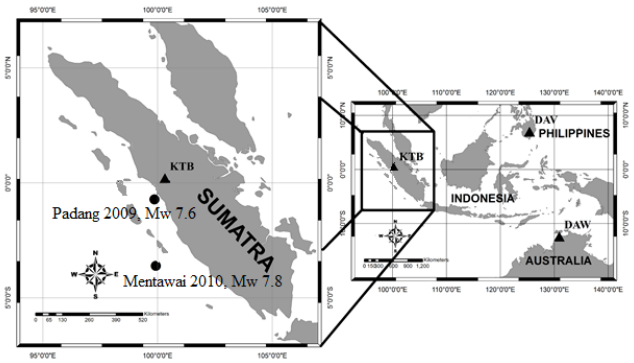

Fig. 1. Distribution epicenter two earthquake investigation [13] and Geomagnetic station Kototabang (KTB, Sumatra) and two station reference Davao (DAV, Philippine) and Darwin (DAW, Australia)

The polarization ratio using power spectral analysis of the ULF emission is a collection contains variety of frequencies are presented in the frequency domain. It is clearly observed that polarization showed a remarkable pre-seismic enhancement [1], Previous research is a possible to determine the pattern of anomalies caused by magnetic disturbances from lithosphere [9-11], and polarization ratio (Z/H) gradual decrease about one month before the Earthquake and recover within 2 week after earthquake [12].

We have been done analyze the Power Spectral Density Spectral (PSD) used with the Welch method of dividing the length of the signal (N data) into several segments, overlapping 50% on each segment [8]. FFT performed on each segment called nFFT the use of type window and type Hamming window of length L = N + 1. Standard deviation need to control and determination onset time. We determination onset time if polarization power ratio Z/H cross moving average from standard deviation.

III. RESULT AND DISCUSSION

From the results of research that has been done by developing a technique polarization power ratio S_Z/ S_H to the timing of onset is still hard to do. But here we got a conviction in which each earthquake occurrence by using spectrum analysis on each component found an intensity anomaly where if there is interference with geomagnetic disturbances external to the component response intensity H has a higher frequency than the component Z. we using Dst Index for control geomagnetic activity in low latitude [8 and 12] in Fig. 2

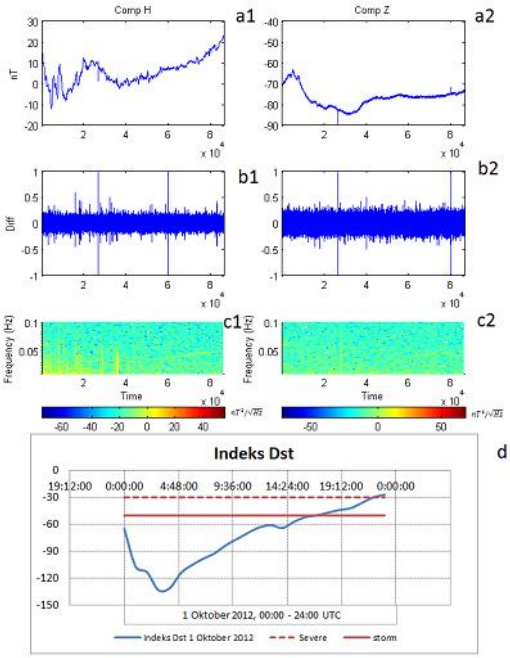

Fig.2 Showing geomagnetic storm (October 1, 2012) with spectrogram in panel c1 and c2 form H Comp. and Z Comp. Dst Index, in Panel d

We showing response frequency if with associated seismogenic, Z comp. have intensity response more than H comp. This is The Padang earthquake September 30, 2009 with a quiet day (no geomagnetic activity) in Fig.2.
Analysis spectrum with polarization rasio S_Z/S_H for determination onset time and lead time to Padang earthquake showing in fig.3.

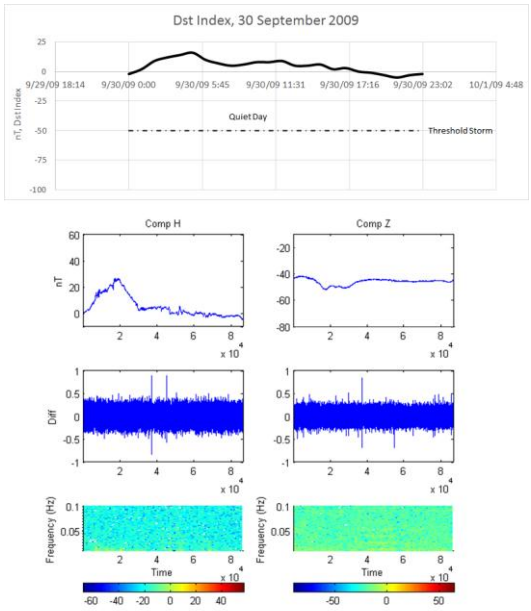

Fig. 3 The associated seismogenic effect for Padang Eq. 30 September 2009 Mw= 7.6 and distance 139 km from KTB, The Comp. Z have response intensity more than H Component.

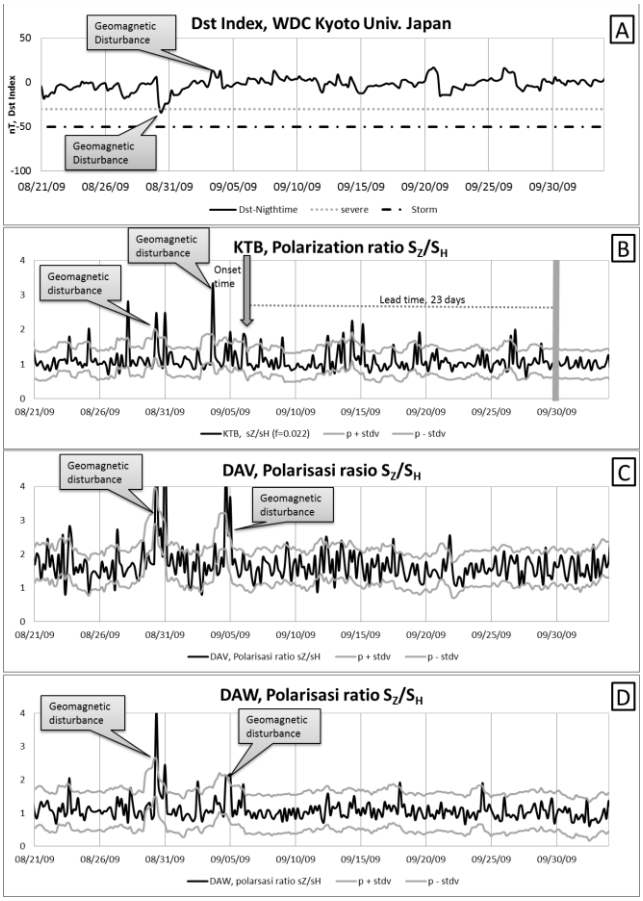

Figure 4 . Top panel (A) is Dst index (black line) (WDC-Kyoto Univ.[14]) in period August 21 – October 10, 2009 was quiet and the middle panel KTB (black line) shown information anomaly ULF emission with onset time September 06 – event (lead time) with shown crossed the line standard deviation (p+σ, p-σ). For below panel is station geomagnetic reference DAV and DAW shown not Information ULF emission all period.

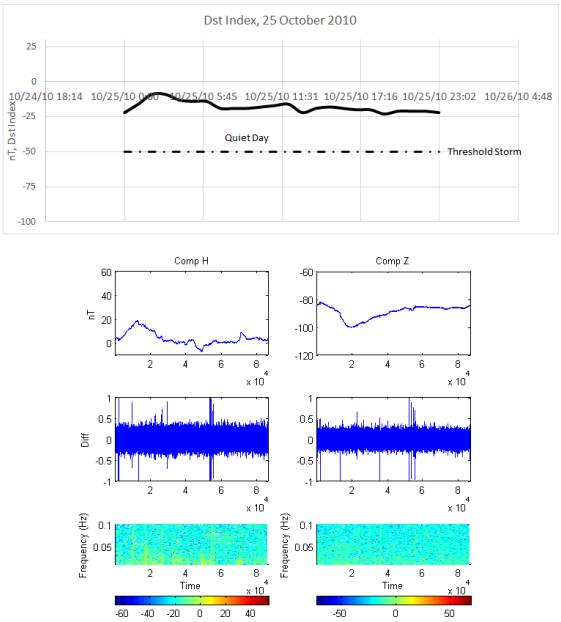

Figure 5. Mentawai earthquake 25 October 2010 showing when event. Top Panel is Dst Index from WDC Kyoto University Japan dan Low panel are comp. H and Z for raw data, diff data and spectrogram.

In Fig.5 low panel in spectrogram showing frequency response in component H and Z. we selected spectrum frequency is f = 0.022 Hz and showing Polarization power ratio for mentawai Earthquake 2010.

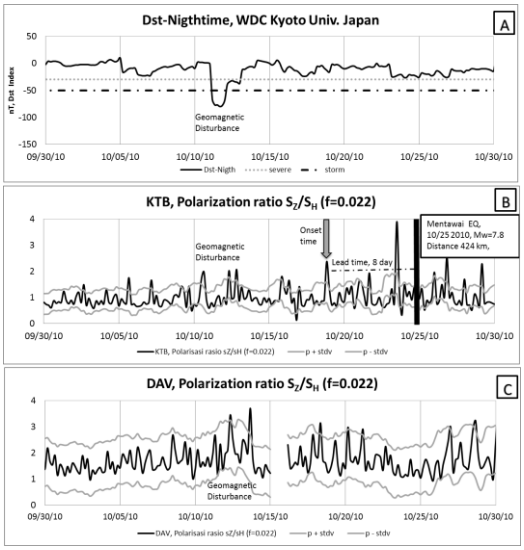

Figure 6. Top panel is Dst index (green line) (WDC-Kyoto Univ.[14]) in period October 16 – 30, 2010 was quite day and the middle panel KTB (blue line) shown information anomaly ULF emission with onset time October 17 – event with shown crossed the line standard deviation (p+σ, p-σ). For below panel is station geomagnetic reference DAV and DAW shown not Information ULF emission all period.

IV. CONCLUSIONS

We have found that electromagnetic frequencies generated from the earthquake source is in the range f = 0.02 to 0.06 Hz for frequencies below or above it is caused by disturbance from outside. Molchanov and hayakawa [11] have modeled the effects of microfracturing which shows the angular frequency < 0.1 Hz. frequency intensity response type effects occur seismogenic the Z component is more dominant than the components of H. we determination onset time using technic polarization rasio Z/H with using standard deviation (p±2 σ) if the signal cross moving average standard deviation we determine as onset time.

Thus the confidence to build an earthquake early warning to the precursor of the ULF emission is in sight, although still far from the earthquake prediction. With the method carried out by previous researchers and the development of methods that we do so we add a new contribution which we can know the objective connection between ULF emission with the magnitude, epicenter distance so that with this method, at least we can know how big an earthquake will the earthquake occurred and the distance of the monitoring stations, even though we have not been able to find out where the fault position is going to happen. Further

ACKNOWLEDGMENT

We thanks to Dr. A. Yoshikawa as a PI: ICSWSE and The part of research has been done in ICSWSE/SERC (International Center Space Weather Science and Education Formerly SERC) Kyushu University Japan to conduct a student visit and to use the data of MAGDAS (JSPS Core to Core Program, B.Asia Africa Science Platforms). Also thanks to LAPAN (National Institute Aeronautic and Space, Indonesia) and STEL (Solar Terrestrial Environment Laboratory) Nagoya University, Japan for Geomagnetic data KTB (Kototabang). The first author grateful acknowledge BMKG for providing the scholarship for his PhD research at Bandung Institute of Technology.

REFERENCES

[1] Hattori, K., Akinaga, Y., Hayakawa, M., Yumoto, K., Nagao, T., and Uyeda, S. (2002): ULF magnetic anomaly preceding the 1997 Kagoshima earthquake, "Seismo- Electromagnetics: Lithosphere-Atmosphere-Ionosphere coupling", edited by M. Hayakawa and O. Molchanov, TERRAPUB, Tokyo. 19-28

[2] Hattori, K., Takahashi, I., Yoshino, C., Isezaki, N., Iwasaki, H., Harada, M., Kawabata, K., Kopytenko, E., Kopytenko, Y., Maltsev, P., Korepanov., V., Molchanov, O., Hayakawa, M., Noda, Y., Nagao, T., and Uyeda, S. (2004): ULF geomagnetic field measurement in Japan and some recent results associated with Iwateken Nairiku Hokubu earthquake in 1998. Phys. Chem. Earth, 29, 481-494, doi: 10.1016/j.pce.2003.09.019

[3] Hattori,K., A.Serita, C. Yoshino, M. Hayakawa, and N. Isezaki., (2006) : Singular Spectral analysis and principal component analysis for signal discrimination of ULF geomagnetic data associated with 2000 Izu Island earthquake swarm, Phys. Chem. Earth, 31,4-9, 281-291, doi:10.1016/j.pce.2006.02.034

[4] Hattori, K., Han, P.,Yoshino, C., Febriani, F., Yamaguchi, H., Chen, C.H.,Investigation of ULF Seismo-Magnetic Phenomena in Kanto, Japan During 2000-2010., (2013) : Case Studies and Statistical studies, *Survey in Geophysic*, 34,293-316,DOI 10.1007/s10712-012-9215-x,

[5] Ismaguilov, V.S. Kopoytenko Yu. A. Hattori K. Voronov P.M. Molchanov O.A. dan Hayakawa M. (2001) : ULF magnetic emissions connected with under sea bottom earthquakes. *Natural Hazards and Earth System Sciences*. 1: 23-31. doi:10.5194/nhess-1-23-2001

[6] Ismaguilov, V.S. Kopoytenko Yu. A. Hattori K. dan Hayakawa M. (2003) : Variation of Phase velocity and gradient values of ULF geomagnetic disturbance connected with the Izu strong earthquake. *Natural Hazards and Earth System Sciences*. 3: 211-215. doi: 10.5194/nhesss-3-211-2003.

[7] Yumoto, K., Ikemoto S., Cardinal, M.G, Hayakawa, H., Hattori, K., Liu J.Y., Saroso, S., Ruhimat, M., Husni, M., Widarto, D.S., Ramos E., McNamara, D, Otadoy R.E, Yumul G., Ebora R., and Servando N.:A new ULF wave analysis for Seismo-Electromagnetics using CPMN/MAGDAS data. Phys. Chem. Earth, Parts A/B/C, 360-366, doi:10.1016/j.pce.2008.04.05, 2008

[8] Ibrahim. G., Ahadi S., dan Saroso S., (2012) : Karakteristik Sinyal Emisi ULF yang Berhubungan dengan Prekursor Gempa bumi di Sumatera, Studi Kasus: Gempa bumi Padang 2009 dan Gempa bumi Mentawai 2010. *Jurnal Meteorologi dan Geofisika*. Vol 13. No.2.81-89

[9] Ida, Y. Yang D. Li Q. Sun H dan Hayakawa M., (2008) : detection of ULF electromagnetic emissions as a precursor to an earthquake in China with an improved polarization analysis. *Natural Hazards and Earth System Sciences.* doi: *10.5194/nhess-8-775-2008*

[10] Karakelian, D. Klemperer, S.L. Fraser-smith A.C. dan Beroza G.C. (2000) : A Transportable system for Monitoring Ultra Low Frequency electromagnetic signal associated with earthquakes. *Seismologica Research Letter*. Vol 71, No.4, 432-436. doi:10.1785/gssrl.71.4.423

[11] Molchanov, O.A., and Hayakawa, M., (1995) : Generation of ULF electromagnetic emissions by microfracturing. Geophys. Res. Lett. 22. 3091-3094, doi:10.29/95GL00781, 1995

[12] Saroso S., Hattori K., Ishikawa H., Ida Y., Shirogane R., Hayakawa M., Yumoto K., Shiokawa K., Nishihashi M., (2008): ULF geomagnetic anomalous changes possibly associated with 2004-2005 Sumatra earthquake. Phys. Chem. Earth. 34. 343-349, doi:10.1016/j.pce.2008.10.065, 2008

[13] BMKG Eq. Catalog, http://www.bmkg.go.id/BMKG_Pusat/Geofisika/Gempa_Dirasakan.bmkg, 2012

[14] WDC, World Data Center for Geomagnetic: http://wdc.kugi.kyoto-u.ac.jp/aeasy/index.html , 2013

G106

On the Influence of DC Railway Noise on Variation Data from Tangerang Geomagnetic Observatories

Relly Margiono
Meteorology and Geophysical Academy
rellymargiono@gmail.com

Mahmud Yusuf
Meteorology Climatology and Geophysical Agency
Jakarta, Indonesia

***Abstract*—Geomagnetic variation data from the observatories in Tangerang (TNG, Indonesia) significantly suffer from disturbances caused by DC electric railways. The aim of this study is to quantify the impact of these disturbances on quantities derived from such data, as the K index of magnetic activity. Therefore, undisturbed data have been reconstructed by means of a moving average filter. The comparison of the K index derived from original and reconstructed data shows an decrease of quiet time segments by 25.92% for TNG. Furthermore, the distribution of the corrected K indices agrees well with the one from the Tuntungan observatory in Medan Indonesia.**

Keywords— Geomagnetic observations; DC railway noise; Moving Average; K index.

I. INTRODUCTION

Geomagnetic observatory must provide variation data that free from interference or noise, because the resulting data reflect only the expected natural conditions without mixed noise originating from man-made. Because of this, the magnetic observatory should be and should remain far enough from man-made disturbances (Jankowski, and Sucksdorff, IAGA 1996). Especially electric rail system running with direct current (DC) should be avoided or placed a safe distance (Nezka et al, 2013). Geomagnetic observatory at least should have distance to the observation building 300 meters from other buildings and at least within 1 km from the railway, if the railroad is electric, the distance has to be several kilometers, and in case of DC trains tens of kilometers, depending on the conductivity of the ground. (Jankowski , and Sucksdorff, IAGA 1996).

In fact, some of the magnetic observatories in Indonesia are located close to several sources of interference and man-made disturbance. This is evident from the variation data were recorded on variometer instrument and have the impact on the natural values of inaccuracies in the determination of the magnetic field around the area. This is what happens on Tangerang geomagnetic observatories (TNG), as can be seen at figure 1, where in 1997 an electric railway line became fully operational. Coupled with the operation of the wholesale market Tangerang in 2001 and residential population are growing rapidly.

From the above issues in the same case in several countries have found some answers. One of the most extreme solutions is to move the magnetic observation station. This is has been done in the magnetic observation station Niemegk in Germany, Uppsala in Sweden and Belsk in Poland (Nezka et al, 2013). The solution to the same problem has been found in Japan. Electric railway system located near the Earth's magnetic observation station Kakioka has changed from DC to AC (Tokumoto and Tsunomura, 1984). The latter emits disturbances only in a limited frequency range and is harmless compared to the first. It is enforced by law in Japan that the rail way company takes into account the needs of geophysical observatories (Y. Minamoto, personal communication in nezka's paper). This is certainly laudable, but unfortunately, unrealistic for most other countries

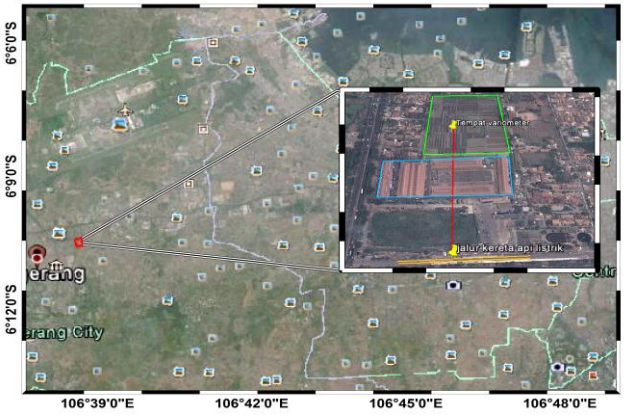

Fig 1. Overview map with positions of Tangerang (TNG). The zoomed-in areas around the observatories demonstrate their proximity to DC railways. TNG observatories with green lines, electrical railroad tracks with a yellow striped, and a wholesale market with blue striped.

Previous research in the same case has been made by (Georgescu et al, 2002), (Pirjola et al, 2007), (Lowes, 2009), and (Neska, 2010), they focused on the mechanism of propagation of disturbances that applying an electric train DC. In this study we have the same intention, but we use a different method. First of all we will show the data of magnetic field variations in the time series, and then determine the k-index for Tangerang data and contrasting with the data k-index of the reference observation stations for which data is not compromised. After that, we will introduce simple methods of filters to eliminate interference in the data.

II. DATA CONTAMINATION

Electric Trains (Commuter)

Electric trains or Mass Rapid Transit is a public transportation service with local coverage available to anyone who pays the cost of which has been determined and is designed to move a large number of passengers at the same time. Ones kinds of mass rapid transit are Kereta API (KA) commuter. The term relates to the operation of the commuter train only at the beginning and end of the working day, devoted to transport consumers who want to go to and or leave the city center. However, the term is also commonly used for all types of freight trains which are not included in the category

Fig 2. Kinds of commuter line that through tangerang city.

Types of Electric Railway (commuter) is a non - AC KRL Economy, Economic KRL AC look Fig 2, KRL Pakuan Ekspress. KRL Economy is a non - AC unit electric train fleet which society is aimed for lower-middle economic class. This class uses the old electric train fleet that did not use the air conditioning (AC). A number of series made by Nippon Sharyo, Hitachi, and BN - Holec. KRL AC Economic same function as the non - AC , a significant difference only lies in the more adequate facilities (air conditioning , new units) and the ticket prices are more expensive . KRL fleet of Ekspress Pakuan Using the same unit with KRL Express. KRL Express is the highest grade in the network Commuter Jabodetabek. Using the same unit with the AC KRL economy, differing only in a more limited station stops, and the ticket prices are more expensive. Maintaining the Integrity of the Specifications.

Electrical system of electric trains

Resources are used as the main power supply to the rail system in Indonesia is obtained from the grid which is then rectified by the rectifier (rectifier) at the substation (sub-station) to be a direct current power with nominal voltage of 1500 VDC great channeled through the upper channel (catenary) and transmitted to the train by using a pantograph (Bien et al, 2006). Pantograph is located on the roof of the carriage. Each pantograph distributes power to electrical installations. Feedback on the installation of high voltage rail is channeled to go back in through the wheels on the wagon. Under conditions of employment, such as conductive channel in Fig. 3, several thousand amperes energized, so that the top of the channel network are voltage losses must be considered.

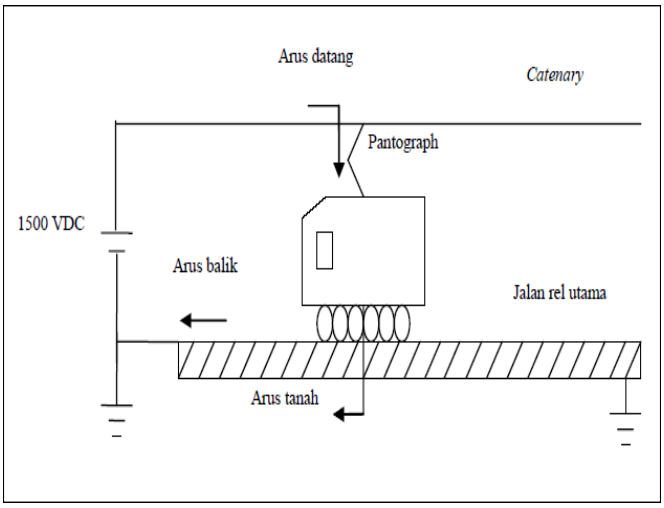

. Fig 3. A simple form of electrical systems KRL and Upper channel network (Catenary) (Biek et al, 2006)

To overcome the voltage loss, then at certain distances (typically every 5 km) mounted substation circuit (sub - station) of the PLN. In addition to the above channel network should remain on track even though exposed to strong winds, hot weather and cold, as well as to other adverse weather conditions

Data Contamination.

At this time we will show about the influence of the electric train to magnetic field variations at tangerang observation. It can be seen that the interference on all components, i.e., components x, y and z-component parts. This disorder can be seen as a noise spike in some components.

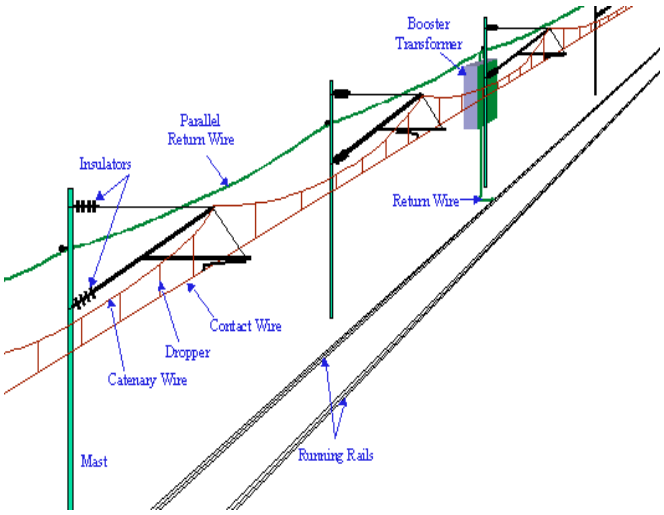

Fig 3. A simple form of electrical systems KRL and Upper channel network (Catenary) (Biek et al, 2006).

A

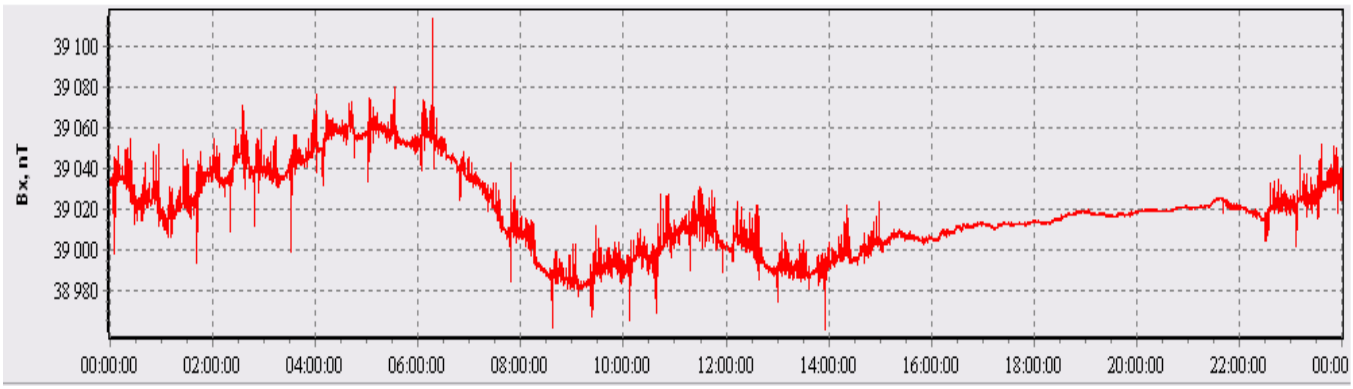

X component 31-08-2013 00:00:00 – 23:59:59

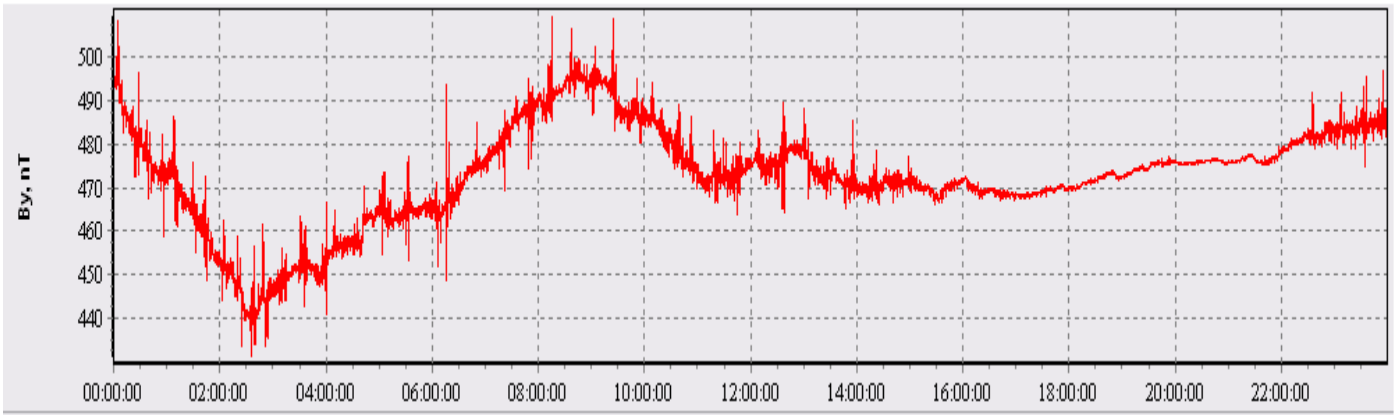

Y component 31-08-2013 00:00:00 – 23:59:59

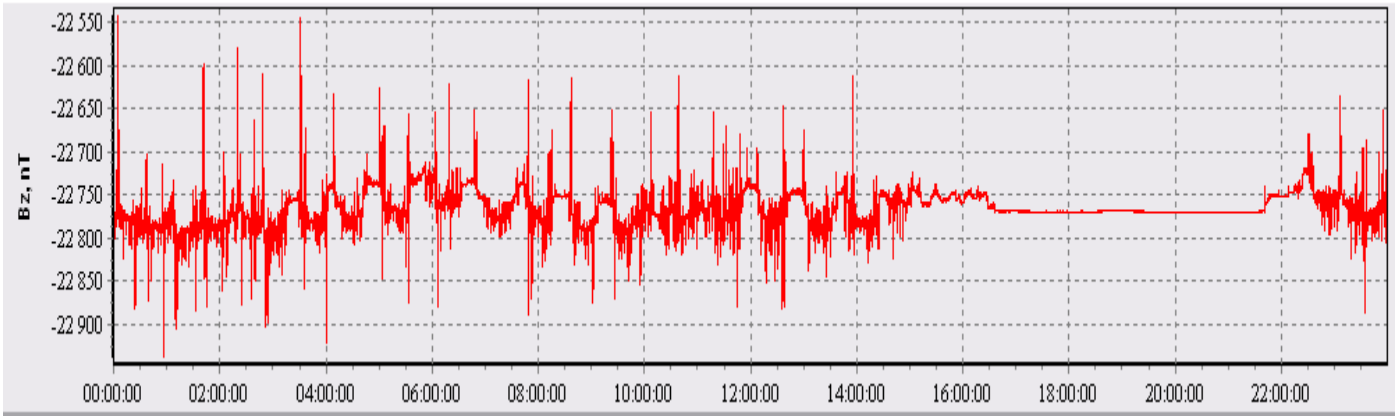

Z component 31-08-2013 00:00:00 – 23:59:59

Fig 4. Magnetic variation signal at tangerang observatory. All of component x, y, z have noise in any time

Disruption caused by electric trains also has an impact on the determination of the K-index. K-index tangerang (TNG) is very difficult to quantify because the noise almost evenly in several components. Compared to the K-index generated by the observation station Tuntungan (TUN), the obtained K-index differences are very large in any time

III. METHOD

In this section a method will be outlined allowing for reconstruction of undisturbed time series data and, thereby, of corrected K indices. We use moving average filter, The moving average is the most common filter in DSP, mainly because it is the easiest digital filter to understand and use. In spite of its simplicity, the moving average filter is *optimal* for a common task: reducing random noise while retaining a sharp step response. This makes it the premier filter for time domain encoded signals. As the name implies, the moving average filter operates by averaging a number of points from the input signal to produce each point in the output signal.

$$y[i] = \frac{1}{M}\sum_{j=0}^{M-1} x[i+j]$$

Equation of the moving average filter. In this equation, x is the input signal, y is the output signal, and M is the number of points used in the moving average. This equation only uses points on *one side* of the output sample being calculated. In this method, we have to try some window width used. If the result is less satisfying then the window can be widened to get maximum results.

IV. RESULT AND DISCUSSION

Reconstructed time series are shown in Fig. 6. It is evident that their noisy character has vanished, but natural features have been preserved. As visible from difference time series between original and corrected data, the order of magnitude of the disturbance amplitudes is 0.01-49 nT for TNG in x component and 0.01-28 nT for TNG in y component and 0.37-190 nT for TNG in z component.

Data reconstruction was performed magnetic field variations of data components x, y and z are impaired. Disturbance data contained in all the components identified as spike noise contained in a certain time frame. In figure 5 can be seen that the interference was in the period 22:30 UTC to 15:00 UTC. In a span of 15:00 UTC until 22:30 UTC identified as the quiet period of the disturbance.

The time of the disturbs occurrence disorder in comparison with the electric train schedule that pass in Tangerang is perfect. We can see in Table 1, the departure of the electric railway in the city of Tangerang start at 22:30 UTC or 05:30 local time. Once observed, the data variation of the magnetic field also began to experience disturbances on that time. Electric railway was completed at 15:00 UTC operates and disorders also completed at the same hour.

Compatibility of the value of the magnetic field disturbance variation with respect to time the operation of an electric railway reinforced by the magnetic field variation of data prior to the change of the electric train schedule . When looking at the data value variations before 1 April 2013 as the attachment to the first, electric trains stop operating at 14:30 UTC, and the value of disturbance also end at the same time.

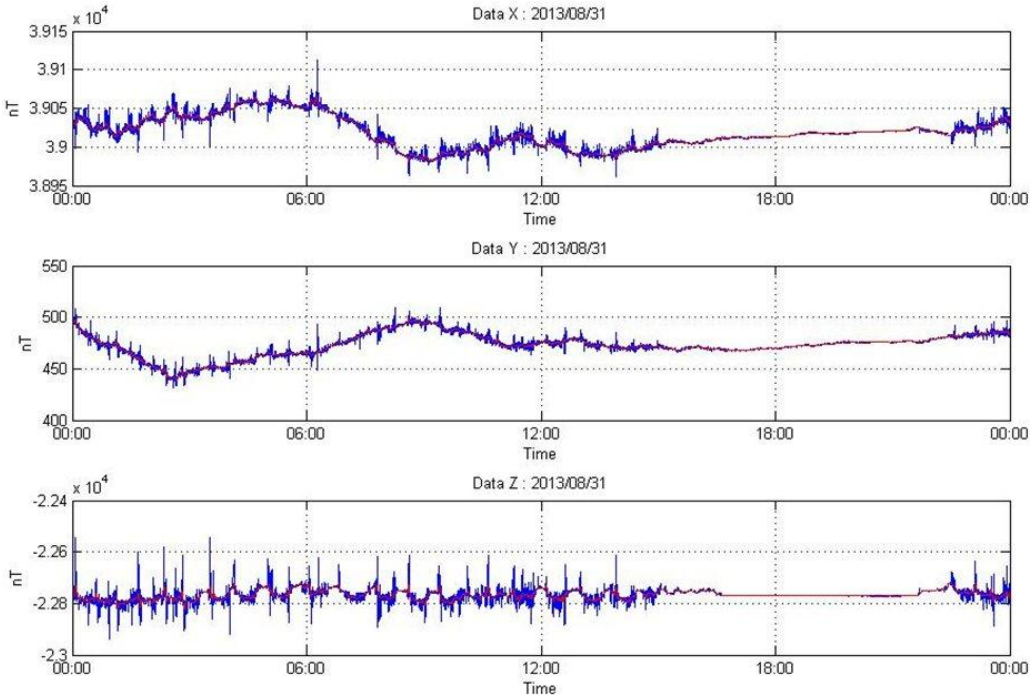

Fig 6. Reconstructed time series of TNG. For comparison, every panel contains the correspondent original time series in blue color and reconstructed data in red color.

From the results of the moving average filter is generated as shown in figure 6 shows that the interference data on the value of the magnetic field variations can be reduced. The result of the reduction depends on the moving average filter window width used. The width of the window used for data reduction is 180 seconds. This is because the window is too wide can cut the authenticity of the data and the window is too narrow can slip off the noise. In the x and y components of the reduction results showed very satisfactory results, but the results of the z component of the reduction is still not optimal. This is because the interference z component very large and require maximum width of the window.

The results of the analysis of the K - index after reduction experienced some significant differences. From Figure 7 it can be seen that the value of the K - index of changes before reaching a few percent reduction. On 26 August 2013 acquired k - index reduction results are close to the k - index reference station. Reference stations used is Tuntungan observation station, because it is a place that away from distractions than Tangerang . It can be seen from the analysis of the k- index , maximum index occurs in 1-3 hours to 13-15 , then the index decreased in 16-18 hours to 19-21, while the index began to rise in the index 22-24 . The decrease and increase in the index is in accordance with the disturbance. Index of 22-24 to 13-15 are the index when operating electric railway. While the minimum index at 16-18 to 19-21 have a minimum value because the electric trains are not operating.

K - Index reconstruction results decreased an average of 21.52 percent before reconstruction. After reconstructing the data taken at the impaired only obtained an average decline of 25.92 percent. The results of k - index correlated with the data reconstruction Tuntungan generate a positive correlation, This shows a strong relationship between the results of reconstruction with the reference value.

V. CONCLUSSION

The conclusions of this study can be summarized as follows: (1) moving average method can reconstruct the variation data disturbance due to electric trains with well; (2). K-index reconstruction results of data has a value that is closer to the reference stations that did not happen due to the disturbance of electric trains.

Acknowledgment we thank to Meteorology and Geophysical Academy that support this paper and Tangerang magnetic observatories that support the data. We thank Mr. Bambang Setio Prayitno head of Tangerang magnetic observatories for consultancy on Moving Average filter during the preparation of the manuscript.

APPENDIX

TABLE 1. THE ELECTRIC TRAIN SCHEDULE THAT PASS IN TANGERANG

Duri	**Tangerang**	**Tangerang**	**Duri**
6:15	6:49	5:30	6:00

6:47	7:21	6:00	6:32
7:20	7:54	6:30	7:04
7:52	8:26	7:02	7:37
8:25	8:59	7:35	8:09
8:56	9:31	8:05	8:42
9:30	10:11	8:40	9:14
10:20	10:56	9:10	9:47
11:10	11:41	9:40	10:11
12:00	12:33	10:25	10:56
12:50	13:21	11:05	11:39
14:00	14:33	12:00	12:33
14:40	15:16	13:00	13:35
15:30	16:06	13:45	14:17
16:18	16:51	14:45	15:16
16:45	17:20	15:35	16:06
17:20	17:54	16:20	16:58
17:52	18:30	17:00	17:37
18:20	18:51	17:35	18:09
19:10	19:41	18:15	18:49
20:00	20:31	19:05	19:39
20:45	21:21	19:55	20:29
21:35	22:05	20:50	21:21

REFFERENCE

[1] Farida, Isky F., (2011), Analisis Kepuasan Pelanggan Terhadap Kualitas Pelayanan Jasa Kereta Api Ekspres Pakuan Jabodetabek (Studi Kasus Kereta Api Ekspres Pakuan Bogor-Jakarta), *Skripsi* IPB

[2] Junge, Andreas (1996), Characterization of an Correction for Cultural Noise, *Surveys in Geophysics* 17:361-391

[3] Lowes, F. J. (2009), DC railways and the magnetic fields they produce – the geomagnetic context, *Earth Planets Space* **61**, i-xv.

[4] Liem Ek Bien, Ishak kasim and Hendry Hartanto, (2006), Sistem Kendali Kereta Otomatis : Jetri Volume 5 no 2.

[5] Marcelo B. P´adua, Antonio L. Padilha, and ´Icaro Vitorello, (2002), Disturbances On Magnetotelluric Data Due To DC Electrified Railway: A Case Study From Southeastern Brazil, *Earth Planets Space*, **54**, 591–596

[6] Maule, C., P. Thejll, A. Neska, J. Matzka, L. Pedersen, and A. Nilsson (2009), Analyzing and correcting for contaminating magnetic fields at the Brorfelde geomagnetic observatory due to high voltage DC power lines, *Earth Planets Space* **61**, 11, 1233-1241.

[7] Neska, A., J. Reda, M. Neska, Y. Sumaruk (2013), On the influences of dc railway noise from belsk and lviv geomagnetic observatories, *Acta Geophysica.*

[8] Pirjola, R., L. Newitt, D. Boteler, L. Trichtchenko, P. Fernberg, L. McKee, D. Danskin, and G.J. van Beck (2007), Modelling the disturbance caused by a dc-electrified railway to geomagnetic measurements, *Earth Planets Space* **59**, 943-949.

[9] Tokumoto,T and S.Tsunomura (1984), Calculation of magnetic field disturbance produced by electric railway, *Mem. Kakioka Maguman. Obs.* **20**, 2, 33-44 (original in Japanese, English translation available).

G107

Lesser Sunda Islands Earthquake Inter-Occurrence Times Distribution Modeling

Indira Puteri Kinasih[1]
1 Mathematical Education Department
IKIP Mataram
Mataram - Indonesia
indiraputeri@gmail.com

Giri Wahyu Wiriasto[2,3], Bulkis Kanata[2,4], Teti Zubaidah[2,5]
2 Electrical Engineering Department
Mataram University
Mataram – Indonesia
3 giriwahyuwiriasto@te.ftunram.ac.id, 4 uqikanata@te.ftunram.ac.id,
5 tetizubaidah@te.ftunram.ac.id

Abstract. **This paper is aimed to analyze and modeling earthquake interoccurence times in Lesser Sunda Islands region using Weibull distribution. The data were classified into three categories, based on its magnitude; weak, medium, and strong earthquake. Cumulative distribution function and hazard rate are also explored in order to obtain the characteristics of earthquake inter-occurrences time data. Empirical result indicates probability and rate of an earthquake recurrence time with a certain magnitude and in a certain time. Medium and weaker earthquake have a bigger chance to occur and it reach 100% probability for the next 60 months. Meanwhile the stronger earthquake has a 75.80% probability of occurrence. It can be seen that the earthquake occurrence probability increase together with time increment.**

Keywords/phrases *: Weibull distribution, interoccurrence times, magnitude, Lesser Sunda Islands, earthquake.*

G108

Horizontal Component Variation in Geomagnetic Stations During Annular Solar Eclipse on January 26th, 2009

I Putu Dedy Pratama, Yosi Setiawan, Daryono
Meteorology and Geophysical Academy
Meteorology, Climatology and Geophysical Agency
Jakarta
checkmate_mail@yahoo.co.id

***Abstract*—Some studies suggest a relationship between the effects of the solar eclipse on the magnetic field recorded at ground-based geomagnetic stations. This study uses 5 seconds data record of the geomagnetic horizontal (H) component at three ground-based geomagnetic stations in Indonesia (Kototabang, KTB; Pelabuhan Ratu, PEL, and Kupang, KUG). These stations are passed by solar eclipse trajectory. The purpose of this study is to analyze the correlation of annular solar eclipse on January 26th, 2009 toward the diurnal geomagnetic variations in H components. We used data from the preceding date of solar eclipse, the date of solar eclipse, and the succeeding date of solar eclipse. The correlation values of H component signal during solar eclipse showed that it is decrease if we compared with the correlation values of preceding and succeeding date. The H component at Kototabang, Pelabuhan Ratu, and Kupang has increased two hours before the eclipse and decreased four hours after the eclipse. The highest change in H-amplitude was observed at Pelabuhan Ratu because its located close to path of solar eclipse. It shows that the solar eclipse affects on the measurement of geomagnetic field especially in H components at ground-based geomagnetic stations which passed by solar eclipse trajectory.**

Keywords—Horizontal Component Variation, Annular Solar Eclipse, Geomagnetic Stations

I. INTRODUCTION

Annular solar eclipse occurred on January 26th, 2009 between 08:00 to 11:00 UTC. The eclipse trajectory starts from the north of Sulawesi and Borneo turning south and passing through the Sunda Strait, across the Indian Ocean and ended in southern Africa. The trajectory map from NASA showed that the peak of solar eclipse occured at 7:58:39 UTC and occuring over the Indian Ocean for 7 minutes and 53.7 seconds.

Some geomagnetic stations in Indonesia are passed by this eclipse, there are Kototabang (KTB), Pelabuhan Ratu (PEL), and Kupang (KUG). The aims of this study are to determine the effect of solar eclipse on the H component of geomagnetic field at geomagnetic stations in Indonesia.

Reference [1], [2], and [3] stated that the greatest disruption in the Earth's magnetic field observations occured in the H component. This study used normalized cross-correlation to compare the H component from magnetometer signal betweenduring the eclipse with a day before and after the eclipse at the same hours.

The most significant changes occured in the ionosphere due to the closest layer to sun. As a result, the reduced sunlight during eclipse allegedly disturbing the ionosphere layer.

Presented in this paper is the study investigating changes in the geomagnetic diurnal variation in H component during the annular solar eclipse on January 26th, 2009 as it affects some geomagnetic stations in Indonesia.

II. DATA

This study used data from the H component of geomagnetic field from the ground-based geomagnetic observation stations: Kototabang (KTB), Pelabuhan Ratu (PEL), and Kupang (KUG) with coordinate information, the eclipse obscuration, and timing of the eclipse showed at Table I.

TABLE I. GEOMAGNETIC STATIONS, GEOGRAPHIC COORDINATE, OBSCURATION, AND TIMING OF JANUARY 26TH, 2009 ECLIPSE AT KOTOTABANG (KTB), PELABUHAN RATU (PEL), AND KUPANG (KUG)

Station	Lat (S)	Lon (E)	Obscuration	Start (UTC)	End (UTC)
KTB	0°13'48"	103°19'12"	75.5%	08:27:57	10:57:54
PEL	7°06'00"	106°36'00"	83.0%	08:19:42	10:50:12
KUG	10°12'0"	123°42'00"	53.4%	08:32:21	-

We used diurnal variation data of the H (horizontal) component from 3 stations the day before, during, and after the eclipse, from 25th to January 27th, 2013. Diurnal data were compared between the events before, during, and after the eclipse.

The coupling between ionosphere, magnetosphere, and Sun-Earth space environment is taken into consideration, and solar activity and magnetic activity during eclipse are checked firstly. According to the data from National Oceanic and Atmospheric Administration (NOAA)/Space Weather Prediction Center (SWPC), from January 25th to 27th, 2009 only on January 25 th, 2009 a sudden impulse occurred at 22:25 UTC.

III. METHOD

Amplitude Change

To determine amplitude change of H component during solar eclipse, we used comparison between a day before, during, and after the solar eclipse. The comparison used time and frequency domain to determine the change that caused by solar eclipse. We changed the signal from the time domain to be frequency domain using discrete Fourier transform.

Cross Correlation

In the analysis of the signal, the comparation signal is done by the cross-correlation method. Cross-correlation methods used in identifying similarity of signal. The calculations with this method is similar to the convolution of two functions which include the reversal signal convolution, shifting, multiplication, and summation, while in the cross-correlation only cover a shift, multiplication, and summation (without reversal).

From the results of cross-correlation is then performed calculations normalized cross-correlation to get the correlation values between the two signals to be compared. In determining the similarity of signals, as in [4], used normalized cross-correlation function:

$$\rho(l) = \frac{r_{xy}(l)}{\sqrt{r_{xx}(0) r_{yy}(0)}} \qquad (1)$$

Where $\rho(l)$ is the normalized cross-correlation value with a range of 0 to 1, $r_{xy}(l)$ is cross-correlation between two signals in function of x and y, $r_{xx}(0)$ and $r_{yy}(0)$ is an auto-correlation in l=0 which has a value equal to the accumulated root mean squareof 2 signals.

IV. RESULTS AND DISCUSSIONS

From the analysis that has been done, comparative results obtained from diurnal variation the day before, during, and after the eclipse. In Kototabang, Pelabuhan Ratu, and Kupang an increase in the H component respectively 15 nT, 50 nT, and 30 nT two hours before the eclipse and decreased respectively by 20 nT, 50 nT, and 40 nT four hours after the eclipse.

Fig. 1 showed the increase in the H component at all stations before the eclipse and decrease after the eclipse. It suggests that the solar eclipse caused an increase in geomagnetic activity in the H component

The highest change of the H component occured in Pelabuhan Ratu because this location is near the eclipse path. The blue box in Fig. 1 showed the timing of the eclipse, it is about 8:00 to 11:00 UTC. Three hours of the H component data for each station were analyzed using Fourier transform spectrum (Fig. 2). The results in the timing of the eclipse showed an increase of amplitude at

frequency below the 0.01 Hz. The increase in amplitude occurred in Pelabuhan Ratu. The maximum obscuration is positively correlated with changes in the value of the H component and the amplitude spectrum.

From the results of the correlation signal (Table II) with normalized cross-correlation formula showed that the correlation between current data with the data before the eclipse decrease (yellow blocks) than the correlation ofthe data before and after the eclipse. It suggests that the eclipse affects the magnetic field observation at H components.

According to [5], [6], and [1] during a solar eclipse the changes in the magnetic field of ionospheric effects are occured. Diurnal variations in the geomagnetic field in a quiet day caused by the flowof dynamo currents in the ionospheric E layer.Solar eclipse caused changes in the ionosphere and magnetosphere component specially in the changes of electron density continuously as in [7].

During the eclipse, partly of the ionosphere deterred from heating and solar radiation. It resulted a change in the flow pattern and observed in the surface as a change in the geomagnetic field. Solar eclipse improve the processes in ionospheric E layer and affect the diurnal variation of the geomagnetic (Solar quiet / Sq).

TABLE II. RESULT OF NORMALIZED CROSS-CORRELATION BETWEEN THE SIGNAL FROM KTB. KUP, AND PEL ON JANUARY 25TH TO 27TH, 2009.

KTBH	25	26	27
25	1	0.5092	0.9245
26	0.5092	1	0.6349
27	0.9245	0.6349	1
KUPH	25	26	27
25	1	0.8679	0.9386
26	0.8679	1	0.8629
27	0.9386	0.8629	1
PELH	25	26	27
25	1	0.994	0.9982
26	0.994	1	0.996
27	0.9982	0.996	1

V. CONCLUSION

Ionization of electromagnetic radiation in the annular solar eclipse January 26th, 2009 influencedthe geomagnetic field on the traversed area and recorded at geomagnetic station as follows: (1) there is an increase in the H component in Kototabang, Pelabuhan Ratu, and Kupang before the eclipse and decrease after the eclipse. (2) There is an increase in the H component spectrum during the eclipse. (3) The highest changes in the H component occurred at Pelabuhan Ratu because this location is near the eclipse path. (4) The normalized cross-correlation value indicated a decrease in the correlation value of the digital signal recording at H component due to the influence of the eclipse.

REFERENCES

[1] A.L. Cullington, “Geomagnetic Effects of The Solar Eclipse, 12 October 1958, at Apia, Western Samoa”, New Zealand Journal of Geology and Geophysics, 5:3, pp. 499-507, 1962.

[2] A.L. Orozco, L.M. Barreto,„”Magnetic effects during the solar eclipse of July 11, 1991”, Geofisica Internacional, Vol. 32, Num 1, pp. 3-13, 1993.

[3] E.V. Onovughe, “Geomagnetic Diurnal Variation during the Total Solar Eclipse of 29 March 2006”, International Journal of Astronomy, 2(4): pp. 51-55, 2013.

[4] J.G. Proakis, D. G. Manolakis, “Digital Signal Processing, Principles, Algorithms, and Application, Third Edition”, Prentice-hall International, INC, New Jersey, 1996.

[5] An Jia-Chun, Wang Ze-Min, E Dong-Chen, Sun Wei, “Ionospheric Behaviour During The Solar Eclipse of 22 July 2009 and Its Effect on Positioning”, Chinese Journal of Geophysics, Vol. 53, No. 5, pp. 731-739, 2010.

[6] Y. Saeki, Y. Minamoto, S. Fujita, S. Nagamachi, “Coupled-Model Numerical Simulation Of Ground Magnetic Fields During The Total Solar Eclipse Of 22 July 2009”, Kakioka Magnetic Observatory Vol.8, No.1, 2, pp. 11-18, 2011.

[7] A. Adam, J. Vero, J. Szendroi,“Solar eclipse effect on geomagnetic induction parameters”. Annales Geophysicae, 23, pp. 3487-3494, 2005.

G109

Changes of the Geomagnetic Signal linked to Tohoku Earthquake on March 11th 2011

Bulkis Kanata1, Teti Zubaidah1, Cipta Ramadhani1, Budi Irmawati2
Department Of Electrical Engineering,2Department Of Informatic University of Mataram
Mataram, Indonesia
uqikanata[at]te.ftunram.ac.id, tetizubaidah[at]te.ftunram.ac.id,
cipta[at]te.ftunram.ac.id, wati[at]te.ftunram.ac.id

Abstract. The geomagnetic fields in atmosphere can be affected by phenomena in the Earth, so that changes of geomagnetic intensity might be used as an indicator of earthquake occurrences. Variations of geomagnetic data have been analyzed in associations with Tohoku Earthquake on March 11th 2011. The Geomagnetic data have been derived from Memambetsu (MMB), Kakioka (KAK) and Kanoya (KNY) Observatories, which are of INTERMAGNET observatories. The analysis was performed by calculating the power spectral density (psd) of ULF signal of Z and H components, then polarization are observed by comparing the psd of Z and of H. The results showed the difference psd of Z and of H between KAK observatory (the nearest position to the epicenter) with MMB and KNY (in some more distances from the epicenter) is quite significant, which can be observed 10 days before the earthquake occurrence. The polarizations of Z/H in KAK indicate a highest change of intensity which occurred at 18 days prior to the earthquake.

Keywords : geomagnetic; psd; earthquake; polarization

G201

Analysis of Harmonic Distortion Effect on Diviation Measurement of Electrical Energy in kWh Meter

Amien Rahardjo
Electrical Engineering
Faculty of Engineering UI
Depok, Indonesia 16424
Email: amien@eng.ui.ac.id

Iwa Garniwa MK
Electrical Engineering
Faculty of Engineering UI
Depok, Indonesia 16424
Email: iwa@eng.ui.ac.id

Faiz Husnayain
Electrical Engineering
Faculty of Engineering UI
Depok, Indonesia 16424
Email: faiz.h@ui.ac.id

Abstract*— The measurement of electrical energy in kWh meter becomes very important because it involves the energy transaction process. When an error occurs in it then it will cause disserve to the consumer and / or producer. This study aims to look at the characteristics of the measurement by the kWh meter, both analog and digital types, which are affected by harmonic distortion which is mounted kWh meters. The results showed that the greater the value of the harmonics on the load it will be more damaging current and voltage waveforms (distorted). As the wave distorted by the kWh meter, the measurement process will be far from the actual values used. In this study, the different in measurement results between Analog kWh-meter and PQA is up to 15% and Total Harmonics Distortion THD-Fi on 2200VA household consumer is 40.86%. For 3500VA the difference is 9.8% with THD-Fi = 12.29%, and for 7700VA 12.8% with THD-Fi = 15.4%. On the other hand, with Digital kWh in 3500VA household consumer, the different measurement results with PQA is equal 4% with THD-Fi = 10.74%. Thus the effect on deviation measurement of electrical energy in Analog kWh-meter is larger than in Digital kWh-meter.

Keywords: Measurement of Electrical Energy; Power Quality; Harmonic Distortion; Analog & Digital kWh Meters, THD

IV. INTRODUCTION

Harmonics is a phenomenon that arises as a result of the use of non-linear load on the power system. This phenomenon can cause problems in terms of quality of power that would eventually lead to a variety of loss and even damage to some of the electrical equipment. Harmonics become a very important issue to be learned and studied because if not treated correctly and immediately, then its impacts will be greater and adversely affect the performance of electrical equipment.

KWh meter is a device used to measure electric power transaction also includes electrical equipment that cannot be separated from the bad influence caused by harmonics. In general, the tool is designed to measure and calculate the power used by the load in the form of current and voltage in pure sinusoidal waveform, so the presence of the ideal waveform (pure sinusoidal) will improve the accuracy of the measurement results by the kWh meter. In other words, if the input waveform is no longer in form of pure sinusoidal because of harmonic distortion effect, then error measurement would be taken place in the kWh meter device. This paper was made to fulfill the author's curiosity about the effects of harmonic distortion on the performance of kWh meters and the possibilities of losses that will occur in the power system when the phenomenon of harmonics present in power system.

V. LITERATURE REVIEW

A. Harmonics

According to IEC 555 - 1982: "Harmonics is sinusoidal voltages or currents having frequencies that are integer multiples of the frequency at the which the supply system is designed to operate-(50Hz or 60 Hz)" which is more or less clear that the harmonics are periodic distortion of the wave sine current, voltage, with a waveform whose frequency is a multiple of the number beyond which the fundamental frequency in the supply system is designed to operate at 50 Hz/60 Hz 11.

While the definition of harmonic distortion that any change in the form of signals generally unintentional and unwanted presence on the system. Harmonics is one of the things that can cause distortion on the voltage waveform and the current fundamentals. This phenomenon arises due to the influence of non-linear load characteristics are modeled as a current source that injects harmonic currents into the power system.

Fundamental frequency of a power system is 50 Hz (in Indonesian). If there is a 2nd harmonic then the wave has a frequency of 100 Hz, the 3rd harmonic has a frequency of 150 Hz and so on so that it can be made a general equation as follows:

$$f_h = f_1 \times n \qquad (2.1)$$

Where: f_h = harmonics frequency; f_1 = fundamental frequency, n = positive integer.

Summation of harmonic wave and distorted wave is a wave that is continuous and periodic (the wave has a period T if f(t)=

f (t + T) for all t). If f (t) is periodic, then the characteristic harmonics can be represented using Fourier series as follows:

$$f(t) = \frac{a_0}{2} + \sum_{h+1}^{\infty} \{a_h.\cos(h\omega_0 t) + b_h.\sin(h\omega_0 t)\} \quad (2.2)$$

where:

$$a_0 = \frac{1}{T}\int_0^T f(t)dt \quad (2.3)$$

$$a_h = \frac{2}{T}\int_0^T f(t).\cos(h\omega_0 t)dt \quad (2.4)$$

$$b_h = \frac{2}{T}\int_0^T f(t).\sin(h\omega_0 t)dt \quad (2.5)$$

In addition, to determine the value of the amplitude of a harmonic wave can be found by the equation:

$$C_h = \sqrt{a_h{}^2 + b_h{}^2} \quad \text{whereas } h \geq 1 \quad (2.6)$$

the value of C as a function of h are often portrayed in a bar chart called "harmonic spectrum"

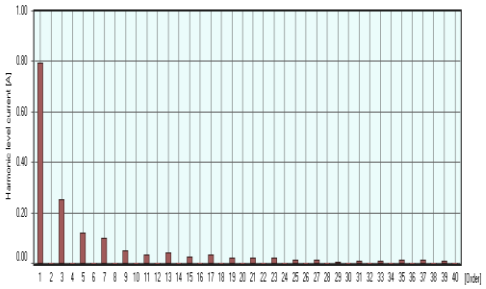

Fig. 1 Harmonic Spectrum

Source of harmonic distortion can be divided into 3 categories:

1. Industrial machines

The machines that are in the industry generally have a converter which is a non-linear load that induces continuous harmonics with arbitrary values. Generally, large-scale industry connected directly to the high voltage network. So the harmonic distortion effect can be fatal to the electrical system.

2. Converter connected to the grid

Converters are connected to the electricity grid can induce large harmonics to the network. Attendance of High Voltage Direct Current (HVDC) system and converter in the battery storage system in the solar power generation system should raise awareness of the influence of the harmonics to the network.

3. Power tools Household

Household appliance such as computers, televisions, and etc is a source of harmonics. This burdens a current source or a DC voltage source. If there are large amounts, it can damage the stability of the system

B. kWh Meters

KWh meter is a common tool used to measure electrical energy. This tool is used by the electricity company to record and analyze the use of electrical energy used by the consumer. In addition, also at the same kWh meter is used as a tool of power transactions because this tool can record how much electrical energy is used up. Electrical energy consumption by consumers, both industrial and domestic use kilowatt unit - hour (kWh) where 1 kWh is equivalent to 3.6 MJ. Thus kWh meter is an appropriate tool used to measure the electrical energy used.

In kWh meter power measurement, components that are comprised of components measuring current and voltage measuring components. KWh meter is widely known in the community is a conventional kWh meter has limited features. KWh meter of this type is referred to as analogue kWh meter. This species is still quite able to read the number of active power consumption well, but are less able to read well so that reactive power kWh meters were created digitally.

KWh meter can read the digital has the advantage of active power and reactive power is unused. In addition, it has the level of accuracy that is better than any analogue kWh meter so that now over PLN encourage consumers to switch to using digital kWh meter.

KWh meter based on its type is divided into two categories, namely:

• Analog KWh Meter

As mentioned before analog kWh meter is already commonly used and the most widely used prior to the creation of digital kWh meter. The main parts of an analogue kWh meter is the coil voltage, coil current, an aluminum disc, permanent magnets, and a mechanical gear that records the number of the rotation is on the device.

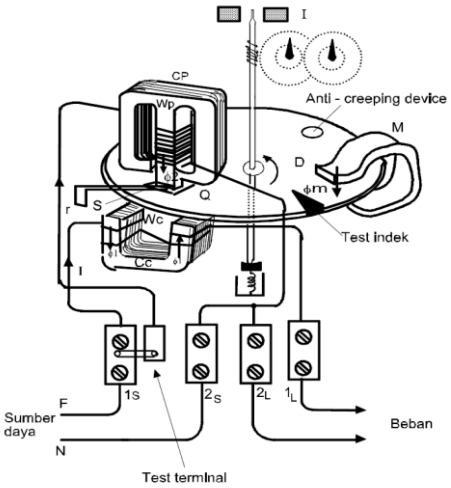

Fig. 2 Analog kWh Meter [1]

From the fig. 2 can be explained on the working principle of an analog meter kWh. At the time of the load current flowing in the coil current I (WC), this current will cause the magnetic flux Φ_1. On the other hand because the voltage is the inductor coil, the coil voltage occurs on the phase difference between current and voltage by 90^o. Current through the coil voltage will also cause magnet flux Φ_2 with different conditions with a 90^o phase Φ_1.

Phase difference between Φ_1 and Φ_2 will cause motion moments on aluminum plate (D) so that the plate rotates in such a way. Round aluminum plates will be forwarded to the registrar wheels / gear mechanical (J) which in turn will run the counter.

The magnitude of the moment of motion / torque that of the aluminum plate is proportional to the magnitude of current I and voltage V, by the equation:

$$T = k .V. I . \text{Cos } \varphi \text{ (Nm)} \qquad (2.7)$$

Where: k = constant (s/rad), V = voltage (volts), I = Current (Amperes), and Cos φ = angle between V and I

From the equation (2.7) it can be seen that the aluminum plate rotation torque (T) will be proportional to the active power (V. I. Cos φ) supplied to the load, so the larger the active power used in the load side round aluminum plate will be faster and vice versa.

- Digital kWh Meter

Digital kWh meter is a measurement tool that has the same function as the analog kWh meter, which measures the amount of electrical energy consumption in units of time. If the analogue kWh meter works on the principle of induction, digital kWh meter works based program designed to microprocessor contained in the digital kWh meter devices.

Fig. 3 Digital KWh Meter [2]

The working principle of a digital kWh meter voltage and current is received by the digital kWh meter will be read separately. Incoming voltage will be read and then passed to a microcontroller. Read currents will also be forwarded to the microcontroller. Inside the microcontroller there is a program that is set up such that the voltage and current will be processed and calculated by the amount of output in the form of electrical energy. The amount in question is active power and energy. So with the digital kWh meter will be able to read electrical energy consumption used by consumers. The instrument used to measure the power used by consumers is kWh meters. This tool has the general form of the input current and voltage measured in a sinusoidal waveform and is used to calculate the power used. If the input waveform is not ideal, it can affect the results of measurements with kWh meter used. Expenses for use in both households and industry have so harmonic distortion measurements using kWh meters are less accurate.

When a measurement error occurs using kWh meter, both customers and producers will lose. Previous research has been conducted to analyze the effect of harmonics on electric energy measurement deviation using analog and digital kWh meter [3]. The type of load used for testing a non- standard energy-saving lamps. However, the results of these measurements have not been compared to estimated system [4]. The system is able to generate estimates of the value of the voltage and current at the fundamental frequency.

With good research and development, the expected estimation system can be used to provide power estimates with more accurate values in the condition of harmonic distortion. If proven to provide a more accurate measurement results, the estimation system can be further developed to be used as the software for kWh meters. These devices are generally having an input in the form of currents and voltages measured in the form of a sinusoidal wave and used to calculate the power used. If the input waveform is not ideal, it can affect the results of measurements with kWh meter used. Expenses for use in both households and industry have so harmonic distortion measurements using kWh meters are less accurate.

VI. METHODOLOGY

To determine the effect of harmonic distortion characteristics caused by the burden of household electrical appliances, testing is carried out in the Laboratory of High Voltage and Electrical Measurements, Department of Electrical Engineering, Faculty of Engineering-University of Indonesia, while for performance testing kWh-meter (Analog and Digital) performed direct on consumer / Household electric customers with a series of tests as follows:

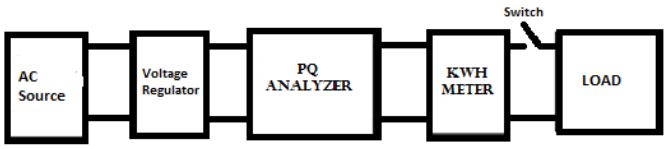

Fig. 4 Schematic testing circuit

VII. RESULTS AND ANALYSIS

In research focused on the problem of harmonic distortion of the load on the network in the form of electrical installation of non-linear loads in particular contained in the household burden. Although the problem of harmonic distortion on household is not great, but the burden of housing in Indonesia is very much the problem of harmonic distortion will

accumulate and have a significant impact on the power system and the readings on the gauges of energy (kWh-meter) PLN.

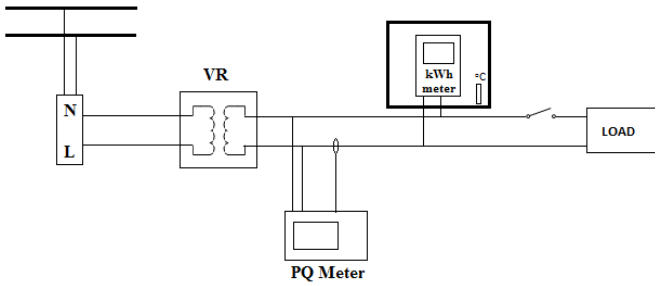

Fig. 5 Layout testing circuit

The cause of the harmonics due to the burdens of non-linear. Non-linear load is derived from electrical equipment that has a saturation value or which have the power electronics components. Identify the type of load carried by recognizing the electrical appliances that have components such as coils, rotating machines (motors), power supply, diode, thyristor, converters, ballasts, and equipment made from semiconductors.

After identification of the load, obtained electrical equipment is a source of harmonics. The equipment is then tested (measured) to investigate the characteristics of voltage and current harmonic distortion, power.

The following are the specifications of electrical equipment, as object measurement:

TABLE I. SPECIFICATIONS LOAD MEASUREMENT OBJECTS

No	Home Appliance Specification[a]		
	Home appliance	*Power (W)*	*Voltage (V)*
1	Compact lamp A	8	170-250
	Compact lamp B	18	170-250
	Compact lamp C	20	170-250
2	Television	65	180-270
3	Air Conditioner	750	220
4	CPU	350	110/220
	Monitor	240	100-240
5	Refrigerator	77	220
6	Dispenser	300	220

[a] All the home appliance has working frequency of 50Hz

As it is known that the true kWh meter is designed to calculate the power (through the current and voltage waveforms that go to the kWh) with the ideal waveform or a pure sinusoidal waveform so that if they are no longer purely sinusoidal then the tool will not be able to work accurately. One thing that can ruin the flow waveform and / or the voltage is harmonic

In general, the more harmonics are generated, the greater the value of %-THD which will then impact on the worsening waveform generated. With poor waveform current / voltage harmonic distortion due to the strong likelihood of error in the measurement. That way, if the tools do not work accurately measuring the possibility of one of the parties will be harmed.

Value of a number of graphs kWh in Fig 6 the harmonic distortion can be seen that in general with increasing harmonic distortion will result in an increase in the value of the measured kWh. This is especially true in kWh analog type, because this type there kWh moving parts / mechanic who is most likely to be influenced by harmonic distortion factor of the kWh. In contrast, the kWh meter digital type is not too affected by harmonic distortion because physically the kWh meter of this type there is no electromechanical parts as well as on the type of analogue kWh meter.

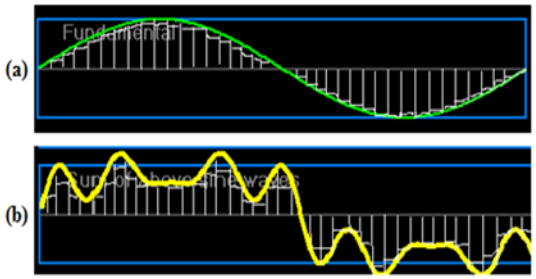

Fig. 6 (a) Illustration Digitally on Ideal Wave Measurements and (b) the Distorted Wave Harmonics [3]

A. The end result of harmonic distortion measurement of household electric appliance in the Laboratory:

TABLE II. MEASUREMENT RESULTS

No	Total Harmonics Distortion (THD)[b]		
	Home appliance	*Voltage (%)*	*Current (%)*
1	Compact lamp	1.66	90.4
2	Television	1.96	126.3
3	Air Conditioner	1.925	111.2
4	Computer	1.388	114.7
5	Refrigerator	1.82	104.5
6	Dispenser	2.00	105.1

[b] All the home appliance measured shared common dominant harmonics distortion in 5th order (250Hz) for voltage and 3rd (150Hz) for current

B. Based on the results of measurements of the energy consumption for 1 (one) week in Household PLN customers.

From the real measurement results in customers Household PLN, indicated that the difference in energy consumption in kWh-meter recorded PLN with the PQA

C. KWh-meter accuracy against PQA:

The higher the current harmonic distortion, the higher the potential deviation kWh-meter readings will be. Based on measurement result, the distortion in measurement result of analog is 2.45 higher than the digital.

TABLE III. MEASUREMENT RESULTS

Customer (VA)	*THD-i (%)*	*THD-v (%)*	Difference PQA and PLN Meter[c]	
			kWh	*%*
2200 with kWh-Analog	40.86	3.78	7.23	15
3500 with kWh-Digital	10.74	3.57	8.84	4
3500 with kWh-Analog	12.29	1.57	15.45	9.8
7700 with kWh-Analog	15.4	2.02	142	12.8

[c.] All PLN Meter measurement results are higher compare with PQA results

VIII. CONCLUSION AND DISCUSSION

Study results show the effect of harmonics distortion on kWh meter are:

1) The magnitude of the deviation of error measurement in the form of energy by the analog and digital kWh meter is affected by the harmonic components in the system. Based on testing, the greater the THD, the larger value of error measurement would be. Irregularities in previous research, the value of the deviation in the measurement due to harmonics can reach 15% (kWh-Analog)
2) The total harmonic distortion factors have more influences on the performance of analog kWh meter compare with the digital kWh meter, with factor 2.45 in 3500VA household consumer.
3) Harmonic filter could be used either on the household electrical installation or in each electrical appliances in order to reduce the harmonics effect in the deviation measurement of energy consumption by analog kWh-meter.

REFERENCES

[1]. Alam, Reza Mighty, "Harmonic Load Effect Analysis (Energy Saving Lamp) The Conductor", Thesis UI

[2]. Amirudin, Arief, "System Hardware KWh Meter Prepaid", KP Reports, Digital London 2009

[3]. Dugan, Roger C., et al., "Electrical Power Systems Quality, Second Edition", McGraw-Hill, 2004.

[4]. Koswara, Firman Indra, "Analysis of the Effect of Harmonics in Power Transformer in the Cement Industry", Thesis, Department of Electrical Engineering-Faculty of Engineering University of Indonesia

[5]. Boromeus SW, "Comparative Analysis of Reading kWh Meter with Analog Digital Meter on Imbalance Charges", the UI Thesis 2008

[6]. Kurnaen, Jemjem, et al ., "Effects of Harmonics on Power Loss and Loss of Electric Power Systems", PT. PLN P3B Jawa Bali

[7]. Kurniawan, Irfan, "Study of the Effect of harmonic performance measurement tool KWh meters as Power Transactions", Depok: DTE FT UI Thesis Book 2011

[8]. Measurement Module: Electrical Measurement Operation

[9]. Nurhidayat, Eka, "Occupational and Environmental Effect of Temperature on Performance Transformer Harmonic Flow", Thesis UI 2010

[10]. Sujatmiko, the Great, "The Effect on Performance Transformer Harmonic Flow", DTE UI 2010

[11]. Tobing, Cristof NH, "The Effect of Harmonics In Distribution Transformer", Universitas Indonesia in 2008

[12]. Sudiarto, Budi, "Analysis of Loss and Loss on Low voltage networks Harmonic Effect Effect On Energy Saving Lamps" UI Thesis 2004

[13]. Falcon, Rafael, "Analysis of Thermal Characteristics and Resistance Dual Core Cable Conductor at NYM 2 x 1.5 mm2 " , Thesis UI 2008

[14]. Sitompul, Andigan D., "Study of the Effect of Temperature Ambient Temperature Characteristics Hotspot on Transformer " , Thesis UI 2011

[15]. Rajani, Ahmad, "Correlation Analysis of Energy Efficient Lamps Against Imposition and Amount of Harmonic Wave Forms", Thesis UI 2012.

G202

Inrush Related Problems Caused by Lamps and Electric Vehicle

J. F. G. Cobben
Electrical Engineering Department,
Electrical Energy System (EES)
Technische Universiteit Eindhoven (TU/e)
Eindhoven, The Netherlands
E-mail: j.f.g.cobben@tue.nl

Niken Arumdati
Energy and Mining Provincial Office of West Nusa Tenggara
Mataram, Indonesia
E-mail: arumdati@gmail.com

***Abstract*— The increase of new types of electronic loads such as electric vehicles and energy saving lamps bring unexpected voltage and current issues. Electronic loads employ circuits with rectifiers and capacitors which withdraw current from the main electricity network that are different compared to the traditional loads like incandescent and standard fluorescent lamps. If the installations are not adapted to the new loads, it may lead to the breakdown of switches or circuit breakers and the overloading of wires or cables and unwanted tripping of protection devices.**

This paper proposes how the risk can be avoided by learning the characteristics of inrush current for various loads, which is done by measuring current waveforms at transient and during steady state. This is useful to estimate the number of loads that can be connected to a switch, and to define factors that should be taken into account for rerating switches.

***Index Terms*— inrush current; energy saving lamps; electric vehicles; current rating.**

I. INTRODUCTION

Recently, energy efficiency initiative and the urgency to save the environment by cutting down the emissions brought a lot of development in the area of electrical power generation and its consumption. As a result, the integration of distributed generation (DG) into the grid and the increasing use of new type of applications such as energy saving lamps and electric vehicles. Align with this development, the interest towards power quality issues is growing. Circuits with rectifiers and capacitors in electronic loads will retrieve current from the grid that are different compared with traditional resistive and inductive loads. The installers and consumers are not aware of the difference in characteristics and will exchange traditional loads by electronic ones without any adaptation in the installation. Meanwhile, the manufacturers are only obliged to provide the standard values of current and power in their documentation. These values exclude all effects that peak currents may cause during start and normal operation or steady state. Additionally, due to the price pressure devices such as energy saving lamps are sold without any adequate filtering resulting in very high starting currents and total harmonic current distortions (THD) that overload the contacts and neutral wires. Consequently, if the installations are not adapted to the new loads, it may lead to the breakdown of switch contacts and circuit breakers, the overloading of wires and unwanted tripping of protection devices.

II. INRUSH CURRENTS

Whenever a heavy load is switched on, or due to re-energizing of the device during voltage recovery following a voltage dip or interruption there is usually a surge of current defined as inrush current. Inrush current occurs because the load contains capacitive or inductive components at its input side. Although the inrush current only appear during the first half cycle and then decay, its magnitude can exceed the steady state current requirements of the load.

Since its magnitude could be higher than the current rating of switches and circuit breakers, inrush current can cause excessive heating of the contacts and eventually lead to contacts degradation, which involves contacts erosion and welding. In addition, high inrush current also cause protection issues such as random false tripping of circuit breaker. In order to avoid these problems, switches or circuit breakers have to be properly sized with high inrush characteristics.

From the previous study [2], there are several factors which affect the amplitude and duration of the inrush current:

1. The voltage switching angle, or when in the first half cycle the circuit is switched on
2. The impedance of the circuit
3. The type of load

III. MEASUREMENT SETUP

The measurement was arranged according to Fig. 1. Basically, the inrush current measurement consists of a series of test starts at different voltage switching angles, and then followed by the measurements of voltage and current. Tie Pie handyscope was used together with a voltage probe and a current clamp to record the voltage and current waveforms. These measurements were saved in .tps file, which is default format of recorded waveforms for Tie Pie handyscope. Recorded data were subsequently processed in Excel and Matlab[1].

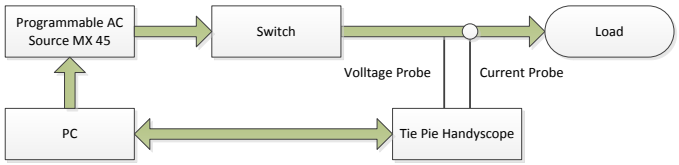

Fig. 1. Diagram of measurement setup

These measurements were conducted with the following load:

1. Several types of CFLs and LED lamps with different rated power, which were 4 W, 8 W, 11 W, 14 W and 20 W;
2. Induction motor with a rated power of 2.2 kW;
3. Transformer with a rated power of 2 kVA;
4. Electric vehicle charging unit with a capacity of 3.3 kW.

IV. MEASUREMENT RESULTS

4.1 LED lamps and CFLs

As seen in Fig. 2, the highest amplitude of inrush current was 0.342 A at 90^0 . Also, it can be seen at the moment when the voltage crossed zero, the amplitude of the inrush current will decrease to 0.230 A. The same pattern repeated again as the voltage switching angle was set to 180^0 and 270^0, but reversed to the negative direction. The same test was done to other LED lamps with different power rating as well, and the results exhibit a similar behavior.

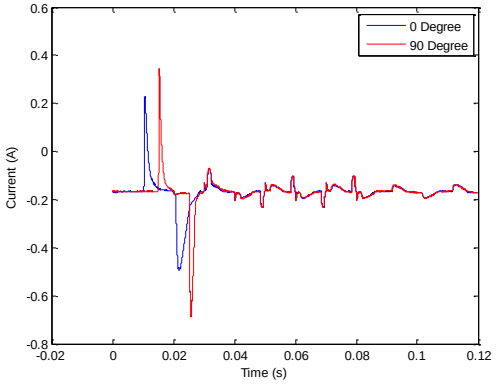

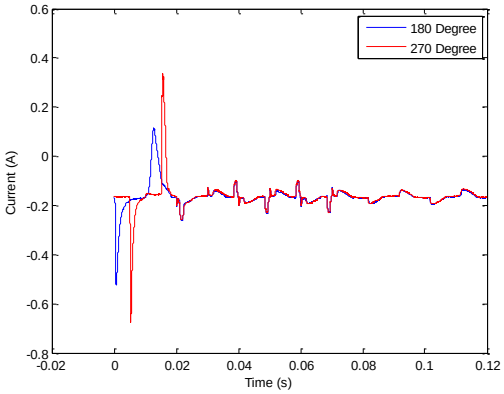

Fig. 2. Inrush current of singe 14 W LED lamp with varying voltage switching angle

The inrush current of a 14 W CFL with varying voltage switching angle are given in Fig. 3. By comparing Fig. 2 and Fig. 3, it can be seen that inrush characteristic of LED lamps has similar pattern with CFLs, both cases it is larger with the switching angle of 90^0 or 270^0 than 0^0 or 180^0. As the voltage was switched on, high peak of inrush occurred at the half of first cycle, and then decayed and the current returned to its steady state.

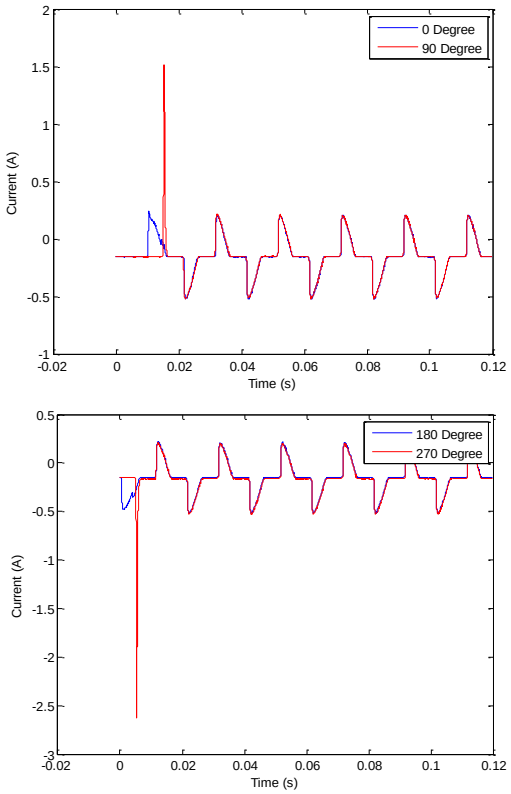

Fig. 3. Inrush current of single 14 W CFL with varying voltage switching angle

When two or more lamps with the same power rating are put together and switched on at the same time, the total inrush current is close to multiplication of the single inrush current. For a greater number of lamps, a similar result can be expected.

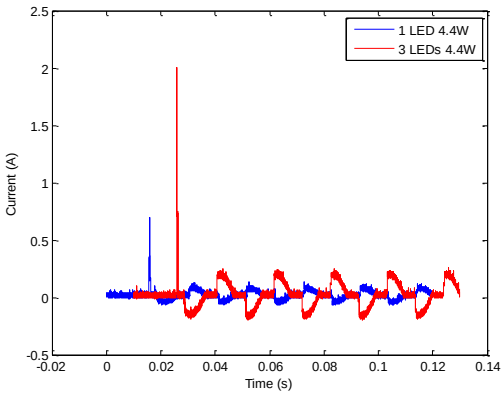

Fig. 4. Inrush current of single 4 W LED lamp and three 4 W LED lamps with switching angle 90^0

4.2 Induction Motors

Current waveforms when motor is started with switching angle 0^0, 60^0, 90^0 and 140^0 are shown in Fig. 5. Result shows that varying switching angle affect the peak values of the inrush current. When the switching angle was set at 0^0, the peak of the inrush current is at its maximum. Whereas, when the switching angle was gradually increased to 140^0, the peak of inrush current was reduced. However in exchange, the time taken to achieve steady state was longer for higher switching angle compared to lower angle. As can be seen in Fig. 5, as the current subsided after the first half cycle, the amplitudes of current at 90^0 and 140^0 are higher than at 0^0 or 60^0, hence it takes longer time to achieve steady state.

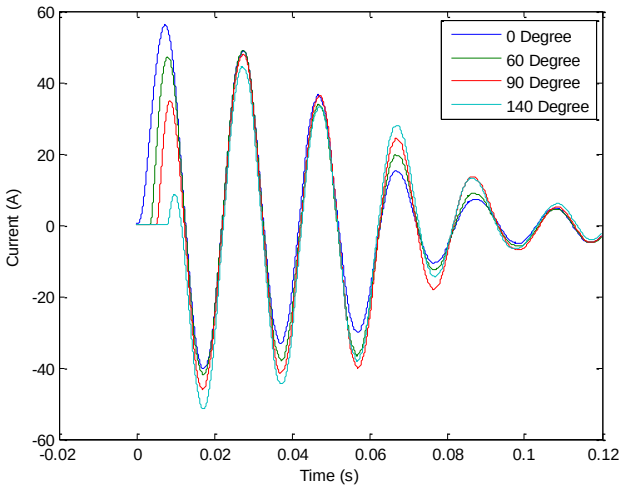

Fig. 5. Inrush current of an 2.2 kW induction motor with varying switching angle

As seen in Fig. 5, the duration of the inrush current is much longer than in the energy saving lamps measurement. Moreover, when the current gradually decrease to its steady state, the process appeared to be smooth.

4.3 Transformers

In this section, the magnetizing inrush current of a transformer with a capacity of 2 kVA was investigated. The primary side of transformer was connected to the AC source MX 45 while the secondary side supplied the load comprises of 16 incandescent lamps connected in parallel, each of them has rated power 40 W. Similar to previous measurement the switching angle then varied between 0^0 to 360^0, with a phase step set to 30^0. The recorded waveforms are presented in Fig. 6.

Fig. 6 shows the inrush current with varying voltage switching angle while the transformer was energized. The highest inrush current of 9.959 A occurred when the transformer was energized at switching angle set to 270^0.

Furthermore, Fourier analysis was used to determine the harmonic content of current at the AC input to primary side of transformer during transient. This information can be useful in analyzing the impact of transformer utilization on the installations.

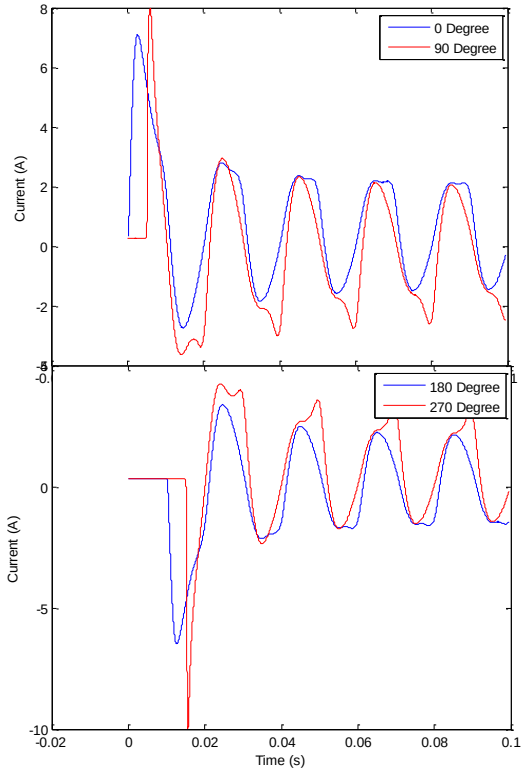

Fig. 6. Inrush current of a 2 kVA transformer with varying voltage switching angle

In Fig. 7, it is noticeable that the magnetizing current of transformer contains a DC component which decayed overtime and high percentage of 2nd harmonic current. These DC components were decreasing as the switching angle was reduced to lower value. As can be seen in Fig. 7, The DC component is gradually decreasing as the angle was set to 180^0, 90^0 and 0^0. Meanwhile, the 2nd harmonic current reached its highest value when the switching angle was set to 90^0 and 270^0, and the lowest when the switching angle was set to 0^0.

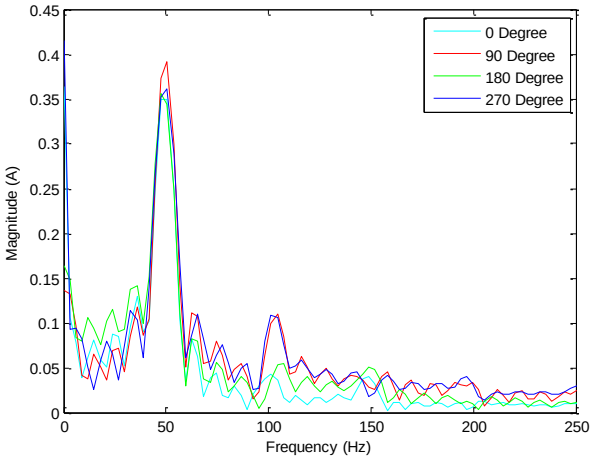

Fig. 7. Harmonic distribution of magnetizing current of transformer with varying switching angle

4.4 Electric vehicle chargers

In this section, a battery powered two seated electric vehicle, manufactured by Renault and marketed under brand name Twizy was measured. Twizy is equipped with 6.1 kWh lithium ion battery. The internal charger is compatible with roadside battery charging facilities as well as the standard 230 V 16 A household electrical supply.

The measurement was performed when the battery is depleted, the state of charge the moment when the measurement was done is 25%. A graph of voltage and current over full charging cycle is shown in Fig. 8.

The graph shows that voltage seemed too continually rise as the battery was charged. Meanwhile, the current behavior was quite different. At the beginning of the charging cycle, the charger withdrawn current around 0.24 A then increased to 9.81 A and reduced to around 8.1 A when the state of charge reached around 40%. There is some correlation between the voltage and the current, as a higher current leads to more voltage drop, but there are also some voltage variations which are definitively caused by other loads. The current remained steady until the state of charge reached 80%. Once the battery reached 80%, the RMS current gradually reduced to 2.51 A. This happened because the charge control circuit restricted the flow of current that flow into the battery. Since once 80% capacity is reached, supplying the same current will not charge the battery at the same rate as if when the battery is fully discharged. Instead, the energy supplied by this excess current is converted into heat that may damage the battery.

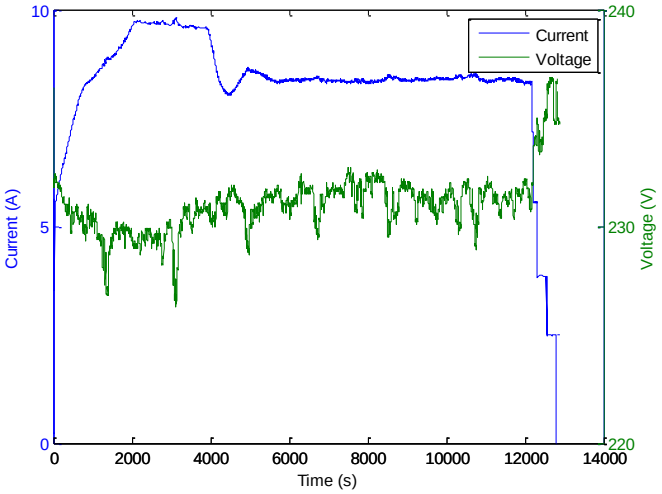

Fig. 8. Voltage and current over full charging cycle

Similar to previous measurement the switching angle then varied between 0^0 to 360^0, with phase step set to 30^0. The recorded waveforms are presented in Fig. 9.

As can be seen in Fig. 9, the highest peak of inrush current happened when the switching angle was set to 90^0. The highest peak was as high as 27.163 A in this study.

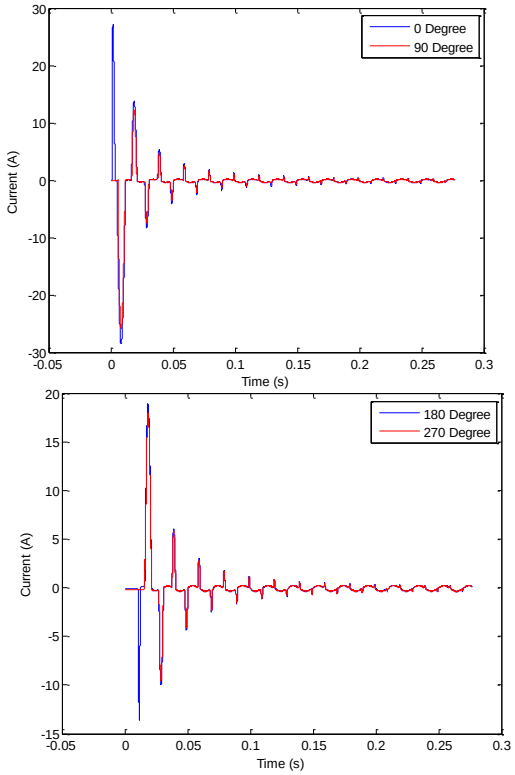

Fig. 9. Inrush current of EV charging with varying voltage switching angle

V. ANALYSIS OF THE MEASUREMENT RESULTS OF CAPACITIVE LOADS

5.1 The effect of switching angle

Loads that are used in the measurements consist of nonlinear loads with capacitive and inductive inrush characteristics. As for capacitive loads, the peak of inrush current can be found from

$$I_c = C\frac{dV}{dt} \tag{1}$$

It describes the dependence of peak of inrush current on the capacitance C and the rate of change for the voltage $\frac{dV}{dt}$. The highest value of $\frac{dV}{dt}$ is reached at 90^0 or 270^0, rather than 0^0 or 180^0. Which means the inrush is mostly affected by parallel capacitance in the charger circuit.

The topology of Twizy charger is not specified by the manufacturer. However, switch mode chargers are the ones most commonly found in residential application. Switch mode chargers works in a similar way as a switch mode power supply.

AC power from the grid is converted to high voltage DC power by a rectifier, and then converted further to a low voltage DC power through a DC-DC converter. The only difference is that it employs additional charge control circuit to regulate current flow into the battery. The circuit has one capacitor connected directly at the input side and another capacitor connected in parallel to the load. This capacitor works as a smoothing capacitor and as a filter to cut off high frequency from DC output.

Another similar pattern is also found in LED lamps. To explain the reason behind it, the topology of electronic driver used in their design need to be looked at. CFLs and low power LED lighting applications typically based on buck or buck boost topologies with capacitor connected in parallel at the input side. Actually, this is one of the methods used to limit harmonic currents of lamps. However, capacitor connected directly to the AC side can have relatively high inrush current, depending on the voltage phase angle the moment it is switched on. According to (1), the higher value of parallel capacitance, corresponds to the higher peak of inrush current values.

Meanwhile, a significant difference exists between continuous operation and energisation of a transformer. In continuous operation, the flux at its negative peak when voltage cross zero point. In the other hand, during energisation the flux has to start at zero, thus the magnetic flux will reach approximately twice its normal peak within voltage waveform's first half cycle. This amount of flux causes saturation of the transformer. In order to prevent the saturation, transformer is switched on when the voltage switching angle is set at 90^0 or 270^0. The starting voltage is also the initial condition, as the rate of change of flux is proportional to the voltage or in the other hand the flux waveform is the integral of voltage waveform, as given by (2) below.

$$\phi = \frac{1}{N}\int e(t)dt \tag{2}$$

With

$$e(t) = E_0 \sin(\omega_0 t) \tag{3}$$

These two waveforms were shifted by 90^0, therefore for inductive loads the highest peak of inrush current occurred at 0^0 and 180^0.

As for induction motor, it is found that at lower switching angle, the peak of inrush current is higher with shorter time to achieve steady state. Meanwhile, at larger switching angle the peak of inrush current is lower with longer settling time. To obtain minimum inrush current and moderate settling time, it is advised to start with higher switching angle, for instance 180^0. Subsequently, the angle is reduced in steps until 0^0 in order to increase the voltage gradually.

RERATING SWITCHES AND CIRCUIT BREAKERS

Switch contacts that connect and disconnect a circuit are exposed to electrical erosion resulting from sparking and arcing. This spark is causing heat in contact surface. The amount of heat dissipated depends on the resistance of the contact, contact material and its current rating. The thermal energy (W) dissipation in contact is calculated by the following equation.

$$W = I_{rms}{}^2 R t_{rms} \tag{4}$$

Where,

I = steady state value of current (A)

t_{rms} = half of the period time, the value is 10ms for 50Hz (s)

R = resistance of the contact material

Eq. (4) calculates the heat dissipation caused by inrush equal to the dissipation during first half cycle with a steady state current. In reality, the nominal current can flow for the whole lifetime of the equipment (e.g. 20 years). Although the duration of the inrush current is short, the heat generated by it

$$I_{rms}{}^2 R t_{rms} = I_{Peak}{}^2 R t_{Peak}$$

Load Type	I_{rms}	I_{Peak}/I_{rms}	t_{Inrush}	t_{Peak}
LED 4 W	0.037 A	7.64	< 1 ms	Infinite
LED 8 W	0.053 A	8.26	< 1 ms	Infinite
LED 14 W	0.068 A	5.03	1.30 ms	Infinite
CFL 11 W	0.068 A	33.76	<1 ms	Infinite
CFL 20 W	0.136 A	25.51	1.44 ms	Infinite
Induction motor 2.2 kW	2.417 A	23.21	11.15 ms	1.30 ms
Transformer 2 KVA	1.307 A	7.62	5.32 ms	Infinite
EV charger 3.3 kW	9.742 A	2.79	1.84 ms	3.47 ms

Table 1. Duration limit of inrush current on contacts

can damage contact material because the peak is much higher than normal operating current. Nevertheless, the temperature increase due to dissipation depends on the thermal time constant of the contact as well, hence the damage doesn't happen as soon as the heat produced exceeds this dissipation in a single half cycle, instead it may degrade the contact surface gradually. As for inrush case, (4) becomes:

(5)

R can be removed, so for duration of current, it can be written as

$$t_{Peak} = \frac{I_{rms}{}^2 t_{rms}}{I_{Peak}{}^2} \quad (6)$$

Where,

I_{Peak} = absolute peak value of inrush current (A)

t_{Peak} = permitted inrush duration on contacts [s]

In previous section, the height (peak) and width (duration) of inrush currents produced by various loads were measured. By substituting those value into (6) and compare the results with the contacts limit from the manufacturer, the duration limit of inrush current on contacts can be calculated. By assuming the ratio of maximum peak current and rated current is 5 [10], hence, if the rated current of contacts as high as 16 A, by taking this value into calculation, the peak current limit equal to 80 A. Furthermore, the peak of current is smaller than I_{rms} or rated current of contacts, the duration limit is described as unlimited. Whereas, in case the magnitude of peak current exceeds the rated current of contacts, then it should be limited to a certain period, as presented in Table 1.

For instance, the induction motor generated inrush current with maximum peak as high as 56.18 A. This peak is higher than rated current of contacts design, but still below the maximum peak 80 A, therefore contacts still able to endure it for maximum 0.0013 s. In case of energy saving lamps (CFLs and LED lamps) and transformer, because the peak of inrush currents were less than rated current of contacts design, the maximum duration of peak current that allowed to flow throughout contacts is infinite.

VI. CONCLUSIONS

High transient current produced by loads the moment it is switched on can create problems on contacts of breaking devices such as switches and circuit breakers. These problems can be contacts welding or false tripping of circuit breakers. The duration of inrush current is normally very short but the peak of current is very high. Duration and peak of inrush current are determined by the following factors:

- Type of load;
- The voltage switching angle;
- The impedance of installations.

Each type of load has its own inrush characteristics, which are defined by their peak current and its duration. Energy saving lamps such as CFLs and LED lamps and EV chargers shared typical characteristics of capacitive loads. The highest peak of inrush current was reached when the loads was switched on close to 90^0 or 270^0. Meanwhile, the highest peak of inrush current occurred at 0^0 or 180^0 for transformer, which is categorized as an inductive load. As for induction motor, it is known that higher switching angle resulted in lower inrush current, but longer time is taken to reach steady state.
Lastly, to cope with the problems caused by inrush current, the contacts of switches or circuit breakers need to be rerated by taking into consideration the following factors.

- The size of the loads;
- The ratio of maximum peak current and rated current;
- Duration of peak current.

I^2t analysis is used to define the current rating. During inrush, even though the duration is short, but the heat generated by it can damage contact material because the peak is much higher than the normal operating current. But the damage doesn't happen immediately after the first cycle of inrush occurs, instead it may degrade the contact surface gradually.

REFERENCES

[1] Cuk, V., Cobben, J. F. G., & Kling, W. L., "Inrush Related Problems caused by Lamps with Electronic Drivers and Their Mitigation," ISBN: 978-1-61804-023-7, pp. 321-326.

[2] Zaltsman, V., "Inrush Current Control for Equipment Powered by UPSs," INTELEC '89 Conference Proceedings, October 1989, Vol. 2, pp. 19.4/1–19.4/7.

[3] Kasztenny, B., "Impact of Transformer Inrush Currents on Sensitive Protection Functions," IEEE Transmission and Distribution Conference and Exhibition, 21-24 May 2006, pp. 820-823.

[4] Wu, L.C., Liu, C. W., Chien, S. E., & Chen, C. S., "The Effect of Inrush Current on Transformer Protection," 38th North American Power Symposium, Taipei, 17-19 September 2006, pp. 449-456.

[5] Nagpal, M., Martinich, T., Moshref, A., Morison, K. & Kundur, P., "Assessing and Limiting Impact of Transformer Inrush Current on Power Quality," IEEE Transactions on Power Delivery, Vol. 21, No. 2, 2006, pp. 890-896. doi:10.1109/TPWRD.2005.858782.

[6] Turner, R. A. & Smith, K. S., "Transformer Inrush Current," IEEE Industry Applications Magazine, Vol. 16, No. 5, 2010, pp. 14-19. doi:10.1109/MIAS.2010.937440.

[7] Steurer, M. & Fröhlich, K., "The Impact of Inrush Currents on the Mechanical Stress of High Voltage Power Transformer Coils," IEEE Transactions on Power Delivery, Vol. 17, No. 1, 2002, pp. 155-160. doi:10.1109/61.974203.

[8] Ebner, A., "Transient Transformer Inrush Currents due to Closing Time and Residual Flux Measurement Deviations if Controlled Switching is used," ETH Zurich, Switzerland, 2007, pp. 1-5.

[9] Veldhuizen, R., "New Loads, New Calculations," [Proposal], Hager Netherlands, 2012, pp. 4.

[10] Hager, "MCCBs and Trip-Free Switches 16A to 1600 A," retrieved from http://download.hager.com/hager.pic/files_download/main_switchgear/Main%20incomming%20devices/New%20MCCBs%20Hager/Catalogue%20pages%20MCCBs%20h3%20NCE E%20GB.pdf

G204

Performance comparison of PWM schemes of dual-inverter fed five-phase motor drives

I Nyoman Wahyu Satiawan,
Ida Bagus Fery Citarsa, I Ketut Wiryajati
Electrical Department, Faculty of Engineering
Mataram University
Mataram, Indonesia
Email : nwahyus@yahoo.com

Mohan V. Aware
Electrical Engineering Department
Visvesvaraya National Institute of Technology
NAGPUR 440011 (INDIA)
Email: mva_win@yahoo.com

***Abstract*— The dual-inverter fed open-end winding configuration can be categorized as a new breed of multi-level converters. The structure is simple and offers a lot of advantages. However the development of suitable PWM schemes is more complicated due to the availability of a large number of switching states and particularly, when it is applied to five-phase motor drives, the existence of the multiple two-dimensional planes further adds the complexity in the development of the proper PWM schemes. A view attempts to develop suitable modulation techniques for the dual-inverter fed five-phase machine drives has been made over the past view years. This paper presents performance comparison of three PWM schemes of the dual-inverter fed five-phase open-end winding motor drives. The quality of the phase output voltages generated by the three PWM schemes are compared and the adequate analyses are provided. The simulation results show that the carrier based phase disposition (PD) PWM scheme enables generate the most excellent output voltage among the three PWM schemes. The Total Harmonics Distortion (THD) of the output voltages generated by the carrier based PWM scheme reduce significantly by 65 % and 15 % in average compared to the THD of the output voltages produced by the URS PWM scheme and the decomposition PWM scheme respectively.**

Keywords—dual-inverter fed; open-end winding; carrier based PWM; Total Harmonics Distortion (THD)

G205

Design of Buck Converter For Photovoltaic System Applications

Ratna Ika Putri
Electronic Department
Malang State Polytechnic
Malang, Indonesia
ikaputri_ratna@yahoo.com

Muhammad Rifa'i
Electronic Department
Malang State Polytechnic
Malang, Indonesia

Supriatna Adhisuwignjo
Electronic Department
Malang State Polytechnic
Malang, Indonesia

***Abstract*—As a tropical country , Indonesia has a huge potential of solar energy as an alternative energy to replace fossil energy is increasingly scarce and expensive. Utilization of solar energy need photovoltaic that will convert solar energy into DC electricity. Advantages of photovoltaic are unlimited energy source, non- pollution, environmentally friendly and low maintenance costs, but PV has low efficiency. To improve efficiency is to operate the PV on maximum power point using maximum power point tracking (MPPT). Dc- dc converter is the heart of the MPPT that will maintain a stable output voltage at the maximum voltage despite changes in temperature and solar irradiation. There are three configurations dc- dc converters that can be used for MPPT is a buck converter, boost converter and buck-boost converter. Buck converter has a better efficiency than other configurations.This paper will analyze, design and simulation of a buck converter circuit for charging batteries using photovoltaic. The design includes the determination of the parameters of the circuit components that accordance with the requirements a photovoltaic system based battery charged.**

Keywords—photovoltaic, buck converter

I. INTRODUCTION

Increasing electrical energy demand are propotional with the growth of population and economic, while availability of fossil energy more scarce and expensive. So we need diversification a renewable energy as an alternative energy. Solar energy is one of the great potential renewable energy in Indonesia. It has the advantages of unlimited avaibility, enviroment- friendly and free pollution. To utilize solar energy requires photovoltaic that convert solar energy to DC electrical energy.

Photovoltaic characteristic depends on light intensity and temperature of junction. Output voltage and current generated is directly proportional with light intensity received [6]. Drawback of photovoltaic is low efficiency so necessary controlling to work in maximum power point (MPP). One of method to define MPP is using MPPT with dc-dc converter. MPPT has advantages is directly measurement of array voltage and thus require lower cost compared than method using solar irradiation measurement and enviroment factor. MPPT using dc-dc converter do not require current measurement so that system becomes simpler [5]. Toobtainoptimumpowercan be doneby usingdc-dc converters as power electronic circuit. Dc-dc converterconnects thephotovoltaicoutputandload. Using abuck converterforphotovoltaicapplicationsproduceshighperformance, efficientandrobust [7].

There are threeconfigurationsdc-dc convertersthatcan beusedforMPPTisa buck converter, boost converterandbuck-boostconverter. Buckconverteris acircuit that generates anoutput voltagelower thanthe inputvoltage, while theboost converterwillgeneratetheoutput voltagegreater thanthe inputvoltage. Buckboost converteroutput voltagewillresult inlarger orsmallerthanthe inputvoltage. The magnitude oftheoutput voltagedc-dc converterdependson the amount ofduty cycle. Buckconverterhas abetter efficiencythanthe other configuration.

Inthis articlewill be designed buck converter for photovoltaic applications. Photovoltaic power for 50WP and buck converters are used to connect between the photovoltaic and battery. The selection of components buck converter will be determined based onusage and simulated using Simulink matlab.

II. PHOTOVOLTAIC

Solar cells will convert solar energy into DC electricity directly . The PV system consists of several solar cells can be connected in series or parallel . The PV system has the advantage that it does not cause pollution, environmentally friendly, low maintenance costs and the availability of solar energy is unlimited and continuous.But the use of PV systems is still rarely used because it has the disadvantage of high cost of installation and low energy conversion efficiency is only about 20 % [2]. Currently the cost of solar energy is estimated at double the cost of fossil energy (coal , oil , etc.). But for the

future, where fossil fuels are very thinned so that the energy costs will increase to equal the cost of solar energy . Until 2000, it was reported to the procurement of solar cell modules to power up to hundreds of kilo –watt. The price of system of per watt of energy generated is about 4.5 U.S. dollars, and in 2005 the price of energy generation system modules with solar cells can be reduced to $ 1 per Watt. The longer inverstasi costs for solar energy is going to go down, so that the operation of the PV system is the most important thing to do is improve the efficiency of the system

Energy conversionefficiency ofsolar cells areassociatedwith themaximum powerpoint(MPP) of PV systems [3]. PVpanelsworkonamaximumpointwhichwillresult inmaximumoutput power. MPPis strongly influencedbysolarirradiation, celljunctiontemperatureandload currentchangesverynon-linear. Solarirradiationandtemperaturechangeswillshift theMPPjunction ofPVsystem. So that the necessaryarrangementstodetermine theMPP. ThePVsystemwillcontinue to operatearoundthe MPPdespitechanges insolarirradiationandthe celljunctiontemperature. Determination ofMPPisalso called themaximum power pointtracking(MPPT). Withtheusing ofthisMPPT,PVsystemefficiencycan be improved.

Characteristics of highly non-linear photovoltaic systems are influenced by external factors. Solar irradiation, ambient temperature and wind speed are the main environmental factors affecting PV system. While the short circuit current (Isc), open circuit voltage (Voc), maximum voltage (Vmax) and current MPP is the main characteristic that shows the IV and PV curves [1]. According to El-Salhi & Bachtiri [4], solar cells are devices that are non-linear and can be expressed as a current source model as shown in Fig 1.

.

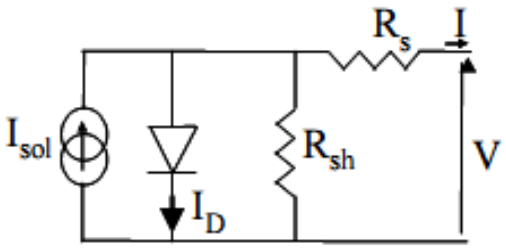

Fig 1. Equivalent Circuit of Solar Cell

III. BUCK CONVERTER

A. Principle of Operation

Buckconverteris acircuitthat convertsthe DCvoltageintoanotherDC voltagewhose valueis smaller. Average outputvoltage ofthe buckconverteris smallerthanthe sourcevoltage. Buck convertercircuitis shownin Fig2. The working principle ofthe circuitdependsonthe condition ofthe switchSwhichhas atwocircumstances, when the switchSis closed(ON) oropen(off) whichswitchSis generallyapower electronics componentssuch asMOSFETs. Operatingmodebuck converterconsistsof two types ofcontinuousanddiscontinuous. Circuitoperatingmodesdependingon thecurrent through theinductor. Incontinuousmodethe inductor currentneverreacheszerowhile indiscontinuousmodewillreach a value ofzerofor a time.

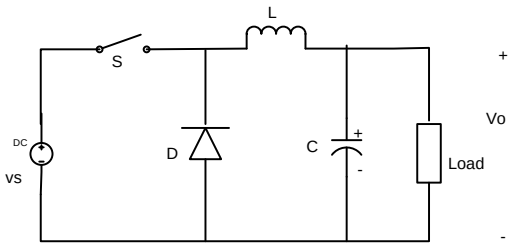

(a) Circuit Diagram

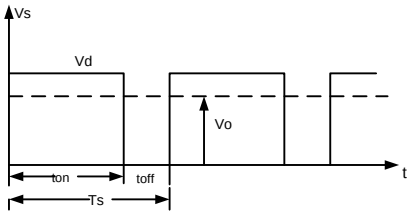

(b) Average Output Voltage

Fig 2. Circuit Diagram and Average Output Voltage of Buck Converter

In most applications,buck converter use continuous modeso thatthe inductor currentnever reacheszeroatfullload conditions. By using thecontinuousmode,the overallperformance of thecircuit willbe betterthan in thediscontinuousmode, otherwise it willproduce amaximumoutput power. Butin themaximum load current smaller,usagediscontinuousmodeis more profitablebecausethe sizeofinductors that usedis smaller so thatthe size of theconverterbecomes smaller. Increasing resistive load in continuos mode buck convertercircuitwillcause it workindiscontinuousmode. The working principleof continuous modebuckconvertercan bedividedinto twoat thetimethe switchis closedandthe switchis open. Fig 3 shown diagram block for system photovoltaic using buck converter.

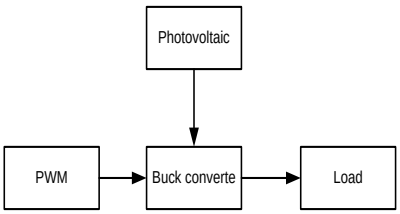

Fig 3. Diagram Block of Photovoltaic System

Mode 1. Switch S is ON.

At the time of the switch in closed condition, diode will be reverse biased and current flows in the inductor L, capacitor

C and load R. The current through inductor will increase while capasitor current have the opposite directions and depending inductor and load current. When inductor current increase, the stored energy will increase too. By using voltage khircoff law, inductor voltage can to be determined by

$$V_L = V_s - V_o \quad (1)$$

and

$$L\frac{di}{dt} = V_s - V_o \quad (2)$$

With finishing eq. [2] will be obtained

$$I_{LON} = \left(\frac{V_S - V_O}{L}\right)t_{ON} \quad (3)$$

where V_S, V_O, V_L, $I_{LON}$and $t_{ON}$are source voltage, output voltage, inductor voltage, inductor current at switch-on condition and time on.

Mode 2 : Switch S, OFF

Atswitchoff, thediodeconducts, the loadis disconnectedto thesource. Inductors that store energywill to flow the current intothe capacitorandthe load. Capacitor current willflowin the opposite directionwith theinductor, so

$$V_L = -V_C = -V_o \quad (4)$$

and

$$L\frac{di}{dt} = -V_o \quad (5)$$

Inductor currentduring switch off can be determined by

$$I_{LOFF} = \left(\frac{-V_O}{L}\right)t_{OFF} \quad (6)$$

where Vc is voltage of capacitor and $t_{OFF}$is switch off period

$$t_{OFF} = T - t_{ON} \quad (7)$$

Based oneq. [3] and[6], the inductor current in one period of

$$I_{LOFF} + I_{LON} = 0 \quad (8)$$

$$\left(\frac{V_S - V_O}{L}\right)t_{ON} + \left(\frac{-V_O}{L}\right)t_{OFF} \quad (9)$$

$$\left(\frac{V_S - V_O}{L}\right)t_{ON} + \left(\frac{-V_O}{L}\right)(T - t_{ON}) \quad (10)$$

With finishing eq. [10] will be obtained

$$V_O = V_S\frac{t_{ON}}{T} \quad (11)$$

$$V_O = V_S D \quad ; 0 < D < 1 \quad (12)$$

Where D is duty cycle.

B. Selection of Components

Buck converter circuit consists of inductor, capacitor, diode, switch and load. The selection ofappropriate componentsplay an important rolein the design ofthe circuitfor the system tooperateoptimally.

1) Switch

Some componentscanbe usedtopowerelectronicswitches, among others; BJTs, MOSFETs, IGBTandCOOLMOS. Transistorsare generallyusedforlow to mediumpower applications. While theMOSFETis avoltagecontrolledcomponents, are better suitedforlow power applicationsandhigh frequencyconverters, IGBTis moresuitable forhigh power applications [7]. For applicationsin50W PV,willbe usedMOSFET aselectronicswitches.

To determine the type MOSFETs that used by determined how much voltage V_{DSS}, I_D, and the maximum frequency that may be imposed on the MOSFET. $V_{DSS}$is the maximum voltage that will be imposed on MOSFET, due to MOSFET input come from photovoltaic output voltage of 20V so V_{DSS}> Vs = 20 Volt. For drain current I_D based on output power so thatI_D> D * Iout.

With D is the duty cycle with a value between 0 and 1, while the desired Iout at 2 amperes, thus ID of 2 amperes. Based on the calculation above, the MOSFET type IRF540 chosen because it has a VDSS of 100 V and I_D of 15 A.

2) Inductor

Inductor valueused dependson theswitching frequencywillalsoaffectthe size of theinductor. The higher theswitching frequency, the value andsize of theinductorisusedalsowill be smaller. Forcontinuous operationtheinductor currentwillalways be greaterthanzeroso that theinductor valuecan be determinedby the equation

$$L = \frac{(1-D).V_o}{2.f.I_o} \quad (13)$$

Where f is switching frequency and I_O is output current.Inductorsareselected usingthe typetoroid, acomponentthat is suitable forhigh frequency applications.

3) Diode

With aswitching frequencyof200KHzthenrequire adiodewitha fastrecoverytimesousedSchottkydiodes. Diodereversevoltagemust beable toface the PVoutput voltage.

4) Capacitor

Capacitance value which used will be influence to ripple output voltage. Capacitor value can be determined by

$$C = \frac{(1-D)V_O}{2f^2LV_{ripple}} \quad (14)$$

Where V_{ripple} is ripple output voltage.

IV. SIMULATION

To determine thecharacteristics of thebuck convertercircuitthathas beendesignedthrough simulationusingSimulinkmatlab. Circuit diagram of buck converterforsimulationas shown inFig4. Based on thecalculation ofthe valueof inductor0.2mH, capacitor4.34μF, source voltage 20Vandswitching frequency200KHz.

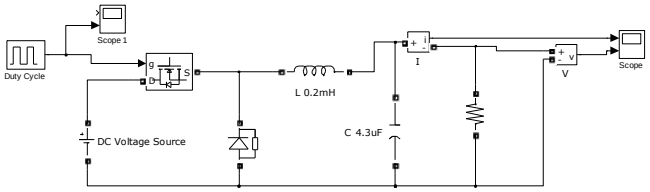

Fig 4. Simulation Buck Converter Circuit

The simulation result of the buck converter at duty cycle 50% as shown in fig 5 and at duty cycle 80% in fig 6.

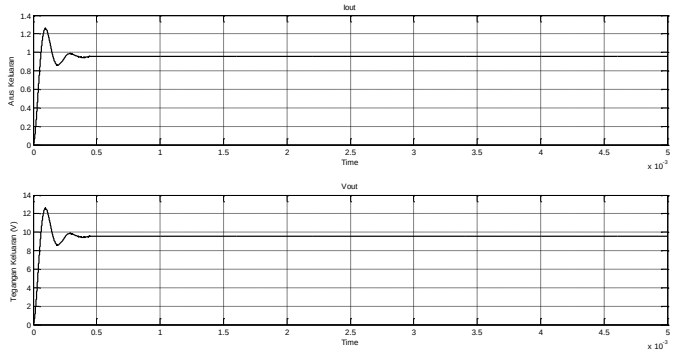

Fig 5. Simulation Result For Duty Cycle 50%

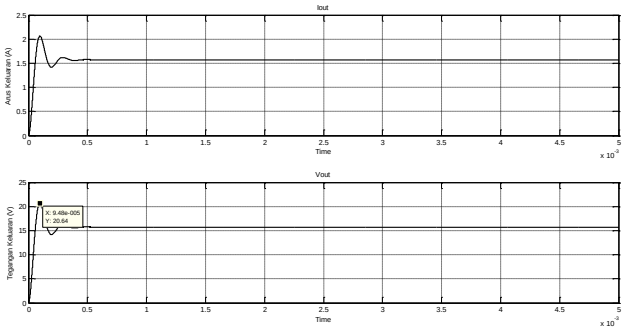

Fig 6. Simulation Result For Duty Cycle 80%

V. RESULT AND DISCUSSION

Based on the simulation results obtained voltage and output current circuit. With aduty cycle of 50% produces a voltage output at steady state conditions at 9.56V. Transient response of output current and voltage have maximum overshoot 31%. While the duty cycle of 80% produces the output voltage of 15.7V at conditions stady state and transient response has a maximum overshoot of 32.5%. By using the parameters of the components designed, the circuit operates in continuous current mode, change the operating mode depending on the value of inductance are used. The greater the inductance value is used then the circuit will operate in continuous mode.

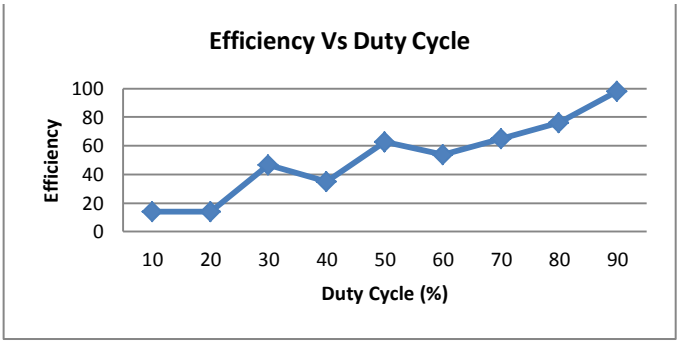

Fig 7. Efficiency to Duty Cycle

Duty cyclechangeswillresult inchanges involtageandoutput power. It alsowillaffect theefficiency ofthe circuit. The relationshipbetweenthe efficiency ofthe circuitwithduty cycleusedis shownin Fig7. The higher duty cycle will increase efficiency of circuit.

VI. CONCLUSION

Buck convertercircuit design for photovoltaic applications have been described. The circuit works incontinuous mode with aswitching frequency of 200 KHz. Determination of the componentsbased onthe needs of photovoltaic systems with duty cyclesettings. The increasing efficiencyis proportional to the circuitduty cycle.

Reference

[1] Aldhobani MS & John Robert. Maximum Power Point Tracking Of PV System Using ANFIS Prediction And Fuzzy Logic Tracking. Proceeding Of The International Multi Conference Of Engineers And Computer Scientists 2008 Vol II. IMECS 2008. Hongkong. 19-21 March 2008

[2] Ayvazyan GY dkk. Maximum Power Operation Of PV System Using Fuzzy Logic Control.Armenian Journal of Physics. Volume 1. 2008.

[3] Chouder A dkk. Simulation of Fuzzy Based MPP Tracker And Performance Comparison With Perturb & Observe Method. Revue des Energies Renouvelables Volume 11 No (4). 2008.

[4] Salhi M & El-Bachtiri, Maximum Power Point Tracking Controller For PV System Using PI Regulator With Boost DC/DC Converter, ICGST-ACSE Journal, ISSN 1687-4811. Volume 8. Issue III. January 2009.

[5] Veerachary Mummadi dkk. Voltage-Based Maximum Power Point Tracking Control of PV System. IEEE Transactions On Aerospace And Electronics Systems Vol 38 No 1. January 2002

[6] Ratna Ika Putri & M. Rifa'i. Maximum Power Point Tracking Control For Photovoltaic Using Neural fuzzy. International Journal of Computer and Electrical Engineering (IJCEE) ISSN 1793-8163.

[7] Syafrudin Masri, Norizah Mohamad, Muhammad Hafeez Mohamed Hariri, Design and Development of DC-DC Buck Converter for Photovoltaic Application. IEEE conference on Power Engineering And Renewable Energy. 2012.

G206

Development of a 20 V-LED driver based on the boost converter using a FPGA module

N. Sulistiyanto, M. Rif´an, O. Setyawati
Electrical Engineering Department
Faculty of Engineering, Brawijaya University
Malang, Indonesia
nnst@ub.ac.id

Abstract— **We present the development of a LED (Light Emitting Diode) driver based on the boost power converter. Several DC to DC converter circuits were modeled using B^{2}SPICE to evaluate their characteristics by varying the components and the duty cycle. The driver´s prototype was realized using a FPGA (Field Programmable Gate Array) module as the switching controller, wherein the simulation using Xilink ISE14.6 and the measurements were successfully performed. The Boost and Cuk converter topologies were investigated to achieve an optimum converter which showed relatively high gain voltage. Duty cycle of 5% up to 25% was required to obtain the driver output voltage of 20V, revealing the efficiency of approximately 90%.**

Keywords— LED driver, power converter, FPGA module, B^{2}SPICE

G207

Development of Microhydro Field Laboratory

under the Program of Science and Technology on Campus Innovation and Creativity

Teguh Utomo And Rini Nur Hasanah
Electrical Engineering Department
Faculty of Engineering
Brawijaya University
Malang, Indonesia
rini.hasanah@ub.ac.id

Mohammad Bisri
Water Resources Engineering Department
Faculty of Engineering
Brawijaya University
Malang, Indonesia
mbisri@ub.ac.id

***Abstract*—Faculty of Engineering Brawijaya University (FT-UB) has a long history in the provision of electricity for community in general, especially through its long-time renown in the field of rural electrification and microhydro power generation activities. The expertise in microhydro power plant (MHP) system has become one of the iconic representations of the Faculty of Engineering in the society. This icon is reflected through its two well-running microhydro field laboratories; one is located in the Kalijari village of Blitar regency whereas the other is in the Bendosari-Batu village of the Malang regency, both are in the province of East Java, Indonesia. The MHP Kalijari supplies electricity for about 60 households of the nearby villages, whereas the MHP Bendosari is so far used by 26 households. The improvement of the field laboratories has been carried out under the program of *Science and Technology on Campus Innovation and Creativity* (*IbIKK Mikrohidro*) financed by the Ministry of Education and Culture of the Republic of Indonesia. It has been prioritized on the construction of the prototype of turbine/waterwheel, the construction/procurement of the components/equipments for a microhydro power plant system (including turbine/waterwheel, generator, Digital Load Controller and dummy load, as well as low-voltage installation panel), establishment of a management system, preparation and development of infrastructure for production, promotion activities and improvement of cooperation. Some positive multiple impacts of the MHP construction would cover the education sector (lighting for households and educational institution buildings), health sector (drugstores, medicaments storage, surgery activities in hospitals, etc.), environment (water utilization and forest/river flow conservation), and even the economic sector of the community.**

Keywords—microhydro; generated power; generator; turbine/waterwheel

I. INTRODUCTION

Currently, there are still many remote villages in Indonesia which have not been reached and are difficult to reach by the service of the national electricity company, i.e. PT PLN (Persero) [1]. On the other hand, local potential of renewable energy could be explored, if existing. For example, if there is a hydropower potential in a village, even on a small scale, rural communities can use it as a primary energy source to meet the needs of electrical energy. Small-scale hydropower plants with installed capacity less or equal to 200 kW are known as microhydro power plant [2].

The continuosly increasing scarcity and price of oil as well as its role as the main direct source of energy among the rural communities which have not been reached by the national electricity grid make the microhydro power an alternative measure for providing electricity at affordable price because water as the primary energy source is available free of charge and throughout the year. The use of micro-hydro electricity in rural areas is mainly for cooking, lighting, and driving machinery of appropriate technology implementation (such as coffee-bean grinder, water pump drive, the corn sheller, poultry incubators, etc.). Therefore the benefit of microhydro electricity during the energy crises era becomes salient to meet the electrical energy needs of people in rural/remote areas and to improve the socio-economic as well as to raise the living standard of society [1].

In Indonesia, the potential for mini/microhydro power plants reaches the value of 450 MW. On the other hand, it is only about 210 MW or 46% of the total potential which has been explored. It indicates that the opportunity to build microhydro power plants is still widely open. These opportunities are supported by the fact that the available water resources as well as the energy market to absorb the generated electricity are there, given that from the electrification ratio it is known that about 32.8% of households in Indonesia are still not electrified.

Based on the existing data of mini/microhydro potential, if it is desired to build microhydro power plants in some rural/remote areas of Indonesia with a capacity of 20 kW/plant at least, then there will be an opportunity to build 12,000 units of microhydro plant. When the plant is built with the maximum capacity of mini/microhydro category, i.e. 200 kW/plant, then there will be an opportunity to build 1,200 units. These facts reflect an enormous market opportunity.

From the previous description it can be clearly seen that a) the opportunity to develop microhydro energy in Indonesia is still widely open, b) the number of competitors in development/procurement of microhydro eenrgy system is still low, considering that to build a microhydro system some involvement of various expertise/specialist skills of multidisciplinary fields are required, c) the prospective consumers of microhydro electricity are still of considerable number as the national electrification ratio is still low (67.2%), meaning that there are still 32.8% of households not electrified and the majority of them are in rural/remote areas, d) the possibility of partnership and cooperation for the development of microhydro energy are still widely open and the involvement of investors/funders and other parties in the construction process is also quite high, such as the cooperation with relevant ministries (Energy, PU, Diknas, PDT, Bappenas, etc.), state-owned companies and enterprises (through CSR), local government (district/city/province), the private sector or non-governmental/other funding organizations [3-9].

II. METHODOLOGY/EXPERIMENTAL

Data collection and analysis techniques in the development of microhydro power plant cover the following steps: a) survey and measurement, b) analysis of hydrology/hydraulics, c) hydromechanical and electrical design followed by the construction of the plant [10].

The power generated by the turbine is called as turbine horse power and can be expressedusing the following equation:

$$P_{turbin} = \frac{\rho g Q H}{1000}\eta_T \quad \text{kW} \qquad (1)$$

where:

ρ = water mass (kg/m^3)

g = gravity (m/det^2)

Q = water flow debit (m^3/det)

H = height difference (m)

η_T = efficiency of turbine (0.75 – 0.9)

Losses arising in the energy conversion process and included in the turbine efficiency cover the volumetric efficiency (η_v), hydraulic efficiency (η_h) and losses arising on the bearings, stuffing boxes of the turbine shaft and the losses due to friction or known as the turbine mechanical losses (η_m).

Hence, the turbine efficiency can be written in the following equation:

$$\eta_T = \eta_v.\eta_h.\eta_m \qquad (2)$$

The manipulation of the two previous formulas will give the equation to find the turbine power, as follows.

$$P_{turbin} = 9.8.Q.H.\eta_T \quad \text{kW} \qquad (3)$$

And then, the power generated by the generator, is called as electric power, can be written the following equation:

$$P_{electic} = 9.8.Q.H.\eta \quad \text{kVA} \qquad (4)$$

Hence, the electric efficiency (η) and the generator efficiency (η_G) can be written in the following equation:

$$\eta = \eta_T.\eta_G \qquad (5)$$

III. RESULTS

Technical specifications of the equipments used in the microhydro power plants of the field laboratories are shown in Table I.

TABLE I. TECHNICAL SPECIFICATIONS OF THE MAIN EQUIPMENTS INSTALLED AT THE MHP FIELD LABORATORIES

No.	Equipment name	Specification
1.	Cross-flow water turbine C4-30B/C4-24	P_{out} 10.6 kW; speed 518 rpm; blade length 550 mm; V-belt mechanical transmission to generator
2.	Over-shoot waterwheel	P_{mech} 4,85 kW; diameter 2.3 mm; blade-number 18; blade width 870 mm; Mechanical transmission system using automobile speed-gears combined with V-belt to generator
3.	Synchronous generator	Three-phase; 380/220V; 50 Hz; 1500 rpm; 15kVA; p.f. 0.85 – 0.90; Continous rating. Single-phase; 380/220V; 50 Hz; 1500 rpm; 2.9kVA; p.f. 0.85 – 0.90; Continous rating.
4.	DLC and dummy-load system	Current sensor ACS 712; Microcontroller ATMega16; TRIAC BTA16-600B; Optocoupler MOC3021; Lamp 100W and 25W (dummy load)
5.	Low-voltage electrical distribution network	One/three-phase systems; 220 Volt; Frequency 50 Hz; Pure radial topology; conductors of bundled cable 4x25 mm2 (main line) and twisted cable 2x10 mm2 (branch line); supporting pylon: concrete/bamboos ± 6m

In terms of non-physical/service activities, the products of this program cover the service/consulting on the study results, the results of field survey, establishment and dissemination of instruction manuals as well as regulation on power generation/distribution, electrical security and safety, and also Standard Operating Procedures.

In terms of physical/field activities the resulted products are various microhydro power plants with installed capacity varying from 1 kW (picohydro) up to a maximum of 200 kW, using either turbines and waterwheels.

Figure 1 shows the powerhouse site of the waterwheel MHP plant Bendosari-Pujon-Malang (PLTMH I), whereas Table II shows the power-house technical data.

Fig. 1. The waterwheel microhydro power plant (PLTMH I) at Bendosari village, Pujon Malang

TABLE II. POWER HOUSE TECHNICAL DATA OF THE WATERWHEEL MHP PLANT BENDOSARI (PLTMH I AND PLTMH II)

Waterwheel	Over-shoot	
	Diameter	2.300 mm
	Number of blades	18
	Width of blade	870 mm
	Mechanical power	4.85kW
Generator	Phase	1; 220/380V
	Electrical power	2.90 kW
	Speed	1500 rpm
	Frequency	50 Hz
	Rating	continuous
Mechanical transmission		Axles and V-belt

Figure 2 shows the second waterwheel MHP in Bendosari-Pujon-Malang (PLTMH II), used also as field laboratory of the Engineering Faculty Brawijaya University whereas Table II also shows the power-house technical data. This second power house has been built with the participation of the third party under the Corporetae Social Responsibility program of a private company (PT Danareksa, Jakarta).

Fig. 2. The second waterwheel MHP (PLTMH II) in Bendosari, Pujon-Malang

Figure 3 shows the powerhouse site of the MHP plant Check Dam V Kalijari-Blitar (PLTMH Kalijari), whereas its technical data is shown in Table III.

Fig. 3. The microhydro power plant at Chekdam V Kalijari, Blitar (PLTMH Kalijari) as the field laboratory of Engineering Faculty Brawijaya University

Figure 4 shows the generator inside the powerhouse of the MHP plant CheckDam V Kalijari-Blitar (PLTMH Kalijari).

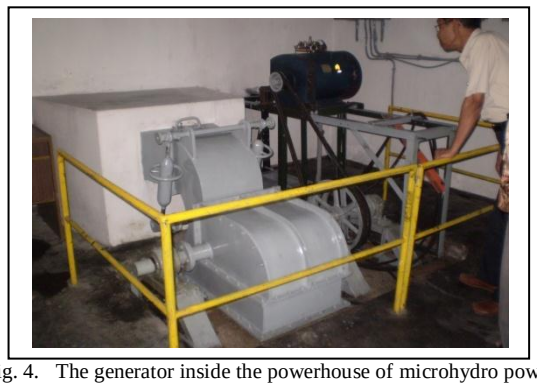

Fig. 4. The generator inside the powerhouse of microhydro power plant at Chekdam V Kalijari, Blitar (PLTMH Kalijari)

TABLE III. POWER HOUSE TECHNICAL DATA OF THE WATERWHEEL MHP PLANT CHECKDAM V KALIJARI (PLTMH KALIJARI)

Turbine	Cross-flow	(Banki)
	Outer diameter	440 mm
	Inner diameter	320 mm
	Runner width	500 mm
	Speed	300 rpm
	Power	15 kW
Generator	Phase number	3
	Capacity	15 kVA
	Speed	1500 rpm
	Frequency	50 Hz
	Rating	continuous
Mechanical transmission using pulley and belt		Ratio 1:5

To support the activities of the program, some in-campus laboratories have been involved, i.e. a) the Mechanical Technology Laboratory of the Mechanical Engineering Department for the production and manufacturing of turbine/waterwheel and mechanical transmission system, including the manufacturing of the prototype of water turbine and generator module, b) the Hydraulics Laboratory of the Water Resources Engineering Department for the analysis of hydrology/hydraulic systems, and c) the Electrical Machines Laboratory for testing the ac generators, transformers, digital load controller (DLC) and the Power System Laboratory for testing modules of low-voltage circuit panel (*PHB TR*), both are at the Electrical Engineering Department [13].

Figure 5 shows the running test of the DLC and dummy-load system system for the MHP at the laboratory of Electrical Machines of the Electrical Engineering Department Brawijaya University.

Fig. 5. Running test of DLC and dummy-load system for the MHP at the laboratory of Electrical Machines of the Electrical Engineering Department Brawijaya University

Figure 6 shows test-model/prototype of water turbine – generator of the *IbIKK Mikrohidro* product, whereas figure 7 shows demonstration module of low-voltage electrical distribution network for the MHP system at the laboratory of Power System Distribution of the Electrical Engineering Department Brawijaya University.

Fig. 6. Test-model/prototype of water turbine – generator of the *IbIKK Mikrohidro* product

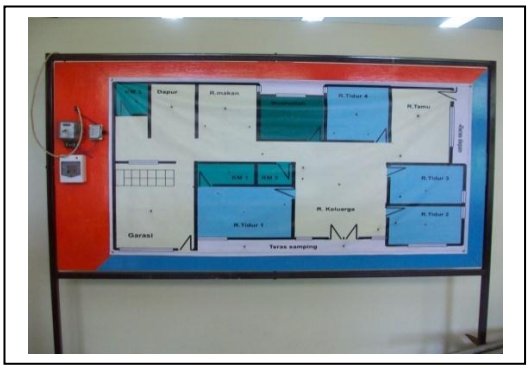

Fig. 7. Demonstration module of low-voltage electrical distribution network for the MHP system at the laboratory of Power System Distribution of the Electrical Engineering Department Brawijaya University

IV. DISCUSSION

There are two types of commercial activities conducted under this *IbIKK Mickohydro* program, including the methods to be used, namely:

1) Service activities, the methods of which include consultation, dissemination of science and technology (design and supervision/monitoring of microhydro development) and education/training.

2) Field activites in the form of the construction of mini/microhydro power systems activities building micro / micro power with the methods used can be: the dissemination of science and technology (construction of MHP) and simulation of science and technology (prototype/model).

The priority activities of this *IbIKK Mikrohidro* program include: a) construction of the prototype of turbine/ waterwheel using the locally available materials based on the existing condition of the field laboratory, and b) preparation of the production systems of equipments supporting the operation and maintenance of the microhydro power plant (including turbine/water turbine, generator, DLC-and-a dummy load system, and low-voltage installation panels). Meanwhile, some supporting activities undertaken to achieve the objectives and target outcomes can be broadly divided into the formation of a management system, preparation and development of production infrastructure of the existing production processes, and also promotional activities to increase more cooperations with other relevant parties [11-12].

From the point of view of quality assurance system, it has been determined to adopt the system ISO 9001: 2000 and the Standard and Manufacturing Operational Procedure (SMOP), in which it is required to demonstrate the ability to provide products which fulfill the prevailing regulation and the demanded requirements with the aim to enhance customer satisfaction. Quality assurance system prevails on the raw material, production process/product development, and up to the end activities, both covering physical and non-physical activities. For the physical activity, product quality assurance begins with the raw materials quality testing in each subsystem of the generation, on the production/development with the focus on the critical points of the development/production chain, and on the final product using running test and commissioning.

Some materials/production tools avalaible for service activities under this program are table for discussion, computer, and printer, while some materials/tools being prepared for the field survey are meter rolls, toolbox, a digital multimeter, digital meter pliers, a Global Positioning System equipment, and a rechargeable flashlight and safety equipments (such as rubber boots, hard hats, safety ladders and gloves).Conclusions

Some conclusions that can be drawn from the program of *Science and Technology on Campus Innovation and Creativity (IbIKK Mikrohidro)* are described as follows.

There are two types of activities carried out under the program, i.e. the service activity and field activity. The service activity includes consulting service, dissemination of science and technology (design and supervision/monitoring of the MHP development), and also training on electrical power and the use of electricity use. The field activity covers the MHP model/prototype simulation and construction.

The prioritized activities are the construction of a prototype of turbine/waterwheel based on the existing condition in the field laboratory, the preparation of the production systems of the equipments supporting the MHP including turbine/water wheel, generator, DLC and a dummy load system, and low voltage installation panels.

The establishment of management systems and the relevant infrastructures has also been carried out, including formation of the management, preparation and development of production infrastructure, and promotion of the activities to enhance much more cooperation with other parties.

Some perspectives can also be previewed concerning the campus innovation and creativity in the field of microhydro power plant to support the autonomy of energy in remote villages, which include the following points.

As the opportunity to develop microhydro power plant in Indonesia is still widely open and the player number in this field is still low, continuous socialization and information on the possibility to take the benefit of microhydro power should always be widely disseminated.

As the prospective consumers of microhydro electricity are of considerable amount, knowing that the national electrifiction ratio is still low, more cooperationa with and active participation of investors/funders and other parties are highly required.

Finally, it is also understood that the concern of the relevant institutions is required to provide any necessary technical assistance to maximize the benefit and to maintain the sustainability of the MHPs.

ACKNOWLEDGMENT

On this opportunity, the authors would like to express their gratitude to the Directorate General of Higher Education of the Ministry of Education and Culture through the Brawijaya University for having financed the realization of this program of *Science and Technology on Campus Innovation and Creativity (IbIKK Mikrohidro)*. Sincere thanks also go to all MHP partners/managers/community groups in Bendosari-Pujon-Malang and Kalijari-Gandusari-Blitar, and to all students of the Engineering Faculty Brawijaya University who have been actively involved in this program.

REFERENCES

[1] B. Mismail, Rural Electrification in Indonesia, Diss. University of Colorado at Boulder, 1980.

[2] Hangzhou Regional Center for Small Hydropower, Small Hydropower: A Textbook Specially Designed for Training Workshop in TCTD Program, Hangzhou, China: HRC-SHP, 2008.

[3] The Technical Team of Engineering Faculty of Brawijaya University, Feasibility Study on the Microhydro Power Development in Malang Regency", Malang: BPP FT UB, 2006.

[4] The Technical Team of Engineering Faculty of Brawijaya University, Detailed Engineering Design of the MHP Sukun River of Malang Regency, Malang: BPP FT UB, 2006.

[5] T. Utomo, H. Santoso, and R.N. Hasanah, Survey on the Microhydro Power Potential in Malang, Malang: BPP FT UB, 2008.

[6] T. Utomo, H. Santoso, and R.N. Hasanah, Research-Action on the Improvement of Output Power Quality of the CheckDam V MHP Kalijar-Blitar, Malang: LPPM UB, 2008.

[7] T. Utomo, H. Santoso, and R.N. Hasanah, Development of a Waterwheeled MHP as an Effort to Supply Electricity to Remote Villages, Malang: LPPM UB, 2009.

[8] T. Utomo, H. Santoso, M. Bisri, M. Shidiq, W. Harsanti, Survey on the Development of Waterwheeled MHP Bendosari, Malang: LPPM UB, 2009.

[9] Technical Team of Engineering Faculty of Brawijaya University, Survey Results on the Operation and Maintenance of the MHP CheckDam V Kalijari-Blitar, Malang: Engineering Faculty UB, 2009.

[10] A. Harvey, Micro-Hydro Design Manual: A Guide to Small-Scale Water Power Schemes, UK: ITDG Publishing, 2006.

[11] Anonymous, "With the proper and wise use, electricity is our friend", Dissemination of the law on electricity (*Undang-undang Republik Indonesia Nomor 20 Tahun 2002 Tentang Ketenagalistrikan*) organized by *Dinas Energi Propinsi Jawa Timur* in cooperation with *Direktorat Jendral Listrik dan Pengembangan Energi*, Surabaya, 26 October 2002.

[12] Anonymous, The law on electrical energy of the Republic of Indonesia "*Undang-undang Republik Indonesia Nomor 20 Tahun 2002 Tentang Ketenagalistrikan"*, Jakarta, 2003.

[13] A.S. Pabla, Electrical Power Distribution, Tata McGraw-Hill Education, 2007.

G208

Resisistivity Structures in Mt. Batur Geothermal Prospect Area in Bali Province, Indonesia

Wahyudi W. Parnadi, Adhiarta P., Widodo

Geophysical Engineering *Department*

Institut Teknologi Bandung
Bandung, Indonesia

Toni Rahadinata

Geological Resource Center (PSDG)
Bandung, Indonesia

***Abstract* — We present resistivity structure in Mt. Batur geothermal prospect area, Bali Province, Indonesia, derived from Magnetotelluric (MT) data. The study area is located in the Mt. Batur caldera, covered by pyroclastic flow and lava. The survey is set up by 40 MT stations, divided into 5 lines that is perpendicular with the main strike in the study area. In this paper, we show 2-D models of shallow and deeper crustal structure. Our overview is focused on low resistivity area (<10 Ωm) and high resistivity area (> 1000Ωm). Our study reveals two zones of low resistivity area at shallow depth which are attributed to fumaroles and steaming ground located near that area. Meanwhile, the high resistivity area at 4 km depth can be interpreted as intrusion of igneous rock.**

Keywords —Geothermal, Magnetotelluric, 2-D model, Mt. Batur; resistivity

I. INTRODUCTION

Indonesia is located within the ring of fire which caused Indonesia to have numerous of volcanoes. The presence of the volcanoes leads to the source of the geothermal energy which is used as alternative energy. This geothermal energy is environment-friendly energy that provides minimum pollution and low emission compared to other energies such as energy from oil and gas.

Mt. Batur, Kintamani, Bali, is one of the active volcanoes in Indonesia which includes in the ring of fire. Located in Kintamani Regency, this volcano is considered as one of the most active volcanoes in Bali and belongs also to Bali's tourism area. With some surface manifestation and geology information near Mt. Batur, we can assume that there is geothermal system below it.

Some physical parameters studied to image subsurface here are temperature, resistivity, density magnetization, and seismicity. Among these, resistivity method is the most successful methods for studying geothermal sites and they are referred to as direct method.

This resistivity method includes magnetotelluric (MT) method, which is sensitive to resistivity structures beneath. The MT method is a passive-surface electromagnetic geophysical technique that measures variations in the earth's natural electromagnetic field to investigate the electrical resistivity structure of the subsurface from depths to tens of kilometers [6].The method belongs to passive method in the sense that it utilizes naturally occurring geomagnetic variations as the power source. Worldwide lightning activity of frequencies from 10,000 to 1 Hz and geomagnetic micro-pulsations of frequencies from 1 to 0.001 Hz provide the majority of natural signals used by the MT method.

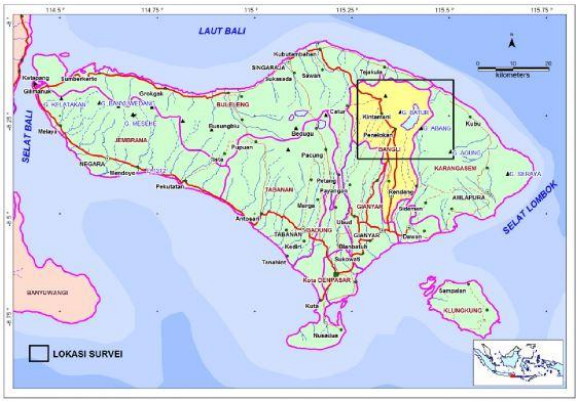

Fig. 1. The squared shape is the area of MT.Batur, Kintamani, Bali

II. SURVEY AREA

Mt. Batur is characterized by Lava Tejakula, steep sided mountains, and ridges of pillow lavas (fig. 1). It also had three times explosion so that it has three calderas. It is located at Bangli regency, Bali province. The main structure at Bali Island is fault that has strike direction mostly oriented to North West – South East with few of it has North East – South West strike direction.

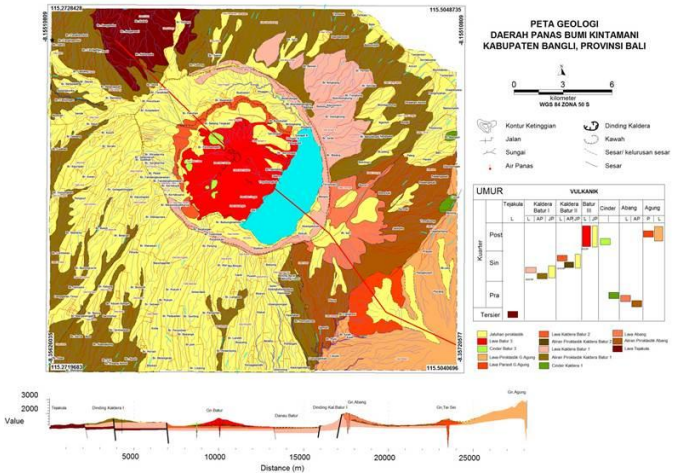

Fig. 2. Mt. Batur Geological Map [5]


Fig. 3. Steaming ground, one of the surface manifestation at the top of Mt.Batur

There are 2 groups of surface manifestation at the top of Mt batur at 2nd crater and 3rd crater. The steaming ground (fig. 3) and the metamorphic rock are located at 2nd crater while the fumarole is located at 3rd crater. The hot spring types as surface manifestation are divided by Boya Bungka Hot Spring group and Songan Hot Spring group.

III. BASIC THEORY

Magnetotelluric is one of geophysical methods that used horizontal component of magnetic field and electric field so that we can observe the vertical variation of earth's electrical conductivity [5]. The magnetic field that used by magnetotelluric method is naturally made by interaction between solar wind and earth's magnetosphere. This interaction causes an electromagnetic fluctuation at the ionosphere and induced earth. The basic concept of MT method is determined by Maxwell's equations.

A. Skin Depth

Electric and magnetic field's variations compared to depth have a limitation. This limit is called skin depth (depth penetration). Skin depth is calculated from real component of wave number (k):

$$k = \sqrt{i\mu_0\sigma\omega} = \sqrt{i}\sqrt{\mu_0\sigma\omega} = \frac{1+i}{\sqrt{2}}\sqrt{\mu_0\sigma\omega}$$
$$= \sqrt{\frac{\mu_0\sigma\omega}{2}} + i\sqrt{\frac{\mu_0\sigma\omega}{2}}$$
$$p(T) = \frac{1}{Re(k)} = \sqrt{\frac{2}{\mu_0\sigma\omega}} \approx 500\sqrt{\rho T} \quad (1)$$

where p(T) is skin depth in meter, ρ is medium resistivity in Ωm and T is period in second.

B. Impedance

Impedance (Z) is a tensor that connecting electric and magnetic field.

$$\vec{E} = \vec{Z}\vec{H} \quad (2)$$

Component of impedance is:

$$\begin{pmatrix} E_x \\ E_y \end{pmatrix} = \begin{pmatrix} Z_{xx} & Z_{xy} \\ Z_{yx} & Z_{yy} \end{pmatrix} \quad (3)$$

C. Impedance of 1D Medium and 2D Medium

In 1D medium, horizontal electromagnetic properties (Ex, Ey, and Hx, Hy) only varies against depth and doesn't have vertical electromagnetic properties.
Impedance for 1D medium described as:

$$Z_{xy} = \frac{E_x}{H_y} = \frac{i\omega\mu_0}{k}\frac{A_x \exp(-kz) + B_x \exp(+kz)}{A_x \exp(-kz) - B_x \exp(+kz)} \quad (4)$$

$$Z_{xx} = Z_{yy} = 0$$
$$Z_{xy} = -Z_{yx} \quad (5)$$

For 2D Medium, the horizontal properties of EM wave differ against lateral condition and depth. Therefore, Simpson and Bahr explain that there are 2 modes of polarization: Transverse Electric (TE mode) and Transverse Magnetic (TM mode). Impedance for 2D medium has a condition:

$$Z_{xx} = -Z_{yy} \text{dan} Z_{xy} \neq Z_{yx} \quad (6)$$

IV. DATA ACQUISITION

We carried out magnetotelluric survey with 40 stations that divided by 5 lines. These lines are perpendicular to the main structure of Mt. Batur which has NW-SE orientation (fig. 5).
The focus area of MT data acquisition is at the location along the side of Batur Lake and at the top of Mt.Batur because of the location of the surface manifestation. We use 2 instruments for this survey, so that we can collect the remote data. The duration of measurement time for each MT station is about 12 until 15 hours for data recording.

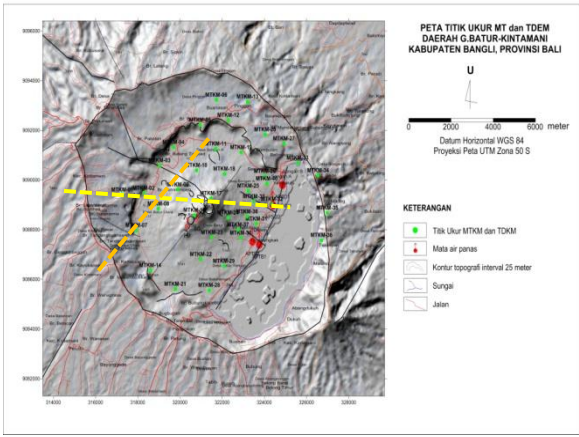

Fig. 4. Station map for MT survey at Mt. Batur, Bali. Orange line is the mark of line 1 and yellow line is the mark of line 2

V. RESULTS AND DISCUSSION

To get the apparent resistivity and apparent phase from the recorded data, we processed it with SSMT2000 program from Phoenix Geophysics. The field data that we get from instrument recording is categorized as time series data, so we have to transform it to frequency series data. This program's main function is the robust process. The step of data field data process on MT survey is described by fig. 5.

Result that generated from robust processing in SSMT2000 program is displayed with MTEditor program. In this program we run the smoothing process. In the smoothing process, we focused on the curve of the apparent resistivity and apparent phase. Fig. 6 shows the course of the raw MT data.

A. 1-D Inversion

Two 1D models were generated using Occam's inversion algorithm. The strategy of the algorithm is to find the solution agreeing with measurement that has the smallest possible roughness. This idea is familiar from the modern methods of data interpolation. There are 2 steps of 1D inversion in WinGlink software: Sounding and X-section.

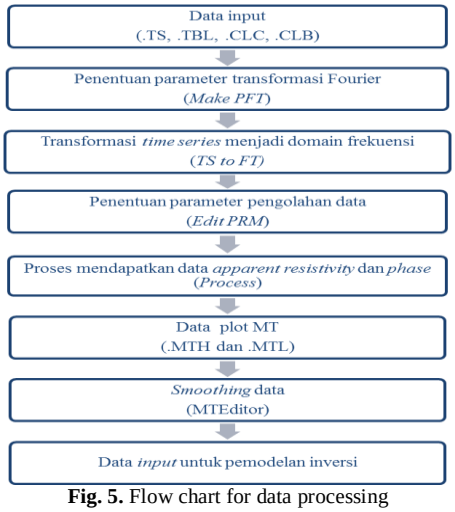

Fig. 5. Flow chart for data processing

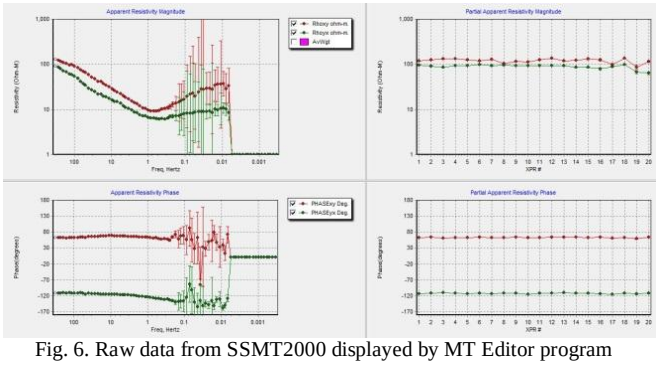

Fig. 6. Raw data from SSMT2000 displayed by MT Editor program

In sounding, 1D Occam models were generated for each station. The iteration for each model is limited by 5 iterations. We use Occam model because it can generate more layer than Bostick model. Fig. 7 shows 1D Occam model from MTKM-09 station for 20 layers.

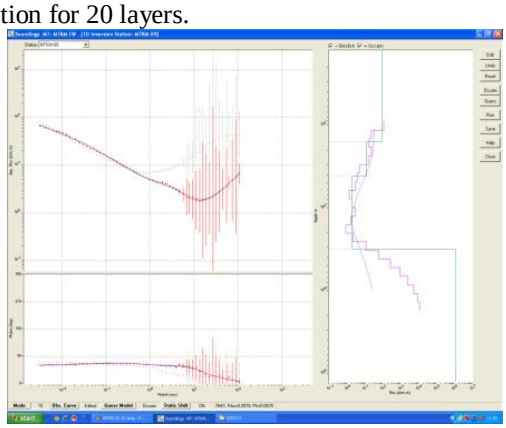

Fig. 7. 1D Inversion at Station MTKM-09

The X-section generates the section for each line of the survey area. Each 1D model that has been generated from sounding step is displayed with color scale. Fig. 8 is the 1D X-section of line 1 and fig. 9 is the 1D X-Section of line 2.

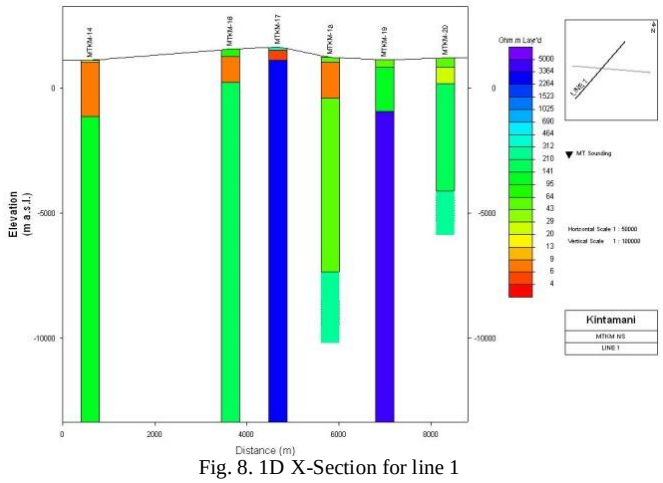

Fig. 8. 1D X-Section for line 1

From 1D inversion X-Section, we can see resistivity value below the surface for each station. In fig. 8, the low resistivity zone shown in station MTKM 14, MTKM 16. MTKM 17 and MTKM 18 have the same range. This low resistivity area may indicate an altered rock. The high resistivity area that displayed at MTKM-17 station in fig. 8 and fig. 9 is matched. Since these 2 lines are approximately perpendicular to eah other, we interpreted this high resistivity area as the intrusion of volcanic rock below Mt.Batur. From 1D model that have been generated, we can not identify the structure below the survey area.

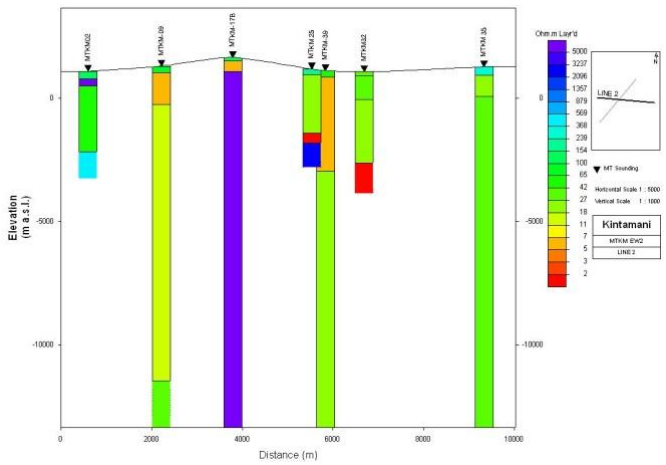

Fig. 9. 1D X-Section for line 2

B. 2-D Inversion

Two 2D models were generated with Non Linear Conjugate Gradient Algorithm (NLCG) [2]. The starting model is a homogenous model with resistivity value of 100 Ωm (fig. 10). We generated model with TE mode and TM mode, and conducted joint inversion of TE and TM mode (fig. 11-16). As we know that TE and TM mode has its own specialty for imaging resistivity value at the subsurface.

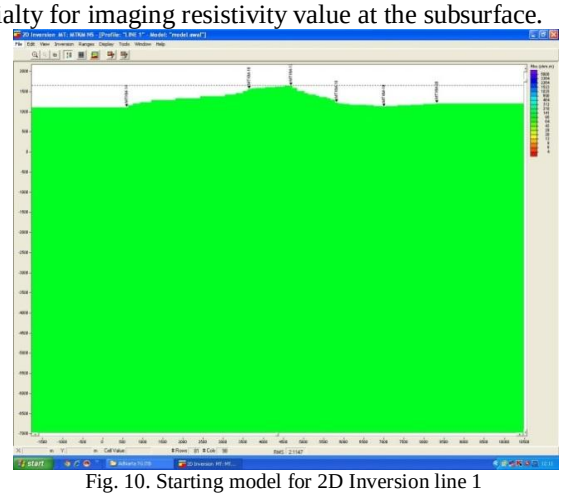

Fig. 10. Starting model for 2D Inversion line 1

The frequency limit for this inversion is 0.01 Hz because the data at the lower frequency is affected with noise. The model is made by 100 times iteration for each model.

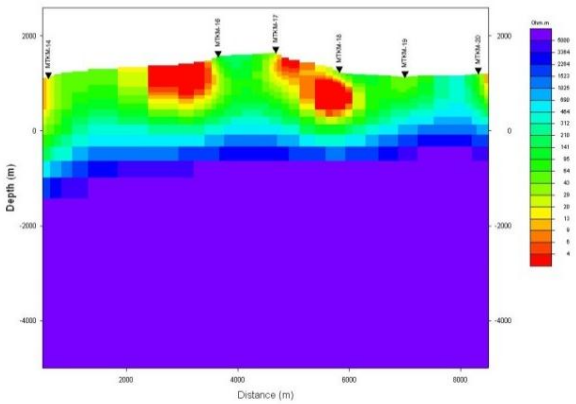

Fig. 11. 2D TE mode inversion model for line 1

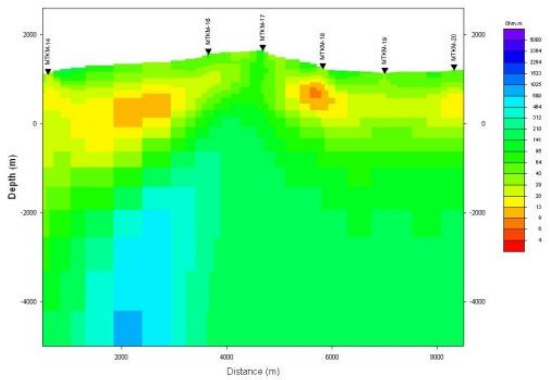

Fig. 12. 2D TM mode inversion model for line 1

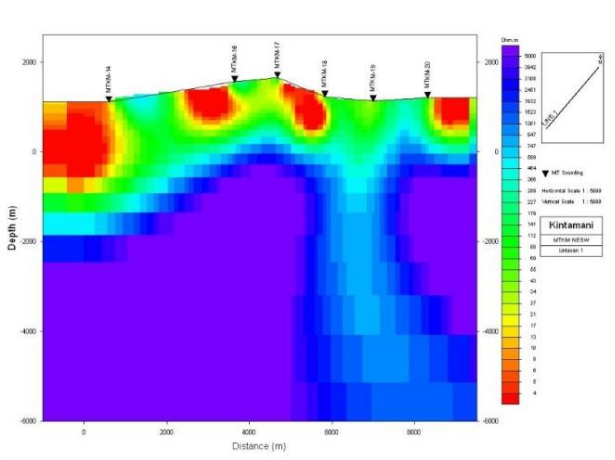

Fig. 13. 2D joint inversion TE and TM model for line 1

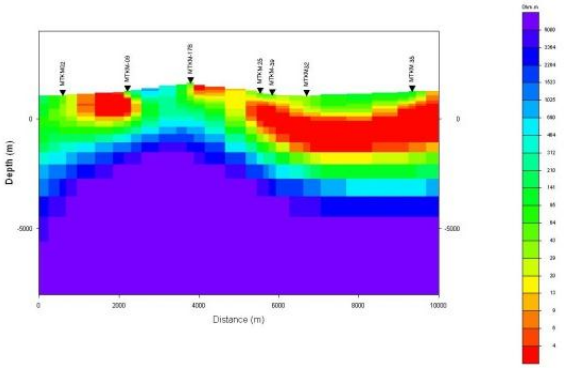

Fig. 14. 2D joint TE mode inversion model for line 2

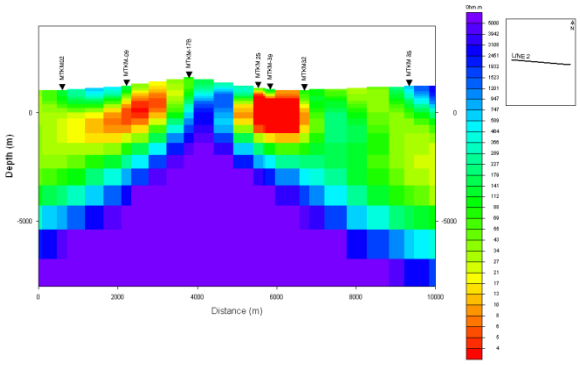

Fig. 15. 2D TM mode inversion model for line 2

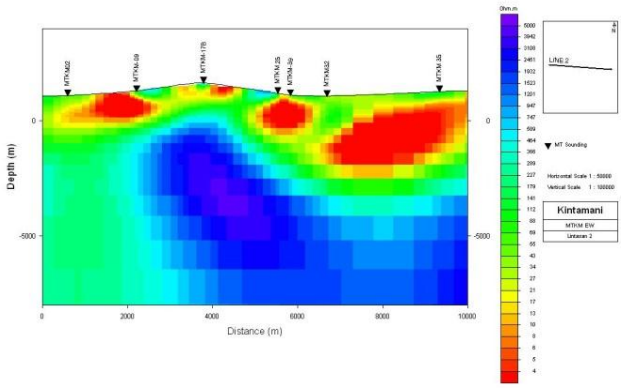

Fig. 16. 2D joint inversion TE and TM model for line 2

C. Discussion and Interpretation

In fig. 17, we made an interpretation for resistivity value at the subsurface below line 1.

We have 6 MT stations at line 1 that provide information about resistivity value at the subsurface until 5 km depth. Line 1 has a steaming ground surface manifestation at the station MTKM-16 near the top of Mt.Batur. The low resistivity area at the depth of 1000 m indicates an altered rock that been heated by the heat source below it. The low resistivity zone that appears below MTKM-16 is discontinued between MTKM-16 and MTKM-17. This anomaly denoted as a fault structure. The low resistivity zone then continued below MTKM-17 until MTKM-18 stations

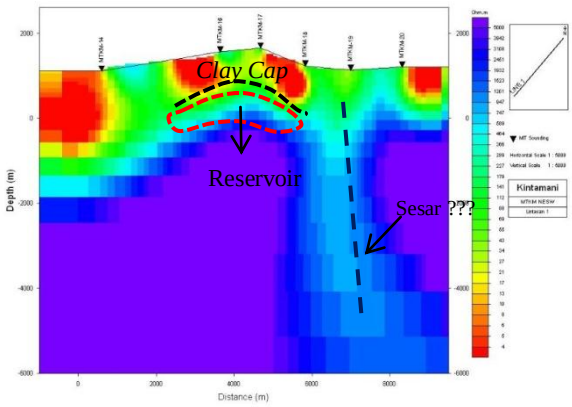

Fig. 17. Interpretation of 2D model for line 1

.The zone with resistivity value between 250 – 300 Ωm is interpreted as the reservoir of the steaming ground at the surface. The discontinued low resistivity zone below MTKM-16 until MTKM-17 stations is interpreted as a fault. This area is also interpreted as reservoir of Mt.Batur's geothermal system. The high resistivity area at depth of 2000 – 5000 m is interpreted as the basement rock of Mt.Batur. This high resistivity anomaly is discontinued below MTKM-19 station and appear again below MTKM-20 station. This discontinue area indicates a fault structure.

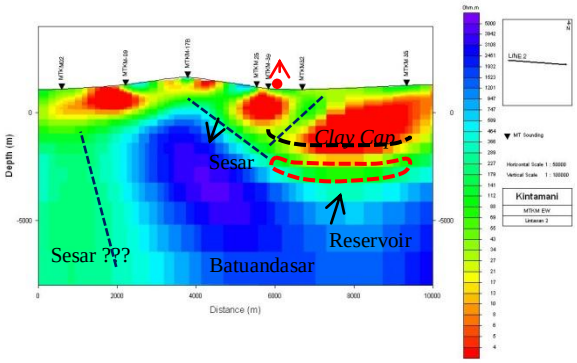

Fig. 18. Interpretation of 2D model for line 2

From the figure 18, we made an interpretation for resistivity value at the subsurface below line 2. There are 7 stations at line 2 that give information about resistivity value at the subsurface until 5 km depth. Line 2 has a Songan hot spring surface manifestation, located between the MTKM-39 and MTKM-32 station alongside of Batur Lake. The low resistivity area with resistivity value between 4 – 8Ωm at the depth of 1000 m with about 500m thickness indicates an association of altered rock that been heated by the heat source below it. This low resistivity area can be indicated as the clay cap of geothermal system at Mt.Batur. This low resistivity area is discontinued below MTKM-39 and MTKM-32 stations. The discontinued zone is associated with fault structure. The area below the low resistivity zone at the depth of 2000 m with resistivity value between 50 – 100 Ωm is associated with reservoir of the Songan hot spring. The high resistivity area at the depth of 2000 – 5000 m below the MTKM-17 station indicates the basement of Mt.Batur that can be associated with rock intrusion.

VI. CONCLUSION

The 2D models from line 1 and line 2 indicate that there is hydrothermal system below Mt.Batur. The clay cap has a resistivity value < 20 Ωm. This layer appears at the depth of 1000 m below the surface with 200 – 500 m thickness. The reservoir of Mt.Batur geothermal system has a resistivity value 50 – 200 Ωm. The top of this reservoir layer is at the depth of 1500 m with 500 m thickness. The high resistivity zone at the depth of 2000 – 5000 m with resistivity value between 1000 – 5000 Ωm indicates the basement of Mt. Batur that associated with rock intrusion. The geothermal prospect area of Mt.Batur is located at Songan Village alongside the Batur Lake. Our study also reveal two zones of low resistivity area at shallow depth which are attributed to fumaroles and steaming ground located near that area. The high resistivity area at 4 km depth can be interpreted as intrusion of igneous rock.

ACKNOWLEDGMENT

A. P. thanks to PSDG for opportunity to be involved involve in its project enabling her to use its result for her final project at the Department of Geophysical Engineering, Institut Teknologi Bandung.

REFERENCES

[1] Cagniard, L., (1953), "Basic Theory of TheMagnetotelluric Method of Geophysical Prospecting", *Geophysics*, 18, 605-635.

[2] Rodi, W., Mackie R.L., (2001), "Nonlinear Conjugate Gradients Algoritm for 2-D Magnetotellurics Inversion", *Geophysics*, 66, 174-187.

[3] Springer, (2012), "Magnetotellurics: Basic Theoritical Concepts", Springer Theses, Springer-Verlag, Berlin Heidelberg

[4] Tikhonov, A.N., (1950), "The determination of the Electrical properties of deep layers of the earth's crust", 73: 295-297.

[5] Tim Survei Terpadu PSDG, (2012), "Laporan Akhir Survei Geologi, Geokimia, dan Geofisika daerah Panasbumi GunungBatur, Kabupaten Bangli, Provinsi Bali", Pusat Sumber Daya Geologi : Bandung.

[6] Vozoff, K. (1991). "The Magnetotelluric Method" in M. N. Nabighian (Ed.), Electromagnetic Methods in Applied Geophysics: Volume 2, Application, Parts A and B (pp. 641-712). SEG. doi: 10.1190/1.9781560802686.ch8

G209

Smart Grid Control with Fuzzy Integrator for Micro Hydro Connected to Low Voltage Distribution PT. PLN (Persero)

Lie Jasa[1], IGA Raka Agung[2], I Putu Ardana[3]
Electrical Engineering Department, Udayana University,
Bali, Indonesia
[1]liejasa@unud.ac.id, [2]puturaka@ee.unud.ac.id,
[3]ardana@ee.unud.ac.id

Ardyono[4], Mauridhy Hery Purnomo[5]
Electrical Engineering Department, Sepuluh Nopember
Institute of Technology Surabaya, Indonesia
[4]priyadi@ee.its.ac.id, [5]hery@ee.its.ac.id

***Abstract*— The capacity of electrical energy supplied by PT. PLN (persero) insufficient to public demand in Indonesia. Micro Hydro Power Plant (MHPP) is a small-scale power plants which relatively easy to developed in remote areas. The generated energy by MHPP must be transmitted to the distribution network. In this study researchers wanted to answer the problems how to make model auto control which connects the MHPP with network distribution of PT.PLN (Persero). The result of this study is MHPP can be auto controlled by controller of I, PI, PID and Fuzzy-I. Smart control of Fuzzy-I controller makes the system to stable with a small overshoot values. It is better than controller of I, PI or PID.**

Keywords— Micro hydro, Energy, Fuzzy

I. INTRODUCTION

Impact of excessive energy use for this is the cause of air pollution, global warming and climate change. Water energy is an environmentally friendly energy source, green, unlimited and renewable nature. All countries in the world today continue to conduct research on water energy, wind and solar, which is used as one of the future energy development policy options. Proven installation of Renewable Energy is currently in parts of the world increased to 30%. [1],[2]

The energy plays an important role for population in the Indonesia. Energy demand is significantly increases every year but the energy resources is limited and decreases. Hydropower [3] is one of clean energy resources in the world. It is also the most reliable and effectively of renewable energy resource. Small hydropower schemes are getting increasingly popular because of its simplicity design, easy in operation, and lower environment.

The energy produced by the micro-hydro power plant (MHPP) should be used by everyone. But the frequency output of MHPP should to match with the frequency of the network distribution PT. PLN (Persero). This research proposes to find model control system about it.

This study focused on discussing the frequency control of the generator mounted on the MHPP to be set for frequency changes (Δf) by using a low voltage reference of PT. PLN(Persero). This control is using fuzzy logic consisting of seven rule member's ship function to control error (*e*) and change of error (*de*).

Block Control of micro hydro set including the components of governor, valves, turbine and generator is made in the transfer function. Fuzzy logic uses to reduce the error from occurring plant using Matlab. Fuzzy logic controller has two input *e* and *de* and one output *u.*

II. LETERATURE REVIEW

A. Hydraulics power theory

Theorem of water flow is used to determine the amount of energy that can be generated from the flowing water. The total extractable hydraulic power from the flowing water is given by the expression of $P_{in} = \rho g Q H$, where Pin is the hydraulic power input to the wheels (W), ρ is the density of water (kg/m^3), g is the acceleration due to gravity (9,81m/s^2), Q is the volumetric water flow rate (m^3/s) and H is the difference in total energy line upstream and downstream of the wheel (m). The angular velocity ω (rad/s) of the wheels is calculated from the number of revolutions N at the given load in revolutions per minute (RPM) of the wheel as: $\omega = 2\pi N/60$. The shaft torque τ (Nm) is the product of the force F of water striking the blades of the water wheel (N) and the moment arm length (m) which, in this case, is the radius of the pulley r. Force is equal to the differences in the mass obtained from the two load cells time the acceleration due to gravity. $\tau = m\ g\ r$. Subsequently the mechanical power output Pout available at the wheel shaft is determined from the measured torque τ and the corresponding angular speed of the wheel ω as : $P_{out} = \omega\ \tau = 2\ \pi\ N\ \tau/60$. By calculating the power of output and input, the mechanical efficiency η of the wheel is therefore: $\eta = (P_{out} / P_{in})100\%$

Automatic control system of micro-hydro is built in a closed loop. First some water are flow in the valve, it continue to the spill way and rotate the turbine.

B. Governor Controller

Control for hydropower plant, hydraulic mechanical governor and electro-hydraulic, PID Controller [4] is used commonly. MHPP in Gambuk, Bali[4],[5],[6] figure 1, without a controller for control the system. Frequency output never stable if load changes. This condition is very difficult when connected with a grid of PT. PLN(Persero).

Figure 1 : Micro Hydro Power Plant

The block control of system micro hydro[7] is set firstly the volume of water that passes through the penstock with a valve . The water from the penstock is to turn a turbine that coupled with the generator. The output of the generator will be paired frequency sensors and compared with a reference frequency of PT . PLN (Persero) . The difference value of frequency will be used by the controller to set the valve again, and so on. As shown in Figure 2

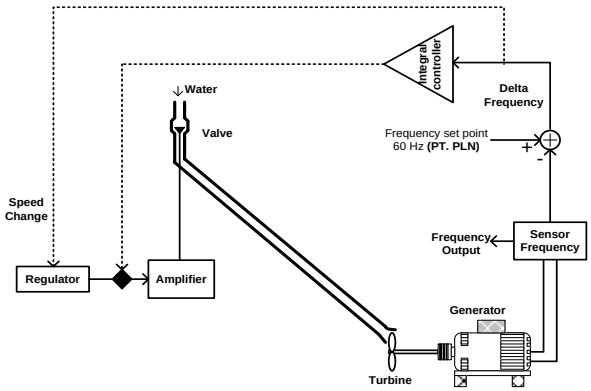

Figure 2 : Design System Control Micro Hydro[5]

C. Micro Hydro Controller

The control system of MHPP been developed in many studies, such as PI control and PID. Everything is based on conventional, because to settings of gain K_i, K_p and K_d by trial and error. In this study the authors emphasize the Fuzzy integrator controller. Alternative controller of MHPP can be choices as shown at figure 3. Where the fuzzy pre-compensation function of regulating of errors that appears before input into the control Integrator.

The equations (1) error as shown in. $y_p = y_{in} - e$ where

$$e = y_{in}-y_p \quad (1)$$
$$e(k) = y_m(k) - yp(k) \quad (2)$$
$$\Delta e(k) = e(k) - e(k-1) \quad (3)$$
$$\mu(k) = Fe(k), \Delta e(k) \quad (4)$$
$$y'_m(k) = y_m(k) + \mu(k) \quad (5)$$

e(k) is the error between the command input $y_m(k)$ and MHPP output $y_p(k)$ and $\Delta e(k)$ is the change in position error. The term $F[e(k), \Delta e(k)]$ is a nonlinear mapping of $e(k)$ and $\Delta e(k)$ base on fuzzy logic. The term $\mu(k) = [e(k), \Delta e(k)]$ represents a compensation or correction term, so that the compensated command signal $y'_m(k)$ is simply the sum of the external command signal $y_m(k)$ and $\mu(k)$.

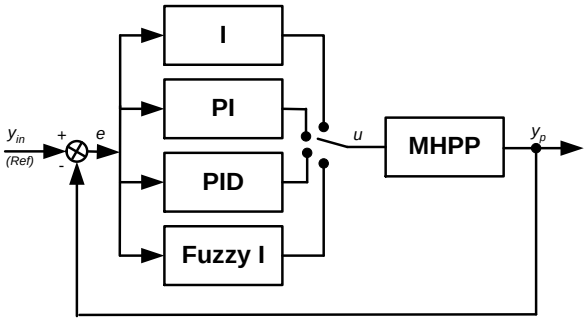

Figure 3 : Alternatif Micro Hidro Controller

The equations governing the I controller are as follows

$$e'(k) = y'(k) - yp(k) \quad (6)$$
$$u(k)=u(k-1) + kie'(k) \quad (7)$$

y_{in} is input reference y_p is output frequency and e is error. Controller changes a value of error until zero or a very small value.

D.Fuzzy Pre-Compensated I C ontroller

Pre-compesated[8] of hybrid fuzzy I controller, was developed to combine the advantages of I controller and fuzzy pre-compesated fuzzy controller. The quantity $e'(k)$ is the pre-compenseted position error between the pre-compenseted position error input $y_m'(k)$ and MHPP output $y_p(k)$, and $\Delta e(k)$ is the pre-compensanted position error. As shown in Figure 4 bellow .

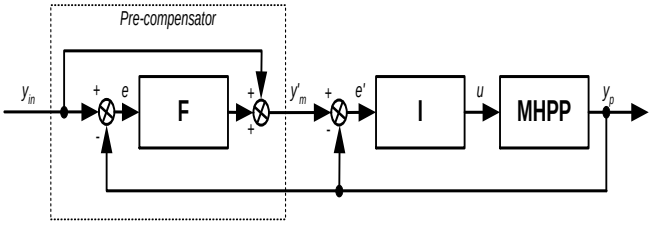

Figure 4 : Block Diagram of Fuzzy Pre-compensated I controller.

D.Data Simulation of MHPP Plants

Data simulation in this paper uses combination data research, total rate capacity change from 50 KW to 5 KW, the normal operating load of 25 KW was changed to 1 KW. This is done to adjust with the existing MHPP plant, detail as shown in Table 1.

Table 1. Data plant MHPP simulation

No	Data	Value
1.	Total rated capacity	5 Kw
2.	Normal Operating Load	1 Kw
3.	Inertia Constant H	7.75 seconds (2<H<8)
4.	Regulation R	10 Hz/pu kW (2<R<10)

Assumption:[5],[9] Load-frequency dependency is linier. Nominal Load = 48%=0.48; ΔPd =3%=0.03. The dumping parameter [4,7],

$$D = \partial p/\partial \quad D = \partial p/\partial \frac{f = 0.48x1}{60x5} = 0.0016\, pukW/Hz$$

Generator parameters are:

Kp = 1/D = 625 Hz/pu kW

$$Tp = \frac{2xH}{f^{0}xD} = 161{,}458\,\text{sec}onds$$

All data of gain parameter use for simulation controller I, PI, PID and Fuzzy-I shown in table 2

Table 2. Data gain simulation

Controller	K_p	K_i	K_d
I	-	-0.00003	-
PI	0.0555	-0.0021	-
PID	0.042156	-0.003253	0.0000246
Fuzzy I	-	0.00075	-

III. FORMULATION OF PLANT MODELS FOR MHPP PLANT

A. PI-PID Controller of Micro Hydro

` The block diagram of the MHPP[9] Plant with PID-Controller is shown in Figure 5. The PID-Controller with the following transfer function is superimposed on the servomotor based governor as $G(s)=K_p+K_i/s+K_d$ s, Where it's K_p = proportional constant, K_i = integral constant and K_d = derivative constant.

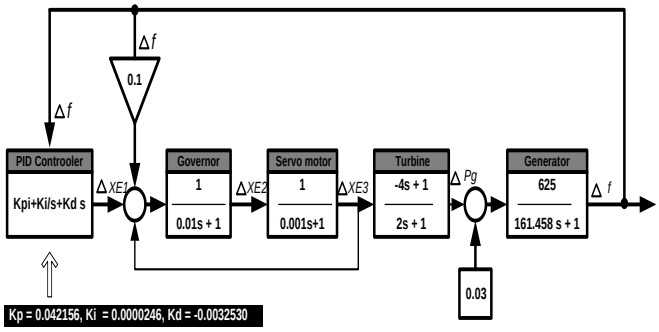

Figure 5. Models of MHPP plant with PID-Controller

B. I-Fuzzy Controller of MHPP

Control model MHPP with pre-compaseted Fuzzy[10],[11],[12],[13],[8] as in Figure 4, is made with blocks model transfer function can be simulated with Matlab. The block Fuzzy logic has a rule 28 with a combination of NB, NM, NS, ZE, PS, PM, PB with membership fucntion as shown in Figure 6.

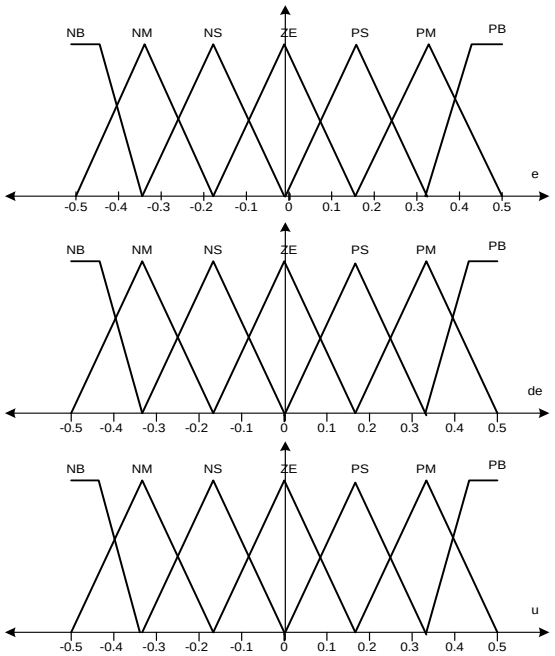

NB : negative big; NM : negative medium; NS: negative small; ZE : zero; PS: positive small; PM : Positive Medium; PB: positive big

Figure 6. The Fuzzy sets of a pre-compensator

Table 2. Fuzzy Rules of Pre-compensator

e \ de	NB	NM	NS	ZE	PS	PM	PB
NB		NB		NB	NM		
NM				NM	NM		
NS				NS	PS		PM
ZE	NB	NB	NM	ZE	PS	PM	PM
PS	NB	NB	NM	PS	PM	PB	PB
PM			NM	PM		PB	
PB			PM	PB			

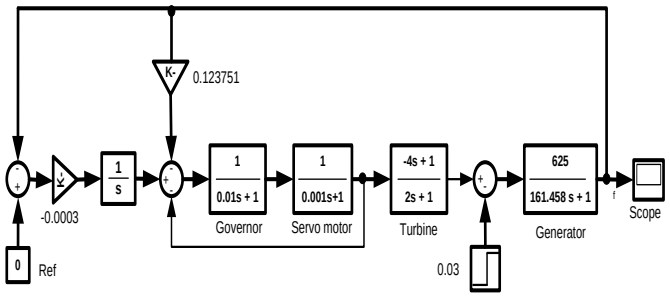

Figure 7. Blok simulation I-control of MHPP

IV. SIMULATION RESULT

Simulation Matlab of MHPP was run to use parameter table 1. Controller of MHPP was replaced by the controller of I, PI, PID and Fuzzy I. Simulation results show that for the I-controller the system stabilized at t = 300 seconds, with overshot between 0 - 0.1 Hz but the system never to the setting point = 0, a decrease of 0.003 Hz.

For the PI controller with K_i = -0.0021 and K_p = 0.0555 showed the system stable at t = 50 with overshoot about 0 to 1.2 Hz. System toward to the setting point 0 Hz. PID controller results with the parameters K_i = -0.003230, K_p and K_d = 0.042156 = 0.0000246 showed the system to be stable at t = 49 seconds with overshot between 0 to 1.1 Hz. System toward to the setting point 0 Hz .

If MHPP using Fuzzy controller-I with parameters K_i = 0.0075 system will be stable at t = 450 with overshoot occurs between 0.01 -0.1 Hz, and the system toward to the setting point 0 Hz. All graph of simulation results can be seen in the figure 9,10,11 and 12.

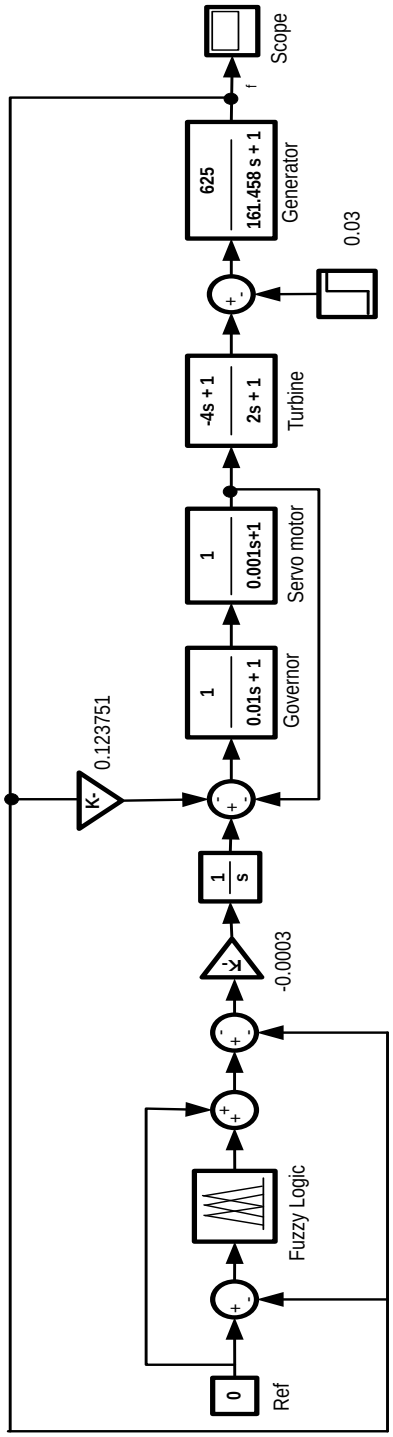

Figure 8. Models of MHPP using fuzzy Controller

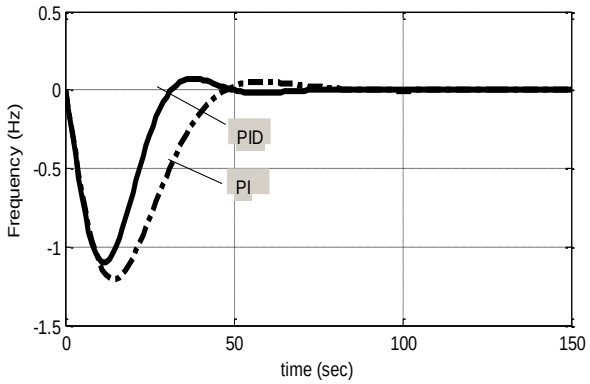

Figure 9. Ouput Δf PI and PID Controller

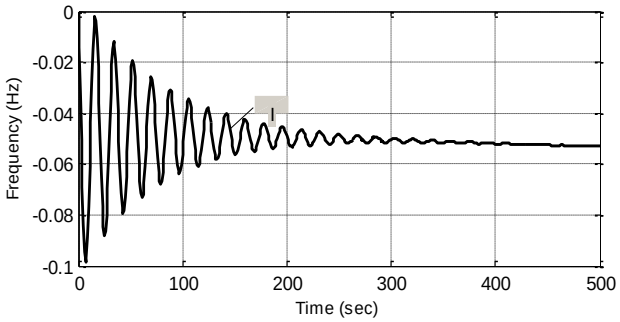

Figure 10. Output Δf of Integrator

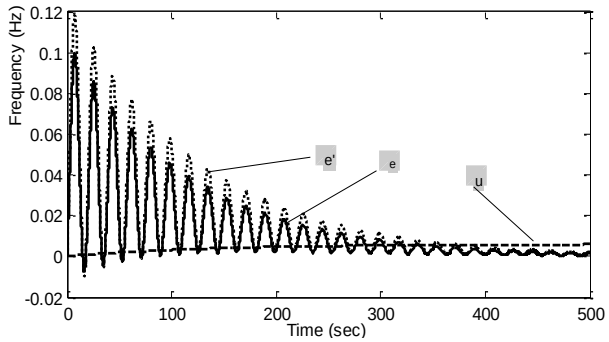

Figure 11. Comperation error controller of Fuzzy I

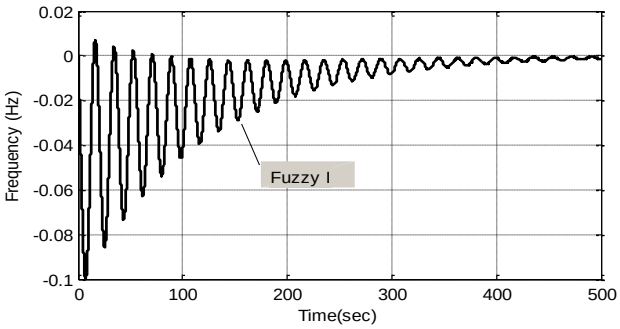

Figure 12. Output Δf of Fuzzy I

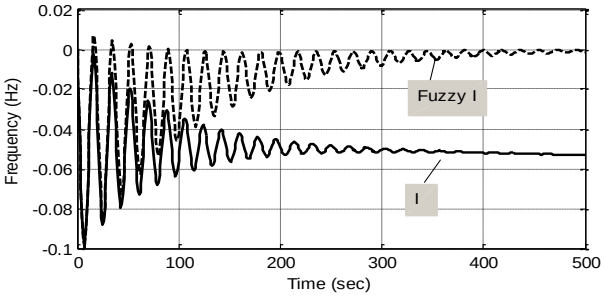

Figure 13. Comperation Output I and Fuzzy I

Comparison between I and Fuzzy-I controller indicates that the value of overshot is almost the same between 0.01 to -0.1 Hz. But with I-controller was system stable 100 seconds faster than the Fuzzy-I, but the system didn't going to the reference point. While Fuzzy-I controller system stable at t = 400 seconds, but the advantage is directly to the setting point.

V. CONCLUSION

MHPP can be controlled with models controller I, PI, PID and Fuzzy-I. Parameters of gain control each controller will be found by with trial and error until is found the system stable. PID controller have the parameters Ki , Kp and Kd, to make a PI controller to eliminate the Kd parameters, but the value of Ki and Kp must be settings again. If making I-controller with to eliminate the parameters of Kp and a value of Ki but must be set back. MHPP plant system is stable with the controller I at Ki = -0.00004, with a PI controller is Ki = 0.0555 and Kp = -0.0021. While the system stable with PID controller is obtained at Ki = -0.003253, Kp and Kd = 0.042156 = 0.0000246.

To build the Fuzzy-I controller, the controller I, is added a pre-Compensator which setting directly by the 28 rule of fuzzy. The results obtained the Fuzzy-I controller was able to make the system MHPP stable at setting point and overshoot values relatively small compared with PI and PID.

ACKNOWLEDGMENT

This research was supported by (1). The Ministry of Culture and Education, under LPPM Udayana University, scheme Research of Unggulan Udayana funding BOPTN 2013. Contract number: 175A.4/UN14.2/PNL.01.03/2013, date 16 Mei 2013. (2). We use Matlab and Simulink licensed for Institut Teknologi Sepuluh Nopember with license number 26833-15780-30897-48803. (3). Muhammad Abdillah from Hiroshima University, Japan that helps found model of control.

REFERENCES

[1] T. H. Ching, T. Ibrahim, F. I. A. Aziz, and N. M. Nor, "Renewable energy from UTP water supply," in *2011 International Conference on Electrical, Control and Computer Engineering (INECCE)*, 2011, pp. 142 –147.

[2] T. Sakurai, H. Funato, and S. Ogasawara, "Fundamental characteristics of test facility for micro hydroelectric power generation system," presented at the International Conference on Electrical Machines and Systems, 2009. ICEMS 2009, 2009, pp. 1 –6.

[3] T. Niimura and R. Yokoyama, "Water level control of small-scale hydro-generating units by fuzzy logic," in , *IEEE International Conference on Systems, Man and Cybernetics, 1995. Intelligent Systems for the 21st Century*, 1995, vol. 3, pp. 2483–2487 vol.3.

[4] L. Jasa, P. Ardana, and I. N. Setiawan, "Usaha Mengatasi Krisis Energi Dengan Memanfaatkan Aliran Pangkung Sebagai Sumber Pembangkit Listrik Alternatif Bagi Masyarakat Dusun Gambuk –Pupuan-Tabanan," in *Proceding Seminar Nasional Teknologi Industri XV*, ITS, Surabaya, 2011, pp. B0377–B0384.

[5] L. Jasa, A. Priyadi, and M. Hery P, "PID Control for Micro Hydro Power Plants Base on Neural Network," in *Proceding Modeling, Identification and Control (AsiaMIC 2012)*, Phuket, Thailand, 2012.

[6] L. Jasa, A. Priyadi, and M. H. Purnomo, "Designing angle bowl of turbine for Micro-hydro at tropical area," in *2012 International Conference on Condition Monitoring and Diagnosis (CMD)*, 2012, pp. 882 –885.

[7] M. Djiteng, *Pembangkitan Energi Listrik*. Jakarta: Erlangga, 2005.

[8] P. Pratumsuwan and C. Thongchaisuratkrul, "Pre-compensation for a Hybrid Fuzzy PID Control of a Proportional Hydraulic System," *www.Intechopen.com*, pp. 202–218, Apr. 2011.

[9] M. Hanmandlu, H. Goyal, and D. P. Kothari, "An Advanced Control Scheme for Micro Hydro Power Plants," in *International Conference on Power Electronics, Drives and Energy Systems, 2006. PEDES '06*, 2006, pp. 1 –7.

[10] E. Özbay and M. T. Gençoğlu, "Load frequency control for small hydro power plants using adaptive fuzzy controller," in *2010 IEEE International Conference on Systems Man and Cybernetics (SMC)*, 2010, pp. 4217–4223.

[11] B. Anand and A. E. Jeyakumar, "Load Frequency Control of Interconnected Hydro-Hydro System with Fuzzy Logic Controller," in *2011 International Conference on Process Automation, Control and Computing (PACC)*, 2011, pp. 1–4.

[12] M. Abdolmaleki, P. Ansarimehr, and A. M. Ranjbar, "A robust fuzzy logic adaptive PI controller for hydro power plants," in *SICE, 2007 Annual Conference*, 2007, pp. 2592–2595.

[13] T. Hiyama, S. Oniki, and H. Nagashima, "Evaluation of advanced fuzzy logic PSS on analog network simulator and actual installation on hydro generators," *Ieee Trans. Energy Convers.*, vol. 11, no. 1, pp. 125–131, Mar. 1996.

G210

A Building Audit Software to Support Energy Management and Conservation

Rini Nur HASANAH, Hadi SUYONO
Electrical Engineering Department
Faculty of Engineering
Brawijaya University
Malang, Indonesia
rini.hasanah@ub.ac.id, hadis@ub.ac.id

WIJONO, Moch DHOFIR
Electrical Engineering Department
Faculty of Engineering
Brawijaya University
Malang, Indonesia
wijono@ub.ac.id, dhofir@ub.ac.id

***Abstract* - Energy audit is one of the plausible efforts to do in energy conservation. This article describes the design and development of a tool being purposed to help in analyzing energy audit data of a building. Some requirements to provide for the success of the task include the knowledge of audit data parameters as well as their computation procedures, the mastering of the programming language to be used, and also logical analysis and criticism to the results of program codes execution. Visual C++ under Visual Studio Integrated Development Environment (IDE) of Microsoft is used as the programming language. Data of four categories of buildings, representing university-, religious-, junior high school-, and kindergarten-buildings are used. The obtained results show that using the chosen programming language and development environment, instruction codes should be grouped as declaration files containing the definition of variables and prototypes names to be used, and implementation files containing the detail instructions to execute. The resulted execution time of the program is relatively fast, with a reasonable tendency to become longer when the available data amount to be processed is larger. The resulted practical software will generally be useful to facilitate the analysis of a building energy audit data, because it covers most measures and analyses to be performed in an energy audit. Moreover, it can also be useful to give an understanding on how energy is used in buildings as well as how to identify opportunities to reduce energy consumption and furthermore to contribute to energy conservation efforts.**

Keywords— building energy audit; software; energy conservation

I. THE IMPORTANCE OF ENERGY AUDIT

Indonesia is a country with large potential of energy resources, but its people's access to energy is still limited. Therefore, the concern of sustainable development must always be borne in mind when taking decision and policy concerning national energy and natural resources management.

In 2011, the president of the Republic of Indonesia issued a legal instruction to save water and energy. In 2012, the Minister of Energy and Mineral Resources issued two regulations, the one dealing with Electrical Energy Saving whereas the other with Management.

Ministry of Energy and Mineral Resources of the Republic of Indonesia enacted all users of energy and energy sources with consumption of energy in all forms greater than or equal to 6000 tonnes of oil equivalent (ToE), or equivalent to 69780 megawatt-hour (MWh) per year, to undertake energy conservation through energy management.

The energy conservation should be done by assigning an energy management, preparing energy conservation programs, carrying out regular energy audits, implementing recommendations resulted from energy audit, and reporting the implementation of energy conservation annually to the Minister, Governor, or Regent/Mayor in accordance with their respective authorities [1].

Energy audits become a very important activity in any energy management strategy. It is stated that energy management must be done by a competent and certified person, and that the audit on the main energy utilization must be conducted on a regular basis at least once every three years.

Meanwhile, the number of certified auditors is still limited compared to the number of buildings to be audited. Audits cost is also expensive, especially if it is desirable to obtain a certified audit results. For organizations/ institutions/large industry with consumption of energy/energy sources exceeding 6000 ToE, which are obliged to conduct energy management and conservation, the audit cost may not be a big problem compared to the possibility of savings that can be obtained, but for users of energy/energy sources less than 6000 ToE which are not required to perform the conservation measures, the audit cost could become a considerable amount being compared to the potential savings to get.

In this paper the design and development of energy audit software is described. The use of software is expected to ease the process of calculation and analysis of the possible energy waste, thus allows to obtain the information about the energy consumption in a building becoming the audit object, possible

waste of resources, and the selection of alternative recommendations to be implemented so that the waste can be reduced or even eliminated. Its use will also be able to reduce the required time and cost of the audit. Furthermore, the results can be used in the implementation of energy management, i.e. the planning of energy conservation program, as well as to increase awareness of users and operators of energy/energy source.

The specific objective of this paper is to describe the design of energy audit parameters algorithm, then its implementation using Visual Studio/Visual C++, to result in an energy audit tool in the form of practical software that is easy to use and interactive for users, so it does not require its use by someone who is already expert and experienced.

II. Energy Audit Data Analysis Tool

In an energy management, to reduce the negative impact of limited generation and transmission capacity, the efforts can be directed to the improvement of efficiency on the load side, known as Demand Side Management [2]. In practice, an in depth audit of all electrical equipments used is necessary.

Energy audits become a very important activity in any energy management strategy. As a consequence, the methodology associated with the improvement of efficiency also becomes very important. However, manual methodologies generally take a long time, more error-prone, and require highly skilled personnel actors [2]. Special technical expertise is needed to enable one to perform an audit on a building efficiently [3].

Accordingly, some researchers have proposed various methods and auditing tools [2-11]. Merwe, et al. (2011) proposed an energy audit tool development to improve the audit process using the methodology for calculating the energy usage profiles at various loads, as well as comparing it to theoretical result.

IEEE Standard 739-1995 can be used as a technical manual in the implementation of energy conservation [12]. This standard provides procedures and techniques that enable the optimization of efficiency in the design and use of any electrical system, taking into account all the aspects (safety, cost, environment, management needs, and so on).

A energy audits software tool was proposed by Prudenzi, et al. (2008). The software is designed and implemented in order to support every step in the implementation of a complete and thorough audit with a focus on energy use in buildings [3].

Maricar, et al. (2005) proposed the use of a web-based application for data mining models for the audit process in the industry [4].

Computational tools proved to be a valuable asset in the field of engineering. Melki, et al. (2009) proposed to design and build software which allows for the simulation and analysis of energy use in a building [5].

Based on the experience already gained by the authors as well as the results of researches previously described, it is known that there are not many energy audit software tools which are specifically dedicated to the type of load as well as standards and regulations applicable in Indonesia [13-14]. Therefore it is purposed in this paper to describe such kind of audit tool. Started with the design of algorithms for an energy audit, followed with the development of the algorithms to results in a software tool, it is tested using the data obtained from the previous audit experience of the authors.

In the future, the software tool can be extended to consider much higher level of complexity of energy/energy sources as well as greater utilization capacity of energy/energy sources.

III. Design and Development Methodology

To design and develop an energy audit software, it is necessary to master the following aspects thoroughly, i.e. the audit data parameters of a building as well as their computational procedures, the logical analysis and criticism to the results of program running, and also the programming language to be used. It begins with the design of algorithms, being followed with its implementation, and then the testing.

The complete steps in designing energy audit software is described in Fig. 1, started with the requirements/specification determination, ended with the maintenance step to correct any error appearing during utilization.

The algorithms design is based on several alternative sequences of steps that could be undertaken in the implementation of a detailed energy audit, as well as tested using data from the audit as ever conducted by the authors at multiple institutions/government agencies [13-14]. So, it becomes imperative to understand and to know the audit process on each system in a building [15].

In general, the audit software includes some blocks that represent the user, output, and also database and data processing blocks. These blocks can be classified into three layers, i.e. presentation layers, business layer, and data layer.

Presentation layer becomes the interface between the business layer and the user. In this layer user can entry some input data, as well as retrieve some output data resulted from the business layer.

The business layer contains the engines used to process data located in the data layer. The engines constitute ‘the brain’ of the software. It is in these engines where all definitions of audit parameters and the procedures to compute them are intertwined to process the data located in the data layer.

In the research the results of which are presented in this article, Microsoft Visual Studio, an integrated development environment (IDE) from Microsoft, has been used to develop console and graphical user interface of this application. The programming language used is Visual C++ which is also supported by Visual Studio.

A set of code files and other resources which are used to build an application is called as solution in Visual Studio. The files in a solution are arranged hierarchically, which might or might not reflect the organization in the file system. The

Solution Explorer, as can be seen in Fig. 2, is used to manage and browse the files in a solution. It provides with an organized view of projects and their files as well as ready access to the commands that pertain to them.

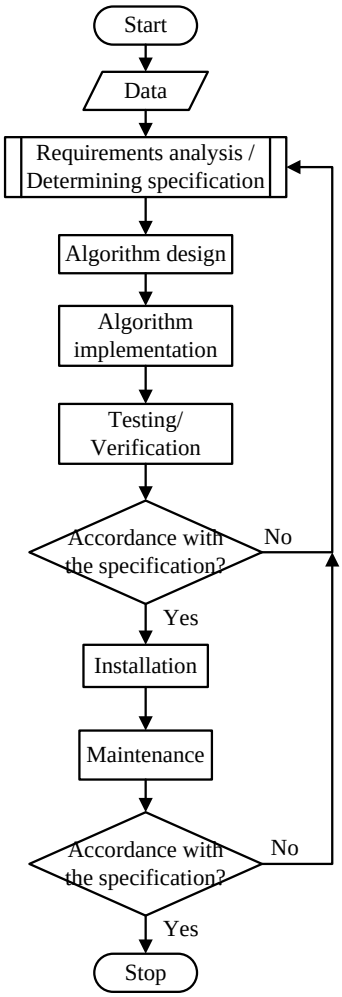

Fig. 1. Steps to follow in designing energy audit software

.

A set of code files and other resources which are used to build an application is called as solution in Visual Studio. The files in a solution are arranged hierarchically, which might or might not reflect the organization in the file system. The Solution Explorer, as can be seen in Fig. 2, is used to manage and browse the files in a solution. It provides with an organized view of projects and their files as well as ready access to the commands that pertain to them.

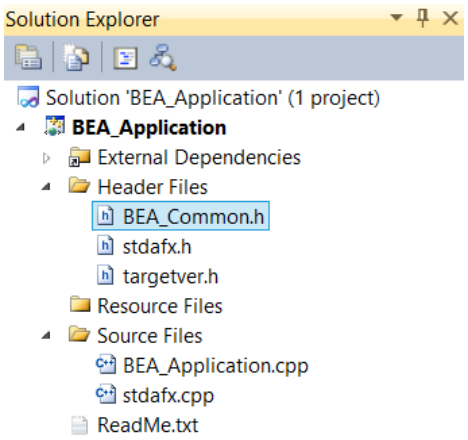

Fig. 2. *Solution Explorer* of Microsoft Visual Studio

Two folders mainly used to write the source codes of application are the Header Files and Source Files. All files in the Header Files folder have an .h suffix, identifying them as header files, whereas in the Source Files folder the files posses a .cpp suffix, even though both of those qualify as source code. A .cpp file is commonly called as an "implementation file", whereas a header file is called as a "declaration file". The main reason would be for separating the interface from the implementation. The header declares "what" a class (or whatever is being implemented) will do, while the cpp file defines "how" it will perform those features.

The separation reduces dependencies so that code that uses the header doesn't necessarily need to know all the details of the implementation and any other classes/headers needed only for that. This will reduce compilation times and also the amount of recompilation needed when something in the implementation changes.

A .cpp file includes the definitions from any header which it includes (because .cpp and header file together become a single 'translation unit'). A header file might be included by more than one .cpp file. The linker typically won't like anything defined in more than one .cpp file. Therefore any definitions in a header file should be inline or static. Header files also contain declarations which are used by more than one .cpp file.

Definitions that are neither static nor inline are placed in .cpp files. Also, any declarations that are only needed within one .cpp file are often placed within that .cpp file itself, instead of in any (sharable) header file.

IV. Results and Discussion

Some declarations and definitons are put in the Header Files, an example of which is shown in Fig.2, BEA_common.h. The source codes in this folder are aimed at defining global variables and the name of prototype functions. Header Files contain information that defines the fundamental Visual C++ codes the project relies on. The files in this folder along with the .dll files will be supplied to the executable files.

As can be seen from Fig. 3, there are no further detailed procedures describe in the source codes.

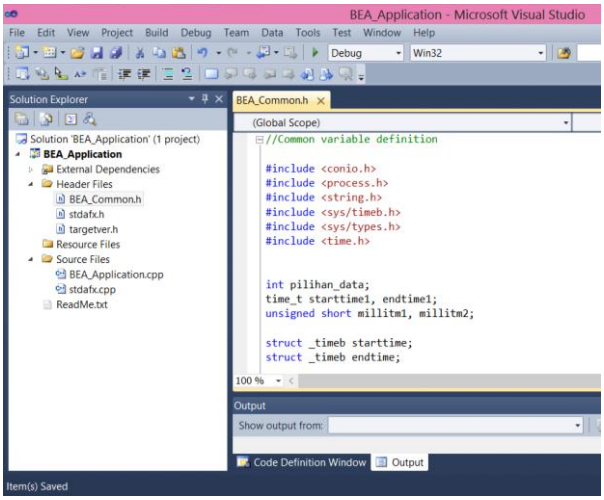

Fig. 3. Display of file source code in the Header Files folder

In Fig. 4, some function definitions are shown, the procedures of which are detailed in the source codes in the Source Files folder.

```
//Functions definition
void Input_Data(void);              //inputting data
void Klasifikasi_Gedung(void);      //determining classification of building
void Display_Data(void);            //displaying data
void Hitung_Rekening(void);         //calculating bill
void Display_Hitung_Rekening(void); //displaying results of bill calculation
void Hitung_Luas_Gedung(void);      //calculating building area
void Display_Luas_Gedung(void);     //displaying result of building area calculation
void Hitung_IKE(void);              //calculating ECI of building
void Display_Hitung_IKE(void);      //displaying result of building ECI calculation
```

Fig. 4. Example of global variable definitions and the name of prototypes in Header Files

In Fig. 5, the detailed procedure on how to calculate the building area is presented. It is more detailed than just the definition of function in Fig. 4.

```
void Hitung_Luas_Gedung(void)
{
    //Calculating the area and volume of the building
    tot_L_gedung = 0.0;     //total buildng area
    tot_V_gedung = 0.0 ;    //total building volume

    for(int i = 1; i<=tot_lantai; i++){
        L_gedung[i] = p_gedung[i]*l_gedung[i];
        V_gedung[i] = p_gedung[i]*l_gedung[i]*t_gedung[i];
        tot_L_gedung = tot_L_gedung + L_gedung[i];
        tot_V_gedung = tot_V_gedung + V_gedung[i];
    }
}
```

Fig. 5. Source code in the Source Files folder

The whole required functions are to be run in the main program, as can be seen in Fig. 6. Using four representative buildings, the data to be processed are classified into four choices of data that must be chosen by the user.

```
Choose the desired building data:
1. Data of University Building (TEUB)
2. Data of Mosque Building
3. Data of Junior High School Building
4. Data of Kindergarten Building
```

Fig. 6. Running the .cpp file, displaying Choice of building data to process

Using the data comparison shown in Table I, the utilization of the designed software has been shown. Fig. 7 and 8 show the example of results of program running.

TABLE I. DATA COMPARISON OF CASE 1 AND CASE 4

Case	Case 1	Case 4
Amount of floors, Amount of meters	2 3	1 1
Building dimensions of each floor, L, W, H	15.00 10.00 4.00 12.00 10.00 4.50	16.00 10.00 6.00
ID meters, Power capacity (VA), Amount of monthly bills	1469096157 105000 12 1469096337 105000 12 1469096346 105000 12	2039539034 1300 12

Fig. 7 is the result when the data are taken from the university building sample (Case 1), whereas in Fig. 8 the data are from the Case 4 (Kindergarten building). The calculation results of buildings area are presented. These results are obtained from the execution of the related procedures detailed in .cpp files, with definitions and functions which are declared in the header files.

A part of the results shown in Fig. 7 and 8 gives the calculation results of area and volume of the buildings, the total energy used, its related bill already paid, the index of energy consumption, and also the potential saving being compared to standard.

```
Calculation of Building Area and Volume
-----------------------------------------------------
| Floor # | L (m) | W (m) | H (m) | A (m2) | Vol (m3) |
-----------------------------------------------------
|  1 | 15.00 | 10.00 | 10.00 | 150.00 | 600.00 |
|  2 | 12.00 | 10.00 | 10.00 | 120.00 | 540.00 |
-----------------------------------------------------
| Total | 270.00 m2 | 1140.00 m3 |
-----------------------------------------------------

ECI and IRPE of Building
-------------------------------------------
Total kWh of Building    : 393555.00 (kWh)
Total Rp of bill of Building     : 528150784.00 (Rp)
Total Building Area      : 270.00 (m2)
ECI of building          : 1457.61 (kWh/m2)
IRPE of building                 : 1956114.00 (Rp/m2)
Standard of Minimum ECI : 210.00 (kWh/m2/th)
Standard of Maximum ECI : 285.00 (kWh/m2/th)
Saving ECI Minimum       : 1247.61 (kWh/m2/th)
Saving ECI Maximum       : 1172.61 (kWh/m2/th)
-------------------------------------------
Start Milliseconds: 233
End Milliseconds: 631
Milliseconds Execution Time: 398
```

Fig. 7. Results of program running for Case 1

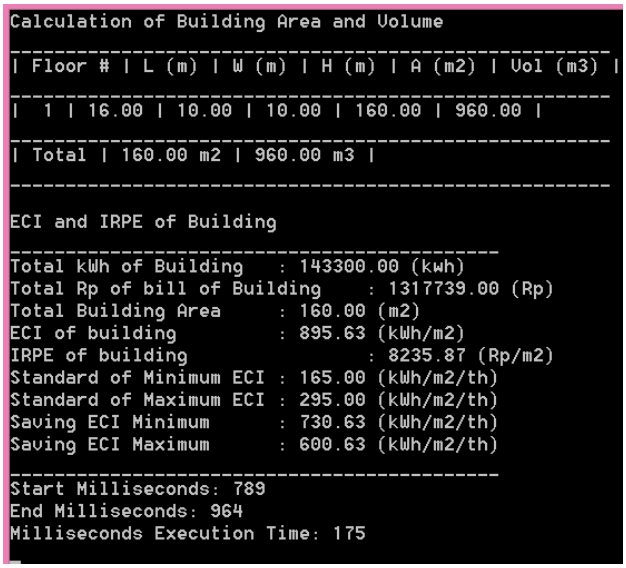

Fig. 8. Results of program running for Case 4

The execution times of both Case 1 and Case 4 are very different, as the amount of data to be processed in Case 1 is higher than that in Case 4, as can be seen from Table II. There are three kWh-meters at the building 1, but only one kWh-meter at the building 4.

The audit software helps in simplifying and reducing the time and cost of energy audit. The results of the study will generally useful to facilitate the analysis of the energy audit, because the resulting practical software covers most measures and analyzes to be performed in an energy audit. Moreover, it gives also an understanding on how energy is used in buildings as well as on how to identify opportunities to reduce energy consumption.

TABLE II. RESULTS OF EXECUTION TIME TESTING

Running no.	Case 1	Case 2	Case 3	Case 4
1	210	120	150	140
2	250	140	110	150
3	270	180	140	130
4	220	160	110	130
5	230	150	150	140
6	280	150	150	120
7	290	140	160	150
8	300	140	140	150
9	240	90	120	110
10	280	90	140	110
Average	257	136	137	133

The audit software helps in simplifying and reducing the time and cost of energy audit. The results of the study will generally useful to facilitate the analysis of the energy audit, because the resulting practical software covers most measures and analyzes to be performed in an energy audit. Moreover, it gives also an understanding on how energy is used in buildings as well as on how to identify opportunities to reduce energy consumption.

V. CONCLUSIONS AND PERSPECTIVES

From the design and development of building energy audit software described in this article, some conclusions can be drawn as follows:

- Processing energy audit data is far easier and faster with the help of a computing tool.
- A computing tool in a form of energy audit software can be designed and built based on the parameters to determine and the corresponding required audit data.
- Recommendations to improve the energy efficiency can be proposed to the energy manager/decision maker based on the implementation results of the software on the available energy audit data.

The design and development of the audit software can also be used to identify potential priorities of measures for energy conservation and savings opportunities, either from the maintenance and operation at a low cost or even no cost at all.

Especially for the industrial/business and trade sectors, in addition to comply with government regulations related to the obligation to conduct an energy audit, it would also be beneficial to reduce the energy cost, which will furthermore reduce the operation and production cost, which can result in an increased profit margins to be gained or product competitiveness in the market.

ACKNOWLEDGMENT

The authors would like to thank the Directorate General of Higher Education of the Ministry of Education and Culture of the Republic of Indonesia through the Brawijaya University for having financed the research, the results of which are presented in this article.

REFERENCES

[1] Anonymous, Indonesian Government Regulation on Energy Conservation No. 70 Year 2009, "*Peraturan Pemerintah Republik Indonesia No. 70 Tahun 2009 tentang Konservasi Energi*", Jakarta, 2009.

[2] J.S. Merwe and H.J. Vermeulen, "Development of an Online Energy Auditing Software Application with Remote SQL-Database Support", 46th International Universities Power Engineering Conference (UPEC), Iserlohn, Germany, pp. 1-6., 2011.

[3] A. Prudenzi, M. Di Lillo, M.C. Falvo, and A. Silvestri, "A software tool for energy audit activities in buildings", International Symposium on Power Electronics, Electrical Drives, Automation and Motion (SPEEDAM), Ischia, Italy, pp. 452 – 456, 2008.

[4] N.M. Maricar and Md. N. Jamal, "Industrial Energy Audit using Data Mining Model Web Application", TENCON 2005 IEEE Region 10, Melbourne, Australia, pp. 1 – 6, 2005.

[5] S. Melki and M. Hayek, "Building simulation tools and their role in improving existing building designs", International Conference on Advances in Computational Tools for Engineering Applications. ACTEA '09, Beirut, Lebanon, pp. 503 – 507, 2009.

[6] R.N. Lahir, et al. "Energy Accounting System for Indian electricity distribution sector", International Power Engineering Conference (IPEC), Singapore, pp. 1006-1013, 2007.

[7] P. Loganthurai, S. Subbulakshmi, and V. Rajasekaran, "A new proposal to implement energy management technique in industries", International Conference on Computing, Electronics and Electrical Technologies (ICCEET), Tamil Nadu, India, pp. 495 – 500, 2012.

[8] A. Omar, N.b. Mariun, and A.M. Radzi, "Software development for energy auditing practice", Student Conference on Research and Development (SCORED), pp. 420 – 423, 2003.

[9] C. Palanichamy, C. Nadarajan, P. Naveen, N.S. Babu, and Dhanalakshmi, "Budget Constrained Energy Conservation-An Experience with a Textile Industry", IEEE Power Eng Rev 17(1):58-58, 1997.

[10] G.W. Ung, P.H. Lee, L.M. Koh, and FH Choo, "A flexible data acquisition system for energy information", International Power & Energy Conference (IPEC), Singapore, pp. 853 – 857, 2010.

[11] JFF Van Rensburg, EHH Mathews, and R. Pelzer, "Energy management audit and recommendations at a tertiary institution", The 9th Industrial and Commercial Use of Energy Conference (ICUE), Cape Town, South Africa, pp. 1 – 6, 2012.

[12] IEEE Standard 739-1995 - IEEE Recommended Practice for Energy Management in Industrial and Commercial Facilities.

[13] The Working Team on Energy Management and Conservation and Power System Engineering, *Task Force on the Operational Implementation of Water and Energy Saving in the Office Buildings of Pamekasan Regency*, Report, Engineering Faculty of Brawijaya University, 2010.

[14] _____, *Analysis of Policy on the Efficiency in Water and Energy Saving Water in the Office Buildings of East Java Province*, Report, Engineering Faculty-PIBLAM of Brawijaya University, 2011.

[15] A. Thumann and W.J. Younger, Handbook of Energy Audits, Lilburn, GA, Fairmont Press, Inc., 2007.

G301

Digital Image Magnification In Two Phase Using Low Pass Filter and Bilinear Interpolation

Cahyo Darujati[1)], Syamsul Anam[2)]
Faculty of Computer Science
Narotama University, UNNAR
Surabaya, Indonesia
cahyo.darujati[1)], syamsul.anam[2)] @narotama.ac.id

Hasan Dwi Cahyono[3)], Agustinus Bimo Gumelar[4)]
Faculty of Computer Science
Narotama University, UNNAR
Surabaya, Indonesia
hasan.dwi[3)],bimogumelar[4)] @narotama.ac.id

Abstract*—Nowadays in digital image processing techniques, magnification process is aims to enlarge the size of the image. *Several previous studies, using this techniques to enlarge the whole object in digital images, sometimes required magnification at a particular object. This research aims to create an application of digital image magnification with two phase. The magnification process is created by two processes, first process is cropping the digital image, and the second process is enlarged filtration process with bilinear interpolation method. The output is a average value of both processes. The final results show a magnification using this method produces values Mean Square Error (MSE) is smaller and the PSNR value 73 % is greater than non-combined method.

Keywords—Digital Image Maginification, Bilinear Interpolation, Low Pass Filter

I. INTRODUCTION

Recently researches on image magnification is almost basic of image processing operations and has many applications in a various area. Image magnification has been attracting a great deal of attention for long, and many approaches have been proposed to date.Nevertheless,bicubic interpolation is still the standard approach since it can be easily computed and does not require apriori knowledge nor a complicated model [10]. Inspite of such conveniencetheimages enlarged bicubically are blurry, in particular for large magnification factors.Digital zooming method generally uses the nearest neighbor interpolation method, which is simpler and faster than other methods. But it has drawbacks such as blocking phenomenon when an image is enlarged, alsoto improve the drawbacks, there exist bilinear interpolation method and the cubic convolution interpolation which commercially used in the software market [5]. The bilinear method uses the average of 4 neighborhood pixels. It can solve the blocking phenomenon but brings loss of the image like blurring phenomenon when the image is enlarged. Cubic convolution interpolation improved the loss of image like the nearest neighbor interpolation and bilinear interpolation. But it is slow as it uses the offset of 16 neighborhood pixels [1,6,8]. A number of methodsfor magnifyingimageshave been proposed to solve such problems. However, proposed methods on magnifying images have the disadvantage that either the sharpness of the edges cannot be preserved or that some highly visible artifacts are produced in the magnified image. Although previous methods show a high performance in special environment, there are still the basic problems left behind. Digital imagery to convey information about the position, size and the inter-relationships between objects. Digital image depicting the spatial information that could recognize. Approximately 75% of the information received by humans is in the form of images [2]. Perceiving human faces is one of the most important functionsforhuman computerinteraction [9].Facial element from human face has been become an object of fascination. It because facial biometrics have an objects element of interest. Objects element of interest include human and non-human bodies, facial expressions, camera positions, and other elements in a scene. In most instances, a live subject, most likely human, is used as the source of data which is transformed into another form. Furthermore to understanding this cognition, it is also increasing interest in analyzing shapes of facial surfaces. Asfacesareoneofthemostexpressivepartsofhuman beings,facedetectionandrecognition areveryimportant topicsformanyapplications [9]. Magnification image is closely associated with high storage size and the media is a plural subject valueable in image processing. Magnification image means changing the number of pixels per image pixel display is only in appearance. Zoom = 1, meaning there is one screen pixel per pixel in the image. Zoom = 2, meaning there are 2 screen pixels per image pixel in both the x and y coordinates. This enlargement is measured by the number of digits calculated numbers or numbers greater than one, which is called magnification. When this number is less than a reference to the reduction in the size of the image, or the so-called minification.

Magnification image is one of the basic image processing operations. Magnification is also a process of enlarging

something only in appearance, not in physical size. In general, the enlargement is divided into two, namely: (i). Linear or transverse magnification - For real images, such as images projected on the screen, size means a linear dimension (eg, in millimeters or inches). (ii). Magnification angle - the placement of objects closer to the eye of the eye usually can focus. Standard methods such as the JPEG standard that can be accepted between lossy methods, but still have good quality results. Magnification related to the size of the image to be able to see more detail, increase resolution, using optics, printing techniques, or digital processing [3,4]. As an example application is image interpolation on regular display satellite imagery to do more sophisticated magnification of the original image. In some literature mentions, most of the image interpolation technique has been developed by interpolating pixels based on the characteristics of the local features such as edge information, the nearest neighbor criteria, [3] proposed a new mathematical technique for image interpolation. This technique is modified by non-local denoising algorithm to perform upsampling and remove noise simultaneously. [11] conducted experiments to enlarge the image by 200% with a PSNR of 36.31. The study was also carried out by [11] section blank pixels with Edge-Adaptive methods in digital image magnification, and conduct experiments on image gray color and RGB color images.

The motivation of this research is to implement an algorithm for digital image magnification that does not require a large amount of user input. A realistic image of the real world will be free of artifacts such as blurring, shadowing and jaggies. The image should include smooth contours and rapid transition edge.

II. LITERATURE

A. Digital Image Magnification

Digital image processing enables the reversible, virtually noise-free modification of an image in the form of a matrix of integers instead of the classical darkroom manipulations or filtration of time-dependent voltages necessary for analog images and video signals. Even though many image processing algorithms are extremely powerful, the average user often applies operations to digital images without concern for the underlying principles behind these manipulations. The images that result from careless manipulation are often severely degraded or otherwise compromised with respect to those that could be produced if the power and versatility of the digital processing software were correctly utilized. Digital image processing makes use of digital computers to process an image. In digital image processing we require two types of information; either the whole input image or some interested information from the user point of view like radius, objects etc. There are various advantages of using digital image processing like preservation of original data accuracy, flexibility and repeatability. Digital image processing includes scaling of image as an important area. Scaling operation plays an important in resizing digital images. Scaling is used for shrinking or zooming of an image. Interpolation is used to find the value of unknown pixels with the help of known pixel values. There is wide variety of image interpolation methods available. Basicly, zooming implies enlargement or magnification of an image for a better view of it. Image zooming known as oversampling.. Zooming is a process of creating new location of pixels and to assign values to new locations. A zooming algorithm takes an image as input and generates a picture of larger size. A zooming algorithm is characterizing good if the required information is acquired after zooming process [12]. PSNR are measures to evaluate the quality of zoomed image. PSNR (peak signal to noise ratio) is a quantitative measure, which is used to compare the quality of an original and zoomed image.

B. Digital ImagesZoomingand Repositioning

Zooming on an image are accomplished by making multiple copies of the pixels of the selected region. It produces an increase in its displayed size, with a corresponding increase in "pixel" size. Although those process does not increase the information content of the region of interest, it can be helpful in the visualization of small structures or for the examination of individual pixel brightness values. There are several useful algorithms available for performing a zoom operation on a digital image. The simplest and most accurate algorithm, known as the **discrete replicating zoom**, performs by displaying multiple copies of each pixel in the area of interest [13]. This algorithm operates in discrete steps, it can produce zoomed images at integral zoom factors of 2x, 4x, and higher. Individual pixels become readily apparent at 4x or higher zoom factors, depending upon the spatial resolution of the image.Fractionally zoomed images can also be obtained by varying the number of copies made of each pixel in the area of interest. The most commonly employed algorithm is known as the **fractional replicating zoom**, which works by copying pixels from the source image into the zoomed image based upon an inexact spatial correspondence between the two. In effect, pixel addresses in the source image are calculated fractionally, based on the ratio between the zoomed image dimensions to the source image dimensions. Because the calculated pixel address is fractional, a decision must be made as to what to do with the fractional part of the address. There are several approaches to this problem. One of the most common, **interpolation**, is based on an estimation of the value between two or more known values, and there are a wide variety of published algorithms to address this type of calculation [13].

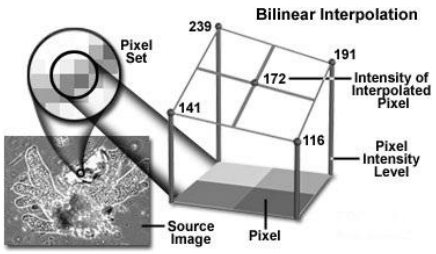

Figure 1. Bilinear Interpolation

An interpolation technique that reduces the visual distortion caused by the fractional zoom calculation is the **bilinear interpolation** algorithm, where the fractional part of the pixel address is used to compute a weighted average of pixel brightness values over a small neighborhood of pixels in the source image. Bilinear interpolation (see Figure 1) produces pseudo-resolution that gives a more aesthetically pleasing result, although this result is again not appropriate for measurement purposes.

C. Bilinear Interpolation Algorithms

Interpolation works by using known data to estimate values at unknown points. Image interpolation works in two directions, and tries to achieve a best approximation of a pixel's color and intensity based on the values at surrounding pixels. The following figure illustrates how resizing / enlargement works [14] :

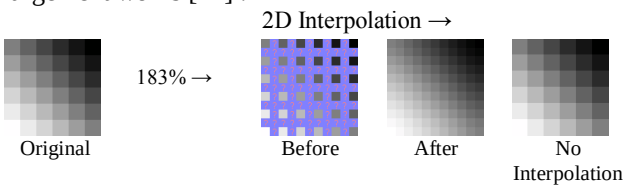

Figure 2. Image Resizing

Pixel values can change far more abruptly from one location to the next. As with the temperature example, the more we know about the surrounding pixels, the better the interpolation will become. Therefore results quickly deteriorate the more stretch an image, and interpolation can never add detail to image which is not already present.Depending on their complexity, these use anywhere from 0 to 256 (or more) adjacent pixels when interpolating. The more adjacent pixels they include, the more accurate they can become, but this comes at the expense of much longer processing time. These algorithms can be used to both distort and resize a photo [14].

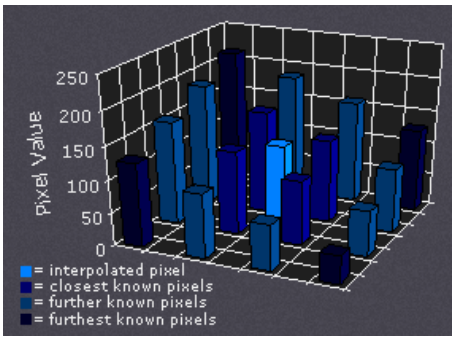

Figure 3. Visualize of bilinear interpolation

Bilinear interpolation considers the closest 2x2 neighborhood of known pixel values surrounding the unknown pixel. It then takes a weighted average of these 4 pixels to arrive at its final interpolated value. This results in much smoother looking images than nearest neighbor.The diagram to the figure 6 is for a case when all known pixel distances are equal, so the interpolated value is simply their sum divided by four.

Scaling an image goes in two ways, making it larger or to make it smaller. By enlarging an image, some new pixels are constructed by means of interpolation. By shrinking, we are tempted to think the right pixels are selected to keep while the others are thrown away, but this is not the case. Unlike nearest neighbor shrinking where pixels are thrown, bilinear shrinking estimates a smaller resolution of the original image. Even though details are lost, almost all the new pixels in the shrunk image do not come directly from their original, but interpolated, indirectly keeping the properties of lost pixels. It should be understood this is not always the case, shrinking image to half size (and smaller) significantly reduce image quality – not much different from nearest neighbor shrinking. This also applies to sizing up more than double the original size [16].

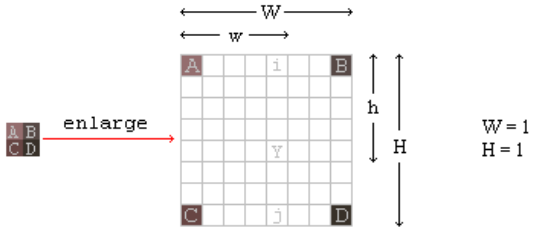

Figure 4. Enlarged image.

For the purpose of this article, explanation will follow the making-it-larger path. So we start by enlarging a small texture such as shown in figure 4. This is not to be mistaken as a requirement to enlarge every single texture found in an image. The objective is finding the colors for all white spaces, including i, j, and Y. First is to find the relation between A, i, and B. Using linear interpolation function (figure 4), we get this equation :

$$\frac{i-A}{w} = \frac{B-A}{W}$$
$$i = A + \frac{w(B-A)}{W}$$
$$i = A + w(B-A) \rightarrow 1 \qquad (1)$$

Do the same for C, j, and D and we get,

$$\frac{j-C}{w} = \frac{D-C}{W}$$
$$j = C + w(D-C) \rightarrow 2 \qquad (2)$$

Now we have two linear interpolation equations. Next is to combine the two equations forming a single equation that is called the bilinear function.

$$\frac{Y-i}{h} = \frac{j-i}{H}$$

$$Y = i + h(j - i) \rightarrow 3 \quad (3)$$

Substituting (1) and (2) into (3) we get,

$Y = A + w(B - A) + h\left(C + w(D - C) - \left(A + w(B - A)\right)\right)$

$Y = A(1 - w)(1 - h) + B(w)(1 - h) + C(h)(1 - w) + D(wh)(4)$

Using (4), all white spaces can now be interpolated.

D. Filtering

Most images are affected to some extent by noise, disturbances in image intensity which are either uninterpretable or not of interest. Image analysis is often simplified if this noise can be filtered out. Image filters may be used to emphasise edges, the boundaries between objects or parts of objects in images. Filters provide an aid to visual interpretation of images, and can also be used as a precursor to further digital processing, such as segmentation. Filters change a pixel's value taking into account the values of neighbouring pixels too. They may either be applied directly to recorded images, or after transformation of pixel values. By utilizing the results of the Fourier transformation. Where the frequency of the image is affected by gradation of colors that exist in the image [7].

One method of filtering an image is to apply a convolution operation to the image to achieve: blurring, sharpening, edge extraction or noise removal. The action of a convolution is simply to multiply the pixels in the neighbourhood of each pixel in the image by a set of static weights and then replace the pixel by the sum of the product. In order to prevent the overall brightness of the image from changing, the weights are either designed to sum to unity or the convolution is followed by a normalization operation, which divides the result by the sum of the weights. In simple terms, perform a weighted average in the neighbourhood of each pixel and replace the pixel's value by the average. The filter is generated by providing a set of weights to apply to the corresponding pixels in a given size neighbourhood. The set of weights make up what is called the convolution kernel and is typically represented in a table or matrix-like form, where the position in the table or matrix corresponds to the appropriate pixel in the neighbourhood. Such a convolution kernel (or filter) is typically a square of odd dimensions, when applied, the resulting image does not shift a half pixel relative to the original image. The general form for a 3x3 convolution kernel looks as follows [17]:

$$\begin{bmatrix} w1 & w2 & w3 \\ w4 & w5 & w6 \\ w7 & w8 & w8 \end{bmatrix} \quad (5)$$

Orif the weights are not designed to sum to unity, then as

$$\frac{1}{sumw}\begin{bmatrix} w1 & w2 & w3 \\ w4 & w5 & w6 \\ w7 & w8 & w8 \end{bmatrix} \quad (6)$$

Where

sumw=(w1+w2+w3+w4+w5+w6+w7+w8+w9). (7)

The simplest convolution kernel or filter is of size 3x3 with equal weights and is represented as follows:

$$\begin{bmatrix} 1/9 & 1/9 & 1/9 \\ 1/9 & 1/9 & 1/9 \\ 1/9 & 1/9 & 1/9 \end{bmatrix} = \frac{1}{9}\begin{bmatrix} 1 & 1 & 1 \\ 1 & 1 & 1 \\ 1 & 1 & 1 \end{bmatrix} = low\ pass\ filter. \quad (8)$$

This filter produces a simple average (or arithmetic mean) of the 9 nearest neighbours of each pixel in the image. It is one of a class of what are known as low pass filters. They pass low frequencies in the image or equivalently pass long wavelengths in the image, i.e. slow variations in image intensity. Conversely, they remove short wavelengthsin the image, which correspond to abrupt changes in image intensity, i.e. edges. Thus we get blurring. Also, because it is replacing each pixel with an average of the pixels in its local neighbourhood, one can understand why it tends to blur the image. Blurring is typical of low pass filters. Low Pass Filter is a filter process that takes images with smooth gradation of intensity and high intensity differences will be reduced or removed [17].

E. PSNR (Peak Signal to Noise Ratio) Analysis

The peak-signal to noise ratio is abbreviated as PSNR is defined as the ratio between signals maximum power and the power of the signals noise. The PSNR is commonly used to measure the quality of the reconstructed images which have been compressed. Each picture element is called as pixel which has color value that can change when an image is compressed and then uncompressed. Signals can have a wide dynamic range, so PSNR is usually expressed in decibels. The signal in this case is the original data and the noise is the error which is introduced due to compression. If the compressed image is closer to original image means which have lower PSNR ratio. The PSNR most easily defined via the mean square error (MSE) for two matrices I and K having dimension of m X n [15].

The PSNR most easily defined via the mean square error (MSE) for two matrices I and K having dimension of m X n. The MSE can be expressed as,

$$MSE = \frac{1}{mn}\sum_{i=0}^{m=1}\sum_{j=0}^{n=1}[I(i,j) - K(i,j)]^2 \quad (9)$$

The PSNR defined as,

$$PSNR = 10\log_{10}\left(\frac{255^2}{MSE}\right) \quad (10)$$

Where I and K represents the matrices that represent the images being compared. The two summations are performed for the dimensions 'i' and 'j' therefore I (i, j) represents the value of pixel (i, j) of image I. The PSNR is expressed in decibels. Typically values for the PSNR in lossy image and video compression are between 30db and 50db.

III. METHOD

The block diagram of the systemimage magnification using the combined method is shown in Figure 5. Image data used is the data image format JPG, BMP, PNG. The image data is carried out first process sampling the image with the desired region by the user, in terms of which regions in the input image to be localized for the magnification process.

After the sampling process is done, then the next step is image filtering process with lower pass filter method and bilinear interpolation.Then the obtained results is an average magnification of the results of the screening process down pass filter and bilinear interpolation. Image sampling process is one stage of the process used to produce a good magnification. The sampling process using the image (xL,yT) and (xR,yB) = coordinates of the upper left corner point and the lower right corner of the image will be sampled, in this case, the sampling is done is to cut a portion of the original image.

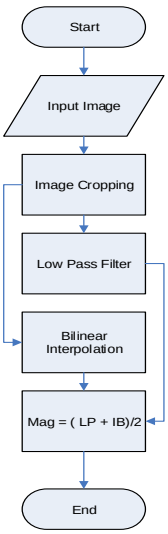

Figure 5. Image Magnification system

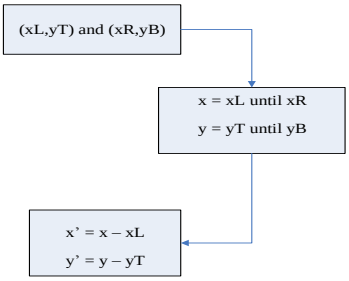

Figure 6. Image sampling process

After the sampling process is performed convolution process image with a low pass filter method, which uses filters in this process - average. The purpose of the process is done is to improve the quality of the original image. To throw a different point with its neighboring points (noise reduction process) then do Low - Pass Filter (LPF) , a filter that takes the form of data on low frequency and disposing of data at high frequencies . The algorithm is described as follows convolution process :

```
For x=0 to picture1.ScaleWidth-1
  For y=0 to picture1.ScaleHeight-1
    z(x,y)=0
    for k1=0 to nFilterX-1
      for k2=0 to nFilterY-1
(x,y)=z(x,y)+H(k1,k2)*I(x+k1,y+k2)
      next k2
    next k1
  next y
Next x
```

The analysis of an image in the frequency domain based on convolution techniques, generally give the output of a linear system can be obtained from the convolution operation between the system impulse response with the input signal. Convolution operation performed by sliding the kernel convolution pixels per pixel, calculate the output pixel f (i, j), and then save it in the new matrix. Convolution is very useful for screening operations (filtering) on the image. In digital image processing, convolution is done on a two-dimensional image.

TABLE I. MSE CALCULATION RESULTS FOR IMAGES WITH EXTENSION JPG , PNG AND BMP

No	Zoom	Size	Peak Signal to Noise Ratio(PSNR)		
			JPG	PNG	BMP
1.	2x	700 x 472	51.4446	51.5822	51.5694
	3x		51.4561	51.5769	51.5659
	4x		51.4594	51.5783	51.5635
	5x		51.4664	51.5478	51.5619
2.	2x	500 x 800	51.4530	51.6784	51.6706
	3x		51.4539	51.6763	51.6665
	4x		51.4585	51.6669	51.6640
	5x		51.4521	51.6169	51.7624
3.	2x	1600 x 1400	55.5323	57.6355	57.7354
	3x		56.1244	57.7243	57.7347
	4x		56.4123	58.9997	57.6365
	5x		56.7465	58.3857	57.7545

TABLE II. THE RESULTS OF THE CALCULATION OF PSNR FOR IMAGE WITH EXTENSION JPG , PNG AND BMP

No	Zoom	Size	Mean Square Error (MSE)		
			JPG	PNG	BMP
1.	2x	700 x 472	0.454	0.452	0.443
	3x		0.453	0.457	0.443
	4x		0.463	0.456	0.443
	5x		0.453	0.456	0.443
2.	2x	500 x 800	0.466	0.459	0.443
	3x		0.466	0.458	0.443
	4x		0.468	0.459	0.443
	5x		0.468	0.459	0.443
3.	2x	1600 x 1400	0.453	0.634	0.623
	3x		0.464	0.652	0.687
	4x		0.465	0.635	0.614
	5x		0.475	0.652	0.634

IV. TEST AND RESULT

The trial results of this research through several stages of the captured image magnification is performed on twelve different trials. Scale enlargement as well as the different image sizes. The scale difference between the sizes in multiresolution is still limited in the fidelity. However, with image processing technology it can be possible to achieve an arbitrary degree of fine detail using a multiresolution representation. In addition to alleviating some of the limitations, multiresolution representations often yield other advantages over uniresolution representations, there is in control, feature detection, compression, and refinement. A representation in multiresolution image, that accommodates different amounts of detail in different parts of the image.

TABLE III. THE RESULTS IMAGE FROM DIFFERENT SCENE

2x	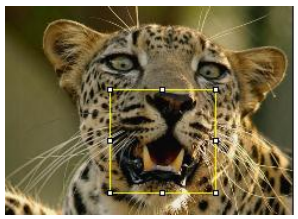	
3x		
4x	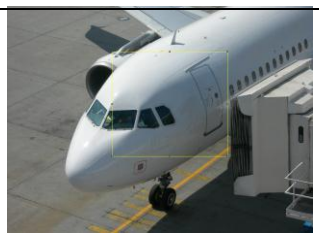	
5x		

From the test results in Table 1, it can be seen that the input image used is the original image that has undergone a process of cutting first with different sizes. Magnification scale is used to make the process of enlargement on each image is different. From Table 1 it can comparing the value of the Mean Square Error (MSE) at each image file extensions are tested.Location of sampling performed well at different locations. The effect of different trials is determine the advantages and disadvantages of this method on digital image magnification. At trial magnification image, a large image of different sizes as well as to determine the value of MSE and PSNR of the magnify iamges. In Table 2 can also be seen that the value of Peak Signal to Noise Ratio (PSNR) which is the smaller the greater the value of MSE and the PSNR value the better the resulting image. In table 1 and 2 can also be seen that the greater the magnification is done then the smaller value of MSE and its PSNR higher. Evaluation results of this pilot study is an attempt magnification image that has been done that the application and the methods used for proper operation in accordance with its function. Although the MSE and PSNR image jpg extension is better than the image bmp extension. This is because the image of the extension jpg is a lossy format, while the extension bmp image is a lossless format, so that the image quality is better. Although if at first glance would not look at all. In addition, the enlarged image do have a higher image quality. This method is designed to reduce the contrast of the image enlarged.

V. CONCLUSION

The conclusion of the research is that the value of MSE is smaller and PSNR value greater than the other methods. By using this combined method produces smoother image but not too appear blurring impression. In this study the process time required magnification is strongly influenced by the size of the image is done bycropping process. In the next stage, this research can be developed by using more robust method in dealing with images sharper color depth and integrate with motion capture system. The speed of the process is also one of the measures that are used when processing the image with a variety of conditions. Applications can also be developed into applications that unsupervised or automatic, both from the beginning of the process to the expected output. In addition to robustness, the method can also be developed into a more adaptive methods.

ACKNOWLEDGMENT

This project research was funded by grant aid Hibah Dosen Pemula 2013 from Directorate General of Higher Education (DIKTI) of the Ministry of Education and Culture of the Republic of Indonesia and Narotama University.

REFERENCES

[1] Biancardi, A., Cinque, L. and Lombardi, L.Improvements to Image Magnification, Pattern Recognition, B.V., 2002.

[2] Notoatmodjo. Prof. Dr. Soekidjo. Prinsip-Prinsip Dasar Ilmu Kesehatan Masyarakat.2nd edition,. Jakarta : Rineka Cipta. 2003.

[3] R. C. Gonzalez, R. E. Woods, 'Digital Image Processing', 2nd ed., Prentice Hall., 2002.

[4] LI Zhiwei, ZHANG Min and WANG Jiechao, "An Image Zooming Technique Based on the Relative Color Difference of Pixels", IEEE Transactions On Image Processing, Vol. 15, No.2, 2006.

[5] Sung-Kwan, Kwang-Baek, Jae-Hyun Cho and Doo-Heon Song, "Image Magnification based on the Human Visual Processing", Vision Systems: Applications, 2007.

[6] Aoyama, K. and Ishii, R. (1993) Image magnification by using Spectrum Extrapolation, IEEE Proceedings of the IECON, 1993.

[7] Glasbey and Horgan, "Image Analysis For The Biological Science, 1994.

[8] Candocia, F. M. and Principe, J. C. (1999) Superresolution of Images based on Local Correlations, IEEE Transactions on Neural Networks, Vol. 10, No. 2, pp. 372-380, 1045-9227.
[9] Darujati, C.; Hariadi, M., "Facial motion capture with 3D active appearance models," *Instrumentation, Communications, Information Technology, and Biomedical Engineering (ICICI-BME), 2013 3rd International Conference on* , vol., no., pp.59,64, 7-8 Nov. 2013.
[10] Hirabayashi and Condat, "A Compact Image Magnification Method WithPreservation Of Preferential Components"
[11] S. Battiato, G. Gallo, F. Stanco, A Locally-Adaptive Zooming Algorithm for Digital Images, Elsevier Science Inc. - Image and Vision Computing Journal , vol. 20, n. 11, pp. 805-812, 2002.
[12] Chadda,Kaur, Thakur, "Zooming Techniques for Digital Images ", IJCST Vol.3, Issue 1, Jan 2012.
[13] http://www.micro.magnet.fsu.edu/primer/java/olympusmicd/digitalimaging/sizepanel/index.html
[14] http://www.cambridgeincolour.com/tutorials/image-interpolation.htm
[15] Yallapurmath et all, Design and Implementation of Image Super Resolution Algorithms, Proceedings of National Conference on Advanced Computer Applications NCACA 2012.
[16] http://tech-algorithm.com/articles/bilinear-image-scaling/
[17] Fred Weinhau, “Digital Image Filtering”.

G302

Outlier Filtering for Hydrogen Temperature and Flow Rate Time series data in Sintering Process

Dede Sutarya
Electrical Engineering Dept., Universitas Pancasila
Jagakarsa, Indonesia
sutarya.dede@univpancasila.ac.id

Adhi Mahendra
Electrical Engineering Dept., Universitas Pancasila
Jagakarsa, Indonesia
Johanes70am@yahoo.com

***Abstract*—The data with free of noise or outliers will not be obtained in the chemical or physical process measurements using due to some kind of noise arising from thermodynamics and quantum effects may not be removed. The extensive use of personal computers in process instrumentation and flexibility of programming software, encourages its use for filtering time series data with satisfactory results. This paper will investigate outlier filtering techniques on time series data of temperature and flow rate of hydrogen gas as result of sensor measurement on the sintering process. The results an optimal parameters on the filtering technique that yields an adequate signal to noise ratio while still maintaining peak signal on the measurement results, Its is very important respect to process safety parameters of hydrogen gas.**

Keywords—outlier; filtering, time series data; sintering process.

I. INTRODUCTION

Outlier is observed data which has significant deviation or anomalies of most of the observations. The outlier may be caused by a spike signal, the sensor measurement errors, noise caused by process equipment, equipment degradation or associated with human error. The data with free of noise or outliers can never be obtained in laboratory measurements using sensors in chemical or physical processes. It is caused by some kind of noise arising from thermodynamics and quantum effects maybe cannot be removed. In some control applications the data outliers will lead to analysis of the data becomes useless because outliers can lead to a mismatch of model specifications, parameter estimates to be biased even produce incorrect analyzes and conclusions. In this paper to overcome the problem of data outliers used median filter as simple filtering method to detect and eliminate outliers in hydrogen temperature and flow rate time series data. The widespread use of computers based for process instrumentation in chemistry and physics, as well as software programming flexibility make use of software for noise detection and filtering [1] , data cleaning outliers [2-4] and median filtering [5-7] widely implemented with satisfactory results.

II. MATERIAL AND METHODS

A. *Sintering Process and Data Acquisitions*

Sintering is a heat treatment applied to a powder compact in order to impart strength and integrity. The temperature used for sintering is below the melting point of the major constituent of the powder metallurgy material. Experimental data are obtained from industrial heat-treating sintering furnace with pure hydrogen atmosphere.

The interfacing of analytical measurement instrumentation to personal computers (PC) for the purpose of online data acquisition has now become standard practice in the modern laboratory. To eliminate the timing uncertainty from temperature and flow rate measurements, a new data acquisition program has been implemented, specific for the furnace. As shown in Figure 1 the data acquisition system (DAQ) diagram for the measured temperature and flow rate of hydrogen. Data collection was conducted during one cycle of sintering process about 36 hours to obtain time series data of hydrogen temperature and flow rate.

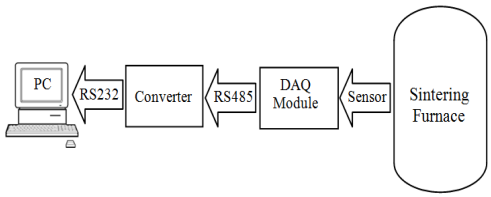

Fig. 1 Data acquisition system for temperature and flow rate measurement.

Experiments and data collection was done by the sintering process parameters as follows: heating rate 250^{o}C/jam, soaking temperature is 1.700^{o}C, the cooling stage was done naturally, and used nitrogen and hydrogen as gas atmosphere in sintering process. Experimental data was measured during the sintering process approximately 36 hours with a total sample of 73.324 data. From the overall data was taken 15,000 time series data of temperature and flow rate of hydrogen gas

and is used as the experimental data in this study, as shown in Figure 2 and Figure 3.

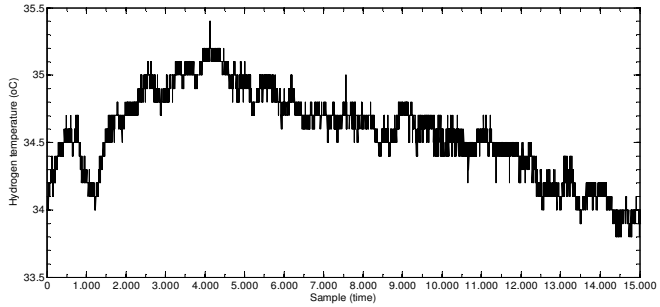

Fig.2 Hydrogen temperature time series data of sintering process

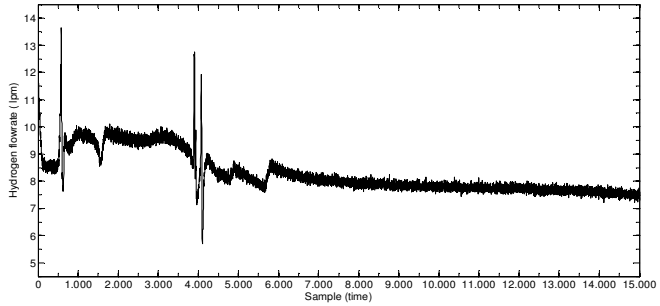

Fig.3 Hydrogen flow rate time series data of sintering process

B. Median Filter

Assuming that the generation of outliers can be explained by the model of the popular additive outliers on the robust-time series analysis [2,8] as follows

$$y_k = x_k + o_k \tag{1}$$

where y_k is the sequence of measurement data, x_k is a sequence of nominal data that we desired and o_k describe the sequence of data that contains outliers. The sequence values of o_k assumed to be zero except for the case of a second time with an o_k value far greater than the nominal visible variation in the data. The search of approximate value x_k based on the observation of current data and previous $y_k - j$ for $k \geq j \geq 0$. In particular the data, y_k , N - 1 and $y_k - j$ stored in the data window W_k with width N.

$$W_k = \{y_k - N + 1, y_k - N + 2, ..., y_k\} \tag{2}$$

The value of the data in the window then arranged by rank to get R_k as follows

$$R_k = \left\{ y^k_{(1)} \leq y^k_{(2)} \leq ... \leq y^k_{(N)} \right\}, \tag{3}$$

and the median y_k^m of the sequence R_k is calculated as follows

$$y_k^m = \begin{cases} y^k_{((N+1)/2)} & for\ N\ odd \\ (y^k_{(N/2)} + y^k_{(N/2+1)})/2 & for\ N\ even \end{cases} \tag{4}$$

The median value y_k^m provides a nominal data as reference compensation current data y_k, then evaluated by determining the distance d_k between y_k and y_k^m , the distance is determined as follows

$$d_k = \left| y_k^m - y_k \right| \tag{5}$$

If the distance exceeds the specified threshold that is Tk ≥ 0, then y_k declared as outliers and replace it with predictive value y_k^m to obtain the data sequence f_k after filtered, with the following conditions.

$$f_k = \begin{cases} y_k & if \quad d_k \leq T_k \\ y_k^{pred} & if \quad d_k \succ T_k \end{cases} \tag{6}$$

The process for removing outliers in the time series data of temperature and flow rate of hydrogen gas is done by varying the size of the sliding window *N*, which aims to find the proper window size with the best signal to noise ratio.

III. SIMULATION RESULTS

In this study, especially the shape of peak of the original signal is very important so it will look the optimal size of the filter window by specifying criteria of mean squared error (MSE) and the lowest signal to noise ratio (SNR) as the greatest width of the window for the optimal filter in this case. To achieve these objectives, in this study used a window size variation is divided into smaller window sizes are 115, 135, 175 and larger window sizes are 215, 235 and 275. Mean squared error and signal to noise ratio criteria were calculated using the following equation.

$$MSE = \frac{1}{N} \sum_{n=0}^{N} (V(n) - V_R(n))^2 \tag{7}$$

$$SNR = \log_{10} \frac{\sum_{n=0}^{N} V_R^2(n)}{\sum_{n=0}^{N} S_R^2(n)} \tag{8}$$

where *N* is the number of time series data, *V(n)* is the original signal before filtered, V_R(n) is the reconstructed signal after

filtered, and $S_R(n)$ is the difference between the original signal and the reconstructed signal after filtered.

MSE and SNR calculation results for the temperature and flow rate time series data of hydrogen gas to eliminate outliers with a small and greater window size are shown in Table 1 and Table 2.

TABLE I. MSE AND SNR VALUES AFTER FILTERED WITH SMALL WINDOW SIZE

Time series data	***Criterion***	**Window size (*N*)**		
		115	***135***	***175***
Temperature	MSE	0,0045	0,0047	0,0052
	SNR	5,3908	5,3693	5,3288
Flow rate	MSE	0,0703	0,0699	0,0657
	SNR	3,0349	3,0373	3,0640

TABLE II. MSE AND SNR VALUES AFTER FILTERED WITH LARGER WINDOW SIZE

Time series data	***Criterion***	**Window size (*N*)**		
		215	***235***	***275***
Temperature	MSE	0,0057	0,0061	0,0067
	SNR	5,2846	5,2613	5,2168
Flow rate	MSE	0,0673	0,0689	0,0705
	SNR	3,0535	3,0436	3,0334

As shown in Table 1 and Table 2, the increase in window size of median filter resulted in an increase the mean squared error followed by a decrease of signal to noise ratio. In other words, the larger window size resulted more progressive performance of median filter while increasing deformation in the signal after filtered to the original signal.

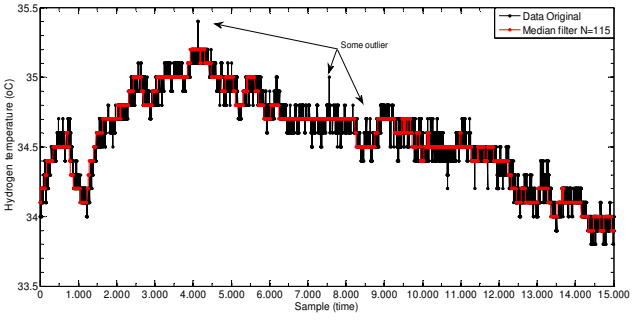

Fig. 4 Some potential outliers in hydrogen temperature time series data with window size N = 115.

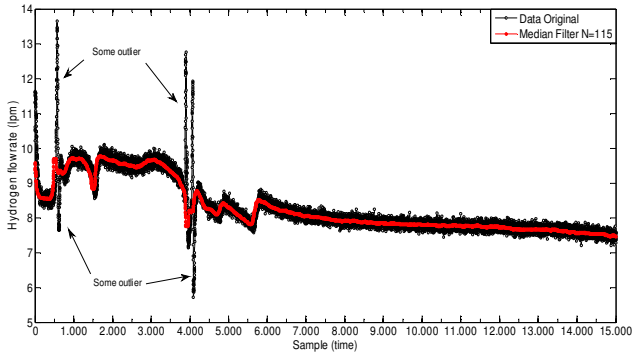

Fig.5 Some potential outliers in hydrogen flow rate time series data with window size N = 115.

Figures 4 and 5 show some potential outliers in the temperature and flow rate of hydrogen time series data using median filter with window size N=115.

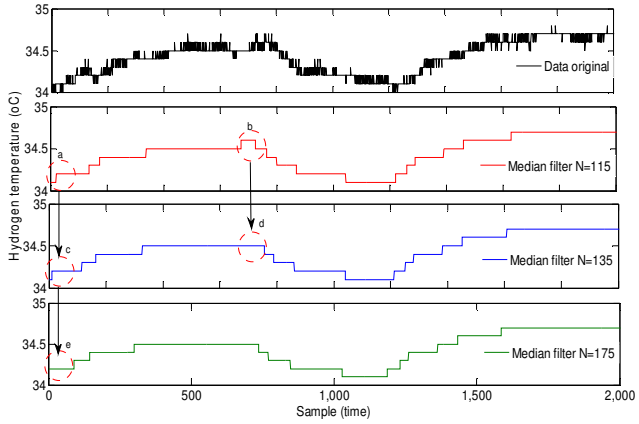

Fig.6 Signal shape comparison before and after filtered with some small size window (a, b, c and d shows the change in shape of the signal corresponding to the addition of the filter window size)

The size of the sliding window filter (moving window size) at a median filter resulting the greater deformation in a signal after filtered as shown in Figure 6 for hydrogen temperature time series data with window size are 115, 135 and 175. Therefore, the selection of the optimal window size of median filter besides considering the value of MSE and SNR are also required the visual observation of the deformation signal at any window size of the filter. This visual observation is an engineering judgment in determining of the optimal size of the median filter window as needed for subsequent analysis.

IV. CONCLUSSION

Implementation of the median filter to the time series data of temperature and flow rate of hydrogen was investigated with a different window size of 115, 135, 175, 215, 235 and 275. The addition of a window size of 20 points resulted in an increase of 0.0002 point of MSE and a decrease of 0.023 point of SNR on the hydrogen temperature time series data. As for time series data of hydrogen flow rate results in an increase of 0.0004 and a decrease of 0.003, MSE and SNR for sequentially. For larger addition of window size resulted more increasing of MSE and more decreasing of SNR. The selection of the optimal window size of median filter besides considering the value of MSE and SNR are also required the visual observation of the deformation signal at any window size of the filter. This visual observation is an engineering judgment in determining of the optimal size of the median filter window as needed for subsequent analysis. However more research is needed to find a more appropriate method for filtering time series data of temperature and hydrogen flow rates were better in the elimination of data outliers while retaining the peaks signal shape of the original data.

ACKNOWLEDGMENT

The authors express their gratitude to the sintering laboratory staff for their assistance during the experiments and to the Ministry of Education and Culture through the Directorate General of Higher Education of Indonesia for financial support in this important work.

REFERENCES

[1] Bhausaheb Shinde, A.R. Dani," Noise Detection and Removal Filtering Techniques in Medical Images", International Journal of Engineering Research and Applications, Vol. 2, Issue 4, p.311-316, July-August 2012

[2] P.H. Menold, R.K. Pearson, F. Allg¨ower," Online outlier detection and removal", Proceedings of the 7th Mediterranean Conference on Control and Automation (MED99) Haifa, Israel - June 28-30, p.1110-1133, 1999.

[3] R. Ganguli," Noise and outlier removal from jet engine healt signal using weighted FIR median hybrid filter", Mechanical Systems and Signal Processing, 16(6), p.967–978, 2002.

[4] [64] Hancong Liu, Sirish Shah, Wei Jiang," On-line outlier detection and data cleaning", Elsevier, Computers and Chemical Engineering, 28, p.1635–1647, 2004.

[5] Lin Yin, Ruikang Yang," Weighted Median Filters: A Tutorial", IEEE Transactions on Circuit and System: Analog and Digital Signal Processing, Vol. 43, No. 3, p. 157-192, March 1996.

[6] Ruikang Yang, dkk," Optimal Weighted Median Filterin Under Structural Constraints", IEEE Transactions on Signal Processing, Vol. 43, No. 3, p. 591-604, March 1995.

[7] H. Hwang and R. A. Haddad," Adaptive Median Filters: New Algorithms and Results", IEEE Transactions on Image Processing, Vol. 4, No. 4, p. 499-502, April 1995.

[8] Martin, R. and V. Yohai,"Influence Functionals for Time Series," Ann. Statist., 14, p. 781-818,1986.

G303

The Implementation of the Advanced Encryption Standard (AES) Encryption Algorithm For Computer File Security

Mokhammad Hendayun, Iwan Abadi, Marulan Heryanto Samosir
Departement of Informatics Engineering
Langlangbuana University (UNLA)
Bandung, Indonesia
hendayun@aol.de , Iwan.abadi69@gmail.com

Abstract-A file is related collection of record or file, that can be translated into archive/data and then stored in secondary storage, such as magnetic disk and magnetic tape. File may contain texts, images, video, audio or combinations of them. Security of computer files is essential to implement, because the files can be stolen by unauthorized person. Therefore we need a method to secure files, method of securing files that are often used include cryptographic. By using the methods of cryptography, files will be encrypted by means of randomizing. Encryption will change the record or text (plain text) into record that can not be read (cipher text). There are several algorithms that can be used to encrypt the file, one of them is Advanced Encryption standad (AES). Hence in this study will be discussed the solutions to problems with file security algorithm using AES, so that the file is safe from people who are not responsible.

Keywords: File Security, Cryptographic, Encription, plain text, cipher text

I. INTRODUCTION

The computer file security is a very important point in the use file on information technology. Processing technology of the computer file can be done from anywhere, because, the communication can be done with the online system. Therefore, how to keeping a file of attack or interference from parties who are not authorized, such things should be notice us. Therefore necessary to secure a methods of the computer files, on method of the computer file security is cryptograph. Cryptography is the science that studies how to keep secure data or messages, from sender to reciver without experiencing interference of the intruder. The security aspects of file security is confidentiality, integrity, availability and authentication. Main process in cryptograph is encryption and decryption. Many of the algorithm with used in cryptography, one of the algorithm is Advanced Encryption Standard (AES).

II. BASIC THEORY

1. Encryption and Decryption

Main process in cryptograph is encryption and decryption. The Encryption is changing the original message (plaintext) into a coded message (ciphertext), while the decryption is to restore the ciphertext into the original message (plaintext) [1]. Overview of the cryptography process can be seen in figure 1 below:

Figure 1 Cryptography Process

2. Advanced Encryption Standard (AES)

The AES is a symetric blok cipher that uses 128 bit, 192 bit or 256 bit keys [2]. For AES 128 bit, The key length and block size can be chosen independently. Each block is encrypted in a certain number of rounds.

3. File

When all the records representing entities of one type are collected together, we call the aggregation a file. Files can be viewed as both logical and physical entities [3]. The file can also be translated archive or data with stored in the storage computer. A file is related collection of record or file, that can be translated into archive/data and then stored in secondary storage, such as magnetic disk and magnetic tape. File may contain texts, images, video, audio or combinations of them. In the information technology necessary to the security file of interference person who do not have access.

III. ANALYSIS AND DESIGN

1. System Description
   The system build called Maru File Protector (MFP). The mechanism of MFP system is:

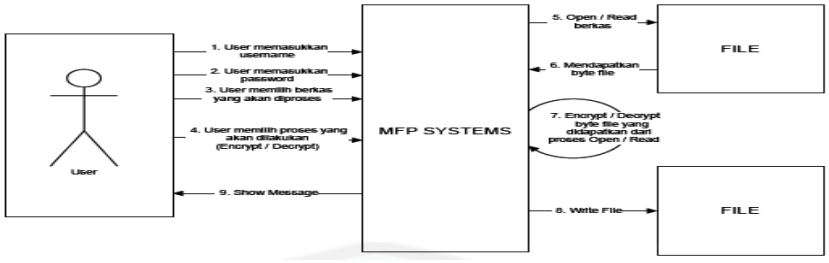

Figure 2 Description of System

TABLE 1 MECHANISM OF SYSTEM

NO	MECHANISM
1	Input username by user
2	Input password by user
3	User memilih file yang akan diproses
4	User memilih proses yang akan dilakukan (enkripsi atau dekripsi)
5	File yang telah dipilih akan dibuka kemudian dibaca untuk mendapatkan byte file
6	Get of byte file
7	Melakukan enkripsi/dekripsi byte file
8	Setelah prose file dienkripsi/didekripsi maka hasilnya dituliskan ke dalam file
9	Show message

2. User of System
   User of system are those that interact directly with the software. In this developed system that interact with the software are user, in the system is referred to as actors.
3. Functional Requirements
   Requirements analysis results in the specification of software's operational characteristics; indicates software's interface with other system elements; and establishes constraints that software must meet [4]. Functional requirements is description of what the system should do. Functional requirements of the system can be seen from the table below:

TABLE 2 FUNCTIONAL REQUIRMENTS

REQUIREMENT NUMBER	REQUIREMENT NAME	DESCRIPTION
MFP-10	Encryption	The system can make changes to the files in the ciphertext
MFP-20	Decryption	The system can make changes to the ciphertext files in the plaintext

Of the functional requirements, the next step is to translate requirements into use cases. Use cases are scenario for understanding system requirements. A use case model can be instrumental in project development, planning, and documentation of systems requirements [5].

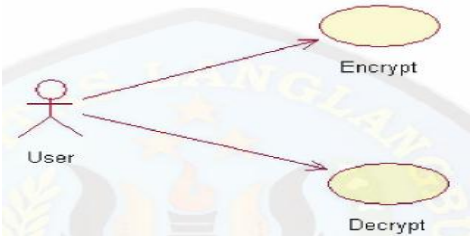

Figure 3 Use cases Diagram

4. Advanced Encryption Standard (AES) Algorithm
   The AES class consists of methods and variables, the following more detailed:

a. AES()
   The method is constructor of AES class
   Input : byte[]arr_keys
   Output :
   Proses : - setting the size of the variable block_state dan block_key
   - Call and running of the method build_sBox(), build__InvsBox(), and build_rCon().

b. setKeys()
   This Method aims to setting of the keys is used:
   Input : byte[]arr_keys
   Output :
   Proses : - Setting variable block_key from arr_keys
   - Form upa-keys or expended keys.

c. Encrypt()
   This Method aims to encryption in the file given to length of variation inputs.
   Input : byte[]arr_plaintext
   Output : byte[]
   Proses : - Get the length from arr_palintext
   - Create an array of result with the length of arr_block*16
   - Perform looping round total block array (arr_block) to encryption for the arr_plaintext

d. Decrypt()

This Method aims to decryption in the file given to length of variation inputs.
Input : byte[]arr_cipher
Output : byte[]
Proses : - Get the length from arr_cipher
- Create an array of result with the length of arr_block*16
- Perform looping round total block array (arr_block) to dekription for the arr_cipher.

e. EncryptByte()
This Method aims to encryption file with length 16 byte
Input : byte[]arr_state
Output : byte[]
Proses : - Conversion from form arrays to form block, setting its value to perform variable block_state
- Call method AddRoundKey() with input value = 0
- Perform looping round Nr – 1, and call method SubBytes(), ShiftRows(), MixColumns(), and AddRoundkey(). For method AddRoundKey() input value is iNr + 1.
- Call method SubBytes()
- Call method ShiftRows()
- Call method AddRoundkey() with input value is Nr.

f. DecryptByte()
This Method aims to decryption file with length 16 byte
Input : byte[]arr_state
Output : byte[]
Proses : - Conversion from form arrays to form block, setting its value to perform variable block_state
: - Call method Addroundkey() with input value is Nr
- Call method InvShiftRows()Call method InvsubBytes()
- Perform looping round iNr > 1, and call method AddRoundKey(), InvMixColumns(), InvShiftRows(), and InvSubBytes(). For method AddRoundKey() input value is iNr-1
- Call method AddRoundkey() with input value is 0.

g. build_sBox()
This Method aims to forming a series of constant matrix called sBox
Input :
Output :
Proses : Setting of value from the variable sBox with matrix 16 X 16

h. build_InvsBox()
This Method aims to forming a series of the substitution box inverse constant matrix called Inv s_Box.
Input :
Output :
Proses : Setting of value from variable iv_sBox and with matrix 16 X16

i. build_rCon()
This Method aims to forming a series of constant matrix called rCon
Input :
Output :
Proses : Setting value from variable rCon and with matrix (Nr + 1) X 4

j. SubBytes()
This Method aims to perform substitution between state box with sBox substitution.
Input :
Output :
Proses : Perform loop for iSubBytes < 16 for sBox substitution block_state

k. InvSubBytes()
This Method aims to perform inverse for substitution between state box with sBox substitution box.
Input :
Output :
Proses : Perform loop for iSubBytes < 16 for substitution block_state to iv_sBox.

l. ShiftRows()
This Method aims to perform cyclic rotation on block_state
Input :
Output :
Proses : Perform loop for iShiftrows < 16 for cyclic rotation.

m. InvShiftRows()
n. This Method aims to perform cyclic rotation on block_state
Input :
Output :
Proses : Perform loop for iShiftRows < 16 for cyclic rotation.

o. MixColums()
This Method aims to do the mixing between block_state with Transformation sBox.
Input :
Output :
Proses : Perform loop for iMixColumns < 4 for do mixing between block_state with Transformation sBox.

p. InvMixColumns()
This Method aims to do the mixing between block_state block_state with Transformation sBox inverse.

Input :
Output :
Proses : Perform loop for iMixColumn < 4 for do mixing between block_state with Transformation sBox inverse.

q. AddRoundKey()
This Method aims to perform XOR between block_state with upa-key in the order. Input : int ipos
Output :
Proses : Perform loop for iAddRoundKey < 16 for merge between block_state with upa-key in the order position the iPos.

r. build_Expansionkeys()
This Method aims to establish a series up-key that will be used for the method AddRoundKey()
Input :
Output :
Proses : - Setting keys for user input is the block_key ke block_w with position 0
- Perform loop iExpand < Nr, for get the upa-key.

s. GFMult()
This Method aims to perform polynomial multiplication.
Input : - byte b
- byte p
Output : int
Proses : - If the multiplier (p) with value 0X01, then return b value.
- If the multiplier (p) with value 0X02, then check b, if value < 128 then give the value of the value of bis shifted 1 bit to the left. If it is greater than 128, then the value of the results in shifted 1 bit to the left at XOR with the multiplier p.
- If the multiplier (p) with value 0X03, then a the result value back to GFMult(b, 0X02) in XOR with GFMult(b, 0X01)
- If multiplier (p) with value 0X09, then a the result value back to GFMult(GFMult(GFMult(b, 0X02), 0X02), 0X02) in XOR with GFMult (b, 0X01)
- If the multiplier (p) with value 0X0b, then a the result value back to GFMult(GFMult(GFMult(b, 0X02), 0X02), 0X02) in XOR with GFMult(b, 0X03)
- If the multiplier (p) with value 0X0d, then a the result value back to GFMult(GFMult(GFMult(b, 0X02), 0X02), 0X02) XOR GFMult(GFMult(b, 0X02), 0X02) and in XOR with GFMult(b, 0X01)
- If the multiplier (p) with value 0X0e, then a the result value back to GFMult(GFMult(GFMult(b, 0X02), 0X02), 0X02) XOR GFMult(GFMult(b, 0X02), 0X02) and in XOR with GFMult(b, 0X02)

t. PacketdTo16()
This Method aims to do package to an array of length 16
Input : byte[]arr
Output : byte[]
Proses : Perform loop for iPacked < iSize to move the conents of arr to variable tmpPackedTo16.

u. SetArrByPos()
This Method aims to do setting 16 byte from array arr_pos
Input : - byte[]arr_input
- int arr_pos
- ref byte[]arr_return
Output :
Proses : Perform loop for iArr smaller than the size of the array arr_input to perform setting of the arr_return in the position of the arr_pos.

v. GetArrByPos()
This Method aims to get 16 byte from the array in order with arr_pos
Input : - byte[]arr_input
- Int arr_pos
Output : byte[]
Proses : Perform loop for iArr value smaller than the size iBatas to get the array of the arr_input in order with arr_pos

5. The File Structure That Have Been Encrypted
Encrypted file structure is as follows:

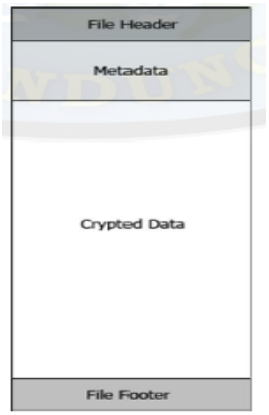

Figure 4 File Structure

IV. IMPLENTATION

The mai menu of the software is to display the encryption and decryption.

Figure 5 The Main Menu

1. The Encryption Process
   The encryption process steps are:
   a. Fill in your username
   b. Fill in your password
   c. Press the button encrypt
   d. Choose a file to the encrypt

2. The Decryption Process
   The decryption process steps are:
   a. Fill in your username
   b. Fill in your password
   c. Press the button decrypt
   d. Chose a file to the decrypt

V. CONCLUSION

The conclusion is:

1. The file security is assured if the encryption is done before the file in sent in a computer network.
2. AES algorithm, is a cryptographic algorithm that produces a good files security.
3. By performing encryption, file security aspects will be fulfiled.

REFERENCES

[1] Munir Rinaldi,"Cryptography", INFORMATIKA, 2006

[2] Brenton Chris, Hunt Cameron,"Network Security", SYBEX Inc. 2003

[3] Harbron R. Thomas, "File Systems; Structures and Algorithms", Prantice-Hall, Inc., 1988

[4] Pressman S Rogers, "Software Engineering", McGraw-Hill International Edition, 2005

[5] Bahrami Ali, "Object Oriented System Development; using the unified modeling language", The Mcgraw-Hill Book Co, 1999

G305

Comparison of K-Means and Agglomerative Hierarchical Clustering Method with Principal Component Analysis in Research Document Analysis

Emi Susilowati
Department of Informatics Engineering
University of Muhammadiyah Jakarta
Central Jakarta 10510
emi_emt@yahoo.com

Dwi Handoko
Badan Pengkajian dan Penerapan Teknologi
Balai IPTEKnet (http://www.bppt.go.id)
Jl. M.H. Thamrin No. 8 Jakarta Pusat
dwihdk@gmail.com

***Abstract*—Clustering is one of text processing techniques which is widely known and has been intensively used in *data mining*. Deciding the appropriate clustering method based on particular case study will produce an optimal cluster. One of deciding techniques is comparing one clustering methods with another. In this study, K-Means Clustering and Agglomerative Hierarchical Clustering Combined with Principal Component Analysis are compared to analyze research documents. Principal Component Analysis is used to reduce data dimension, since there are abundant features, approximately 5803 features, extracted from the documents. The result of K-Means and Agglomerative Hierarchical Clustering with PCA comparison based on validation test shows that K-Means produced lowest Sum of Square Error (SSE) which is 10088.4313 with number of features is 100. It can be concluded that chosen methods, K-Means, for the number of class k=9 generated labels automatically, thus we can get the meaning for each chosen method. The extracted meanings become new valuable knowledge from the dataset of research documents. Based on 9 classes that has been mentioned, we can see research trends for food security category. As for several years later, the best theme on food security is still around expansion of production land and reduction of land loss, while the topic of research is related to test of multi-location expectation furrow and creation of superior varieties.**

Keywords—clustering, k-means, hierarchical agglomerative clustering, principal components analysis, food security;

I. INTRODUCTION

Science and technology will be a force for the advancement of Indonesia , and also become a source of pride in the nation's life , when the research and development of science and technology and science and technology utilization activities carried out in harmony and mutually reinforcing (National Research Agenda, 2010). Research is very important in determining whether or not a developed and developing countries . So what about the development of science and technology (science) in Indonesia ? " Science Indonesia has reached its nadir . Research institutions we already marginalized , a phenomenon which can be directly seen from the poor quality of research results . The scientific community and the general public have been shoulder to shoulder pressing research quality " (Terry Mart , Reuters May 8, 2006 edition) . Low science and research activities in Indonesia outline caused by several factors such as : the establishment of a national seed research theme is not based on the competencies of Human Resources (HR) ; lack of international collaboration ; less optimal performance reviewer team ; lack of raw determination to the research criteria good for all disciplines ; lack of government intervention in improving the quality of national research (TerryMart , http://staff.fisika.ui.ac.id/tmart/nadir.html , access October 8, 2011).

Research Incentive Program is a program funded by the Ministry of Research and Technology in building science and technology associated with the development of the National Innovation System . Ministry of Research and Technology along with the National Research Council (DRN) sets out a number of products targets to be achieved through Intensive Research Program . For the 2010 fiscal year provided 50 product targets are translated into 294 activities by giving priority to the seven (7) areas of focus of the development of science and technology as listed in the National Short-Term Development Plan (RPJPN) and the 2005-2025 National Medium Term Development Plan (RPJMN) 2010 -2014 , one of them is the field of food security . The number of research activities at the Research Incentive Program conducted by academics and researchers produce data in the form of course report documents the results of research in large numbers . In the research report documents containing the data : title research ; agencies ; budget ; field of research ; locations ; year ; abstract ; etc. . These data when administered using certain techniques can yield valuable information in the form of knowledge. Techniques or methods are known as data mining. Han, J. and Kamber , M. (2006:7) , Provide the definition of data mining as the process of discovering interesting knowledge from large amount of data stored in databases , data warehouses , or other information storage . Cluster techniques include techniques that are well known and widely used in data mining . The main purpose of the methods or techniques cluster is a grouping of a number of data or objects into clusters (groups) so that in each cluster will contain the data as closely as possible. Clustering is one of the unsupervised learning techniques which do not need to train

them or in other words there is no learning phase (Santosa , Budi . 2007:33) .

Clustering techniques can be used for document clustering research reports , so that the expected output of the clustering process can yield valuable information in the form of knowledge (knowledge) is needed as to identify trends or trends in any category of research focus areas of science and technology development , research themes what is in demand by the academics and researchers , institutions involved in the research , any location that is frequently used in research and much more valuable information that can be obtained from extracting data from documents of research reports . Selection of the appropriate cluster method will produce the optimal cluster . One way of selecting the appropriate cluster method is to perform a comparison between the cluster method to cluster the other methods . In this study discusses the results of the analysis report documents the results of a comparison study using a cluster of K - Means and Hierarchical Agglomerative Clustering with Principal Components Analysis . Use of Principal Component Analysis is used to reduce the dimension of data that has a large amount because featrure (word unique money) in this study is 5828 . To obtain a quality cluster can not be determined based on a subjective opinion , but must go through testing the validity of the cluster . In this study the validity of the clusters are used for the K - Means and Agglomerative Hierarchical Clustering is the Sum of Squared Error (SSE) . Expected from the comparison of the two methods can be seen right cluster method based on the determination of optimal clusters based on the validity of the cluster that has the value of Sum of Squared Error is the smallest that can be analyzed to document and interpret research reports Research Incentive Program based automatic label formed.

II. FOUNDATION FRAMEWORK FOR THINKING

According to (Chakrabarti et al., 2009:3), "Data mining is defined as the process of discovering patterns in the data. The patterns discovered must be meaningful in that they lead to some advantage, usually an economic advantage. The Data is present in substantial quantities Invariably ". In this definition submitted that as the process of data mining to find patterns in the data. Patterns discovered must be meaningful and bring some advantages, usually an economic advantage. Data is always there in large numbers.

The definition of data mining is also proposed Han, J. and Kamber, M. (2006:7), "Data mining is the process of discovering interesting knowledge from large amounts of the data stored in databases, data warehouses, or other information repositories". Data mining is the process of discovering interesting knowledge from large amount of data stored in databases, data warehouses, or other information storage.

A. Partitioning Method

K-Means is the most popular and very easy to understand in partitonal clustering algorithm. The main idea of the K-Means can be described in the following steps (Arriyani, 2010):

1. Determine the desired number of clusters k

2. Initialize k cluster center (centroid) by random / random

3. Place each data object to the cluster or nearby. The proximity of the two objects is determined by the distance. Distance used in the K-Means algorithm is Euclidean Distance.

4. Recalculate the cluster centers cluster membership now. Cluster center is the average (mean) of all the data or objects within a particular cluster. Back again to step 3 until no more objects moving clusters.

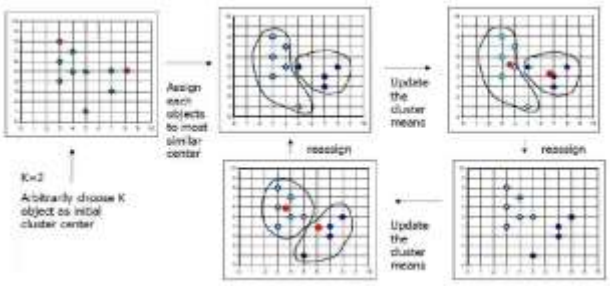

Fig. 1. Examples of K-Means Algorithm
Source: Han, J. and Kamber, M. (2001)

B. Hierarchical Method

Agglomerative hierarchical clustering algorithm to consider starting the process all the data as a set of initial clusters. Then clusters are combined in a larger group, this process continues over and over until you have the desired group. Agglomerative algorithms can be described in 3 steps (Chen, 2004):

1. Change object attribute into the distance matrix

2. Place each object as a cluster (if it has N objects, meaning have N clusters at first.

3. Repeat step two until the number of clusters is one, by the way:

   a. Combine the two (2) nearest cluster

   b. Update the value of the distance matrix

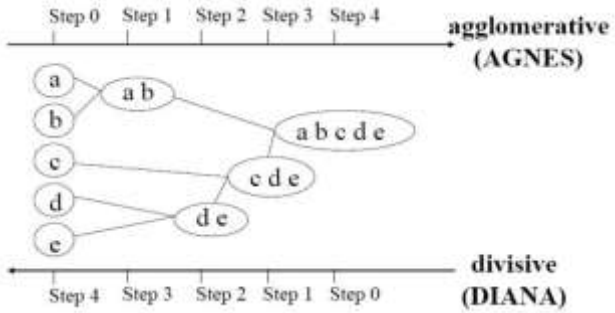

Fig. 2. Agglomerative and divisive Hierarchical Clustering Data Objects {a, b, c, d, e}

C. Principal Component Analysis

The dimensions of the data is determined by the number of features on the object. One method used to reduce the number of dimensions of the data is PCA (Principal Component Analysis). PCA procedure basically aims to simplify the observed variables by means of shrinking (reducing)

dimension. This is done by eliminating the correlation between the independent variables through the transformation of the independent variables to the origin of a new variable that is not correlated at all (Soemartini, 2008). With the help of matlab software, can use PCA procedure to reduce high correlated variables so as to assess which variables are truly worthy to be included in subsequent analyzes.

III. RESEARCH METHODOLOGY

This research was conducted in several stages in the framework described in Figure 3.1.

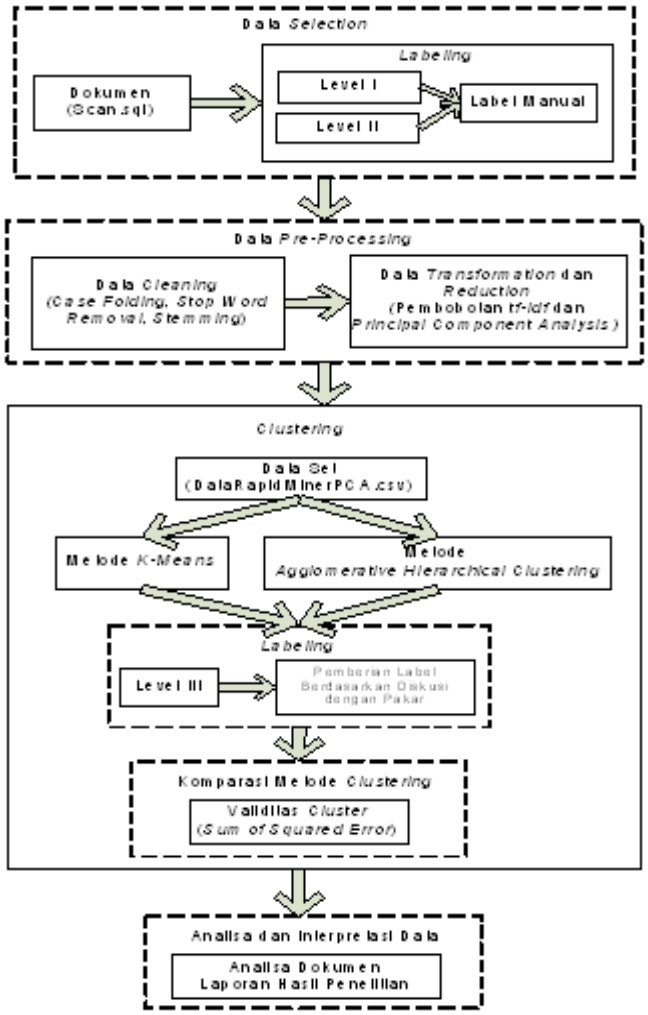

Fig. 3. Research Framework

A. Data Selection

In this study, the data used is document research reports Research Incentive Program in 2010 in food security, amounting to 391 documents in the form of structure query language (SQL) and then transformed to forms xml extension to facilitate the processing of data. The first step in data processing is a research report documents labeling or labeling manually, by the provision of food security categories for level I and level II for 5 subcategories. Sample report documents the results of research in the field of food security in 2010 is as follows:

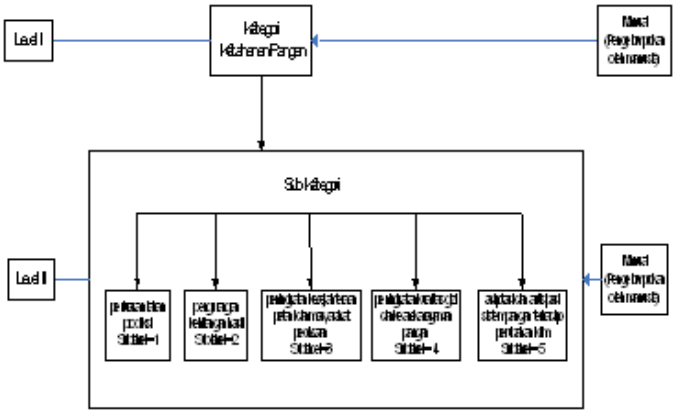

Fig. 4. Document Field Research Report on Food Security Source: Agency for the Assessment and Application of Technology (BPPT, 2010)

Fig. 5. On the Labeling Process Document Manually (Grouping by humans)

B. Data Preprocessing

To get the most out of data preprocessing stage used in the Java programming language and matlab. Data preprocessing stage is conducted in this study as follows:

1. Beheading words (tokens) in a document with the aim to facilitate the elimination of punctuation, numbers and words that are included in the stop word. Making all the words contained in the document to lowercase everything (case folding). Only the letter 'a' to 'z' that can be processed. The goal is to eliminate the duplication of the word.

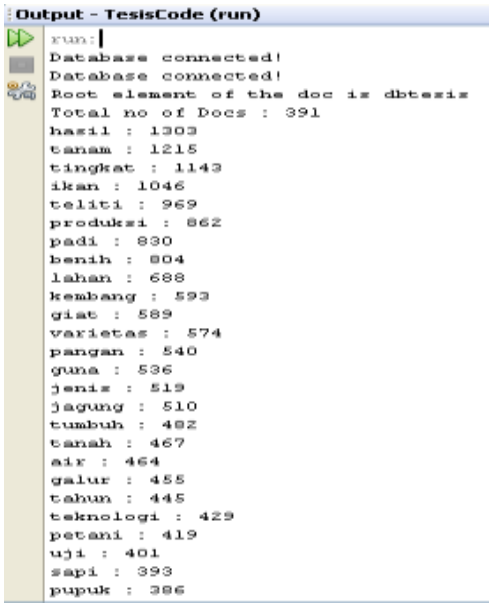

Fig. 6. Token process or decoding of words in a document

2. Making all the words contained in the document to lowercase everything (case folding). Only the letter 'a' to 'z' that can be processed. The goal is to eliminate the duplication of words.

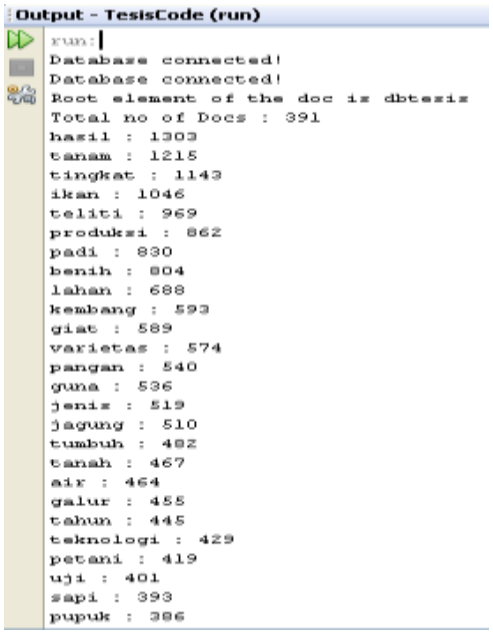

Fig. 7. Token process or decoding of words in a document

3. Do stop word or words that have no meaning but has a frequency of occurrence is very frequent in the document.

Fig. 8. Examples of words include Stop Word

4. Change all said additive into the base word (stemming)

id	term	stem
1	pengembangan	kembang
2	pembangkit	bangkit
3	peningkatan	tingkat
4	mendukung	dukung
5	pembuatan	buat
6	memanfaatkan	manfaat
7	meningkatkan	tingkat
8	pemakaian	pakai
10	kehandalan	handal
11	kesiapan	siap
12	kebijakan	bijak
13	mendorong	dorong
14	peralatan	alat
15	peranan	peran
16	pertumbuhan	tumbuh
17	ketahanan	tahan

Fig. 9. Examples of the results stemming the words in the document

5. Data transformation or data transformation is a process by which data is transformed into a form that can be in mining-right. The way that the object word (term) can in mining-it is a way of weighting the word using TF-IDF (Term Frequency - Inverse Document Frequency). Here is an example of a data matrix containing the results of weighting features 19 objects and 5 attributes.

TABLE I. SAMPLE DATA MATRIX FEATURE WEIGHTING RESULTS

-1.3847	2.481939	1.667287
-1.25787	-1.60353	-0.6839
-0.83293	0.789304	1.675255
-1.09657	-1.46045	1.89896
-1.50955	-1.72425	0.276499
-1.47843	-1.7297	-1.28111
-1.00914	-1.47069	1.303258
-0.71909	0.911802	2.255076
-1.44674	-1.64476	1.595621
-1.53786	-1.73888	1.264755
-0.59976	-1.30967	0.852068
-0.35283	7.387291	1.855891
-1.56131	-1.79753	0.042046
-1.30633	-1.68313	0.95556
-1.52221	0.670898	2.081172

In the table above can be explained from the data that the report documents the results of research into a form that can be transformed in ¬-right-mining to be understood by the data mining tool. Transformation of the data in this study using feature weighting tf-idf approach (term frequency - inverse document frequency).

6. Data reduction or data reduction is a way to reduce the number of data dimensions. The dimensions of the data is determined by the number of features on the object. One method used to reduce the number of dimensions of the data is PCA (Principal Component Analysis). PCA procedure basically aims to simplify the observed variables by means of shrinking (reducing) dimension. This is done by eliminating the correlation between the independent variables through the transformation of the independent variables to the origin of a new variable that is not correlated at all (Soemartini, 2008). With the help of matlab software, can use PCA procedure to reduce the independent variables are highly correlated so as to assess which variables are truly worthy to be included in subsequent analyzes.

TABLE II. EXAMPLE OF CALCULATION RESULTS FEATURE WEIGHTING USING PCA (DATA MATRIX CONTAINING 15 3 OBJECTS AND ATTRIBUTES)

-1.3847	2.481939	1.667287
-1.25787	-1.60353	-0.6839
-0.83293	0.789304	1.675255
-1.09657	-1.46045	1.89896
-1.50955	-1.72425	0.276499
-1.47843	-1.7297	-1.28111
-1.00914	-1.47069	1.303258
-0.71909	0.911802	2.255076
-1.44674	-1.64476	1.595621
-1.53786	-1.73888	1.264755
-0.59976	-1.30967	0.852068
-0.35283	7.387291	1.855891
-1.56131	-1.79753	0.042046
-1.30633	-1.68313	0.95556
-1.52221	0.670898	2.081172

The table above can be explained as follows, from the original data feature weighting totaling 391 objects (m) and 5803 attributes / term (n) is then calculated using a PCA with the help of matlab software, feature weighting calculation results obtained by PCA with the object number 391 and the number of attributes 100.

C. Clustering

This study used comparison of two methods, namely K-Means clustering and Agglomerative Hierarchical Clustering by Principal Components Analysis which serves to reduce the dimension of data that has a large amount. To measure the distance between two points proximity euclidean distance is used as the data dimension suitable for many of the most popular and used to calculate the dissimilarity, dissimilarity calculating formula is shown in equation 1.

$$d(i,j)=\sqrt{(x_{i1}-x_{j1})^2+(x_{i2}-x_{j2})^2+\cdots+(x_{in}-x_{jn})^2}, \quad (1)$$

D. Cluster Validity

The validity of the cluster is the procedure to assess the quality of clustering results and find a good strategy for cluster-specific applications. The validity of this cluster aims to find an optimal cluster and can interpret the pattern of the resulting clusters. In this study the validity of clusters used is Sum of Squared Error (SSE). The smaller the value of SSE will be better. Here is a formula of the SSE:

$$\mathrm{SSE} = \sum_{i=1}^{K} \sum_{x \in C_i} dist(\mathbf{c}_i, \mathbf{x})^2 \quad (2)$$

In equation 2 Sum of Squared Error (SSE) is used to determine the clustering result is better, if the initialization centroidnya different. In this study to find the optimal cluster from the comparison method K-Means and Agglomerative Hierarchical Clustering is used on the calculation of the smallest SSE. Techniques to minimize the value of SSE is to increase the value of k (Atastina, ITT Telkom).

E. Clustering Comparison Method

In this research, comparative method of K-Means and Hierarchical Agglomerative Clustering based on the results of the cluster, the processing time and the value of Sum of Squared Error (SSE).

F. Data Analysis and Interpretation

Based on the selection method of the best clusters were compared between the 2 methods, namely: K-Means and Agglomerative Hierarchical Clustering clusters are obtained optimal results. The resulting optimal clusters can be used to analyze the report documents the results of research by way of interpreting the data in the cluster formed. The results at this stage of the analysis and interpretation of this data can find new information that is interesting and valuable.

IV. RESULT AND DESCRIPTION

A. K-Means clustering

In the K-Means method, should be determined in advance the number of clusters desired. In this study, the number of clusters (k) that is used is k = 5, k = 7, k = 9. Here is the result of the clustering of each predefined number of clusters from the beginning of the K-Means method.

TABLE III. RESULTS OF K-MEANS CLUSTERING (K = 5)

label / cluster	Perluasan Lahan Produksi	Pengurangan Kehilangan Hasil	Peningkatan Kesejahteraan Petani dan Masyarakat Pedesaan	Peningkatan Kualitas Gizi dan Keanekaragaman Pangan	Adaptasi dan Antisipasi Sistem Pangan Terhadap Perubahan Iklim	Label	Anggota Cluster
0	13	6	4	2	0	Pengembangan Budidaya dan Teknologi	25
1	1	0	0	0	0	Evaluasi Sosial Ekonomi	1
2	22	1	0	0	0	Uji Multilokasi Galur Harapan	23
3	24	0	1	1	0	Pengkajian Penerapan Kebutuhan dan Sistem Penyediaan Ket	26
4	11	2	0	0	0	Pengkajian Teknologi Reproduksi	13
5	223	36	22	9	10	Pemberdayaan Keterse Unggul	382
6	1	0	0	0	0	Kajian Keterkaitan Produksi, Perdagangan dan Konsumsi	1
						Jumlah Data Set	381

TABLE IV. RESULTS OF K-MEANS CLUSTERING (K = 7)

label / cluster	Perluasan Lahan Produksi	Pengurangan Kehilangan Hasil	Peningkatan Kesejahteraan Petani dan Masyarakat Pedesaan	Peningkatan Kualitas Gizi dan Keanekaragaman Pangan	Adaptasi dan Antisipasi Sistem Pangan Terhadap Perubahan Iklim	Label	Anggota Cluster
0	13	6	4	2	0	Pengembangan Budidaya dan Teknologi	25
1	1	0	0	0	0	Evaluasi Sosial Ekonomi	1
2	21	0	0	0	0	Uji Multilokasi Galur Harapan	21
3	0	1	0	0	0	Assesed Usaha Tani	1
4	15	3	1	0	0	Pengkajian Teknologi Reproduksi	19
5	23	0	1	1	0	Pengkajian Penerapan Kebutuhan dan Sistem Penyediaan Kebutuhan	25
6	3	0	0	0	0	Reproduksi dan Mobilitas Sapi Kembar	3
7	220	35	21	9	10	Pemberdayaan Keterse Unggul	295
8	1	0	0	0	0	Kajian Keterkaitan Produksi, Perdagangan dan Konsumsi	1
						Jumlah Data Set	381

TABLE V. RESULTS OF K-MEANS CLUSTERING (K = 9)

label / cluster	Perluasan Lahan Produksi	Pengurangan Kehilangan Hasil	Peningkatan Kesejahteraan Petani dan Masyarakat Pedesaan	Peningkatan Kualitas Gizi dan Keanekaragaman Pangan	Adaptasi dan Antisipasi Sistem Pangan Terhadap Perubahan Iklim	Label	Anggota Cluster
0	296	44	27	12	10	Pemberdayaan Keterse Unggul, Pengkajian Penerapan Kebutuhan dan Teknologi Reproduksi	389
1	1	0	0	0	0	Evaluasi Sosial Ekonomi	1
2	1	0	0	0	0	Kajian Keterkaitan Produksi, Perdagangan dan Konsumsi	1
						Jumlah Data Set	381

B. Agglomerative Clustering with hierrachical Clustering (AHC)

AHC clustering method, not determined in advance the number of clusters desired, since the number of clusters obtained from the cutting (cut off) the right dendogram based on the largest gap of each stage and then specify the number of clusters are formed based on the results of the cut-off.

TABLE VI. AGGLOMERATIVE HIERARCHICAL CLUSTERING RESULTS CLUSTERING (AHC)

label / cluster	Perluasan Lahan Produksi	Pengurangan Kehilangan Hasil	Peningkatan Kesejahteraan Petani dan Masyarakat Pedesaan	Peningkatan Kualitas Gizi dan Keanekaragaman Pangan	Adaptasi dan Antisipasi Sistem Pangan Terhadap Perubahan Iklim	Label	Anggota Cluster
0	296	44	27	12	10	Pemberdayaan Keterse Unggul, Pengkajian Penerapan Kebutuhan dan Teknologi Reproduksi	389
1	1	0	0	0	0	Evaluasi Sosial Ekonomi	1
2	1	0	0	0	0	Kajian Keterkaitan Produksi, Perdagangan dan Konsumsi	1
						Jumlah Data Set	381

AHC clustering method, not determined in advance the number of clusters desired, since the number of clusters obtained from the cutting (cut off) the right dendogram based on the largest gap of each stage and then specify the number of clusters are formed based on the results of the cut-off.

C. Comparison of value Sum of Squared Error (SSE)

From the results of running the Sum of Squared Error (SSE) of 20 times running by considering the number of features from the range of 100 up to 400 objects. SSE is obtained as follows:

TABLE VII. COMPARISON OF THE RESULTS OF SSE VALUE

Cluster	*K-Means*			AHC
Objek	k=5	k=7	k=9	
100	**10754.928**	**10184.21173**	**10088.431**	**10849.704**
150	12555.056	11997.8994	11683.569	12506.799
200	13859	13280.9117	13070.446	13724.117
250	14614.999	14330.6002	14237.411	14623.203
300	15363.228	15045.5535	14903.604	15252.708
350	15736.686	15494.1683	15319.227	15689.444
400	15935.178	15695.6816	15518.633	15888.821
Rata2	14117.011	13718.4323	**13545.903**	**14076.4**

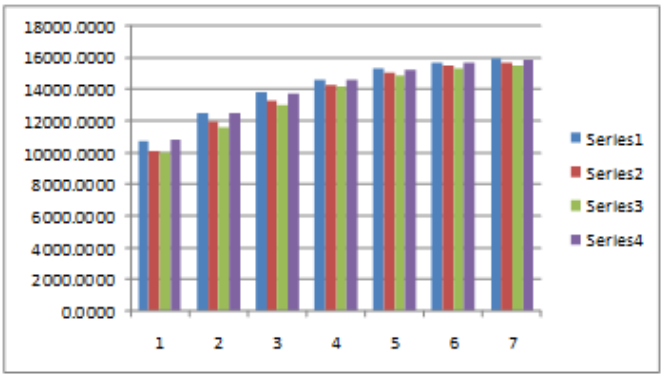

Fig. 10. Comparison of the results of SSE value for the K-Means method (k = 5, k = 7, k = 9) and AHC Methods

Based on Table VII. and figure 10 on the results of the comparison value of SSE, SSE average value for K-Means is the smallest number of clusters 13545.9030 at k = 9 and Agglomerative Hierarchical Clustering (AHC) has an average value of the SSE at 14076.3995. This indicates that the average value of the best (smallest) value of SSE is the number of K-Means cluster of nine (9). This means that the method of K-Means cluster with the number nine (9) to find members of each cluster are more similar than the AHC method.

D. Selected Results Clustering Analysis Method

Clustering results are used to make the analysis and interpretation of the data is the result of clustering using K-Means elected dengann number of clusters k = 9. This is because the value of the SSE of the K-Means method is smaller than the AHC method, which means that the error in the method of K-Means clustering smaller.

TABLE VIII. RESULT CLUSTERING METHOD CHOSEN BY K-MEANS (K = 9)

label cluster	Perluasan Lahan Produksi	Pengurangan Kehilangan Hasil	Peningkatan Kesejahteraan Petani dan Masyarakat	Peningkatan Kualitas Gizi dan Keanekaragaman	Adaptasi dan Antisipasi Sistem Pangan Terhadap	Anggota Cluster	Label
1	13	6	4	2	0	25	Pengembangan Budidaya dan Teknologi
2	1	0	0	0	0	1	Evaluasi Sosial Ekonomi
3	21	0	0	0	0	21	Uji Multilokasi Galur Harapan
4	0	1	0	0	0	1	Asuransi Usaha Tani
5	15	3	1	0	0	19	Pengkajian Teknologi Reproduksi
6	23	0	1	1	0	25	Pengkajian Pemetaan Kebutuhan dan Sistem Penyediaan Kebutuhan
7	3	0	0	0	0	3	Reproduksi dan Mobilitas Sapi Kembar
8	220	35	21	9	10	295	Pembentukan Varietas Unggul
9	1	0	0	0	0	1	Kajian Keterkaitan Produksi, Perdagangan dan Konsumsi
					Jumlah Data Sets	391	

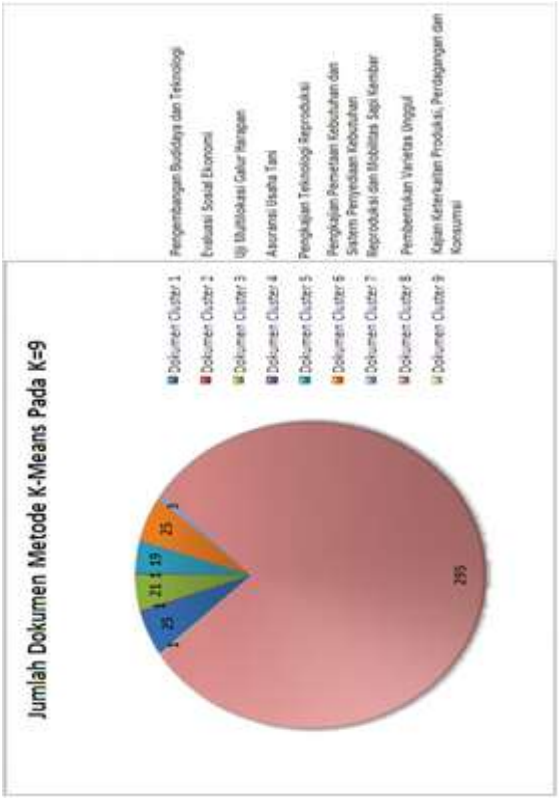

Fig. 11. Number of documents per-Cluster

Explanations for Table VIII. and Figure 11 are follows:

1. For Cluster 1 is a class where researchers concentrated on the theme of food security research subcategories expansion of production, reduction of yield loss, improving the welfare of farmers and communities, and improving the nutritional quality and diversity. Making more research topics range of Aquaculture Development and Technology.
2. For Cluster 2 is a classroom in which researchers concentrate on the theme of food security research subcategories expansion of production. Making research topics on Economic Social Evaluation. Small number of members can be considered as outliers or extreme data state that is different from the rules in general. It can be concluded that in 2010, the research topics that discuss the socio-economic evaluation is very rare.
3. For cluster 3 is the class in which the researchers concentrated on the theme of food security research subcategories expansion of production. Making all research topics range from about Strains Hope multilocation trials.
4. For cluster 4 is a class in which the researchers concentrated on the theme of food security research subcategories reduction in yield loss. Making research topics about Farm Insurance. Small number of members can be considered as outliers or extreme data state that is different from the rules in general. It can be concluded that in 2010, the research topics that discuss Farm Insurance is very rare.
5. For cluster 4 is a class in which the researchers concentrated on the theme of food security research subcategories reduction in yield loss. Making research topics about Farm Insurance. Small number of members can be considered as outliers or extreme data state that is different from the rules in general. It can be concluded that in 2010, the research topics that discuss Farm Insurance is very rare.
6. For cluster 6 is a class where researchers concentrated on the theme of food security research subcategories expansion of production, improving the welfare of farmers and communities and increased nutritional quality and diversity. Making more research topics range of Mapping Needs Assessment and Provision System Requirements.
7. For cluster 7 is a class where researchers concentrated on the theme of food security research subcategories expansion of production. Making all research topics range of Reproduction and Mobility Cattle Twins.
8. For cluster 8 is a class where researchers concentrated on the theme of food security research subcategories expansion of production, reduction of yield loss, improving the welfare of farmers and communities, and improving the nutritional quality and diversity, and Adaptation and Food Systems Against Climate Anticipation. Making more research topics range from about Development Establishment Varieties.
9. For cluster 9 is the class in which the researchers concentrated on the theme of food security research subcategories expansion of production. Making research topics on Assessment of Trade Linkages, Production and Consumption. Small number of members can be considered as outliers or extreme data state that is different from the rules in general. It can be concluded that in 2010, the research topics that discuss Linkage Study of Trade, Production and Consumption extremely rare.

E. Research Implications

The results of the comparison method of K-Means and Hierarchical Agglomerative Clustering with PCA based validation test smallest SSE values obtained can be concluded that the chosen method is the method of K-Means for k = 9, the label is automatically generated to obtain meaning for each selected cluster method, meaning that produced is knowledge (knowledge) is a valuable new set of documents from a set of data research reports. Of the nine (9) classes can be seen above the trend of the future for research on food security category of research that still revolves around the theme of excellent research on Land Expansion of Production and Reduction of Loss results, the research topics related to strain Hope multilocation trials and Formation of Varieties.

V. Conclusion and Recommendation

A. Selected Results Clustering Analysis Method

From the results of research conducted on the data selection to analysis and interpretation of data for analysis report documents the results of research using the comparison method of k-means and agglomerative hierarchical clustering with principal component analysis it was concluded that data mining techniques can be used to analyze the report documents the results of research based clustering procedure because of the comparison method of K - means and Hierarchical Agglomerative clustering with PCA based validation test values obtained Sum of Squared Error (SSE) smallest , this means that the chosen method is the method of K - means for k = 9 is a method with optimal clustering results where cluster labeling method that has elected to have a sense of knowledge (knowledge) is a valuable new set of documents from a set of data research reports . Of the nine (9) classes that have been formed by clustering automatically by the program and labeling (labeling) involving food security experts can be seen in the future research trends for categories of food security research that excellent research theme still revolves around the expansion of production and loss reduction the results of the research topics related to the formation or assembly of high-yielding varieties or clones or varieties of seeds .

B. Selected Results Clustering Analysis Method

For subsequent studies that combine partitioning methods and hierarchical methods. Calculations performed prior to the K-Means method and proceed with the calculation method of Agglomerative Hierarchical Clustering. To reduce the number of dimensions for the large amounts of data can use the Singular Value Decomposition or Principal Component Analysis. To get the optimal cluster can use two (2) test the validity as well as to increase the level of accuracy of the results of the cluster, such as the F-Measure and Purity.

Acknowledgment

The authors would like to thank Department Head of Informatics Engineering, and Dean of Faculty of Engineering University of Muhammadiyah Jakarta that have given a chance to participate AEMT conference as speaker.

References

[1] Chris Ding dan Xiaofeng He. *Principal Component Analysis and Effective K-Means Clustering*

[2] Chapman, et all., 2000. CRISP-DM 1.0 : *Step by Step Data Mining Guide*, CRISP-DM *Consortium*

[3] Han, J. dan Kamber, M (2001) . Data Mining : *Concepts and Techniques First Edition*, Morgan Kaufmann

[4] Han, J. dan Kamber, M (2001) . Data Mining : *Concepts and Techniques Second Edition*, Morgan Kaufmann

[5] Kusrini dan Luthfi, Emha Taufiq (2009). Algoritma Data Mining, Andi Publisher, Yogyakarta

[6] Santosa, Budi. (2007). Teknik Pemanfaatan Bisnis Dengan Data *Mining*, Graha Ilmu

[7] Rizky, Wibisono, Kusnendar. (2009). Perbandingan *Clustering Based on Frequent Word Sequence* dan *K-Means* Untuk pengelompokan Dokumen Berbahasa Indonesia

[8] Umran, Munzir dan Abidin, Taufik Fuadi (2009). Pengelompokkan Dokumen Menggunakan *K-Means* dan *Singular Value Decomposition* : Studi Kasus Menggunakan Blog

[9] Tajunisha dan Saravanan (2010). *An Increased Performance of Clustering High Dimensional Data Using Principal Component Analysis*

G306

LEVEL PREDICTION OF PNEUMONIA IN CHILDREN TIME RANGE BASED BREASTFEEDING, IMMUNIZATION STATUS, NUTRITION USING K-MEANS

Yusriel Ardian
Faculty of Information Technology, University of Malang
Kanjuruhan
acilnet@yahoo.com

Wiji Setiyaningsih
Faculty of Information Technology, University of Malang
Kanjuruhan
wiji_setiya@yahoo.co.id

Abstract - At the core contribution of which can be obtained from the results of this study are related parties of the neighborhood health center level, health centers and hospitals, particularly hospitals that become the object of study can obtain information that supported accurate data about the importance of exclusive breastfeeding, immunization and nutrition in toddlers, in order to suppress or minimize disease of children under five will be. Related parties as early as possible to disseminate to the public the relationship between exclusive breastfeeding, immunization and nutritional status on disease susceptibility that can be suffered by a toddler.NWith the implementation of K - Means algorithm in the process of knowledge about high clusterisasi pneumonia in toddlers based immunization status, the time range of exclusive breastfeeding, and nutrition status of children under five, are expected to contribute grouping and determination of the most appropriate number of clusters/accurate to predict the value of level of frequency/frequency of visits toddler to the hospital for treatment . The proposed plan of activities to collect and study the literature relating to the concept of DM clustering, which uses K-Means algorithm . Literature sources such as text books, papers, journals, scientific papers.

Keywords : clustering, K-Means, Pneumonia, ISPA, nutrition, immunization, exclusive breastfeeding.

I. PRELIMINARY

ISPA is a disease affecting one or more of the parts and the respiratory tract from the nose (upper line) to the alveoli (bottom line) including adneksanya networks, such as the sinuses, middle ear and pleural cavity. While the infection that attacks the lower respiratory tract (lungs) one of which is pneumonia. Pneumonia is an acute inflammatory process in the lung tissue (alveoli) due to infectious germs that cause respiratory distress. Pneumonia is dangerous because it can lead to death, because the lungs are not able to function to get oxygen to the body (Depkes RI, 2007). Pneumonia has become a health problem in the world because of the high death rate. This does not just happen in developing countries, but also in developed countries.

According to research conducted Mery and Widyaiswara (2012), which attacked pneumonia in infants is influenced by the mother's level of education, immunization status, exclusive breastfeeding, and nutritional status of children under five. Meanwhile, according to Dea and Yandofa (2012) found a significant association between nutritional status on the incidence of pneumonia in young children, and there is a significant association between breast feeding on the incidence of pneumonia in young children.

The World Health Organization (WHO) in 2005 estimated deaths from pneumonia in children under five worldwide about 19 percent or about 1.6 to 2.2 million. Of which about 70 percent occur in developing countries, especially Africa and Southeast Asia. World Pneumonia Day (WPD) reported that Indonesia is the country with the incidence of pneumonia 6th rank in the world. In Indonesia, pneumonia is the third cause of death after cardiovascular and tuberculosis. Pneumonia in children under five mortality rate in Indonesia is estimated at 21%. The morbidity rate was estimated at 250 to 299 per 1,000 children under five each year.

Dr. I. Boediman, Sp. A (K) in the World Pneumonia Day 2010 seminar revealed that the child has a healthy immune system that protects the lungs from germs. Child with a weak immune system such as child malnutrition, especially because not exclusively breastfed, vitamin A deficiency and measles has a high risk of pneumonia (Sutriyanto, 2011). The high rates of respiratory tract infections in infants related to environmental sanitation, inadequate health services and with low immunization coverage. Respiratory tract infections in infants are also influenced by the pattern of breastfeeding and complementary feeding. In infants who had been given food before the age of 4-6 months or even a few moments after

birth can lead to infants susceptible to disease infection (LIPI, 2004).

According to Professor Guido Moro Macedonis Melloni Maternity Hospital of Milan about two- thirds of the benefits of breastfeeding the baby's immune system is in the stomach , so it is important to pay attention to what the baby is eating and drinking . That is why baby mothers breastfed newborn desperately need especially during the first 6 months of life.

As the baby 's first food , it turns out not only nutrients breast milk is perfect for baby and closer emotional relationship between mother and baby, but at the same time provide protection for beneficial breastfeeding strengthens the natural immunity of newborns . So many benefits of breast milk for the baby, ten magic among other things: 1). Breast milk strengthens the immune system. The main components of the immune system builder ASI is a prebiotic. 2). Breastfeeding lowers the risk of allergies. 3). Breastfeeding lowers the risk of gastrointestinal disease, such as diarrhea and improve immunity in the digestive system. 4). Breastfeeding lowers the risk of respiratory problems , such as colds and coughs. 5). Breast milk is rich in AA | DHA that support the growth of children's intelligence. 6). Breast milk contains natural prebiotics to support the growth of intestinal flora. 7). Breast milk composition proper nutrition and a balanced (where asi only have one).

Health Ministry data shows, breast milk can reduce mortality by 17 percent in the new birth (neonatal) and 12 per cent in children under five years old. Newborn mortality rate nationally is 34 per 1,000 live births and the mortality rate of children under five years old to 44 children per 1,000 live births. Regrettably, the rate of exclusive breastfeeding in the country is still very low. Only about 22 percent of mothers giving birth to her baby exclusively breastfed. The results of recent research investigators showed that infants who received complementary foods before 6 months of age (non- exclusive breastfeeding) would be more frequent diarrhea, constipation, respiratory infection (Soraya , 2005) (Suprihadi, 2010).

Based on the description of the literature review studies mentioned above, the knowledge of the high pneumonia in toddlers is an important thing that needs to be investigated, particularly by common factors known to mothers who have children under five as immunization status, time range of exclusive breastfeeding, and nutritional status in toddlers.

There is a field of science that is able to solve the problem is data mining. Data mining is an activity that includes the collection, use historical data to determine the regularities, patterns or relationships in large data sets. One of the major tasks of data mining is the clustering of clustering where the data is grouped not have any examples of groups (Santosa, 2007).

One clustering method which can be used as a solution to these problems is the method of K - Means, as was done by the researcher Dwi Noviati (2012) for regional revenue budget, or Budi and Patdono for market segmentation.

With the implementation of the K-Means algorithm in the process of knowledge about high clusterisasi pneumonia in toddlers based immunization status, time range of exclusive breastfeeding, and nutritional status of children under five, are expected to contribute grouping and the determination of the most appropriate number of clusters/accurate to predict the value of level of frequency/frequency of visits toddler to hospital for treatment. In essence the contribution that can be obtained from the results of this study are related parties of the neighborhood health center level, health centers and hospitals, particularly hospitals that become the object of study can obtain information that supported accurate data about the importance of exclusive breastfeeding, immunization and nutrition in infants, in order to suppress or minimize disease of children under five will be. Related parties as early as possible to disseminate to the public the relationship between exclusive breastfeeding, immunization and nutritional status on disease susceptibility that can be suffered by toddlers.

II. LITERATURE NUTRITIONAL STATUS AND THE BREASTFEEDING TODDLERS

Many factors affect the high number of deaths from pneumonia in children under five, namely: age, gender, malnutrition, low birth weight, breastfeeding status, immunization status, kepadatanhunian, ventilation, air pollution in the home. The high incidence of pneumonia primarily affects infants and toddlers age group. Toddlers with poor nutrition will be more susceptible to pneumonia than infants with normal nutrition for endurance factor is less. Infectious diseases alone would cause infants do not have the appetite and lead to malnutrition. In a state of malnutrition, infants are more susceptible to pneumonia attack even longer (Dea Yandofa, 2012).

One of the risk factors that play a role in the incidence of pneumonia in children is nutritional status, where the interaction between infection and protein-energy malnutrition (PEM) has long been recognized, both conditions synergistic, mutual influence, which predisposes to the other one. In PEM, decreased body resistance and virulence of pathogens causing stronger balance will be disturbed and infection, whereas one of the main determinants in maintaining that balance is the nutritional status of children . Immune system in infants or toddlers not yet completely formed. Therefore, the baby will be more susceptible to infections if they do not get adequate nutrition. This is reinforced by research Rusepno (2005) which says that nutrition and infection are factors that affect the growth of children in developing countries, including Indonesia. Plus the delay in providing nutrition services will result in damage that is difficult and may not even be helped (Dea Yandofa, 2012).

III. RESEARCH METHODS

Implementation methods of research used in writing this time is the experimental method. Experimental method is a

design study that identified a causal relationship (Sudaryono et al: 45, 2011).

The explanation of this research method is as follows:

A. Literature Study

By collecting and studying the literature relating to the concept of DM clustering, which uses K-Means algorithm. Literature sources such as text books, papers, journal, scientific papers, and supporting websites.

B. Archive Data Collection

To find the necessary information, the author conducted data collection archives.

C. Preprocessing Of Data

Preprocessing the data include:

• Selection of data

To select a data set (dataset) which will be used in this paper, namely the data range time exclusive breastfeeding, immunization status, and nutrition.

• Cleaning

To clean the data, the complete data, removing duplicate data, remove noise.

• Transformation of data

To format the data to be ready clustered.

D. Clustering Using K-Means Algorithm

Stage of the process where data is already dipraproses in the cluster by using the workings of K-Means algorithm.

• Select the number of clusters k. Initialize k cluster centers can be done in various ways. How random is often used, the cluster centers are given by the initial value and the random numbers are used as initial cluster centers.

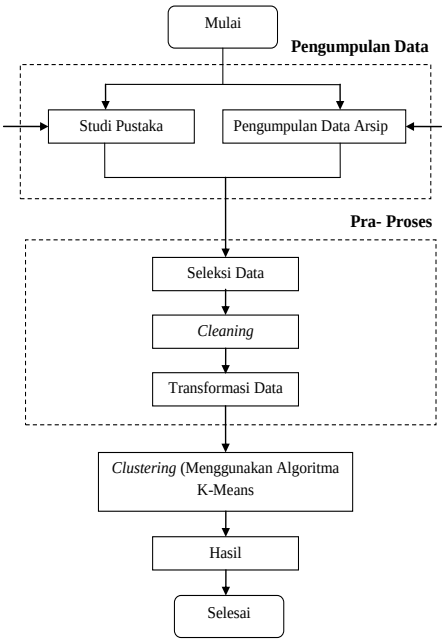

Figure 1. Stages of Research

E. Place each data/object to the nearest cluster, proximity of the two objects is determined by the distance between the two objects . Similarly, the proximity of the data to a particular cluster is determined by the distance between the data center of the cluster. In this stage, the data need to be calculated for each distance to each cluster center. The closest distance between the data at a particular cluster will determine the data included in the cluster where. As for the distance calculation using the formula Eulidean.

$d(x, y) = \sqrt{(xi - yi)^2 + (xi - yi)^2}$ ..... (1)

• Recalculate the center of the cluster with cluster membership now . Center of the cluster is the average of all the data/objects within a particular cluster. Calculations by determining the centroid/center of the cluster.

$C(i) = x1 + x2 + x.. + x... \Sigma x$ ..... (2)

• The shortest distance between the center of the cluster with the data/object determines the position of a cluster of data/objects. For example, a data/object A has the shortest distance to the cluster center compared to one another, then the data/object A went into cluster 1.

• Reassign each object by using the new cluster centers. If the center of the cluster is no longer changed, then the process is complete pengclusteran. If changed, then go back to step no.3 to the cluster center does not change anymore.

• Once the process is complete pengclusteran, it will be calculated the value of each cluster SSE. SSE value depends on the number of clusters and how the data are grouped into clusters such. The goal is to obtain a partition (fixed number of clusters) which minimizes the total square error. The smaller the value of SSE, the better the clustering results. Here's how the SSE.

$SSE = (Ci)^2 + (Ci)^2 + (C..)^2 + (C..)^2$ ..... (3)

F. Analysis Of The Results Clusterisasi

Stages to analyze the results already obtained in the clustering process.

IV. DISCUSSION

A. Aspects of Assessment

Aspects value obtained from the City Health Office in Malang, where its aspects, among others:

a. Exclusive breastfeeding status

Exclusive status data contains values YES and NO

a. Immunization Status

Exclusive status data contains values YES and NO

c. Nutritional intake

Exclusive status data contains values and LESS GOOD

B. System Design

Context Diagram

The following is a general overview of the system K-Means method for Disease Pneumonia high Knowing Striking Toddler Time Range Based on exclusive breastfeeding, immunization and nutrition status in the context diagram form.

In general the system can be described that the admin role is to provide input to the system in the form of data on the number of pneumonia patients based on three aspects of previous years (the value for each cluster), which serves as the training data. Next the user can provide input the number of patients by 1 symptom/cluster to predict the amount based on other symptoms. The results of prediction are also able to demonstrate the prediction of the overall rate of patients with pneumonia symptoms/clusters.

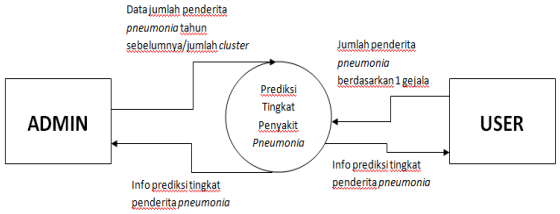

Figure 2. Prediction Context Level Diagram of Pneumonia Patients

C. Data Flow Diagrams (DFD Level I)

The following description of the system K-Mean Method For High Knowing Pneumonia Patients Striking Toddler Time Range Based on exclusive breastfeeding, immunization and nutrition status in the form of Data Flow Diagrams (DFD Level I).

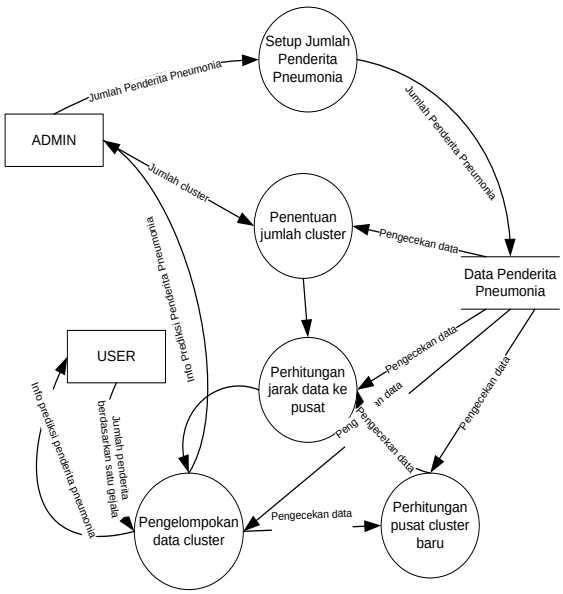

Figure 3. Data Flow Diagrams (DFD Level I) Predicted Rate Pneumonia Patients

In DFD level I explain step-step completion prediction using K-Means method. Starting from the master setup process training data pneumonia number of people with previous years (the value for each cluster), so that the training data are stored in files. Next training data used for the calculation of the K-Means method, starting from the centroid calculation, calculation of distances, to obtain the value of sum square error (SSE).

D. Database Design

Application of K-Means method to determine the height of pneumonia in toddlers is based on data summary contracted pneumonia caused due to problems of time range of exclusive breastfeeding, immunization status, and nutritional intake needed to use one table as training data for the prediction of future data beracuan six last year . Adapaun design training data tables are as follows:

TABLE 1. TRAINING DATA TABLE PNEUMONIA

Nama Field	Tipe Data	Keterangan
code Year	Byte	Code as the reference year data summary per year
breast milk	Integer	Number of people per year who contracted pneumonia as a result of problems on exclusive breastfeeding
immunization	Integer	Number of people per year who contracted pneumonia as a result of immunization issues
Nutritional intake	Integer	Number of people per year who contracted pneumonia as a result of problems with the intake of nutrients

E. Discussion on Application of K-Means Method

In this study using three aspects of the issue on breastfeeding, immunization, and nutrition intake, with the last six years of training data as follows:

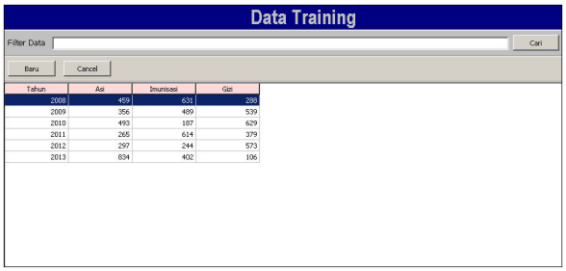

Figure 4. Training Data Pneumonia Patients Per Year

In this stage the researcher determines the value of the centroid into two parts, ie having 3 and 2 centroid centroid. This is done to determine where the most amount of good centroid, as in the formulation of the K-Means cluster most smallest value will be the value of the most well clusters. Here is the process of calculating the application of K-Means method to predict the rate of pneumonia disease that strikes children under five years in the future in Malang, due to the

impact of the frequency of exclusive breastfeeding, immunization status and nutritional intake, with beracuan on public health training data the last six years.

F. Initial Centroid Calculation

Clusterisasi phases using K-Means algorithm, beginning with the formation of clusters in a dataset are 3 clusters (exclusive breastfeeding, immunization, and nutrition intake), with 2 parameter testing, namely, 3 and 2 values centroid centroid value.

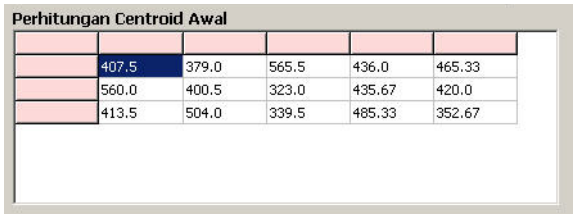
Perhitungan Centroid Awal

	407.5	379.0	565.5	436.0	465.33
	560.0	400.5	323.0	435.67	420.0
	413.5	504.0	339.5	485.33	352.67

Figure 5. Initial Centroid Calculation

3 centroid calculation to obtain C0, C1, and C2 for each cluster. 3 For the calculation of the centroid is obtained from the sum of two values for each aspect of the training data is divided by 2. As for the centroid obtained 2 C0, and C1, which is obtained from the sum of three values for each aspect of the training data is divided by 3.

Calculation of Distance Early

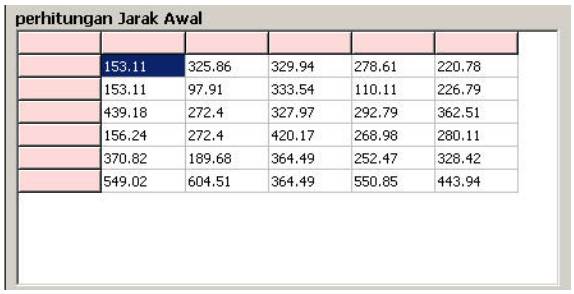
perhitungan Jarak Awal

	153.11	325.86	329.94	278.61	220.78
	153.11	97.91	333.54	110.11	226.79
	439.18	272.4	327.97	292.79	362.51
	156.24	272.4	420.17	268.98	280.11
	370.82	189.68	364.49	252.47	328.42
	549.02	604.51	364.49	550.85	443.94

Figure 6. Calculation of Distance Early

In this step the distance calculations carried out to determine the distance of each outcome data on the number of clusters (k) at each centroid. Perform calculations to determine the distance of each data with initial centroid, using the formula euclidiance distance. Here are the results for 3 centroid distance calculation, and 2 centroid.

Centroid Calculation for Iteration 1

Based on how the K-Means algorithm as specified value clusters (k) and then calculate the distance between the centroid and data on each of each centroid. In this stage, the calculation returns a value to the centroid of each cluster, called iterations, until the value has not changed from the previous centroid.
3 centroid calculation to obtain C0, C1, and C2 for each cluster. 3 For the calculation of the centroid is obtained from the sum of two values for each aspect of the training data is divided by 2. As for the C0 2 centroid obtained from the sum of two values for each aspect of the training data is divided by 2, and C1 were obtained from the sum of 4 values for each aspect of the training data is divided by 4.

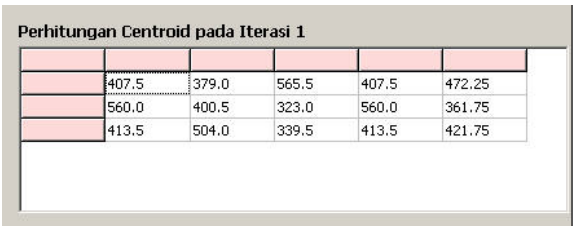
Perhitungan Centroid pada Iterasi 1

	407.5	379.0	565.5	407.5	472.25
	560.0	400.5	323.0	560.0	361.75
	413.5	504.0	339.5	413.5	421.75

Figure 7. Centroid Calculation for Iteration 1

3 centroid value for iteration 1 to step 3, the results remained similar to 3 centroid in step 1, then the iteration is stopped.
Centroid value for iteration 2 to 1 step 3, with the result 2 DIFFERENT centroid in step 1, then the second calculation.

Distance calculation for Iteration 1

Distance calculations for iteration 1 is done, because the value of 2 centroid step 3, with the result DIFFERENT 2 centroid value in step 1. Perform calculations to determine the distance of each data with initial centroid, using the formula euclidiance distance. Here are the results for 3 centroid distance calculation, and 2 centroid.

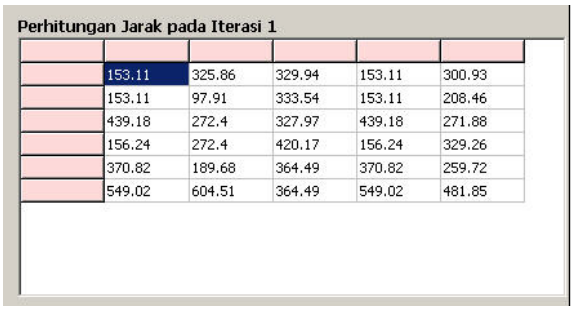
Perhitungan Jarak pada Iterasi 1

	153.11	325.86	329.94	153.11	300.93
	153.11	97.91	333.54	153.11	208.46
	439.18	272.4	327.97	439.18	271.88
	156.24	272.4	420.17	156.24	329.26
	370.82	189.68	364.49	370.82	259.72
	549.02	604.51	364.49	549.02	481.85

Figure 8. Distance calculation for Iteration 1

Centroid Calculation for 2nd Iteration

3 centroid calculation to obtain C0, C1, and C2 for each cluster. 3 For the calculation of the centroid is obtained from the sum of two values for each aspect of the training data is divided by 2. As for the C0 2 centroid obtained from the sum of two values for each aspect of the training data is divided by 2, and C1 were obtained from the sum of 4 values for each aspect of the training data is divided by 4. In the following table the result of the calculation of the centroid for iteration 2.

Perhitungan Centroid pada Iterasi 2

	407.5	379.0	565.5	407.5	472.25
	560.0	400.5	323.0	560.0	361.75
	413.5	504.0	339.5	413.5	421.75

Figure 9. Centroid calculations for iteration 2

3 centroid value for the 2nd iteration step 5, the result is still the same with 3 centroid in step 3, then the iteration is stopped.

Centroid value for iteration 2 to 2 step 5, the result is still the same with 2 centroids in step 3, then the iteration is stopped.

Calculation of Value Sum Square Error (SSE)

In this phase will be calculated from the centroid value iteration results, if the results of the SSE value gets smaller, the better the results clusteringnya. There will be 2 testing parameters in calculating the value of SSE, the results will be used as a determinant of the cluster where the most good.

SSE

3 Centroid 461,004.5

2 Centroid 528,853.25

Based on the calculation of the smallest value of SSE SSE is the value of 3 centroid, it can be concluded as the best cluster in a research trial in the case of training data from 2008 to 2013 prediction of pneumonia disease that strikes children under five years in the future in Malang, due to the impact of frequency Exclusive breastfeeding, immunization status and nutrient intake.

G. Cluster Determination of Initial Training Data

Based on the calculation of the smallest value of SSE SSE is the value of 3 centroid, it can be concluded as the best cluster, so as to create two clusters based on the training data as follows:

Cluster Pertama (C0) : Rendah

TAHUN	ASI EKSKLUSIF	IMUNISASI	ASUPAN GIZI
2008	459	631	288
2009	356	489	539

Cluster Kedua (C1)

TAHUN	ASI EKSKLUSIF	IMUNISASI	ASUPAN GIZI
2010	493	187	629
2011	265	614	379
2012	297	244	573
2013	834	402	106

Figure 10. Cluster Final Determination

Based on the results of the K-Means clustering, then the pattern of the results obtained from each cluster. Here's an explanation of each cluster on each member of the cluster:

• Members of the data on the first cluster (C0) has a characteristic value for the problem at the estimated value of exclusive breastfeeding from 459 to 356, for the immunization of the estimated value of 631 to 489, and for the nutritional intake of 288 to 539.

• Members of the data on the second cluster (C1) has a characteristic value for the problem at the estimated value of exclusive breastfeeding from 439 to 834, for the immunization of the estimated value of 187 to 402, and for the nutritional intake of 629 to 106.

Clustering results of K-Means prediction can be illustrated in the following chart:

Figure 11. Prediction of Final Determination of Cluster Graphs

V. CONCLUSION

As for the conclusion that the bias obtained from research progress report K-Means Method To Learn The high Pneumenia Disease Based Attacks Toddler Time Range of exclusive breastfeeding, immunization status and Nutrition:

• There is a relationship between the time range of exclusive breastfeeding, immunization and nutrition status of the low height of the toddler pneumonia.

• With the K-Means method can predict the level of toddlers aged patients with pneumonia associated with variable time range of exclusive breastfeeding, immunization and nutrition status.

VI. SUGGESTION

Advice from the results of the progress of this study are as follows:

• Training data can be copied again to get more accurate results.

• Aspects supporting predictions can be developed even more with the development of pneumonia symptoms experienced by the community.

3 . Applications are made to be developed in the form of early detection of disease pneumonia using online media so that the public can easily access it.

REFERENCES

[1] ___. 2013. The benefits of exclusive breastfeeding for the baby. http:// http://www.botolkacaasi.com. March 11, 2013

[2] Fanada, Mery and Young, Widyaiswara. 2012. Factors Associated With Disease Occurrence Pneumonia In Toddlers In Palembang Kenten Work Area Health Center in 2012.

Provincial Training Agency. South Sumatra

[3] Nango, Dwi Noviati. 2012. The application of K-Means Algorithm for Clustering Data Local Budget In District Xyz. Department of Informatics. University of Gorontalo

[4] Rahman, Vionny. 2012. Do you know what are the contents of the milk?. http://www.duniaanak.org. March 11, 2013.

[5] Santoso, Budi. 2007. Applied Data Mining with MATLAB. First Edition. Graha Science. Yogyakarta

[6] Widyawati, N. 2010. Comparison of Clustering Based On frequest Word squence (CFNS) and K-Means clustering Documents To Speak Indonesian . Faculty of Mathematics and Natural Sciences. UPI. duo

[7] Yafonda, Dea. 2011. Nutritional status and breastfeeding in Genesis Against Pneumonia In Toddlers Work Area Health Center Ambacang Kuranji Padang District of the Year 2011. Faculty of Nursing. Universitas Andalas

G307

Parallel Programming to Increase Performance of Binary Search Tree

Cipta Ramadhani
JurusanTeknikElektro
FakultasTeknikUniversitasMataram
Nusa Tenggara Barat, Indonesia
cipta@te.ftunram.ac.id

Wahyu Ramadhani
STMIK SyaikhZainuddin NW
NadhatulWathanAnjani
Nusa Tenggara Barat, Indonesia
Wahyurama2@gmail.com

Abstract—**Binary Search Tree is one of the most useful fundamental data structure for dynamic datasets. It can be used to sort numerical data, character string and any other data in a sophisticated way. However, the performance in term of running time for Binary Search Tree (BST) increases when a data become large, especially for data mining and detecting pattern in DNA sequences. To increase speed performance of Binary Search Tree, there are several strategies were applied such as using super computing or conducting parallel programming. In this research we applied parallel programming by using Message Passing Interface (MPI) to sort numerical data. This method is more efficient and less cost compare with using super computing. The basic idea of parallel programming is dividing root into sub-root and executing sub-root simultaneously on multiple cores. MPI provides a set of send and receive function that allow data to be processed on multiple cores. This method is very useful to find data faster than in a sequential way, but the consequence is the coding time takes little bit longer than usual.**

Keywords—Binary search tree, Message passing interface, Parallel programming.

I. INTRODUCTION

Binary search tree (BST) is a binary tree where the root node values is greater than its left children and smaller than its right children. We can represent tree search by a linked data structure in which each node is an object. In addition to a key value, each node contains attributes left, right and parent that point to the nodes corresponding to its left child, right child and its parent respectively. The operations that can be performed on BST including searching, insertion, deletion and other queries. Basic operations on a binary search tree take time proportional to the height of the tree. For a complete binary tree with n nodes, such operations run in O($\log_n$) for the worst-case time. However, the performance in terms of running time for BST increases when data become larger and that case becomes a big deal if we run BST to process data mining which contain different data type. To overcome this problem, parallel programing can be applied as a solution to reduce time consuming problem of BST.

A. *Why Parallelization*

Parallelization is another optimization technique to further enhance the performance. The goal is to reduce the total execution time proportionally to the number of cores used. If the serial execution time is 20 seconds for example, executing the parallel version on a quad core system ideally reduces this to 20/4 = 5 seconds. [1]

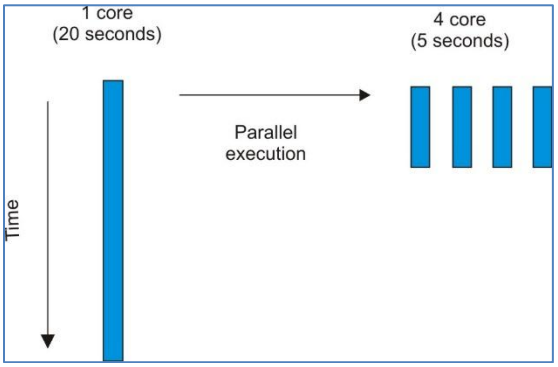

Figure 1 Parallelization reduces the execution timer

The significant difference here is that unlike tuning for serial performance, with parallelization more than one core is executing the program. So the goal must use these additional cores as efficiently as possible to reduce the execution time. Butperformance improvement is not guaranted. Depending on the application characteristics, the parallel programming model selected, the implementation of the parallelism in the application, the system software and the hardware used, one might see little or no performance improvement when adding cores. in some cases enabling more cores can degrade performance when compared to single core execution.

B. What is Parallel Programming

Parallel programming is a computer paradigm where multiple processors attempt to cooperate in the completion of a single task. The basic idea is dividing task into sub-task and executing sub-tasks simultaneously on the multiple cores. In the parallel programing paradigm, there are two memory models: shared memory and distributed memory. Shared memory is a piece of memory that can be allocated and attached to an address space. Thus, process that have this memory segment attached will have access to it. Otherwise, distributed memory has its own rule. On distributed memory processing nodes have access only to their local memory, and access to remote data was accomplished by request and reply messages[2].

C. The Basic Idea of MPI

MPI is ran on distributed memory paradigm. Several computers on the network are used to process a large amount of data. Before conducting the parallelism, the data on the server must be divided into parts and send it to a particularly processor. After processing a part of the data, particular processor will send it back to the server. By using this concept, the problem of running time can be reduce.

The MPI programming requires that the parallelism is coded explicitly by the programmer. Therefore, the programmer is responsible for analyzing and identifying the algorithm/application. The programmer must know how to conduct mechanism of send and receive the data. In addition to send and receive mechanism, communication process must be identified specifically. As a result, programming using MPI tends to be hard and intellectually demanding. However, on the other hand, properly written the MPI programming can often achieve very high performance and scale to a very large number of process[3].

D. Contribution

This research is dedicated to researcher who want to process a large amount of data which bounded by time consuming problem.The aim of this paper is to evaluate performance in term of running time of BST by using parallel programming. Several kind of strategy such as searchings and deletion problem will show the benefit of using MPI. The other main goal is also to reduce device cost. Instead of using super computer, scientist may use several computer with a reduce price.

II. RELATED WORKS

MPI has been widely used in many research field, for example in Local Area Network. It constructed distributed parallel computing based on LAN to solve the problem of scientific computing of geophysical exploration explaining. It can distribute massive complex scientific computing tasks to multiples mainframes in the LAN, and use the idle CPU resources from workstation to complete scientific computing problem cooperatively[4]. In another field, parallel programming is used to detect pattern in DNA sequence. By using parallelized paradigm, a better performance in term of running time can be achieved[5]. In BST concept, some researcher has also conducted. Kakako tree A BST with caching is added. the time complexity of BST varies between O(n) and O(log n) depends upon the number of nodes that are present in left and right children. Kakao Tree is a new data structure which is a variant of BST with some initial nodes act like caching.[6]

In this paper, numerical data will be used to show the benefit of parallel programming by using BST structure.

III. METHODOLOGY

On this paper, we will measure and analyze running time of BST using MPI. Several procedure, such as searching and deletion data is conducted to show the advantage of using parallel programming.

A. Materials

During the experiment, we used several computer for running the parallelizing. In addition to several computer, switch and cables will be used to support traffic data among the computer. One computer is set up as a server and the other as slave. Because every slave will process a part of data with their own resource, computer server will divide the data in to a part and send it to every single slave. Figure 3.1 below describe a computational model of parallel programming.

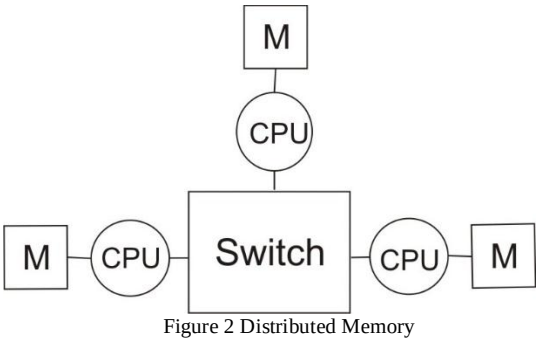

Figure 2 Distributed Memory Multiprocessor

Each computer slave will use their own memory to process the data which already send by the server. After process on each slave has been completed, output data is sent back to the server. And the process will be terminated.

B. Description of experimental scenario.

The parallel operations of BST are implemented using Linux Debian. Our experiment will be divided into two part. First scenario is to find the lowest value in the numerical data by using Domain decomposition method. Step one, computer server has to divide the data into parts and send each part to the slave. Each of computer slave will find the lowest value in its data BST algorithm and send it back to the server. Furthermore, on the computer server, all data which derived from the slave will be process again on the computer server to get the lowest value. Finally the process is terminated. figure 3 below show the procedure of domain decomposition method

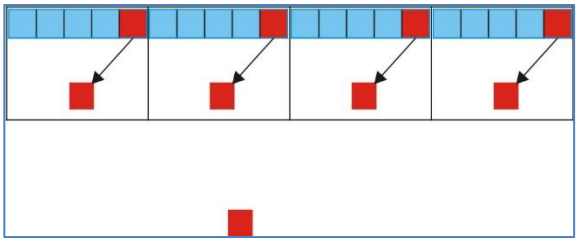

Figure 3Domain Composition method

Slightly different to the first scenario, the second scenario will find a single value in BST using the same procedure with the first scenario. It used a Domain decomposition method.

Parallelizing model used Domain decomposition model to spread all of data to the computer slave. By using Domain decomposition model, every computer slave must maintain its own data which is already sent by computer server. On each scenario, different data size will be used to show the trend of speed performance in BST. In this experiment, we used dual core processor. Therefore, each computer will have two cores for running the parallelizing. For example, if we have four computers in the experiment, we will have eight cores which can be used to process each part of the data.

The parallel operations are implemented using c++. For this experiment, we conducted two cases such as searching and finding the minimum value of the data. In each case, scanning data must be conducted at the beginning. After completing the scanning process, whole data must be divided by a total number of computer so that each core will get the same number of data to process. Then, each core will conduct insertion process with its own data. after all scanning and insertion process have done, searching and finding value can be conducted.

IV. RESULTS

The focus in this research is to know about the performance of BST in term of the running time by using parallel programming idea. In order to achieve the result, we used different number of computers in each experiment so that the differences of running time in each process can be found clearly.

In the first experiment, we will find the lowest value in a large amount of data. The target value will be placed manually in the code program. Figure 4 shows the benefit of using parallel programming.

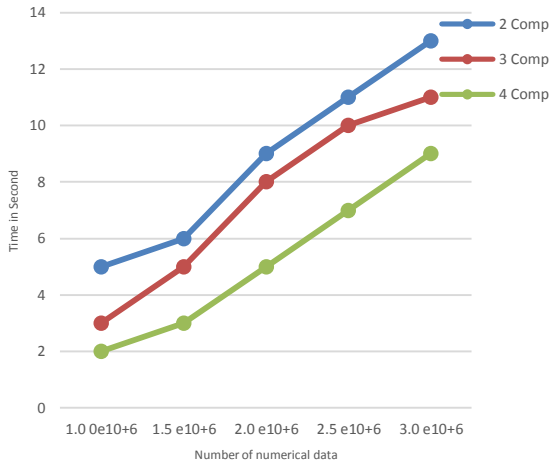

Figure 4Find the lowest value's scenario

in figure 1 shown above, The best performance of BST derived by using eight cores (four computer). If we used just two or three computers the running time becomes larger. It means that the more computer we used the better performance we have. From these research we known that by utilizing a parallel programming, we can reduce the running time of BST very significant rather than using just one computer. by using one computer, it takes more than 100 second to get the lowest value. But if we used two or three computer, the running time of BST can be reduced significantly.

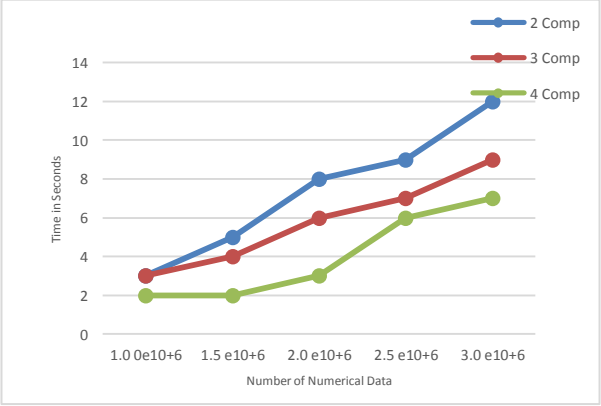

Figure 5Searching's scenario

With the same procedure, the searching process is conducted in the second experiment. We used different number of computer show the performance of BST. In a searching process, the worst case problem should be used to see the maximum process in BST. By using this idea, the changing of time speed in parallel programming can be found clearly. Figure 2 shows that by adding a number of computer continuously, the time value for the searching process can be reduced

V. CONCLUSION

This paper introduced the benefit of using parallel programming. In this research, we have shown that parallel programming can be used to increase the performance of BST in term of time speed. The best performance of BST is derived by using eight cores (four computer). If we used just two or three computers the running time becomes larger. It means that the more computer we used the better performance we have. In sharp contrast to its benefit, parallel programming can notbe used if we used it to process small data. it is happened because the time speed of BST is more affected by communication process among the computer not by its computational process.

VI. FUTURE WORKS

The next research, we plan to process DNA sequence or protein sequence by using parallel programming. It is important because DNA sequence have as many as 64 million different strings that need to be taken into account.

VII ACKNOWLEDGMENT

We are very grateful to Indonesian Ministry of Research and Technology under SINas 2014. We are also gratefuly thanks to Miss Teti and Miss Bulkis for their valuable assistance.The department of electrical engineering, which has provided the opportunity to conduct this research in Lab. Kendali Digital. Also, we would like to say thanksto LilisNugrahani, Helmibaskara and toharsagara for their support, especially in producing of numerical data.

REFERENCES

[1] Oracle, Parallel Programming with Oracle Developer Tools., 2010.
[2] Harry F. Jordan ICASE, Shared versus Distributed Memory Multiprocessor. January, 1991.
[3] Message Passing Interface Forum. *MPI : A Message-Passing Interface Standard*. 2009.
[4] Qing Guan, Jienhe Guan"*The Realization of Parallel Computing in LAN*, IEEE Journal 2012.
[5] Jian Feng, Daniel Q Naiman and Bret Cooper *"A Parallelized Binary Search Tree"*.K Inform Tech Engg 2011.
[6] Rajesh Ramachandran *"Kakkot Tree- A Binary Search Tree with Caching"*IEEE Journal 2012.

.

G308

Fall Detection System for Elderly Based on Android Smartphone

Made Liandana, I Wayan Mustika, and Selo
Department of Information Technology and Electrical Engineering
Universitas Gadjah Mada
Jalan Grafika No.2 Kampus UGM, Yogyakarta, Indonesia
Email: liandana.mti.18a@mail.ugm.ac.id, {wmustika, selo}@ugm.ac.id

***Abstract*—Physical ability of elderly person will degrade as the aging process occurs, thereby increasing the potential for falls. Falls on the elderly will have serious impact such as injury or even death if they do not get help immediately. Aid can be given more quickly if the occurrence of falls can be immediately detected. This paper study the fall detection technique using Android smartphone. The proposed technique computes the total acceleration and tilt angle from accelerometer sensor in smartphone. Fall is detected based on total acceleration and sum of difference of total acceleration. The tilt angle is used to mark whether a forward fall, backward fall, fall to the left, or fall to the right. The results show that the proposed technique has a sensitivity of 90% and specificity of 94% in a total set of 490 movements.**

***Index Terms*—Elderly, accelerometer, total acceleration, sum of difference of total acceleration, tilt angle, Android.**

I. Introduction

Physical ability of elderly person will degrade as the aging process occurs, thereby increasing the potential for falls. Approximately 50% of nursing home residents fall at least once a years, while 40% of them fall more than once [1]. According to the research in [2] 28% to 35% of people, aged above 65, fall at least once a year. Another study stated that one of two people, aged 80 or over, have experienced falls [3]. Number of persons, aged 60 years and over was 841 millions in 2013 and it is estimated that nearly 2 billion of person aged 60 years and over in 2050 [4]. Thus, falls affect millions of people (especially the elderly) and may result in significant injuries.

The fall of the person can be described as uncontrolled movements from standing or sitting position to a lying or almost lying position [3]. Fall will certainly have a direct impact on health, such as increase of mortality, morbidity, disability, and frailty [5]. Therefore, a system that can detect the uncontrolled movement such as fall is needed.

Yu [6] categorizes methods of fall detection into three approaches: wearable device, ambiance device, and camera-based. Among three approaches, wearable device has a relatively low cost and ease to configure [6]. Wearable devices can be worn on clothes or part of certain body, or held by the user. Smartphone and microcontroller can be designed as a wearable devices, because they have a relatively small size and enough computational capability to process data.

Chen *et al.* use microcontroller as a processing unit to generate total acceleration and tilt angle on z-axis from accelerometer sensor [7]. The proposed system has sensitivity of 95% and specificity of 100%. Sensitivity is ability of system to identify fall. Specificity is ability of system to detect non fall activities. Falls detection technique using accelerometer sensors on smartphones have been done by previous works [8] [9] [10]. Feature extraction on acceleration of accelerometer sensor can use method Signal Magnitude Area (SMA), Signal Magnitude Vector (SVM), and Tilt Angle (TA). The results obtained from feature extraction are used as a parameter to detect fall [8]. Fang *et al.* [10] use the total and vertical accelerations to distinguish fall with normal activity. This method has a sensitivity of 72% and specificity of 73%. Dai *et al.* [9] use the same method with Fang, but they add time window. Referencing to the dynamic of free fall, velocity can be used as a parameter whether fall has occurred or not [11] [12].

This paper study the fall detection technique using Android smartphone. The proposed technique uses total acceleration, sum of difference of total acceleration, and tilt angle. Tilt angle consist of three, namely, tilt angle based on x-axis, y-axis, and z-axis. Tilt angles are used to mark the fall direction, whether a forward fall, backward fall, fall to the left, or fall to the right. All of parameters, such as total acceleration, sum of difference of total acceleration, and tilt angle are generated by accelerometer sensor in Android smartphone. This paper focus on developing methods for improving sensitivity and specificity based on Android smartphone.

The remainder of this paper is organized as follows. Section II describes the design of the proposed system. The experimental results are represented in section III. Section IV concludes the paper.

II. System Design

A. System Overview

The proposed system uses a smartphone with Android operating system. The accelerometer sensor has three axis, namely x-axis, y-axis, and z-axis, which can create sensing data in three-dimentional space. The x-axis forms horizontal line, y-axis forms vertical line, and z-axis leads to front and back of screen device (see Fig. 1a). As shown in Fig. 1b, smartphone is attached on the left waist. The device has placed

firmly on the belt, so that the position of device does not change during falls.

As shown in Fig. 2, there are three important parts of fall detection processes, namely total acceleration, sum of difference of total acceleration, and tilt angle. First, acceleration from sensor accelerometer is filtered by high pass filter. After that the total acceleration is calculated. Fall is detected by comparing the total acceleration, sum of difference total acceleration, and tilt angle with the threshold values.

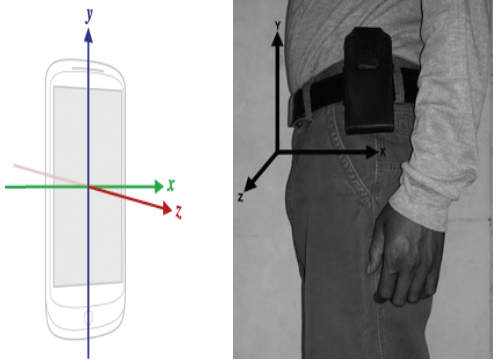

(a) [13] (b)

Fig. 1: (a) X-axis, y-axis, z-axis on smartphone. (b) Smartphone attached on left waist.

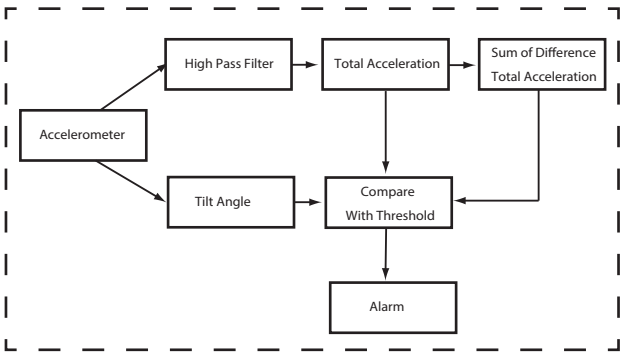

Fig. 2: Process of fall detection.

B. Algorithm of Fall Detection

Acceleration on accelerometer sensor is affected by mass of the device, force, and gravity. Fig. 3 shows that when the smartphone is placed horizontally, acceleration of x-axis, and y-axis is 0 m/s^2, while z-axis is 9.81 m/s^2.

To get the actual value of acceleration, the influence of gravity and noise can be removed by filtering. There are two filters that can be applied, namely high pass filter and low pass filter. Bylemans *et al.* [14] used two filters to reduce the effect of gravity and noise. However, this study only uses a high pass filter such as Eq. (1). Fig. 4 shows the results of a high pass filter, where the acceleration in the z-axis is close to zero when the smartphone is placed horizontally. In other words, the effect of gravity is reduced using filter.

$$\begin{aligned} ACCHPavg &= ACCnew * 0.1 + ACCHPavg * 0.9 \\ ACCHPFiltered &= ACCnew - ACCHPavg, \end{aligned} \tag{1}$$

where ACCnew is data obtained from each axis of accelerometer, ACCHPavg is acceleration that has been isolated from force of gravity, and ACCHPFiltered is result of high pass filter.

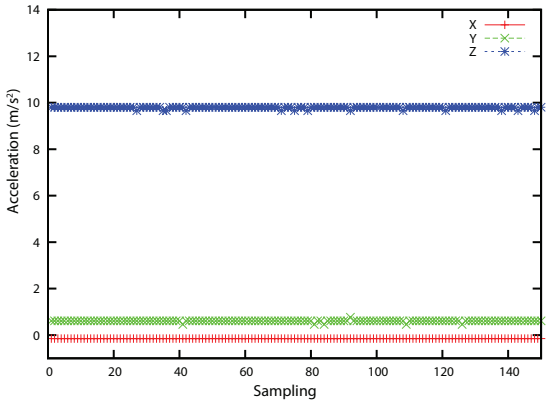

Fig. 3: Acceleration without filtering.

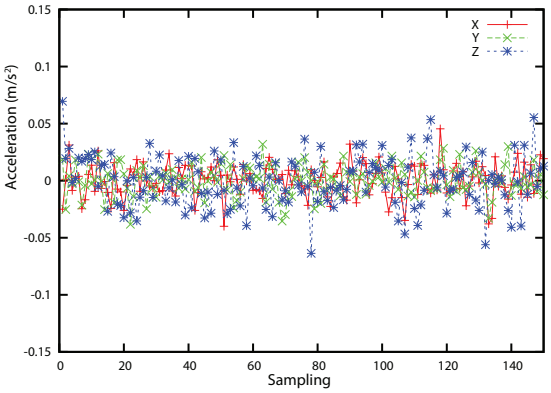

Fig. 4: Acceleration with filtering.

In the fall detection process, the accelerometer sensor continuously monitors acceleration of a smartphone along three axes. After filtering process, total acceleration (AT) is calculated using Eq. (2). As indicated in Eq. (2) A_x, A_y, and A_z, are the acceleration in the x, y, z axes, respectively. Generally, movements of fall are faster than normal activities, so that total acceleration caused by falls is higher than that of normal activities. As shown Fig. 5, total acceleration soars from normal activities (such as walking) to the position of the falls, and then decreased significantly when the body begins

to lay. In addition, falls and normal activity are distinguished by using sum of difference of total acceleration SDif. It is calculated by Eq. (3). SDif is calculated if AT reaches a peak that is caused by a fall.

$$AT = \sqrt{A_{x^2} + A_{y^2} + A_{z^2}} \tag{2}$$

$$SDif = \sum_{i=0}^{6} AT_{i+1} - AT_i \tag{3}$$

Fall is an uncontrolled movement from a standing position to a lying position. The position of standing and lying can be differentiated by using tilt angle. The position of lying caused by falls is used to mark the direction of fall, such as forward fall, backward fall, fall to the left, or fall to the right. Each position of lying that caused by falls, has differences of tilt angle with others activities.

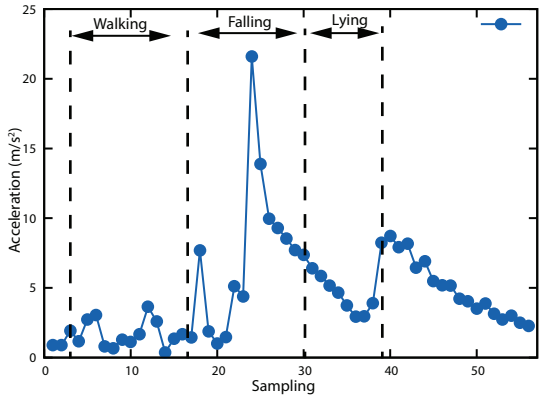

Fig. 5: Acceleration with filtering.

In this study, tilt angles are calculated based on acceleration that is generated by the accelerometer sensor on x-axis, y-axis, and z-axis. As indicated in Eq. (4)-(6), the tilt angles of three axes are denoted by TA_x, TA_y, TA_z and gravity is denoted by G. Chen *et al.* [7] used tilt angle to identify fall, but they only used single angle on z-axis.

$$TA_x = \arccos(A_{x/G}) \times (180/pi) \tag{4}$$

$$TA_y = \arccos(A_{y/G}) \times (180/pi) \tag{5}$$

$$TA_z = \arccos(A_{z/G}) \times (180/pi) \tag{6}$$

Tilt angles that are generated by sensor accelerometer depend on the position of smartphone. Fig. 6 shows the up position, left position, right position, back-up position, and front up position of smartphone. Tilt angles based on position of smartphone (see Fig. 6) are shown by Table I.

Normally, position of smartphone on standing position, lying face down, lying face up, lying on the left side, and lying on the right side, are shown in Fig. 6a-6e respectively. This condition applies if the smartphone is attached on the left

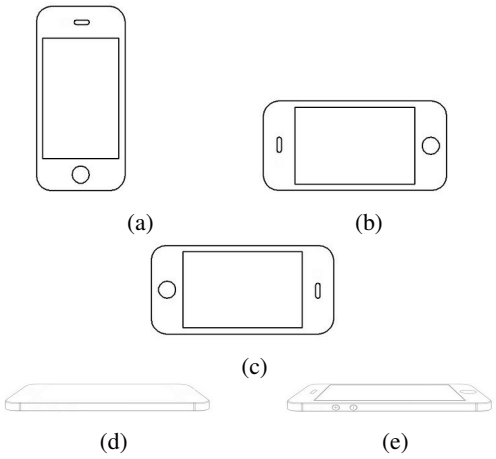

Fig. 6: (a) Up position. (b) Left position. (c) Right position. (d) Back-up position. (e) Front up position.

TABLE I: Tilt angle based on smartphone position

Position	TA_x	TA_y	TA_z
Up	90	0	90
Left	0	90	90
Right	180	90	90
Back-up	90	90	180
Front up	90	90	0

waist as shown Fig. 1. In reality, tilt angles of lying that are caused by fall are not always the same with the tilt angles that are shown Table I. However, it can be approached using the minimum and maximum values as shown in Table II.

TABLE II: Aproach of tilt angle

Position	TA_x		TA_y		TA_z	
	Min	Max	Min	Max	Min	Max
Lying face down	0	45	75	115	75	115
Lying face up	140	180	75	115	75	115
Lying on the left side	75	115	75	115	140	180
Lying on the right side	75	115	75	115	0	45

To determine threshold of total acceleration AT_{Th} and sum of difference of total acceleration $SDif_{Th}$, extensive experiments are performed (200 times). Since it is high risk to conduct the experiment on the elderly, the non-elderly is used as the subject of experiment. AT_{Th} of greater than or equal to 11 m/s^2 and $SDif_{Th}$ of less than or equal to -2 m/s^2 were based on experiments.

If the total acceleration is greater or equal to 11 m/s^2 in certain sample, it is marked as AT_0, and next samples are marked as AT_1 to AT_7 respectively, as shown in Fig. 7. Based on AT_0 to AT_7 the sum of difference of total acceleratioan can be calculated. When AT is greater or equal to AT_{th}, and SDif is greater or equal to $SDif_{th}$, tilt angles TA_x, TA_y, and TA_z are calculated, then they are observed along samples AT_0 to AT_7. If contains tilt angle as shown in Table II, it is can be

categorized as fall.

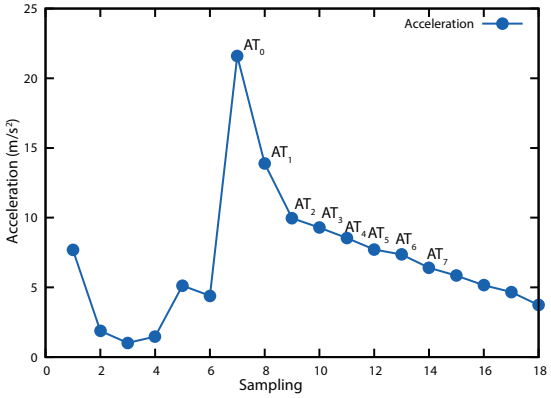

Fig. 7: Calculating SDif along AT_0 to AT_7.

III. Results

A. Experiment Design

Tests are carried out on three subject who have weight about 60-75 kg and height 170-180 cm. Mattress that is used in the experiments has high about 25 cm from floor. Table III shows the design of experiments.

TABLE III: Experiment Design

Category	Instruction
Forward fall	Ending Lying
	Ending Lateral Position
	With Recovery
	On the Knees
Backward fall	Ending Lying
	Ending Lateral Position
	Lateral Position
	With Recovery
Fall to the left	Ending Lying
	With Recovery
Fall to the right	Ending Lying
	With Recovery
Normal Activities	Sitting Down-Stand Up
	Lying Down-Rising Up
	Walking
	Bending Down-Rising Up
	Running

Performance of fall detection system can be measured by sensitivity and specificity. There are four parameter that are used in measuring the performance. True positive (TP), means that fall occurs, the system can correctly detects. False positive (FP), means that the system detects fall when no fall occurs. True negative (TN), means that system does not detect fall when no fall occurs. False negative (FN), means that the system does not detect fall but fall occurs.

$$Sensitivity = \frac{TP}{TP + FN} \quad (7)$$

$$Specificity = \frac{TN}{TN + FP} \quad (8)$$

B. Experiment Results

Experiments are conducted in 490 movements, which is categorized into fall by 365 movements, and normal activities by 125 movements. Since it is high risk to conduct the experiment on the elderly, the non-elderly is used as the subject of experiment. We also compare result without SDif and result with SDif. The results are shown in Table IV and V.

TABLE IV: Experiment results

Category	Times	Without SDif		With SDif	
		True	False	True	False
Forward fall	92	85	7	85	7
Backward fall	93	86	7	86	7
Fall to the left	90	83	7	83	7
Fall to the right	90	76	14	76	14

TABLE V: Experiment results in normal activities

Category	Times	Wihtout SDif		With SDif	
		True	False	True	False
Sitting Down-Stand Up	25	0	25	0	25
Lying Down-Rising Up	25	3	22	3	22
Walking	25	0	25	0	25
Bending Down-Rising Up	25	0	25	0	25
Running	25	4	21	4	21

Numbers of true positive (TP) and false positive (FP) are determined based on fall categories as shown in table IV, and true negative (TN) and false negative (FN) are determined based on normal activities as shown in Table V. Number each of parameter is shown in Table VI.

TABLE VI: Number of parameter

Parameters	Scheme without SDif	Scheme with SDif
True positive (TP)	330	330
True negative (TN)	118	118
False negative (FN)	7	7
False positive (FP)	35	35

TABLE VII: Comparing our scheme with previous work

Proposed	Sensitivity	Specificity
Previous work [10]	56.67%	66.39%
Scheme without SDif	90.41%	94.4%
Scheme with SDif	90.41%	94.4%

Based on the results as shown in Table VII, the proposed scheme with SDif and without SDif have sensitivity of 90.41% and specificity of 94.4%, which improves the performance of system compared to that of previous work [10]. Tilt angle

based on x-axis, y-axis, and z-axis is one factor that caused the proposed scheme better sensitivity and specificity than previous work. There are no difference between proposed scheme with SDif and without SDif, this may be due to the sampling rate of the accelerometer in smartphone is low.

IV. Conclusions

In this paper, we have proposed technique uses total acceleration and sum of difference of total acceleration (SDif) to identify falls. We also use tilt angle to mark whether a forward fall, backward fall, fall to the left, or fall to the right.

The proposed technique with SDif and without SDIf have sensitivity of 90% and specificity of 94% from 180 movements. It is important to note that the combination of AT and SDif can only mark a drastic changes in acceleration that are caused by falls. Sometimes normal activities produce drastic changes in acceleration, so that they will be detected as a fall. Exploring the factors that influence the performance of the proposed scheme is left as our future work.

References

[1] T. Rein, *Falling in Old Age: Prevention and Management*. New York: Springer Publishing Company, 1998.

[2] S. Khawandi, B. Daya, and P. Chauvet, "Implementation of a monitoring system for fall detection in elderly healthcare," *Procedia Computer Science*, vol. 3, no. 0, pp. 216 – 220, 2011.

[3] N. Noury, P. Rumeau, A. Bourke, G. Laighin, and J. Lundy, "A proposal for the classification and evaluation of fall detectors," *IRBM*, vol. 29, no. 6, pp. 340 – 349, 2008.

[4] (2012) World population prospects the 2012 revision. [Online]. Available: http://esa.un.org/wpp/Documentation/pdf/WPP2012_HIGHLIGHTS.pdf

[5] A. Shumway-Cook, M. Ciol, J. Hoffman, B.J.Dudgeon, K. Yorkston, and L. Chan, "Falls in the medicare population: incidence, associated factors, and impact on health care," *Phys Ther*, vol. 89, pp. 324–332, April 2009.

[6] X. Yu, "Approaches and principles of fall detection for elderly and patient," in *e-health Networking, Applications and Services, 2008. HealthCom 2008. 10th International Conference on*, Jul 2008, pp. 42–47.

[7] D. Chen, W. Feng, Y. Zhang, X. Li, and T. Wang, "A wearable wireless fall detection system with accelerators," in *Robotics and Biomimetics (ROBIO), 2011 IEEE International Conference on*, Dec 2011, pp. 2259–2263.

[8] Y. He, Y. Li, and S.-D. Bao, "Fall detection by built-in tri-accelerometer of smartphone," in *Biomedical and Health Informatics (BHI), 2012 IEEE-EMBS International Conference on*, Jan 2012, pp. 184–187.

[9] J. Dai, X. Bai, Z. Yang, Z. Shen, and D. Xuan, "Perfalld: A pervasive fall detection system using mobile phones," in *Pervasive Computing and Communications Workshops (PERCOM Workshops), 2010 8th IEEE International Conference on*, Mar 2010, pp. 292–297.

[10] S. H. Fang, Y.-C. Liang, and K. M. Chiu, "Developing a mobile phone-based fall detection system on android platform," in *Computing, Communications and Applications Conference (ComComAp), 2012*, Jan 2012, pp. 143–146.

[11] C. C. Wang, C. Y. Chiang, P. Y. Lin, Y. C. Chou, I. T. Kuo, C. N. Huang, and C. T. Chan, "Development of a fall detecting system for the elderly residents," in *Bioinformatics and Biomedical Engineering, 2008. ICBBE 2008. The 2nd International Conference on*, May 2008, pp. 1359–1362.

[12] R. Tiwari, A. Singh, and S. Khan, "Using android platform to detect free fall," in *Information Systems and Computer Networks (ISCON), 2013 International Conference on*, Mar 2013, pp. 161–163.

[13] Sensorevent. [Online]. Available: http://developer.android.com/images/axis_device.png

[14] I. Bylemans, M. Weyn, and M. Klepal, "Mobile phone-based displacement estimation for opportunistic localisation systems," in *Mobile Ubiquitous Computing, Systems, Services and Technologies, 2009. UBICOMM '09. Third International Conference on*, Oct 2009, pp. 113–118.

G309

Poverty Mappingin Mataram by Multi-Criteria Fuzzy Approach

Misbahuddin
Dept. of Electrical Engineering
University of Mataram
Mataram, Indonesia
misbah@te.ftunram.ac.id

Heri Wijayanto
Dept. of Informatic Engineering
University of Mataram
Mataram, Indonesia
heri@te.ftunram.ac.id

Muhsyaf Saipul Arni
Dept. of Accountancy
University of Mataram
Mataram, Indonesia
saipul.am@gmail.com

Abstract*—this research developed a software as a support system to define the poverty level of households in Mataram town. To measure the poverty level of households, we used fourteen attributes of poverty as indicators that are grouped into four sets, i.e., shelter, food, clothing, and other indicator. Multi criteria fuzzy logic method to poverty measurement is used to obtain category of poverty level. The poverty level is grouped into three categories, i.e., near poor, poor, and very poor. Besides, two additional parameters are fuzzy average and fuzzy weight. The fuzzy average is used to determine the category of a poverty attribute whilst the fuzzy weight is used to determine the determinant factor of poverty degree in a sub district or a village region. The result of analysis shows that there are five of fourteen poverty criteria indicated as both very poor category and very strong factors of poverty degree. Moreover, there are eight of fourteen poverty criteria indicated as the poor category. Indeed, only one of fourteen poverty criteria is indicated as near poor category. In conclusion, 93.07% of the households in Mataram town are classified as poor, 6.65% are classified as very poor, and 0.28% are classified as near poor.

Keywords*—poverty, multi criteria fuzzy, fuzzy average, fuzzy weight

I. INTRODUCTION

Poverty is still one of the main problems that is faced by Indonesia. in Indonesia, the number of poor people in September 2012 amounted to 28.59 million (11.66 percent) with the composition of poor people in the city of 10.51 million (8.60 percent) and the number of poor people in the village as much as 18.08 million people (14.70 percent) [1]. The province of West Nusa Tenggara (NTB) is one of the 10 provinces with the largest number of poor people in Indonesia. NTB provincial poverty rate remained at position six of the 33 provinces in Indonesia. The number of poor people in September 2012 was 828,330 people (18.02 percent) with the composition of the population of the urban poor in 415,380 people (21.65 percent) and the number of poor people in rural 412,940 people (15.41 percent) [2]. Mataram city also has anumber of sizeable poor populations that are equal to 60.636 people (15.41 percent) [3].

Aid delivery of the government's poverty alleviation programs is considered less on target by some of the societies. Actually, it does not mean that it has undesired purposes, but it is mostly caused by the lack of poor people data that consists of the number and addresses. Besides that, generally, each ministery or institution has self definition and criterion about poverty. Consequently, poverty tends to be partially understood, and its alleviation tends to be sectorial. It causes the difficulty of preventing program continuity and the trend of launching the new program that is not the continuation of previous programs. Antecedents of it are the weakness of the method of the poverty rate criteria of the people/household and the region categorized poverty rate criteria. The faced obstacles today are the difficulty of determining people/household poverty rate criteria and the region's poverty rate criteria in Mataram town. Criteria that are used for reckoning poverty rate today, mostly are based on classical method. It is based on score approaches that were done by many researchers [4-7].

Based on the explanation of the problems above, It is urgent to solve a solution by intensive research on developing a criterion model of level poverty that can analyze comprehensively, strongly and accurately the poverty level. A potential approach for these requirements is multi criteria fuzzy logic. Furthermore, this model is implemented in a software that can analyze poverty level and determine the determinant's factors of poverty level. This software is expected as a tool that can help government of Mataram town on the poverty alleviation programs.

II. RELATED WORKS

Poverty is the complex phenomenon that needs holistic approach for developing alleviation program strategy. Effective policies and program's construction for handling several poverty dimensions, especially on the limited resource available, has become a challenging task for government in the world, and also Indonesia. It pushes researchers to study about poverty in urban or rural areas.

Measurement of multidimensional poverty by using weight calculation approach and stated in axiom form of

aggregation procedure for obtaining index classes against inequality of poverty was used in [8]. Fuzzy logic approach to measure poverty that based on monetary variables for differentiating poor and rich people was used in [9]. The methodology for analyzing multi criteria fuzzy for describing poverty structure and presenting structural representation of implication pattern that exists between the poverty descriptors that differ from the specific context scene on a geographical region selected was proposed in [10].

This research used multi criteria fuzzy analysis approach that based on 14 poverty indicators (is taken from Statistics Center Board *(Badan Pusat Statistik (BPS))*[7]. Next, determining fuzzy poverty criteria becomes clear criteria, and then it can be obtained poverty criteria that close to real situation.

III. METHODOLOGY

The stage of the research was divided into four steps, there were: 1) survey for collecting poor household in Mataram town, 2) Creating a poverty criteria model by multi criteria fuzzy approach, 3) Designing and coding software, and 4) analyzing data by multi criteria fuzzy.

A. Survey of poor household

For obtaining the description of poverty in Mataram town, survey was done on sixsub-districts, and 50 villages.The steps of this survey were:

a. Poor household survey was conducted for obtaining 14 indicators of poverty according to BPS, that was grouped on 4 main groups, there are[7]:
   (1) Shelter groups
      a) The type of shelter building floor;
      b) The wide of shelter building floor;
      c) The type of shelter building wall;
      d) The type of toilet facility;
      e) The source of light
   (2) Food groups
      a) Frequency of daily eating;
      b) Beef/chicken/milk consumption in a week;
      c) Drinking water source;
      d) Energy source for daily cooking.
   (3) Clothing groups
   Annual buying of new clothes.
   (4)Other groups
      a) Ability for taking medicine;
      b) Salary of the head of household;
      c) Highest education of the head of household;
      d) Ownership of expensive things that more than Rp. 500.000.

Based on those 14 poverty indicatorsabove; therefore, it can be analyzed by multi criteria fuzzy for obtaining:

1. Category of the poor household for each of 14 poverty indicators.
2. Category the poor household with 3 (three) categories, there are: very poor, poor, and near pooron each sub-districts and villages.
3. Dominant poverty indicator that causes the poor household on a villages or sub districts.

b. Sampling technique

Interview is used as sampling method and the smallest unit is a household. By considering with that term, so this measurement approach is called by household approach. The term of household was defined as a person or people that stay on a part of a building or single building and usually eat from a single kitchen.

The steps of collecting data were as below:firstly, the poor household datais taken from the government's Mataram town. Sampling of the poor household useproportional random sampling method. From 74.833 of the available poor household data are taken 2% on each village; therefore, there are 361 obtainedpoor household.Next, collecting data was conducted by mean of direct interview andfulfillingquestionnaire.Choosinghousehold on each village is conducted randomly by considering to household representation in a village.

B. Modelling Poverty Criteria by Multi Criteria Fuzzy Logic Approach

On classical set theorem,A poverty indicator, for example, salary of the head of household, can be only categorized into two states, there are poor (state 1) for the salary that is below poverty line, and rich (state 0) for the salary that is above the poverty line. However, fuzzy set theorem gives more than two states, for example: near poor, poor, and very poor by degree of membership exists in between 0 and 1. Therefore, fuzzy set theorem is appropriate to use for poverty model.

Generally, multi criteria fuzzy that is used in this research are:

1) Decide a population of a village A with the number of household observed is *n*,thus household set is obtained as A = $\{a_1, a_2, a_3, ..., an\}$.
2) For each household has poverty criteria attribute*k*, X = $\{x_1, x_2, x_3, ..., x_k\}$.
3) Membership degree of fuzzy set A from household i^{th} by (i=1, 2, 3 , ..., n) against j^{th} attribute by (j=1, 2, ..., m) can be defined as:
   $$\mu_A\left(X_j(a_i)\right) = x_{ij}, 0 \le x_{ij} \le 1 \quad (3)$$
   where,
   $x_{ij} =$ 1 ifhouseholdnumber*i*doesnothasattributenumber*j*,
   $x_{ij} = 0$ if household number *i*has attribute*j*, and
   $0 \le x_{ij} \le 1$if household number *i* has attribute jby intensity of having on the interval (0,1).
4) The degree of membership function of poverty attribute that is cumulative(as salary or wide of floor)from fuzzy set A (set of household)number-i can be calculated by:
   $$\mu_{A_j} = \begin{cases} 1 & if\ 0 \le x_{ij} \le x_{pj} \\ \frac{x_{ij}-x_{Pj}}{x_{Rj}-x_{Pj}} & if\ x_{pj} \le x_{ij} \le x_{Rj} \\ 0 & if\ x_{ij} \ge x_{Rj} \end{cases} \quad (4)$$

where,

x_{Pj} poor limit for variabel j^{th}

x_{Rj} rich limit for variabel j^{th}

$x_{Pj} < x_{Rj}$

5) The degree of membership for poverty attribute that is qualitative (as floor type or wall type) from fuzzy set A (set of household) number-*i*can be calculated by:

$$\mu_{A_j} = \begin{cases} 1 & if\ 0 \le x_{ij} \le x_{pj} \\ \frac{x_{Rj}-x_{ij}}{x_{Rj}-x_{Pj}} & if\ x_{pj} \le x_{ij} \le x_{Rj} \\ 0 & if\ x_{ij} \ge x_{Rj} \end{cases} \quad (5)$$

where,

x_{Pj} poor limit for variable j^{th}

x_{Rj} rich limit for variable j^{th}

$x_{Pj} < x_{Rj}$

6) Poverty household index from fuzzy set A can be defined as: [11]

$$f(x_i) = \frac{\sum_{j=1}^{k} \mu(x_{ij}) w_j}{\sum_{j=0}^{k} w_j} \quad (6)$$

where,

i : (1, 2, 3, ..., n)

w_j : weight of attribute number-*j*

$\mu(x_{ij})$: degree of special membership of the household number-*i* on the attribute number -*j*

7) Poverty household index gives a value intervalin 0 – 1; it means that if index value is a closer value to 1, this household is poorer. Defining the class interval for obtaining category of poor household can be calculated by Walpole's formula [7]:

$$Interval = \frac{Nt-N0}{K} \quad (7)$$

where,

Nt : highest value

N0 : lowest value

K : number of class

thus,

$$Interval = \frac{1-0}{3}$$

$= 0.33$

Therefore, interval class is obtained:

1. ≥ 0 dan ≤ 0.33 :near poor category
2. $0.33 >$ dan ≤ 0.67 :poor category
3. $0.67 >$ dan < 1 :very poor category

8) Village poverty index is calculated based on the average of poor household indexes of village or sub-districts. Classification of village or sub-district poverty indexes follows the classification of category poor household method.

9) Determinant factor of poverty level can be measured by the weight of each village or sub-districts poverty attribute[12]:

$$W_j = -\ln\left\{\frac{1}{n}\sum_{j=1}^{k} \mu(x_{ij})\right\} \quad (8)$$

C. Designing and Coding Application Software of Multi Criteria Fuzzy

Application software that was developed in this step was used for analyzing data.

C.1. Database design

Database is used for storing data that had been written on the questionnaire.Questionnaire consists of place recognition, household member, and14 questions.

C.2 User Interface Design

User interface is a facility on a software that is used to conduct interaction between user and computer. In this research user interace was made under web platform, thus it can be accessed from any computer in the local network. This interface has main function that is used for manipulating data in the database. Therefore user can entry data to database or read stored data.

Fig. 1 shows an interface for viewing the results of the calculation process. It is a list about poverty data that is based on the type of house floor in Ampenan sub-district. This research has 91 interfaces that similar to the interface that is shown in Fig. 1, although those have different type of poverty criteria.

No	Kecamatan	Kelurahan	Jenis Lantai Bangunan Tempat Tinggal							
			Kategori							
			Mendekati Miskin		Miskin		Sangat Miskin		Fuzzy	
			Jumlah	Persentase	Jumlah	Persentase	Jumlah	Persentase	Average	Weight
1	Ampenan	Dayan Peken	4	25	12	75	0	0	0.41	0.9
2		Bintaro	1	16.67	4	66.67	1	16.67	0.54	0.61
3		Ampenan Tengah	1	25	2	50	1	25	0.56	0.58
4		Ampenan Utara	1	14.29	5	71.43	1	14.29	0.54	0.62
5		Kebon Sari	2	40	3	60	0	0	0.4	0.92
6		Pajeruk	0	0	11	91.67	1	8.33	0.51	0.68
7		Taman Sari	1	33.33	2	66.67	0	0	0.42	0.88
8		Banjar	2	50	2	50	0	0	0.34	1.06
9		Ampenan Selatan	0	0	5	71.43	2	28.57	0.56	0.59
10		Pejarakan Karya	0	0	10	100	0	0	0.46	0.77
		Total	12	16.22	56	75.68	6	8.11	0.47	0.75

Fig. 1. Interface of The Calculation Results

IV. RESULT AND DISCUSSION

A. Poverty Characteristic

Poverty indicator that is used by Statistics Center Board (*Badan Pusat Statistik*, BPS) for detecting poor household is grouped into 4 main groups, there are: shelter, food, clothing, andother.

For obtaining poverty indicators in Mataram town is done by survey on fivesub-districts that consists of 50 villages, and the number of samples is 361 respondents.Next, fuzzy method is performed to obtain the description of the poverty level in each village.Besides that,analysis of indicators was done to measure the weight of poverty attribute. This step is performed in every village and sub-districts, and then; determinant factor of poverty is obtained.

B. Shelter Group Indicators

These indicators contain: the type of building floor, the wide of building, the type of building wall, toilet facility, and main light source.

B.1 The Type of Building Floor

Five choices of the floor type are: high-quality ceramics, low quality ceramics, cement, low quality bamboo/wood, andground floor. The choice can be a combination of them. Average value of this choice is mapped to fuzzy set by equation (5).

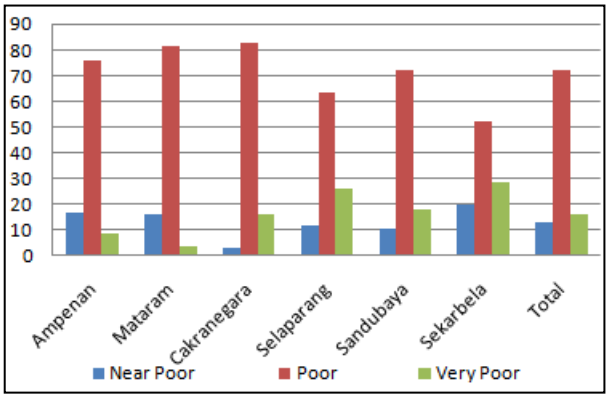

Fig. 3. Percentages of Sub-districts poor household composition Based on The type of building floor in Mataram.

Based on the chart shown in Fig. 3, the type of building floor criteria shows poor household in Mataram majority in poor category. Poor category has 71.75% and contrast, near poor is 12.74% and very poor is 15.51%.

B.2 The Wide of Shelter Building

The second indicator in this group is the wide of shelter building that is a quantitative criterion. The limit of poverty is given that is 3 m^2/person, whereas the limit of wealth is 9 m^2/person. The value of floor wide is divided by the number of family member, and then it is mapped to be fuzzy set by equation (4) for obtaining the degree of its membership.

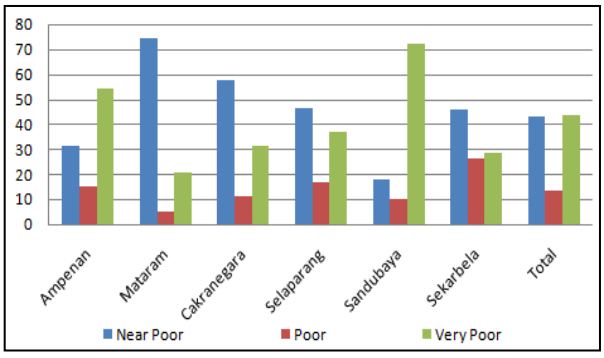

Fig. 4. Percentages of Sub-districts poor household composition Based on The wide of building floor in Mataram

B.3 The type of Shelter Building Wall

The third criterion of this group is the type of shelter building wall. There are 5 choices for the type of wall: medium or high-quality wall, wall without plaster, medium or low-quality wood, bamboo, and sago pal leaves. Respondent is permitted to choose more thanoneof them and then the average of this combination is mapped to fuzzy set by equation (5).

Based on Fig. 5, the result of analysis of this indicator is known that there are 67.87%, 26.04%, and6.09%,of poor households are included in category near poor, poor, and very poor.

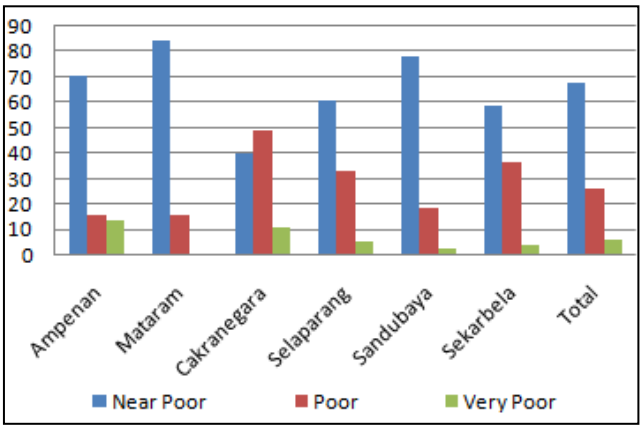

Fig. 5. Percentages of Sub-districs poor household composition Based on The type of building wall in Mataram.

B.4. Toilet Facility

Fourth criterion in this group is toilet facility. There are 5 choices: private facility and it is located inside the house and it is ≥ 2.5 m², private facility and it is located inside the house and it is <2.5 m², private facility and it is located outside of house, public facility, and none. In this criteria alse posible to chose more than one option and the average value of this choice is mapped to fuzzy set by equation (5).

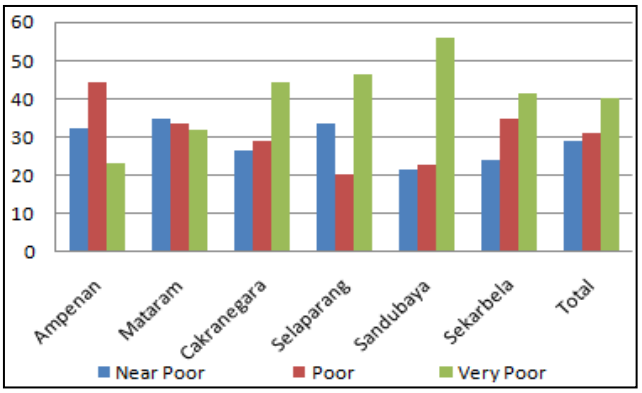

Fig.6. Percentages of Sub-districs poor household composition Based on The type toilet facility in Mataram.

Based on Fig. 6, the result of analysis presents 28.81%, 31.02%, and 40.17%, poor households areincluded in near poor, poor, and very poor category.

B.5. Main Light Source

Fifth criteria of this group is the main source of light that has 5 options, there are: electricity ≥ 1300 Watt, electricity≥900 Watt. Electricity≤450 Watt, electricity that is shared by neigborhoodand not electricity. The choice

can be more than one options and the average value of tis choices is mapped to fuzzy set by equation (5).

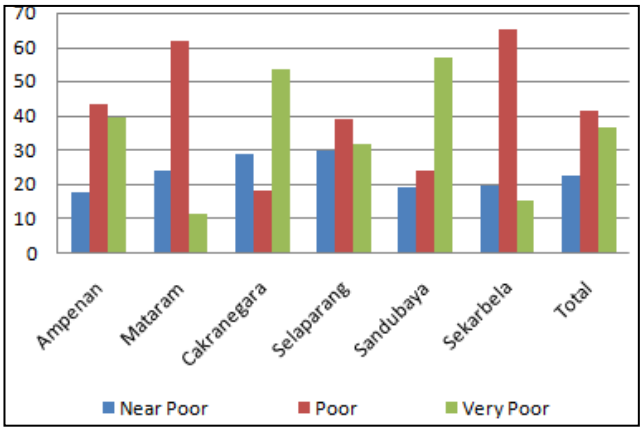

Fig. 7. Percentages of Sub-districts poor household composition Based on The source of light in Mataram.

Based on Fig. 7.It is known that 22.44%, 41.27%, and 36.29%, of poor households are included in near poor, poor, and very poor category.

C. Food Group Indicators

This indicators have questions about: daily eating frequency, weekly buying of beef/milk/chicken, drinking water facility, daily cooking energy source.

C.1. Daily Eating Frequency

The first criteria in this group is daily eating frequency that has 5 options, there are: eat as desired, more than three times per day, three times, two times, and one times per day. The choice can be combinations of those options. The average value of this combinations was mapped to fuzzy set by equation(5).

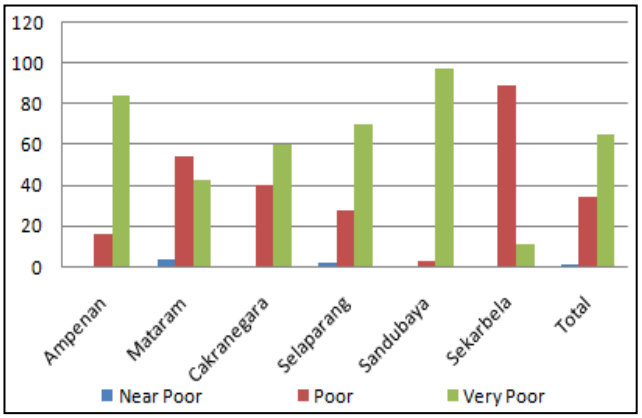

Fig. 8. Percentages of Sub-districts poor household composition Based on The Daily Eating Frequency in Mataram.

Based on Fig. 13,the result of this indicator analysis is known that 0.83%, 33.8%, and 65.37% of households in Mataram town are included in near poor, poor, and very poor category.

C.2. Weekly Consumption of Beef/Chicken/Milk

Second criteria of this group is ability of consuming beef/chicken/milkin a week that has 5 options, there are: everyday, five/sixtimes, three/four times, one/twotimes, andnever. The choice can be combination of 5 options and the average value of this is mapped to fuzzy set by equation(5).

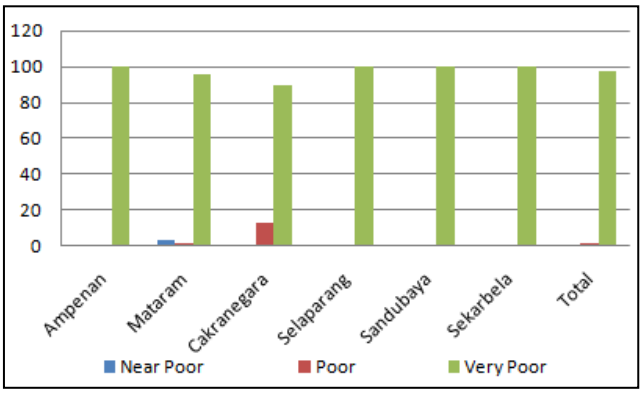

Fig. 9. Percentages of Sub-districts poor household composition Based on The Weekly Consumption of Beef/Chicken/Milk in Mataram.

Based on Fig. 9,the result of analysis in this criteria is known that 0.55%, 1.94%, dan 97.51% of householdsare as characteristic of near poor, poor, andvery poor.

C.3. The Source of Drinking Water

The third criteria of group of food is type of drinking water source that has 5 options, there are: botled water, water suplier company (PDAM), water pump, well, and river/unprotected spring/rain water. The choice can be combination of them and the average value that choice is mapped to fuzzy set by equation(5).

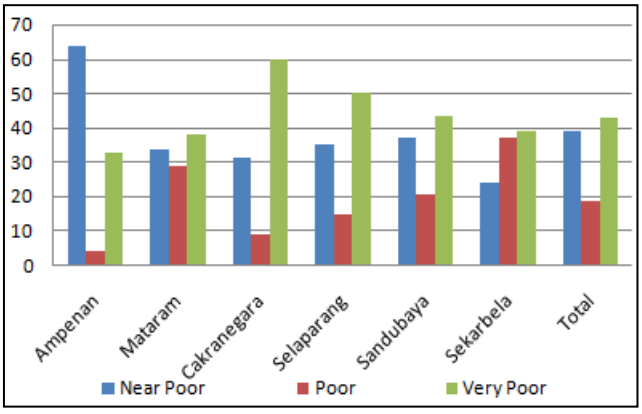

Fig. 10. Percentages of Sub-districts poor household composition Based on Drinking Water Source in Mataram.

Based on Fig. 17 and 18,it is known that 39.06%, 18.28%, and 42.66% of poor householdsare the characteristic of category near poor, poor, and very poor.

C.4 The Type of Energy Source for Daily Cooking

The last criteria in this group is the type of energy source of daily cooking that has 5 options, there are: electricity, gas (Liquid Petroleum Gas,LPG), biogas, stone oil, andwood/charcoal. The choice can be combination of that options and the average value of it is mapped to fuzzy set by equation (5).

Based on Fig. 11, the result of this analysis shows that 26.59%, 6.65%, and 66.76% of poor households are the characteristic of near poor, poor, and very poor category.

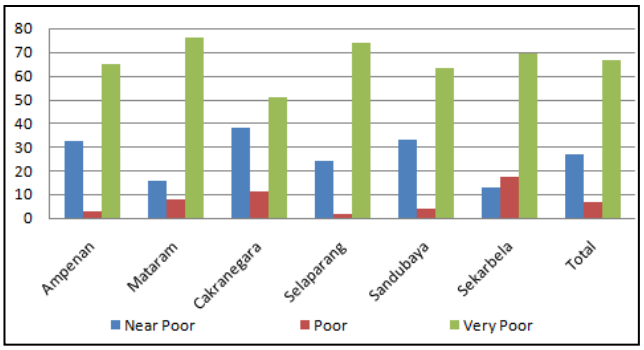

Fig. 11. Percentages of Sub-districs poor household composition Based on Energy Soure of daily Cooking in Mataram.

D. Clothing Indicator Group

Indicator in this group is only one, that is the annual buying of new cloth.

D.1. Annual buying of new cloth

It has 5 options that are everytime, three cloths in a year, two cloths in a year, a cloth in a year, and never. The choice can be combination of those options and the average of thischoice is mapped to fuzzy set by equation (5).

Based on Fig.12, the result of analysis shows that 3.88%, 10.53%, and 85.6% of poor households are as characteristic of near poor, poor, and very poor category..

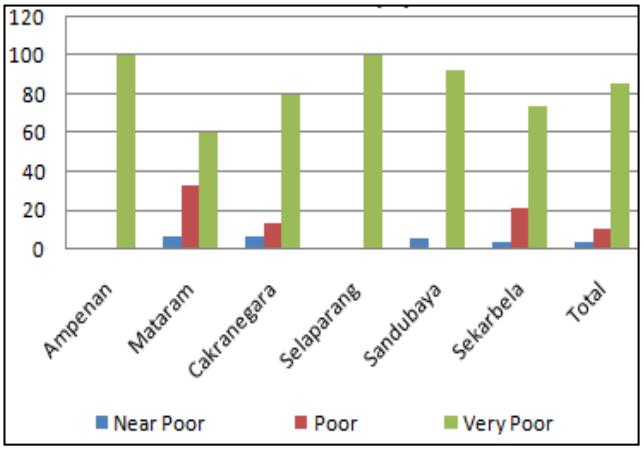

Fig. 12. Percentages of Sub-districs poor household composition Based on Annual Buying of New Cloth in Mataram.

E. Others Indicators Group

This indicators group has questions about: the ability of taking medicine, salary of household head, the heighest education of household head, and the ownership of expensive things (at least Rp. 500.000).

E.1. The Ability of taking Medicine

The first indicator in this group is the ability of household to take medicine if one of the household member is getting sick. This indicator has 5 options, there are: physician practice/private clinics, government health centers (*Pusat Kesehatan Masyarakat, PUSKESMAS*) / hospitals without public health insurance (*Jaminan Kesehatan Masyarakat, JAMKESMAS*), PUSKESMAS / hospitals with JAMKESMAS, shaman/healer, andnone. The choice can be combination of those 5 options, and the average value of this choice is mapped to fuzzy set by equation(5).

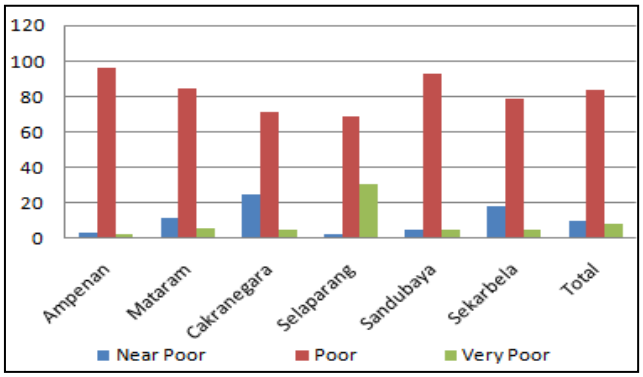

Fig. 13. Percentages of Sub-districs poor households composition Based on the ability of taking medicine in Mataram.

Base on charts in Fig.13, the result of analysis on this indicator is known that 8.86%, 83.66%, and 74.48% of poor households are categorized in near poor, poor, and very poor category.

E.2. Salary of The Household Head

The second indicator in this group is the salary of hosehold head that is qualitative attribute. The limit of poverty that has setted based on city poverty border in rupiah/capita/mounth (BPS, 2012), whereas border of wealth is determined based on regional minimum salary (*Upah Minimum Regional, UMR*). The amount of household head income is devided by the number of family member is mapped to fuzzy set by equation (3.2) for obtaining membership dgree. By this membership degree is obtained poverty degree shown in Fig. 14.

Based on Fig 14, the result of analysis shows that 1.66%, 2.22%, and 96.12% of poor households are categorized in near poor, poor, and very poor category.

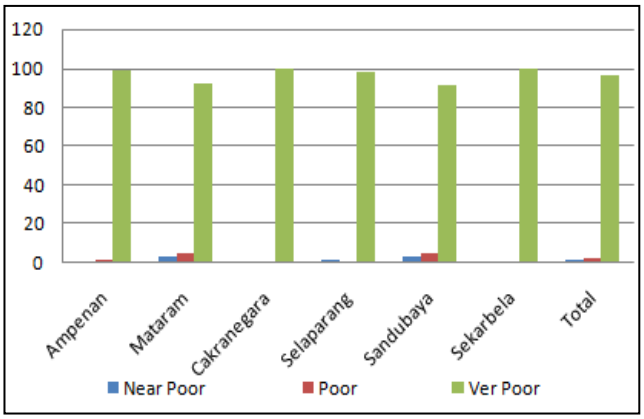

Fig. 14. Percentages of Sub-districts poor households composition Based on Salary of household head in Mataram.

E.3. The Highest Education of Household Heads

The third criteria in this group is the highest education of household head that has 5 options, there are: university graduates, senior high school graduates, yunior high school graduates, elementary school graduates, and not pass elementary school /uneducated. The choice can be combination of those 5 options and the average of this choice is mapped to fuzzy set by equation(5).

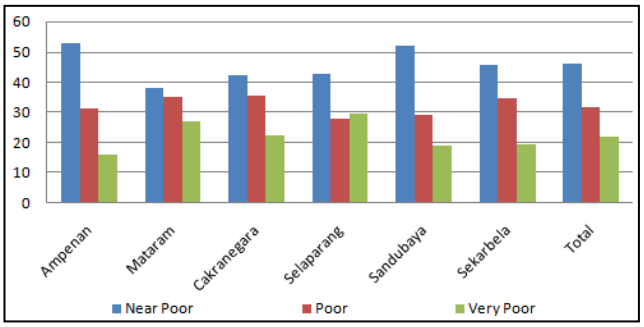

Fig. 15. Percentages of Sub-districts poor households composition Based on the Highest Education of Household Head in Mataram.

Based on Fig.15, the result of analysis in this indicator is obtained 46.26%, 31.86%, and 21.88% of households are categorized in near poor, poor, and very poor ategory.

E.4 Expensive Things Ownership

The last criteria of all indicators is the expensive thing ownership that is easy to sell by price Rp. 500.000 ore greater. This ownership is devided into 10 types, there are: gold saving, TV, livestock (goats/cow/horse), fowls, motor cycle, farmland, laptop, phonecell, andthe others.If a household has one of the this things then these household is given value by 1 and if not is given value by 0. The total of those value is mapped to fuzzy set by equation(5).

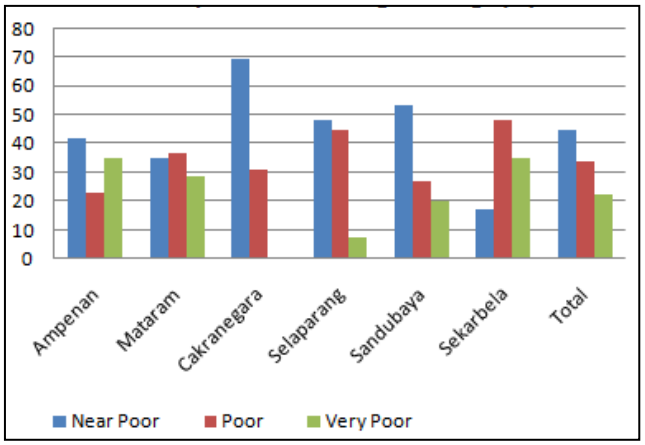

Fig. 16. Percentages of Sub-districts poor households composition Based on the Ownership of expensive things in Mataram.

Based on Fig.16, the result of analysis shows that 44,32%, 33,52%, and 22,16% of poor household are categorized in near poor, poor, and very poor category.

F. Characteristics of Poverty Degree Based on 14 Indicators

Chart in Fig. 17 presents the recapitulation of all fuzzy weigh calculations. First 5 indicators are as characteristic of very poor category, because those value is below then 0.4. These five indicators ordered from smallest are salary of household head, beef/chicken/milk consumption, annual buying of cloth, daily eating frequency, and energy source for daily cooking. And then, 8 indicators remain are as characteristics of poor category, because those fuzzy weight values are in between 0.4 to 1, there are toilet facility, main source of light, type of shelter floor, the source of drinking water, ability of taking medicine, shelter wide, ownership of expensive things, and education. Besides that, only one category is as characteristic of near poor category, these is the type of shelter wall.

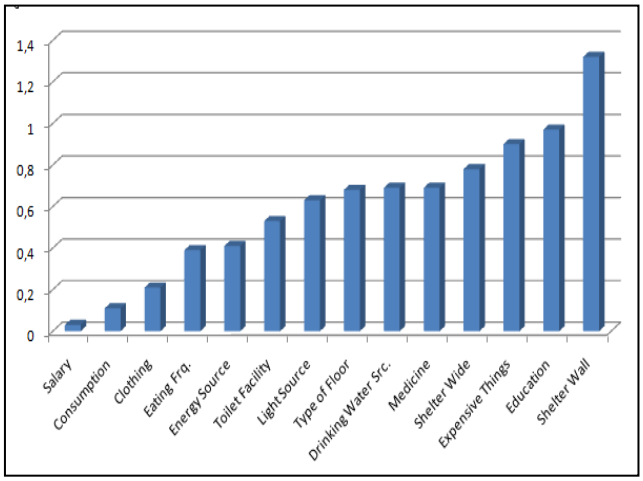

Fig. 17. Characteristics of Poverty Degree Based on 14 Indicators

G. Composition of Poor Households in Mataram

Poor households categories compositions in every subdistrics is presented in Fig. 18. The majority category in every subdistrics is poor category that has values in between a little below 90% to near 100%. Only Cakranegara has near poor category that is only in around 3%. Each subdistrics have very poor category although those are relative low to poor category that those are in below 17%. Selaparang has the highest percentage in this category and contrastly, Sekarbela has the smallest percentage.

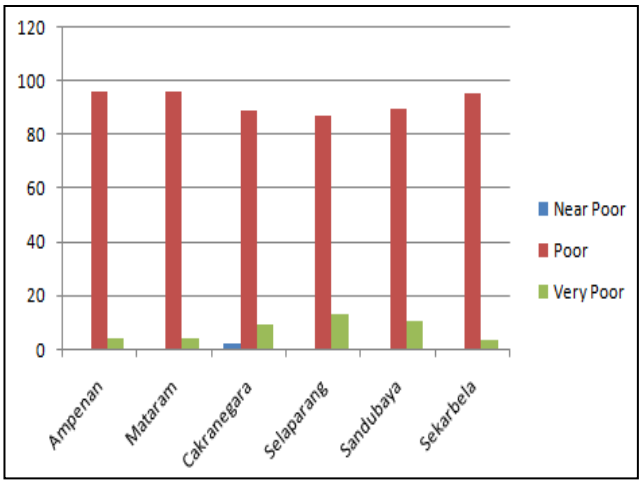

Fig.18. Poor Household Percentages in each sub districts in Mataram Town

The total amounts of poor poverty category composistion in Mataram town is shown in Fig. 19. Poor category is 93.07%, very poor is 6.65%, and near poor is only 0.28% from 361 samples that had been taken.

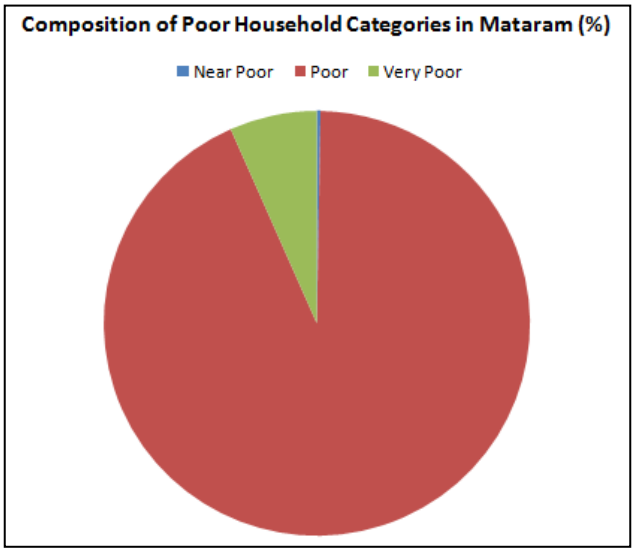

Fig.19. Poor Household Percentage in Mataram Town.

V. CONCLUSIONS

Based on the result of analysis of the application software, it can be summarized as follows:

1. There are 5 (five) criteria of poverty are indicated as characteristic of very poor category, there are: daily eating frequency, the ability of consuming beef/chicken/milk in a week, the source of energy for daily cooking, annual buying of new cloth, and the salary of household head.
2. There are 8 (eight) poverty criteria are indicated as characteristic of poor category. There are the wide of shelter building floor, the type of shelter building floor, toilet facility, main source of light, the source of drinking water, the ability of taking medicine, the highest education of the head of household, and the ownership of expensive things.
3. Only 1 (one) criterion that is indicated as characteristic of near poor category, it is the type of shelter building wall.
4. Generally, poverty category in Mataram shows that poor households in Mataram can be categorized in near poor category that has percentage is 0.28%, poor category is in 93.03% , and very poor category is in 6.65%. This composition is obtained from survey that had conducted before of 361 respondents.

VI. FUTURE WORKS

1. This research is hopped to be continued in the second year, 2014, for integrating with Geographical Information System (GIS). Therefore, this system can help Mataram Government on the mapping task of poverty in Mataram.
2. A lot of poverty degree information is presented in this application that can be used on the Decision Support System (DSS).

ACKNOWLEDGMENT

The authors would like to acknowledge the Directorate General of Higher Education of Indonesia for providing the funding research. The authors would also like to acknowledgethe surveyors.

REFERENCES

[1] BPS, “Berita Resmi Statistik”, No.06/01/ TH.XVI, 2 Januari 2013, http://bps.go.id/ data_uploads/brs/kemiskinan_02jan13.pdf.
[2] BPS Nusa Tenggara Barat, “Berita Resmi Statistik”, No. 6/01/52/TH.VII, 2 Januari 2013,http://ntb.bps.go.id/data_uploads/brs/brs-2013-01-02 kemiskinan.pdf.
[3] BPS Nusa Tenggara Barat, “Berita Resmi Statistik”, No. 35/07/52/Th. V, 1 Juli 2011, htttp://ntb.bps.go.id/fileupload/BRS_Kemiskinan_Maret_2011.pdf.
[4] Foster, J.E., and Shorrocks, A.F., “Poverty orderings. Econometrica”, Springer-Verlag, 1988.
[5] Xu, K., and Osberg, L., “The social welfare implications, decomposability, and geometry of the Sen family of poverty indices”. Canadian Journal of Economics, 2002.

[6] Chakravarty, S.R., "A deprivation-based axiomatic characterization of the absolute Bonferroni index of inequality", Journal of Economic Inequality, 2007.
[7] PKDSP Fakultas Ekonomi Universitas Brawijaya, "Faktor-Faktor Kemiskinan di Perkotaan dan Alternatif Kebijakannya Di Kota Mojokerto", Universitas Brawijaya, Malang, 2009.
[8] Bossert W., Chakravarty S. R., and D'Ambrosio C., "Multidimensional poverty and material deprivation", Department of Economics and CIREQ, University of Montreal, 2009.
[9] Giordani P., and Giorgi G. M., "A Fuzzy Logic Approach To Poverty Analysis Based OnThe Gini And Bonferroni Inequality Indices, Dipartimento di Statistica, Probabilità e Statistiche Applicate Sapienza", Università Roma, 2010,
[10] Annoni P., Fattore M., and Rainer B., "Analysing the Structure of Poverty by Fuzzy Partial Order", Dept. of Economics, Business and Statistics, University of Milan, Milan, 2011.
[11] Cerioli A., and Zani S., "A fuzzy approach to the measurement of poverty, in: Income and Wealth Distribution, Inequality and Poverty", Dagum C. & Zenga M. (Eds.), Springer-Verlag, Belin, 1990.
[12] Anonim, "Multi-dimensional Measure of Poverty Using The Fuzzy Approach, Studies for economic and econometrics", University of Pretoria, 2005.

G310

Socialization and Visualization of City Transport Using Google Maps API

Falahah
Informatics Department
Widyatama University
Jl. Cikutra no. 204 A, Bandung, Indonesia
falahah@widyatama.ac.id

Abraham Mikhael Dolok
Informatics Department
Widyatama University
Jl. Cikutra no. 204 A, Bandung, Indonesia
abrahammikhael@gmail.com

Abstract –
Traffic jam is a classic problem that has always faced by big cities. One source of traffic jam is the number of private vehicles used by people in everyday mobility. Therefore, some of the city government initiated the program to encourage people to use public transport, such as in Jakarta and Bandung. The evidence suggests there are still many people, especially certain circles or urban migrants, who are reluctant to use public transportation services because they do not know the complete information of public transportation such as the route and tariff. On the basis of the problems we are trying to build an application to introduce public transportation service and pricing estimates.
This web -based GIS application built using the Google Maps API technology that can display interactive maps and easy to use. This application is equipped with various facilities such as public transportation data entry, visualization routes, calculates distance, public places are impassable, route planning and calculation of the total tariff for two particular points on the map. The application contains information about 39 tracks and 78 routes. The application is expected used by local government to socialize the public transportation, especially city transport.

Keywords: traffic jam, GIS, Google Maps, route, visualization

I. INTRODUCTION

Traffic jam and unmanaged public transportation is a common problem in big cities. Some solution has been introduced to serve citizen better, such as building better transportation system, provide more roads and many more. But, there also some constraint in implementing the solution such as limited budget, limited spaces, priority conflict and so on.

The idea of public mass transportation has considered as a suitable solution. But it needs time, space and money to be realized. For some cities in Indonesia, build infrastructure to support public mass transportation is not easy. For example, building a new train route, provide new road, or build new transportation system such as TransJakarta. The constraint varies from budget, space, local culture and local system that tend to resist new system.

Bandung, famous as Paris van Java, is facing the same problem. Data from the Local Government stated Bandung has a population of 2.4 million. The level of vehicle ownership is high at 146.73 Bandung / 1000. The average vehicle ownership is 101.29 / 1,000 people. 0.8 Mobility vehicles in Bandung trip. While public transport in Bandung there are trains and buses. The use of trains is high at 3 million. For bus itself there are 3 kinds of Small Bus (sort of public transportation), Medium Bus and Large Bus [7].

Bandung has 36 route of small bus to serve the mobility of citizen. The local government has a program to empower and utilize the public transportation by improving the quality of public transportation services and promote them among the resident. The problem is how to promote it better, especially for urban migrant, since they do not familiar with local condition. To resolve this problem, we proposed a system to support people finding information about public transportation in Bandung, using web based application that can present spatial information. The system is expected give the user better information about route, distance and tariff for public transportation so it can help the citizen more familiar with the public transportation.

II. MAPPING USING GOOGLE MAPS API

A. Spatial and Non Spatial Data

Spatial data is geographic data related to the actual appearance of objects on the surface of the earth, such as administrative boundaries, hydrologic boundaries, land use, potential and soil characteristics, and hydrological and building irrigation networks[9]. Spatial data obtained from maps, aerial photographs, satellite imagery, statistical data and other.

Non-spatial data is the data in the form of text or numbers (commonly called attributes), tabular form of the data that is

linked to spatial data. This relationship allows the user to understand the meaning of the spatial object. Information about the attributes of a spatial object is shown as a row of data records in the attribute table. Explain the non-spatial data or spatial data as a basis to describe the spatial data.

B. Google Maps

Google Maps is a web mapping service application and technology provided by Google, powering many map-based services, including the Google Maps website, Google Ride Finder, Google Transit,[12] and maps embedded on third-party websites via the Google Maps API.[12] It offers street maps and a route planner for traveling by foot, car, bike (beta), or with public transportation. It also includes a locator for urban businesses in numerous countries around the world. Google Maps satellite images are not updated in real time, however, Google adds data to their Primary Database on a regular basis, most of the images are no more than 3 years old.

Like many other Google web applications, Google Maps uses JavaScript extensively.[13] As the user drags the map, the grid squares are downloaded from the server and inserted into the page. When a user searches for a business, the results are downloaded in the background for insertion into the side panel and map; the page is not reloaded. Locations are drawn dynamically by positioning a red pin (composed of several partially transparent PNGs) on top of the map images. A hidden *iFrame* with form submission is used because it preserves browser history. The site also uses JSON for data transfer rather than XML, for performance reasons. These techniques both fall under the broad Ajax umbrella. The result is termed a slippy map[13] and is implemented elsewhere in projects like OpenLayers.

C. Google Maps API

After the success of reverse-engineered mashups such as chicagocrime.org and housingmaps.com, Google launched the Google Maps API in June 2005[12] to allow developers to integrate Google Maps into their websites. It is a free service, and currently does not contain ads, but Google states in their terms of use that they reserve the right to display ads in the future.

By using the Google Maps API, it is possible to embed Google Maps site into an external website, on to which site specific data can be overlaid. Although initially only a JavaScript API, the Maps API was expanded to include an API for Adobe Flash applications (but this has been deprecated), a service for retrieving static map images, and web services for performing geocoding, generating driving directions, and obtaining elevation profiles. Over 1,000,000[12] web sites use the Google Maps API, making it the most heavily used web application development API.

There are four types of maps available within the Google Maps API. In addition to the familiar "painted" road map tiles, the Google Maps API also supports other maps types. The following map types are available in the Google Maps API:

- ROADMAP displays the default road map view. This is the default map type.
- SATELLITE displays Google Earth satellite images
- HYBRID displays a mixture of normal and satellite views
- TERRAIN displays a physical map based on terrain information.

The main requirement to be able to use the Google Maps API is to get the API Key. API key is a code which is the interface between the web applications that we created with the function performed. The steps to get the API Key is as follows:

1. Having a Google account.
2. Log in to the Google APIs Console page: https://code.google.com/apis/console.
3. Start a new project by selecting the Create Project menu.
4. Selecting the menu "Services", select one of the services that will be used, such as "Google Maps API v3" and change the status to "On"
5. Select the "API Access", Google will include the API key is ready for use, for example:
   ```
   ABQIAAAA8tt4eKTuBZMVnLJfP2BZrBT2yXp_ZAY8_ufC
   3CFXhHIE1NvwkxS4Rz1LFzG0odNPtk8VLkdrQF5grA
   ```
6. API key is then inserted at the script file that will access the web page functions available on google maps service is maps.google.com, as the following example:
   ```
   <script type="text/javascript"
   src="http://maps.google.com/maps/api/js?sens
   or=true&amp;key=ABQIAAAA8tt4eKTuBZMVnLJfP2BZ
   rBT2yXp_ZAY8_ufC3CFXhHIE1NvwkxS4Rz1LFzG0odNP
   tk8VLkdrQF5grA"></script>
   ```

Furthermore, earlier key can be used to insert a map from Google Maps on the web application as follows:

1. Incorporating Maps API Javascript into our HTML (Javascript snippet like the above example).
2. Creating a div element with the name map_canvas to display the map, example:

   ```
   <div id="map_canvas" style="width:600px;
   height:600px"></div>
   ```

3. Create some literal objects to save the properties on the map, example:

   ```
   var map = new
   google.maps.Map(document.getElementById("map
   _canvas"), myOptions);
   ```

4. Write a Javascript function to create map object, such as:

   ```
   function initialize() {
   var latlng = new google.maps.LatLng(-6.4,
   106.8186111);
   var myOptions = {
   zoom: 13,
   center: latlng,
   mapTypeId: google.maps.MapTypeId.ROADMAP
   ```

```
};
```

Setting the map is determined by the position you want to appear as in step 4 above, namely by entering longitude and latitude (map coordinates).

Parameter determines the zoom level you want. The smaller the value, the farther you are from the ground. A value of 0 will show a map of the whole world. The maximum value is 19.

MapTypeId parameter determines the type of map to be displayed, and there are four options, such as ROADMAP, SATELLITE, TERRAIN, and HYBRID.

5. Initiate map in on-load event at body tag of HTML, example:
```
<body onload="initialize()">
```

III. VISUALIZATION OF CITY TRANSPORT

A. The Problem in Public Transportation

Transportation system is a conjunction of some components or related object to move people or goods using vehicle accordance with the advancement of technology[5]. The system consists of the transports and the management that manage the transports.

Mode of transport (or means of transport or transport mode or transport modality or form of transport) is a term used to distinguish substantially different ways to perform transport. The most dominant modes of transport are aviation, land transport, which includes rail, road and off-road transport, and ship transport. Each mode has its own infrastructure, vehicles, and operations, and often has unique regulations. Each mode also has separate subsystems. On this paper we only discuss about road transportation.

The management of transportation falls into two categories which are marketing management and selling of transportation services, and management of traffic.

Public transportation, in this paper, limited to road transportation, is a transportation system using in the city, or a regency using automobile or bus that has fixed and specific route and destination, both scheduled or unscheduled.

Each destination is distinguished by color or number. The tariff usually is defined by local government, but short-distance passenger or students usually pay in lower tariff. The route or trajectory for public transportation is set by local government.

Formally, the public transportation can stop only in specific point such as a bus stop, but actually, especially in Bandung, the drivers will stopped their vehicle anywhere to pick or drop the passenger. The violation of rules is common happen such as pick the passenger or good over capacity, the door is not closed properly and many more. The violations are ignored by the officer because of weakness in applicable laws.

The problems in public transportation have strong related with the people and rules. Some of problem such as: the inconvenience environment in the vehicle, undisciplined drivers and passenger, and criminality problem[11].

Bandung, the capital of West Java, is facing the problems of public transport as well as other cities in Indonesia. The existence of public transportation is not properly empowered and some problem arise such as undisciplined driver and passenger, unbalanced distribution on public transportation to serve certain area and others, are often blamed to be the cause of traffic jam problem. The other problem of traffic jam also caused by unbalanced of amount of road users compare to roads space. It leads to an initiative to empower the public transportation to reduce the amount of vehicles in the road, especially in peak time. The initiatives include improvement of transportation system, make public transportation more comfortable and socialize the system to the citizen. It involved some stakeholders such as Transportation authority department, local government, transportation management, and the citizen.

Mosca and Zito has built the application for mapping public transport in Adelaide [10] using ArcGIS. The system can display the bus route and coordinate of bus position. But in Indonesia, recently we did not find the GIS-based system which can display the route of public transportation in the city.

B. Socialization and Visualization Transportation System

Based on problem according to public transportation as described previous, we try to provide a system to support the promotion program of using public transportation among the citizen. The system will provide visualization of public transportation route and give some information such as the tariff, public place on the route and total cost for certain route. The system should provide some functional requirement such as:

1. The system can display information about the route, tariff and distance for each route.
2. User can use the system to make a travel plan, by simulate some alternative route and calculate the distance and tariff for each alternative. It can be done interactively.
3. The system can display public place which are famous or relative important for the citizen such as mall, government office, hospital, and so on.
4. Administrator system can manage the master data such as route, tariff, road name, category, and public place.

The reference data using in this system is based on Bandung Government Decree according to public transportation, route and tariff, which consist of 36 routes. The public places describe in this application are classified into some categories such as: restaurant or café, entertainment, education, tourism, health services, government office, transportation, and public services.

The system functionality can describe as Figure 1 below. The system will manage by an administrator who will maintain the

data and tagging the map. User, anybody who can access the web, can view the map that will display the route and public places. User also can search certain route and make a travel plan. The system will display the route, distance and total tariff that is accumulated from transportation passes the route.

The identified data modeled by conceptual data model as displayed in Figure 2. The main entities are trayek, route, public place, street, and tariff. Each trayek has a route, which can differ from incoming and outgoing route. Each trayek has a tariff which is defined by government rules. Each route will consists some streets and based on the street route we can calculate the distance.

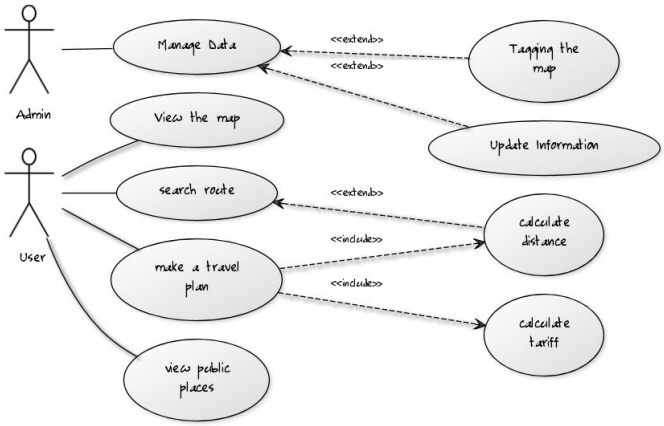

Figure 1. Use Case Diagram

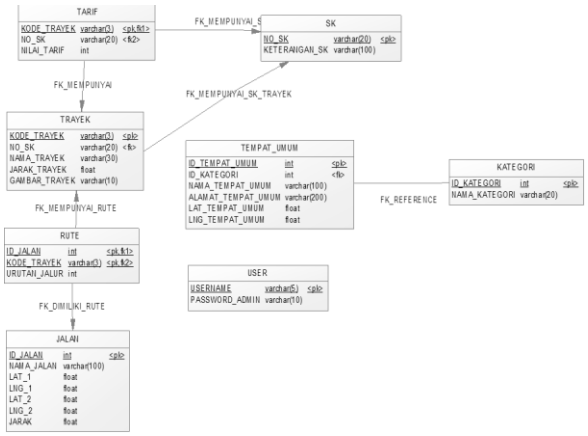

Figure 2. Conceptual Data Model

User can access the application through main panel which consist 2 options. User can choose between display the route or display the public places.

The main panel displays the map and user can choose the available trayek in dropdown text.

Figure 3. Main Panel for User

After user chosen a specific trayek, application will display the route of chosen trayek with different color between incoming and outgoing route (Figure 4), because some of them have different route. It can helps the user to decide the right trayek if they want to visit certain places. The system also display a photo and information about the trayek, and tariff in flat condition (not depends on distance).

Figure 4. Panel for display the route

Figure 5 display the panel for all public places. User can chose to display specific categories such as education, health services, or government office by clicking the menu above. The map also combined with trayek and route so the user can choose the right trayek to reach their destination places. Map also show different icon for different category of public places.

Figure 5. Public Places

The system is not implemented yet and also need some improvement such as integrated with other transportation mode (train or busses). The difficulties on this system is for administration when entering the street path data, because they have to divide the street path into some section and input each section to present the complete route. But, since it need to be done only once, the administrator can do it step by step until we can present the data completely. Another constraint of this system is the system will works well if there is internet connection available, in other words, the performance of this system depends on quality of internet connection.
The system was built without intelligent features such as shortest path and intelligent search because of lack of data on city traffic jam and other statistic data according to city transport problem.

CONCLUSION

Based on analysis and development of system which can display the map of city transport above we can conclude some point as bellow:

1. Google Maps can help us to present spatial information easily and it give us lots of opportunity to build some system and present the information spatially so it more informative than before.
2. The feature of Google Maps, through API facility, has implemented as a tools to build the system which can display the route of public transportation in Bandung. This system is expected to help the government promote the public transportation uses between the resident as a solution in reducing traffic jam and transportation problems.
3. The system is developed to display public transportation which has some features such as display the route, calculate the tariff and distance between two places, display public places and help user to make a simple travel plan.
4. The system was designed to display only small bus type of public transportation since it is a main transportation mode in Bandung.
5. The system need internet connection to operate well so the system performance is also depends on the quality of internet connection.

In the future, we expect can improve the system by adding some extended feature such as improving the search alternative so user can using vary search option, integrated the system into public transportation mode such as big Bus or train mode.

REFERENCES

[1] Asep Iskandar P. Pengenalan MapInfo. http://student.eepis-its.edu/~raisputra/GIS/ Map%20Info/pengenalan%20 mapinfo .pdf

[2] Bappenas, Modul Arc GIS Dasar. http://p3b.bappenas.go.id/handbook/docs/15.%20%20Modul_ ArcGIS/Modul_ArcGIS_Dasar.pdf

[3] Dinas Perhubungan Kota Bandung, "Surat Keputusan Walikota Bandung Nomor: 551.2/KEP.400-Bag.Hukham/2008. Daftar tarif angkutan penumpang umum di Kota Bandung." Mei-2008.

[4] Hidayat, Rahmat.2005. Jenis-jenis Peta dan Fungsi. Bandung:Garis Pergerakan.

[5] Hubdat. Direktorat Jendral Perhubungan Darat. http://www.hubdat.web.id

[6] Iskandar, Abubakar.1998. Sistem Transportasi Kota. Jakarta: Direktorat Bina Sistem Lalu Lintas dan Angkutan Kota.

[7] Jurnal Kajian HMS 2 – Transportasi Kota Bandung & Angkot Day, Kominfo, Dec 11, 2013, accessed from : http://ima-g.ar.itb.ac.id/ima-g/?p=656

[8] Google. Documentation Google Maps Javascript API Versi 3. http://code.google.com/apis/maps/documentation/javascript/maptypes [23 Juni 2011].

[9] Pharasta, Eddy.2002. Konsep-konsep Dasar Sistem Informasi Geografis . Bandung: Informatika.

[10] Mosca, Nicola, and Zito, Rocco, "Positioning needs for public transport", Proceedings of Australasian Transport Research Forum 2011. 28-30 September 2011

[11] Virtuemagz .Quantum GIS. http://virtuemagz.com/quantum-gis.html.

[12] Zhang, Jingyuan and Shi, Hao, "Geospatial Visualization using Google Maps : A Case Study on Conference Presenters", Proceeding of the Second International Multi-Symposiums on Computer and Computational Sciences,(IMSCC '07), p:472-476, 2007.

[13] http://www.bimbingan.org/masalah-angkutan-umum.htm

[14] https://developers.google.com/maps/documentation/javascript/maptypes

[15] http://www.w3schools.com/googleapi/google_maps_types.asp

[16] http://en.wikipedia.org/wiki/Google_Maps

G311

SIG-based Earthquake Information System

Wina Witanti[1)]
[1)]Computer Science, Basic Science Faculty
Universitas Jenderal Achmad Yani
Jl. Jendral Sudirman, Cimahi
Indonesia
[1)]wina.witanti@lecture.unjani.ac.id

Falahah[2)], Yuliana[3)]
[2,3)]Informatics Department,
Universitas Widyatama
Jl.Cikutra no.204 A Bandung
Indonesia
[2)]falahah@widyatama.ac.id
[3)]yoe.lia91@gmail.com

Abstract— Indonesia has been known as an area prone to earthquakes, volcanic or tectonic earthquakes either. Therefore, it is essential to disseminate information to the public about the earthquake to raise awareness of the dangers of earthquakes as early as possible.

The GIS-based earthquake information system has available but the content has not been able to accommodate all the available information because there are many tools which are not available .The system is not equipped with several important features such as geospatial data are not managed properly so that the news delivered incomplete and has not been linked to the news location. Map shown is also not equipped with the grouping by district or tagging earthquake prone areas.

Based on these issues, we develop a geographic information system mapping earthquake which consist of important information such as data summary earthquake in Indonesia (1629-2013), the latest earthquake news, earthquake-prone maps, epicenter of the earthquake, and seismic data search by province, years, and the desired magnitude. The system is built utilizing the Google Maps API and Quantum GIS to create maps prone to earthquakes and management of spatial data.

Keywords:earthquake, map, GIS, Google Maps, Quantum GIS

I. INTRODUCTION

Indonesia is a country that has high risk in earthquake. It caused by its tectonic position which is among Asia and Australia plate, and also by the "ring of fire" or the area where a large number of earthquakes and volcanic eruptions occur in the basin of the Pacific Ocean. The line passes Indonesia from the North Maluku to West Java. It puts Indonesia into most dangerous location for earthquakes.

In the other side, the awareness of disaster caused by earthquake in Indonesia is not familiar among the citizen, because the earthquake with serious damage is rarely happens. But, recently, this country is woken by some earthquake events that caused serious damaged for example big tsunami in Aceh, earthquake in Yogyakarta, tsunami in Pangandaran, and many more.

The awareness of earthquake hazard arises among people in Indonesia and they start to learn about earthquake more intensive than before. The presence of internet technology and ease of access of information make the earthquake information distributed easier than before.

It leads the government to provide suitable information about earthquake, so the people can find information about earthquake easily.

Directorate of Volcanology and Geological Hazard Mitigation (PVMBG) has provided a website that contains information about earthquake. The website was developed with some information and also be equipped with the map so it can display the information spatially. The website also implemented the GIS technology, but the information provided is not complete and there are many tools which are not accessible by the user. This condition leads us to build a website which implement GIS technology to display information about earthquake more complete than the ones has provided by PVMBG. The aim of this system is to facilitate the public to find out information about earthquake in detail manner such as location of frequent earthquake, environmental damage caused by the earthquake, as well as areas that are prone to earthquakes. The system has earthquake data in Indonesia from 1629 -present. These data were obtained from a catalogue of destructive earthquake in Indonesia from the Center for Volcanology and Geological Hazard Mitigation (PVMBG) Bandung and BMKG website Meteorology, Climatology and Geophysics (BMKG). Mapping using Google Maps API

II. LITERATURE REVIEW

A. Geographic Information Systems

Geographic Information Systems (GIS) is a computer-based system (CBIS) is used to store and manipulate geographic information. GIS is designed to collect, store, and analyze objects and phenomena where geographic location is an important characteristic or critical to be analyzed. Thus GIS is a computer system which has the following four capabilities

in handling geographically referenced data: (a) input, (b) data management (storage and retrieval), (c) the analysis and manipulation of data, and (d) output [3].

A GIS can be thought of as a system that provides spatial data entry, management, retrieve, analysis, and visualization functions. The implementation of a GIS is often driven by jurisdictional (such as a city), purpose, or application requirements. Generally, a GIS implementation may be custom-designed for an organization. Hence, a GIS deployment developed for an application, jurisdiction, enterprise, or purpose may not be necessarily interoperable or compatible with a GIS that has been developed for some other application, jurisdiction, enterprise, or purpose. What goes beyond a GIS is a spatial data infrastructure, a concept that has no such restrictive boundaries.

Geographic data in question here is a spatial data characteristics are:

1. Has geometric properties such as coordinates and location.
2. Related to aspects such as space parcels, city, area development.
3. Dealing with all the phenomena that are in the earth, for example, the data, the incidence, symptoms or object.
4. Used for certain purposes, such as analysis, monitoring or management.

Most of the GIS using the concept of "layer" (layer). Each layer represents a geographic feature in the same area and then all the layers are stacked with each other to get complete information. Each layer can be thought of as a transparent plastic containing only certain images. Users can select the desired transparent-transparent and then superimposed each other so that would be obtained image is a combination of a number of transparent.

B. Earthquake

Earthquake / earthquake is a vibration or shock that occurs in the earth's surface due to the release of energy from the sudden that creates seismic waves. Normal earthquakes caused by the movement of the earth's crust (tectonic plates). Frequency region, referring to the type and scale of earthquakes experienced over a period of time.

Earthquakes are measured using observations from seismometers. The moment magnitude is the most common scale on which earthquakes larger than approximately 5 are reported for the entire globe. The more numerous earthquakes smaller than magnitude 5 reported by national seismological observatories are measured mostly on the local magnitude scale, also referred to as the Richter scale. These two scales are numerically similar over their range of validity. Magnitude 3 or lower earthquakes are mostly almost imperceptible or weak and magnitude 7 and over potentially causes serious damage over larger areas, depending on their depth. The largest earthquakes in historic times have been of magnitude slightly over 9, although there is no limit to the possible magnitude. The most recent large earthquake of magnitude 9.0 or larger was a 9.0 magnitude earthquake in Japan in 2011 (as of October 2012), and it was the largest Japanese earthquake since records began. Intensity of shaking is measured on the modified Mercalli scale. The shallower an earthquake, the more damage to structures it causes, all else being equal.

C. Google Maps

Google Maps is a web mapping service application and technology provided by Google, powering many map-based services, including the Google Maps website, Google Ride Finder, Google Transit,[12] and maps embedded on third-party websites via the Google Maps API.[12] It offers street maps and a route planner for traveling by foot, car, bike (beta), or with public transportation. It also includes a locator for urban businesses in numerous countries around the world. Google Maps satellite images are not updated in real time, however, Google adds data to their Primary Database on a regular basis, most of the images are no more than 3 years old.

Like many other Google web applications, Google Maps uses JavaScript extensively.[13] As the user drags the map, the grid squares are downloaded from the server and inserted into the page. When a user searches for a business, the results are downloaded in the background for insertion into the side panel and map; the page is not reloaded. Locations are drawn dynamically by positioning a red pin (composed of several partially transparent PNGs) on top of the map images. A hidden *iFrame* with form submission is used because it preserves browser history. The site also uses JSON for data transfer rather than XML, for performance reasons. These techniques both fall under the broad Ajax umbrella. The result is termed a slippy map[13] and is implemented elsewhere in projects like OpenLayers

III. RESEARCH APPROACH

A. Requirement Analysis

The information about natural disaster, especially earthquake, is handled by Meteorology, Climatology and Geophysics (BMKG) Office. BMKG has several agencies in the areas of seismicity which aims to help inform the earthquake in Indonesia. One of the related office is Volcanology and Geological Hazard Mitigation (PVMBG) in Bandung. PVMBG already built a web-based information system about earthquake, which can access through the address http://www.vsi.esdm.go.id.

The web site consist three (3) contents which are about earthquake, the earthquake and map of publication.

The first step in this research is exploring the website and conducting an interview on the Center for Volcanology and Geological Hazard Mitigation (PVMBG). After exploring the existing system we found some problems, such as:

1. The existing website of earthquake could not accommodate all the required information because there are many tools that could not executed.
2. Geospatial data that is not managed properly so that the news delivered incomplete, both in mapping and news content.

3. There is no content mapping in detail is shown with a particular coloration to indicate areas prone to earthquakes are grouped according to the districts in Indonesia.

To resolve this problem, we try to develop new system using GIS technology to create the map of earthquake in Indonesia. The map will display the earthquake information statistically and accompany with some detail information for each earthquake event such as magnitude and the damage caused by earthquake.

The system is expected can provide information to the people and supported by the main contents such as:

1. Breaking news, information about recent earthquake.
2. Maps and Information, information about the region in Indonesia that have experienced earthquakes since 1629-now in spatial format.
3. Each area that have experienced earthquakes is marked with a dot on a map, and the news is displayed bellow.
4. The area which has more frequent earthquake is marked with specific colors.

Spatial data contained on this map was made using GIS quantum. The new system is expected to run better than the previous, its can provide accurate information to the users and can expand for more feature and facility in the future.

B. System Design

Based on requirement that has defined above, we design the system and present it using some diagram such as Data Flow Diagram for process modeling and ER Diagram to present the data model.

The highest level of DFD shows two external entity which involved in this system, Admin as system administrator and the user. The user can be anyone who can access the website. User can view the content, send the comment and read the comment respond. Admin has responsible to keep the data up to date and reply the comment from users.

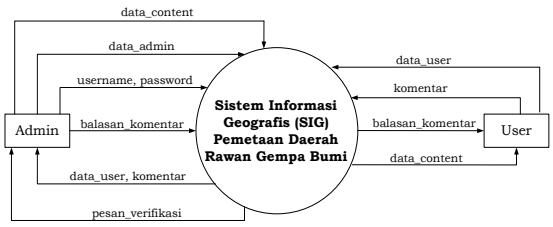

Figure 1. DCD System

As derived process from DCD we define four main process which are manage admin data, manage content, manage shoutbox (comments) and manage the category(of the news). We define the data and the news which entered to the system as the content for simplifying the process.

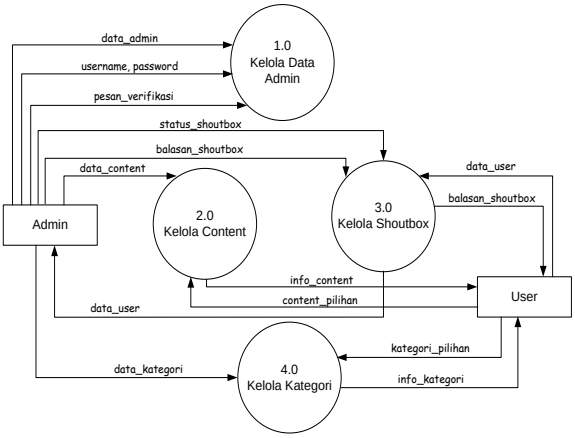

Figure 2. Data Flow Diagram Level 0

Based on data element defined in DFD, we build the data model and present it on ER Diagram as shown on Figure 3. The diagram consists of 6 entities and the earthquake information is put on "titik gempa" or the center of earthquake.

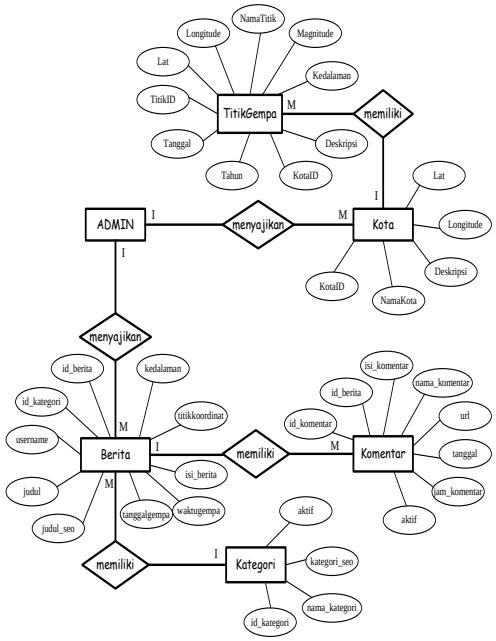

Figure 3 ER Diagram

The next step is transforming the ER Diagram to become the table relationship diagram. To support the system we use 6 table as describe in figure 4.

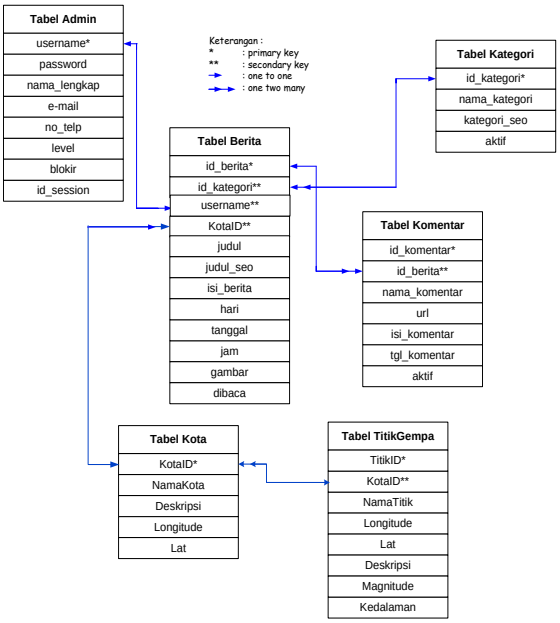

Figure 4 Table Relation

The website was developed using CMS approach so the admin can manage the content easily. As an admin, we can manage the content using main panel as shown in Figure 5

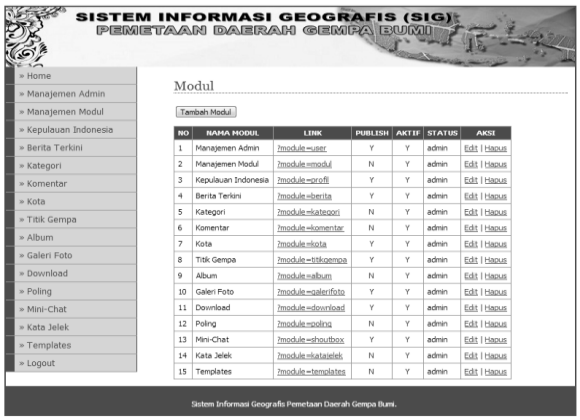

Figure 5. Main Panel for Content Management

Admin can input the earthquake data using the panel as shown in figure 6. The panel shows the city, earthquake epicenter and the impact of earthquake into human or environment

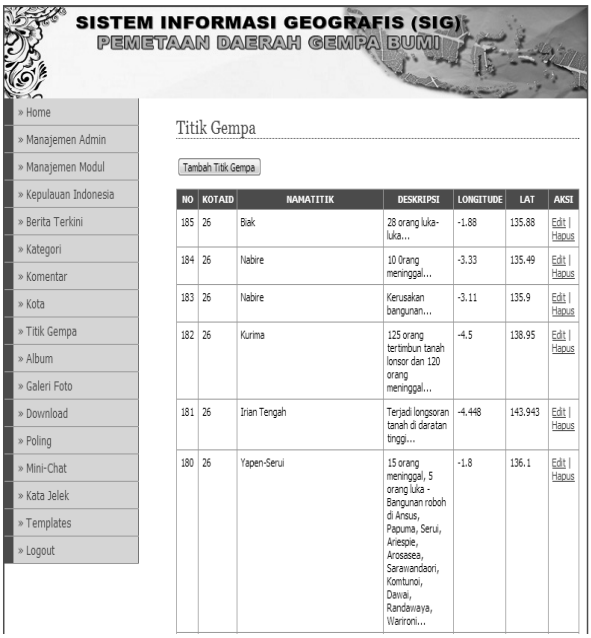

Figure 6. Main Panel for Earthquake Events

Users can see all information in one page that consists of recent news, video, image and comments according to earthquake events (figure 7). Users also can explore more using advanced menu such as display the map, searching the data (figure 8) and download the interest file.
The system also can show the area which has specific range of earthquake event, for example, we classify the area as high risk earthquake prone, middle, and low based on history of earthquake event in the certain area. Figure 9 show the map

Figure 7. Main Menu for Users

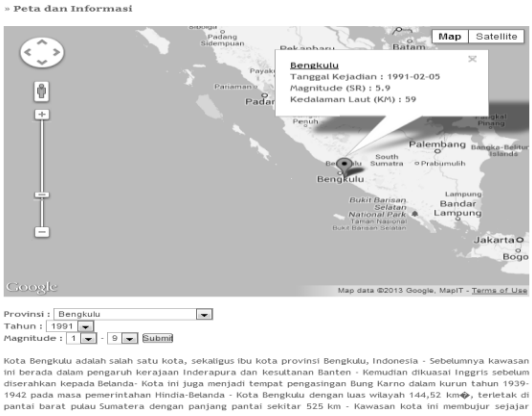

Figure 8. Searching Facility

Figure 9. Map of earthquake region

The data using in this application is entered manually and based on past information. If the system already installed and hosted, we can add some additional features such as connected with earthquake station or detector so the data can update automatically. The system also not include tsunami prediction because of mainly tsunami is caused by high magnitude of earthquake which has epicenter in ocean area. In this application we focused on mapping the area that has more frequent earthquake so the people can make consideration in planning and building the infrastructure in the specific area.

CONCLUSION

Based on implementation of GIS Application in mapping the earthquake prone areas in Indonesia, we can conclude some interesting issue as follow:

1. We can make a Geographic Information Systems (GIS) Mapping Earthquake Prone by using maps that have been digitized and provide features which include the provincial earthquake, year and magnitude , as well as showing seismic area with coloring based on the amount of the number of earthquakes that have occurred in the area.
2. Digitizing the map is done using Quantum GIS to create, store and process spatial data. The data then is stored in MySQL as textual database and using Google Maps API as supported tools to present the spatial data easily.
3. The website can display the information about earthquake more detail because it has news, video and has equipped with searching facility and the earthquake event for each area which categorized based on frequency. It expected to help the user to know which area with high risk of earthquake.

In the future, we can explore and expand the features of this website by adding some integrated data such as data from satellite, completing missed earthquake information, and keeping the data up to date so it can be important reference for the citizen.

REFERENCES

[1] Adam Suseno dan Ricky Agus T., S.T., S.Si, M.M. 2012. Penggunaan *Quantum GIS* Dalam Sistem Informasi Geografis. Bogor: Gunadarma.

[2] Aronoff, Stanley. 1989. Geographic Information System: A Management Perspective. Otawa, Canada: WDL Publications.

[3] Bildirici, I.O, and Ulugtekin, N.N., "Web Mapping With Google Maps Mashup : Overlaying Geodata", A special joint symposium of ISPRS Technical Commission IV & AutoCarto in conjunction with ASPRS/CaGIS 2010 Fall Specialty Conference November 15-19, 2010 Orlando, Florida

[4] Demers, M.N. 1997. *Fundamentals of Geographic Information Systems*. New York: John Wileys dan Sons, Inc.

[5] Gunarto, Thomas Yuni. 2008. *Gempa Bumi*. http://staffsite.gunadarma.ac.id/thomasyg/index.php?stateid=download&id=8195&part=files (akses : 23 Maret 2013).

[6] HM, Jogiyanto 2005. Pengenalan Komputer Dasar Ilmu Komputer Pemrograman, Sistem Informasi. Yogyakarta: Andi.

[7] Pheby. 2012. Bab 2 – Teori Penunjang. http://digilib.its.ac.id/public/ITS-NonDegree-7526-7405040025-bab2.pdf (akses: 25 Maret 2013).

[8] Harsiti. 2009. *Entity Relationship*. http://harsiti09.files.wordpress.com/2009/10/v-entity-relatinal-diagram.doc (akses: 01 September 2013).

[9] Hartono, Jogiyanto . 2005. Pengenalan Komputer Dasar Ilmu Komputer Pemrograman, Sistem Informasi. Yogyakarta: Andi.

[10] Hidayat, Rahmat, dkk. 2005. Geografi dan Koordinat Peta. Bandung : Garis Pergerakan.

[11] Irsyam, Masyhur, et.al, "Development of Seismic Hazard and Risk Maps for New Seismic Building and Infrastructure Codes in Indonesia", Proceeding the 6th Civil Engineering Conference in Asia Region: Embracing the Future through Sustainability.

[12] Malik, Abdullah. 2012. Pengertian, Fungsi dan Jenis Peta. Jepara. URL :

[13] http://farid-rizky.blogspot.com/2012/12/pengertian-fungsi-dan-jenis-peta.html (akses : 05 September 2013).

[14] Mutiarani, Afifi. 2012. Skala Gempa Bumi. Surabaya. URL : http://fiflowers.wordpress.com/geofisika/gempabumi/skala-gempabumi/ (akses : 05 September 2013).

[15] Prahasta, Eddy. 2002. Konsep – konsep Dasar Sistem Informasi Geografis. Bandung : Informatika.

[16] Prihatna, Henky. 2005. Kiat Praktis Menjadi Webmaster Profesional. Jakarta : PT. Elex Media Komputindo.

[17] Rapper J. dan Green N. 01 Maret 1994. *Gis Tutor 2 for Microsoft Windows*. Milton Road, Cambridge CB4, 4ZD, UK: *Longman GeoInformation 307 Cambridge Science Park*.

[18] Sajo, Daud. 2009. Pengertian-Peta. URL : http://geografi-bumi.blogspot.com/2009/09/pengertian-peta.html (akses : 25 Maret 2013).

[19] Setiawan, Dita. 2012. Sistem Informasi Pemetaan Pengungsi Menggunakan *Openlayers Framework*. http://repository.amikom.ac.id/files/Publikasi_06.11.1049.pdf (akses : 23 Maret 2012).

G312

Denoising Acoustic Emission Signal Using Wavelet Transforms for Determining the Source Location Micro Crack on Concrete

I Gede Pasek Suta Wijaya
Informatics Engineering and Electrical Engineering Dept.
Engineering Faculty, Mataram University
Jl. Majapahit 62 Mataram
Mataram Lombok, Indonesia
gpsutawijaya@te.ftunram.ac.id

Ni Nyoman Kencanawati
Civil Engineering Dept.
Engineering Faculty, Mataram University
Jl. Majapahit 62 Mataram
Mataram Lombok, Indonesia
nkencanawati@ts.ftunram.ac.id

Abstract*—Acoustic emission (AE) technique is developed to locate damages in concrete interior. However, the AE signal consists of much noise which makes the determination of first time amplitude of AE signal be difficult to be carried out. In fact, the determination of this parameter is a significant part for locating the source of damage in concrete. Therefore, one of the denoising methods called as wavelet based denoising is proposed. In this case, some wavelet bases functions are investigated to find out the proper wavelet bases function to perform the denoising of AE Signal. From the experimental data, the best wavelet bases function for this case is Coiflet, which provide better SNR than others wavelet families. In addition, the result of the denoising has been implemented for determining cracks location, which can be performed easier than that of without denoising methods.

***Keywords*— damage concrete, acoustic emission signal, denoising, wavelet, and SNR**

.

G401

Particle Swarm Optimization for Wireless Sensor Network Deployment Design by Taking Account of Barrier Position and Attenuation

Masjudin, I Wayan Mustika, and Widyawan
Department of Electrical Engineering and Information Technology
Universitas Gadjah Mada
Jalan Grafika No.2, Yogyakarta, 55281 Indonesia
Email: mas_judin@yahoo.com, {wmustika, widyawan}@ugm.ac.id

***Abstract*—Connectivity in the deployment of sensor nodes is an important part of the Wireless Sensor Network (WSN). The existence of barrier such as wall introduces damping or attenuation to power transmit of WSN, in which can degrades the communication range among nodes. This research studies the deployment system of WSN in indoor environment with barrier based on Particle Swarm Optimization (PSO) algorithm. PSO optimizes the position of WSN by providing global best position solution at each iteration. Different number and position of barrier are used to show the effect of the presence of a barrier on the deployment results. The simulations show that the deployment of sensor networks using PSO algorithm in indoor environment with barrier generates network solutions in which their connections are maintained on transmit power variation, number of barrier and their position.**

Keywords—connectivity, deployment, WSN, PSO, barrier

I. INTRODUCTION

Wireless Sensor Network (WSN) is a computer network that consists of several intercommunicating computers are equipped with one or several sensors [1]. WSN technology has many advantages in its implementation such as small size, low power consumption and use wireless communications so that suitable for any condition of environment. Deployment of nodes is a fundamental problem that must be solved in a WSN. Proper placement of nodes can reduce the complexity of routing problem in WSN such as data fusion, communication between nodes and the other [2]. In addition, the proper placement of sensor nodes can extend the life-time of WSN and thus, maintain a good connectivity among nodes.

Barrier such as wall, building, block house, or unpredicted barrier often exists in sensing area. It significantly affects the connectivity and coverage area of sensor node and therefore it may affect the deployment solution of sensor nodes. The existance of barrier reduces the communication range between sensor nodes. Deploying WSN without considering the barrier is very likely to result holes in coverage area and needs to spend longer time on deploying sensor node. The existance of barrier reduces the communication range between sensor nodes.

Research on the effects of radio wave propagation of mobile radio communications in indoor indicate that the largest attenuation occurs in the rooms are dominated by the concrete wall. This suggests a strong correlation between attenuation and propagation constant of a room [3].

Generally, researchers use the optimization algorithm to solve the WSN deployment problems in indoor environment with or without barrier. Several researcher have tried to offer new algorithms such as robot deployment algorithm to overcome unpredicted obstacles and to optimize the distribution area for the minimal sensor nodes [4]. Additionally, the Obstacle-Resistant Robot Deployment (ORRD) algorithm involves the placement of node design policy, serpentine movement policy, the obstacles handling, and boundary width. The algorithm can quickly deploy minimal number of sensor nodes covering the sensing area and handle regular or irregular obstacles [5].

Other researchers used Particle Swarm Optimization algorithm to control the mobility of nanosensor in WSN with the objective to increase the life-time and improve the network performance of the nanosensor. Simulation results show that the proposed optimization algorithm improves the network coverage by better utilization of neighbour nodes. The results also demonstrate that the algorithm increases nanosensor life-time [6]. The PSO algorithm has been applied in the deployment of sensor nodes to reduce the complexity and improve the quality of service (QoS) of WSN applications. Simulation results show that the proposed algorithm generates superior results in comparison with the traditional deployment on coverage area [7].

Particle Swarm Optimization (PSO) algorithm also has been implemented in developing sensor nodes in free space

area (Line Of Sight). Simulation Results show that the sensor nodes can form a network with well maintained connectivity [8].

Since most papers are not consider the influence of the position and type of barrier in the area of distribution, this paper studies the wireless sensor networks deployment using Particle Swarm Optimization algorithm (PSO) by taking account of barrier position and attenuation. PSO algorithm was used as optimization method because it has several few operational function and parameters thus makes the PSO algorithm faster in execution [9].

II. RADIO WAVES PROPAGATION MODELS

Wireless communication system has been known for two condition: LOS (Line of Sight) and NLOS (Non Line of Sight). In LOS condition, obstacles does not exist between the sender and receiver. If this criterion does not met, then the received signal strength will decrease drastically. NLOS condition, the signals that has arrived at the receiver experiences attenuation, reflection, scattering and refraction. We assumed that the barrier has a certain attenuation value and there are no reflections, signal shadowing or interference wave, then the propagation loss in indoor environment with barrier (L) in decibel can be calculated by Eq. (1) [10].

$$L = 32{,}44 + 20 \log f + 20 \log d + (\sum Br) \qquad (1)$$

with

L : propagation loss
f : frequency in MHz
d : distance between transmitter and receiver (in Km)
Br : attenuation value of barrier.

Where d (in Eq. 1) is the distance between transmitter and receiver in the network, we get from the Euclidean distance formula and can be expressed in Eq. (2).

$$d = \sqrt{(x_i - x_j)^2 + (y_i - y_j)^2} \qquad (2)$$

x_i,y_i and x_j,y_j is represented the position coordinat of sensor node at the deployment area.

The received signal strength at the receiver can be formulated as as shown in Eq. (3).

$$Pr = Pt + Gt + Gr - ((32{,}44 + 20\log f + 20\log d) + \sum Br) \qquad (3)$$

where

P_t : power transmit
G_t : gain antenna of transmitter

III. G_R : GAIN ANTENNA OF RECEIVERPARTICLE SWARM OPTIMIZATION ALGORITHM

The PSO algorithm was first introduced by Kennedy and Eberhart in 1995 [11]. PSO is apopulation based optimization algorithm inspired by social behavior of animals such as fish movements (school of fish), herbivore animals (herd), and birds (flock). Each object of animals is simplified into a particle. Three basic concepts of PSO is evaluating, comparing and imitating.

PSO begins with a set of particles (solutions) are generated randomly. Then the quality of each particle is evaluated using the fitness function. Furthermore, the particles will fly in the space by following the optimum particle. At each generation (iteration), the position of each particle is updated based on the two best fitness values. The first is the best achievement by a single particle which is known as *personal best* (p_{best}) and the second is the best achievement by all particles which is called *global best* (g_{best}). After discovering the best values, each particle i at position Xi update its velocity vector and position based on the following Eq. (4).

$$v_i^{k+1} = v_i^k + c_1 r_1^k \left(p_{best_i}{}^k - x_i^k\right) + c_2 r_2^k \left(g_{best_i}{}^k - x_i^k\right)$$
$$x_i^{k+1} = x_i^k + v_i^{k+1} \qquad (4)$$

Fig. 1. Shows the flow chart of optimization with PSO algorithm:

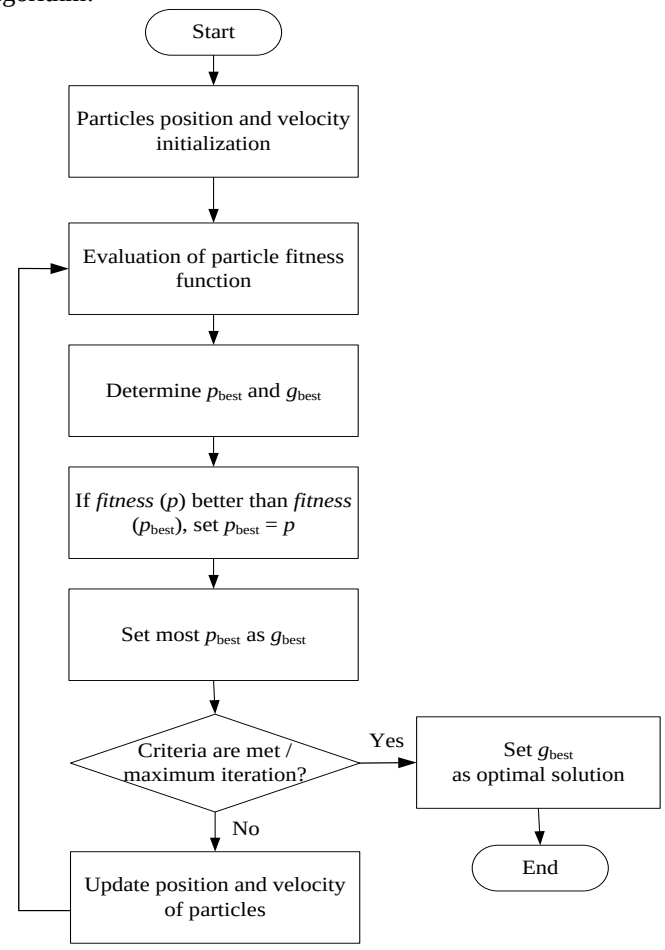

Fig. 1. Flowchart of optimization with PSO.

In this study, PSO parameters are:

A. Swarm

Swarm is a collection of particles that make up the population. The recommended range of swarm size is 20-60. The small size of swarm can lead to trapped at local optimum even if the process is very fast. In contrast, the large sizes of

swarm rarely get stuck in local optimum, but the process is much longer. In this study we used 30 with consideration of time efficiency and the achievement of solutions to approach the global optimum.

B. Particle

Particle (denoted by *Xi*) is asolution which is randomly generated and optimized to produce a good solution. This study concern to the optimization of the sensor nodes position when they are deployed in the area by taking account of barrier position and attenuation. The particles that are implemented represent the position of the sensor nodes in two dimension (2D) space with square deployment area. The distribution area is a square with maximum room size of 500 x 500 m^2. Representation of the particle can be seen in Fig. 2.

$X_{1,1}$	$X_{1,2}$	$X_{1,3}$	. . .	$X_{1,j}$
$X_{2,1}$	$X_{2,2}$	$X_{2,3}$	. . .	$X_{2,j}$
. . .	. . .	. . .	. . .	. . .
$X_{i,1}$	$X_{i,2}$	$X_{i,3}$	. . .	$X_{i,j}$

Fig.2 Particle representation

$X_{i,j}$: position of particle *i* and node *j* in 2D space
i : the size of swarm
j : the number of sensor node

The $X_{i,j}$ are retricted to the lower limit (Xa = 0.0 and the upper limit of (Xb = size of deployment area).

C. Fitness Function

The fitness function of this study is determined based on the power received and the number of connections with the following provisions:

1) Required power receive for a successful connection is -110 dB. If the power received is less than -110 dB, the node is not connected. Retrictions minimum power received by a node greater than -110 dBm because the radio frequency range of the TR 52B can reach 700 m (1.2 kb/s) and 500 m (19.2 kb/s), but actually the distribution area specified in the test is not more wide than TR 52B specification.
2) The deployment is designed to connect all sensor nodes in the network in full mesh form (each node connected to all nodes with direct connection). However, partial mesh form (each node connected to all nodes but does not direct connection, connection can by pass through the other node) are also allowed. Because of those influences, the number of connections have also been calculated in the fitness function.

Based on these scenarios, the proposed fitness function is defined by Eq. (5)

$$F(Xi) = \sum_0^{j-1} Pr_k(Xij) - \sum 2^{n_{ij}-1}.C \qquad (5)$$

where

$F(X_i)$ = fitness function of particle *i*.
$Pr_k(Xij)$ = the best power received by particle *i* sensor node *j*.
n_{ij} = number of detected nodes in particle *i* sensor node *j* (the number of connections).
C = constant value (30).

$Pr_b(X_{ij}) = \min [Pr(X_{ij})] \geq (-110 \text{ dB})$
$Pr_b(X_{ij})$ is the best signal received by a sensor node *i* particle *j*. The goal of determine $2^{n_{ij}-1}$ and choosen value of C = 30 are to make balance value between sum of power receive and sum of the number connection, so no one value is dominant to the other.

D. Learning Rate

Learning rate used in this study is $c_1 = 1.3$ and $c_2 = 2.8$ with consideration for balancing between cognitive part and social part in PSO.

E. Constriction Factor

Another parameter that is known in PSO algorithm is the constriction factor. This parameter was introduced by Clerc with the aim to ensure the faster convergence in PSO algorithm [12]. Value of constriction factor (K) is given by Eq. (6).

$$K = \frac{2}{|2-\varphi-\sqrt{\varphi^2-4\varphi}|},\ \varphi = \varphi_1 + \varphi_2,\ \varphi > 4. \qquad (6)$$

with $\varphi_1 = c_1 = 1.3$ and $\varphi_2 = c_2 = 2.8$

The equation to update the velocity and the new position of particle by entering the constriction factor value is defined by Eq. (7).

$$v_i^{k+1} = K.v_i^k + c_1 r_1^k \left(p_{best_i}{}^k - x_i^k\right) + c_2 r_2^k (g_{best_i}{}^k - x_i^k)$$
$$x_i^{k+1} = x_i^k + v_i^{k+1} \qquad (7)$$

with provisions :

$$v_i^{k+1} = 0, \text{ if } x_i^k < X_{\min} \text{ or } x_i^k > X_{\max}$$
$$x_i^{k+1} = \begin{cases} x_i^k + v_i^{k+1} \text{if } X_{\min} < x_i^k + v_i^{k+1} < X_{\max} \\ X_{\max} \text{ if } x_i^k + v_i^{k+1} > X_{\max} \\ X_{\min} \text{ if } x_i^k + v_i^{k+1} < X_{\min} \end{cases}$$

X_{min}= lower limit

X_{max} = upper limit

v_i^{k+1} = velocity of particle *i* at iteration *k* + 1

x_i^{k+1} = position of particle *i* at iteration *k* + 1

IV. DISCUSSION AND RESULT

The proposed scheme is simulated using two simulation models: single barrier simulation model and two barriers simulation models.

A. *Testing Scenario*

The testing process of this study following restriction:

1) Using various level of power transmit of IQRF TR 52B (according to the datasheet) that is -25 dB, -28 dB, -31 dB, -34 dB. The number of sensor nodes is 10. The frequency is 868 MHz and the maximum iteration is 50.
2) The distribution area is divided by a barrier into 1, 2 and 3 space with barrier location can be changes.
3) The barrier that is assumed is a brick wall with 6 dB attenuation values, the glass with 2 dB and wood with 2.85 dB [13].

B. *Testing Result*

In this study, experimets are conducted by combining the value of c_1 and c_2 according to the range suggested in Zhang's study [14]. Considering the number of possible combinations, the value of c_2 is fixed to 1.3 and value of c_1 can be changed. The combination values of c_1 is 2.75, 2.8, 2.9, 3.0 and the latest by exchanging the value of c_1 and c_2 by c_1 = 1.3 and c_2 = 2.8. The experiments were performed with the same initial position and power transmit (-25 dB) in a room without barrier. The result is shown as in Fig. 3.

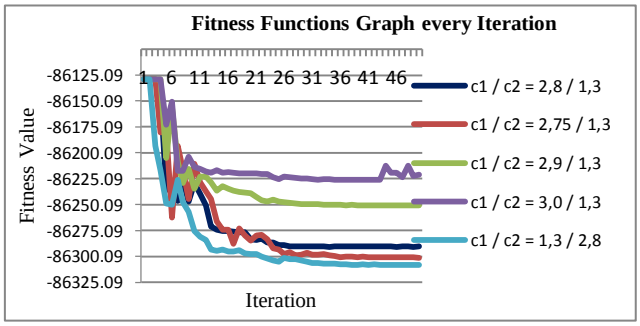

Fig. 3. Comparison the rate of convergence with different values of learning rate in the room without barrier.

As shown in Fig. 3, the combination of the value of c_1 = 2.8 and c_2 = 1.3 produces faster convergence rate. Thus, the value for the learning rate in this study is set to c_1 = 2.8 and c_2 = 1.3 for all simulation models.

1) *Single Barrier Simulation Model*

Deployment of sensor nodes is tested in the area with a single barrier, in which the barrier location coordinates is on the x axis and shifted by a certain values. Fig. 4 shows the results of the deployment in the room by different type and locations of barrier at power transmit -25 dB.

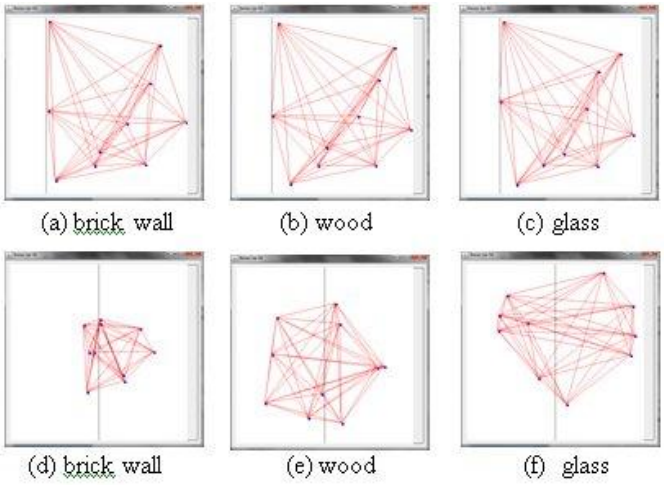

Fig. 4. Results of the deployment in the room with single barrier by different type and locations of barrier at transmit power of -25 dB.

As shown in Fig. 4, it can be inferred that the type and positions of barrier affect the deployment solution. For the simulation with the barrier position at x = 100 (Fig. 4 (a) to (c)), the room with brick wall has the average of communication range at 269.0681 meters, wood barrier at 269.0831 meters and glass barrier at 268.2368 meters. The simulation models with barrier position at x = 250 ((Fig. 4 (d) to (f)), the average of communication range is shorter than the barrier position at coordinates x = 100. The average of communication range in the room with brick wall at 142.5302 meters, wood barrier at 223.6971 meters and glass barrier at 254.9477 meters. Based on Table I, we can saw that on transmit power -25 dB, barrier position at middle (x = 250) has better communication range average than barrier position at the edge (x = 400) (wood and glass barrier). It caused the large transmit power and small attenuation make the nodes have long distance but still connected each other. Table II show that decrease of transmit power (-28 dB), just glass barrier by middle position (x = 250) has better communication range average than edge position (x = 400). For the transmit power -31 dB and -34 dB (show in Table III and IV), all the barrier types in the middle position has a shorter average of communication range than barrier position on the edge (x = 100 and x = 400).

Table I shows the network form and average of communication range with different types and location of barrier and transmit power is -25 dB, while Table II shows the network form and average of communication range with different types and location of barrier as Table I but using -28 dB transmit power.

Table I. Network form and average of communication range of single barrier simulation model on -25 dB transmit power.

Type of barrier	Barrier position	Form of network	Average of communication range (m)	Standar deviation (m)
Without barrier	x = 0	Full mesh	331,9966	136,2241
Brick wall	x = 100	Full mesh	269.0681	116,2596
	x = 250	Full mesh	142.5302	59.6028
	x = 400	Full mesh	278.8911	117.3982

Wood	x = 100	Full mesh	269.0831	115.3094
	x = 250	Full mesh	223.6971	85.0946
	x = 400	Full mesh	219.4241	94.6968
Glass	x = 100	Full mesh	268.2368	114.1623
	x = 250	Full mesh	254.9477	111.1347
	x = 400	Full mesh	227.4202	114.1347

Table II. Network form and average of communication range of single barrier simulation model on -28 dB transmit power.

Type of barrier	Barrier position	Form of network	Average of communication range (m)	Standar deviation (m)
Without barrier	x = 0	Full mesh	220.4852	85.5224
Brick wall	x = 100	Full mesh	218.2637	87.8383
	x = 250	Full mesh	97.1036	48.5407
	x = 400	Full mesh	202.6215	92.3733
Wood	x = 100	Full mesh	218.2637	87.8384
	x = 250	Full mesh	165.5994	80.3555
	x = 400	Full mesh	204.7691	84.1624
Glass	x = 100	Full mesh	218.2637	87.6364
	x = 250	Full mesh	201.1755	78.0586
	x = 400	Full mesh	192.5653	78.6488

TABLE III. NETWORK FORM AND AVERAGE OF COMMUNICATION RANGE OF SINGLE BARRIER SIMULATION MODEL ON -31 DB TRANSMIT POWER.

Type of barrier	Barrier position	Form of network	Average of communication range (m)	Standar deviation (m)
Without barrier	x = 0	Full mesh	142.5265	60.4873
Brick wall	x = 100	Full mesh	146.8617	57.5128
	x = 250	Full mesh	127.5731	58.9135
	x = 400	Full mesh	148.1423	62.5463
Wood	x = 100	Full mesh	143.8315	60.2588
	x = 250	Full mesh	129.4584	49.6890
	x = 400	Full mesh	148.1423	62.5464
Glass	x = 100	Full mesh	143.8315	60.2588
	x = 250	Full mesh	120.5877	48.1129
	x = 400	Full mesh	148.1423	62.5463

TABLE IV. NETWORK FORM AND AVERAGE OF COMMUNICATION RANGE OF SINGLE BARRIER SIMULATION MODEL ON -34 DB TRANSMIT POWER.

Type of barrier	Barrier position	Form of network	Average of communication range (m)	Standar deviation (m)
Without barrier	x = 0	Full mesh	111.0409	46.9630
Brick wall	x = 100	Full mesh	106.8776	41.4769
	x = 250	Full mesh	72.3909	33.7546
	x = 400	Full mesh	110.9631	46.9000
Wood	x = 100	Full mesh	106.8776	41.4769
	x = 250	Full mesh	91.2346	40.3804
	x = 400	Full mesh	111.0409	46.9630
Glass	x = 100	Full mesh	106.8776	41.4769
	x = 250	Full mesh	92.3332	38.8686
	x = 400	Full mesh	111.0409	46.9630

Based on the results as shown in Table I to IV, we can conclude that the position and type of barriers affect the distribution results. All of the simulation models with different types of barrier, generally, barrier positions on the edge (barrier position coordinates are x = 100 or x = 400) have a longer average of communication range compare with the simulation models by the barrier in the middle position (coordinates x = 250). It is because the large power with small attenuation make the nodes have long distance but still connected each other, the position of the barrier in the middle may affect the nodes position are balanced, and the position of the nodes are spread evenly. In the general, a brick wall barrier in the middle (coordinate x = 250) produces a shortest average of communication range than the other types like wood and glass barrier because the brick wall has the greatest attenuation (6 dB). Wall of glass has average a longer communication range for most small attenuation (2 dB) compared to the brick wall (6 dB) and wall of wood (2.85 dB).

2) Two Barrier Simulation Models

In this simulation models, space is divided in three sections by two barrier. The barrier placed sequentially at x_1 = 100 and x_2 = 400, x_1 = 225 and x_2 = 275, and the last is the coordinates at x_1 = 167 and x_2 = 333.

Fig. 5 shows the results of the deployment space of two barriers with the same location that is x_1 = 225 and x_2 = 275, but with different transmit power.

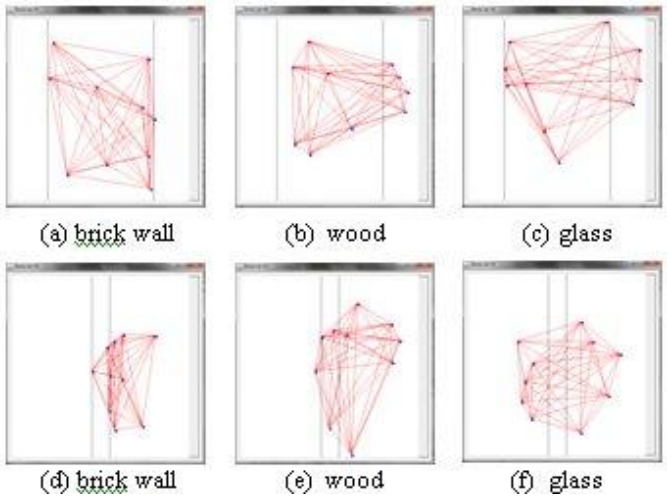

Fig. 5. Results of the deployment in the room with two barrier by different type and locations of barrier at transmit power -25 dB.

As shown in Fig. 5, it can be inferred that the number, type and position of barrier affect the deployment solution. For the simulation with the barrier position at x_1 = 100 and x_2 = 400 (Fig. 5 (a) to (c)), the room with brick wall has the average of communication range at 243.4523 meters, wood barrier at 221.7073 meters and glass barrier at 257.8703 meters. The simulation models with the barrier position at x_1 = 225 and x_2 = 275 ((Fig. 5 (d) to (f)), the room with brick wall has the average of communication range at 143.9456 meters, wood barrier at 200.7037 meters and glass barrier at 198.0752 meters. From this results, it can be inferred that addition of barrier affect the deployment result. The average of communication range with two barrier is shorter than single barrier. Its caused addition of barrier give addition attenuation or damping, so the power receive at the receiver is weaker and communication range would be short. As same as single barrier, two barrier simulation model with barrier position at

the middle (x_1 = 225, x_2 = 275 and x_1 = 163, x_2 = 333) give simulation result with shorter range communication average than barrier position at the edge (x_1 = 100, x_2 = 400).

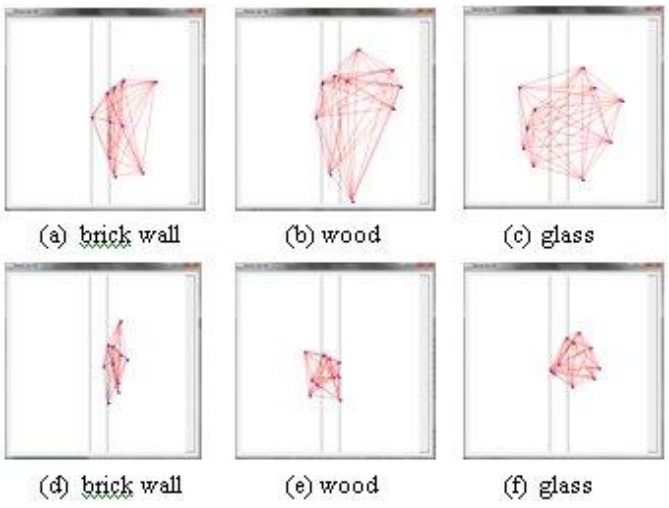

Fig. 6. The deployment result in the room with two barrier and the same position of barrier at transmit power of -25 dB and -34 dB.

Fig. 6 (a) to (c) uses the transmit power of -25 dB with barrier position at x_1 = 100 and x_2 = 400, while Fig. 6 (d) through (f) uses same types and position of barrier but different level of transmit power (*Pt* = -34 dB). As shown in Fig. 4, the deployment results in six form of networks with different qualities. Greatest transmit power (-25 dB) would result in longest average of communication range (Fig. 6 (a) to (c)). In contrast, smallest transmit power (-34 dB) will produces a smallest or average shortest communication range (Fig. 6 (d) to (f)). All deployment as shown in Fig. 6, the connections are maintained well, although two deployment results like Fig. 6 (d) and (e) form a partial mesh network, but it still connected because IQRF sensor nodes are multi hop. These results can satisfy the required conditions in the evaluation of the fitness function.

Table V. Network form and average of communication range of two barrier simulation model on -25 dB transmit power.

Type of barrier	Barrier position	Form of network	Average of communication range (m)	Standar deviation (m)
Without barrier	x = 0	Full mesh	331.9966.	136.1224
Brick wall	x_1 = 100 x_2 = 400	Full mesh	243.4523	102.1281
	x_1 = 225 x_2 = 275	Full mesh	143.9456	70.5699
	x_1 = 167 x_2 = 333	Full mesh	157.5310	68.5041
Wood	x_1 = 100 x_2 = 400	Full mesh	221.7037	95.5415
	x_1 = 225 x_2 = 275	Full mesh	200.9286	98.9501
	x_1 = 167 x_2 = 333	Full mesh	210.4026	82.9512
Glass	x_1 = 100 x_2 = 400	Full mesh	257.8703	102.1283
	x_1 = 225 x_2 = 275	Full mesh	198.0752	102.1271
	x_1 = 167 x_2 = 333	Full mesh	199.9742	102.1281

Table VI. Network form and average communication range of two barrier simulation model on -34 dB transmit power.

Type of barrier	Barrier position	Form of network	Average of communication range (m)	Standar deviation (m)
Without barrier	x = 0	Full mesh	111.0409	46.9630
Brick wall	x_1 = 100 x_2 = 400	Full mesh	106.8787	41.4809
	x_1 = 225 x_2 = 275	Partial mesh	76.4955	41.2702
	x_1 = 167 x_2 = 333	Full mesh	99.7524	39.4909
Wood	x_1 = 100 x_2 = 400	Full mesh	106.8787	41.4808
	x_1 = 225 x_2 = 275	Partial mesh	81.4545	34.1273
	x_1 = 167 x_2 = 333	Full mesh	98.2872	38.7986
Glass	x_1 = 100 x_2 = 400	Full mesh	106.8787	41.4809
	x_1 = 225 x_2 = 275	Full mesh	83.5506	34.7054
	x_1 = 167 x_2 = 333	Full mesh	97.9347	39.0145

Table V shows the network form and the average of communication range with different types and location of barrier and transmit power is -25 dB, while Table VI shows the network form and the average of communication range with different types and location ofbarrier as Table V but using -34 dB transmit power.

As shown in Table V and VI we can conclud that the distribution results not only affect by position and type of barriers but also by level of transmit power and the number of barrier. If we compare Table V with Table VI, we find that increasing the number of barrier and decreasing the level of transmit power produces different solution. Lower transmit power (-34 dB) with two barrier simulation model produces worse solution than the single barrier. On the position of the barrier in the middle, barriers from wall and wood produce a partial mesh network forms. All of the simulation models with different types of barrier, barrier positions on the edge (barrier position coordinates are x_1 = 100 and x_2 = 400) have a longer average of communication range than with the simulation models by the barrier in middle position (coordinates x_1 = 225 and x_2 = 275). From three simulation models, the position of the barrier x_1 = 225 and x_2 = 275 with brick wall barrier type generates the shortest range communication and barrier positions x_1 = 100 and x_2 = 400 and glass wall barrier type produces longest communication range.

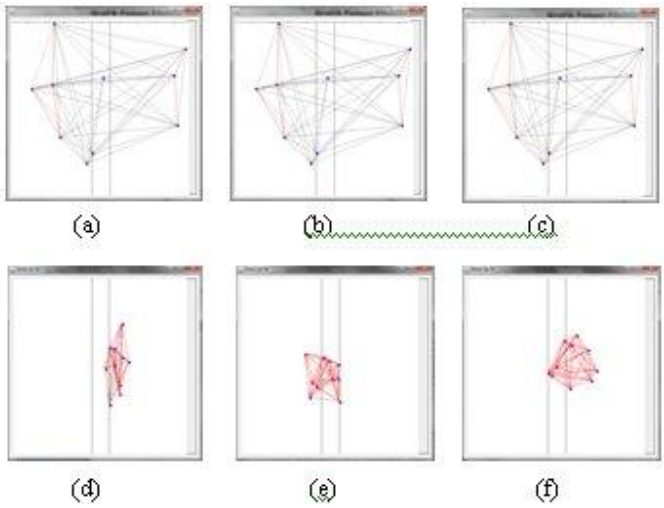

Fig. 7. Comparison deployment result with and without optimization using PSO algorithm: (a) brick wall, (b) wall of wood, (c) wall of glass ((a) to (c) without optimization), (d) brick wall, (e) wall of wood, (f) wall of glass ((d) to (f) with optimization).

Fig. 7 (a) to (c) shows the deployment result on power transmit of -34 dB in the room with different barriers without optimization. The result is worse for all simulation models (the room with brick wall, wall of wood and wall of glass barrier). All of solutions form partial network. However, in fact there is only few connection occured, which is shown with grey line to indicate that the received power of sensor node is less than -110 dB and therefore, it does not fullfil the connection. In WSN, partial network is not allowed.

Fig. 7 (d) to (f) shows the deployment result in the room with different barrier like Fig. 7 (a) to (c) but using optimization with PSO algorithm. All of deployment results successfully establish connection with the network. The room with brick and wood walls forms partial mesh, but it is still allowed in accordance to the limits of testing scenario.

Based on the comparison results of the deployment as shown in Fig. 7, the deployment with PSO algorithm successfully forms a network with good connectivity. The fitness function that is applied using PSO algorithm successfully makes the well maintained network connection. Optimization with PSO algorithm shows better performance when compared to that of the traditional random deployment. Traditional random deployment (without optimization) gives a poor solution with partial network form. After optimization with PSO algorithm is done, the solution can form a network with well maintained connections for all transmit power levels (-25 dB, -28 dB, -31 dB and -34 dB).

Based on all the deployment results can be concluded that the deployment results are affected by the distance between nodes, the position and type of barrier, and level of the transmit power. In this study, optimization of PSO algorithm using the proposed fitness function shows good performance and results compared to the traditional deployment without PSO algorithm.

V. CONCLUSSION

In this research, we have proposed wireless sensor networks deployment using Particle Swarm Optimization (PSO) algorithm by taking into account barrier position and attenuation. The room with a number of barriers and greater attenuation values (two barrier and brick wall) provides greater attenuation to the transmit power and result in shorter average of the communication range. Largest transmit power (-25 dB) produces a network with longest average communications range and better network connection than that using smallest transmit power (-34 dB). PSO algorithm also shows good performance to produces a solution where connections are maintained compared to that of the traditional deployment (without optimization).

REFERENCES

[1] D. E. Culler, H. Wei, "Wireless Sensor Networks*"*, Communications of the ACM, 2004, 47(6): 30-33.

[2] R. Bischoff, J. Meyer, G. Feltrin, *Wireless sensor network platforms.* In Encyclopedia of Structural Health Monitoring, Chichester, UK: John Wiley & Sons Ltd, 2009.

[3] Indrawati, Amir D, "Analisa korelasi konstanta propagasi terhadap redaman propagasi gelombang radio dalam ruang pada komunikasi bergerak", *Jurnal Litek*, 2009, Volume 6 No. 1, hal 11 – 14.

[4] Chang Chih-Yung, Sheu Jang-Ping, Chen Yu-Chieh, dan Chang Sheng-Wen, "An Obstacle-Free and Power-Efficient *Deployment* Algorithm for Wireless Sensor Network," IEEE Systems, Man and Cybernetics, Part A: Systems and Humans 39 Issue: 4: 795 – 806, 2009.

[5] C.Y. Chang, C.C. Tsun, C.Y. Chieh, C.H. Ruey, "Obstacle-resistant deployment algorithm for wireless sensor networks", *IEEE Vehicular Technology*, 2009, 58: 6: 2925-2941.

[6] M. Abbasi, M.S.A. Latiff, "Mobility control to improve nanosensor network life-time based on particle swarm optimization", *International Journal of Computer Applications* (0975 – 8887), 2011, Volume 30 No.4.

[7] M. Abbasi, M.S.A. Latiff, A. Modirkhazeni, M.H. Anisi, "Optimization of wireless sensor network coverage based on evolutionary algorithm", *IJCCN: International Journal of Computer Communications and Networks*, 2011, Volume 1.

[8] Z. Saharuna,Widyawan, S. Sumaryono, "Deployment jaringan sensor nirkabel berdasarkan algoritma particle swarm optimization", *Gadjah Mada University*. 2012.

[9] R.L. Haupt, S.E. Haupt, *Practical Genetic Algorithm, 2nd Ed*. Hoboken, New Jersey: John Wiley & Sons, Inc. 2004.

[10] M. Lott, I. Forkel, "A multi-wall-and-floor model for indoor radio propagation", *IEEE*, 2001, 0-7803-6728-6/0I.

[11] R.C. Eberhart, Y.H. Shi, "comparing inertia weight and constriction factors in particle swarm optimization*"*, *Congress on Evolutionary Computing*, 2000, Vol. 1, pp.84-88.

[12] M. Clerc, J. Kennedy, "The particle swarm explosion, stability, and convergence in a multidimensional complex space*"*. *IEEE Trans. Evolutionary Computation*, 2002, Vol. 6(1):58-73.

[13] P. Shamanna, "Simple link budget estimationand performance measurements of Microchip sub-GHz radio modules", *Microchip Technology Inc*. 2013.

[14] L.P. Zhang, H.J. Yu, S.X. Hu, "Optimal choice of parameters for particle swarm optimization*"*, *Journal of Zhejiang University, SCIENCE*, 2005, 6A(6):528-534.

G402

Circularly Polarized Stack-Patch Microstrip Array Antenna for Mobile Satellite Communications

Muhammad Fauzan Edy Purnomo
Electrical Department
Faculty of Engineering, University of Brawijaya
Malang, Indonesia
mfauzanep@ub.ac.id

***Abstract*— Nowadays, the knowledge of science and technology, especially in the field of mobile satellite communication is developing hugely and rapidly. It is included the development of the ground station antenna as transceiver signal to make a good conducted communication between the satellite and terminal station at the earth. Moreover, as geostationary satellites are remotely located (about 36,000 km) from the earth, the incoming wave is very weak. Consequently, it is required that the antenna for mobile satellite communications has a high gain in the case multimedia communications performing large-capacity data communication is aimed.**

In order to obtain a good performance antenna to clarify suitably result on frequency characteristic, return loss, and radiation pattern, and also to obtain a simple configuration such as small, light and low profile, a left-handed circularly polarized stack-patch microstrip array antenna is proposed [1]-[2].

The antenna configuration instead of receiver and transmitter which is combined becomes array antenna at frequency target 2.48 GHz and at 2.63 GHz, respectively. The antenna was calculated by the Method of Moments using probe-fed pentagonal array antenna as radiating patch and triangular array antenna as parasitic patch with dielectric relative permittivity 2.17 and loss tangent 0.0009.[3]-[6]

In this paper, it discuss about the performances of that antenna at *El*=48° with calculation results. The calculated results both receiver and transmitter antenna at *El*=48° are satisfied about 5 dBic gain, and the 3-dB axial ratio beamwidth. The whole azimuth range about more of 120° for each beam coverage in the conical-cut direction also satisfy for mobile satellite applications, especially for Japan areas.

Keywords—circularly polarized; stack-patch; receiver and transmitter; array antenna

I. INTRODUCTION

Nowadays, the knowledge of science and technology, especially in the field of mobile satellite communication is developing hugely and rapidly. It is included the development of the ground station antenna as transceiver signal to make a good conducted communication between the satellite and terminal station at the earth. However, high gain could not easily be achieved because of the isotropy in the conical-cut direction. In contrast, the beam generated by satellite-tracking systems [7] is always turned towards the satellite position even when the azimuth angle of the mobile station varies. Therefore, such antennas have the possibility to reach a higher gain compared to the conical beam antennas. Every antenna has good antenna characteristics. However the one of the most remarkable disadvantage is the cost, weight and volume. It is expected that the antenna for the next generation of mobile satellite communication is small, thin and high performance [8].

In terms of keeping the stable mobile communications, antenna system gain is required as higher as possible. Furthermore, in terms of mounting the general car roof, compact design with high performance is required. In this reason, gain enhancement of triangular patch antenna is necessary. For getting that purposed, in this paper, a simple stack-patch satellite-tracking left-handed circularly polarized six-element array antenna in using both of reception (2.48 GHz) and transmission (2.63 GHz), whose beams are electrically switched in three azimuth directions, is investigated. The switching is realized by use of a simple on/off feed control rather than by a phase shifter. The composition and performance of an antenna designed for mobile satellite applications are described. Numerical analyses both receiver and transmitter antenna are shown and discussing.

II. CONFIGURATION OF ARRAY ANTENNA

The antenna structure of six-element array antenna is depicted in Fig. 1 (ε_r = 2.17, loss tangent 0.0009). The array antenna instead of three pentagonal patch antennas as radiating for its reception and transmission which each element directly fed by three probe feed located on the beneath of the construction. In the top of the construction is laid three isosceles triangular patches as parasitic elements. The proper feeding location on the radiating patch is chosen for matching with 50 Ω input feed. For more strength of matched with 50 Ω, air-gap is inserted at the area between the fed elements and the parasitic elements. Moreover, the function of feeding is to trigger the dominant mode and higher mode, to make circular polarized and to reduce the coupling with element one half. While, the other air-gap function is to wide bandwidth and to increase the gain. Similar with the air-

gap function, for more stability of it, the parasitic element operated for not only that purposed, also for making smooth circular polarized and to adjust coupling with the element beside it. In matter of coupling, the distance between apex of both transmission and reception element to center point of array are set 9.7 mm and 19.7 mm, respectively. It is meant to reduce isolation with each closer patch and thus to get sufficient gain for obtaining the minimum requirement 5 dBic. Usually, for decreasing coupling to patch element closer each other, need the distance between central of patch element (in this case 1/3 *h*, where *h* is a height of patch antenna) to the other closer patch element (*d*) is based on the formula 0.5 λ < *d* <λ, where λ is wavelength of used. Furthermore, based on investigate in simulation (seen Fig.1) that both of coupling and current distribution are increased parallel with counter-clockwise moved, for example coupling patch *R1T1* (*S-21*) > coupling patch *R1T3* (*S-23*) (seen Fig.2). In the otherwise manner coupling and current distribution become decreased. The construction of this antenna makes possible to excite the two near-degenerate orthogonal modes of equal amplitudes and 90°dimension phase difference for left-handed circular polarized (LHCP) operation. The dimension of the construction is 160 mm and 6.4 mm in diameter and height, respectively.

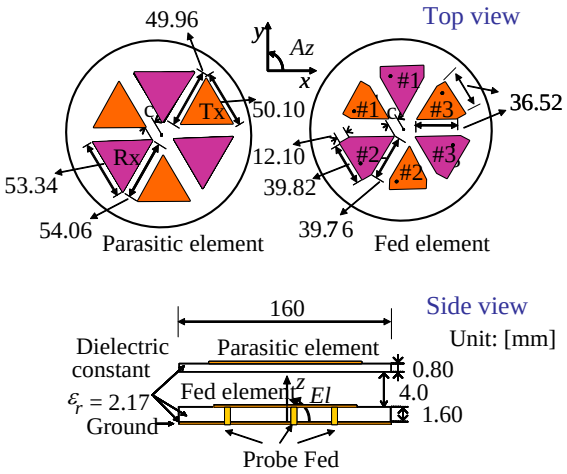

Fig. 1. The construction of 6-elements array antenna

III. RESULT

Fig.2 shows that the bandwidth of reception, Rx (*S-11*) and transmission, Tx (*S-22*) of simulation results below -10 dB are 7.79% and 6.21%, respectively. At the frequency target in Rx=2.48 GHz, and Tx=2.63 GHz the value of *S*-parameter of simulation results are about -11.48 dB and -23.45 dB, respectively. The isolation between elements located closed with each other is less the target isolation 20 dB, i.e. about 12 dB until 20 dB.

Fig.3 illustrated the simulation results of frequency characteristic both Rx and Tx at the frequency targets 2.48 GHz and 2.63 GHz are 6.9 dBic (gain), 0.009 dB (axial ratio) and 5.69 dBic (gain), 0.18 dB (axial ratio), respectively. Moreover, the 3 dB axial ratio bandwidth gets both of Rx and Tx in simulation results about 1.99% and 1.69%, respectively.

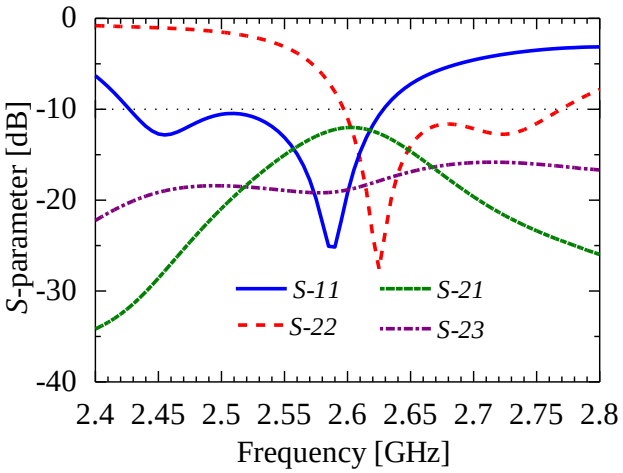

Fig. 2. *S*-Parameter

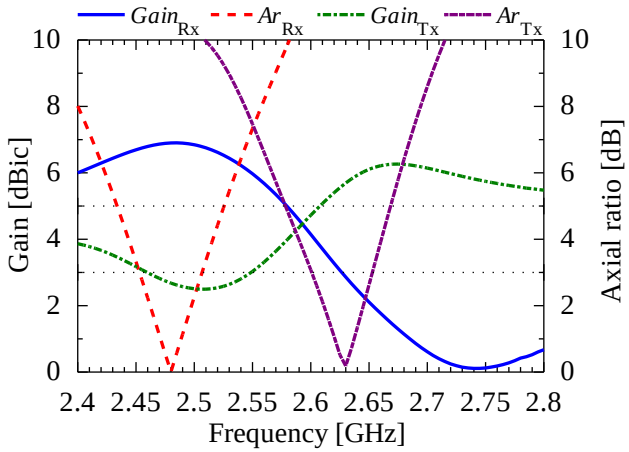

Fig. 3. Frequency Characteristic

The axial ratio satisfies the target less than 3 dB and the gain more than 5 dBic at elevation angle *El* = 38° - 58° both of Rx and Tx in simulation results as shown in Fig.4. This condition achieved by one of three ports is switched OFF, and the others bias ON. These mechanism make a beam could be directed suit with the target desired.

The beam of the antenna is generated by a simple ON OFF mechanism that consists in one out of three radiating elements is turned off. For that reason, there are three OFF states beam switching mechanism i.e. #1 OFF, #2 OFF, and #3 OFF. By considering the mutual coupling between fed elements, their phases and distances, the beam direction can be varied. Furthermore, the two fed elements theoretically will generate a beam shifted of -90° in the conical-cut direction from the element which is switched OFF. For example, when element Rx #1 which located at azimuth, *Az*=90° switched OFF, the beam is directed towards the azimuth angle *Az*=0° (seen Fig.1).[5]

The simulation results of gain and axial ratio characteristics of the beam switching in the azimuth plane are shown in Fig.5. The simulated results of Rx show the axial ratio increases for each OFF condition, but the 3-dB axial ratio

coverage of the simulated result both Rx and Tx can cover 360° in the conical-cut plane at *El* = 48°. Moreover, the beam is possibly switched at minimum gain about 6.5 dBic for Rx and about 5.8 dBic for Tx. This elevation is applied at Kanto (Japan) area.

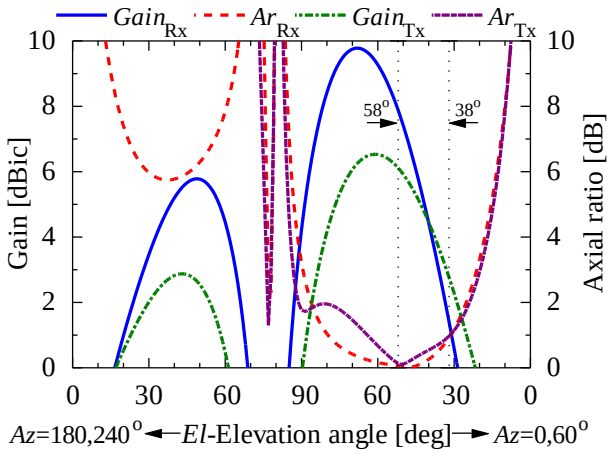

Fig. 4. Elevation cut plane, patch 1off, azimuth Tx=0^0, Rx=60^0

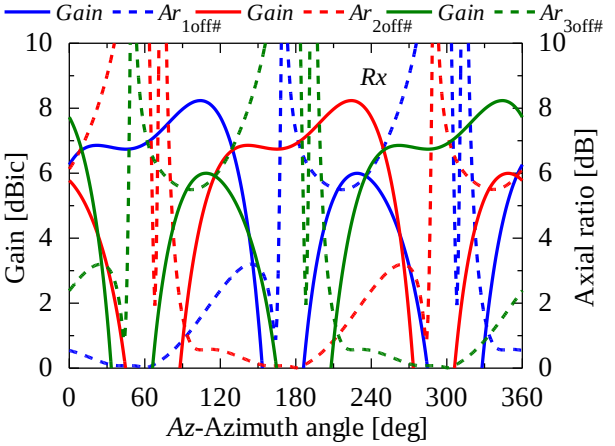

(a) Reception (Rx)

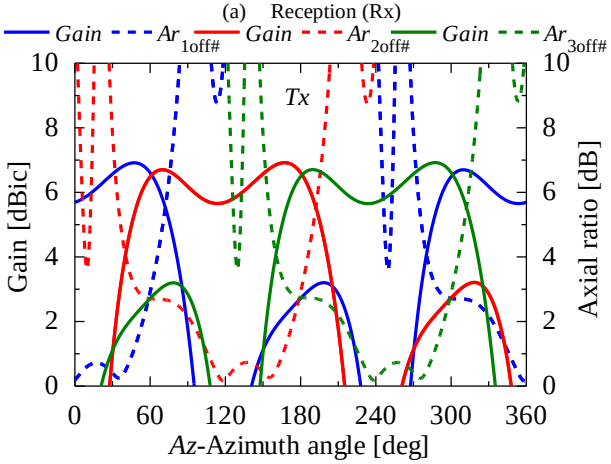

(b) Transmission (Tx)

Fig. 5. Conical cut plane, elevation 48^0

IV. Conclusion

The construction of dual band six-elements array antenna for mobile satellite communications is presented in simulation results. The simulation results for elevation angle *El* = 48°, express that radiation pattern characteristics are satisfied in the azimuth direction both of at the target frequency 2.48 GHz for reception, and at frequency target 2.63 GHz for transmission. Furthermore, the beam switching characteristics both of Rx and Tx show that gain and axial ratio are more than 5 dBic and less than 3 dB, respectively. In addition, both of reception and transmission that the gain above 5 dBic and the axial ratio below 3 dB can be obtained at elevation angles 48° as latitude of Kanto (Japan) area.

References

[1] T.Tanaka, T.Houzen, M.Takahashi, and K. Ito, "Circularly Polarized Printed Antenna Combining Slots and Patch", IEICE Trans.Commun., VOL.E89—B, 2006.

[2] Delaune D., J. T. Sri Sumantyo, M. Takahashi and K. Ito,"Circularly Polarized Rounded-Off Triangular Microstrip Line Array Antenna", IEICE Trans. Commun., vol. E89-B, no. 4, April 2006.

[3] J. T. Sri Sumantyo, K. Ito, and M. Takahashi, "Dual band circularly polarized equilateral triangular patch array antenna for mobile satellite communications", IEEE Trans. Ant. Prop., vol. 53, pp. 3477-3485, Nov. 2005.

[4] Basari, Muhammad Fauzan Edy Purnomo, Kazuyuki Saito, Masaharu Takahashi, and Koichi Ito, "Antenna System for ETS-VIII Land Vehicle Communications", Proceedings of IJJSS2008, Chiba, Japan.

[5] Muhammad Fauzan Edy Purnomo, Basari, Kazuyuki Saito, Masaharu Takahashi, and Koichi Ito, "Developing Antenna for ETS-VIII Applications", Proceedings of IJJSS2008, Chiba, Japan.

[6] Sri Sumantyo, J.T., Ito, K., Delaune, D., Tanaka, T., Onishi, T., and Yoshimura, H.,"Numerical analysis of ground plane size effects on patch array antenna characteristics for mobile satellite communications", Int. J. Numer. Model. Electron. Netw. Devices Fields, 2005, 18, (2), pp. 95-106

[7] Yamamoto, S. , Tanaka, K. , Wakana, H. , and Ohmori, S.,"An antenna tracking system for land mobile satellite communications systems", IEICE Tech. Rep., 1990, 90, (51), (in Japanese)

[8] Delaune D., T. Tanaka, T. Onishi, J. T. Sri Sumantyo, and K. Ito, "A simple satellite-tracking stacked patch array antenna for mobile communications experiments aiming at ETS-VIII applications", IEE Proc. Microwave Antennas Prop., vol. 151, no. 2, pp. 173 - 179, Apr. 2004.

G403
Angle of Arrival Using Cross Yagi-Uda Antennas

SatriaGunawanZain
Electrical Engineering, Makassar State University
Yogyakarta, Indonesia
Wawan38@yahoo.com

Adhi Susanto , Thomas Sriwidodo
Electrical Engineering, GadjahMada University
Yogyakarta, Indonesia

WahyuWidada
National Institute of Aeronotics and Space
Bogor, Indonesia

***Abstract*—this paper discusses Angle of Arrival method using cross Yagi-Uda antennas. The method is based on ratio of signal strength from receives of nine cross Yagi-Uda Antennas. Just little research explores the potentials of radiation patent of Yagi-Uda antennas to estimate Angle of arrival. The proposed method is using radiation patent of nine Yagi-Uda antennas that is placing on different direction. The Antennas that have same direction as the signal emitter reach highest signal strength. Based on ratio between highest signal strength of ones antennas received and its neighborhood signal strength, the azimuth and elevation angle of arrival can be calculated. The performance of our method is investigated by simulation of AOA method using cross Yagi-Uda Antennas.**

***Keywords*—angle of arrival, azimuth and elevatioan angle, cross Yagi-Udaantenas, ratio signal strength**

I. INTRODUCTION

Determining azimuth and elevation angle of arrival from source of the radio emission isgreat importance for retrieving the position of objects. Various methods have been produced such as Received Signal Strength (RSS) [1] - [4], Time Difference of Arrival (TDOA) [5] - [6], Difference Phase of Arrival (DPOA)[7], Difference of Arrival (DOA)[8] and Angle of Arrival (AOA)[9]. AOA methods have not been fully studied to estimate the azimuth and elevation angles simultaneously.

AOA methods have been developed such as in the use of Omni directional antenna array which is arranged in a circular to the ESPRIT method for estimating the direction of emission sources [8]. The uses of beam lobe (radiation pattern) directional antennas have not been much explored. It can be found in the use of beam lobe for AOA study [10]. This method can be used to fly at low speed vehicle but will find it hard to follow the movement of a vehicle flying at high speed like a rocket.

The use of the radiation pattern of Yagi antenna has also been studied by Sayrafian-pour and Kaspar [6]. In his research revolves Yagi antennas are used at the receiver and transmitter. Transmitting antenna rotated 360 degrees to each movement of the receiving antenna Θ degrees. The method is applied to determine the position of the emission sources in a building. The method is claimed to have better results than the use of MUSIC and ESPRIT algorithms [9]. Potential use Yagi antenna for AOA methods have the opportunity to study further. Exploration of the use polaradiasi Cross Yagi-Uda antenna in azimuth and elevation angle estimation simultaneously has never been done. This paper will discuss the use Yagi-Uda antenna Cross to estimate the azimuth and elevation angles simultaneously.

II. METHODOLOGI

A. Received Signal Model

Powerful radio signal that is captured by the receiver of a radio transmitter at a certain point is modeled by Bahl and Padmanabhan [1] with equation (1).

$$P(d)[dbm] = P(do)[dbm] - 10nlog\left(\frac{d}{do}\right) - \begin{cases} nW * WAF & nW < C \\ C * WAF & nW \geq C \end{cases} \quad (1)$$

Where n is the path loss by an increase in the distance P (do) is the signal power at the reference distance and d is the distance between the transmitters to the receiver. C is the maximum number of reflections that can infer the magnitude of the received signal strong, nW is the number of reflections between the transmitter and the receiver, and the WAF is the attenuation factor of the barrier.

B. Model of Cross Yagi Uda

Yagi-Uda antennas are cross Yagi antennasthat have a cross-shaped element. Fig. 1 shows the physical appearance of crossYagi antenna and Fig. 1b shows the radiation pattern.

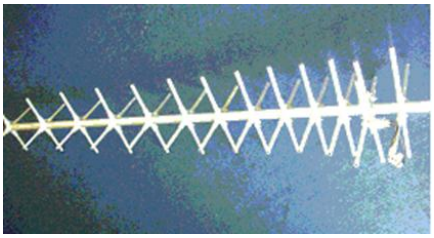

(a) Physical appearance of Cross Yagi-Uda

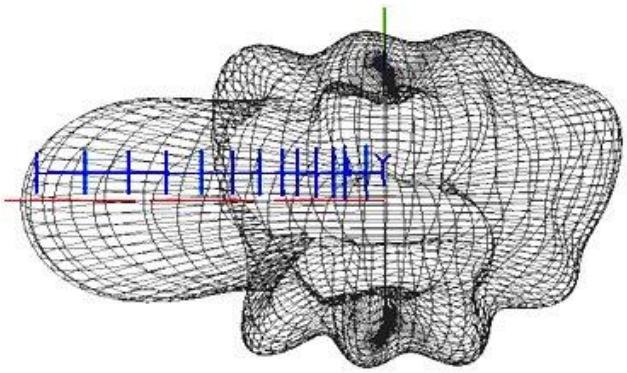

(b) Radiation pattern of CrosYagi Antenna

Figure 1.Cross YagiUda antenna and radiation pattern

The composition of cross Yagi antennas is created using a 3x3 configuration. Each antenna has different direction angles. Figure 2 shows the configuration of Cross Yagi-Uda antennas used.

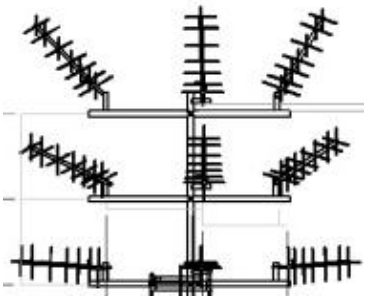

Figure 2. Configuration of nine Yagi-Uda antennas

Fig. 2 shows nine CrossYagi-Uda antennas with different direction angles. Antenna 1th amplifies the signal received (rx) with the gain G(α-sa, β) because the antenna is directed at a different angle then the amplified signal is received in accordance with the received antenna gain angle. Nine antennasassumed have the same radiation pattern, so that the radio signals that come in will be strengthened by each antenna. If the antennas are arranged horizontally directed to different direction angles of Sa^o and vertical antennas are arranged with different directions of Sb^o, then signal strength will be received and the equation can be written as follows:

$$rx = St + nW \quad (2)$$

$$P_k(\alpha, \beta) = rx + A_k \qquad k = 1,2,\ldots\ldots 9 \quad (3)$$

Pk in dbm is a signal strength measured at the k-th antenna. Ak is the k-th antenna gain to the value specified in equation 4.

$$A_k = \begin{bmatrix} G(\alpha - sa, \beta) \\ G(\alpha, \beta) \\ G(\alpha + sa, \beta) \\ G(\alpha - sa, \beta + sb) \\ G(\alpha, \beta + Sb) \\ G(\alpha + sa, \beta + sb) \\ G(\alpha - sa, \beta + 2sb) \\ G(\alpha, \beta + 2sb \\ G(\alpha + sa, \beta + 2sb) \end{bmatrix}$$

C.RSS 9 Antennas

Using radiation pattern of Figure 2 and equation 1, nine signal strength antennas can be calculated using interpolation equation 4 with the following equation:

$$P_k(\alpha, \beta) = \sum_{i=0}^{n} \sum_{j=0}^{m} L_{ij}(\alpha, \beta) P_k(\alpha_i, \beta_j) \quad (4)$$

Pis signal strength measured by antennak-th. The signal strength depends on gain of azimuth (α) and elevation angle (β) of antennas. L_{ij} is polynomiallangrage which can be determined by equation (5) below.

$$L_{ij}(\alpha, \beta) = L_i(\alpha_r) L_j(\beta_s) (6)$$

$$L_i(\alpha) = \prod_{r=0, r \neq i}^{n} \frac{(\alpha - \alpha_r)}{(\alpha_i - \alpha_r)} \quad (7)$$

$$L_j(\beta) = \prod_{s=0, s \neq j}^{m} \frac{(\beta - \beta_s)}{(\beta_i - \beta_s)} \quad (8)$$

$$L_{ij}(\alpha_r, \beta_s) = \begin{cases} 1 & i = r, j = s \\ 0 & otherwise \end{cases} \quad (9)$$

Where n and m is a count of α and β data.Signal Strength of nine antennas can be calculated using equation (2-8).

(2)

D. Estimation of Azimuth and Elevation Angle

Angle of arrival estimation is based on received signal strength of ninecross Yagiantennas. The highest signal strength received by one antenna indicatesthat the location of emission source has same direction of the antenna. To determine estimationof azimuth and elevation angles, signal strength of the highest received antenna is comparedto its

neighborhood signal strength then interpolated to the lookup table.

Figure 3 shows a coverage area of nine antennas. The red mark indicates the maximum signal strength and the blue mark indicates the neighborhood signal strength. The comparison of signal strength of the red mark with blue mark in the left or right side is used to determine horizontal ratio (Ra). The comparison of red mark with the above or below side is used to determin the vertical ratio (Rb). Both horizontal ratio and vertical ratio are used to interpolate to the lookup table in determining the azimuth and elevation angle.

Figure 3.Illustrate coverage area of nine antennas

Figure 3a shows the highest signal sensed by antennas first. To calculate the horizontal ratio (Ra), signal strengthof the first antenna compared to signal strength of second antenna. By comparing the signal strength of first antenna and fourth antenna, the vertical ratio (Rb) can be obtained. Figure 3b show the second antenna sensed a highest signal strength. To calculate the horizontal ratio, signal strength of second antenna compared with one of the both higher signal strength of first or third antenna.Vertical ratio calculated by comparing signal strength of second antenna and fifth antenna. Figure 3c indicated that fifth antenna sensed the highest signal strength. To calculate the vertical ratio, the signal strength of fifth antenna compared to one of both higher signal strength of fourth or sixth antenna.Vertical ratio (Rb) obtained by comparing signal strength of fifth antenna with one of both higher signal strength of second or eighth antenna.

Azimuth and elevation angles are estimated by interpolating the sum of horizontal ratio square and vertical ratio square into lookup table (equ. 11-13). The lookup table is mapping of vertical and horizontal ratio that corresponding to the azimuth and elevation angles.

$$\mathrm{R} = R_\alpha{}^2 + R_\beta{}^2 \qquad (10)$$

$$\alpha(\mathrm{r}) = \sum_{i=0}^{n} L_i\,(r)\alpha(r_i) \qquad (11)$$

$$\beta(r) = \sum_{i=0}^{n} L_i\,(r)\beta(r_i) \qquad (12)$$

$$L_i(r) = \prod_{j=0;j\neq i}^{3} \left(\frac{r - r_j}{r_0 - r}\right) \qquad (13)$$

First of all the lookup table produced by placing the transmission radio in front of nine Yagi antennas. The antennas rotate in azimuth and elevation direction. In each degree of the nine signal strength, azimuth angle and elevation angle will captured then saveit to memory. This file is processed using the above algorithm to obtain the mapping of horizontal ratio and vertical ratio that corresponds to the azimuth and elevation angle.

III. SIMULATION RESULT

A. Radiation Pattern of Nine Antennas

Based on data radiation patent of cross Yagi-uda antenna obtained by MMANA software, the radiation pattern of nine antennas with configuration like Figure 2 can be shown as Figure 4.which Sa and Sb are 40 degree.

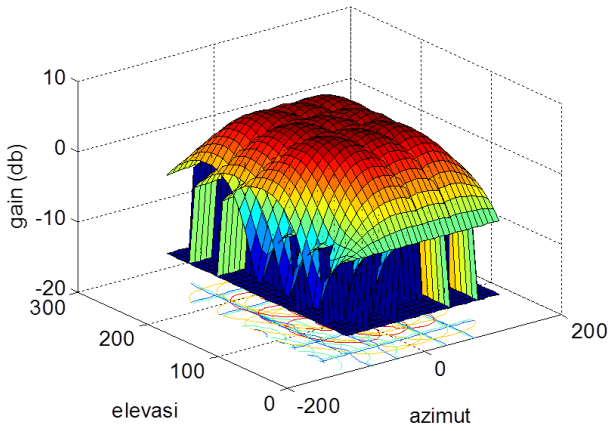

Figure 4.Radiation Paternof Nine Cross Yagi antennas

B. LookupTable

Lookup tableis mapping ofvertical and horizontal ratio that correspond to the azimuth and elevation degree. To retrieve data lookup table, the nine antennasare rotated towards the left to the right and top to down. For each degree change direction, the nine antennas measure and capture of the ninesignal strength data and direction angle (azimuth and elevation).Each data is processed using algorithm that has been described in Chapter 2 to obtain lookup table. By using nine antennas, the lookup tablewill generate 22 files. Table 1 shows lookup table files.

TABEL 1.LOOKUPTABLE DATA

The Highest Strength	Neighborhood	Ratio	Note	Lookup tabel
PA1	PA2	Ra		LT1
PA1	PA4	Rb		LT2
PA2	PA1	Ra	P1>P3	LT3
PA2	PA3	Ra	P3>P1	LT4
PA2	PA5	Rb		LT5
PA3	PA2	Ra		LT6
PA3	PA6	Rb		LT7
PA4	PA5	Ra		LT8
PA4	PA1	Rb	P1>P7	LT9
PA4	PA7	Rb	P7>P1	LT10
PA5	PA4	Ra	P4>P6	LT11
PA5	PA6	Ra	P6>P4	LT12
PA5	PA2	Rb	P2>P8	LT13
PA5	PA8	Rb	P8>P2	LT14
PA6	PA5	Ra		LT15
PA6	PA9	Rb		LT16
PA7	PA8	Ra		LT17
PA7	PA4	Rb		LT18
PA8	PA7	Ra	P7>P9	LT19
PA8	PA9	Ra	P9>P7	LT20
P8	P5	Rb		LT21
P9	P8	Ra		LT22
P9	P6	Rb		LT23

Figure 5.shows lookup tablein LT1 and LT2. The axis x is azimuth ratio and axis y is elevation ration. Both azimuth and elevation ratio have correlated to the azimuth angle (Fig. 5a) and elevation angle (Fig. 5b). The graph describes the content of a lookup table that is used to estimate the azimuth and elevation angles by interpolation.

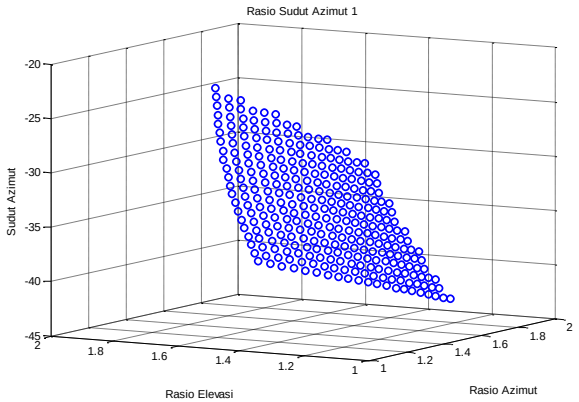

(a) Azimuth Angle

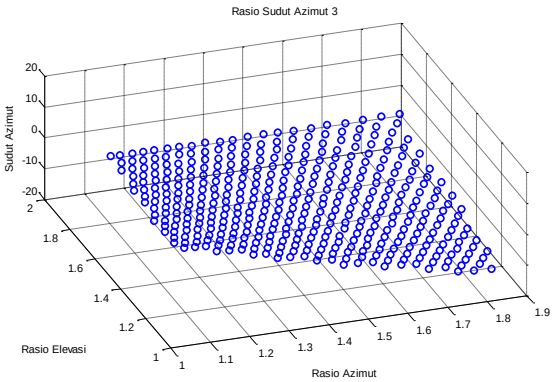

(b) Elevation Angle

Figure 5. Lookup tablefile LT1 and LT2

At the time of measurement, if the first antenna receives highest signal strength,ratio (R) in eq. 10is interpolated to lookuptable LT1 (Fig. 5a) to derive azimuth angle. To derive the elevation angle ratio (R) is interpolated to lookup table LT2 (Fig. 5b).

Similarly, when highest signal strength is detected by second antenna, the azimuth angle will be derived by interpolated R value to LT3 (PA1>PA3) or LT4 (PA3>PA1). Elevation angle is derived by interpolation of the R value to look up table LT5.Furthermore,when the highest signal strength is detected by antenna 3,4,5,6,7,8,9,the lookup tableused isin accordance with the rules in Table 1 .

C. Estimation of rocket direction

To clarifythe algorithm in estimating the azimuth and elevation angles that have beendeveloped, the motion of the rocket is simulated. The rocket contains a radio transmitter that continuesemittingat 465 MHz frequency. At the receiver, 9 Yagi antennas with 3x3 configuration as shown in Fig. 2 areplaced few feet behind the launching pad rocket.

Continuously, the radio signals transmitted from the payload rocket are received by nine cross Yagi-uda antennas. Nine signal strengthsare received and processed using the algorithm discussed in Chapter 2 to generate the azimuth and elevation angles.

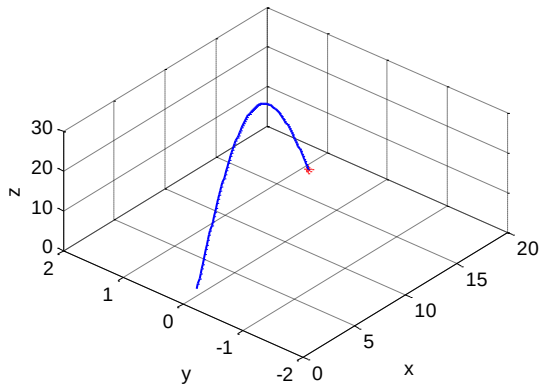

Figure 8. Rocket trajectory

The signal strength from transmitter which moves can be calculated using equation 2-8. The simulation results of signal strength measurements by nine antennas can be seen in Figure 9. By using equation 10-13, azimuth and elevation angle can be calculated. Figure 9b and Figure 9c shows the estimation results of azimuth and elevation angle of the rocket motion.

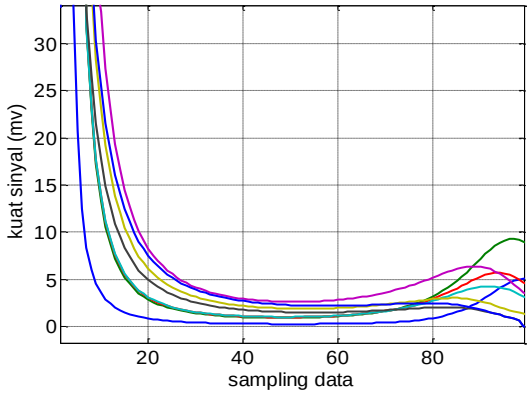

(a) Signal Strength of nine Antennas

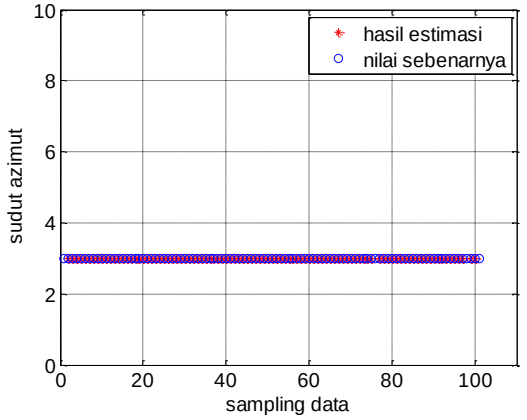

(b) Estimation of azimuth angle

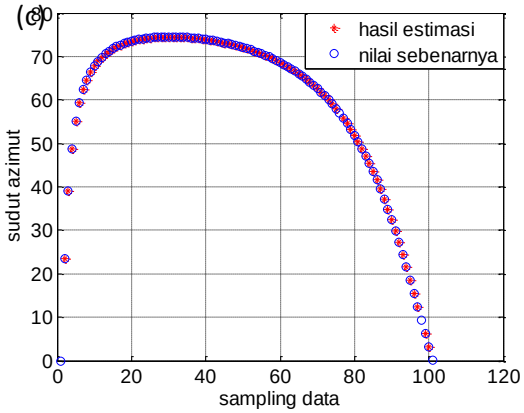

(c) Estimation Elevation angle

Figure 9.Simulation result of azimuth and elevation angle of arrival

Fig. 9 shows estimation of the azimuth and elevation angle. The star red mark indicates the estimation and the circle blue mark indicates the true value. Noise measurements of Figure 10 shows a very small value which proves that this method can be applied to detect location of the source emission radio and estimate the direction of movement of the rocket.

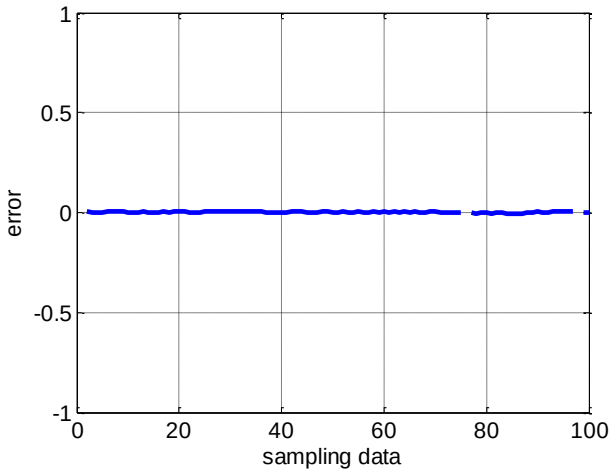

(a) Error of azimuth angle

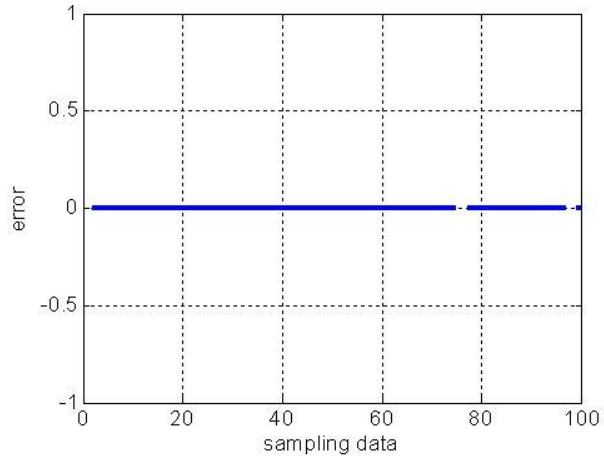

(b) Error Elevation angle

Figure 10.Error of azimuth and elevation angle

III. CONCLUTION

Estimation of azimuth and elevation angle based on radiation pattern of nine Yagi-uda antennas can be proven to work by simulating and estimating the direction of rocker motion in three dimensions. The algorithm developed in this study uses interpolation of the sum of horizontal ratio square and vertical ratio square into its corresponding lookup table. The horizontal ratio is obtained by comparing the highest signal strength of one antenna to its neighborhood signal strength of right or left side. The vertical is ratio obtained by comparing its signal strength to its neighborhood at above or below its side.

REFERENCES

[1] P. Bahl and V. N. Padmanabhan, "Radar: An In-Building RF-based user Location and Tracking System", IEEE INFOCOM, Mar.2000.

[2] A.E. Waadt, C. Kocks, S. Wang, G. H. Bruck, P. Jung,"Maximum Likelihood Localization Estimation based on Received Signal Strength", International Symposium on Applied Sciences in Biomedical and Communication Technologies (ISABEL), Nov 2010.

[3] F. Yin, C. Fritsche, F. Gustafsson, A. Zoubir, " Received Signal Strength-Based Joint Parameter Estimation Algorithm For Robust eolocation In LOS/NLOS Environments", IEEE International Conference on Acoustics, Speech and Signal Processing (ICASSP), May 2013

[4] P.L. Yu and B. M. Sadler,"Receive Signal Strength Gradient Estimation For Mobile Network", Military Communication Conference, Nov. 2010

[5] M. Elhefnawy and W. Ismail, "New Technique to Find the Angle of Arrival", Japan-Egypt Conference Electronics, Communications and Computers (JEC-ECC), March 2012.

[6] C. Liu, J. Yang, F. Wang, "Joint TDOA and AOA location algorithm", Journal of System Engineering and Electronics, Vol. 24, No. 2, April 2013.

[7] H. Chen, T. Lin, H.T. Kung, C. Lin, Y. Gwon, "Determining RF Angle Arrival using COTS antenna arrays: A Field Evaluation," , Military Communications Conference, Nov 2012.

[8] O. A. Oumar, M.F. Siyau, T. P. Sattar, "Comparison between MUSIC and ESPRIT Direction of Arrival Estimation Algorithms for Wireless Communication System", IEEE International, May 2012.

[9] K. Sayrafian-Pour, D. Kaspar, "Source-Assisted Direction Estimation Inside Buildings", IEEE International Conference on Computer Communications, April 2006.

[10] S. Jenvey, J. Gustafsson, F. Henriksson, "A PortbleMonopulse Tracking Antenna For UAV Communications",Intenational Unmanned Air Vehicle System Conference, April 2007

G404

SIMULATION ATTENUATION FROM RAIN CELL MOVEMENT FOR WIMAX CHANNEL TRANSMISSION IN LOMBOK

Made Sutha Yadnya[1]
[1]Jurusan Teknik Elektro Universitas Mataram,
Nusa Tenggara Barat
msyadnya@unram.ac.id

I Wayan Sudiarta[4]
[4]Jurusan Fisika Universitas Mataram,
Nusa Tenggara Barat
wayan.sudiarta@unram.ac.id

Haniah Mahmudah[2] , Ari Wijayanti[3]
[2,3]JTE Politeknik Elektronika Negeri Surabaya
Jawa Timur
[2]haniah@eepis-its.edu, [3]ariw@eepis-its.edu

Achmad Mauludianto[5]
[5]Jurusan Teknik Elektro ITS
Surabaya, Jawa Timur
[5]maulud@ee.its.ac.id

Abstract*—Rain attenuation from rain condition in tropical maritime is intruder for high frequency transmission, then attenuation can lead to communication breakdown. Rain rates in tropical signal are very significance fluctuations, these situations should be able to adapt for mobile communication, and one solution is adaptation instrument for rain attenuation in domain spatial and domain temporal. This research is conducted by wireless channel models transmission of WiMAX (Worldwide Interoperability for Microwave Access) transmission. Channel transmission is classified spatially into rural and urban conditions. Data is obtained directly from measurement results raingauge. Accuracy prediction for the mobile adaptation of the cell, assuming rain rate is not stationary, rain can move to anywhere by wind to other cell caused by "heavy attenuation". The results are indexs cell correlation of 0.1315dB/km in urban and 0.1143dB/km in rural.

Keywords: WiMAX, channel, fading.

I. INTRODUCTION

Climate change is a problem that is likely to constitute a threat to all mankind on this earth. Conditions in Indonesia in the tropics is not favorable because in the years preceding the rainy season and dry can be predicted accurately. For the measurement of instantaneous rain in a matter of minutes with millimeters per hour (mm / h) has not been conducted in the NTB, globally many researchers have studied and generate predictions but not in accordance with the area / place and time. This study was conducted as a child of the nation of Indonesia to be able to cope with floods and landslides. Indonesia is a maritime country that has scattered islands from Sabang to Merauke management requires a strategy for handling the climate change. Climate change specifically in the high rainfall and long will be crucial once the disaster. In this case the communication is expected to persist even in rainy conditions. Wireless technology is so fast, it can be seen with the naked eye the increasing use of cellular phones, in addition to the evolving wireless technology is also used to access the internet. WiMAX is one of the variants of communication and information technology that works on the network and the WiMAX. In other words, the WiMAX is the trade name standart certification is given to the manufacturer of telecommunications equipment which works in the WiMAX network interoperability and already meets the required quality. Standart WiMAX used IEEE 802.16. Modulation for mitigation per channal used OFDM [1].

Channel obtained by a channel which varies according to the exact distribution of rainfall fell on the links (lines) wireless communication. Communication was very disturbed at a very high rainfall. Permittivity value of rain also influence damping (disturbance) is happening. Slope falling rain and strong winds or even more trends will greatly exacerbate the occurrence of typhoons on the quality of communication [2].

Correlation characteristics of rain on the number of papers have reported some empirical models of spatial rainfall. Morita-Higuti produce precipitation method of spatial structure that is represented in a correlation coefficient of rainfall precipitation measurements for ten years in Japan. This method is very successfully applied to the prediction of rain attenuation in the application of statistical diversity for satellite-earth links in Japan. Capsoni et al produce another model of spatial correlation of radar observations in Italy. Lin propose an empirical model of spatial correlation of specific attenuation measurements of rainfall using rain gauge in North America. Given the spatial variations for specific attenuation and rainfall from one location to another location dependent climate, topography, precipitation type and others, the implementation of mitigation techniques should use the correlation coefficient corresponding to that location. While the spatial model specific damping Lin also approached to Surabaya. This suggests that the rain cell to Surabaya very large spatial correlation of

rainfall and rain attenuation statistics from this study is recommended as one of the parameters in the implementation of diversity techniques in Surabaya, on the application of mitigation techniques such as rain attenuation site diversity. Model rainfall spatial correlation coefficient and the specific attenuation vary from one location to another, for the climate in Japan [3].

In the fall of water in the study of heavy rainfall can be divided into 2 groups, i.e. stratiform and convective rain. Characteristics stratiform rain is rainfall is less than 25 mm / h and the uneven effect that tends to rain a longer duration than convective. While the characteristics of convective rain has high rainfall above 25 mm / h , a short duration when the rain more than 15 minutes would be more evenly , and very brief coverage is usually accompanied by storms in certain areas . The percentage measureament in certain period of time (usually within 1 year), so to say the percentage of time 0:01 % (R0.01), this means that the amount of rainfall that exceeded the average rainfall measurements over a period of 0:01 % in a year (70.63 min) under these conditions is quite high chance of rain. For wireless communication channel in order Gigahertz (millimeter wave) is very influential in transmitting the signal integrity of the communication [4].

From observation made by Morita-Higuti using rain gauge synchronization and produce a model of spatial correlation as a function of distance in the equation where is the correlation coefficient as a function of distance and the value of α ranges from 0.2-0.3 /km. Through radar observations in Italy, Capsoni et al propose another type of model of spatial correlation of rainfall as a function of distance as shown by the equation where is the correlation coefficient as a function of distance and the value of α ranges 0.46km-half. A typical WiMAX basestation transmits at power levels of approximately +43 dBm (20 W), and the mobile station typically transmits at +23 dBm (200 mW). For adaptation can uses another technique to address the link imbalance is adaptive modulation. [5].

Since measureament rain rate 50 (fifty) years into a very unique research in Spain. The uniqueness of the rain that has rainfall distribution is almost the same every year for fifty years, while the research generating different things because of the climate change (climate change). In measurements in Barcelona (Spain) for fifty years that tends to have a lognormal distribution caused by rainfall that comes periodically. In this case the rainfall can be said to be stationary in the distribution function that falls on the surface of the ground (measured by the measuring instrument). The size of the existing rainfall depends on the time. The most fundamental things appear because rain is very heavy and it takes time to narrow the proper fade margin calculations [6]. For propagation channel during the rain has been studied predict rain if the team that produced some of its models for signal transmission millimeters [7]. Attenuation from atmosphiric gases, clouds and rain used difference numbers effec in channel communication. Focus at rain attenuation trasmission 5.7 GHz in milliter standart impact in micro cell under 1 km in rain measureament 12.5 mm/h the number is 0.0313 dB [10].

Communication design for 4G rain attenuation should be included in the count of tropical climates because the wind changed suddenly, changes in the signal received from the channel made by the sender of the satellite must be above threshold Mitigation satellite or teresterial communication is choice for communication still fine and faster trasmission data [11]. Data loggers with RTC and SD card modules as well as other additional sensors will be used in our future studies in mapping weather patterns in Lombok. Analysis of weather data will also be conducted to understand weather variability and to develop weather models[12].

II. METHODOLGY OF RESEARCH

Transmission signal for channal WiMAX used radio frequentely in 2300MHz until 3400MHz. Multiple path fading effect is problem in transmit signal. It will make the received signal can weaken or strengthen in accordance with the movement of the receiver directly correlated with the signal path that rises and falls caused no direct path and the reflected in channel part by part if intruder from colour noise. Diffraction does not pass LOS Diffraction mechanisms in other words a greater attenuation of the original signal. Channel model wireless communication system applications LOS to NLOS. Static channel variations and dynamic changes with time series to observe the variation of the canal needs to be known in the channel change numbers statistical ensemble are the same and ergo dig city. Fast fading channel rapidly changing in minor condition and slow changing channels run private fading slow this is in mayor condition.

This paper focuses on the transmission on a communication channel with a frequency wave Giga herzt (3.4 Hz). Asumsion compared in two different areas (urban and rural), the two variations of the same conditions but in different places of measurement shown at Fig.1. Rainy conditions that have fluctuated rain fell and the amount of rain that falls. Undisturbed transmission channel tried to be simulated and analyzed as decision design to use millimeter waves in Indonesia, especially Mataram. The gap between urban and rural for air distance is 11 km. Detection of the propagation channel using a digital filter requires stability in order to produce the corresponding (matching) between sender and receiver. Filter made for necessary stability of the pole and zero in accordance with the scope of the existing channel. Communication is accomplished with either depending on channel conditions especially on the wireless channel (wireless). Rain intensity measurements made requires a model that can be studied from an existing system, the desired expectation (expected values) is known to the average observed. To expected the average function g (X) of a discrete random variable X can as follows:

$$E\{g(X)\} \cong \sum_{i=1}^{n} g(x_i)P(X = x_i) \quad (1)$$

Valid of all the events that occurred from a random function from measureament rain is data time series. This happens not only of discrete signal events but also in signal continue. There are two values that must be considered in the random condition that the average value (mean) and standard deviation or variance can as follows:

$$E\{X\} = \mu_x = \sum_{i=1}^{n} x_x P(X = x_x)$$

$$E\{(X - \mu_x)^2\} = \sigma_x{}^2 = \sum_{i=1}^{n} (x_i - \mu_x)^2 P(X = x_i) \quad (2)$$

$$X_{t,N} = \sum_{u=1}^{t} (x_u - \mu_N)$$

$$S_N = \left[\frac{1}{N} \sum_{i=1}^{N} (y_i - \hat{y}_N)^2 \right]^{\frac{1}{2}} \quad (3)$$

$$y(n) = -\sum_{i=1}^{p} a(i)y(n-i) + \sum_{j=0}^{q} b(j)v(n-j) \quad (4)$$

With modification Mercer's theory which state that:

$$K_{XX}(t_1, t_2) = \sum_{n=1}^{\sim} \lambda_n \phi_n(t_1)\phi_n^*(t_2). \quad (5)$$

Assume K-L expansion of white noise, than the autocorrelation factor must be integral equation :

$$K_{XX}(t_1, t_2) = \sigma^2 \delta(t_1 - t_2)$$

$$\sigma^2 \int_{-T/2}^{T/2} \delta(t_1 - t_2)\phi(t_2)dt_2 = \lambda\phi(t_1)$$

$$\sigma^2\phi(t) = \lambda\phi(t) \quad \text{for } (-T/2 \le t_1 \le +T/2)$$

Simple detection problem in a fading channel is White Gaussian noise. For simplicity, let us assume a flat fading model where the channel has represented by a single discrete-time complex filter. Random process plus white noise in K-L expansion for noisy process:

$$Y(t) = X(t) + W(t) \quad (6)$$

The rain-fade margin is a function of the rain rate(mm/hour). Therefore, for a particular system availability goal and rain zone, the rain-fade margin has computed, and the system's range is established. Illustrates the link range model, depicting the downlink, which is thelink in the direction from the PMP hub to the remote site. The hub is broadcasting with EIRP of P dBm. (EIRP is the product of transmit power and transmit antenna gain, expressed in dBW or dBm.)

The signal experiences propagation loss, L, and loss due to rain fade, F. The receiver sensitivity is R dBm. In dB, the total path loss equals P – R, which also equates to L+F. Improving receiver sensitivity increases the allowable path loss, therefore increasing the range. The fade component is a function of the attenuation per kilometer for a given rain rate and distance. The total path loss has given by:

Path loss = L + Fade Rate x Range (in km) (7)

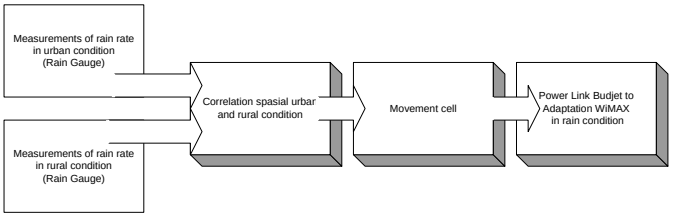

Fig. 1 Correlation from Data Measurements for Power Link Budjet WiMAX Transmission

III. MEASUREAMENT AND ANALSYS DATA

Use of software simulation using Matlab version 2009a . Results of measurements made at two different locations deffrence group generate data at each measurement in the same group , but the correlation between the group . Figures 3 and 4 show the relationships between each group of measurements. To show the correlation between the group and Figure 6 position in the condition probability of rainfall in the same time and Figure 7 simulate the distribution of the two different locations. In the millimeter wave transmission of order Giga hertz will cause fat problems, especially when the rain passes through or crosses from the track. One objective of the simulation in this case to know if the path past the 2 BTS rain , according assuming the maximum distance between them is 5.3 km . Distance between urban (city) and rural (village) in the air distance is 10.1 miles. In accordance with the power of the transmitter (Tx) and receiver (Rx). In the group of cells form a circle assumed that the maximum radius of 250 meters of air distance. Need to get value of this correlation can be used to generate predictions of rain in the future in case of rain distribution according to the measurement results. The complete rain gauge of the data logger The software Code Vision AVR [12] and an ISP programmer are used to program the ATMega8L and to download data store in the microcontroller using serial data communication. To save the battery power, it is essential to used power management facilities of the microcontroller. Beside that the timer of microcontroller needs also to be programmed and checked for its accuracy. Some adjustment of timer may be required to get correct interval of time. Data Logger shown at Fig. 2.

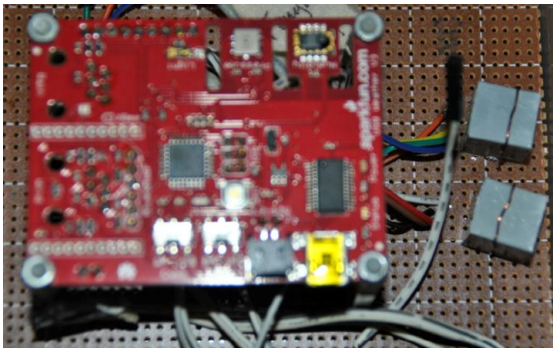

Fig. 2 Logger and Rain Gauge

IV. CONCLUSION

Progress simulation attenuation shown at Fig. 3 until Fig. 10. Fig. 3 until Fig. 5 in unban condition, Fig. 6 until Fig. 8 in rural condition. Fig. 9 Power spectral density urban and Fig. 10 Power spectral density in rural.

Correlation value in urban values obtained using correlation analysis is very bad for the link Pustik 0.0496 and Engineering, 0.0484 to link Pustik and Algriculture Lab, as well as for Engineering Lab and Agricultural Lab better is 0.4442, rain Attenuation from measurent in 1 km is 0.131 dB, the rain rate condition maximum at 201 mm/h. As for rural values between 1 and 2 Sesaot is 0.7278 distance 3.5 km north to south, for Sesaot 2 and 3 distance 3.5 km north to south are the most well 0.7231 Sesaot 1 and 3 is 0.9174 . distance 7 km north to south. Rain Attenuation from measurent in 1 km is 0.1143 dB, the rain rate condition maximum at 167 mm/h. Accuracy prediction for the mobile adaptation of the cell, asumsy rain rate is not stationary, rain moved anywhere by wind to other cell is made of heavy attenuation. The results are indexs cell coorleration average of 0.1315dB/km in urban and 0.1143dB/km in rural.

V. DISCUSSTION NEXT RESEARCH

Simulation results channel in the rain until the Year 2013 is still being conducted research to obtain perfect results. In terms of mobile communications in the movement poses a very significant effect on the transmission channel, therefore disgn for an early warning system to be tested accuration rainy conditions. Rainy conditions are potentially disrupt the path (link) and will damage the direction of the antenna due to heavy rain accompanied by wind storms tend. Classification of rainfall from this study must be studied further to generate predictions communication mintages rain condition for mobile comunication system.

ACKNOWLEDGMENT

This paper research project supported by JICA PREDICT-ITS (2006-2007), Research Grant A2 Elektro Engineering Department, Universitas Mataram (2008), Higher Education Grant DP2M Competence 2009 and 2010. Information and Computer Technology Center, Universitas Mataram in 2011, Desentralisation Fundamental Found from Higher Education Grant DP2M 2013, specifically for this publication found is assisted by Jurusan Teknik Elektro Universitas Mataram 2014.

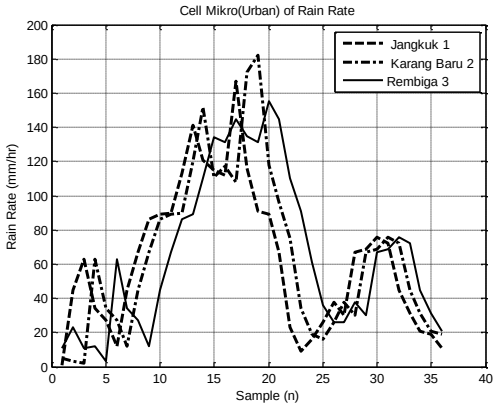

Fig. 3 Movement Cell in Urban

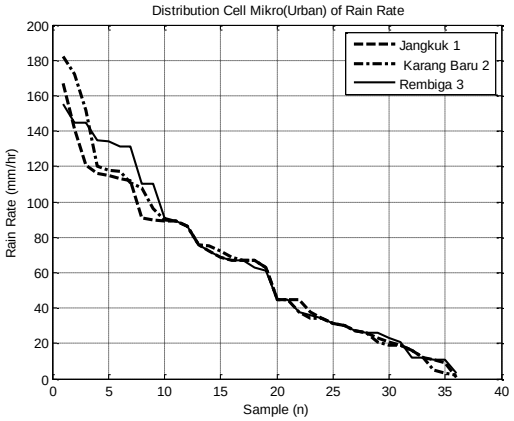

Fig. 4 Probability Rain Rate in Urban

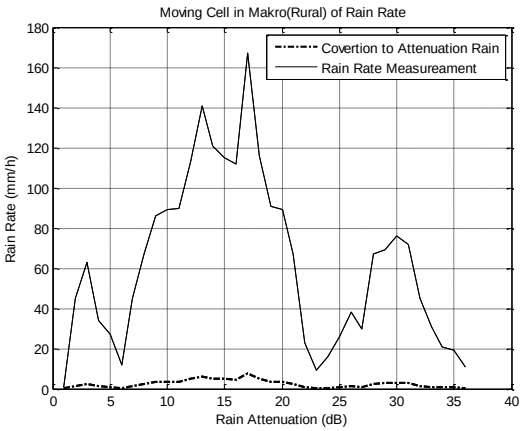

Fig. 5 Movement Cell in Rural

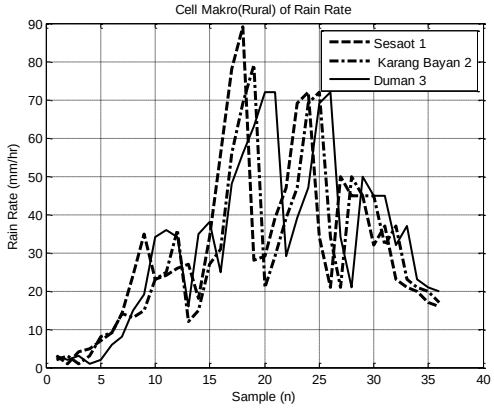

Fig. 6 Movement Cell in Rural

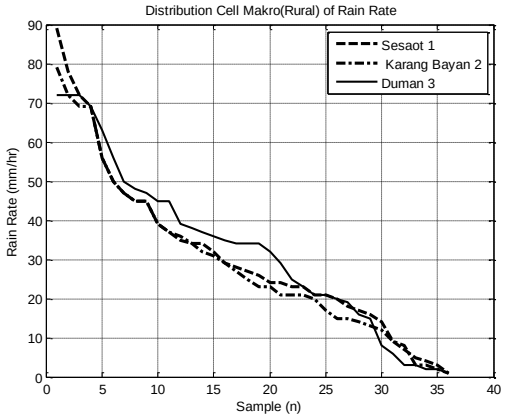

Fig. 7 Movement Cell in Rural

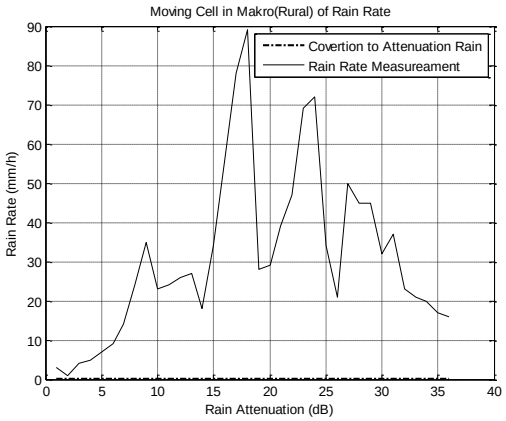

Fig. 8 Movement Cell in Rural

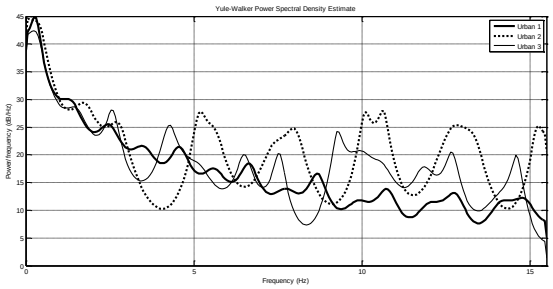

Fig. 9 Power Spectral Density Urban

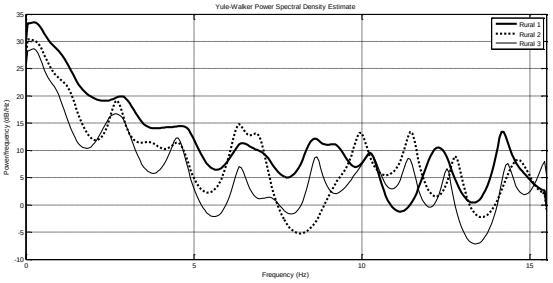

Fig. 10 Power Spectral Density Rural

REFERENCES

[1] Yaghooby H (2009), "Mobile WiMAX Update and 802.16m" Intel Corporation 2009, WiMAX Forum March 2009.

[2] Yadnya, M.S, Mauludiyanto .A, Hendrantoro.G (2008a) "*Statistical of Rain Rate for Wireless Channel Communication in Surabaya*",WOCN 5-7 May 2008 Surabaya-Indonesia, IEEE, ISSN 978-1-4244-1980-7-08.

[3] Yadnya, M.S, Mauludiyanto .A, Hendrantoro.G (2008b) "*Akaike Information Criteria Application to Stationary and Nonstationary Rainfalls for Wireless Communication Channel in Surabaya*", ICTS 5 August 2008 Surabaya-Indonesia, ISSN 1858-1633 , pp 292-299.

[4] Morita.K & Higuti , 1976, " Prediction Method of Rain Attenuation Distribution of micro-millimeter waves ", Rev Electr.communication Lab vol 24, no 7-8, pp 651-688.

[5] Saitou N, Endo Y, Shibuya Y (2008), "Mobile WiMAX Base Station Archetecture and RF Technology ", Fujitsu Science Technology Journal, pp 325-332.

[6] Burgueno, E. Vilar, M. Puigcerver 1990,*"Spectral Analysis of 49 Years of Rainfall Rate and Relation to Fade Dynamics",* IEEE TRANSACTION ON COMMUNICATION Vol.38 no.9 pp(1359-1366)

[7] Yadnya, M.S, Mauludiyanto .A, Muriani, Hendrantoro.G ,Wijayanti.A ,Mahmudah. H(2007), "*Simulation of Rain Rate and Attenuation in Indonesia for Evaluation of Millimeter-wave Wireless System Transmission*", ICSIIT 26 Juli 2007,pp376-381

[8] Yadnya, M.S, Mauludiyanto .A, Hendrantoro.G (2008c) "*Simulation of Rain Rates for Wireless ChannelCommunication in Surabaya* ", Kumamoto ICAST 14 Maret 2008, pp 139-140.

[9] Suryani T, Hendrantoro.G (2013). "Block-Type Arragement with Alternating Polarity for Mitigation in Mobile OFDM System",Journal of Communication Software and System Vol. 9 no 8, 11865-6421/09.8391 CCIS pp78-183.

[10] Guissard. A (1980). "Study of the influence of the atmospheric on the perfomance on an imaging microradiometer ", ESTEC european Space Agency. Contact 4142/79/NL/DG(SC).

[11] Yadnya, M.S, Sudiarta I.W (2013), "Cell Movement of Rain Rate Imfact in Satellite and Mobile Comunication Based on Tropical Maritime", American Scientific Publisher Advance Science Vol. 4, 400–407, 2013.

[12] Sudiarta I.W, Yadnya, M.S, Mardiana L, Kauripan I.K, (2013), "Measurements of Surface Air Temperatures in Lombok with Low Cost Miniature Data Loggers", ICTAP 3rd International Conference on Theoretical and Applied Physics 2013 Universitas Negeri Malang Malang-Indonesia, AIP.

G405

Android Based Indoor Navigation Application using Earth's Magnetic Field Pattern

Case Study: UNIVERSITAS MULTIMEDIA NUSANTARA

Rijal Widhi Permadi[1], Maria Irmina P.[2]
Computer Science, Universitas Multimedia Nusantara
Scientia Garden, Jl. Boulevard Gading Serpong,
Tangerang, Indonesia
[1]rizalwidhi@gmail.com, [2]maria@umn.ac.id

KanisiusKaryono
Computer Engineering, Universitas Multimedia Nusantara
Scientia Garden, Jl. Boulevard GadingSerpong,
Tangerang, Indonesia
karyono@umn.ac.id

***Abstract*—An indoor navigation application can be built by utilizing the pattern of Earth's magnetic field which is unique at each location. In previous research, users have to record magnetic values all the way inside the building site before the application can be used. By utilizing built-in magnetometer sensors, magnetic values on the X and Y axis that captured by the sensor will be stored in a database and used as a reference point. This research uses the fingerprinting method for creating the magnetic database. There are two main phases in the research process, the first phase is to create magnetic field map database and the second is creating Android application for positioning. This research implements two magnetic data comparison functions, which are random function and first position function. The result shows that the maximum error position value is 116.54 meter for random function. While first position function returns a smaller number, which is 18.83 meters. It can be concluded that indoor navigation with magnetic database yield better accuracy compared to indoor navigation using GPS. This approach can become reliable solution if there are no communication channels to convey the message or to triangulate the position in emergency situation.**

Keywords—earth magnetic field, magnetometer, navigation, mobile, fingerprinting method

I. INTRODUCTION

People always say that they find it difficult to know their own position or looking for a location when they enter a new building. A building plan along with general information on each floor is unable to provide the position in real-time. This position information is very beneficial especially in emergency situation. However, this problem can be solved with the use of navigation applications in mobile devices (smart phones), which has been commonly used in everyday life. In such condition we cannot only rely on the position data which need communication channels to convey the message or to triangulate the position.

Many prototypes of indoor navigation have been developed in recent years. However, most of the prototypes require an external device. One of the devices that developed for the navigation system in the building utilizes the value of the Earth's magnetic field as a reference [1].

Using the magnetometer which has now become standard sensor in recent smart phones, it is possible to develop an indoor navigation application without external devices. Magnetometer is a sensor that can be used to measure the strength and show the direction of the Earth's magnetic field. The use of the magnetometer was based on case studies conducted by IndoorAtlas [1]. This study was conducted to create The Android application for indoor positioning using the Earth's magnetic field on the X, Y, and Z axis based on a magnetic field map that has been stored in the magnetic field map database.

II. MAGNETIC FIELD

A. Earth's Magnetic Field In Cartesian coordinates

At any location, the Earth's magnetic field can be represented as a three dimensional vector. Using a Cartesian coordinate system, the X-axis is the angle towards the north geographicalpole, Y-axis is east geographical pole and Z-axis pointing down. Declination angle (*D*) measures the angle between the Earth's geographic north pole and magnetic north pole [2].

In addition, there are deviations toward Earth's geographic and magnetic compass, the needle itself also had positions that are not flat. Horizontal direction deviation was due to the magnetic lines of force is not parallel to the surface of the earth (in horizontal plane). As a result, the compass needle that points toward the north pole, will deviate either upward or downward to the earth's surface. The deviations in the compass needle will form an angle to the plane surface of the Earth. The angle formed by the compass needle's north pole with a flat surface is called the angle of inclination *I*.

Declination angle (*D*) can be obtained by

$$tanD = Y/X, \quad (1)$$

thus, the total magnetic field strength (*F*) is,

$$F = \sqrt{X^2 + Y^2 + Z^2} \quad (2)$$

And the inclination angle (*I)*

$$\tan I = Z/\sqrt{X^2 + Y^2} = Z / H \quad (3)$$

where *H* is the magnetic force on the horizontal field in X,Y and Z axis[2].

B. Tri-axial Magnetometer

Magnetometer is an instrument for measuring the strength of a magnetic object. Embedded magnetometers in smartphones can measure the strength of Earth's magnetic field through a three different direction known as tri-axial magnetometer [3]. T*ri-axial* magnetometer sensor on a *smartphone* represented by X, Y and Z axis that prescribed by the right hand rule in accordance with the Lorentz force. X is the horizontal plane and points to the right, Y is on the vertical plane and points to the front and Z is pointing up, which can be described in the figure 1.

According to the *develeoper.android.com* as an official website of Android application development,the magnetic field sensor on Android will measure the magnetic force on tri-axis way. The sensor direction does not change even if the user rotating the screen orientation.

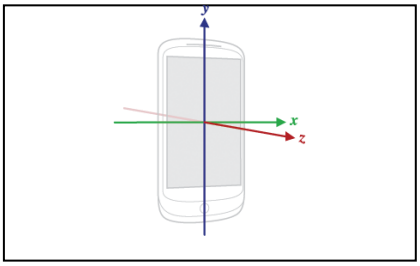

Figure 1. Smartphone sensor direction[3].

The amount of magnetic force in the direction to X, Y and Z can be used for the calculation of the magnetic field strength *F* (total) [2], where

$$F = \|Bx + By + Bz\| \quad (4)$$

in x, y and z axis.

C. Magnetic Field Fingerprinting Map

A methodology called "fingerprinting" is widely used where signal propagation is unpredictable, this method allows the system to use a lot of samples on a wide area [4]. The method is to put some value (eg: earth magnetic value) into the database and mapping it on a map. Fingerprinting method for localization is called scene analysis, one of its application is the mapping of signal strength on WiFi network in a building [5].

Fingerpinting carried out in two phases, the offline and online phase. In offline phase, the magnetic data at each location will be collected into a database and mapping it according to the earth magnetic strength's value. The X, Y and Z value that stored in the database are obtained from tri-axial magnetometer sensor. In the online phase, the magnetic field values obtained by the device user will be compared with the existing data in the magnetic database [6].

The placement of device will not affect the Earth's magnetic values, but it actually only affect the recorded values. For this study the device is placed at the bottom of the chest.This posisition give a better results compared to the wrists, legs and shoulders with the average value of the magnetic difference reaches 20% [7].

Magnetometer sensor which is used for measure the earth magnetic field is also be affected by static magnetic field. The database of magnetic field should be updated if some environment on a building has changed drastically, by providing new database record near the affected environment.

III. SATELITE BASED POSITIONING

A. GPS

GPS stands for "Global Positioning System". GPS is a satellite navigation system used todetermine ground position and velocity (location, speed, and direction). GPS was first developed by the U.S. Department of Defense which is used for military purposes. In general, the use of GPS for outdoor navigation activities have 50 to 150 meters accuracy rate when using cell tower triangulation, while the use of GPS satellite sensors directly provide a higher level of accuracy, which is able to achieve accuracy of 1 to 10 meters [8] .

B. Positioning in GPS

GPS works by collecting data obtained from each satellite signal continuously, the data are in the form of information about when the signals are transmitted using atomic clocks that located on satellites and which satellites that sent the data. Afterwards, data are processed in GPS receiver to determine the position of the distance of a sateite signal sender and the distance between each near satellites [9].

A coordinate knows as waypoint (latitude and longitude) will be obtained from the sampling of its locations. Then, by applying satellite trilateration method, the GPS will counts the approximate position of the receiver.

Trilateration is a method for finding a relative position using a circular geometry. The triangulation or trilateration works by comparing the position of a satellite receiver with other satellites, each satellite has a different distance to the receiver. So, the point of intersection between the three satellites is estimated to be a receiver position [10].

If there are not enough satellites, the trilateration method can not be done. GPS will use a method known as absolute or point positioning, where a position will be determined using only one satellite. The accuracy of the receiver position is not accurate and is intended only for navigation.

IV. MAGNETIC FIELD PATTERN POSITIONING

Refering to a fingerprinting method, which is divided into two phases, storing the magnetic value into a database (offline phase) and data comparison (online phase). This study implemented two applications, the first application is "GeoRecorder" that used to capture the value of the Earth's magnetic field from a location. This application read the magnetic value using magnetometer sensor obtained by a device from a location and stor into a text file.

The second application is "Emone" (*Earth magnetic observed navigation evince*) that used by the user to inform their position. This application use OSMdroid library for showing the building map and the navigation process, also the navigational menu like zoom and scroll map.

A. GeoRecorder

GeoRecorder system is initialized by registering the magnetometer sensor on the device. If there is no magnetometer sensor, then the application will display error message information and the application is forced to stop. Besides a magnetometer sensor, the system also uses GPS to get the latitude and longitude values that used as the reference point during the map binding process. If the coordinates obtained using GPS are inaccurate inside a building, then this coordinates is only being used as a check values where the reference points are generated from the position reference in outer position of the building where the value of GPS satellites positioning have adequate precision (sufficient PDOP values).

After the sensors have been registered, the application will record the magnetic values along with the coordinates in one position per second and calculates the average of the magnetic values that obtained. It is used to minimize the possibility of error when the magnetic sensor captures a value that is skewed from the actual value. This because of the value that read by a magnetic sensor can be varied and changes so fast. Finally, the system will create a new text file for data placeholders. The system will continue to repeat until the application is stopped and sufficient data is generated for generating the magnetic database map. The flow chart of this application can be seen in figure 2.

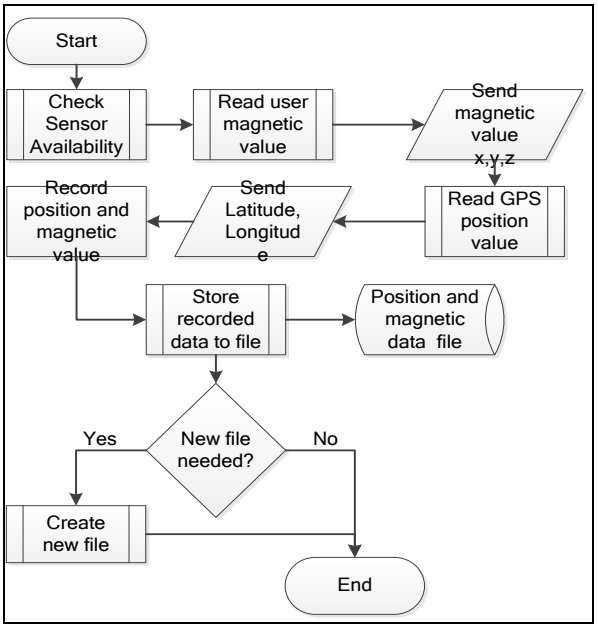

Figure 2. Flow Chart of theGeoRecorder Application.

B. Emone

The functions for sensor checking system and magnetic reader system used on the Emone application are adopted from GeoRecorder application. Slight modification is needed because Emone does not require a data storage menu. Application initialized by loading a map of a building or specific area and then continued to load the entire magnetic database for positioning. The magnetic database is then converted into arrays to speed up the positioning process. Furthermore, the system will prompt the user to perform calibration at predetermined points shown on the map. Calibration process is used to correct the deviation of magnetic value acquired by different devices other than the device used to generate the reference magnetic data values stored in a database.

Calibration process produces a constant calibration values used to reduce or add value of magnetic sensors that obtained by user. The system will perform comparison of magnetic values which are read by the sensor device every second. Such data will be compared with magnetic values database that has been deposited into the array to determine the user location. Finally, the system will show the user's position on a map based on latitude and longitude obtained from the previous process. The flow chart of this application can be seen in figure 3.

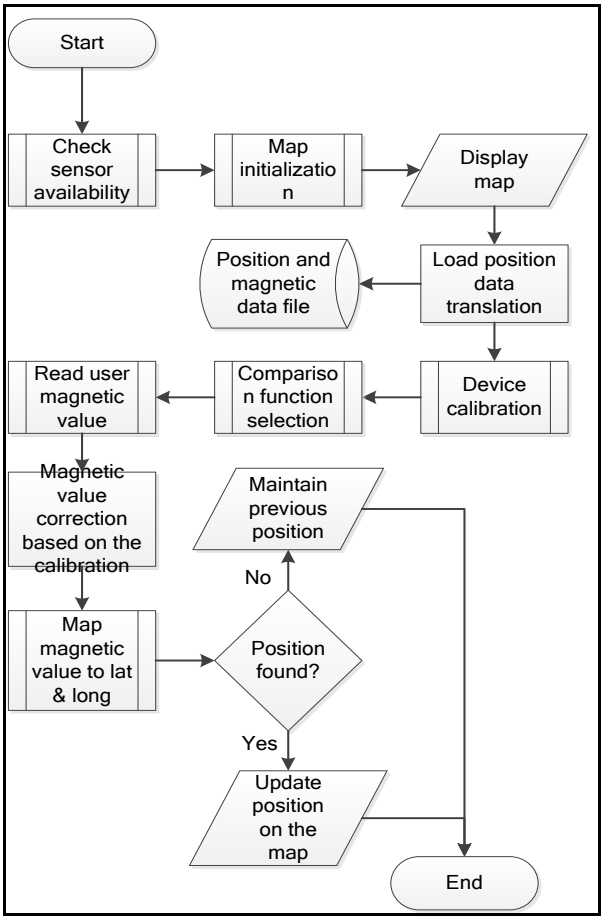

Figure 3. Flow Chart of theEmone Application.

C. *Collecting and Mapping Earth's Magnetic Field*

Magnetic field data collection is collected in two directions, by a vertical and a horizontal directions referring to a map layout of buildings that is used in this application. The retrieval is done using a device that has been equipped with GeoRecorder applications. Magnetic data were taken with the certain value of distance on each single floor. Here are the steps for taking a magnetic value at a location.

1) Device placed on a tripod with a box that can help minimizethe magnetic interference from outside
2) Positioning device at 105 cm above the ground, or positioning at abdominal of user
3) The user place the device in the middle of the floor and pressing the record button on the application
4) Application will store the magnetic value and write it into a text.

Once the magnetic data collected into a text file, then the value will be mapped to form the magnetic latitude and longitude position using the reference of latitude and longitude position information on MapInfo. Using the maps published in MapInfo, we can bind the value of the magnetic placement with placement assistance point. Finally, the entire text file that contains the value of the magnetic field and its position will be imported into a database using SQLite Manager Application. The results of magnetic data on building floor plan are shown in figure 4.

Figure 4. Magnetic sensor placement during data gathering on building floor plan.

V. MAGNETIC COMPARISON FUNCTION MAPPING

In this study, we use two comparison functions for comparing the magnetic values obtained by user with the magnetic field map database that has been created before. The comparison process produces a coordinate that will be used for determining the user position.

A. *Random Function*

Random function will compare the value of the magnetic field that obtained by the user with all the magnetic data contained in the database. These are the procedures that performed on the random function:

1) Comparing the X-axis magnetic field value in the database with the X-axis obtained by user
2) Accommodate the sequence (rowid) from the value on the X-axis between the same user and the database
3) Increase or decrease the range with difference of 0.1 to obtain the same magnetic values between users and database
4) Comparing the Y-axis magnetic values on database with user based on sequence (rowid) that obtained before
5) If the difference in the value of the Y-axis is not greater than or equal to the limit, then the comparing process is successful.

B. *First Position Function*

First position function will find a position of the point of departure from the previous position, at the first, it will use the latitude and longitude values at the starting point of calibration position. Then, the system will search for magnetic values in the database which are located near the area, and discard (filter) the magnetic values which have much difference with the user magnetic value. These are the procedures that performed on the first position function:

1) Check the current user coordinate location and find the magnetic value on X-axis and Y-axis in the database that was near the area

2) Comparing the value of magnetic X-axis and Y-axis obtained by user with database where area has been limited
3) Widen the comparison are by adding the value of the latitude and longitude of 0.00001 if there is no magnetic values are equal or adjacent.

VI. RESULT AND DISCUSSION

This study performed using three different devices for testing purpose, Xperia X10 mini, Galaxy Chat, and Nexian Journey. All those devices are used to see how much distance errors obtained by each device. After each calibration device and conducted 10 trials to the specified point. Table I shows the result of the error for the random function and the results of the error for first position function. Figure 5 shows the error rate in units of meters on each device and comparison functions are used.

The results of a series of trials that have been done show that:

1) Looking at the error position ratio obtained from the three different devices, there is no significant difference in error distance between the device with other devices. This is due to the differences of magnetic value that read by each sensor device has been corrected by a calibration process.
2) There is relatively high value of error obtained on random functions, which reached 116.54 meters. That is because there are several magnetic values identical at different coordinates. The algorithms used in the random function does not compare the new coordinates that obtained with the previous position coordinates, as implemented in the first position function algorithm. So that, algorithms on random function will display the position on the map if there is any value equal or close to the databases magnetic values obtained by the user.
3) Broadly speaking, the searching process and comparison functions are carried out by first position takes longer than random functions. It can be seen that the application will get some delay when updating the location at a time. This delays could become a problem when the user walks so fast and the position has not been updated.

TABLE I. ERROR COMPARISON RESULT

Device	**Random Function**		
	Max. Error (meter)	***Average Error (meter)***	***Std. Dev.***
Xperia X10 mini	116.2	27.1	30.14
Galaxy Chat	116.54	24.51	25.58
Nexian Journey	110.65	24.89	26.77
Device	**First Position Function**		
	Max. Error (meter)	***Average Error (meter)***	***Std. Dev.***
Xperia X10 mini	13.25	6.08	4.28
Galaxy Chat	17.64	7.45	4.05
Nexian Journey	18.83	6.61	3.43

4) Algorithms on random functions comparison focuses on the X-axis, while the algorithm on the function compares first position in both X and Y-axis to find the nearest position. This makes first position function is more accurate for get a new location and does not display the displacement distance is too far when compared with the random function.
5) From the test results, the value of magnetic influence on the Z-axis will be generated if the altitude of the device is not the same. In this research, users are not required to hold the device at a high position. Therefore, if the user holds the device in the same location with a different height, the Z value that obtained by sensor will always be different. Therefore, comparison using the Z-axis value were eliminated.

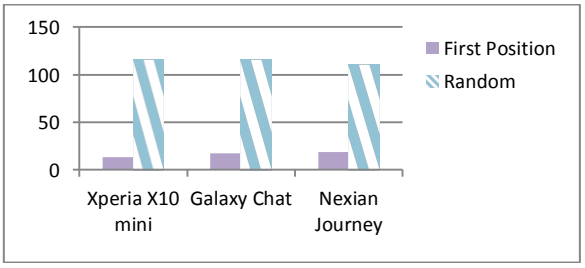

Figure 5. The maximum number of error between devices.

6) Errors or gaps can occur due to magnetic data comparison in the incomplete data-record. When the user is in a position other than horizontal and vertical position, the magnetic values that caught in such position will not match the value of the magnetic owned by the database. Therefore, to get a more accurate position of the user, the magnetic database should be created not only using the horizontal and vertical position only, but also with every axis.

VII. CONCLUSIONS

Earth's magnetic field can be used as a reference for navigation within a building. Magnetic field values obtained from the results of the study have a unique value and there is a pattern of sequential magnetic values at some point the location. This pattern makes first position function has an average error rate of 6.7 meters.

The use of magnetic database as a reference for acquire the user's position is potential to replace one's duty to

accommodate magnetic values. Despite the value of the maximum error at 18.83 meters, the magnetic database has been able to be used as a reference to determine the location of where the users with fairly accurate position. This position errors caused by the reading process on Earth's magnetic field value at a position besides vertical and horizontal directions, which is not stored inside the magnetic database that has been made.

The use of the earth's magnetic field as a navigation reference inside a building gives better results when it's compared with the GPS for navigation inside a building.

REFERENCES

[1] IndoorAtlas Ltd., "Ambient magnetic field-based indoor location technology", pp.1-5, Jul. 2012.

[2] Haris Muhammad A., "Use of Earth's Magnetic Field for Pedestrian Navigation", University Of Calgary, 2011.

[3] James Steele, Nelson To, Shane Conder& Lauren Darcey.*The Android Developer's Collection (Collection)*. Addison-Wesley Professional, 2011.

[4] Binghao Li, Thomas G., Andrew G. Dempster & Chris R., "How feasible is the use of magnetic field alone for indoor positioning?", in *International Conference on Indoor Positioning and Indoor Navigation*, pp. 1-7, Nov. 2012.

[5] Christian B. & Martin K., "Fingerprinting Based Localisation Revisited", in *International Conference on Indoor Positioning and Indoor Navigation*, pp. 1-3, Nov. 2012.

[6] Eung Sun K. & Yong K., "Indoor Positioning System Using Geomagnetic Anomalies for Smartphones", Samsung Advanced Institute of Technology, pp. 1-5, 2012.

[7] Kai K., Gernot B,, Paul L., "Can Magnetic Field Sensors Replace Gyroscopes in Wearable Sensing Applications?*", Embedded Systems Lab University Passau, Passau*, pp1.-4, 2012.

[8] Jeff Hightower, "Mobile Location Technologies", Intel Labs, 2012.

[9] Ivis, F. "Calculating Geographic Distance: Concepts and Methods". In *Proceedings of the 19th Conference of Northeast SAS User Group*, Philadelphia, PA, USA, Sept. 2006.

[10] *Bajaj R.*, S. L. Ranaweera, and D. P. Agrawal, "*GPS*: *Location-Tracking Technology*", *IEEE Computer*, Apr. 2002.

G406

Implementation of Haar Wavelet Transform on Xilinx Spartan-3E FPGA

Risanuri Hidayat[1],Sasmito Aji[2], Litasari[3]
[1,2,3] Department Electrical Engineering, Engineering Faculty University of GadjahMada
University of GadjahMada (UGM)
Jln. Grafika 2 Yogyakarta 55281 INDONESIA

***Abstract*—This paperdiscussesthe efficient and accurate implementation ofthe discreteHaarWavelet Transform (HWT) by selection of the best fit filterbank structure and data format. Implementation ofthe Haarwavelet transform is performed onXilinxSpartan-3E Field ProgrammableGateArray(FPGA) and it is intendedforprocessing of voice signals. By using thelatticefilter bank structureandfixed-point data format, the implementation ofHaar Wavelet Transform withsix decomposition levels require only 5% of FPGA's slices and give accuracy 98.9%.**

Keywords—Discrete Wavelet Transform (DWT), Haar Wavelet Transform (HWT), Field Programmable Gate Array (FPGA), Filter Bank, Data Format, Decomposition.

I. INTRODUCTION

Currentlymanypapers discuss about discrete wavelet transform (DWT)either its usefulnessor its implementation process both insoftwareandhardware. One of thehardwarecan be usedfor theimplementation of theDWT is Field Programmable Gate Array (FPGA). Thereare manypapersthat discussthewavelet transformonFPGAespecially for signal processing and also the optimization to improve the speedandthe efficiency of FPGA's resources[1, 2, 3, 4, 5, 6].

The paperthat focuses on FPGAcan't be separatedfrom theoptimizationto improvethe efficiency of FPGA's resources becausethe resourceswhich availablein theFPGA is limited. So it must be find the techniquesandmethods in order to get optimal, efficient, and accurate of FPGAimplementation. Almost all ofpapers about FPGAalwayshavediscussionaboutcomputing speed, the resources efficiency andalso the result accuracy.

Thereare manypaperdiscussing the implementation and optimization ofDWTonFPGA thatusedforimageandvideoprocessing [2, 4, 6, 7, 8, 9, 10].Inimageandvideoprocessing, DWTis usedforcompressionandde-noising. Besides usedforimage processing, implementation of DWTonFPGAis alsousedforvoicesignalprocessing [11].Althoughthere aremany papers thatimplementDWT on FPGA, there islimited paper that studies about the performance ofthefilterbankstructureand data formatin the DWT.

The study on the filter bank structure and the data format is important to produce an efficient and accurate implementation of DWT. This paper discusses the implementation of filter bank structure and data format in DWT in order to get an efficient and accurateimplementation of DWT. There are two types of filter bank structure that studied i.e.polyphase and lattice and also three types of data formats including one floating point and two fixed point data format. Besides focus on the filter bank structure and data format, this paper also discuss about the effect of the decomposition level on the FPGA's resources. The DWT is implemented on FPGA Xilinx Spartan 3-E (XC3S500E-4FG320)

II. HAAR WAVELET TRANSFORM (HWT)

In the analysis process ofDWT, the input signal x[k] entered into the low pass filter (L) and highpass filter (H). Those filters separate the signal into low and high frequency with the same length and number of data. To eliminate data redundancy, the filtering stage is followed by down sampling (↓). In the synthesis process, the signal will be up sample (↑) and then passed to low pass filter (L ') and highpass (H'). The process of DWT is show in Fig.1. Low pass and high pass filter of HWT is shown in (1) [12].

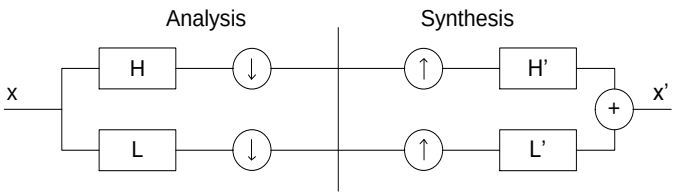

Fig. 1. Analysis and Reconstruction of DWT [13]

$$L=\left[\frac{1}{\sqrt{2}} \quad \frac{1}{\sqrt{2}}\right] \qquad H=\left[\frac{1}{\sqrt{2}} \quad -\frac{1}{\sqrt{2}}\right]$$
$$L'=\left[\frac{1}{\sqrt{2}} \quad \frac{1}{\sqrt{2}}\right] \qquad H'=\left[-\frac{1}{\sqrt{2}} \quad \frac{1}{\sqrt{2}}\right] \quad (1)$$

A. Filter Bank Structure

Toperformthe HWT, low passandhigh passfilter must bearranged to formfilter bank. Filter bank structure affects thecomputationso thatthe selection of the best fit filter bank structure can giveoptimal computation. There areseveraltypes offilterbanks structure such as direct form, polyphase, lattice, andlifting. Inthis paper will be focused on polyphase and lattice filter bank structure. Polyphaseand thelattice filter bankis shownin Fig.2and Fig.3. Those filter bankscan be expressedby(2) and(3).

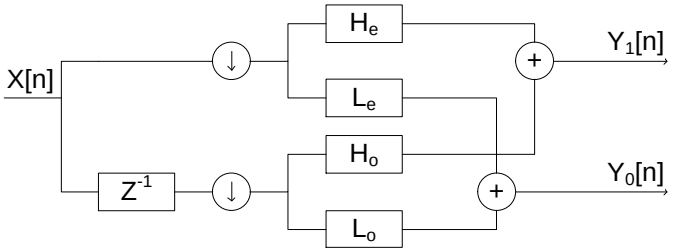

Fig. 2.PolyphaseFilterbank Structure

$$\begin{bmatrix} Y_0 \\ Y_1 \end{bmatrix}=\begin{bmatrix} L_e & L_o \\ H_e & H_o \end{bmatrix}\begin{bmatrix} X_e \\ z^{-1}X_o \end{bmatrix}=\begin{bmatrix} \frac{1}{\sqrt{2}} & \frac{1}{\sqrt{2}} \\ \frac{1}{\sqrt{2}} & -\frac{1}{\sqrt{2}} \end{bmatrix}\begin{bmatrix} X_e \\ z^{-1}X_o \end{bmatrix} \quad (2)$$

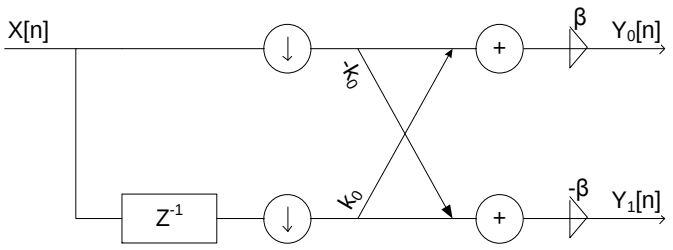

Fig. 3.Lattice Filterbank Structure

$$\begin{bmatrix} Y_0 \\ Y_1 \end{bmatrix}=\begin{bmatrix} \beta & k_0\beta \\ k_0\beta & -\beta \end{bmatrix}\begin{bmatrix} X_e \\ z^{-1}X_o \end{bmatrix} \; with\; k_0=1 \;\&\; \beta=\frac{1}{\sqrt{2}} \quad (3)$$

B. Data Format

The data format influences the result accuracy of HWT. The data format shall be compromised to computational resources. There are three types ofdata formatthat studied including of two types of fixed point data formats and the floating point data format. The data format is shown in Fig. 4, Fig. 5 and Fig. 6. In the fixed-point data formats, there are 18-bit data, consist of sign bit, integer and fraction. One fixed-point data format consists of a 3-bit integer and 14-bit fraction and called Fixed Point-I, while anotherfixed point data format consists of a 4-bit integer and 13-bit fraction and called as Fixed Point-II. The floating point data will consist of a 1-bit sign (S), 8-bit exponent (Exp) and 23-bit mantissa (M). And can be expressed with floating point can be expressed by (4) [14].

$$N=(-1)^S 2^{(Exp-127)} M \quad (4)$$

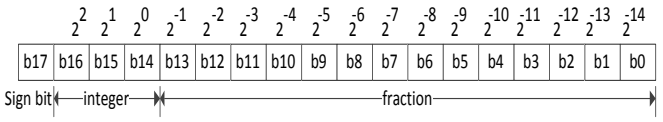

Fig. 4.Data Format Fixed Point-1

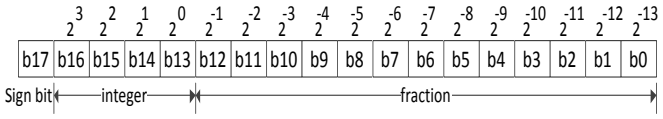

Fig. 5.Data Format Fixed Point-II

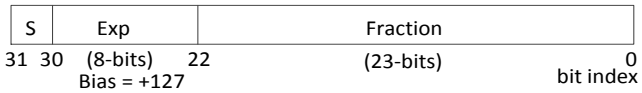

Fig. 6.Data Format Single Precision Floating Point[14]

III. METHODOLOGY

The implementation of HWT includes implementation on software and FPGA. Implementation of HWT on software is required to get data reference as comparison for implementation of HWT on FPGA. To perform HWT on FPGA, the input datais entered to FPGA from computer by using serial communication and the result of HWT will be sent back from FPGA to the computer in the same serial communication lines. As input datais used voice signals that originating from the pronunciation of the vowel "I". This voices signal is saved in wav format and cut into 64 data points. Each data point is represented by 18-bit fixed point or 32-bit single precision floating point.

To givean optimal and efficient of HWT, the best fit of filter bank structure, data format and the decomposition level is selected. Some HWT programs with different filter bank structures, data formats, and decomposition level are written and implemented on FPGA by using Verilog HDL. The usage of FPGA's resources including slice flip-flop, Look Up Table (LUT), slice, Input Output Block (IOB), Random Access Memory (RAM) and Multiplier arestudied for different implementation.The computation process of HWT on the FPGA can be illustrated by Fig. 7.

The implementation of HWT with the minimal use of FPGA'sresources will give better efficiency. Beside of efficiency aspect, thispaper also examines the accuracy of

HWT implementation. The accuracy is obtained by comparing the HWT results with data reference. The input data come from voice signal is entered to FPGA and the result of HWT on FPGAs is sent back to computer to be compared todata reference in order to get accuracy.

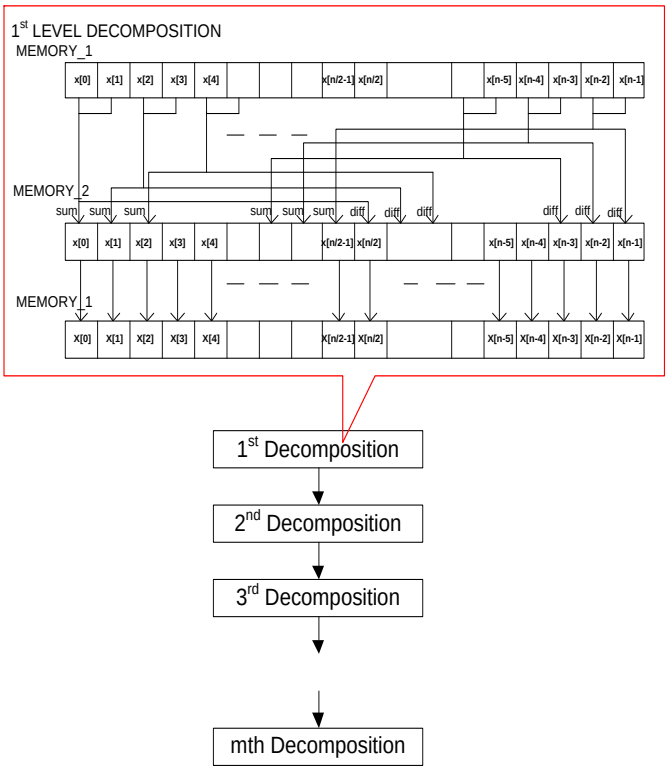

Fig. 7. Decomposition Process on FPGA

IV. RESULT AND DISCUSSION

An efficient of HWT is obtained by the selecting filter bank structure, data format, and the decomposition level.

A. Selection of Filter Bank Structure

There are two filter bank structures that studied, they are polyphase and lattice. FPGA's resources required to implement the HWT with polyphase filter bank structures is shown in Table I and for lattice filter bank structure is shown in Table II. From Table I and Table II, it can be obtained that the lattice structure requires less of FPGA resources.So lattice structure is more efficient than polyphase structure. If both implementation of HWT are tested, it give 99.67% accuracy (error = 0.33%) for the polyphasestructure and 99.65% accuracy (error = 0.35%) for the lattice structure.Both implementations of HWTwith polyphase and lattice structure give good accuracy.

TABLE I. RESOURCES FOR HWT WITH POLYPHASE FILTERBANK STRUCTURE

Logic Utilization	Decomposition [a]	Total Program [b]
No. of Slice Flip-Flop (max. 9312)	339 (3%)	653 (5%)
No. of LUT (max. 9312)	471 (5%)	1553 (16%)
No. of Slice (max. 4656)	287 (6%)	862 (18%)
No. of IOB (max. 232)	42 (18%)	13 (5%)
No. of RAM (max. 20)	3 (15%)	3 (15%)
No. of Multiplier 18x18 (max. 20)	4 (20%)	4 (20%)

a. Resource required for decomposition program
b. Resource required for total program including Input data processing, decomposition, and output data processing

TABLE II. RESOURCES FOR HWT WITH LATTICE FILTERBANK STRUCTURE

Logic Utilization	Decomposition [a]	Total Program [b]
No. of Slice Flip-Flop (max. 9312)	160 (1%)	478 (5%)
No. of LUT (max. 9312)	346 (3%)	1417 (15%)
No. of Slice (max. 4656)	190 (4%)	763 (16%)
No. of IOB (max. 232)	42 (18%)	13 (5%)
No. of RAM (max. 20)	2 (10%)	2 (10%)
No. of Multiplier 18x18 (max. 20)	1 (5%)	1 (5%)

B. Selection of Data Format

Thereare threedata formatsthat studied including fixedpoint-I, fixedpoint-II, and singleprecisionfloating point. The implementation of HWT with three types of data format use lattice filter bank structure. Latticefilter bank structure givesefficientimplementation of HWT based on part IV.A.The FPGA's resourcesrequired for implementation of HWT with three type data format are shown in Table III, Table IV, and Table V.

TABLE III. RESOURCES FOR HWT WITH FIXED POINT- I DATA FORMAT

Logic Utilization	Decomposition [a]	Total Program [b]
No. of Slice Flip-Flop (max. 9312)	160 (1%)	478 (5%)
No. of LUT (max. 9312)	346 (3%)	1417 (15%)
No. of Slice (max. 4656)	190 (4%)	763 (16%)
No. of IOB (max. 232)	42 (18%)	13 (5%)
No. of RAM (max. 20)	2 (10%)	2 (10%)
No. of Multiplier 18x18 (max. 20)	1 (5%)	1 (5%)

TABLE IV. RESOURCES FOR HWT WITH FIXED POINT-II DATA FORMAT

Logic Utilization	Decomposition [a]	Total Program [b]
No. of Slice Flip-Flop (max. 9312)	160 (1%)	478 (5%)
No. of LUT (max. 9312)	346 (3%)	1417 (15%)
No. of Slice (max. 4656)	190 (4%)	763 (16%)
No. of IOB (max. 232)	42 (18%)	13 (5%)
No. of RAM (max. 20)	2 (10%)	2 (10%)
No. of Multiplier 18x18 (max. 20)	1 (5%)	1 (5%)

TABLE V. RESOURCES FOR HWT WITH FLOATING POINT DATA FORMAT

Logic Utilization	Decomposition [a]	Total Program [b]
No. of Slice Flip-Flop (max. 9312)	1789 (19%)	2187 (23%)
No. of LUT (max. 9312)	1930 (20%)	3411 (36%)
No. of Slice (max. 4656)	1422 (30%)	2221 (47%)
No. of IOB (max. 232)	70 (30%)	13 (5%)
No. of RAM (max. 20)	2 (10%)	2 (10%)
No. of Multiplier 18x18 (max. 20)	4 (20%)	4 (20%)

Based on Table III, Table IV, and Table V, both fixedpoint data formats require the same number of resources even though the data formats havedifferent number of integer and fraction. So the fixed point data format will require the same number of resourcesas long as it has the same data size. The

floating point data format requires more resources compared to fixed point data formats. As the example, the total FPGA slice required for floating point data format is 600% higher than fixed point data formats. Although thenumber of FPGA'sresources in floating point data format is higher, the floating point data format offers excellent accuracy and very wide data range. Those advantages are not owned by the fixed point data format.

In the fixed point data format,data range and accuracy sometimes give opposite direction or effect. To get better accuracy, the number of fraction shall be increased, but this will make narrower data range. Therefore before usingfixed point data format, the inputdata range and the expected accuracy shall be considered and compromised. After that the appropriate fixed point data format can be determined.

Considering the large number of FPGA's resources which is required for implementation of HWT with floating point data format, then the usage of fixed point data format is good choice. Beside efficient in the usage of FPGA's resources, the implementation of HWT with fixed point data format can also give good accuracy. As the evidence, when using fixed point data format with lattice structure for implementation of HWT, its accuracy is 99.65%(as per part IV.A).

C. Effect of Decomposition Level on FPGA Resources

It has been implemented the HWT with several decomposition level from 1st up to 6th decomposition level. The implementation of HWT uses lattice structure and fixed point data format. The numbers of FPGA's resources required for implementation are shown in Table VI to TableX. The FPGA'sresource for implementation of HWT with 1st decomposition has been shown in Table IV.

TABLE VI. RESOURCES FOR HWT WITH 2ND DECOMPOSITION LEVEL

Logic Utilization	Decomposition[a]	Total Program [b]
No. of Slice Flip-Flop (max. 9312)	168 (1%)	485 (5%)
No. of LUT (max. 9312)	385 (4%)	1462 (15%)
No. of Slice (max. 4656)	208 (4%)	789 (16%)
No. of IOB (max. 232)	42 (18%)	13 (5%)
No. of RAM (max. 20)	2 (10%)	2 (10%)
No. of Multiplier 18x18 (max. 20)	1 (5%)	1 (5%)

TABLE VII. RESOURCES FOR HWT WITH 3RD DECOMPOSITION LEVEL

Logic Utilization	Decomposition[a]	Total Program [b]
No. of Slice Flip-Flop (max. 9312)	176 (1%)	492 (5%)
No. of LUT (max. 9312)	434 (4%)	1506 (16%)
No. of Slice (max. 4656)	236 (5%)	811 (17%)
No. of IOB (max. 232)	42 (18%)	13 (5%)
No. of RAM (max. 20)	2 (10%)	2 (10%)
No. of Multiplier 18x18 (max. 20)	1 (5%)	1 (5%)

TABLE VIII. RESOURCES FOR HWT WITH 4TH DECOMPOSITION LEVEL

Logic Utilization	Decomposition[a]	Total Program [b]
No. of Slice Flip-Flop (max. 9312)	186 (1%)	505 (5%)
No. of LUT (max. 9312)	428 (4%)	1502 (16%)
No. of Slice (max. 4656)	230 (4%)	807 (17%)
No. of IOB (max. 232)	42 (18%)	13 (5%)
No. of RAM (max. 20)	2 (10%)	2 (10%)
No. of Multiplier 18x18 (max. 20)	1 (5%)	1 (5%)

TABLE IX. RESOURCES FOR HWT WITH 5TH DECOMPOSITION LEVEL

Logic Utilization	Decomposition[a]	Total Program [b]
No. of Slice Flip-Flop (max. 9312)	189 (2%)	506 (5%)
No. of LUT (max. 9312)	467 (5%)	1529 (16%)
No. of Slice (max. 4656)	250 (5%)	820 (17%)
No. of IOB (max. 232)	42 (18%)	13 (5%)
No. of RAM (max. 20)	2 (10%)	2 (10%)
No. of Multiplier 18x18 (max. 20)	1 (5%)	1 (5%)

TABLE X. RESOURCES FOR HWT WITH 6TH DECOMPOSITION LEVEL

Logic Utilization	Decomposition[a]	Total Program [b]
No. of Slice Flip-Flop (max. 9312)	193 (2%)	511 (5%)
No. of LUT (max. 9312)	518 (5%)	1601 (17%)
No. of Slice (max. 4656)	276 (5%)	858 (18%)
No. of IOB (max. 232)	42 (18%)	13 (5%)
No. of RAM (max. 20)	2 (10%)	2 (10%)
No. of Multiplier 18x18 (max. 20)	1 (5%)	1 (5%)

If Table IV and Table VI to Table X are described in graphics, it will be obtained Fig. 8. From Fig. 8, it clear thatthe increasingof decompositionlevel does not significantly affectto the increasing of FPGA resources.At6thdecomposition level, the implementation of HWTonly require FPGA resources that1% higher compared to the implementation of HWT with 1st decomposition level. When tested, the HWT with 6th decomposition level give 98.13% accuracy forfixed point-Idata formatand98.90% forfixed point-IIdata format.

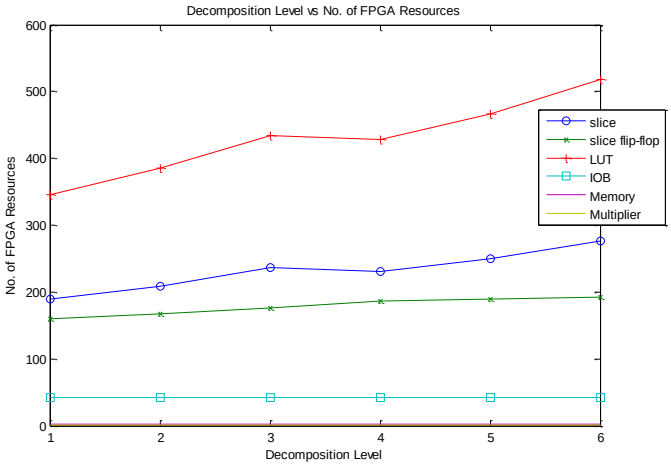

Fig. 8. Decomposition level and Resources of FPGA

Based on part IV.A, IV.B and IV.C, the implementation of HWT requires small number of FPGA's resources if it uses an appropriate filter bank structure and data format. By using the lattice structure and fixed point data format, the implementation only require 4% of slice for HWT with 1st decomposition level and 5% of slice for HWT with 6thdecomposition level. Lattice structure canreduce the computation, reduce memory usage and reduce multiplier significantly. It only needs two memories and single multiplier to implement HWT with the lattice structure.

The data format affects the usage of FPGA's resources. Single precision floating point data format offers excellent accuracy and wide data range, but require more FPGA's resources. As an example the number of slice required for floating point data format is 600% higher than fixed point data format. Fixed point data format requires less of FPGA, so it more efficient. Beside that, it can give good accuracy as long as the number of integer and fractionis matched to the range of signal to be processed. Although fixed point data format has different number of integer and fraction, the HWT will requiresame number of FPGA's resources as long asthat fixed point data format has same data width.

An increasing of decomposition level does not increase the number of FPGA resources significantly. Because when decomposition level increases, the number of data being processed decreases into half of the original number. The implementation of HWT with 6thdecomposition level only requires FPGA's resources 1% higher compared to HWT with 1st decomposition level. But at 6thdecomposition level, the accuracyis decreasing to 98.9% from 99.67% at 1st decomposition level. The decreasing of accuracy is affected by rounding error propagationthat occurs from the 1stdecomposition level up to 6thdecomposition level.

V. CONCLUSION

This paper successfully implements the discrete HWT on Xilinx Spartan-3E FPGA (XC3S500E FG320) with good efficiency and accuracy. An efficient and accurate HWT implementation is obtained by selectingthe best fit filter bank structure and data format. Lattice structure and fixed point data format give efficient and accurate implementation of HWT. Beside that the decomposition level will not increase the usage of FPGA's resources significantly. The implementation of HWT with 6thdecomposition level only requires5% of slices and gives 98.9% of accuracy. The efficient and accurate implementation of HWT will provide flexibility for further development of HWT especially for more complex signal processing.

REFERENCES

[1] M. Angelopoulou, K. Masselos, P. Cheung and Y. Andreopoulos, "A Comparison of 2-D Discrete Wavelet Transform Computation Schedules on FPGA," 2006.

[2] Q. Huang, Y. Wang and S. Chang, "High Performance FPGA Implementation of Discrete Wavelet Transform for Image Processing," 2011.

[3] M. Guarisco, X. Zhang, H. Rabah and W. Serge, "An Efficient Implementation of Scalable Architecture for Discrete Wavelet Transform On FPGA," in *IEEE*, 2007.

[4] M. Katona, A. Pizurica, N. Teslic, V. Kovacevic and W. Philips, "FPGA Design and Implementation of a Wavelet Domain Video Denoising System".

[5] P. Gupta and S. K. Lenka, "A Novel VLSI of Architecture of High Speed 1D Discrete Wavelet Transform," *International Journal of Electrical and Electronic Engineering (IJEEE)*, vol. 3, no. I, pp. 79-85, 2013.

[6] H. Sahoolizadeh and A. Keshavarz, "A FPGA Implementation of Neural / Wavelet Face Detection System," *Australian Journal of Basic and Applied Science*, pp. 379-388, 2010.

[7] A. Benkrid, K. Benkrid and D. Crookes, "Design and Implementation of a Generic 2-D Orthogonal Discrete Wavelet Transform on FPGA," in *11th Annual IEEE Symposium of Field Programmable Custom Computing Machine (FCCM'03)*, 2003.

[8] K. H. Talukder and K. Harada, "Haar Wavelet Based Approach for Image Compression and Quality Assessment of Compressed Image," *IAENG International Journal of Applied Mathematics*, 2006.

[9] R. M. Jiang and D. Crookes, "FPGA Implementation of 3D Discrete Wavelet Transform for Real-Time Medical Imaging," IEEE, 2007.

[10] A. Ahmad, P. Nicholl and B. Krill, "Dynamic Parial Reconfiguration of 2-D Haar Wavelet Transfrom (HWT) for Face Recognition System".

[11] J. Chilo and T. Lindblad, "Hardware Implementation of 1D Wavelet Transform on an FPGA for Infrasound Signal Classification," in *IEEE Transaction on Nuclear Science Vol. 55*, 2008.

[12] M. Vetterli and J. Kovacevic, Wavelet and Suband Coding, New Jersey: Prentice Hall PTR, 2007.

[13] M. Steinbuch and M. Van de Molengraft, Wavelet Theory and Application a Literature Study, Eindhoven: Eindhoven University Technology Department of Mechanical Engineering Control System Group, 2005.

[14] R. Wood, J. McAllister, G. Lightbody and Y. Yi, FPGA-based Implementation of Signal Processing Systems, Wiltshire, United Kingdom: John Wiley & Sons, 2008.

G407

A Robust Method of Encryption and Steganography Using ElGamal and Spread Spectrum Technique Based on MP3 Audio File

Priadhana Edi Kresnha
Department of Informatics Engineering
University of Muhammadiyah Jakarta
Central Jakarta 10510
priadhana.edi@informatika.ftumj.ac.id

Aini Mukaromah
Faculty of Computer Science
University of Mercu Buana
Kebon Jeruk, West Jakarta 11650
ainialmukaromah@yahoo.co.id

***Abstract*—Security is one of the most important things to be considered when exchanging message, particularly when the message exchanged is top secret message. In this research, a tool is developed to encrypt the message and hide it into a digital object. Encryption method used is ElGamal Encryption, and the object where the message hidden is mp3 audio file. The part in mp3 file used for attaching the message is homogenous frame. This process is enhanced with spread spectrum method and pseudo noise modulation to make the encrypted message more randomized and harder to decrypt. The result shows that the sound quality of the original file and stego-file are almost the same. The noise produced by the message is measured by calculating Error rate and PSNR (Peak Signal to Noise Ratio) between original file and stego-file.**

Keywords—Encryption; Mp3 file; Spread Spectrum; Steganography; Stego-Object;

I. INTRODUCTION

Security is one of the most important things to be considered when exchanging message, particularly when the message exchanged is top secret message. The importance of concealing the message has been considered since ancient age which makes the theory of cryptography becomes one of the oldest theories that human made.

One of the oldest cryptography methods which have ever been made is Caesar cipher. It is also known as shift cipher, Caesar's code, or Caesar shift. It is one of the simplest and most widely known encryption techniques. It works by shifting the order of the alphabet by some fixed number. Other advance shifting method was then discovered. The newer one uses key to shift the order of alphabet. The example of this one is vigenere encryption.

Along with encryption, steganography as a method to conceal the message has been emerged as well. Differ from encryption which converts the message into unreadable form, steganography tries to hide a message into an object. The oldest steganography method was hiding the message on a courier head. Before writing the message on the courier head, his hair had to be cut. The message was then written on his bald head. After writing the message, the courier had to be quarantined for approximately three months, while waiting until the hair grew up again. The courier would be sent to the field commander to convey the message from the supreme leader. Later on the courier had to be killed to prevent the message uncovered by unauthorized person.

In this research, both encryption and steganography are used to conceal the message. Encryption is used so that no unauthorized person can read the message, and steganography is used so that no unauthorized person realizes that the object being sent contains a message, thus an effort to break encryption codes or do cryptanalysis action can be avoided. This way, exchanging message can be more secure.

There are several studies on cryptography and steganography technique, particularly digital steganography. The most used digital steganography technique is Least Significant Bit (LSB). This technique manipulates bits which give insignificant changes when they are modified. It has been generally known that computer processes data in digital form which consists of bit 0 and 1 only. The bits are combined to represent a single value of data. I.e. a character is represented by the combination of 8 bits (1 byte). Therefore a character can be valued from 0 to 255.

In digital file, particularly multimedia file, a single value data can be represented by various numbers of bits. I.e.jpeg file, each pixel of every channel (Red, Green, and Blue) is represented by 8 bits. By changing the least significant bit, the modification cannot be seen clearly. For example, if the red value of the pixel is 255, after the least significant bit has been changed, it becomes 254. For human, this changed will not affect the sense of the picture. But if the modified bit is the most significant bit, the value will decrease into 128 and this will drastically change the sense of the picture. This kind of technique has been conducted by [1,2,3].

LSB is able to be implemented in audio file as well. In [1] MPEG formatted Audio becomes the cover file to conceal the message. It uses two-steps algorithm to embed watermark bits into higher LSB layers. However in that paper no encryption method is implemented to enhance message security. In [4] LSB is implemented to hide the message into uncompressed digital audio, but again, it is not enhanced by encryption technique to increase security level. In [3], LSB audio steganography and encryption techniques are implemented. The encryption process uses sum of all ASCII form of the key to create XOR modulation bits. These bits become the encryption key, and the encryption is done by doing XOR modulation between bits form of the message and XOR operator bits. The used key is symmetric key, so the sender and recipient share the same key. When decrypting the message, the recipient inserts the same key as the sender did when he encrypt the message.

In this research, combination of various encryption and steganography techniques are conducted to provide more powerful message concealing method. The file used for steganography is mp3 audio file. Audio file is chosen since the capacity is bigger than text or image file, and it is not as complicated as video file. Mp3 format is chosen since it is the most widely known and used compared to other audio formats. Another steganography studies using Mp3 file format have been conducted by [5,6,7,8]. Encryption method used in this research is ElGamal Encryption. The encrypted message is embedded in the homogenous frames of mp3 audio file. Before embedding the message into the file, the encrypted message is enhanced with spread spectrum method and XOR modulation to improve its randomness. This way, the security of the message can be improved without significantly affecting the quality of audio file.

This paper consists of several parts; Section 2 contains general information about encryption and steganography method. Detailed process of encryption is explained in section 3. Steganography process is explained in section 4 and its subsections. Quality measurement technique to assess stego-object is elaborated in section 5. Implementation of the method and its result is explained in section 6. The last section, section 7, contains conclusion and further development of the system.

II. METHODS

Generally, steganography process is described in Fig 1. First, cover object has to be prepared, and then the message is inserted into that cover object using some key. After the cover object has been inserted by the message and become stego-object, this stego-object is sent to the recipient. The recipient will open this stego-object using some key, and derive the message from the object.

In the proposed method, steganography is combined with other encryption technique to improve its security. The process of the proposed method is shown in Fig 2. First, cover object and message have to be prepared. The message is then encrypted using ElGamal Encryption. Encryption result is then converted into bits. In this bit form, the bits are spread using spread spectrum technique and modulated by pseudo noise signal. This noise signal is the XOR modulator which used to randomize the encrypted bits. The result of modulation is then inserted into mp3 file as noise. Mp3 file which has been inserted by the message is called stego-audio.

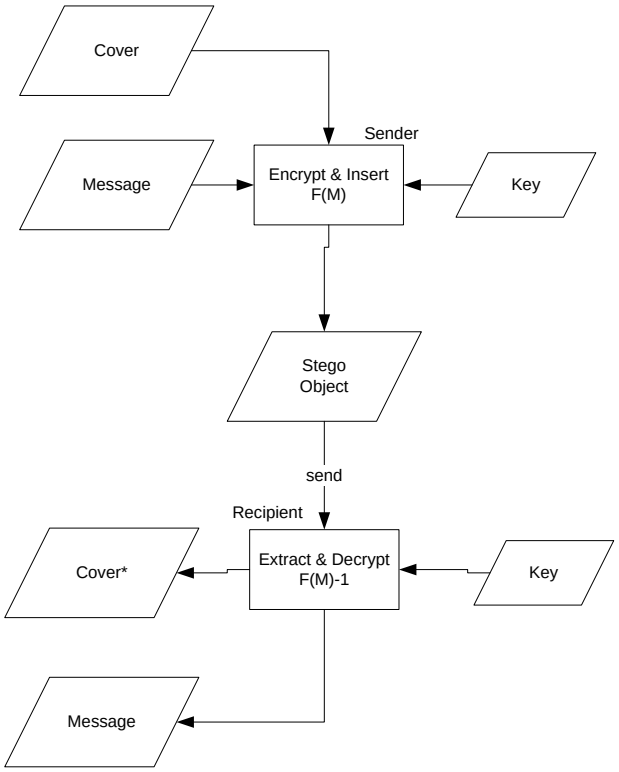

Fig. 1. General Steganography Process.

III. ENCRYPTION

Encryption method used in this research is ElGamal encryption. Elgamal Encryption is an asymmetric key encryption algorithm based on the Diffie-Hellman key exchange. Unlike [3], this research uses asymmetric key to encrypt the message. The sender and the recipient don't share the same key. The sender encrypts the message using recipient's public key, and the recipient decrypts the encrypted message using his own private key.

Elgamal encryption was originally used for digital signature, but was later modified so it can be used for encryption and decryption. Elgamal is currently used in security software developed by GNU Privacy Guard, recent versions of PGP. The security of this algorithm lies in the difficulties to solve discrete algorithm problem [9,10].

Discrete algorithm problem : *if p is prime number, g and y are random natural numbers, find x which satisfies following formula,*

$$g^x \equiv y(\mathrm{mod}\ p) \quad (1)$$

IV. STEGANOGRAPHY

There are several processes conducted before embedding the message into the file. First, converts the encrypted message

into bits form. Conversion is done for each character, and each encrypted character is not necessarily consists of 8 bits. It depends on the number of bits used in ElGamal encryption process. Normally, the number of bits used in encryption process is 64 bits. It means that a place consists of 64 bits must be prepared in stego-file for each character. This makes the length of the message become a major issue, since the capacity of stego-file to store the message is very limited, depends on the number of homogeneous frames provided by the stego-file. The more bits used for each character, the less number of characters can be inserted into the same file. Therefore the number of bits used in the encryption process is decided no more than 15 bits. This way, a longer message can be inserted into the file

After converting the message into bit form, spread spectrum process is done to the message, followed by XOR modulation and insertion into the file. Those processes are explained in the following subsections.

A. Spread Spectrum

In Spread Spectrum technique, secret message is encoded and spread to every available frequency spectrum. It transmits a narrow information signal band in a broad band channel [5,11].

In the steganography process, signal spreading is used to increase the level of redundancy. Redundancy magnitude is determined by a *cr* scalar multiplier. The length of the message bit after spreading is *cr* times of its initial length.

B. XOR Modulation

In this process, the enrypted message which has been converted into bits form and spread with some spreading coefficient (*cr*) is modulated by *pseudo-noise signal*. This *pseudo-noise signal* is generated randomly using *Linear Congruential Generation* (LCG) algorithm [12]. LCG is one of the oldest and best known pseudorandom generator algorithm. The generator is defined based on the following recurrence equation:

$$x_{n+1} = (ax_n + b)(\mathrm{mod}\, m) \qquad (2)$$

Where

$0 < m$, m is the modulus

$0 < a < m$ is the multiplier

$0 \le b < m$ is the increment

x_n is the current sequence of pseudo random value

x_{n+1} is the next sequence of pseudo random value

.

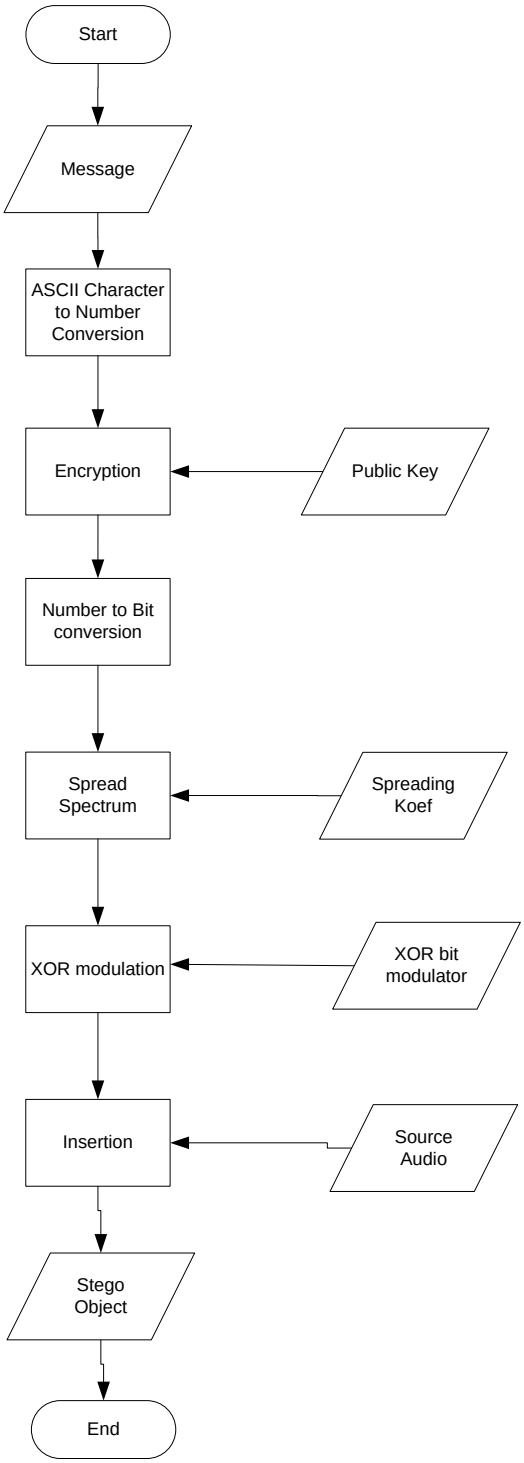

Fig. 2. Steganography Process in this study.

C. MP3 Homogenous Frame

The part of mp3 file which is used to embed the message is homogeneous frame. This frame consists of bit 1 only.If it is converted into the decimal,the value in this frame simply contains -1. Not every mp3 file has homogeneous frame. Therefore not all mp3 files can be inserted by the message.

Only files with homogeneous frames are able to be inserted by the message.

Homogenous frame can be seen as multiple '*ff*' character in some part of mp3 file. The example is shown in Fig.3.

Fig. 3. Homogenous Frame in an Mp3 File.

After inserting the message into the file, the homogenous frame in Fig.3 becomes Fig.4.

Fig. 4. Homogenous Frame After Inserted By Message.

The length of the message after encryption and steganography process, and ready to be inserted into the file can be computed using the following formula,

$$L = n * \omega * cr \tag{3}$$

Where L is message length (in bits), n is the number of characters in the message, ω is the number of bits used in encryption process, and cr is spread spectrum coefficient ratio.

On the other hand, The capacity provided in mp3 file to insert message can be calculated as follows,

$$SP = \tau * 8 * \varsigma - \left(2 * \left(\xi + \zeta\right)\right) \tag{4}$$

Where SP is the capacity provided, τ is the number of homogenous frame, ς is the number of byte provided in each frame, ξ is the number of header bit, and ζ is the number of footer bit.

To check whether the message can be inserted or not, the result of equation 3 and 4 are substracted using the following formula,

$$RS = SP - L \tag{5}$$

Where RS is remained message space. If $RS \geq 0$, then the message can be inserted.

V. Quality Audio Measurement

Two techniques are used to measure the quality of the audio, subjective and objective. Subjective measurement is done by listening to the stego-file and compare it with the initial file, while objective measurement is estimated by computing Error rate and PSNR (Peak Signal to Noise Ratio) of stego-file.

Error rate is calculated using this following formula,

$$ER = \frac{1}{m}\sum_{i=1}^{m}\left|x_1(i) - x_0(i)\right| \tag{6}$$

andPSNR is calculated using the following formula,

$$PSNR = 10 *^{10} \log\left(\frac{\sum_{i=1}^{m} x_1^2}{\sum_{i=1}^{m}\left(x_1 - x_0\right)^2}\right) \tag{7}$$

Where x_0 is the cover signal intensity and x_1 is the stego signal intensity.

A good audio quality is achieved when the error rate is low while the PSNR is high. Lower error rate and higher PSNR means better stego-object audio quality.

VI. Implementation and Result

Several mp3 files and messages are prepared to test the system. Mp3 files and their information are listed in Table I, while messages and their size after encryption and spread spectrum process are listed in Table II.

TABLE I. MP3 File with various size for testing

Name	File Size (bytes)	Capacity (bytes)
Mary.mp3	1423176	2576
Converstion.mp3	2152590	3976
Relaxing_instrumental_music.mp3	2357255	133288
Maid with the Flaxen Hair.mp3	4113874	1004065
Sleep Away.mp3	4842585	1436464

TABLE II. Message with various size for testing

Name	Size (bytes)
Coy knows pseudonoise codes	1620
Can you can a can as a canner can can a can?	2640
Send toast to ten tense stout saints' ten tall tents	3120
Six sick hicks nick six slick bricks with picks and sticks	3480
Peter Piper picked a peck of pickled peppers. A peck of pickled peppers Peter Piper picked. If Peter Piper picked a peck of pickled peppers, Where's the peck of pickled peppers Peter Piper picked?	11760

To simplify the writing, each mp3 file is represented from 1 (*mary.mp3*) to 5 (*Sleep Away.mp3*), and the message is

represented from A (*Coy knows pseudonoise codes*) to E (*Peter Piper picked a peck of pickled peppers. A peck of pickled peppers Peter Piper picked. If Peter Piper picked a peck of pickled peppers, Where's the peck of pickled peppers Peter Piper picked?*). Errorrate and PSNR of the combination between mp3 file and the message are shown in Table III and IV.

TABLE III. ERROR RATEMATRIX

Mp3\Msg	A	B	C	D	E
1	0.0016	-	-	-	-
2	$1.5x10^{-4}$	$2.2x10^{-4}$	$2.7x10^{-4}$	$2.8x10^{-4}$	-
3	$7.5x10^{-4}$	$9.5x10^{-4}$	$1.2x10^{-3}$	$1.5x10^{-3}$	$4.9x10^{-3}$
4	$3.3x10^{-6}$	$5.8x10^{-6}$	$7.2x10^{-6}$	$7.6x10^{-6}$	$3.1x10^{-5}$
5	$6.8x10^{-6}$	$9.0x10^{-6}$	$1.1x10^{-5}$	$1.2x10^{-5}$	$2.5x10^{-5}$

TABLE IV. PSNR MATRIX

Mp3\Msg	A	B	C	D	E
1	17.9851	-	-	-	-
2	26.5147	25.1752	24.4314	24.4003	-
3	19.8028	19.5011	18.0854	16.8738	11.2900
4	59.3997	56.0651	54.7537	54.4367	48.2227
5	58.1832	57.7936	57.1564	56.7710	53.5136

The result shows that there is a tendency more file size and capacity makes error rate lower and PSNR higher. On the other hand, more message size makes error rate higher and PSNR lower. The graphic of the result can be seen in Fig.5 and 6. To make it easy to see, the value in error rate graph is converted into log10 and added by 6.

In first mp3 file experiment, only first message can be inserted into the file. Other message cannot be inserted since the capacity for carrying the message is not big enough. Therefore neither error rate nor PSNR can be estimated. The same goes with second mp3 for last message.

The advantage of this steganography technique is that the size of stego-object does not change. It does not increase nor decrease, because it modifies the file in bit level, not byte nor signal magnitude.

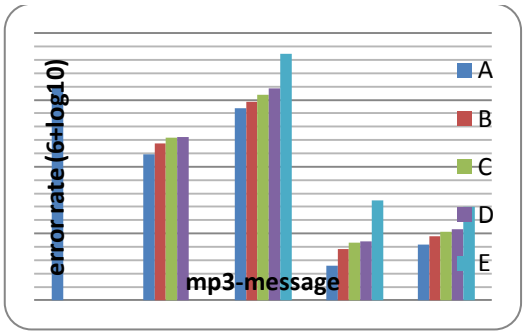

Fig. 5. Error Rate Graph

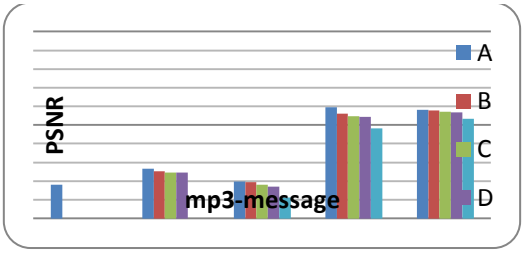

Fig. 6. PSNR Graph

VII. CONCLUSIONS

Elgamal Encryption and Steganography using spread spectrum and pseudonoise modulation have been successfully implemented in this research. The quality of stego-file is estimated using error rate and PSNR. The quality depends on file size and message length. The experiment shows there is a tendency that PSNR becomes lower and error rate becomes higher when the size of stego-file is smaller or the length of the message is larger. The less PSNR is, the lower quality stego-file will be obtained. The advantage of this technique is stego-file size does not change. It makes the quality of stego-file can be maintained and reduces the suspicion towards the stego-file.

ACKNOWLEDGMENT

The authors would like to thank Department's head and Faculty's Dean for the support to join the 1st AEMT conference. This research was funded in part by Faculty of Engineering University of Muhammadiyah Jakarta (http://ftumj.ac.id/).

REFERENCES

[1] Cvejic, N., and Seppanen, T, "Increasing Robustness of LSB Audio Steganography Using A Novel Embedding Method", in *The International Conference on Information Technology : Coding and Computing (ITCC'04)* IEEE, 2004.

[2] Pangaribuan, F, "Application Development of Encrypted Message Concealment Using Mars Method on Image with LSB Image Zang Method", B.S. thesis, Department of Informatics and Electro Engineering, Bandung Institute of Technology, Bandung, Indonesia, 2008.

[3] Sridevi, R., Damodaram, A., Narasimham, S, "Efficient Method of Audio Steganography by Modified LSB Algorithm and Strong Encryption Key with Enhance Security", Journal of Theoretical and Applied Information Technology (www.jatit.org), 2009.

[4] Utami, E, "Steganography Application Based on Least Bit Modification Approach Using Uncompressed Digital Audio File", Journal of DASI, Vol. 10, No. 1, 2009.

[5] Baskara, T, "The Study and Implementation of Steganographic Based on MP3 Audio Using Spread Spectrum Technique", B.S. thesis, Department of Informatics and Electro Engineering, Bandung Institute of Technology, Bandung, Indonesia, 2008.

[6] Herianto, "Cryptography Software Development Based on MP3 Audio File Using Parity Coding Technique in Mobile Phone Device", B.S. thesis, Department of Informatics and Electro Engineering, Bandung Institute of Technology, Bandung, Indonesia, 2008.

[7] Atoum, M., S., Ibrahim, S., Sulong g., M-Ahmad., A. "MP3 Steganography: Review", IJCSI International Journal of Computer Science Issues, Vol. 9, Issue 6, No 3, November 2012.

[8] Pinardi, R., Garzia, F., Cusani, R. "Peak-Shaped-Based Steganographic Technique for MP3 Audio", Journal of Information Security, vol. 4, pp. 12-18, 2013.

[9] Munir, R, Cryptography, Bandung : Infomatika, 2006.

[10] Tsiounis, Y., Yung, M. “On the Security of ElGamal Based Encryption”, Springer-Verlag Berlin Heidelberg, LNCS 1431, pp. 117-134, 1998.

[11] Winanti, W, "Message Concealment Based on JPEG Compressed Image Using Spread Spectrum Method", B.S. thesis, Department of Informatics and Electro Engineering, Bandung Institute of Technology, Bandung, Indonesia, 2008.

[12] Hallgren, S. "Linear Congruential Generators over Elliptic Curves". CS94 -143 , Dept. of Comp. Sci., Cornegie Mellon Univ, 1994.

G408

Check Out System Using Passive RFID Technology in Wholesale Supermarket

Gede Angga Pradipta, I Wayan Mustika, and Selo
Department of Information Technology and Electrical Engineering
Universitas Gadjah Mada
Jalan Grafika No.2 Kampus UGM, Yogyakarta, Indonesia
Email: angga.mti.18A@mail.ugm.ac.id,{wmustika, selo}@ugm.ac.id

***Abstract*—The aim of this paper is to improve reading accuracy and precision of passive tags on shopping cart. The proposed system, which is embedded on shopping chart, consists of a RFID (Radio Frequency IDentifier) reader. The reader temporarily records items that put in the shopping chart. At the check out counter, the proposed system transmits data to central server, while the RFID reader at the check out counter reads all items that pass to it. The central server then matches the data from the proposed system and the data obtained from check out counter. The checkout process is successfully done when both data are identical. Otherwise, a warning message is generated. Customer can monitor the total purchase by letting the reader identifies the items in the shopping chart. The results show that using the combination of both checking systems, the accuracy can be improved up to 18 percent by compared to that of using single checking system.**

***Index Terms*—Passive RFID ,Supermarket,RFID reader,RFID Tag,Check out counter,Accuracy.**

I. Introduction

As a commercial business, grocery stores, and similar shopping establisments play an important role in today's economy. [1] said, the supermarket sales in Indonesia are growing with rates of 13-15 % on 2012. With increasing purchasing power of consumers from year to year, producers face challenges in improving the customer's convenience. Problems in stock management and customer data have to be eliminated in order to improve the customer's convenience and ensure that the system can operate properly. According to [2], identification technique using bar code which is done for each individual item requires line of sight between barcode and reader. In contrast RFID identification technique allows automatic multi tag reading when the one or more tags enter the coverage area of the reader. Thus, implementation of RFID technology is expected to enhance the customer comfort and convenience when shopping in a supermarket.

Research on the implementation of RFID and Internet of Things (IoT) in supermarket have been done to improve the comfort and convenience when shopping [3]-[4]. Zhengshan studied the use of RFID technology in a supermarket [5]. The authors utilized the IoT and active RFID for searching position and monitoring availability of goods. At check-out counter, mobile payment was used for transaction. The goals of using mobile payment system is to reduced queue at the check-out counter. Monitoring goods informations using shopping cart which is mounted with RFID reader has been investigated [6]. In this research each shelf mounted with a reader to monitor the stock of goods. The system automatically updates the data to the central server when the items on the shelf have been reduced. Rong *et al*. [4] developed a guidance system in supermarket based on wireless technique and IoT. The system consists of active RFID tags on the shelf and hand held devices that is embedded with a RFID reader. The device receives product information when it is close to the tag.

The design and implementation of a new intelligent advertisement and shopping guide system for large supermarkets has been investigated by Ningyuan [3]. The wireless touch screen device is integrated in shopping cart. It can automatically broadcast the commodities advertisement when the cart is moving in large supermarket. Customer can easily search the commodity who they need with help of electronic guide services.

However, most researches do not pay attention on the accuracy and precision of the identification tags on product. A supermarket should ensure that is no fault occur during transactions on the check out counter. The tags that overlap with each other on shopping cart may be undetectable by reader and thus the products are not recorded to the system.

In this paper, double checking system is proposed. The aim of this paper is to improve reading accuracy and precision of passive tags on shopping cart. The proposed system, which is embedded on shopping chart, consists of a RFID (Radio Frequency IDentifier) reader. The reader temporarily records items that put in the shopping chart. At check out counter, the proposed system transmits data to central server, while the RFID reader at the cashier gate reads all items that pass to it. The central server then matches the both data. The checkout process is successfully done when both data are identical. Otherwise, a warning message is generated.

The reminder of this paper is organizedas follows. Section II describes the system overview of the proposed system. The experimentals and results are represented in section III. Section IV concludes the paper.

II. System Overview

The overall structure of proposed system is divided into three main layers which handle the entire task of the system as follows.

- First layer. This is client layer, which processes the data and generate the system output.
- Second layer. This is communicaton service layer, which is responsible for two-way communication between systems that use radio frequency data transmission and application on cashier.
- Third Layer. This is the data service layer, which is mainly responsible for providing the basic data for communication layer.

The proposed check out system aims to increase the accuracy of reading tag on goods and also improve the security in purchasing. Besbes [7] studied an intelligent check out system using camera at the cashier to determine the movement of customer if they already close to the gate cashier and selected puchase goods approach the checkout system. Thus, RFID reader is activated and identification of goods is started. According to that scenario, validation process of total goods and data items is executed only at cashier gate. Thus, the opportunity of items is not detected using the RFID reader is high as the selected purchase items are piled up on shopping cart. In the proposed system, double checking consists of the first checking system at the shopping cart for temporary selected purchase items and final checking system at the check out counter gate for final validation and transaction.

Every goods that is temporarily recorded on shopping cart will be compared with data obtained by RFID reader at cashier gate. This can be explain as follows. When the customer shopping cart passes through the cashier gate, system identifies each item by the RFID reader. At the same time the data is compared with data recorded in the system attached on shopping cart. Transaction can be completed when both data are identical. Otherwise, warning message is generated and the manual checking for the unidentified item should be done. Fig.1 shows the basic design of system.

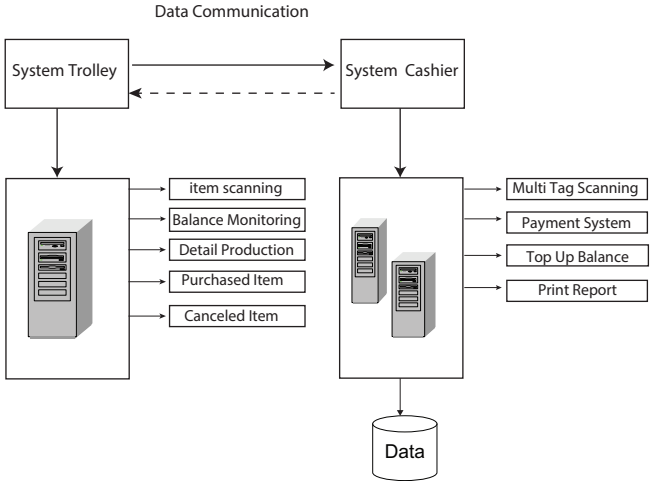

Fig. 1: Design of basic structure system.

III. Check Out System Design

A. RFID System in Shopping Cart

In the supermarket, every customer will take a shopping cart to transport the selected purchase items to the checkout counter during shopping. This research proposed a system with RFID technology embedded in the shopping cart. The embedded system will display the detail information when an item is handed in the vicinity of the RFID reader on the shopping cart.

Scenario of the proposed on shopping cart can be explained as follows:

- Customer enters the supermarket and selects one shopping cart.
- Embedded system on the shopping cart read the customer ID as appear in the customer card member. Customer ID and shopping cart ID will be used as parameters for every transaction. It is that assumed every customer have a card member for payment.
- Customer information and customer balance will be displayed when the card is read by the system.
- Each selected item has to be handed close to the RFID reader on shopping cart to record the temporary purchased items.
- When an item is read by system, detailed information such as a item description, producer, price, expired date, etc.will be shown in the monitor. The total of temporary purchased item is also shown in the monitor.
- When a customer wants to cancel the purchase of an item, she rescans the item to the reader and select the menu in the system for cancellation so the total temporary purchased item will be adjusted.
- Finally if the customer passes the check out counter. The system perfoms multitag reading using RFID reader to the items in the shopping cart and both data will be analyzed by the central server.

The workflow of embedded system on shopping cart is shown in Fig. 2.

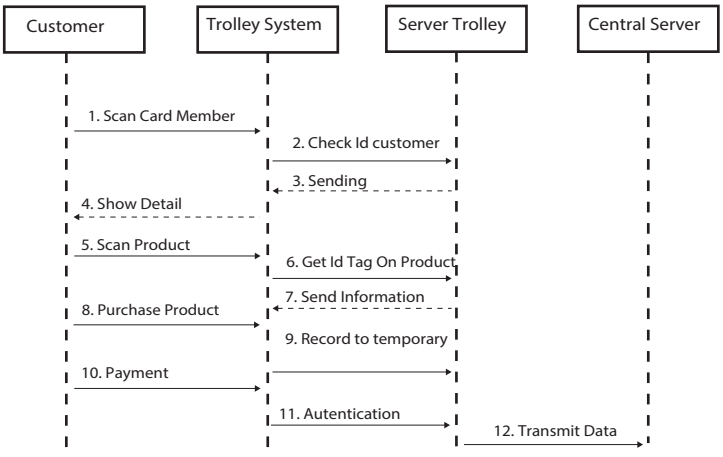

Fig. 2: Trolley system work flow

The advantages of using this system is not only for increasing accuration and security on cashier but also for improving the customer convinience. This system can monitoring directly the balance information at the shopping cart. Every goods that has been scanned will directly decrease balance of customer temporarily until they are ready to make a payment on cashier. With that way, customer can controlling their purchase goods by looking into information of last balance. Moreover customer can get detail information about goods which they want by scanning it on reader at shopping cart. After customer finish to select goods and ready for payment on the cashier, then shopping cart system will transmit data of goods which is recorded on temporary shopping list to central cashier system. Fig. 3 show the example of system on shopping cart.

Fig. 3: Shopping cart system [8].

B. RFID System On Cashier

Every item in supermarket is attached a tag that has unique identity. The system performs multi tag reading when shopping cart customer passes the reader. The proposed system uses RFD210P integrated ultra high frequencies(UHF)Gen-2 Reader Writer that work at 960MHz. This reader is an entry level reader that reads and writes electronic labels or tags and complies with ISO-18000-6B standard and EPC Class 1 G2. According the reader specification, mulitag scanning can be done with maximum read range up to 4 meters. Smart card is assumed to be used by customer for transaction in which the system automatically detects the customer ID and reduce the balance of customer during transaction. Specification of the smart card is Gen 2 blank UHF card with frequency of 860MHz-960MHz.

To avoid the phenomenon of lining up at check out counter waiting for payment, customers purchase the product through shopping cart and scan product to be recorded as temporary purchased items. After purchasing, when customer walk through the check out counter, the shopping cart will wirelessly transmits the data of temporary purchased items, customer ID, and shopping cart ID. The flow chart system on check out counter is shown in Fig. 4.

Both systems on shopping cart and check out counter have database to record any data related to the transaction process. Database at shopping cart system records the data of temporarily purchased items on shopping cart based on customer ID and shopping cart ID. The system read tags of

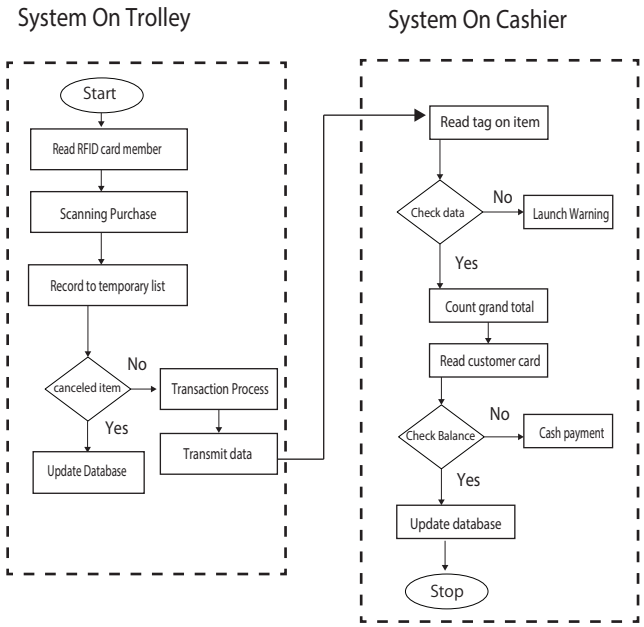

Fig. 4: Flow chart cashier system.

items on shopping cart and compare it with data from shopping cart based on the customer ID and shopping cart ID. If data of both system are matched, then field paid status on database set true. To avoid error occur if same customer purchase item in other time with same product and same shopping cart. System automatically check field that status paid is false. The scheme of comparing field is shown Fig. 5.

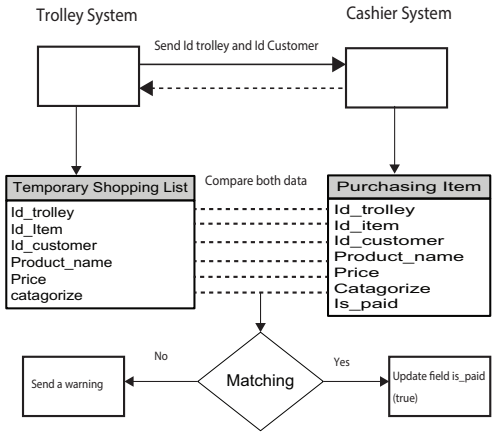

Fig. 5: Comparing data system.

IV. Experimentals and Results

A. Experiments of Single Checking System

To evaluate the effectiveness of the proposed system we will comparing single checking system and double checking system. The result will show which method is better. Some experiments are conducted including to estimate the maximum

capacity of shopping cart. According to the [9], the standardized shopping cart in hypermart has a maximum volume of 180 liters with 99.5 cm in length, 59 cm in width and 50 cm in height. In this experiment, the selected purchase items are assumed as a pile of boxes that has various size but not exceed the maximum capacity of the shopping cart. Maximum carried items that can be included in the shopping cart are calculated by dividing volume of the cart with a total volume of purchased item. The maximum number of tags on the shopping cart can be calculated as in Eq.(1).

$$Tag_{max} = \frac{L_t \times W_t \times H_t}{L_b \times W_b \times H_b} \quad (1)$$

$$L_t : Lengthtrolley, W_t : Widthtrolley, H_t : Heighttrolley$$
$$L_b : Lengthboxes, W_b : Widthboxes, H_b : Heightboxes$$

The volume number of shopping cart is $99.5cm \times 59cm \times 50cm = 293525cm^3$ and the volume of box is $30cm \times 25cm \times 35cm = 26250cm^3$ then the maximum capacity is

$$\frac{293252}{26250} = 11,185 \quad (2)$$

Based on result above, 11 tags RFID are used in this experiment as shown in Table I, experiment is conducted to determine the reading accuracy of RFID readerin a certain distance at the check-out counter gate.

TABLE I: ACCURACY EXPERIMENT

Experiments		
Distance (cm)	Time (s)	Accuracy %
50	4	100
100	22	81.3
150	55	56.2
200	65	43.8
250	73	25
300	78	18.75

As shown in Fig. 6, the reading accuracy decreases as the distance between the tag and reader increases. In order to improve the accuracy we propose the double checking system.

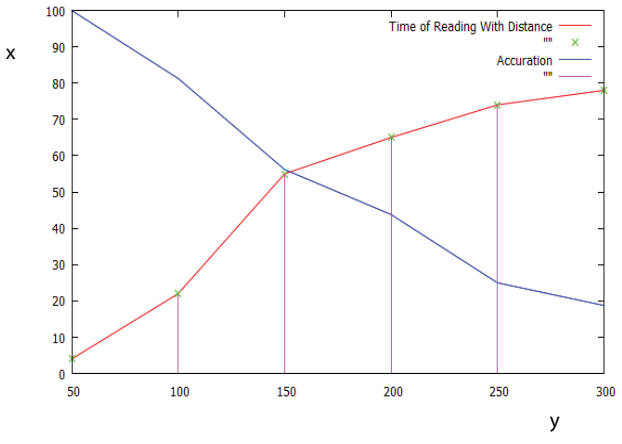

Fig. 6: Accuration reading tag based on distance.

B. Experiments of Double Checking System

In this experiment, the data recorded in the embedded shopping cart system will be compared with the data read at the check-out counter. If the RFID reader at the check-out counter can not detect all tags on shopping cart then the missed data will be copied from the embedded system on shopping cart. Scheme of adding the missed is shown in Fig. 7.

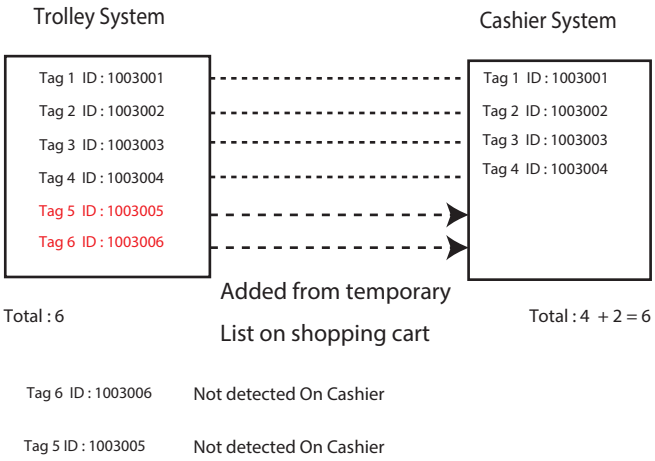

Fig. 7: Scheme of checking an adding unread items

Security and accuracy become an important part to measure reliabilty of the proposed system. The experiment scenario is explained as follows:

- In this experiment, it is assumed that 9 out of 11 tags on shopping carts have been scanned and recorded in the temporary database. However, 2 tags are not scanned and stored in temporary purchased items.
- Three boxes are used as barrier between tags where every box has width 30 cm, 25 cm, and 20 cm.
- Maximum distance is 50 cm and the experiment is conducted 50 times.

The result one checking system is shown in Fig.8.

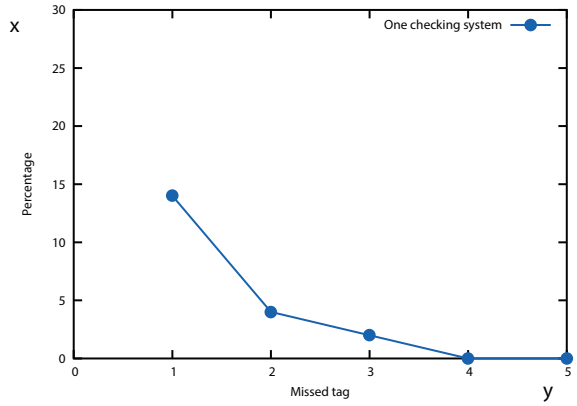

Fig. 8: Percentage of missed tag.

Fig. 8 shows that using one checking system, the reading accuracy is 78%. This come from 14% of 1 missed tags , 4% of 2 missed tags , and 4% of 3 missed tags.

With double checking system, missed tag is only 4% from 50 times experiments as shown in Fig. 9. Thus the reading accuracy from the double checking system is 96%. The result is shown in Fig.9.

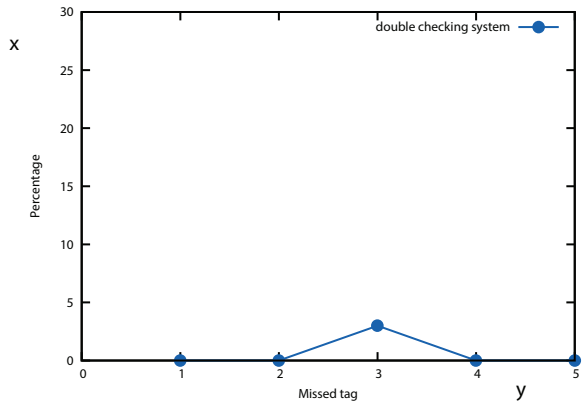

Fig. 9: Percentage of missed tag.

V. Conclusion

In this paper we have proposed double checking system to improve reading accuracy and precision of RFID tag on check out counter. The proposed system, which is embedded on shopping chart, consists of a RFID (Radio Frequency Identifier) reader and the reader temporarily records items that put in the shopping chart. At the check out counter, the proposed system transmits data to central server, while the RFID reader at the cashier gate reads all items that pass to it. The central server then matches the data from the proposed system and the data obtained from cashier gate. The advantages of the proposed system for customers are to monitor and controll amount balance during the shopping in supermarket.

According to the experiments with one checking system, accuracy of reading tag at check out counter is about 78% which is measured from 50 times experiments. The proposed double checking sytems reduce the percentage of missed tag about 18 % and thus the accuracy increases up to 96% compared with single checking system. In this study, shown that using double checking system is better than single checking system based on accuracy and precision to detected tag.

References

[1] W. rahajo jati, "Dilema ekonomi : Pasar tradisional versus liberalisasi bisnis ritel di indonesia," pp. 119–132. [Online]. Available: http://fe.um.ac.id/wp-content/uploads/2013/02/JESP-Ed.-4.-Vol.-2-Nov-

[2] P. G. A. R. White G, Gardiner G, "A comparison of barcoding and rfid technologies in practice," pp. 119–132, 2007.

[3] W. Ningyuan, Z. Zengwei, C. Jianping, C. Yuanyi, and L. Jin, "Advertisement and shopping guide system for large supermarkets based on wireless sensor network," in *Computer Science and Automation Engineering (CSAE), 2012 IEEE International Conference on*, vol. 2, May 2012, pp. 518–522.

[4] R. Chen, L. Peng, and Y. Qin, "Supermarket shopping guide system based on internet of things," in *Wireless Sensor Network, 2010. IET-WSN. IET International Conference on*, Nov 2010, pp. 17–20.

[5] Z. Luo and H. Wang, "Research on intelligent supermarket architecture based on the internet of things technology," in *Natural Computation (ICNC), 2012 Eighth International Conference on*, May 2012, pp. 1219–1223.

[6] A. C.Hurjui, "Monitoring the shopping activities from the supermarkets based on the intelligent basket by using the rfid technology," 2008.

[7] M. A. Besbes and H. Hamam, "An intelligent rfid checkout for stores," in *Microelectronics (ICM), 2011 International Conference on*, Dec 2011, pp. 1–12.

[8] [Online]. Available: http://www.geeksugar.com/Shopping-Carts-Get-Upgrade-LCD-Screens-114584

[9] [Online]. Available: http://www.rajarakminimarket.com/barang/trolley-supermarket.html

G409

Instrumentation of Carbon Monoxide to Indentify Traffic Jams

Siti Sendari
Department of Electrical Engineering,
Faculty of Engineering, State University of Malang
Malang, Indonesia
siti.sendari.ft@um.ac.id

Yuni Rahmawati
Department of Electrical Engineering,
Faculty of Engineering, State University of Malang
Malang, Indonesia
yuni.rahmawati.ft@um.ac.id

***Abstract*—This paper studies the influence of the number of motor vehicles to the level of carbon monoxide (CO). While the number of motor vehicles' increases significantly and affects many traffic jams, it could be indicated by the high CO level in the air. This indication is used to observe the points of the traffic jams in Malang, i.e., Jl. Sukarno-Hatta and Jl. Sumbersari as the samples of heavy traffic. These roads have characteristic, such as, similar users, two ways, and close to each other, while Jl. Sukarno-Hatta has more open air and plants comparing to Jl. Sumbersari. The observation showed that the levels of CO have significantly been affected by the number of vehicles. This result is used to design a detector system of traffic jams in Malang.**

Keywords—Instrumentation; Carbon Monoxide; Traffic jams

I. INTRODUCTION

The number of motor vehicles' increases significantly, which causes air pollution to be twice at 2000 since 1990, and it could be ten times at year 2020 [1]. Moore said that increasing the number of motor vehicles at a point of roads influences the high level of the pollution [2]. Transportation and gas combustion are the main pollution sources, there are five air pollution, i.e., PM10 (*particulate matter, 10μ or smaller*), SOx, CO, NOx, VOCs (*volatile organic compounds /hydrocarbon*). Among those sources, CO is the biggest polluter [3], while it can be dangerous if the level of this gas is high.

Another problem faced by the developing countries is that increasing the number of vehicles is not followed by expanding of roads, so there are many traffic jams occur. This situation also happens in Malang-Indonesia, which is shown in the website of the government [4]. There are at least 15 points where the traffic jams always occur, the two of them are Jl. Sukarno-Hatta and Jl. Sumbersari. These points are studied in this research, because they have characteristics, such as, the users of the roads are similar, those roads are two ways, and they close to each other, while the topography of these roads is different, that is, Jl. Sukarno-Hatta has more open air and plants comparing to Jl. Sumbersari.

Based on those reasons, this paper studies the instrumentation of CO gases to indicate the traffic jams. The

TABLE 1. PEAK TIME ON JL.SUMBERSARI

Direction / day	Morning	Daylight	Afternoon	Vol.Max (vehicles/hour)
Sumbersari-Dinoyo				
Monday	06.45 – 07.00	12.15 – 12.30	14.45 – 15.00	1066,80
Friday	06.15 – 06.30	11.00 – 11.15	14.45 – 15.00	1090,80
Saturday	06.45 – 07.00	12.15 – 12.30	16.45 – 17.00	1047,20
Dinoyo-Sumbersari				
Monday	06.45 – 07.00	09.45 – 10.00	15.45 – 16.00	1265,40
Friday	06.45 – 07.00	09.45 – 10.00	15.15 – 15.30	1266,40
Saturday	06.45 – 07.00	10.15 – 10.30	16.45 – 17.00	1259,40

calibration of gas sensors is done according the data logging of CO gases at Jl. Sukarno-Hatta and Jl. Sumbersari, which represents of all situations of traffic jams in Malang.

The rest, this paper is organized as follows. Section II describes the gas sensor to indicate the traffic jams. Section III describes the method to calibrate the sensor. Section IV shows the results, and Section V is devoted to conclusions.

II. GAS SENSORS TO INDICATE TRAFFIC JAMS

A. CO Gases

Carbon and Oxygen can combine to produce carbon monoxide (CO) as a result of imperfect combustion, where this gas is odorless, tasteless and colorless at the ambient air temperature. Furthermore, CO can also be potential as a dangerous toxin, which able to be bound strongly with hemoglobin [1]. In 1992, WHO revealed that 90% of CO in urban air comes from motor vehicle's emission. Thus, increasing the number of motor vehicles' influences the high CO levels.

On the other hand, the traffic density is shown by a comparison between the volume of traffic represented by the number of passing vehicles, and the road capacity represented by the ability of the road to pass a number of vehicles. When the capacity of the road does not be enhanced, while the huge number of vehicles passes on the roads, it causes disruption on the road, so that the speed of the motor becomes unstable and causes imperfect combustion; thus, the pollution is increased more [5].

The CO levels in urban area are quite varied depending on

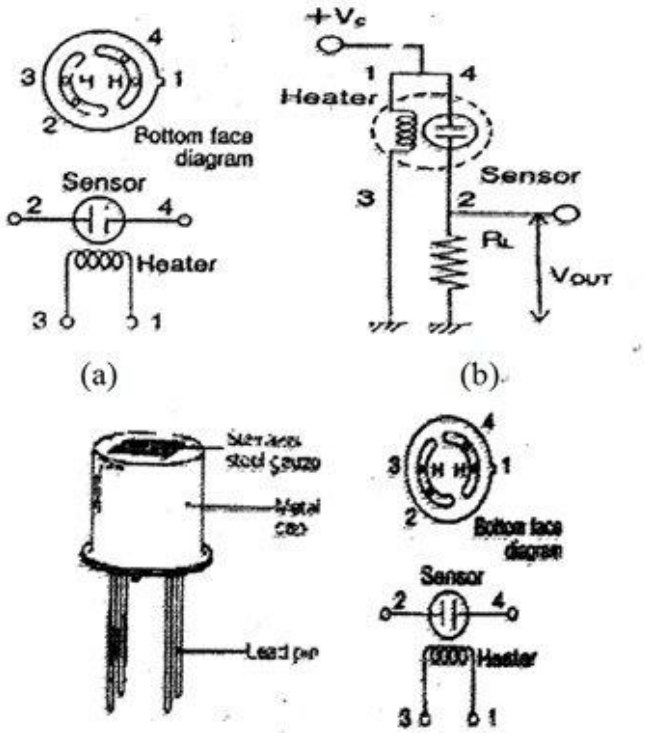

Figure 1. Gas sensor of AF series

(a). Pin configuration (b) Method to calibrate, (c) Physical graph

(source : tic film gas sensr gas AF-series data sheet)

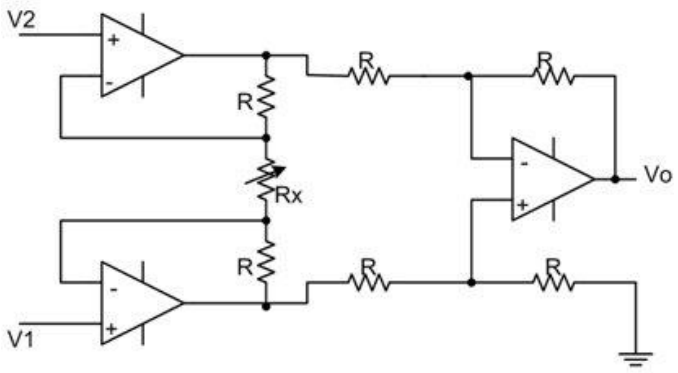

Figure 2. Instrumentation Amplifier Circuit

the density of motor vehicles that use gasoline. Generally, maximum levels of CO are found to coincide in the rush hours in the morning and evening. Besides of that, the weather and topography of the surrounding streets also influence the levels of CO. Winayati [6] studied the peak time of the rush hours on Jl. Sumbersari as shown in Table [1]. These peak times are used as the base time of this paper.

B. Selecting Gas Sensor

In order to detect the CO level on the roads, the gas sensors are needed. One of the types is the AF series, which is produced from thick films. This sensor works by binding and uptake of gases on the surface of it, which is related to the decreasing resistance of the sensor. The pin configuration, a method to calibrate, and a physical graph of gas sensor is shown in Fig. 1.

The resistance of the gas sensor (Rs) can be calculated from the output voltage (V_{OUT}) as follows

$$Rs = \frac{Vc - V_{OUT}}{Vout} \cdot R_L \qquad (1),$$

where, V_C is the common voltaje, and R_L is the load resistance. The sensitivity of the sensor is defined as a comparison between the resistance of the air contaminated by the gas (R_{GAS}) and that of the uncontaminated air (R_{AIR}).

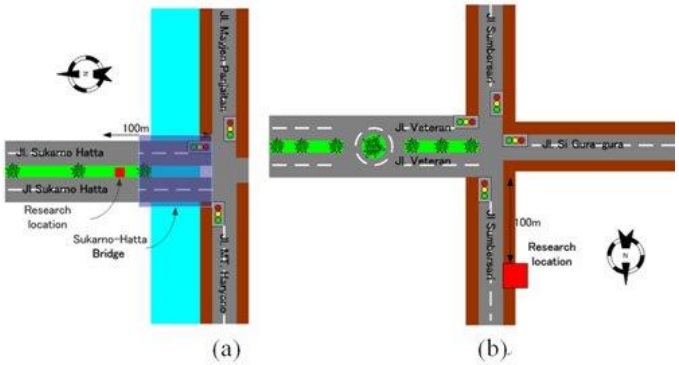

Figure 3. 3 Map of the research location
(a). on Jl. Sukarno-Hatta
(b). on Jl. Sumbersari

C. Signal Conditioning for Gas Sensor

A Signal conditioning is needed to change the level of a signal so it can be suitable for the other components. An instrumentation amplifier can be applied as a signal conditioning, which is developed using Op-Amps as shown in Fig. 2.

An instrumentation amplifier has some advantages; that is, it has high impedance inputs, and the gain of the amplifier can be tuned easily and appropriately by setting the variable resistance Rx. The gain of instrumentation amplifier is defined as follows,

$$\frac{V_o}{V_1 - V_2} = 1 + \frac{2}{a}, \quad a = \frac{Rx}{R} \qquad (2),$$

where, V_1 and V_2 are the voltage input at the channel (+) and that at the channel (-), respectively. V_o is the output voltage of the instrumentation amplifier, which is proportional to the differential inputs (V_1-V_2). The characteristics of the instrumentation amplifier are (1) the gain is determined by Rx, (2) the impedance inputs are high and are not changed when the gain is changed, and (3) the output Vo is only depended on V_1 and V_2 and is not depended on the common mode.

III. RESEARCH METHODS

The research is done using the steps as follows.

The first step is done by selecting the appropriate location, Since there are more than 15 points where the traffic jams always occur [4], Jl. Sumbersari and Jl. Sukarno-Hatta are selected. The reasons are the different topograph of those roads, i.e., Jl. Sumbersari is a two-way street, which has narrow width and has little open air, while Jl. Sukarno-Hatta is a wide street, where it has more open air and green line in the middle of the street. The characteristic of these roads are shown in Fig. 3. The differences are used as bases comparation of the CO level to the topograph.

The second step is to select the appropriate data. The time selected is a busy hour ranging from solitary – normal – busy – normal. This step is selected to observe the influence of the volume street to the CO level. According to Winayati's

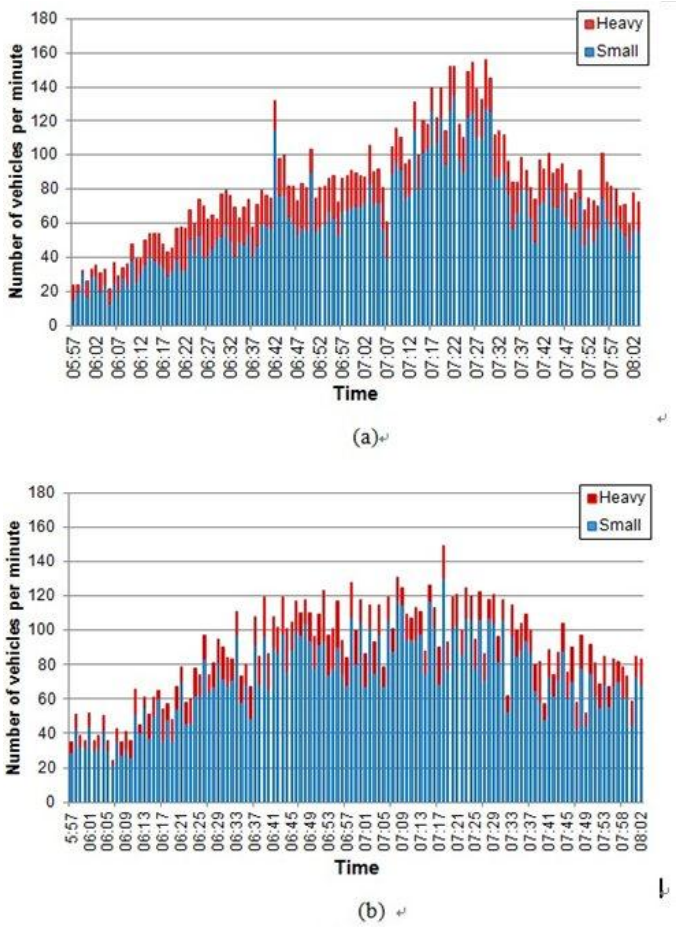

Figure 4. Number of vehicles passes on the street
(a). on Jl. Sukarno-Hatta
(b). on Jl. Sumbersari

research [6], this research is done at the peak time on Jl. Sukarno-Hatta and Jl. Sumbersari, which occurs at 06.00 – 8.30 a.m., here, the data is counting every minute.

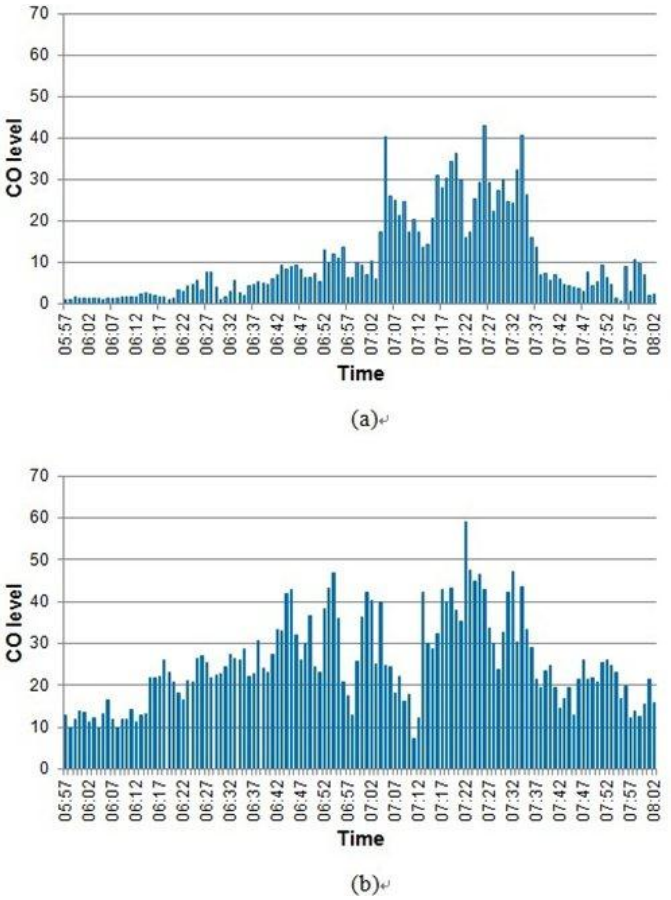

Figure 5. CO level on the street
(a). on Jl. Sukarno-Hatta
(b). on Jl. Sumbersari

TABLE 2. NUMBER OF VEHICLES PASSES ON JL. SUKARNO-HATTA AND JL.SUMBERSARI

	Small	Heavy	Total
Jalan Sukarno-Hatta			
average	63	19	82
max	135	30	156
Jalan Sumbersari			
average	72	15	86
max	130	29	149

The third step is to determine the research variables, i.e., independent and dependent variables represented by the number of vehicles and the CO level, respectively. Here, the number of vehicles is grouped by three categories, i.e., small, heavy, and total representing motors, cars, and total of motors and cars.

The fourth step is the mechanisms of data retrieval. The traffic density is calculated as the number of vehicles passed the street per minute, which is counted based on the video records taken at the times. On the other hand, the CO level is taken using data logger using EL-USB-CO [7]. This

instrument count six times per minute; then the average level per minute is used. This data is used as calibration of sensor used in the system designed.

The fifth step is the mechanisms of analysis data. The analysis is carried out by calculating (1) vehicles' volume, (2) CO levels, and (3) influence of the number of vehicles to the CO levels.

The last step is an experiment to calibrate the sensor, here AF sensor is used, which convert the CO level to the suitable voltage.

IV. Results

The measurement of the traffic density, CO level, and the influence of the number vehicles to the CO level are shown as follows.

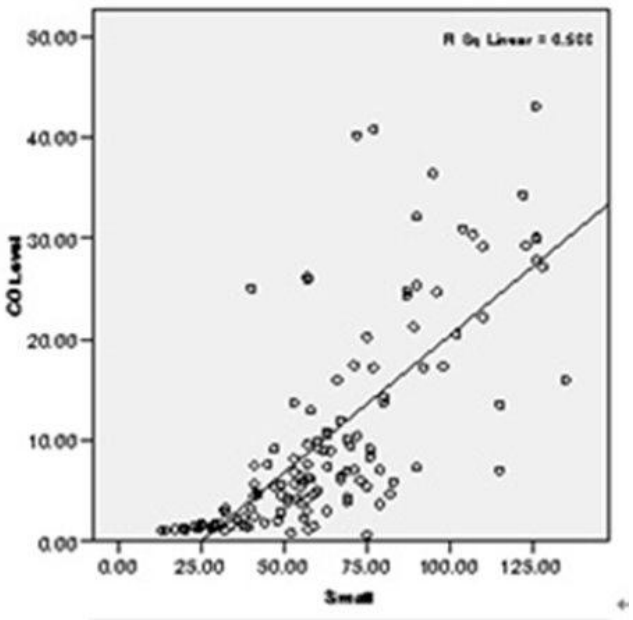

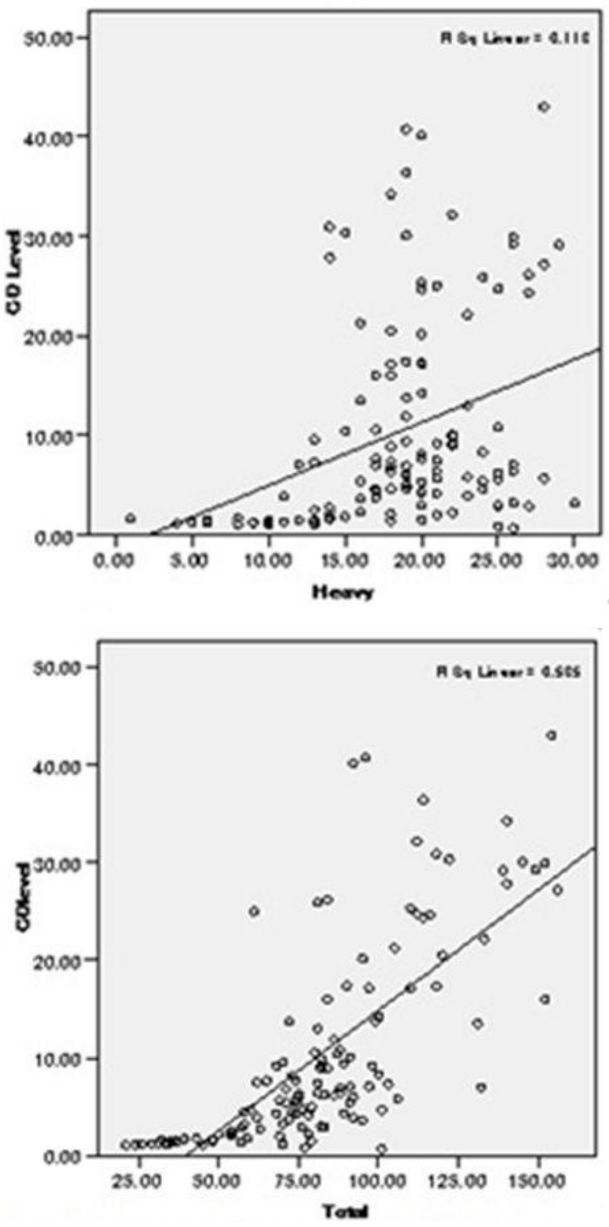

Figure 6. Influences of vehicles number to CO level on Jl.Sukarno-Hatta

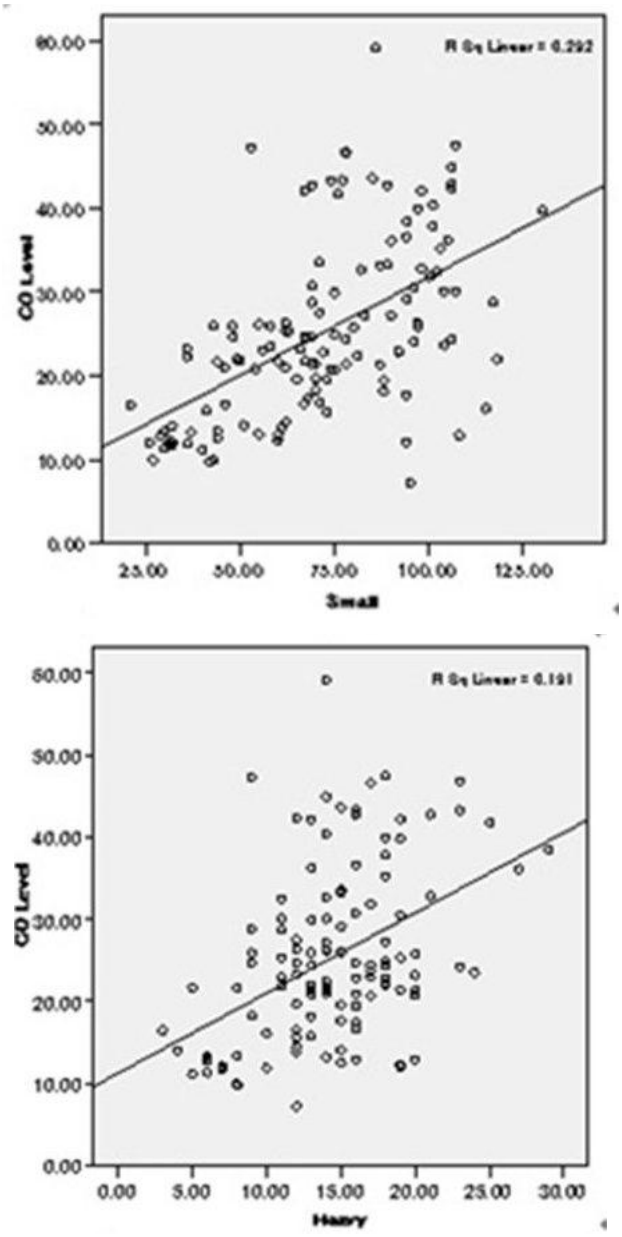

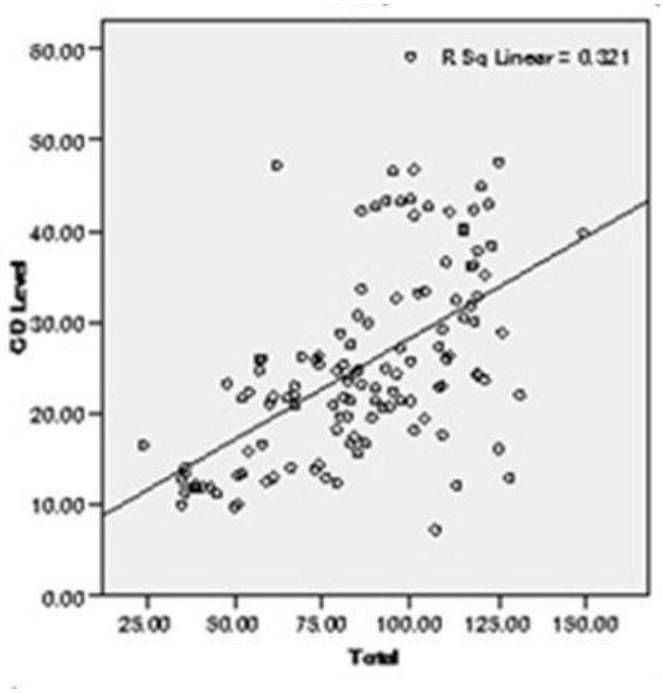

Figure 7. Influences of vehicles number to CO level on Jl.Sumbersari

TABLE 3. INFLUENCE COEFFICIENTS OF THE VEHICES' NUMBER TO THE CO LEVEL

Location	Type of vehicles	Coefficient	t-test	sig
Jl. Sukarno-Hatta	Small	Y=-6.747+0.271X	1.69e-45	0.000
	Heavy	Y=-1.370+0.634X	1.69e-13	0.000
	Total	Y=-9.792+0.247X	5.39e-56	0.000
Jl. Sumbersari	Small	Y=8.297+0.235X	2.01e-46	0.000
	Heavy	Y=11.278+0.975X	6.71e-25	0.000
	Total	Y=5.969+0.223X	9.24e-60	0.000

TABLE 4. T-TEST OF CO LEVELS ON Jl.SUKARNO-HATTA AND Jl.SUMBERSARI

	Jl. Sukarno-Hatta	Jl. Sumbersari
Mean	10.39	25.15
Stdev	10.35	10.63
t-statistic	-11.21	-
p-value (1-sided)	3.22e-24	-

A. Measurement of Volume of Density Traffic

The measurements of the traffic density on Jl. Sukarno-Hatta and Jl. Sumbersari are counted at the busy hours; that is, at 06.00 to 08.30 a.m. as shown in Fig. 4. The figure shows that the peak number of vehicles on Jl. Sukarno-Hatta is at 7.00 to 7.30 a.m., while that on Jl. Sumbersari is at 6.30 to 7.50 a.m. As shown in Table. 2, the maximum number of the vehicles which was passed on Jl. Sukarno-Hatta is 156, while Jl. Sumbersari is 149. It is because that Jl. Sukarno-Hatta is wider than Jl. Sumbersari. However, the average of the vehicles on Jl. Sumbersari is larger than Jl. Sukarno-Hatta; it is because that Jl. Sumbersari narrower than Jl. Sukarno-Hatta. Then it is supposed that the CO level on Jl. Sumbersari higher than Jl. Sukarno-Hatta

B. Measurement CO level

The measurements of the CO level on Jl. Sukarno-Hatta and Jl. Sumbersari are shown in Fig. 5. The average and highest level of CO on Jl. Sukarno are 10.4 ppm and 43 ppm, respectively, while those on Jl. Sumbersari are 24.6 ppm and 59.2 ppm.

Although the number of vehicles which pass on Jl. Subersari is smaller than those on Jl. Sukarno-Hatta, and since the characteristics of Jl. Sumbersari are narrow and has no much open air compared to Jl. Sukarno-Hatta, the CO level on Jl. Subersari is higher than Jl. Sukarno-Hatta It is confirmed that the topograph of the road can influence the level CO level.

C. Influence of Number of Motor Vehicles to CO Level

The influences of the number of motor vehicles to the CO level on Jl. Sukarno-Hatta and Jl. Sumbersari are analyzed using regression analysis, which was performed using SPSS 15. These analyses are carried out to observe the influences of the small, heavy and total vehicles on the CO level. The scattered charts of are shown in Fig. 6 and Fig. 7.

The coefficients of influences of the number of vehicles to the CO level are shown in Table 3. The results show that the significance is less than 0.05, which mean the influence of the number of the vehicles influent significantly to the CO levels.

D. Influence of topography to CO level

In order to observe the influence of the topographies on Jl. Sukarno-Hatta and Jl. Sumbersari to the CO level, a comparison test is conducted using independent t-test. The CO level on Jl. Sukarno-Hatta, which are collected from 5.57 a.m. to 8.03 a.m, is compared to that on Jl. Sumbersari. The comparative results show that F value is 0.95, while F table is 1.34. It means that data is homogenous. The influence of the topography is analyzed using t-test as shown in Table 4.

This results show that the CO levels on Jl. Sukarno-Hatta and Jl. Sumbersari are different significantly with p value 3.22e-24, which mean the topographies of those roads influence the CO levels. The averaged CO levels on Jl. Sumbersari are higher than those on Jl. Sukarno-Hatta, i.e., 25.15 ppm and 10.39 ppm, respectively.

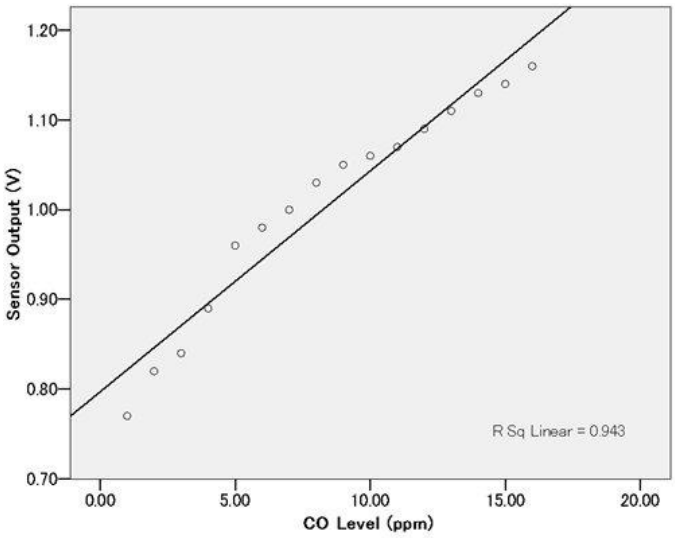

Figure 8. Gas sensor calibration

E. Calibration of Gas Sensor Based on CO Levels

The results of the CO levels of the previous steps are used as the base for calibrating the gas sensors, where this sensor is used as an input of the traffic density indicator. This gas sensor converts the CO levels to the electric voltage so it could represent the actual situations on the roads. The conversion of the CO levels to electric voltage is shown in Fig. 8.

The result of the sensor calibration is analyzed using linier regression, which shows that the relation between CO levels and voltage levels can be expressed as $Y = 0.797 + 0.025X$, here Y is the sensor output and X is the CO level. In order to use the output sensor as a traffic density indicator, the sensor is connected to the signal processing, where the output sensor changes from 0 V to 4.49V when the CO levels vary from 0 ppm to 50ppm.

V. CONCLUSIONS

This research shows the CO levels can be used as an indicator of a traffic density, that is, increasing the number of vehicles on the roads, it can influence the CO levels. Furthermore, The results also show the different CO levels, while the topograph of the road is different. So, when designing an indicator of a traffic density, it also should consider the topograph of the roads.

The future work of this research is going to design an integrating system which could collect the data from traffic density indicators.

REFERENCES

[1] Health Department of Indonesia. 1999. *Parameters air pollutants and Its Impact on Health*. www.depkes.go.id/downloads/udara.pdf.

[2] Moore, C., 2004, "Mutu Udara Kota, Seri Makalah Hijau" Redaktur: Howard Cincotta, Penerjemah: Tim Penerjemah IKIP Malang, US Embassy Jakarta.Peraturan, Pemerintah Republik Indonesia (Presiden) Nomor 41 Tahun 1999 tentang Pengelolaan Pencemaran Lingkungan.

[3] Woldenviro. 2006. *Air Polution*. www.worldenviro.com/airp.html 6 March 2013

[4] The government of Malang, Web GIS of Roads in Malang. www.pemkot-malang.go.id., 6 March 2013

[5] Syaukat, A. 2002. Study on Influences of Vehicles' Motor and Environment to CO levels on *Jl. Maliboro*, *Yogyakarta*. Media Teknik Majalah Ilmiah Teknologi No. 4 Th. XXIV November 2002, ISSN 0216-3012.

[6] Winayati. 2004. Relation Between Volume, Speed, and Traffic Density of Motor Cycle to Other Vehicles. Thesis of Brawijaya Postgraduate Program, Specialzed on Transportation Engineering.

[7] http://www.testequipmentdepot.com/lascar/dataloggers/elusbco.htm?gclid=CMDW8qPb1bsCFc9U4godDXgAbg

G410

CHANNEL ESTIMATION USING LEAST SQUARE ESTIMATION (LSE) ORTHOGONAL FREQUENCY DIVISION MULTIPLEXING (OFDM) SYSTEM

Muhamad Asvial and Indra W Gumilang
Electrical Engineering Deparment, Faculty of Engineering Universitas Indonesia,
Kampus UI Depok 16424,
asvial@ee.ui.ac.id and gumilang_indra@hotmail.com

Abstract–Orthogonal Frequency Division Multiplexing communication system is now starting to be widely used because of the high-speed data transfer. OFDM data transfer speeds can reach 100 Mbps. However, the high speed OFDM system transmits data makes it susceptible to fading and noise generated by the channel. Fading and noise can result errors in the transmission of bits. Therefore, we need a technique that can reduce the error that occurred. One technique widely used is the estimated channel. Channel estimation is useful to reduce the changes that occur when the transmitted bits. In this thesis, will be explained one of the least square method of channel estimation with pilot symbol receipts. This estimator will estimate the channel containing the Rayleigh fading and AWGN to the receiver moving at certain speeds.

Key Words – channel, estimation, OFDM, fading, pilot,

I. INTRODUCTION

Orthogonal Frequency Division Multiplexing (OFDM) are widely applied in mobile communication technology today because of the high transmission speed and bandwidth usage effectiveness when compared to its predecessor generation. This is why the OFDM technology has been proposed for broadband wireless access standards such as IEEE 802.16 (WiMAX) and as a core technique for the Long Term Evolution (LTE) fourth-generation wireless mobile communications [1]. But besides that, fading and noise is still a major problem in mobile communications because it can lead to errors and decrease the signal quality. Because, the higher data transfer rates the higher the required signal quality. Therefore, many, many ways used to overcome fading and noise in mobile communications. One way to do this is to estimate the channel[2]. Estimation channel using a variety of random distributions used to model the fading or noise occurs. In OFDM, channel estimation is needed, especially in fast fading channel, ie when the channel impulse response varies very rapidly with time.

In this journal will be explained about the system model channel estimation with pilot-assisted method using least squares estimation and simulation will be performed using a MATLAB program to find the performance of the channel estimation. Pilot-assisted channel estimation using pilot symbols inserted in the OFDM symbol. Pilot symbol is a signal that has previously been known that the effects of changes in the channel signal can be easily predicted. This technique is widely applied because of its ease in implementation and accurate in predicting the damage [3].

II. CHANNEL ESTIMATION

Channel estimation is a technique used in the transmission that aims to predict or estimate the channel impulse response (CIR) or the impulse response of a channel to the signal sent. Effect changes to the sent signal generated by the channel estimation must be done so that the detection signal becomes more accurate information.

In general, channel estimation can be grouped into three types, the pilot assisted channel estimation, blind channel estimation, and decision directed channel estimation. Pilot assisted channel estimation works by sending a pilot symbol

which is a sequence of bits that we have previously seen, along with the information to be sent. The pilot symbol is used to determine the pattern changes. Furthermore, with the pattern of these changes we can know the impulse response of channels. Hereinafter, with the interpolation method then information signal before passing through channel can we expect, so the error that occurred can be minimized. Unlike the pilot assisted channel estimation, blind channel estimation on the pilot symbols are not used to estimate the channel. Because we do not have to allocate specific bandwidth to transmit the pilot symbols, become more efficient use of bandwidth when compared with the the pilot assisted channel estimation techniques. Although the accuracy of estimating, the pilot assisted channel estimation techniques are still superior. Furthermore, the final estimation technique is the decision directed channel estimation. The basis of this technique is to use channel estimates obtained from the previous OFDM symbol channel estimation. Furthermore, the new estimate is obtained, is used to estimate the next. This technique is superior in estimating the bandwidth but in estimating is not better when compared with the pilot assisted channel estimation.

III. SYSTEM DECRIPTION

A. *Pilot Symbol*

As mentioned earlier, the pilot symbol is a row of bits that have previously been known. Previous recipients have learned the value of pilot symbols to be transmitted by the transmitter. Pilot symbols are sent with paste on the OFDM signal block of information. And then along with the pilot symbol signal information sent to the recipient. In general, there are two basic preparation of the pilot symbols are:

a. Block-type pilot, by including a pilot symbol into all subcarrier within a certain time within a specific time period. In addition to the previous recipient already knows the value of pilot symbols, the receiver also has to know when the pilot symbols transmitted simultaneously.
b. Comb type pilot, that is provided a special allocation of frequencies used to transmit pilot symbols every time. The sender determines the subcarrier which has previously been used to transmit pilot symbols.

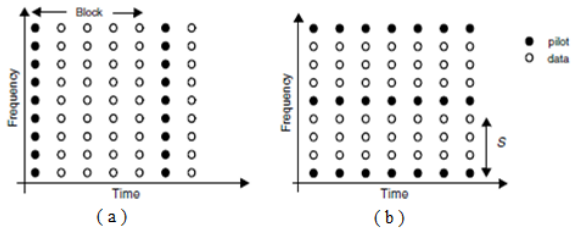

Figure 1. Two Types of Pilot Symbol Arrangement (a) Block-type Pilot Arrangement (b) Comb-type Pilot Arrangement.

The arrangement of the pilot symbol on the type of block, the pilot symbols transmitted simultaneously in all the subcarriers at specified intervals. Therefore, the estimate used in the data symbol is the same for a finite time to do an estimate for the next time interval.

For the arrangement of the pilot symbol on the type of comb, a total N_p pilot symbol of the signal $X_p(m), m = 0,1,\dots,N_p - 1$ are uniformly inserted into the signal $X(k)$. That is, of the total N subcarriers are divided into groups where one group N_p consists of $L = N/N_p$ group, the first subcarrier is used to transmit pilot signals modulated on the k-th subcarrier OFDM can be written as

$$X(k) = X(mL + l) \tag{1}$$

$$X(k) = \begin{cases} X_p(m), & l = 0 \\ data\ informasi, & l = 1,2,\dots L-1 \end{cases} \tag{2}$$

In these simulations will be used the arrangement of comb type pilot symbol. With a known pilot symbol value is transmitted and then when passing through the channel, the receiver can compare the value of pilot symbols that have previously been identified by the pilot symbol is changed through the channel. Furthermore, with the a channel estimation algorithm technique we can get his channel impulse response.

In the channel estimation block type, the pilot symbols transmitted by all subcarrier periodically. And further channel estimation is also performed regularly at the pilot symbol is sent. Therefore, these estimates are very suitable for frequency selective fading channel where there is need for different estimates on each individual subcarrier. Type channel estimation is also very appropriate when applied to slow fading channel with channel characteristics that have relatively fixed because of changes in the arrangement of block type pilot symbol estimation done at the interval at which pilot symbols sent.

While in non-pilot symbol estimation only followed by the pilot before.

On the other hand, the arrangement of comb type pilot symbol for pilot symbols are inserted at intervals of a fixed subcarrier at all times then this technique is more suited to fast channel fading. Impulse response at Fast fading channel varies very rapidly in each OFDM symbol, therefore the estimate needs to be done every time. This makes the comb type channel is more robust against fast fading. This technique is also suitable on flat fading channel where each frequency component of the signal fading experienced a relatively fixed magnitude. CIR value for subcarrier non-pilot (which contains the data) is estimated using the approach with the interpolation techniques.

Therefore, in OFDM systems where the channel is considered as flat fading or fast fading channel, preparation techniques comb type pilot symbol of a very good thing to do. At the end of this thesis, will be simulated OFDM system using comb-type pilot assisted channel estimation.

B. Least Square Channel Estimation

In general, there are many methods used in estimating channel. The number of methods is based on the reduction of error that occurred by comparing the pilot symbols are initially sent and received. Besides the method of least squares, method of channel estimation is widely used is the minimum mean square (MMSE), best linear unbiased estimator (BLUE), and adaptive boosting (AdaBoost) [4]. However, least square channel estimation was chosen because it is easier and very simple to apply. The difference technique is based on an algorithm taking CIR value of the comparison of known pilot symbol.

In OFDM systems, transmitters modulate a series of bits into symbols PSK / QAM, performed IFFT operation on the symbol to turn it into a signal in time domain, and further sent through the channel. Received signal is usually distorted by the channel characteristics. To repair bit sent, the effects of channel estimation should be expected or done. The equation of the received signal to the channel impulse response can be written into the equation

$$\boldsymbol{Y} = \boldsymbol{XH} + \boldsymbol{W} \qquad (3)$$

where **Y** is the received signal, **H** is the impulse response of channel, **W** is the noise, and **X** is the signal sent and each is written into the

$$\boldsymbol{Y} = \left[Y[0]\ \ Y[1] \ldots\ Y[N-1]\right]^T \qquad (4)$$

$$\boldsymbol{H} = [H[0]\ \ H[1] \ldots\ H[n-1]]^T \qquad (5)$$

$$\boldsymbol{W} = \left[W[0]\ \ W[1] \ldots\ W[N-1]\right]^T \qquad (6)$$

$$\boldsymbol{X} = \begin{bmatrix} X[0] & 0 & \ldots & 0 \\ 0 & X[1] & & \vdots \\ \vdots & & \ddots & 0 \\ 0 & \cdots & 0 & X[N-1] \end{bmatrix} \qquad (7)$$

$\boldsymbol{X}$ is written in the form of a diagonal matrix since we assume all orthogonal subcarrier.

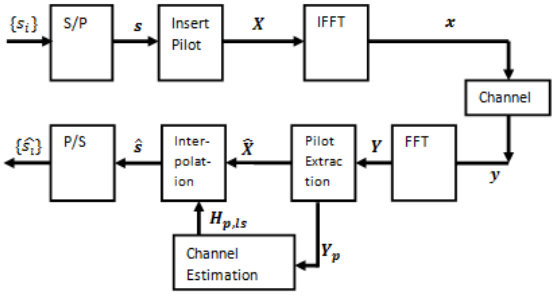

Figure 2 Chart flow channel estimation

channel estimation is done by searching channel impulse response estimation, $\boldsymbol{H}_{p,ls}$, by using pilot symbols. We assume the entire subcarrier orthogonal and ICI did not occur between them. Then, the pilot symbols for the N subcarrier is represented with the a diagonal matrix

$$\boldsymbol{X_p} = \begin{bmatrix} X_p[0] & 0 & \ldots & 0 \\ 0 & X_p[1] & & \vdots \\ \vdots & & \ddots & 0 \\ 0 & \cdots & 0 & X_p[N-1] \end{bmatrix} \qquad (8)$$

where $X_p[k]$ denote the pilot symbol on k-th subcarrier with $E\{X_p[k]\} = 0$ and $Var\{X_p[k]\} = \sigma_x^2, k = 0,1,2 \ldots, N-1$. Given that the impulse response as a pilot channel and pilot symbol $\boldsymbol{H_p}$ received $\boldsymbol{Y_p}$ represented as

$$\boldsymbol{Y_p} = \boldsymbol{X_p H_p} + \boldsymbol{W} \qquad (9)$$

Based on equation (9) the estimated channel impulse response $\widehat{\boldsymbol{H}}_{\boldsymbol{p}}$ is determined by the equation

$$\frac{\boldsymbol{Y_p}}{\boldsymbol{X_p}} = \boldsymbol{H_p} + \frac{\boldsymbol{W}}{\boldsymbol{X_p}} = \boldsymbol{\hat{H}_p} \quad (10)$$

The basic principle of Least Square Channel Estimation is by minimizing the error by using the method of Least Square Approach [6]. If $x[n$ is the signal sent and received signal after passing through channel, then error $\varepsilon[n]$ that occur can be formulated into the equation

$$\varepsilon[n] = y[n] - x[n] \quad (11)$$

and least square error $J(\theta)$ that is the square value of $\varepsilon[n]$ is

$$J(\theta) = \sum_{n=0}^{N-1} (x[n] - y[n])^2 \quad (12)$$

With the substitution $x[n]$ with the $\boldsymbol{Y_p}$ and y [n] with the $\boldsymbol{\hat{H}_p X_p}$ in equation (9) is obtained

$$J(\theta) = (\boldsymbol{Y_p} - \boldsymbol{\hat{H}_p X_p})^H (\boldsymbol{Y_p} - \boldsymbol{\hat{H}_p X_p}) \quad (13)$$

$$J(\theta) = (\boldsymbol{Y_p}^H - \boldsymbol{\hat{H}_p}^H \boldsymbol{X_p}^H)(\boldsymbol{Y_p} - \boldsymbol{\hat{H}_p X_p})$$

$$J(\theta) = \boldsymbol{Y_p}^H \boldsymbol{Y_p} - \boldsymbol{Y_p}^H \boldsymbol{\hat{H}_p X_p} - \boldsymbol{\hat{H}_p}^H \boldsymbol{X_p}^H \boldsymbol{Y_p} + \boldsymbol{\hat{H}_p}^H \boldsymbol{X_p}^H \boldsymbol{\hat{H}_p X_p})$$

Where $(.)^H$ is the conjugate transpose operation. Minimum value of J (θ) is achieved when $\frac{\partial J(\theta)}{\partial \hat{H}}\Big|_{\hat{\boldsymbol{H}}} = 0$, so that the obtained equation[5]

$$\frac{\partial}{\partial \boldsymbol{H}^H} J(\theta) = -\boldsymbol{X_p}^H \boldsymbol{Y_p} + \boldsymbol{X_p}^H \boldsymbol{X H} = 0$$

$$\boldsymbol{H_{p,ls}} = (\boldsymbol{X_p}^H \boldsymbol{X_p})^{-1} \boldsymbol{X_p}^H \boldsymbol{Y_p}$$

$$\boldsymbol{H_{p,ls}} = \boldsymbol{X_p}^{-1} \boldsymbol{Y_p} \quad (14)$$

where $\boldsymbol{\hat{H}_{p,ls}}$ is the impulse response least squares channel estimation. So that the pilot signal estimation based on least squares criteria is given with

$$\boldsymbol{\hat{H}}_{p,ls} = [H_{p,ls}(0)\, H_{p,ls}(1)\, H_{p,ls}(N_p - 1)]^T = \boldsymbol{X}_p^{-1}\, \boldsymbol{Y}_p$$

$$= \left[\frac{Y_p(0)}{X_p(0)} \;\; \frac{Y_p(1)}{X_p(1)} \;\; \cdots \;\; \frac{Y_p(N-1)}{X_p(N-1)}\right]^T \quad (15)$$

C. Interpolation

After an estimate done and the estimated channel impulse response least squares $\boldsymbol{\hat{H}_{p,ls}}$ the obtained, interpolation technique is then performed. Interpolation is used to obtain the estimated channel impulse response in all OFDM symbols are sent. Two channel estimates obtained from the adjacent pilot symbols used for channel estimation on the data between them. There are various types of such one-dimensional interpolation, linear interpolation, cubic spine-interpolation, low-pass interpolation, and second-order interpolation. What is meant by this is a one-dimensional, we can interpolate with the review of one dimension only, and can we consider the frequency or time dimension. However, that will be used in channel estimation is linear interpolation here.

When the pilot symbols are distributed in the OFDM block by using structures such as comb-type pilots, interpolation carried out to obtain channel impulse response on the overall structure of the data subcarrier. By using interpolation, the estimated channel at the k-th subcarrier containing the information data in which $mL < k < (m+1)L$ is given with

$$\boldsymbol{\hat{H}}(k) = \boldsymbol{\hat{H}}_{p,ls}(mL+1), \quad 0 < l < L \quad (16)$$

$$\boldsymbol{\hat{H}}(k) = \left(1 - \frac{l}{L}\right) \boldsymbol{\hat{H}}_{p,ls}(m) + \frac{l}{L} \boldsymbol{\hat{H}}_{p,ls}(m+1) \quad (17)$$

Where L is the number of subcarrier groups in comb-type and $\boldsymbol{\hat{H}_{p,ls}}$ is the carrier impulse response estimation. The value of $\hat{H}(k)$ of each subcarrier is inserted at the beginning of the equation

$$\boldsymbol{\hat{X}} = \boldsymbol{Y}/\boldsymbol{\hat{H}} \quad (18)$$

In order to obtain the estimated value of the signal being sent or $\hat{X}[k]$ for all subcarriers.

IV. PERFORMANCE PARAMETERS

A. BER

BER or bit-error-rate is the ratio of the number of error bits or bits having errors with the all bits sent in the transmission of signals through a channel during a certain time interval. Bit error probability is the expected value of the BER. Therefore,

the BER can be determined by calculating the bit error probability.

Calculation of the BER on the AWGN channel is calculated by the integral Gaussian probability density function. Bit error rate for BPSK and QPSK written in equation

$$P_b = \frac{1}{2} erfc\left(\sqrt{\frac{E_b}{N_0}}\right) \quad (19)$$

However, due to the channel impulse response h, the energy bit to noise ratio becomes $\frac{|h|^2 E_b}{N_0}$. So that the bit error probability becomes

$$P_{b|h} = \frac{1}{2} erfc\left(\sqrt{\frac{|h|^2 E_b}{N_0}}\right) = \frac{1}{2} erfc(\sqrt{\gamma}) \quad (20)$$

where $\gamma = \frac{|h|^2 E_b}{N_0}$. h is a random variable from the Rayleigh distribution, therefore $|h|^2$ is chi-square distribution with two degrees of freedom. Since $|h|^2$ is chi-square distribution, then γ is also a chi-square distribution. Probability density function γ that is

$$P(\gamma) = \frac{1}{E_b/N_0} e^{\frac{-\gamma}{E_b/N_0}} \quad , \gamma \geq 0 \quad (21)$$

By substituting equation (20) into equation (21) so that we get

$$P_b = \int_0^\infty \frac{1}{2} erfc\left(\sqrt{\gamma}\right) p(\gamma) d\gamma \quad (22)$$

Equation (2.23) can be simplified into

$$P_b = \frac{1}{2}\left(1 - \sqrt{\frac{(E_b/N_0)}{(E_b/N_0)+1}}\right) \quad (23)$$

Because $\frac{E_b}{N_0} = SNR \,.\frac{B}{R}$ then we can change the above equation becomes

$$P_b = \frac{1}{2}\left(1 - \sqrt{\frac{SNR}{SNR + B/R}}\right) \quad (24)$$

Where B is the bandwidth and R is the bit rate signal. In [7] described the Least Square Error Estimation with the equation SNR

$$SNR_{LSE} = \frac{P_{LSE}}{N_{LSE}} \quad (25)$$

where P_{LSE} is the signal power and noise power N_{LSE} are respectively defined as

$$P_{LSE} = \left[\frac{1}{K}\sum_{i=0}^{K-1} Re\{y(i,j)\hat{h}(i,j)a^*(i,j)\}\right]^2 \quad (26)$$

and the noise power N_{LSE} is defined as

$$N_{LSE} = \frac{1}{K}\sum_{i=0}^{K-1} |y(i,j)|^2 - P_{LSE} \quad (27)$$

where a is the amplitude of the QPSK modulated signal, $\hat{h}$ is the channel estimate, y is the received signal and i, j is the pilot carrier and the symbol index. Therefore, with the SNR value substituted in equation (24) with the SNR_{LSE} in equation (25) then we get the estimated signal BER.

B. Throughput

Throughput indicates the size of the number of data bits of information that is successfully delivered or the other in terms of number of packet symbols that are not experiencing an error in transmitting. Throughput is strongly influenced by the magnitude of the BER in the transmission of data. Throughput can be calculated with the equation,

$$Throughput = R(1 - PER) \quad (28)$$

where PER is *packet error rate* and R is data rate transmission.

C. Channel capacity

Channel capacity is defined as the amount of information that can be transmitted through the channel. Channel capacity of a known CIR can be written using equation

$$C = log_2\left\{\det\left(1 + \frac{P_{LSE}}{N_{LSE}} * (\widehat{\boldsymbol{H}}_{ls})^{\boldsymbol{H}}\widehat{\boldsymbol{H}}_{ls}\right)\right\} \quad (29)$$

or can we write with the

$$C = log_2\{\det(1 + SNR_{LSE} * (\widehat{\boldsymbol{H}}_{ls})^{\boldsymbol{H}}\widehat{\boldsymbol{H}}_{ls})\} \quad (30)$$

where $\widehat{\boldsymbol{H}}_{ls}$ is the channel response estimation and SNR_{LSE} is signal to noise estimation.

V. SIMULATION RESULTS AND ANALYSIS

Simulation least square channel estimation is made using the software MATLAB 7.8.0 (R2009a). This simulation aims to see the performance of least squares to estimate channel bit error rate, throughput, and channel capacity for the increased signal to noise ratio or SNR. For comparison, channel estimation is also carried out on various types of digital modulation, that is BPSK, QPSK, 16-QAM, and 64-QAM. The simulation was carried out on a stationary receiver and a moving receiver that generates a frequency shift or Doppler frequency of 100 Hz. The following are also included constellation each signal digital modulation on the value of SNR = 10 dB and SNR = 20 dB. This simulation has the following parameters:

System Parameter	Value
Number of subcarrier	256
Number of pilot simbol	32
Number of data subcarrier	224
Guard interval ratio	¼
Channel Length	16
Modulation	BPSK, QPSK, 16-QAM, 64-QAM
Frequency Doppler	0 Hz dan 100 Hz
SNR	0 – 30 dB
IFFT size	256

In this simulation used 256 subcarriers where 32 subcarriers are used to transmit the pilot symbols so that the number of subcarriers is used to transmit data as much as 224. Or in another sense, one block of OFDM subcarriers is divided into 32 groups, each consisting of 8 subcarriers where the subcarriers beginning of each subcarriers group is used to transmit the pilot symbol. The system is maintained to avoid inter-symbol interference (ISI), hence the guard interval must be greater than the length of channel. Therefore, the channel length of 16 is added guard interval ratio of 1/4 or 64. In the system, do not over-sample so that the number of points equal to the number of IFFT subcarriers which is equal to 256.

A. BER

This section will explain the change of BER based the increase of SNR on a variety of modulation techniques with the stationary receivers and mobile receivers that produce the Doppler shift frequency of 100 Hz. For comparison, are included BER images system that do not use channel estimation techniques. Red straight line graph shows change of BPSK BER against SNR, while successively to green, blue, and black is a graph of BER of each modulation technique for QPSK, 16-QAM, and 64-QAM. BER calculations in these simulations are performed with the Monte Carlo technique that is sent bit by comparing the elements one by one with the elements of the received bits.

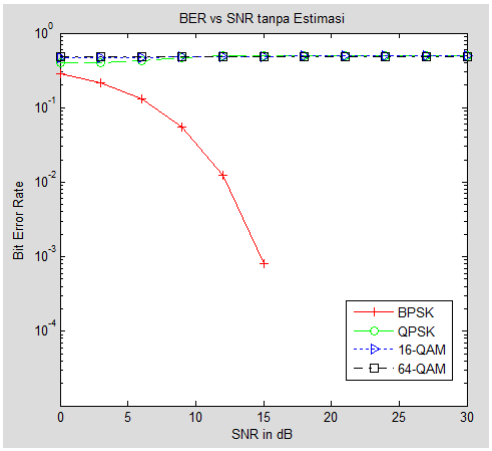

Figure 3 BER vs SNR with the Doppler frequency = 0 Hz without any estimation technique

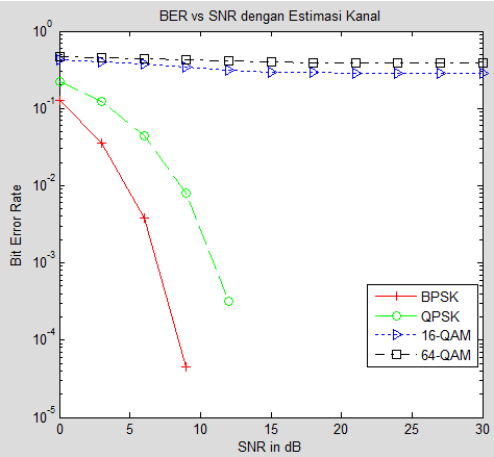

Figure 4 BER vs SNR with the Doppler frequency = 0 Hz with the estimation techniques

In comparison, Figure 3 to Figure 4, the channel estimation can improve the BER value along with increasing SNR on BPSK and QPSK modulation techniques. However, for 16-QAM and 64-QAM, BER relative fixed although given the increase of SNR. At the SNR = 15 dB, the BER of 16-QAM and 64-QAM BER value does not decrease even after it was given increase of SNR. Accordingly as previously described, least square channel estimation cannot give a good effect on the BER at 16-QAM modulation technique and 64-QAM. Least square channel estimation works by finding the CIR obtained from the pilot symbols. In the high-order modulation techniques such as 16-QAM and 64-QAM, it seems like this is not good technique to be applied. The reason is, the higher order it will be more and more also the distribution of random numbers generated from the information which finally resulted in the possibility of CIR generated increasing irregularly. CIR irregularity is used extensively to estimate the value of bits that were previously sent. This makes the higher order modulation, channel estimation techniques to be applied poorly.

If we look at the picture, still there is a reduction the BER, but this did not mean. In contrast, in BPSK and QPSK modulation techniques, channel estimation managed to fix BER. Seen on the value of SNR = 9 dB, the BPSK and QPSK originally had BER value = $5.5\text{x}10^{-2}$ and $44.6\text{x}10^{-1}$, with the channel estimation technique BER at SNR equal to $4.5\text{x}10^{-5}$and $7.9\text{x}10^{-3}$.

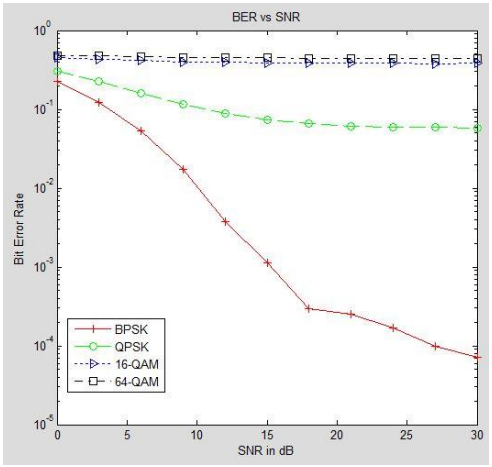

Figure 5 BER vs SNR with the Doppler frequency = 100 Hz estimation technique

At any receiver moves, the channel estimation technique is shown in Figure 5, the BER is improved although still not as good as fixed receiver.

B. Throughput

Throughput of a system is very dependent on the packet error rate (PER) of the system. PER is also directly proportional to the BER that occur. The smaller the value of the BER will be smaller then the value of PER is also vice versa. Figure 6 shows the graphical relationship with the SNR on the throughput of modulation BPSK, QPSK, 16-QAM, and 64-QAM with Doppler frequency of = 0 Hz.

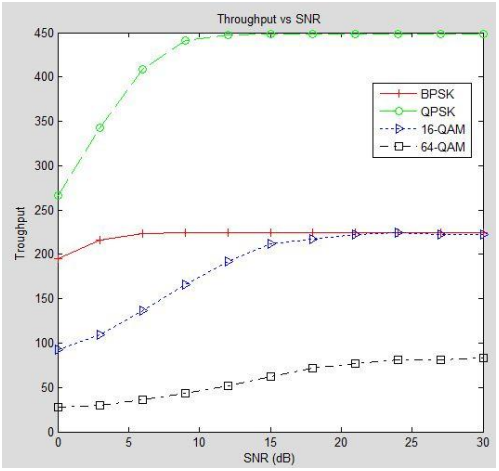

Figure 6 Throughput vs SNR in the Doppler frequency = 0 Hz

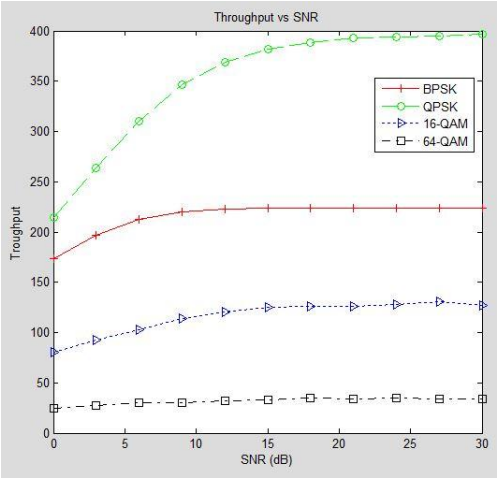

Figure 7 Throughput vs SNR in the Doppler frequency = 100 Hz

In the picture shown that at low SNR, which represents the channel conditions are poor, low-performance throughput from the system. In addition, the higher-order modulation, throughput is also higher. However, as discussed earlier, the simulation is estimated least square channel works effectively on BPSK and QPSK modulation, therefore the throughput graphs look better than 16-QAM and 64-QAM. Both modulation BER is very high, it is this which makes it smaller throughput of BPSK and QPSK although the 16-QAM and 64-QAM has a higher order.

Doppler frequency that occur can make the BER increases, if the graph in Figure 6 compared to the graph in Figure 7 looks throughput in Figure 7 is more sloping. It may be noted on the value of SNR = 6 dB. In BPSK and QPSK modulation throughput values in Figure 7 respectively about 210 and 310 whereas in Figure 6 for the same SNR value throughput 225 and 340.

C. Channel capacity

Figure 8 and Figure 9 shows the graphical capacity of the canal system with least square channel estimation at the receiver is stationary (Doppler frequency = 0 Hz) and the receiver are moving (frequency Doppler = 100 Hz). In the picture shown that the higher-order modulation of the channel capacity increases. This is because the higher-order modulation so the more bits are transmitted at the same time and make the canals increased capacity.

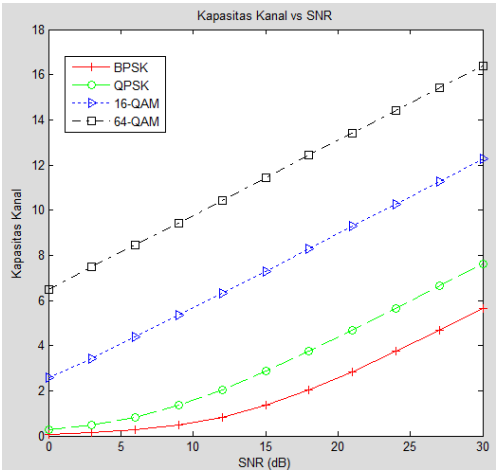

Figure 8 Channel Capacity vs SNR in Doppler frequency = 0 Hz

Seen in the figure, the capacity of the channel to move receiver a little bigger than a stationary receiver. This is because there is a the channel response matrix is greater in moving conditions due to the increasing number of multipath fading that occur.

VI. CONCLUSION

From the simulation results and analysis has been done, then get some conclusions relating to the least square the channel estimation performance.

1. The channel estimation least square working optimally on BPSK and QPSK modulation techniques, but not when applied at higher modulation techniques such as 16-QAM and 64-QAM. In BPSK and QPSK modulation techniques, the channel estimation managed to fix the value of BER. Seen on the value of SNR = 9 dB, the BPSK and QPSK originally had BER value = $5.5\text{x}10^{-2}$ and $4.6\text{x}10^{-1}$, with the channel estimation techniques SNR value at the same BER be $4.5\text{x}10^{-5}$ and $7.9\text{x}10^{-3}$. While the 16-QAM and 64-QAM is relatively fixed.
2. In a moving receiver, the channel estimation may work well despite an increase of the value of the BER when compared with a stationary receiver. BER for BPSK, QPSK, 16-QAM, and 64-QAM for mobile receiver that generate the Doppler frequency of 100 Hz is $1.7\text{x}10^{-3}$, $1.1\text{x}10^{-1}$, $4\text{x}10^{-1}$, $44.5\text{x}10^{-1}$.

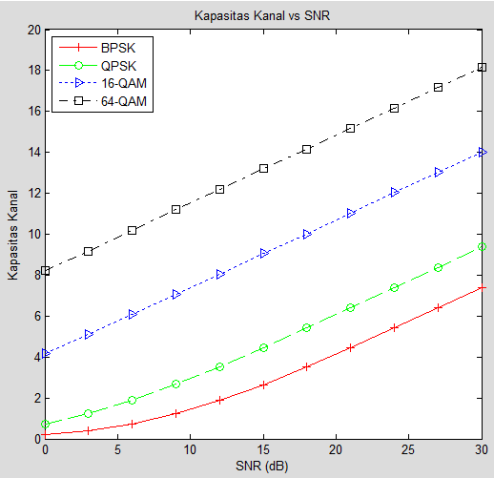

Figure 9 Channel Capacity vs SNR in the Doppler frequency = 100 Hz

3. The capacity of the channel at the moving receiver slightly larger than a fixed receiver because the channel response matrix in conditions that make moving the greater capacity of canals to be enlarged accordingly. Figure 4.9 is obtained from each modulation BPSK, QPSK, 16-QAM, and 64-QAM capacity of canals by 5.6, 7.6, 12.25, and 4.16 for the value of SNR = 30 dB. Value of the highest throughput on the system with least square the channel estimation is achieved by QPSK modulation technique for 448, BPSK, 224, and further 64-QAM, 222, and the last 16-QAM, 83. optimally the channel estimation in the QPSK and BPSK, which makes the BER her down and this also makes PER declined but because the throughput is proportional to the QPSK data rate therefore have greater throughput than BPSK. Similarly, 64-QAM and 16-QAM. Only, the resulting BER and PER in the channel estimation on the modulation technique is very bad
4. Value of the highest throughput on the system with least square the channel estimation is achieved by QPSK modulation technique for 448, BPSK, 224, and further 64-QAM, 222, and the last 16-QAM, 83. optimally the channel estimation in the QPSK and BPSK, which makes the BER her down and this also makes PER declined but because the throughput is proportional to the QPSK data rate therefore have greater throughput than BPSK. Similarly, 64-QAM and 16-QAM. Only, the resulting BER and PER in the channel estimation on the modulation technique is very bad.

VII. REFERENCE

[1] Yushi S. dan Martinez E. (2006) *Channel Estimation in OFDM Systems*, Freescale Semiconductor.

[2] Holma, H. dan Toskala A. (2009) *LTE for UMTS: OFDMA and SC-FDMA Based Radio Access*, New York:John Wiley & Sons.

[3] Xiaodai D., Wu-Sheng Lu, & Anthony C.K.S., (2006) *Linear Interpolation in Pilot Symbol Assisted Channel Estimation for OFDM.*

[4] Pradhan, P.K., Faust, O., Patra, S.K. & B.K. Chua., (2010) *Channel Estimation Algorithms for OFDM Systems*. National Institute of Technology Rourkela.

[5] Gladwin, S. Joseph, Salivahanan, S. (2010). *Channel Estimation in OFDM System over Wireless Channels*. Proc. of Int. Conf. on Control, Communication and Power Engineering 2010

[6] Kay, Steven M., (1993) *Fundamental of Statistical Signal Processing: Estimation Theory*, Prentice Hall.

[7] Barrera, M., Betancur, L., Navarro, A. (2009). *Novel SNR Estimation Algorithm for MB OFDM Ultra Wide Band Communications*. Communications, 2009. LATINCOM '09. IEEE Latin-American Conference. Mendellin.

G411 Design of Low Noise Amplifier for 2.35 GHz Long Term Evolution (LTE) Application

Fitri Yuli Zulkifli, Eufrasia Inti Alphatia Putri, Basari and Eko Tjipto Rahardjo
Antenna, Propagation and Microwave Research Group (AMRG)
Dept. of Electrical Engineering, Faculty of Engineering, Universitas Indonesia
Kampus Baru UI Depok, Indonesia

***Abstract*—In this paper, a Low Noise Amplifier (LNA) for Long Term Evolution (LTE) application is designed with the centre frequency at 2.35 GHz. Low Noise Amplifier is used to amplify the received low power RF signals. The LNA design uses inductive source degeneration with 24 dB voltage gain (S_{21}) and 4.5 V supply voltage. The Field Effect Transistor (FET) is used to design this LNA. The simulation result shows bandwidth of 282 MHz, with stab fact 0.659, VSWR 1.43, and noise figure is 1.185 dB at frequency 2.35 GHz. The Advanced Design Software (ADS) is used to simulate and show the specifications of the design.**

Keywords—Low Noise Amplifier, LTE, Noise Figure, FET

I. INTRODUCTION

Wireless communication is greatly improved and developed in this modern technology. Therefore, the technology that requires a communication system which can transmit a large amount of data continues to increase rapidly from the first generation (1G) technology to the present generation (4G) technology. 4G technology is the latest technology which is mobile broadband technology. Long Term Evolution (LTE) is a standard for wireless data communication technology and the evolution of the standard GSM/UMTS.

LTE consists of many types of equipment/devices to build the big system. One device needed is the RF receiver which usually consists of Low Noise Amplifier (LNA). To be used in multi-standards Radio Frequency (RF) technology for LTE, LNA is designed in the receiver and located at the first stage of a wireless communication near the antenna. It is often located very close to the antenna, thereby making losses in the feed-line less critical. The antenna receives small signal with large noise from the transmitter, therefore, the LNA amplifies the signal with contributing noise as low as possible to the next stage of the receiver. It is important to design LNA with low noise and high gain to meet a great specification.

Researches have been developed and have proposed the design of LNA for multi-bands applications [1], [2]. It is used for LTE and WLAN applications at the frequency of 2.35 GHz - 2.4 GHz. The LNA design in [1] has reached the highest gain of 22.5 dB while and in [2] achieved the lowest noise figure around 2 dB. In this paper, the LNA design is proposed to work with the center frequency of 2.35 GHz, provides a better noise figure which is less than 2 dB, and with a higher gain which is higher than 22.5 dB.

Design and simulation of the LNA is conducted by using Advanced Design Software (ADS).

II. DESIGN OF THE LNA

LNA is one of the most critical building blocks in modem integrated radio frequency (RF) transceivers for wireless communications. For low noise, the amplifier needs to have a high amplification in its first stage. Therefore Hetero Junction Field Effect Transistor (HJ-FETs) is used, which are not energy efficient, but reduce the relative amount of noise. Input and output matching circuits are used for the device matching. The matching technique uses the values of load and source reflection coefficients. Biasing is designed using large resistors, because energy efficiency is not of primary concern, and a large resistor prevents leakage of the weak signal out of the signal path or of noise into the signal path.

In designing LNA to meet all the standards, the first step is to determine the specification for the LNA. The second step is to choose the transistor and determine the DC bias to know the LNA operation. Transistor selection is the most important step in designing LNA. The transistor should provide high gain, low noise figure, low power consumption while preserving an easy matching frequency of operation. And the third step is to determine the input and output impedance of the LNA.

Figure 1 shows the LNA which uses an inductive source degeneration topology. M_1 is the common-source stage with the source inductive degeneration to provide enough power gain. M_2 is the common-gate stage that provides isolation for the input and output stages. Good matching can improve power transformation and noise performance. The common-gate transistor M_2 can reduce the Miller effect of the parasitic gate-drain capacitance of M_1, the input impedance of the input stage (M_1) can be written as [3], [4]:

$$Z_{in} = s(L_g + L_s) + \frac{1}{sC_{gs1}} + \frac{g_{m1}L_s}{C_{gs1}}, \quad (1)$$

Where C_{gs1} is the parasitic gate-source capacitance of M_1 and g_{m1} is the transconductance of M_1.

$$L_s = \frac{R_s C_{gs1}}{g_{m1}}, \tag{2}$$

and

$$(L_s + L_g) = \frac{1}{\omega_0^2 C_{gs1}}, \tag{3}$$

Where ω_0^2 is the operation frequency.

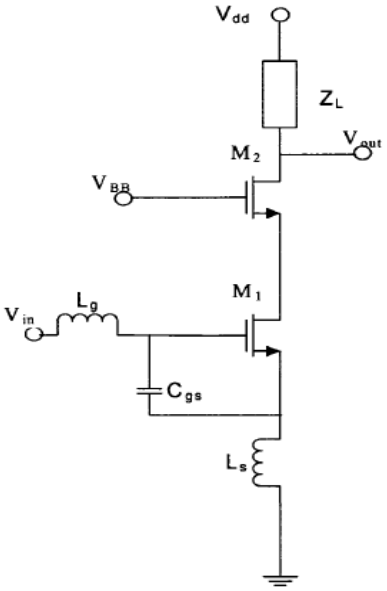

Fig 1. LNA with the Inductive Source Degeneration Topology [5]

For a LNA to work well, input matching must be achieved as well as a good noise figure performance. The porpose of input matching is to generate low input return loss across the entire bandwidth without adding more noise. The input matching network is implemented by second-order Chebyshev bandpass filter to achieve the wideband matching as shown in Fig. 2.

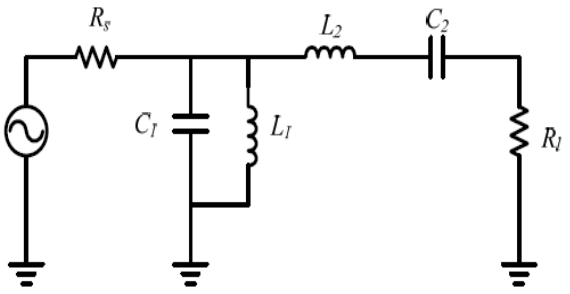

Fig 2. The Second-order Chebyshev Bandpass Filter

The LNA proposed in this paper is depicted in Fig. 3. The input impedance includes L_1, C_1, C_p, L_g, L_s, and C_{gs1}, can be written as [3], [4]:

$$Z_{in} = s(L_g + L_s) + \frac{1}{sC_T} + \frac{g_{m1} L_s}{C_T}, \tag{4}$$

To obtain matching condition, the source resistor R_s and load resistor R_l are 50Ω. The source inductor L_s of M_1 is used to generate a real term for input impedance matching. Set C_1 and L_1 in Fig. 2 equal to C_1 and L_1 in Fig.3,

$$C_1 = (C_{gs1} + C_p) = C_2, \tag{5}$$

and

$$L_1 = (L_g + L_s) = L_2 \tag{6}$$

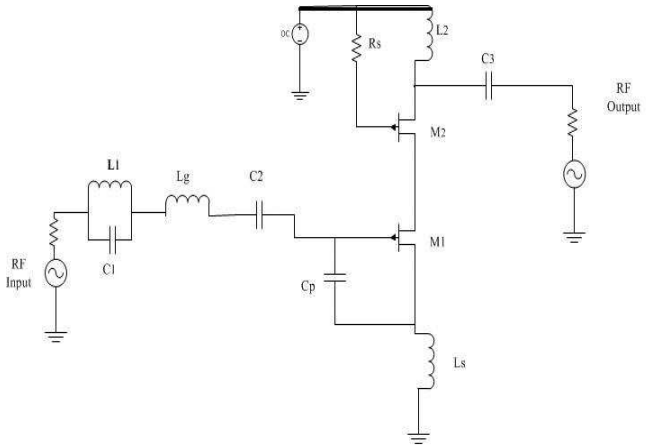

Fig 3. Design of the proposed LNA

III. SIMULATION RESULTS

In this section, the simulation results of the LNA for LTE application is discussed. The LNA design has been simulated using ADS. The simulated S-parameter results are shown in Fig. 4 to Fig. 5. The diagram curve in Fig. 4 shows the return loss, while in Fig. 5 shows the VSWR result of the simulation.

Fig. 4 indicates the characteristic return loss (S_{11}) of the LNA. The simulation result shows the S_{11} is -15.032 dB at 2.35 GHz. The simulated LNA bandwidth is 282 MHz (S11 ≤ -10dB).

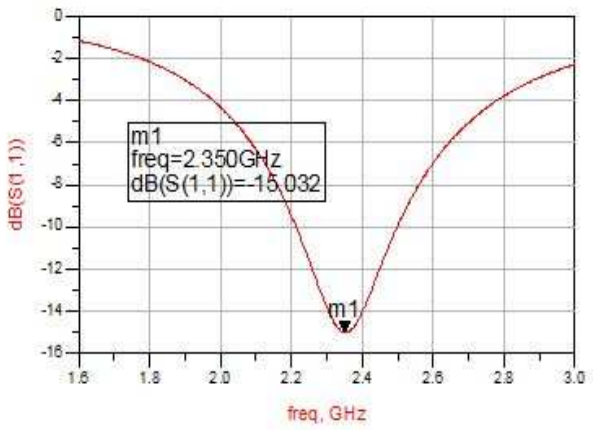

Fig. 4. Return Loss Diagram of the LNA

In Fig. 5, For VSWR < 2, the LNA bandwidth shows similar result as in Fig. 4. At the center frequency 2.35 GHz, VSWR simulated result is 1.431. This result is below the specified specification VSWR < 2.

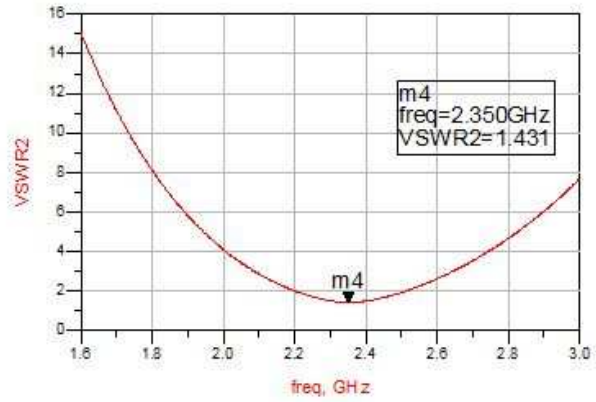

Fig. 5. VSWR Diagram of the LNA

Figure 6 shows the simulated gain (S_{21}) result of the LNA. The gain is 24.023 dB achieved at frequency 2.35 GHz.

Fig. 6 Gain Diagram of the LNA

The simulated noise figure of the LNA at the frequency 2.35 GHz is 1.185 dB which is shown in Fig. 7, the noise figure is less than 2 dB, therefore, this parameter has met the desired specifications which is < 2 dB.

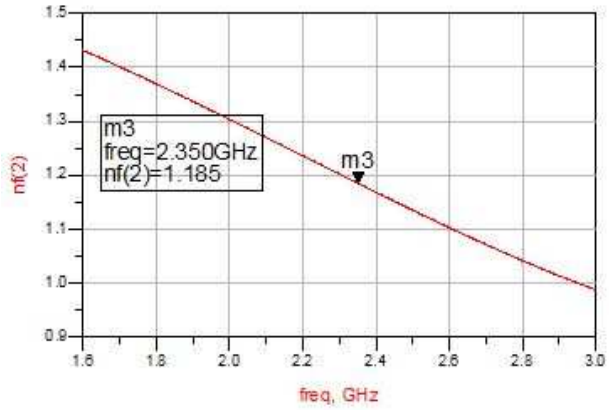

Fig. 7 Noise Figure of the LNA

An LNA is stable if it has a value of the parameter stab fact (K) is bigger than one (K >1). If K is less than one, then the LNA is in an unstable condition. Instability causes LNA experiencing oscillation, which will affect the performance of the LNA. Based on the simulation results in Fig. 8, it shows that at the frequency 2.35 GHz, the LNA design is in unstable condition. The Stab fact value is 0.659.

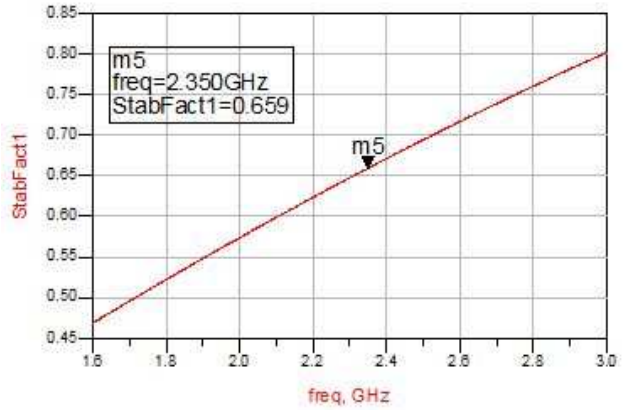

Fig. 8 Stability Factor Diagram of the LNA

From all of the simulated results of the proposed LNA, Table 1 shows all of the parameter results.

Table 1. Performance Summary of the LNA

Parameters	Specification	Simulation Result
Return Loss	< -10 dB	-15 dB
Gain	> 10 dB	24 dB
NF	< 2 dB	1.1 dB
VSWR	< 2	1.4
Stab Fact	> 1	0.6

IV. CONCLUSION

This paper proposes the LNA design with concurrent input and output matching networks for LTE application communication standards at the frequency 2.35 GHz. The simulated result shows bandwidth of 282 MHz. At frequency 2.35 GHz the parameter stab fact is 0.659, VSWR is 1.43, return loss is -15.032 dB, noise figure is 1.185 dB and gain above 24 dB. The LNA design shows good results which has reached the purposed specification of the LNA.

REFERENCES

[1] Sambit, D., Ashudeb D., Tarnn K. B., "A Gain Boosted Fully Concurrent Dual-Band Interstage Matched LNA Operating in 900 MHz/2.4 GHz with sub-2dB Noise Figure," Communication Control and Computing Technologies (ICCCCT), 2010 IEEE International Conference. India. 2010

[2] Sambit D., Kunal D., Ashudeb D., Tarun K. B., "Fully Concurrent Dual-Band LNA Operating in 900 MHz/2.4 GHz Bands for Multi-Standard Wireless Receiver with sub-2dB Noise Figure," Third International Conference on Emerging Trends in Engineering and Technology. India. 2010

[3] Shaeffer K. Derek, Lee H. Thomas, "A 1.5-V, 1.5-GHz CMOS Low Noise Amplifier," IEEE Journal Of Solid-State Circuits, Vol. 32, No. 5, May 1997.

[4] Pozar, D. M. 2005. Microwave Engineering Third Edition.John Wiley & Son.Amherst.

[5] Chih, L. Hsiao, and Yi L. H., "A Low Supply Voltage Dualband Low Noise Amplifier Design," The 13th IEEE International Symposium on Consumer Electronics (ISCE). 2009.

G501

Three-Dimensional Mapping of Static Magnetic Fields over a Semi Anechoic Chamber

Teti Zubaidah, Bulkis Kanata, Paniran

Applied Electromagnetic Research Group
Electrical Engineering Dept. of Mataram University
Jl. Majapahit 62, Mataram-Lombok, INDONESIA
E-mail: tetizubaidah@te.ftunram.ac.id; uqikanata@te.ftunram.ac.id; paniran@te.ftunram.ac.id

***Abstract*— Geomagnetic field is a kind of natural potential field in the Earth. A three years research for exploration of this field has been conducted in the Lombok Island-Indonesia, where extreme geomagnetic anomalies with two very strong dipolar structures exist. The research aims to construct a system to collect and concentrate geomagnetic fields, in order to possibly use the concentrated fields for geomagnetic power plants or to integrate the system with a fields picking-up scheme by means of wireless power transfer. The designed geomagnetic concentrator system has been tested in a self arranged semi anechoic chamber with a pair of Helmholtz coil, induced with DC currents to simulate the regional ambient static geomagnetic fields. Several tests have proven the performance of system in one dimensional space. This paper presents results of detailed three dimensional measurements of static magnetic fields in the semi anechoic chamber. Static magnetic fields over the entire chamber are drawn in their magnitudes and directions, by interpolating data obtained in regular grids of 50 cm x 50 cm. In specific areas, where the Helmholtz coil is placed, extra grids of 25 cm x 25 cm are inserted to sharpen fields' depictions. Results show that by inducing 1 A current on each of coils will produce magnetic fields, concentrated over the surrounding area of Helmholtz coil. The intensities of magnetic fields over this area are about 15,000 - 45,000 nT, which can be used to model the geomagnetic fields of the Lombok Island. Using the results of 3D field mapping, it will be possible to get the optimum placement of the geomagnetic concentrator system when it is tested on the chamber.**

Keywords— Anechoic chamber; Geomagnetic fields; Helmholtz coil; Lombok Island

.

G502

APPLICATION OF MT AND GRAVITY METHOD TO POTENTIAL ANALYSIS OF KEPAHIANG GEOTHERMAL, BENGKULU

Boko Nurdiyanto
Upstream Technology Center
PT Pertamina
Jakarta, Indonesia
boko.suwardi@pertamina.com

Yunus Daud
Post Graduate Program of
Geophysics Reservoar
FMIPA, UI
Jakarta, Indonesia

Ahmad Zarkasyi
Center for Geological Resources
Geological Agency
Bandung, Indonesia

Abstract*— An analysis of geothermal potential in Kepahiang-Bengkulu area using gravity and MT measurements of PSDG has been done. The analysis was conducted on 286 gravity points and 37 MT points spread over the southern part of Mount Kaba to Babakan Bogor hot springs. Kepahiang geothermal system is related to the volcanic activity of Mount Kaba which is still preserving the residual heat from the magma. Based on the gravity residual anomaly, the structure that controls the emerging Sempiang hot springs is estimated to be Sempiang fault that in near north-south direction, while Babakan Bogor hot springs is estimated to be controlled by the Sumatra fault. The cap rocks scatter around Sempiang hot springs start from near ground surface with thickness of between 1500 meters to 2500 meters. Cap rock is a unit of Young Lava of Kaba with resistivity < 10 Ohm-m and density is 2.2 gr/cm^3. Geothermal reservoir is estimated to be located under the cap rocks scatter around Sempiang hot springs as indicated by values of 10-60 Ohm-m in resistivity and density is 2.4 gr/cm^3. The top of reservoir is estimated to be 1500 meters below the ground surface, these rocks are volcanic products of Old Kaba in form of either lava or pyroclastic. Kepahiang geothermal prospect area scatters 19 km^2 wide around Sempiang hot springs which is bound by contrast resistivity and fault. It has potential geothermal of 133 MWe with the assumption of reservoir temperature (geochemistry) is 250 ^{0}C. Calculation of geothermal potential is included in the classification of expected reserves, as well as the extent and thickness of reservoir rock and fluid physical parameters are estimated based on data integrated geosciences detail depicted in the model tentatively.

Keywords— Kepahiang Geothermal, Gravity, MT

I. INTRODUCTION

Geothermal energy is one of the environmentally friendly alternative energy. The total potential of geothermal energy in Indonesia is estimated at 27 GW, which is the largest geothermal potential in the world. Data compilation is carried out by the Ministry of Energy and Mines has identified no less than 256 geothermal prospect areas in Indonesia. Indonesian geothermal systems in the hydrothermal systems generally have high temperatures (>225 °C), only a few of them that have moderate temperatures (125-225 °C). So the potential for power generation in case undertaken [1]. But that has installed power capacity recently reached 1,200 MW, or about 4% of the existing potentials [2]. The problem faced is that most of the geothermal field can not be utilized due to the lack of technical data for characterization, so it can not attract investors for further development [2].

Geothermal field development requires a gradual process that is quite long and requires a substantial investment costs. Before the geothermal potential can be harnessed as a source of energy, there must be initial steps are done, a study to determine the character of the geothermal system in terms of geology, geophysics and hydrology, as well as estimates of stored energy reserves.

The purpose of this study was to determine the geothermal system, and calculate potential prospects based on MT and gravity data analysis in Kepahiang, Bengkulu.

II. STUDY AREA

A. Regional Geological Setting

Sumatra located along the southwestern edge of the continental Sunda plate and on the western edge of the Sunda arc, oceanic crust beneath tilted subducted towards the north - northeast [3]. Subduction beneath the western edge of Sumatra was initiated at the beginning of Permian [3].

Regional fault system along Sumatra is a result of the subduction system, the pressure generated by the oblique collision between the Indian-Australian plate and the Eurasian plate appearances process becomes a means of geothermal resources in Sumatra associated with volcanoes. Figure 1 shows that the pattern of tectonic region as a whole is very complex and shows many asperities. There are four patterns of

lineaments (fault) that can clearly be observed on radar image, ie: Pattern lineament (fault) Northwest-Southeast, Northeast-

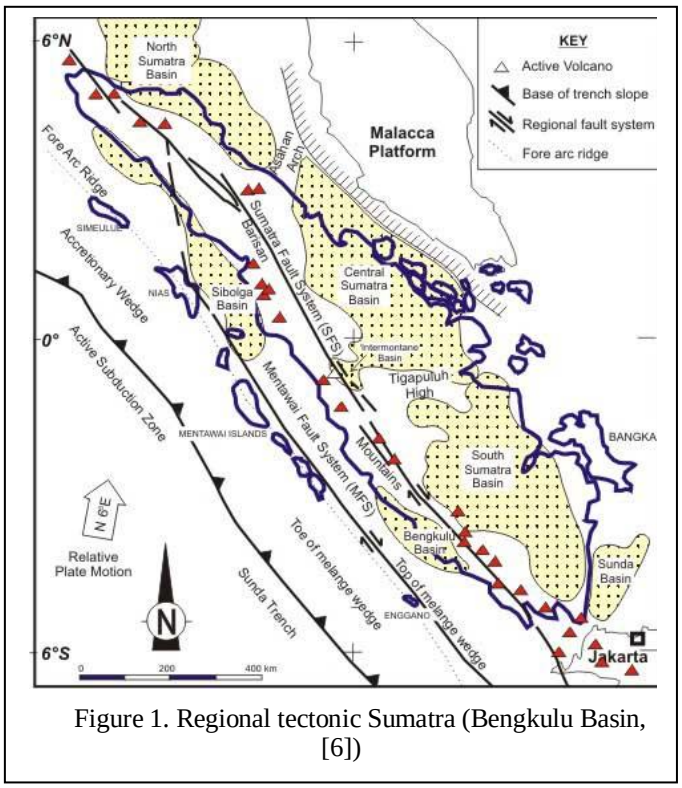

Figure 1. Regional tectonic Sumatra (Bengkulu Basin, [6])

Southwest, North-South and East-West. Fault structures trending Northeast-Southwest, namely: the Great Sumatran Fault Zone, especially those who are active in this area also shows the complexity of the structure of a fault zone termination [4]. Termination of this fault zone consists of many segments of the fault zone that forms the transtension zone and the step-over zone-compressional between fault segments [5].

B. Manifestations of Kepahiang Geothermal

Geological data of Kepahiang geothermal area indicate the presence of impermeable rock that has the properties of the clay mineral montmorillonite and kaolinite types, they are quite high in the area around the manifestation of Sempiang alteration, rock alteration that forms a type of argillic to advanced argillic. The alteration appears pyroclastic flows and lava of Mount Kaba products. The cap rock is in the Sempiang fault zone structures trending almost north south. In addition to the data alteration, other possibilities that can be interpreted as the cap rock is massive Young Kaba Lava and not yet strongly fractured [7].

Manifestations of the Kepahiang geothermal and the surrounding area (Figure 2) consists of fumaroles, solfatara, hot springs, rock alteration and craters accompanied by sublimation of sulfur that quite thick at the top of Mt. Kaba (temperature 96-360 °C). There are two groups manifestations, the first group is Sempiang group located at the headwaters Air Putih (Bukit Itam area), consisting of the appearance of the hot springs, fumaroles and rock alteration. The second group is Babakan Bogor group found in the Babakan Bogor village, manifestations such as appearance of 2 hot springs and cold springs [8].

The manifestations outside of the research area are hot springs in the northwestern part of the leg Mt. Kaba (Suban and Tempel Rejo hot springs), in the eastern part (Sindang Jati hot springs) and in the southern part (Bayung hot springs) [7].

Kusnadi [7] shows the hot water fumaroles of Kaba crater and Sempiang hot springs are sulfuric acid type, whereas Babakan Bogor 1, Bogor Babakan 2, Sindang Jati, Suban, Tempel Rejo, and Bayung hot springs are bicarbonate type. All of the hot springs in the immature zone water and interaction of the fluid with the rock in hot conditions, also mixed with surface water (meteoric water). Babakan Bogor 1 and Bogor Babakan 2 hot springs are no indication that the hot water interact with the volcanic system before it reaches the surface. Based on geotermometer gas shows reservoir temperatures estimated at 250 °C [7].

III. METHODOLOGY

A. Research Data

Measurement data used in this study are land gravity and magnetotelluric. Geological and geochemical information were used for support the analysis of the potential of geothermal energy. Measurement data obtained from the results of land acquisitions carried out by the Center for Geological Resources (PSDG). Measuring point spread in the southern part of Bukit Kaba up to Babakan Bogor hot springs.

Gravity measurement as much as 286 points with spacing are approximately 250 meters, while the MT data by 37 points with the distance between the measurement are 1000 meters to 2000 meters. Coverage of research area are 9250 x 8740 meters (Figure 2).

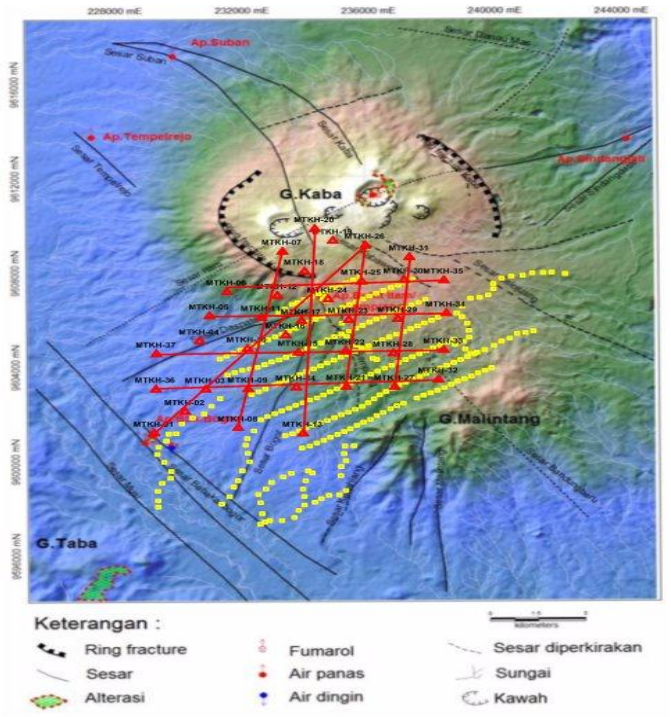

Figure 2. Red triangle are Gravity measurement points; Yellow box are MT measurement points and the red line is the line of 2D MT models

B. *Data Processing*

Gravity data processing is done to reduce the factors that affect the gravity data become complete Bouguer anomaly [9] [10]. To determination regional and residual anomalies using second orde polynomial method [11]. In a cross-sectional modeling the subsurface residual anomaly map created by Surfer software and GravPro-X. Calculation of depth estimation models using spectrum analyzer and to determine the type of geological structure using SVD analysis.

MT data processing begins with quality control data is done by looking at the time series of the electric field components (Ex, Ey) and magnetic field components (Hx, Hy, Hz) of each measurement data from each station within a certain time interval, and then carried out the selection of data where there is no many distractions. Processing time series data [11] performed with SSMT 2000 and editing is done using MT-Editor.

Static correction done using statistical averaging methods [12] [13] and 2D inversion modeling performed on the nine line. Four line in south-north direction, four line in east-west direction and one line in southwest-northeast direction that passes through the Babakan Bogor and Sempiang hot springs. 2D modeling is done by WinGLink and 3D visualization using GeoSlicer-X.

IV. Results and Discussion

A. *Gravity Methods*

Gravity observation value (g_{obs}) in the base station is 977863.9776 mGal. The average value of the surface density (density topography) using Parasnis method [9] in the study area is 2.40 gr/cm^3.

Figure 5 (top) shows the regional anomaly map with a range of values between 22 to 68 mGal. The pattern of high values anomalous in the middle with trending northeast-southwest. Value rises in the middle because of rocks are arranged by the old volcanic rock that properties more massive, while in the southeast and northwest, anomalous values relatively decrease due to the rocks that arrange the area are young volcanic rocks.

Residual anomalies (Figure 5:bottom) shows alignment patterns contour between the low and high anomalies quite sharp. Range residual anomalous values ranging from -7 to 21 mGal. The alignment patterns indicate that controlling fault structures or geothermal systems in the study area.

Alignment contour of high and low anomaly dominant trending northwest - southeast, it is interpreted as the main active fault structure of the Sumatra fault and is the structure that controls Babakan Bogor hot spring manifestation. The other is a alignment contour of high and low anomaly trending nearly north - south, this alignment indicates a fault structure trending. These fault is interpreted as structure that control Sempiang hot spring manifestation.

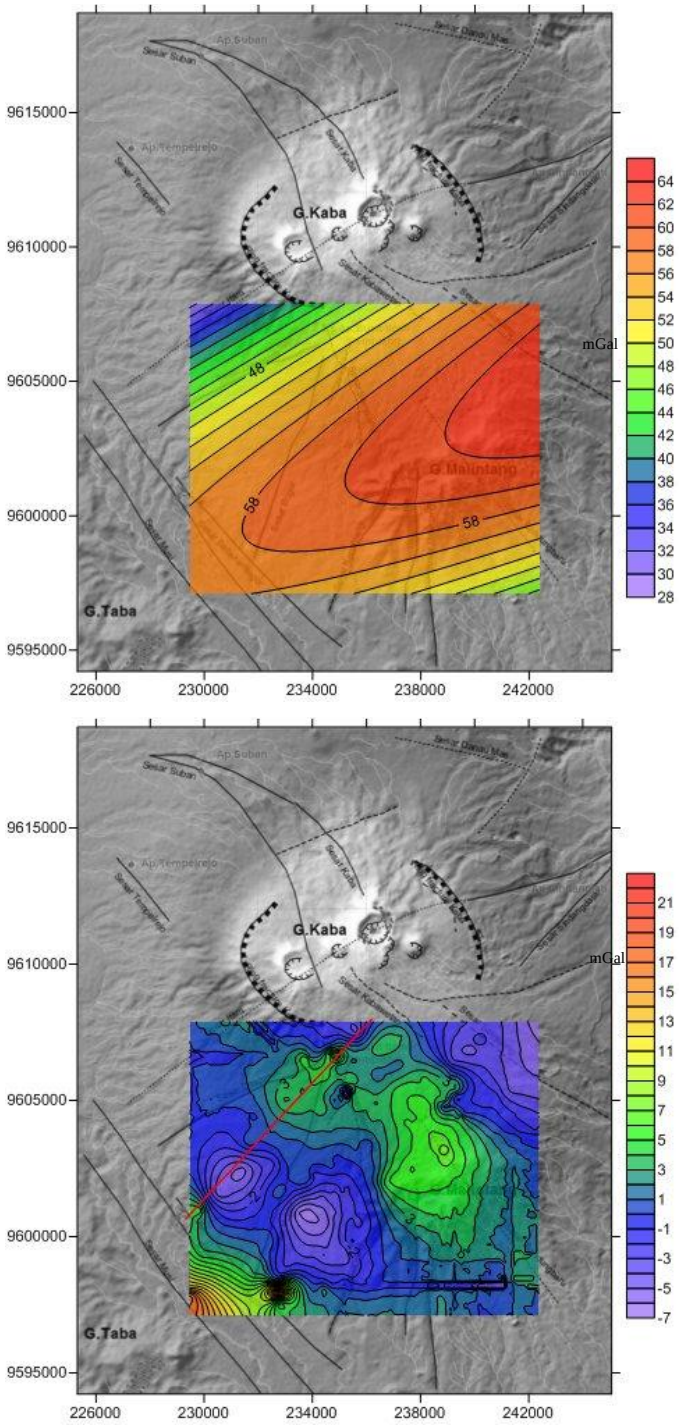

Figure 5. Map of regional anomaly (top) and residual anomaly map of Kepahiang geothermal area (bottom)

In calculating the estimated depth of the response by spectrum analysis on six line in the complete Bouguer anomaly contour. The estimated depth of the response to each line is 2178 m, 1905 m, 3511 m, 3282 m, 2604 m and 1737 m, in order to obtain the average depth of response is used as model input cross section of the subsurface gravity method is 2500 meters.

mGal

Second vertical derivative (SVD) of Bouguer anomaly was calculated by the Elkins method [15]. This method to determine the type of geological structures modeling. In determining the criteria for the type of fault structures using correlation $\left(\frac{\partial^2 g}{\partial z^2}\right)_{maks} > \left|\frac{\partial^2 g}{\partial z^2}\right|_{min}$ for normal fault and $\left(\frac{\partial^2 g}{\partial z^2}\right)_{maks} < \left|\frac{\partial^2 g}{\partial z^2}\right|_{min}$ for thrust fault. Two profiles that represent of the response of the geological structure are showed in figure 6, and based on existing criteria indicate that the anomalies are the normal fault.

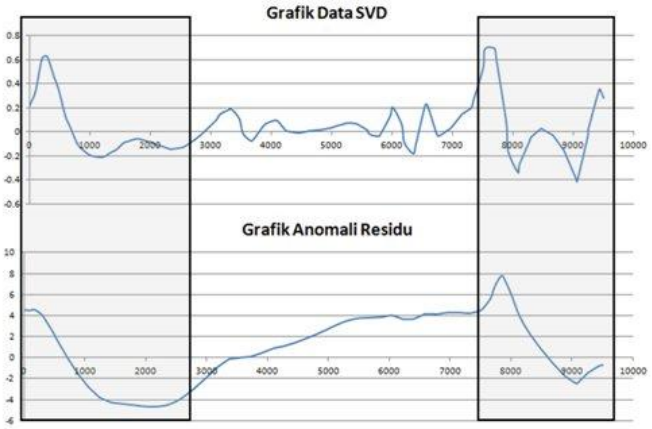

Figure 6. Graph of line A –A' for SVD (top) and residual anomaly data (below)

Inversion model of residual anomaly is also made using the Zondmag2D, the result (Figure 7) shows the variation of density between 1.94 to 2.88 gr/cm^3 along the line A –A'. The line trending southwest - northeast which is the alignment of the Babakan Bogor hot springs towards the Sempiang hot spring. In the southwestern and northeastern parts there has been density contrast represent a fault structures that control the appearance of the Babakan Bogor hot springs and Sempiang hot springs.

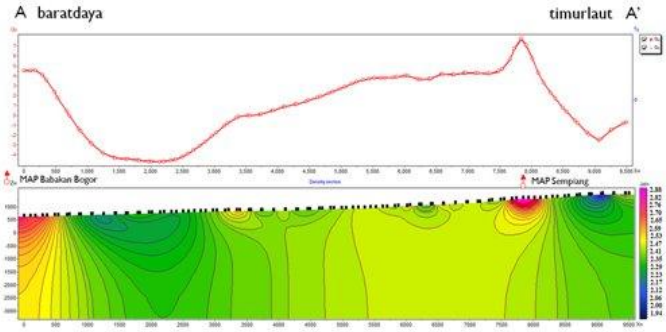

Figure 7. 2D cross-sectional model of gravity inversion results. Figure line A –A'as shown in Figure 5

Based on geological surface information, the results of spectral analysis, SVD analysis and 2D gravity inversion model, then made a cross section model of the subsurface structure. Figure 8 shows the subsurface modeling of the gravity with anomaly of topography density is 2.4 gr/cm^3 in line A –A'.

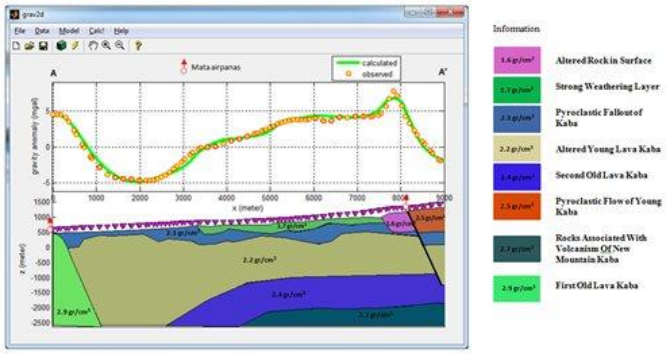

Figure 8. 2D cross-section model of gravity in Kepahiang geothermal area. Figure line A –A'as shown in Figure 5

A cross section models of Gravity shows geological structures, they are lithology contact and fault which are control the manifestation of Babakan Bogor and Sempiang hot spring. Rock density varies from 1.6 to 2.9 gr/cm^3. In the early part of the line (southwestern) contained 2.9 gr/cm^3 rock density that interpreted as Lava of First Old Kaba, then there is a lithological contact, below layer has a density of 2.2 gr/cm^3 interpreted as Young Kaba Lava are undergoing process of alteration that has decreased in density value and upper layer is the pyroclastic fallout of Kaba (2.1 gr/cm^3), and on the surface there is a layer that has undergone strong weathering with a density of 1.7 gr/cm^3. Layer beneath the Young Kaba Lava there is a layer of Second Old Lava Kaba with density of 2.4 gr/cm^3, while the lowest density (1.6 gr/cm3) in the northeastern part of an area of geothermal manifestations are thought to be the location of the rock changes due to the influence of the activity of the Kepahiang geothermal system. In northeastern section there is pyroclastic flow of Young Kaba with density 2.5 gr/cm^3, bounded by the fault that controls Sempiang hot spring. At the depth of 2000 meters there looks rock with a density of 2.7 gr/cm^3, this rock are interpreted as lithologies related to volcanism of New Mount Kaba.

B. MT Method

2D resistivity model from MT measurement in Kepahiang geothermal area at 9 line that trending southwest-northeast, south-north and west-east (Figure 3) are shown in the vertical and horizontal cross-section to describe the distribution layer with low, medium and high resistivity.

2D resistivity model of line 1 (Figure 9) shows a distribution of low resistivity values extending from the southwest to the northeast. This low resistivity scattered from near the surface to 2500 meters depth with a thickness between 1500 to 2500 meters. Low resistivity are interpreted as the response of the rock alteration that serves as the cap rock geothermal system in this area. At the bottom of this layer, scattered moderate resistivity values. Resistivity that located between the Babakan Bogor hot springs and Sempiang hot springs are interpreted as a response of the geothermal reservoir, while the high resistivity values next to northeastern Sempiang hot springs are interpreted as a reservoir associated with the volcanism of Mount Kaba.

In the cross-section of the Babakan Bogor hot springs and Sempiang hot springs seen the contrast of resistivity values are interpreted as an indication of lithological contacts and fault structures. Contrast resistivity values seen in the north-east, around the point MTKH-25, interpreted as an indication of the caldera structure located around the peak of Mount Kaba.

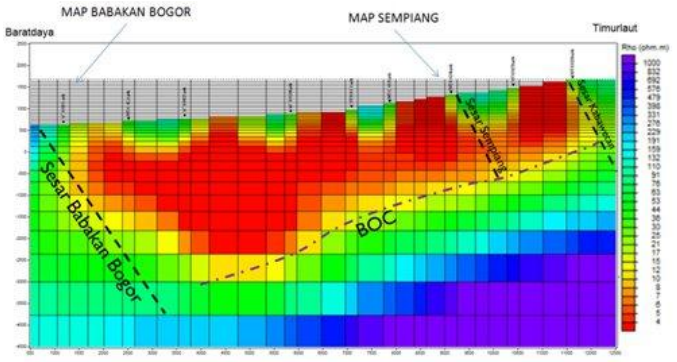

Figure 9. 2D resistivity model of the line 1

Figure 10 (top) is shown resistivity model of line 2-5 in the south – north direction and figure 10 (bottom) is shown resistivity model of line 6-9 in the west – east direction. Figure 11 shows the resistivity model results in a horizontal cross-section.

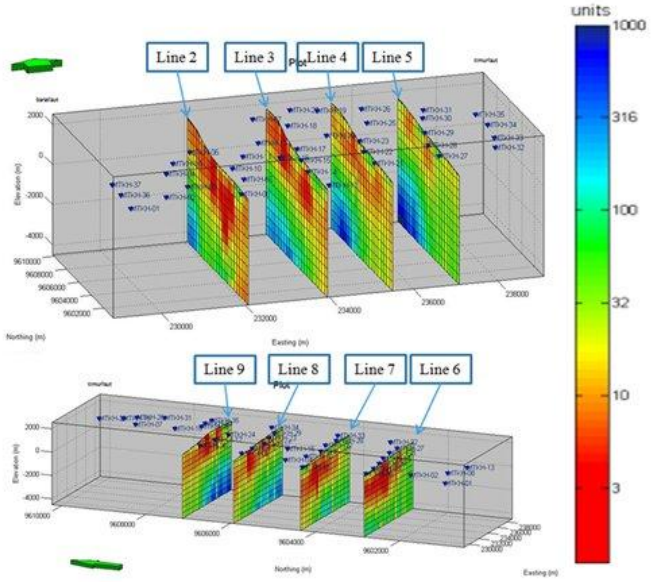

Figure 10. Resistivity model in a vertical cross-section

From Figure 10 and 11 clearly visible scatter of low resistivity (<10 Ohm-m) that extends from the southwest to the northeast. In the northeastern part of the low resistivity are spread from near the surface to a depth of about 1500 meters, towards the south-west of this low resistivity thicken up to 2500 meters. Low resistivity are interpreted as the response of the rock alteration that serves as the cap rock geothermal system.

At the bottom of this layer, scattered moderate resistivity values with depth following the thickness of the layers of cap rock. The resistivity are interpreted as a response of the geothermal reservoir. High resistivity values are in the northeast to form a dome with the top of the dome in the northeast of research area. These rocks are interpreted as volcanic rocks associated with the volcanism of Mount Kaba. Distribution of the cap rock, reservoirs and volcanic rock possibility still being towards the north of studied area (towards the top of Mount Kaba).

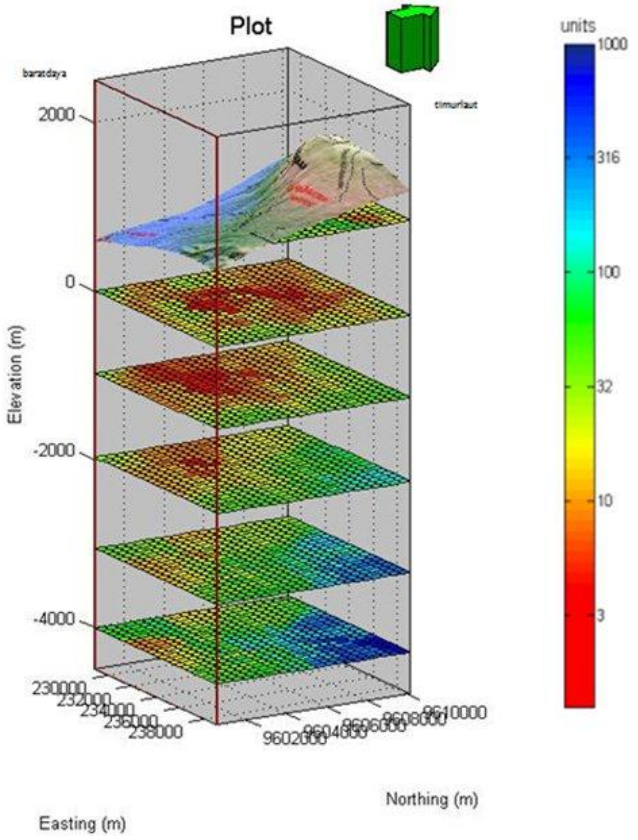

Figure 11. Resistivity model in a horizontal cross-section

C. Kepahiang Geothermal Systems

Formation of geothermal systems in Kepahiang particularly in the area of Kaba in the framework of plate tectonics is closely related to the magmatic arc path. Kepahiang geothermal system model is very similar to the model proposed by Bogie, et al. [16] is a model of volcanic geothermal systems (magma reservoir). Reservoir of geothermal system is a reservoir of hydrothermal system, ie where the geothermal reservoir system containing steam, water or a mixture of both, depending on reservoir pressure and temperature [17].

These systems are thought to form due to the interaction of tectonic plates stretch of rock that is as thick as 64-145 km which floats on the asthenosphere. These plates move slowly and constantly push each other and one of them will subducted under the other plate. Because of the heat in the astenosfere and heat due to friction, the tip of the slab crushed melt, has a high temperature (magmatism process). The existence of this hot

rock causes the temperature gradient in the area to be larger than the average gradient temperature.

As a result of the subduction system, pressure or compression produced by the oblique collision between the Indian-Australian plate and the Eurasian plate resulted in regional fault that extends along the island of Sumatra, which is a means for the emergence of geothermal sources associated with young volcanoes. According Saptadji [1] also concluded that geothermal systems in Sumatra are generally controlled by regional fault systems associated with the Sumatra fault system. Sumatra geothermal reservoirs in sedimentary rocks which generally occupy has undergone several tectonic deformation or faulting at least since the Tertiary until Resen. This led to the formation of secondary porosity or permeability in sedimentary rocks are dominant in the end produces geothermal reservoir permeability is large. Judging from the characteristics of the geothermal system has a high enough temperature associated with young volcanic activity.

Geothermal fluid contained in the hydrothermal reservoir comes from surface water, among other rainwater (meteoric water) that penetrate the bottom surface of the slopes of Mount Kaba and from outside the Kaba complex area, and heated by a heat source. The water will enter through cracks into the permeable rock. The surrounding rocks are the source of heat from magma, then the heat will be propagated through the rock (by conduction) and through the fluid (by convection). Heat transfer by convection occurs basically due to the buoyant force (bouyancy). Water because of gravity always has a tendency to move down, but if the water is in contact with a heat source, there will be heat transfer to the water temperature becomes higher and the water becomes lighter. This situation causes more hot water moving upward and cooler water moves down to the bottom, resulting in water circulation or convection currents.

Rocks in hydrothermal systems is a natural rock fracturing. In the study area there is a geological fault structure which allows the water to flow through cracks and or permeable rock, and then appeared on the surface. Phase change occurs on its way to the surface, when the water temperature has reached the saturation temperature or the temperature of the boiling point. So that the fluid in the form of steam-water mixture and form a vapor phase only. This leads to the types of geothermal surface manifestation became very diverse, there are hot springs, fumaroles, cold springs and rock alteration that each has different characteristics despite its close proximity.

By looking at the manifestations of hot springs, fumaroles and alteration (acid) in the area Sempiang hot springs estimated as the upflow of geothermal systems Mount Kaba, while Babakan Bogor, Suban, Tempel rejo, Sindang Jati hot springs on the bottom slopes of Mount Kaba estimated is outflow zone of the geothermal system Mount Kaba (Geochemistry).

Heat source on Mount Kaba geothermal system associated with Quaternary volcanic system that still has a heat content and complex active volcano Mount Kaba is type A. History of the volcanic eruption of Mount Kaba has experienced in 1951 and the formation of the crater Volkgesang (Directorate of Volcanology, 1990) and in 2004 a hydrothermal eruption (freatomagmatik) at Kaba large crater. Based on these data, the heat source in this system is estimated to originate from volcanism of New Kaba Mountain product.

The cap rock is estimated to be rock alteration and Young Kaba Mountain product that has not undergone fractured and alteration process (density 2.2 gr/cm3). This alteration of rocks have different physical properties that are not unchangeable rocks, one of which is the resistivity of rocks. In geothermal systems in volcanic areas, rock alteration that serves as the cap rocks generally give low resistivity value of the response, while the rock which serves as a reservoir to respond resistivity values higher than the cap rock. Based on the results of MT in Kepahiang geothermal area, low resistivity values (<10 Ohm-m) is interpreted as the response of the rock alteration (the cap rock) scattered around the Sempiang hot springs and dilated toward Babakan Bogor hot springs. This low resistivity began to spread near the surface of the soil to a depth of about 2500 meters with a thickness of between 1500 meters to 2500 meters (Figure 12).

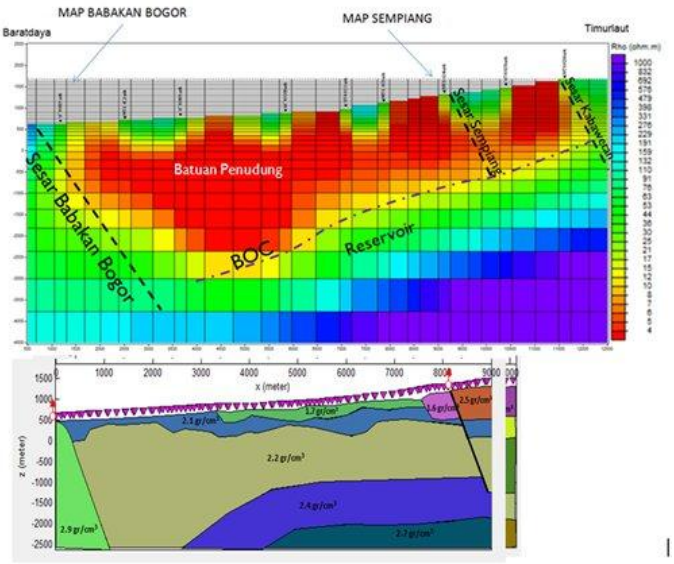

Figure 12. Subsurface cross section model based on gravity and MT method

Geothermal reservoir is estimated to be under the rock alteration as indicated by resistivity values between 10-60 Ohm-m and density 2.4 gr/cm^3 scattered around the Sempiang hot springs and dilated toward Babakan Bogor hot springs. The highlight of the reservoir is estimated to be in the north Sempiang hot springs with a depth of about 1500 meters below the ground surface. Based on geological data, this rock is a product of the Old Kaba Volcanic lava or pyroclastic.

From the results of 3D visualization based on the resistivity model (Fig. 13) and the gravity model and supported by geological and geochemical information, and then made a conceptual model of the Kepahiang geothermal system (Figure 14). Conceptual image of the model can be explained that the Sempiang hot springs is upflow zone and Babakan Bogor hot springs is outflow zone. So the geothermal prospect areas located around Sempiang hot springs.

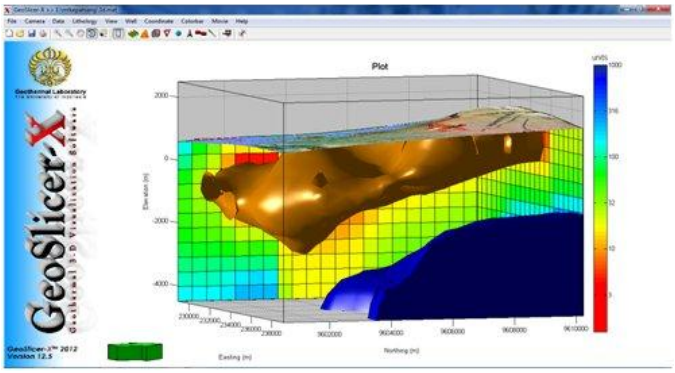

Figure 13. 3D visualization results based on resistivity models using GeoSlicer-X

D. Prospect area of Kepahiang Geothermal

By considering the geochemical and geological data, from the processing of gravity and MT is then used to determine the prospect areas of Kepahiang geothermal. The area is localized using the base of conductor map (BOC) which is the lower limit of the cap layers so the distribution of reservoir can be determined. The prospect area of Kepahiang geothermal that calculated from BOC which bounded by fault and depth of BOC is 19 km^2 (Figure 15).

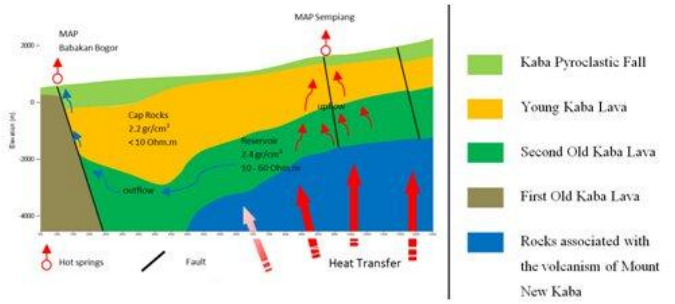

Figure 14. Conceptual model of Kepahiang geothermal system by gravity and MT methods

Calculation of the geothermal energy potential uses the basic principles of volumetric methods, geothermal reservoir is considered as a form of a box whose volume can be calculated by multiplying the widespread distribution and thickness. The approach model used was lumped parameter models that assume a uniform reservoar parameters [18].

Volumetric method used in the resource class hypothetical until proven. Some assumptions are needed to estimate the heat energy equal to the electrical energy. Assumptions used: 1 km thick reservoir, recovery factor = 50%, conversion factor = 10%, lifetime = 30 years.

Lump parameters equation:

$$Q = K \times A \times (Tres - Tcut\ off) \quad (1)$$

Where K = 0.1 (conversion factor for thermal energy contained in the thermal fluid) and K = 0.19 (for the heat energy contained in the fluid and rock formations), A = area of the prospect; Tres = reservoir temperature; tcut off = temperature cut-off

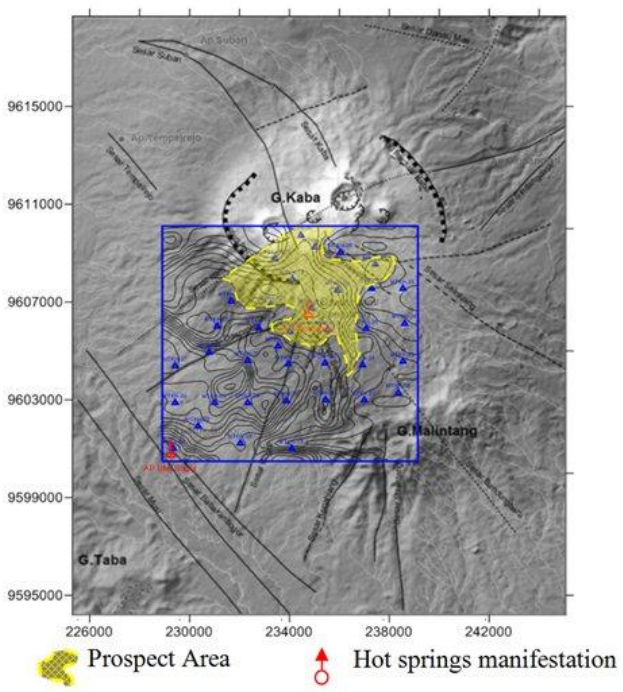

Figure 15. Prospect area map of Kepahiang geothermal

Information based on geology, geochemistry and geophysics, geothermal prospect areas in the study area is as shown in Figure 5.5. Kepahiang geothermal prospect areas are around the Sempiang hot springs bounded by contrasting resistivity and geological structure has a 19 km^2 area. Reservoir temperature based on geochemical analysis is 250 ^{0}C, based on SNI classification is a high-temperature reservoir classification (>225 ^{0}C) so the temperature cut-off used 180 ^{0}C [18] and K is used 0.1 then the area of Kepahiang geothermal energy potential is calculated as follows,

Q = 0,1 x 19 x (250 – 180) = 133 Mwe

Kepahiang geothermal area with approximately 19 km^2 prospect area has a geothermal potential of 133 MWe. Based on ISO Classification Geothermal Energy Potential in Indonesia in 1999, the calculation of potential geothermal reserves are included in the expected reserves classification, the extent and thickness of reservoir rock and fluid physical parameters are estimated based on data integrated geoscience described in detail tentative models [18].

V. CONCLUSION

The results of the Kepahiang geothermal system analysis based on analysis of gravity and MT as well as geological and geochemical information can be summarized as follows:

1. Kepahiang geothermal system in a volcanic geothermal system associated with Quaternary volcanic system with a heat source in this system is estimated to originate from volcanism of New Kaba Mountain product.

2. Based on the residual gravity anomalies, structures that control the appearance of the hot springs in the area Sempiang estimated Sempiang fault trending nearly north-south. While the Babakan Bogor hot springs is estimated controlled by the Sumatra fault.
3. The cap rocks scattered around the Sempiang hot springs and widened towards the Babakan Bogor hot springs, starting near the ground surface to a depth of about 2500 meters with a thickness of between 1500 meters to 2500 meters. The cap rock is a unit of the altered Young Kaba Lava with resistivity values < 10 Ohm-m and density 2.2 gr/cm^3.
4. Geothermal reservoir is estimated to be under the cap rocks as indicated by resistivity values between 10-60 Ohm-m and density 2.4 gr/cm^3. Volcanic rock is a product of the Old Kaba either lava or pyroclastic.
5. Kepahiang geothermal prospect area scatters 19 km^2 wide around Sempiang hot springs which is bound by contrast resistivity and fault. It has potential geothermal of 133 MWe with the assumption of reservoir temperatur (geochemistry) is 250 ^{0}C.
6. Calculation of potential geothermal reserves is included in the classification of expected reserves, the extent and thickness of reservoir rock and fluid physical parameters are estimated based on data of integrated geoscience detail depicted in the tentative models.

ACKNOWLEDGMENT

The first author is very grateful to the Center for Geological Resources (Geological Agency) for providing the Gravity and MT data. Also, the author would like to thank the PT NewQuest Geotechnology for facilitating the data processing.

REFERENCES

[1] Saptadji, N.M., 2009. Karakterisasi Reservoir Panas Bumi. Training "Advanced Geothermal Reservoir Engineering, 6 – 17 Jumi 2009. ITB

[2] Tjahjono, B.S.E., Arsadi, E.M., Syuhada dan Arifin, J. 2010. *Penyelidikan Geologi dan Geofisika untuk Inventarisasi Potensi Panasbumi di Kabupaten Rejang Lebong, Bengkulu*. Laporan Akhir Tahun 2010 Kegiatan Program Insentif Bagi Peneliti dan Perekayasa, Lembaga Ilmu Pengetahuan Indonesia

[3] Gafoer, S., Amin, T. C., and Pardede, R., 1992. *Geologi Lembar Bengkulu, Sumatra*. Puslitbang Geologi, Bandung. 91 halaman

[4] Natawidjaja dan Sieh, 1994. Neotektonik dari sistem sesar Sumatra, *Prosiding hasil-hasil penelitian puslitbang geoteknologi LIPI 1994*. LIPI, Bandung

[5] Natawidjaja dan Ruslan, 1994. Kondisi Tektonik Serta Hubungannya dengan Kegempaan dan Aktivitas Gunung Api Di Daerah Rejang Lebong, Bengkulu. *Prosiding hasil-hasil penelitian puslitbang geoteknologi LIPI 1994*. LIPI, Bandung

[6] IAGI, 2009. *Cekungan Bengkulu*, diakses pada tanggal 16 April 2012. http://geologi.iagi.or.id/2009/03/22/cekungan-bengkulu/

[7] Kusnadi, D., Nurhadi, M., Suparman. 2011. Penyelidikan Terpadu Geologi dan Geokimia Daerah Panas Bumi Kepahiang, Kabupaten Kepahiang, Bengkulu. *Prosiding Hasil Kegiatan Pusat Sumber Daya Geologi Tahun 2010*. PSDG, Bandung

[8] Arsadipura, S., Kholid, M., Djukardi, D. 2011. Penyelidikan Geofisika Terpadu Gaya Berat, Geomagnet dan Geolistrik Daerah Panas Bumi Kepahiang, Kecamatan Kaba Wetan, Kabupaten Kepahiang, Provinsi Bengkulu. *Prosiding Hasil Kegiatan Pusat Sumber Daya Geologi Tahun 2010*. PSDG, Bandung

[9] Telford, W. M., Geldart, L.P., Sheriff, R.E., Keys D.A., 1990. *Applied Geophysics 2nd edition*. Cambridge University Press.

[10] Blakely, R. J., 1995, Potential Theory in Gravity and Magnetic Applications, Cambridge University Press.

[11] Purnomo, J., Koesuma, S., Yunianto, Y., 2013. Pemisahan Anomali Regional-Residual pada Metode Gravitasi Menggunakan Metode Moving Average, Polynomial dan Inversion. *Indonesian Journal of Applied Physics (2013)* Vol.3 No.1 halaman 10

[12] Vozoff, K., 1991, The Magnetotellruic Method, Chapter 8, Electromagnetic method in applied geophysics-Applications part A and part B, edit by Corbett, J.D., published by Scociety of Exploration Geophysicists, p.641-711.

[13] Sulistyo, A. 2011. Koreksi Pergeseran Statik Data Magnetotelluric (MT) Menggunakan Metode Geostatistik, Perata-rataan, Dan Time Domain Electromagnetic. Skripsi Program Studi Fisika, FMIPA, UI

[14] Jiracek, G.R. 1985. Near Surface and Topografic Distortion In Electromagnetic Induction. San Diego State University

[15] Elkins, T.A., 1951, The Second Derivative Method of Gravity Interpretation. *Geophysics*, 16, 29-50

[16] Bogie I., Lawless J.V., Rychagov S. and Belousov V. 2005. *Magmatic-Related Hydrothermal Systems: Classification of the types of geothermal systems and their ore mineralisation*. Geothermal and mineral resources of modern volcanism areas (proceedings of the International Kuril-Kamchatka field workshop, July 16 - August 6, 2005), Publishing house ÖTTISK¨", 2005. 460p

[17] Edwards, L. M., Chilingar, G. V., Rieke, H. H., and Fertl, W. H. *Handbook of Geothermal Energy*, Gulf Publishing Company, 1982, Chapter 2

[18] Badan Standarisasi Nasional-BSN, 1999. Metode Estimasi Potensi Energi Panas Bumi. Standar Nasional Indonesia, SNI 13-6171-1999, ICS 73.020

G503

Three-dimensional Inversion of Magnetic Resonance Sounding (MRS) for Groundwater Detection

Warsa Warsa, Hendra Grandis, Wahyudi W Parnadi, and Djoko Santoso
Applied Geophysics Research Group
Faculty of Mining & Petroleum Engineering ITB
Bandung, Indonesia
warsa@gf.itb.ac.id

Abstract*—We consider the resulting 3-D inversion using inversion modeling, which have been motivated by a developed theory and the recent application of the magnetic resonance sounding (MRS) technique to detecting and mapping of subsurface groundwater. MRS is a non-invasive method which directly detects the groundwater existence from surface measurements. A pulse current, at a proper frequency, is transmitted into a loop. After hydrogen atoms of water molecules in the subsurface are energized by pulses of alternative current, the magnetic resonance field produced by the H protons is measured within the same loop. MRS can be generalized to have two observables: initial amplitude and decay time. The aim of inversion is to extract the information, i.e., the value and distribution of two physical parameters of subsurface: water content and subsurface properties (pore and grain size). We presented a general formulation for inverting initial amplitude and decay time of MRS data to recover a 3-D distribution of groundwater. The forward problem was solved using integral equation method in the spatial domain. An improved Levenberg-Marquardt strategy has been employed to solve the inverse problem. Two synthetic examples have illustrated the basic functionality of the inversion algorithm, and the real data results have shown the applicability in a larger-scale field example. (*Abstract*)

Keywords—MRS; groundwater; 3-D inversion; water content; decay time (key words)

G504

Magnetotelluric Investigations in Wai Umpu Geothermal Prospect Area Lampung Province, Indonesia

Wahyudi W. Parnadi, Widodo, Ryanti W. Savitri
Geophysical Engineering Department
Bandung Institute of Technology (ITB)
Bandung, Indonesia

Ahmad Zakarsyi
Subsurface Department
Geological Resource Center (PSDG)
Bandung, Indonesia

***Abstract*— The PSDG previous research estimated that "Wai Umpu 1" hot spring in Wai Umpu geothermal prospect area reflects a reservoir temperature of 160 °C – 195 °C. From geological observation, the main fault structure in that area is Wai Umpu Fault, which has a strike direction of NE – SW and the area is dominated by volcanic rocks. Many joints are also found along fault line. "Wai Umpu-1" hot spring is controlled by these geology structures. These previous research and field observation lead us to carry out continuing study in that area, which is aimed at determining its resistivity structure to a depth of 4 km.**

For this purpose, we carried out field measurement using Audiomagnetotelluric (AMT) and Magnetotelluric (MT) methods. The work presented in this paper is the result of 1-D and 2-D inversion model from 8 MT soundings. We compare inversion models using 1-D Bostick transformation, 1-D Occam, and 2-D Nonlinear Conjugate Gradient (NLCG) algorithms. The study result reveals the existence of strike as indicated from geological data and a low resistivity zone at shallow surface to a depth of 2 km that is most probably associated with partial melting and intrusion at greater depth.

***Keywords*— Geothermal; Magnetotelluric; 1-D and 2-D models; Wai Umpu Lampung**